

Inhibitory and metabolic effects of diabetes on yolk sac-derived endothelial-macrophage progenitors in postnatal murine tissues

Sanuri Rashmitha Liyanage

A thesis submitted to The University of Adelaide
in candidature for the degree of Doctor of Philosophy
in the School of Medicine, Faculty of Health and Medical Sciences

December 2022



THE UNIVERSITY
of ADELAIDE

School of Medicine

Faculty of Health and Medical Sciences

The University of Adelaide

South Australia

&

Vascular Research Centre

Lifelong Health Theme

South Australian Health & Medical Research Institute

South Australia

Table of contents

TABLE OF CONTENTS	II
TABLE OF FIGURES	VIII
TABLE OF TABLES	XI
ABSTRACT	XII
DECLARATION	XIV
ACKNOWLEDGEMENTS	XVI
CONFERENCE PRESENTATIONS.....	XIX
AWARDS	XXI
PUBLICATIONS.....	XXII
ABBREVIATIONS.....	XXIII
PROTEIN ABBREVIATIONS.....	XXVII
GENE ABBREVIATIONS.....	XXXII
1. INTRODUCTION.....	1
1.1 THE RECIPROCAL INTERACTIONS BETWEEN MYELOID AND ENDOTHELIAL CELLS	2
1.2 THE ANCESTRAL LINK BETWEEN MACROPHAGES AND ENDOTHELIAL CELLS	7
1.2.1 <i>Development of the embryonic haematopoietic system.....</i>	<i>7</i>
1.2.2 <i>Maintenance of postnatal tissue macrophages</i>	<i>14</i>
1.2.3 <i>Haemangioblasts and haemogenic endothelium: two possible candidates for bipotent progenitors for haematopoietic and endothelial cells.....</i>	<i>16</i>
1.2.4 <i>Development of the embryonic vascular system</i>	<i>19</i>
1.2.5 <i>Origins of postnatal endothelial cells</i>	<i>20</i>
1.3 DIABETES MELLITUS	22
1.3.1 <i>Epidemiology.....</i>	<i>22</i>
1.3.2 <i>Maintaining glucose homeostasis</i>	<i>22</i>
1.3.3 <i>Classification of diabetes mellitus</i>	<i>26</i>
1.4 THE EFFECT OF DIABETES ON MITOCHONDRIAL BIOLOGY	34

1.4.1	<i>Basic physiology of aerobic respiration in steady state</i>	34
1.4.2	<i>Mitochondrial dysfunction in type 1 and type 2 diabetes</i>	41
1.4.3	<i>Mitochondrial reactive oxygen species in steady state</i>	45
1.5	WOUND REGENERATION IN HEALTHY AND DIABETIC SKIN	52
1.5.1	<i>Anatomy and functions of skin in steady state</i>	52
1.5.2	<i>Cellular components of steady state skin</i>	53
1.5.3	<i>Mechanisms of wound healing in steady state</i>	58
1.5.4	<i>Mechanisms of impaired wound healing in diabetes</i>	69
1.6	THE RESPONSE AND ADAPTATION OF THE SKELETAL MUSCLE TO DIABETES	78
1.6.1	<i>Skeletal muscle characteristics in physiological conditions</i>	78
1.6.2	<i>Skeletal muscle development</i>	80
1.6.3	<i>Cellular components of muscle regeneration</i>	82
1.6.4	<i>Skeletal muscle in diabetes</i>	89
1.6.5	<i>Cellular mechanisms of diabetes impaired ischaemic repair</i>	92
1.7	DISCOVERY OF YOLK-SAC DERIVED ENDOTHELIAL-MACROPHAGE PROGENITORS AS A NOVEL BIPOTENT SOURCE OF MACROPHAGES AND ENDOTHELIAL CELLS	101
1.7.1	<i>EndoMac progenitors in adventitia of murine arteries</i>	101
1.7.2	<i>EndoMac progenitors in murine skin and skeletal muscle</i>	105
1.7.3	<i>EndoMac progenitors in healthy and diabetic human vasculature</i>	108
1.8	PROJECT SCOPE	109
2.	MATERIALS AND METHODS	111
2.1	GENERAL MATERIALS	112
2.1.1	<i>Equipment</i>	112
2.2	MATERIALS	115
2.3	REAGENTS	119
2.4	SUPPLEMENTED CULTURE MEDIA	124
2.4.1	<i>Dulbecco's Modified Eagle's Medium, High Modified (DMEM)</i>	124
2.4.2	<i>Endothelial Cell Growth Media (EGM)</i>	124
2.4.3	<i>Freezing Media</i>	124
2.4.4	<i>Iscove's Modified Dulbecco's Medium (IMDM)</i>	124
2.5	ANIMAL PROCEDURES	125

2.5.1	<i>Animal ethics</i>	125
2.5.2	<i>Mice</i>	125
2.6	PREPARATION OF SINGLE CELLS	127
2.6.1	<i>Preparation of aortic, skin, and skeletal muscle cells</i>	127
2.6.2	<i>Preparation of brain cells</i>	127
2.6.3	<i>Preparation of blood</i>	127
2.6.4	<i>Preparation of bone marrow (BM)</i>	128
2.6.5	<i>Cell counts and viability</i>	128
2.7	IN VIVO TECHNIQUES.....	129
2.7.1	<i>Streptozotocin (STZ)-induced type 1 diabetes model</i>	129
2.7.2	<i>Hind limb ischaemia</i>	129
2.7.3	<i>Wound healing</i>	131
2.8	IN VITRO METHODS	133
2.8.1	<i>Primary cultures</i>	133
2.9	IMMUNOSTAINING	137
2.9.1	<i>Immunofluorescence labelling and confocal microscopy</i>	137
2.9.2	<i>Cytoimmunofluorescence</i>	137
2.10	PROTEIN ANALYSIS.....	141
2.10.1	<i>Flow cytometry</i>	141
2.11	MOLECULAR BIOLOGY TECHNIQUES.....	147
2.11.1	<i>RNA isolation from cells and tissues</i>	147
2.11.2	<i>RNA quantification</i>	147
2.11.3	<i>Bulk-RNA-sequencing</i>	148
2.12	STATISTICAL ANALYSIS	150
3.	UNDERSTANDING THE HETEROGENEITY OF ENDOTHELIAL-MACROPHAGE PROGENITORS	
	151	
3.1	INTRODUCTION.....	152
3.2	METHODS IN BRIEF	155
3.2.1	<i>Overview</i>	155
3.2.2	<i>Statistical analysis</i>	156
3.3	RESULTS	157

3.3.1	<i>Immunophenotypic characterisation of EndoMac progenitors</i>	157
3.3.2	<i>Aortic EndoMac progenitors are angiogenic and possess bipotent differentiation capacity</i>	162
3.3.3	<i>EndoMac progenitors are bipotent at a clonal and single cell level</i>	165
3.3.4	<i>Effect of different tissue source on the biology of EndoMac progenitors</i>	168
3.3.5	<i>Tissue-related effects on the angiogenic and differentiation capacity of EndoMac progenitors</i>	172
3.3.6	<i>Transcriptomic comparison of EndoMac progenitors from different tissue sources</i>	176
3.3.7	<i>STZ-induced hyperglycaemia is associated with fewer EndoMac progenitors with limited clonal renewal capacity in aorta</i>	191
3.3.8	<i>Aortic progenitors have diminished differentiation and angiogenic capacity from diabetic mice</i>	195
3.3.9	<i>Diabetic aortic progenitors are prone to double-stranded DNA breaks</i>	198
3.3.10	<i>Effects of in vitro exposure to high glucose on aortic progenitors</i>	201
3.4	DISCUSSION	204
	LIMITATIONS AND FUTURE DIRECTIONS	207
	CONCLUSION	208

4. INHIBITORY EFFECTS OF DIABETES ON YOLK-SAC DERIVED ENDOTHELIAL-MACROPHAGE PROGENITORS IN MURINE SKIN AND WOUND HEALING 209

4.1	INTRODUCTION.....	210
4.2	METHODS IN BRIEF	213
4.2.1	<i>Overview</i>	213
4.2.2	<i>Statistical analysis</i>	214
4.3	RESULTS	215
4.3.1	<i>High glucose attenuates stem-like and angiogenic properties of skin EndoMac progenitors</i>	215
4.3.2	<i>High glucose inhibits mitochondrial metabolic activity of skin EndoMac progenitors</i>	219
4.3.3	<i>Skin EndoMac progenitors function at lower metabolic capacity when exposed to high glucose</i>	223
4.3.4	<i>STZ-induced hyperglycaemia is associated with fewer EndoMac progenitors in skin</i>	228
4.3.5	<i>Diabetic skin EndoMac progenitors are more prone to DNA damage and mitochondrial abnormalities</i> 234	
4.3.6	<i>Diabetic skin EndoMac progenitors have diminished differentiation and angiogenic capacity in vitro</i>	238
4.3.7	<i>Diabetes impairs wound healing with diminished expansion of EndoMac progenitors after wound injury</i> 241	
4.3.8	<i>Transfer of non-diabetic but not diabetic progenitors promotes wound healing in diabetic skin</i>	260

4.4	DISCUSSION	271
	LIMITATIONS AND FUTURE DIRECTIONS	275
	CONCLUSION	277
5.	INHIBITORY EFFECTS OF DIABETES ON YOLK-SAC DERIVED ENDOTHELIAL-MACROPHAGE PROGENITORS IN MURINE SKELETAL MUSCLE AND ISCHAEMIA	278
5.1	INTRODUCTION.....	279
5.2	METHODS IN BRIEF	283
5.2.1	<i>Overview</i>	<i>283</i>
5.2.2	<i>Statistical analysis</i>	<i>284</i>
5.3	RESULTS	285
5.3.1	<i>High glucose attenuates stem-like and angiogenic properties of SkM EndoMac progenitors.....</i>	<i>285</i>
5.3.2	<i>Effects of high glucose on the mitochondrial and metabolic activity of SkM progenitors.</i>	<i>289</i>
5.3.3	<i>SkM EndoMac progenitors' function at a lower metabolic capacity when exposed to high glucose</i>	<i>293</i>
5.3.4	<i>Streptozotocin-induced hyperglycaemia induces a systemic inflammatory state.....</i>	<i>298</i>
5.3.5	<i>STZ-induced hyperglycaemia is associated with fewer EndoMac progenitors in SkM.....</i>	<i>302</i>
5.3.6	<i>Diabetic SkM progenitors are more prone to DNA damage and possess mitochondrial abnormalities.</i>	<i>308</i>
5.3.7	<i>Diabetic SkM EndoMac progenitors have diminished differentiation and angiogenic capacity</i>	<i>312</i>
5.3.8	<i>Diabetic SkM has reduced capacity for ischaemic repair with delayed expansion of EndoMac progenitors</i>	<i>315</i>
5.3.9	<i>SkM progenitors arise from YS EMPS and show reduced expansion early post-ischaemia in diabetes.</i>	<i>326</i>
5.3.10	<i>Transfer of non-diabetic but not diabetic progenitors promotes perfusion recovery after ischaemia in diabetic SkM.....</i>	<i>339</i>
5.4	DISCUSSION	350
	LIMITATIONS AND FUTURE DIRECTIONS	355
	CONCLUSION	357
6.	GENERAL DISCUSSION.....	358
6.1	GENERAL OVERVIEW AND KEY FINDINGS	359
6.2	BRIDGING EXISTING KNOWLEDGE GAPS	366
6.2.1	<i>Why defining the function of EndoMac progenitor cells in diabetes is important?</i>	<i>370</i>
6.2.2	<i>EndoMac progenitor origins and tissue heterogeneity</i>	<i>371</i>

6.2.3	<i>Mitochondrial and metabolic function of EndoMac progenitors</i>	378
6.3	FUTURE DIRECTIONS AND RESEARCH AREAS OF INTEREST	382
6.3.1	<i>Type 2 diabetes</i>	382
6.3.2	<i>Studying EndoMac progenitors in human skin and muscle</i>	382
6.3.3	<i>EndoMac progenitors as a potential therapy for diabetic tissue repair</i>	384
6.3.4	<i>Rescuing EndoMac progenitors by targeting mitochondrial dysfunction</i>	385
6.4	CONCLUSION	388
7.	APPENDICES	389
8.	REFERENCES	396

Table of figures

FIGURE 1.1: MACROPHAGES AND ECs ARE INTIMATELY INVOLVED IN ANGIOGENIC PROCESSES.....	6
FIGURE 1.2: THE SUCCESSIVE WAVES OF MURINE HAEMATOPOIETIC DEVELOPMENT.....	12
FIGURE 1.3: ORIGINS OF TISSUE-RESIDENT MACROPHAGES.....	13
FIGURE 1.4: INSULIN SIGNALLING PATHWAY.....	24
FIGURE 1.5: GLUCOSE HOMEOSTASIS IN THE HUMAN BODY.....	25
FIGURE 1.6: THE STAGES OF CELLULAR AEROBIC RESPIRATION.....	36
FIGURE 1.7: OXIDATIVE PHOSPHORYLATION- THE ELECTRON TRANSPORT CHAIN	39
FIGURE 1.8: REACTIVE OXYGEN SPECIES PRODUCTION IN THE ELECTRON TRANSPORT CHAIN AS A RESULT OF ELECTRON LEAK	47
FIGURE 1.9: THE FOUR PHASES OF WOUND HEALING AND THE SPECIFIC TIMELINES IN MURINE WOUND HEALING	68
FIGURE 1.10: MECHANISMS OF WOUND HEALING IN HEALTHY VERSUS DIABETES.....	76
FIGURE 1.11: THE ROLE OF MACROPHAGES IN PROMOTING MYOCYTE RECOVERY	88
FIGURE 1.12: FACTORS AFFECTING DIABETIC ISCHAEMIC REPAIR.....	99
FIGURE 1.13: ENDOMAC PROGENITORS IN POSTNATAL TISSUES.....	104
FIGURE 1.14: SUMMARY OF CURRENT FINDINGS ON TISSUE-RESIDENT ENDOMAC PROGENITORS.	107
FIGURE 1.15: CENTRAL HYPOTHESIS: PROPOSED INHIBITORY EFFECTS OF DIABETES ON ENDOMAC PROGENITORS.....	109
FIGURE 3.1: AORTIC ENDOMAC PROGENITORS GIVE RISE TO CFU-M	161
FIGURE 3.2: AORTIC ENDOMAC PROGENITORS FORM COMPLEX SPROUTS AND CORDS IN MATRIGEL™ CONTAINING NEW ECs AND MΦs	164
FIGURE 3.3: ENDOMAC PROGENITORS ARE CAPABLE OF BIPOTENT DIFFERENTIATION AT A CLONAL AND SINGLE CELL LEVEL	167
FIGURE 3.4: ENDOMAC PROGENITORS DISPLAY TISSUE-SPECIFIC DIFFERENCES IN THEIR CLONOGENIC, RENEWAL AND METABOLIC PROPERTIES.....	171
FIGURE 3.5:TISSUE-RELATED EFFECTS ON THE ANGIOGENIC AND DIFFERENTIATION CAPACITY OF ENDOMAC PROGENITORS.....	175
FIGURE 3.6: DIFFERENTIAL GENE EXPRESSION SIGNATURES OF AORTIC, SKIN AND SKM ENDOMAC PROGENITORS	181
FIGURE 3.7: HYPERGLYCAEMIA IS ASSOCIATED WITH FEWER ENDOMAC PROGENITORS IN AORTA	194

FIGURE 3.8: DIABETIC AORTIC CFU-M PROGENITORS HAVE DIMINISHED DIFFERENTIATION AND ANGIOGENIC CAPACITY	197
FIGURE 3.9: DIABETIC AORTIC PROGENITORS ARE PRONE TO DOUBLE-STRANDED DNA BREAKS	200
FIGURE 3.10: HIGH GLUCOSE INHIBITS CLONAL EXPANSION OF ENDO ^{MAC} PROGENITORS <i>IN VITRO</i> AND ALTERS THEIR METABOLIC ACTIVITY	203
FIGURE 4.1: HIGH GLUCOSE ATTENUATES STEM-LIKE AND ANGIOGENIC PROPERTIES OF SKIN ENDO ^{MAC} PROGENITORS.	218
FIGURE 4.2: EXPOSURE TO HIGH GLUCOSE LEVELS DAMPEN THE MITOCHONDRIAL FUNCTION OF SKIN PROGENITORS	222
FIGURE 4.3: SKIN ENDO ^{MAC} PROGENITOR FUNCTION AT A LOWER METABOLIC CAPACITY UNDER HIGH GLUCOSE.....	227
FIGURE 4.4: STZ-INDUCED DIABETES IS ASSOCIATED WITH FEWER ENDO ^{MAC} PROGENITORS IN SKIN.....	230
FIGURE 4.5: DIABETES ATTENUATES THE CLONAL RENEWAL CAPACITY OF SKIN ENDO ^{MAC} PROGENITORS.....	233
FIGURE 4.6: DIABETIC SKIN ENDO ^{MAC} PROGENITORS ARE MORE PRONE TO DNA DAMAGE AND MITOCHONDRIAL ABNORMALITIES.....	237
FIGURE 4.7: DIABETIC SKIN PROGENITORS HAVE DIMINISHED CORD-FORMING CAPACITY.....	240
FIGURE 4.8: DIABETES IMPAIRS WOUND HEALING OF INJURED SKIN.....	243
FIGURE 4.9: DIABETES LAUNCHES A DELAYED INFLAMMATORY RESPONSE FOLLOWING WOUND INJURY.....	247
FIGURE 4.10: DIABETIC SKIN HAS DIFFERENT CONTENT OF PROGENITORS, MΦS AND ECs DURING WOUND HEALING.	251
FIGURE 4.11: KINETICS OF YS-DERIVED CELLS IN NON-DIABETIC AND DIABETIC WOUNDS DURING HEALING.	255
FIGURE 4.12: REDUCED CELL PROLIFERATION AND INCREASED APOPTOSIS IN DIABETIC WOUNDS IMMEDIATELY POST-INJURY.	259
FIGURE 4.13: NON-DIABETIC ENDO ^{MAC} PROGENITORS ACCELERATE WOUND HEALING IN DIABETIC SKIN.	264
FIGURE 4.14: TRANSFER OF NON-DIABETIC BUT NOT DIABETIC ENDO- ^{MAC} PROGENITORS ENGRAFT, ACCUMULATE, AND DIFFERENTIATE IN DIABETIC WOUNDS.....	267
FIGURE 4.15: TRANSFERRED NON-DIABETIC DONOR ENDO ^{MAC} PROGENITORS INCREASE OVERALL NUMBERS OF PROGENITORS, MΦS AND ECs IN RECIPIENT WOUNDS.	270
FIGURE 5.1: HIGH GLUCOSE ATTENUATES CLONAL, RENEWAL AND ANGIOGENIC PROPERTIES OF SkM PROGENITORS....	288
FIGURE 5.2: EXPOSURE TO HIGH GLUCOSE LEVELS DAMPEN THE MITOCHONDRIAL FUNCTION OF SkM PROGENITORS....	292
FIGURE 5.3: SkM ENDO ^{MAC} PROGENITORS FUNCTION AT A LOWER METABOLIC CAPACITY UNDER HIGH GLUCOSE.....	297
FIGURE 5.4: STZ-INDUCED HYPERGLYCAEMIA INDUCES A MORE INFLAMMATORY STATE IN PERIPHERAL BLOOD.....	301
FIGURE 5.5: HYPERGLYCAEMIA IS ASSOCIATED WITH FEWER ENDO ^{MAC} PROGENITORS IN SkM.	304
FIGURE 5.6: DIABETIC SkM ENDO ^{MAC} PROGENITORS HAVE LIMITED CLONOGENIC RENEWAL CAPACITY	307

FIGURE 5.7: DIABETIC SkM PROGENITORS ARE MORE PRONE TO DNA DAMAGE AND POSSESS MITOCHONDRIAL ABNORMALITIES.....	311
FIGURE 5.8: DIABETIC SkM CFU-M PROGENITORS HAVE DIMINISHED DIFFERENTIATION AND ANGIOGENIC CAPACITY .	314
FIGURE 5.9: DIABETIC MICE DISPLAY REDUCED PERFUSION RECOVERY AFTER HIND LIMB ISCHAEMIA.....	318
FIGURE 5.10: KINETICS OF PROGENITORS, MΦS AND ECs IN NON-DIABETIC AND DIABETIC ISCHAEMIC SkM.	324
FIGURE 5.11: SkM PROGENITORS ARISE FROM EMBRYONIC YS AND SHOW DELAYED EXPANSION POST-ISCHAEMIA IN DIABETES.	330
FIGURE 5.12: YS EMPs MAKE A MAJOR CONTRIBUTION TO EC RECOVERY AND EXPANSION AFTER ISCHAEMIA.....	334
FIGURE 5.13: PROLIFERATIVE STATUS OF YS-DERIVED POPULATIONS.	338
FIGURE 5.14: NON-DIABETIC ENDOMAC PROGENITORS RESCUE PERFUSION RECOVERY IN DIABETIC ISCHAEMIC MUSCLE.	342
FIGURE 5.15: NON-DIABETIC PROGENITORS ENGRAFT AND DIFFERENTIATE IN DIABETIC ISCHAEMIC MUSCLE.	346
FIGURE 5.16: EFFECT OF NON-DIABETIC DONOR PROGENITORS ON OVERALL NUMBERS OF PROGENITORS, MΦS AND ECs IN RECIPIENT SkM.	349
FIGURE 6.1: ENDOMAC PROGENITORS AS A NEWLY IDENTIFIED SOURCE FOR THE RENEWAL OF YS-DERIVED TISSUE MACROPHAGES AND ENDOTHELIAL CELLS.	360
FIGURE 6.2: THE ROLE OF ENDOMAC PROGENITORS IN TISSUE REPAIR IN STEADY STATE AND PATHOLOGICAL DISEASE.	364
FIGURE 6.3: DISCOVERY OF CFU-M FORMING PROGENITORS IN HUMAN BLOOD VESSELS.....	369
FIGURE 6.4: ENDOMAC PROGENITORS PRODUCED DIFFERENTIATED ECs BUT NOT EVPs AT DAY 14 POST-ISCHAEMIA..	377
FIGURE 6.5: MACROPHAGE COLONY FORMING UNITS IN HUMAN SKIN AND SKELETAL MUSCLE.....	383
APPENDIX 7.1: RAW DATA FILES FOR BULK-SEQUENCING ANALYSIS.....	390
APPENDIX 7.2: LIBRARY SIZES OF SAMPLES ANALYSED BY RNASeq.	391
APPENDIX 7.3: NORMALISED COUNTS DISTRIBUTION.	392
APPENDIX 7.4: FLUORESCENCE MINUS ONE CONTROL FOR STZ- AND STZ+ SKIN AND SkM FRESH TISSUE AND MATRIGEL	393
APPENDIX 7.5: FLUORESCENCE MINUS ONE CONTROL FOR STZ- AND STZ+ WOUNDS AND HIND LIMB ISCHAEMIA SkM	394
APPENDIX 7.6: ENDOMAC PROGENITORS ARE LARGELY PREVALENT IN SKINS DERMIS THAN THE EPIDERMIS.	395

Table of tables

TABLE 1.1: THE BREAKDOWN OF ATP YIELD DURING AEROBIC RESPIRATION.....	40
TABLE 1.2: THE LOCAL AND SYSTEMIC FACTORS THAT IMPAIR THE WOUND HEALING PROCESS.....	66
TABLE 2.1: EQUIPMENT AND SOFTWARE	112
TABLE 2.2: MATERIALS AND SUPPLIERS	115
TABLE 2.3: REAGENTS, CHEMICALS AND SUPPLIERS.....	119
TABLE 2.4: MITOCHONDRIAL INHIBITORS	136
TABLE 2.5: REAGENTS USED FOR IMMUNOSTAINING	139
TABLE 2.6 :REAGENTS USED FOR FLOW CYTOMETRY	143
TABLE 3.1: GENES MOST DIFFERENTIALLY EXPRESSED IN ENDOMAC PROGENITORS BETWEEN AORTA AND SkM	183
TABLE 3.2: GENES MOST DIFFERENTIALLY EXPRESSED IN ENDOMAC PROGENITORS BETWEEN AORTA AND SKIN	184
TABLE 3.3: GENES MOST DIFFEERENTIALLY EXPRESSED IN ENDOMAC PROGENTIROS BETWEEN SkM AND SKIN.....	185
TABLE 3.4: GENE ONTOLOGY TERMS AND PATHWAYS OVER-REPRESENTED IN AORTIC VERSUS SKIN ENDOMAC PROGENITORS.....	186
TABLE 3.5: GENE ONTOLOGY TERMS AND PATHWAYS OVER-REPRESENTED IN SkM VERSUS SKIN ENDOMAC PROGENITORS	188
TABLE 6.1: SUMMARY OF ENDOMAC PROGENITOR PREVALENCE, STEMNESS AND FUNCTION ACROSS THREE TISSUES....	375
TABLE 6.2: SUMMARY OF MITOCHONDRIAL ASSAY RESULTS FOR PROGENITORS FROM DIFFERENT TISSUES FOR NON- DIABETIC (STZ ⁻) AND DIABETIC (STZ ⁺) MICE.	381
TABLE 6.3: TABLE SUMMARISES DIFFERENT CLASSES OF POTENTIAL DRUG CANDIDATES TO ADDRESS METABOLIC AND MITOCHONDRIAL DYSFUNCTION.....	387

Abstract

Macrophages (MΦs) and endothelial cells (ECs) share an intimate relationship which helps mediate tissue inflammation and neovascularisation. Both cells display considerable heterogeneity, which is a product of tissue and disease context and their complex ontogeny. Converging evidence indicates developmental overlap whereby some tissue MΦs and ECs arise from a common embryonic source, namely yolk sac (YS) erythromyeloid progenitor cells. Although it is widely considered that YS-derived MΦs and ECs are maintained after birth by proliferative self-renewal, our group has recently identified YS-derived bipotent endothelial-macrophage (EndoMac) progenitors as an alternative source for their postnatal renewal in different tissues.

This thesis addresses several knowledge gaps relating to EndoMac progenitors. In Chapter 3, we demonstrate that FACS-isolated and culture-derived progenitors from mouse aorta are Lin⁻CD45⁺CD11b⁻F4/80⁻Sca-1⁺c-Kit⁺ and express the receptors for fractalkine (CX₃CR1) and macrophage colony-stimulating factor (CSF1R). Crucially, we also establish the bipotency of EndoMac progenitors at a single cell level. Progenitors from different tissues (aorta, skin, skeletal muscle [SkM]) exhibit important similarities, with subtle tissue-related variations in clonal renewal, angiogenic capacity and gene expression. Finally, with a view to understanding their metabolic regulation, we study the effects of high glucose on aortic progenitors and identify glucose-induced reductions in their clonogenic and angiogenic capacity, as well as their DNA integrity.

Chapter 4 extends these findings by examining the effects of hyperglycaemia on skin progenitors using a streptozotocin-induced mouse model of type 1 diabetes, given that diabetes impairs skin wound healing. Exposure to high glucose *in vitro* and hyperglycaemia *in vivo* inhibits the clonal expansion, renewal, differentiation and angiogenic capacity of skin EndoMac progenitors. This is

associated with reduced mitochondrial viability and metabolic function. Using lineage-mapping techniques, we reveal that diabetes attenuates the rapid burst of proliferative accumulation of YS-derived progenitors in early skin wounds. This is accompanied by blunting of the expansion of YS-derived MΦs and ECs in later stages of wound repair. Finally, we show that progenitors from non-diabetic skin can engraft, differentiate and promote wound repair when transplanted into recipient diabetic wounds, whereas these salutary properties are severely diminished for diabetic progenitors.

In Chapter 5 we investigate how high glucose affects EndoMac progenitors from SkM, with focus on understanding how diabetes impairs perfusion recovery in peripheral ischaemia. High glucose and hyperglycaemia inhibit the key properties of these cells, while also dampening their metabolic activity. Lineage-tracing demonstrated that under non-diabetic conditions, hind limb ischaemia is associated with early proliferative accumulation of YS-derived progenitors, followed by sequential expansion of MΦs and ECs, such that YS is the source of up to 55% of MΦs and 80% of ECs in ischaemic SkM. This is severely reduced in diabetes. Lastly, we demonstrate that transplantation of non-diabetic SkM progenitors promotes perfusion recovery of ischaemic limbs in diabetic mice, with these cells engrafting and differentiating into both endothelial and myeloid progeny within recipient tissue.

In summary, this thesis provides new insights about the properties of EndoMac progenitors across different mouse tissues, while also revealing that diabetes has striking effects on their function, metabolic activity and reparative potential. This provides a novel framework to help understand how diabetes impairs wound repair and vascularisation of ischaemic tissue.

Declaration

I certify that this work contains no material which has been accepted for the award of any other degree or diploma in my name, in any university or other tertiary institution and, to the best of my knowledge and belief, contains no material previously published or written by another person, except where due reference has been made in the text. In addition, I certify that no part of this work will, in the future, be used in a submission in my name, for any other degree or diploma in any university or other tertiary institution without the prior approval of the University of Adelaide and where applicable, any partner institution responsible for the joint award of this degree. I give permission for the digital version of my thesis to be made available on the web, via the University's digital research repository, the Library Search and also through web search engines, unless permission has been granted by the University to restrict access for a period of time. I acknowledge the support I have received for my research through the provision of an Australian Government Research Training Program Scholarship.

.....

Sanuri Rashmitha Liyanage

Date: 10/12/22.....

This thesis is lovingly dedicated to my parents, Priyanthi and Ari, whose interest in this, as in all my ventures, were never less than my own.

Acknowledgements

I am deeply indebted to my primary supervisor A/Prof. Peter Psaltis without whom this thesis would not have been possible. Thank you does not begin to express how grateful I am for your unwavering and ongoing support. Your words of encouragement, intelligence, and wisdom throughout the past four years have shaped me and my appreciation for science. You have made all of us critical thinkers and better researchers and I am forever thankful. Thank you to my secondary supervisors, A/Prof Christina Bursill and Prof. Claudine Bonder for your invaluable advice, input, and support. You are an inspiration to all women scientists. I am honoured to have been your student.

Dr. Mohammad Hassanshahi, you have been an excellent mentor. I hope you know that you continue to inspire me and have played an integral role in my realising my passion for science. I am grateful I can call you my friend and for all the advice you've carefully given me- thank you. Dr Shiwani Sharma, your input made this thesis what it is, and I am grateful for your time, valuable expertise, and insight into this project.

Thank you to the SAHMRI flow cytometry group- Dr Randall Gross and Jarrad Goyne, for supporting all my experiments. Your themed music and Netflix projections have kept me going during my very long days at the flow core suite.

I am extremely lucky to know the amazing people at the Vascular Research Centre at SAHMRI. Dr Joanne Tan, Khalia Primer, Emma Solly, Victoria Nankivell, Laura Wilsdon, Zahra Lotfollahi, Lauren Sandeman, Lukah Dykes, Benjamin Pullen, and Jake White. Thank you to the Psaltis group past and present- Dr Nisha Schwarz, Dr Deb Toledo-Flores, Dr Aaron Long, Catherine Cornish, Pich Chhay, Helia Abdollahi, Sylvia Kurevska, Alex Tran and Dr Tam Nguyen. You gave true meaning to the phrase *it takes a village*. Thank you for always nudging me forward, especially during the days I dragged my feet.

A special thank you to Thalia Salagaras for your kindness, honesty, and constant support during my time with the Psaltis group. You held my hand through the rollercoaster ride that was my PhD and words cannot express the deep appreciation I have for you. Thank you for always being the voice of reason at times when things are tough. My fondest memories with you involve dissecting complicated multicultural recipes online during our incubation times.

Dr. Sanuja Fernando and Dr. Anna Williamson, you have been my right hand, my older sisters, my guideposts, and my family away from home. I am so lucky to know two extremely talented, driven, and genuine human beings that have left behind enormous shoes for me to fill. Thank you for dragging me away from work and insisting I have fun. I will continue to cherish our weekly dinners, movie nights, high-altitude hikes (much to my dismay) and for the best advice. A massive thank you to my best friend, Sanj for always being there no matter what. You and I have raised each other ever since we moved to Adelaide, and you have always been my biggest cheerleader. Thank you for letting me practice all my presentations with you and for earnestly listening to me talk about science. Your words of encouragement and impromptu catchups when I have been overwhelmed this year, got me through the hardest parts.

To my childhood friends Tharani, Thari and Chathu thank you for constantly keeping me going at times throughout by PhD. I am who I am because of your love and encouragement since our first day in kindergarten. Even though we are now spread across three continents, you have been a constant presence in my life. Thank you for flying down, keeping me company at late hours in the night when I was writing, and for all the laughs we've had.

Thank you to my beautiful family back home in Sri Lanka: to my six aunts for constantly checking up on me and for all the great home food you send my way. I am incredibly proud to have been raised by you. Thank you to my army of cousins and for the weekend trips when I'm stressed. I love each one of you.

To my two brothers, Navodh and Heshitha: your constant love and support during this endeavour got me to the finish line. There will never be enough right words to thank you for the childhood you shared with me. Therefore, I believe our catchphrase seems quite fitting here- *“No one will ever have my back as you will”*. To my happy-go-lucky forever puppy Hatchi, you are the best gift I have and will ever receive. You make me smile especially on the hard days.

Finally, thank you to my parents and my ultimate inspiration, Ari and Priyanthi. Mum and Dad, you taught me that I could be whomever I wanted to be and you supported me through it all. This thesis is as much yours as it is mine. Thank you for everything you’ve done and for everything you continue to do for me every day. I love you always.

Conference presentations

Oral presentations

S. Liyanage, A. Williamson..., PJ Psaltis. Inhibitory effects of diabetes on yolk-sac derived Endo-Mac progenitors in murine skin and muscle. Australian Vascular Biology Society, Adelaide, South Australia, 2021

S. Liyanage, A. Williamson..., PJ Psaltis. Inhibitory effects of diabetes on yolk-sac derived Endo-Mac progenitors in murine skin and muscle. South Australian Health and Medical Research Institute Seminar (SAHMRI), Adelaide, South Australia, 2021

S. Liyanage, A. Williamson..., PJ Psaltis. Finding a new saviour in the war against diabetic amputations. University of Adelaide, 3-minute thesis competition, Adelaide, South Australia, 2021

S. Liyanage, A. Williamson..., PJ Psaltis. Finding a new saviour in the war against diabetic amputations. South Australian Health and Medical Research Institute Showcase (SAHMRI), Adelaide, South Australia, 2022

S. Liyanage, A. Williamson..., PJ Psaltis. Inhibitory effects of diabetes on yolk-sac derived Endo-Mac progenitors in murine skin and muscle-Oral presentation. International Society for Stem-cell research, San Francisco, USA, 2022

S. Liyanage, A. Williamson..., PJ Psaltis. Inhibitory effects of diabetes on yolk-sac derived Endo-Mac progenitors in murine skin and muscle. Australian Society for Medical Research (ASMR), Adelaide, South Australia, 2022

Poster Presentations

S. Liyanage, A. Williamson..., PJ Psaltis. Inhibitory effects of diabetes on yolk-sac derived Endo-Mac progenitors in murine skin and muscle. Florey Conference, Adelaide, South Australia, 2021

Awards

S. Liyanage, A. Williamson..., PJ Psaltis. Finding a new saviour in the war against diabetic amputations. South Australian Health and Medical Research Institute Showcase (SAHMRI), Adelaide, South Australia, 2022, 3-minute thesis winner.

S. Liyanage, A. Williamson..., PJ Psaltis. Finding a new saviour in the war against diabetic amputations. University of Adelaide, 3-minute thesis competition, Adelaide, South Australia, 2022, Faculty top 6 finalist.

S. Liyanage, A. Williamson..., PJ Psaltis. Finding a new saviour in the war against diabetic amputations. University of Adelaide, 3-minute thesis competition, Adelaide, South Australia, 2021, Faculty top 6 finalist.

Publications

Publications arising from this thesis

Williamson, A., Toledo-Flores, D., Liyanage, S., Hassanshahi, M., Dimasi, C., Schwarz, N., Fernando, S., Salagaras, T., Long, A., Di Bartolo, B., Drummond, G., Vinh, A., Chandrakanthan, V., Tan JTM., Bonder, C., Nicholls, S., Bursill, C., and Psaltis, P. Self-renewing tissue-resident endothelial-macrophage progenitor cells originate from yolk sac and are a local source of inflammation and neovascularization in postnatal aorta. *Nature Cell Biology (in revision)*. Submitted on BioRxiv.

Williamson, A.*, Liyanage, S.*...., Bonder, C., Bursill, C., and Psaltis, P. Divergent roles of Yolk sac-derived EndoMac Progenitor cells in Skin Wound Healing and Melanoma Growth, *in preparation*. *Co-first author

Williamson, A., Liyanage, S....., Bonder, C., Nicholls, S., Bursill, C., and Psaltis, P. Yolk sac-derived EndoMac progenitor cells in murine skeletal muscle contribute to neovascularisation and perfusion recovery after hind limb ischaemia, *in preparation*.

Patents arising from this thesis

Methods and compositions for promoting neovascularisation. *Provisional patent pending*.

Abbreviations

2-NBDG	d-glucose analog 2-[N-(7-nitrobenz-2-oxa-1,3-diazol-4-yl) amino]-2-deoxy-D-glucose
4-HNE	4-Hydroxynonenal
AGM	Aorta gonad mesonephros
anti-GAD	Anti-glutamic acid decarboxylase
APC	Antigen-presenting cells
ATP	Adenosine triphosphate
BB	Biobreeding
BLCFC	Blast colony forming cells
BL-CFC	Blast colony forming cell
BM	Bone marrow
BMMC	Bone marrow-derived mononuclear cells
cAMP	Cyclic adenosine 3', 5'-monophosphate
CFU	Colony forming unit
CHD	Coronary heart disease
CLI	Critical limb ischaemia
CLP	Common lymphoid cell
cMoP	Common monocyte progenitors
CMP	Common myeloid cell
d	Day
DFU	Diabetic foot ulcers
DHPA	10-acetyl-3,7-dihydroxyphenoxazine
DIO	Diet induced obese

E	Embryonic day
EC	Endothelial cell
ECAR	Extracellular acidification rate
EndoMac	Endothelial-macrophage progenitors
EPCs	Endothelial progenitor cells
EPR	Electron paramagnetic resonance
ESC	Embryonic stem cell
EVP	Endovascular progenitors
FACS	Fluorescence activated cell sorting
FADH	Flavin adenine dinucleotide
FAP	Fibroadipogenic progenitors
FMNH₂	Reduced flavin mononucleotide
GMP	Granulocyte/macrophage progenitor
GPX	Glutathione peroxidase
GSH	Glutathione
H₂O₂	Hydrogen peroxide
HOCl	Hypochlorous acid
HSPC	Haematopoietic stem and progenitor cell
i.p.	Intraperitoneal
ICAM-1	Inter-cellular adhesion molecule-1
iPSC	Induced pluripotent stem cells
Leprdb	Leptin receptor mutant db/db
LIMA	Left internal mammary artery
Lin	Lineage

LT-HSC	Long-term haematopoietic stem cells
M2-like	Alternatively activated
MDP	M Φ (monocyte)/dendritic precursors
MEP	Megakaryocyte/erythroid progenitor
MIC	Muscle interstitial cells
MPTP	Mitochondrial permeability transition pore
mRNA	Messenger RNA
MSC	Mesenchymal stem cells
MΦ	Macrophage
NADH	Nicotinamide adenine dinucleotide
NO	Nitric oxide
NOD	Nonobese diabetic
ns2Akita	Akita type 1 diabetic mice
O₂^{•-}	Superoxide radical
OCR	Oxygen consumption rate
OH[•]	Hydroxyl radical
ONOO⁻	Peroxynitrite
PAD	Peripheral artery disease
PBMC	Peripheral blood mononuclear cells
Q	Ubiquinone
RBC	Red blood cell
ROS	Reactive oxygen species
Sc-RNA seq	Single cell RNA-sequencing
SDEC	Somite-derived EC

SDF-1	Stromal derived factor 1
SkM	Skeletal muscle
SMC	Smooth muscle cell
ST-HSC	Short-term haematopoietic stem cells
STZ	Streptozotocin
SV	Saphenous vein
T1D	Type 1 diabetes
T2D	Type 2 diabetes
TAM	Tamoxifen
T_c	Cytotoxic T cell
Th1	Activated T-helper cell
VCAM-1	Vascular cell adhesion molecule-1
w	Week

Protein Abbreviations

ATF6	Activating transcription factor 6
Acta2	Smooth muscle actin
ANG	Angiopoietin
ANG1	Angiopoietin 1
ANG2	Angiopoietin 2
BH2	Dihydrobiopterin
BH4	Tetrahydrobiopterin
CCR2	C-C Chemokine Receptor Type 2
CD11b	Integrin Alpha M
CD11c	Integrin Alpha X
CD133	Prominin-1
CD14	Cluster of Differentiation 14
CD143	Cluster of Differentiation 146
CD144	VE-Cadherin/CDH5
CD16	Cluster of Differentiation 16
CD206	Cluster of Differentiation 206
CD209	C-type Lectin Domain Family 4 Member f
CD31	EC adhesion molecule
CD34	Cluster of Differentiation 34
CD36	Cluster of Differentiation 36
CD4	Cluster of Differentiation 4
CD40	Cluster of Differentiation 40

CD43	Cluster of Differentiation 43
CD45	Cluster of Differentiation 45
CD5	Cluster of Differentiation 5
CD56	Cluster of Differentiation 56
CD62L	Cluster of Differentiation 62 ligand
CD64	Cluster of Differentiation 64
CD8	Cluster of Differentiation 8
CD86	Cluster of Differentiation 86
CD93	Cluster of Differentiation 93
CDK4/6	Cyclin-dependent kinase 4/6
c-Kit	Proto-oncogene c-KIT
Cnn1	Calponin
CSF1R	Macrophage Colony-Signalling Factor 1 Receptor
CX3CR1	CX3C Chemokine Receptor 1
CXCL8	C-X-C motif chemokine ligand 8
DL4	Delta-like ligand 4
EGF	Epidermal growth factor
eNOS	Endothelial nitric oxide synthase
F4/80	EGF-like Module-containing Mucin-like Hormone Receptor-like 1
FGF	Fibroblast growth factor
FL	Foetal liver
Flk1	Vascular endothelial growth factor protein
GDF3	Growth differentiation factor 3

GLUT4	Glucose transporter type 4
Gr-1	GPI-linked Myeloid Differentiation Marker
GSK-3	Glycogen synthase kinase 3
HIF1	Hypoxia-induced factor
HLA	Human leucocyte antigen
HSP27	Heat shock protein 27
HSP47	Heat shock protein 47
HSP70	Heat shock protein 70
HSP90	Heat shock protein 90
ICAM	Inter-cellular adhesion molecule
ICAM-1	Inter-cellular adhesion molecule-1
IFN-γ	Interferon- γ
IGF-1	Insulin-like growth factor 1
IKK-β	I κ B kinase β
IL-10	Interleukin-10
IL-13	Interleukin-13
IL-1α	Interleukin-1 α
IL-1β	Interleukin-1 β
IL-4	Interleukin-4
IL-6	Interleukin-6
IL-8	Interleukin-8
iNOS	Inducible nitric oxide synthase
IRE-1	Inositol-requiring enzyme 1
IRS-1	Intracellular substrate-1

JNK	c-Jun amino-terminal kinase
Ly6C	Lymphocyte Antigen 6 C
Ly6G	Lymphocyte Antigen 6 G
Lyve1	Lymphatic Vessel Endothelial Hyaluronan Receptor 1
MAPK	Mitogen-activated protein kinase
MCK	Muscle creatine kinase
MCP-1	Monocyte chemotactic protein 1
MerTK	Proto-oncogene Tyrosine-Protein Kinase MER
MHCII	Class II Major Histocompatibility Complex
MHCII	Major histocompatibility complex II
MIF	Migration Inhibitory Factor
MMP	Matrix melanoprotease
MMPs	Matrix metalloproteinases
MRC1	Mannose receptor 1
MRF	Myogenic regulatory factor
NF-κB	Necrosis factor-κB
NLPR3	NOD-like receptor family pyrin domain containing 3
NOS	Nitric oxide synthase
PD1	Program-death 1
PDGF	Platelet-derived growth factor
PDL-2	Program-death 2
PEPCK	Phosphoenolpyruvate carboxykinase
PERK	PKR-like ER kinase

PI3K	Phosphatidylinositol 3-kinase
PlGF	Placental growth factor
PKC	Protein Kinase C
PRR	Pattern-recognition receptor
Sca-1	Stem cell antigen
SM22	Smooth muscle protein 22
Ter119	Glycophorin A
TGFβ	Tumour growth factor-β1
Tie2	Angiopoietin-1 Receptor
TLR	Toll-like receptors
TNF-α	Tumour necrosis factor-α
UPR	Unfolded protein response
UPR8	Unfolded protein response 8
VCAM	Vascular cell adhesion molecule
VEGF	Vascular endothelial growth factor
VEGFR1	Vascular growth factor receptor 1

Gene abbreviations

<i>1110002E22Rik</i>	RIKEN cDNA 1110002E22 gene
<i>2310002L09Rik</i>	RIKEN cDNA 2310002L09 gene
<i>A3243G</i>	Mitochondrial tRNA ^{Leu} (UUR) gene
<i>Abcc9</i>	ATP-binding cassette, sub-family C (CFTR/MRP), member 9
<i>ACE</i>	Angiotensin converting enzyme
<i>Angpt1</i>	Angiopoietin 1
<i>Ano5</i>	Anoctamin 5
<i>Arsi</i>	Arylsulfatase i
<i>Atp1b1</i>	ATPase, Na ⁺ /K ⁺ transporting, beta 1 polypeptide
<i>Atp2a1</i>	ATPase, Ca ⁺⁺ transporting, cardiac muscle, fast twitch 1
<i>Brachyury</i>	Mesodermal gene T
<i>C130073E24Rik</i>	RIKEN cDNA C130073E24 gene
<i>C6</i>	Complement component 6
<i>Cacng1</i>	Calcium channel, voltage-dependent, gamma subunit 1
<i>Car3</i>	Carbonic anhydrase 3
<i>Casq2</i>	Calsequestrin 2
<i>Cbr2</i>	Carbonyl reductase 2
<i>Cd163</i>	Cluster of Differentiation 163
<i>Cd300a</i>	CD300A molecule
<i>Cd96</i>	CD96 antigen

<i>Cdh15</i>	Cadherin 15
<i>Ces1f</i>	Carboxylesterase 1F
<i>Chrng</i>	Cholinergic receptor, nicotinic, gamma polypeptide
<i>Ckm</i>	Creatine kinase, muscle
<i>Cldn2</i>	Claudin 2
<i>clock</i>	Circadian rhythm gene
<i>CLR</i>	C-type lectin receptor
<i>Clu</i>	Clusterin
<i>c-Myb</i>	Myb proto-oncogene
<i>Cntn1</i>	Contactin 1
<i>Colec11</i>	Collectin sub-family member 11
<i>Comp</i>	Cartilage oligomeric matrix protein
<i>Cpz</i>	Carboxypeptidase Z
<i>CtsG</i>	Cathepsin G
<i>Cx3cr1</i>	Chemokine (C-X3-C motif) receptor 1
<i>Dchs1</i>	Dachsous cadherin related 1
<i>Ddr1</i>	Discoidin domain receptor family, member 1
<i>Disp2</i>	Dispatched RND transporter family member 2
<i>Egr1</i>	Early growth response 1
<i>Emx2</i>	Empty spiracles homeobox 2
<i>Enc1</i>	Ectodermal-neural cortex 1
<i>Eomes</i>	Eomesodermin
<i>Erv3</i>	Endogenous retroviral sequence 3
<i>F13a1</i>	Coagulation factor XIII, A1 subunit

<i>Fcgrt</i>	Neonatal fc receptor
<i>Fcna</i>	Ficolin 1
<i>Fgfr4</i>	Fibroblast growth factor receptor 4
<i>Fhl1</i>	Four and a half LIM domains 1
<i>FLK1</i>	Foetal liver kinase 1; vascular endothelial growth factor receptor 2
<i>Flt1</i>	FMS-like tyrosine kinase 1
<i>Folr2</i>	Folate receptor beta
<i>Fosb</i>	Protein fosb
<i>Fxyd2</i>	FXYP domain-containing ion transport regulator 2
<i>Galnt14</i>	Polypeptide N-acetylgalactosaminyltransferase 14
<i>Gm10354</i>	Predicted gene 10354
<i>Gm13522</i>	Predicted gene 13522
<i>Gm14066</i>	Predicted gene 14066
<i>Gm16485</i>	Predicted gene 16485
<i>Gm17019</i>	Predicted gene 17019
<i>Gm21955</i>	Predicted gene, 21955
<i>Gm9758</i>	Predicted gene 9758
<i>Gpr141</i>	G protein-coupled receptor 141
<i>H2ac6</i>	H2A clustered histone 6
<i>Hdc</i>	Histidine decarboxylase
<i>Hexa</i>	Hexosaminidase A

<i>Hey2</i>	Hairy/enhancer-of-split related with YRPW motif 2
<i>HLA</i>	Human leucocyte antigen
<i>Hoxb9</i>	Homeobox B9
<i>Hpn</i>	Hepsin
<i>Ier3</i>	Immediate Early Gene
<i>Ifi205</i>	Interferon activated gene 205
<i>Igfn1</i>	Immunoglobulin-like and fibronectin type III domain containing 1
<i>IL-12</i>	Interleukin 12
<i>Il1r2</i>	Interleukin 1 receptor, type II
<i>Il23r</i>	Interleukin 23 receptor
<i>Irx1</i>	Iroquois homeobox 1
<i>Irx5</i>	Iroquois homeobox 5
<i>Ism1</i>	Isthmin 1, angiogenesis inhibitor
<i>Kcnq5</i>	Potassium voltage-gated channel, subfamily Q, member 5
<i>Klf4</i>	Kruppel-Like Factor 4
<i>Klhl31</i>	Kelch-like 31
<i>Klhl40</i>	Kelch-like 40
<i>Lhfp11</i>	Lipoma HMGIC fusion partner-like 1
<i>Lum</i>	Lumican
<i>Lyz1</i>	Lysozyme 1
<i>Lyz2</i>	Lysozyme 2
<i>Map7d2</i>	MAP7 domain containing 2

<i>Mboat2</i>	Membrane bound O-acyltransferase domain containing 2
<i>MCK</i>	Muscle creatine kinase
<i>Meiosin</i>	Meiosis initiator
<i>Mfap2</i>	Microfibrillar-associated protein 2
<i>Mfap4</i>	Microfibrillar-associated protein 4
<i>Mgp</i>	Matrix Gla protein
<i>Mrc1</i>	Mannose Receptor C-type 1
<i>My5</i>	Myogenic Factor 5
<i>Mybph</i>	Myosin binding protein H
<i>Myh2</i>	Myosin, heavy polypeptide 2, skeletal muscle, adult
<i>Mymk</i>	Myomaker, myoblast fusion factor
<i>MyoD</i>	Myoblast Determination Protein 1
<i>Myog</i>	Myogenin
<i>Nfasc</i>	Neurofascin
<i>Notch</i>	Neurogenic locus notch homolog protein 1
<i>Npr3</i>	Natriuretic peptide receptor 3
<i>Nrn1</i>	Neuritin 1
<i>Nxpe5</i>	Neurexophilin and PC-esterase domain family, member 5
<i>Pax7</i>	Paired box 7
<i>Pdgfd</i>	Platelet-derived growth factor, D polypeptide
<i>Pdk4</i>	Pyruvate dehydrogenase kinase, isoenzyme 4

<i>Plac8</i>	Placenta-specific 8
<i>Plppr3</i>	Phospholipid phosphatase related 3
<i>Ppp1r3a</i>	Protein phosphatase 1, regulatory subunit 3A
<i>Prg4</i>	Proteoglycan 4 (megakaryocyte stimulating factor, articular superficial zone protein)
<i>Prrg4</i>	Proline rich Gla (G-carboxyglutamic acid) 4 (transmembrane)
<i>PU.1</i>	Spi1 gene
<i>Pvalb</i>	Parvalbumin
<i>Rbfox1</i>	RNA binding protein, fox-1 homolog (C. Elegans) 1
<i>Rps6ka2</i>	Ribosomal protein S6 kinase, polypeptide 2
<i>Runx1</i>	Runt-related transcription factor 1
<i>Scara3</i>	Scavenger receptor class A, member 3
<i>SCI</i>	T-cell acute lymphocytic leukemia protein 1
<i>Scp2-ps2</i>	Sterol carrier protein 2, pseudogene 2
<i>Sfrp2</i>	Secreted frizzled-related protein 2
<i>Sgca</i>	Sarcoglycan, alpha (dystrophin-associated glycoprotein)
<i>Slc16a3</i>	Solute carrier family 16 (monocarboxylic acid transporters), member 3
<i>Slc6a12</i>	Solute carrier family 6 (neurotransmitter transporter, betaine/GABA), member 12
<i>Slc6a13</i>	Solute carrier family 6 (neurotransmitter transporter, GABA), member 13
<i>Spats2l</i>	Spermatogenesis associated, serine-rich 2-like
<i>Spry4</i>	Sprouty RTK signaling antagonist 4
<i>Tbx15</i>	T-box 15

<i>Tbxas1</i>	Thromboxane A synthase 1, platelet
<i>Thbs2</i>	Thrombospondin 2
<i>Thy1</i>	Thymus cell antigen 1, theta
<i>Timd4</i>	T-cell Immunoglobulin and Mucin Domain Containing 4
<i>Tlr8</i>	Toll-like receptor 8
<i>Tnfsf11</i>	Tumor necrosis factor (ligand) superfamily, member 11
<i>Tnni1</i>	Troponin I, skeletal, slow 1
<i>Trdn</i>	Triadin
<i>Trpc4</i>	Transient receptor potential cation channel, subfamily C, member 4
<i>Trpv1</i>	Transient receptor potential cation channel, subfamily V, member 1
<i>Tslp</i>	Thymic stromal lymphopoietin
<i>Usp17le</i>	Ubiquitin specific peptidase 17-like E
<i>VEGF-A</i>	Foetal liver kinase 1; vascular endothelial growth factor receptor 2
<i>WNT</i>	WNT1 protein gene
<i>Wt1</i>	WT1 transcription factor
<i>Xirp2</i>	Xin actin-binding repeat containing 2
<i>Zic1</i>	Zinc finger protein of the cerebellum 1
<i>Zmat4</i>	Zinc finger, matrin type 4

Chapter 1

1. Introduction

1.1 The reciprocal interactions between myeloid and endothelial cells

Neovascularisation, or new blood vessel formation, is an integral process in the development, growth and repair of mammalian tissues. Vasculogenesis and angiogenesis are the two major processes by which new blood vessels form and grow. While vasculogenesis typically refers to the *in situ* differentiation and development of vasculature from mesodermal precursors, called angioblasts during prenatal development, angiogenesis is defined as the formation of new blood vessels from existing ones by two distinct mechanisms: (i) the migration, proliferation and sprouting of endothelial cells (ECs) and (ii) intussusceptive microvascular growth (1).

In embryonic development, vasculogenesis gives rise to the primitive vascular plexus inside the embryo, comprising the dorsal aorta and vitelline veins, as well as the extra-embryonic yolk sac (YS) circulation (2). The further establishment of a mature vascular network occurs by angiogenesis, which enables expansion of the developing circulation to regions that are thus far avascular. Well-characterised stages of angiogenesis include the activation of ECs via growth factors, such as vascular endothelial growth factor (VEGF)-A and basic fibroblast growth factor (bFGF), degradation of the basement membrane, proliferation and migration of ECs that coordinate the outward growth of an endothelial “tip” cell, with the adjacent expansion of “stalk” cells (3, 4). Subsequently, the vasculature is stabilised by the establishment of a new basement membrane and secretion of other cytokines, including platelet-derived growth factor (PDGF) and angiopoietin-2 (ANG2) which attract other cells to support ECs such as pericytes (5). The endothelium is composed of a monolayer of cells that lines blood vessels and is responsible for a number of key regulatory functions of the vascular system. It provides a semi-permeable membrane for the transfer of nutrients and retrieval of waste products, regulates monocyte adhesion and subsequent infiltration at tissue sites, promotes vasodilation and

inhibits inflammation, and thrombosis. Further remodelling via intussusception occurs by splitting pre-existing vessels to sprout new vessels (1).

Among the various cellular interactions that are essential for successful vascular remodelling, macrophages (MΦs) have long been recognised for their pro-angiogenic activity encompassing both the secretion of pro-angiogenic soluble factors, as well as their physical support of sprouting blood vessels (6). MΦs are the body's first line of defence against invading pathogens (7), and play crucial roles in tissue homeostasis, morphogenesis, and pathophysiological conditions, involving tissue injury, inflammation and repair (8). They phagocytose microbes and activate specific adaptive immune responses via antigen presentation. MΦs are also a source of multiple growth factors that can enhance EC proliferation and/or survival in a paracrine fashion during angiogenesis. These include VEGF-A, placental growth factor (PIGF) (9), C-X-C motif chemokine ligand 8 (CXCL8), interleukin (IL)-1 β , tumour-necrosis factor- α (TNF α) and bFGF2 (10). Furthermore, MΦs promote the remodelling of the perivascular matrix by secretion of proteases and provide survival and/or “guidance” cues, like semaphorins, to the ECs, which are important for EC migration and the directional growth of new blood vessels (11-13). Finally, MΦs proliferate and engage in tight cell-to-cell contact with sprouting blood vessels by expanding their filopodia to facilitate the “bridging” of endothelial sprouts during vascular anastomosis (14) (**Figure 1.1**).

Conversely, there is also evidence that MΦs exert anti-angiogenic properties via secretion of vascular growth factor receptor-1 (VEGFR-1), a potent anti-angiogenic factor that can sequester VEGF-A and limit its bioavailability. This has been shown to be related to non-canonical WNT signalling in MΦs (15). Interestingly, at selected anatomical sites MΦs appear to tightly regulate angiogenesis by

limiting the formation of excessive vessel branches. In the hyaloid vasculature this role is performed by WNT7B-secreting MΦs which sensitise ECs to ANG2 and induce EC apoptosis (16).

The promotive and regressive effects of angiogenesis by MΦs prompts the question of whether these opposing functions are executed by distinct MΦ subtypes or simply different activation states. Although now superseded, the historical classification of MΦs was broadly divided into (i) classically (M1-like) and (ii) alternatively (M2-like) activated subtypes. The gene expression signatures of MΦs equipped with pro-angiogenic activity are largely consistent with anti-inflammatory M2-like MΦs. Therefore, polarisation into specific functional states might largely be shaped by vessel-derived signals (17). In support of this, there is mechanistic evidence to show that ECs in turn can influence MΦ plasticity to mediate inflammation and angiogenesis by secretion of CSF1/M-CSF that promotes selective growth and differentiation of MΦs from monocytes (18). Further, ECs provide a niche for the progressive differentiation of M2-like MΦs characterised by the increased expression of M2-like markers [TIE2, mannose receptor (MRC1)], from haematopoietic progenitor cells (HPCs) (19). He *et al.* has shown that this relies on direct cell-cell interaction between HPCs and ECs, rather than regulation by soluble factors (18). Mechanistically, it was also discovered that EC-derived CSF1 promoted HPC development and MΦ survival in co-cultures, whereas MΦ-produced VEGF-A improved the EC monolayer's long-term stability. This confirms the bidirectional relationship between MΦs and ECs throughout the formation, maturation and remodelling of neovessels.

Importantly, while excessive angiogenesis is a hallmark of diseases, such as cancer and atherosclerosis, insufficient blood vessel formation can lead to non-healing ulcers, tissue ischaemia and infarction, especially in the presence of atherosclerotic disease of the coronary, cerebral and

peripheral vasculature. A lack of balance between pro- and antiangiogenic cues is considered one of the most crucial features that distinguishes physiological from pathological angiogenesis (1).

Interim conclusion

To comprehend and target neovascularisation in physiological and pathological settings, a greater knowledge of how these close connections between MΦs and ECs are so well-orchestrated is required

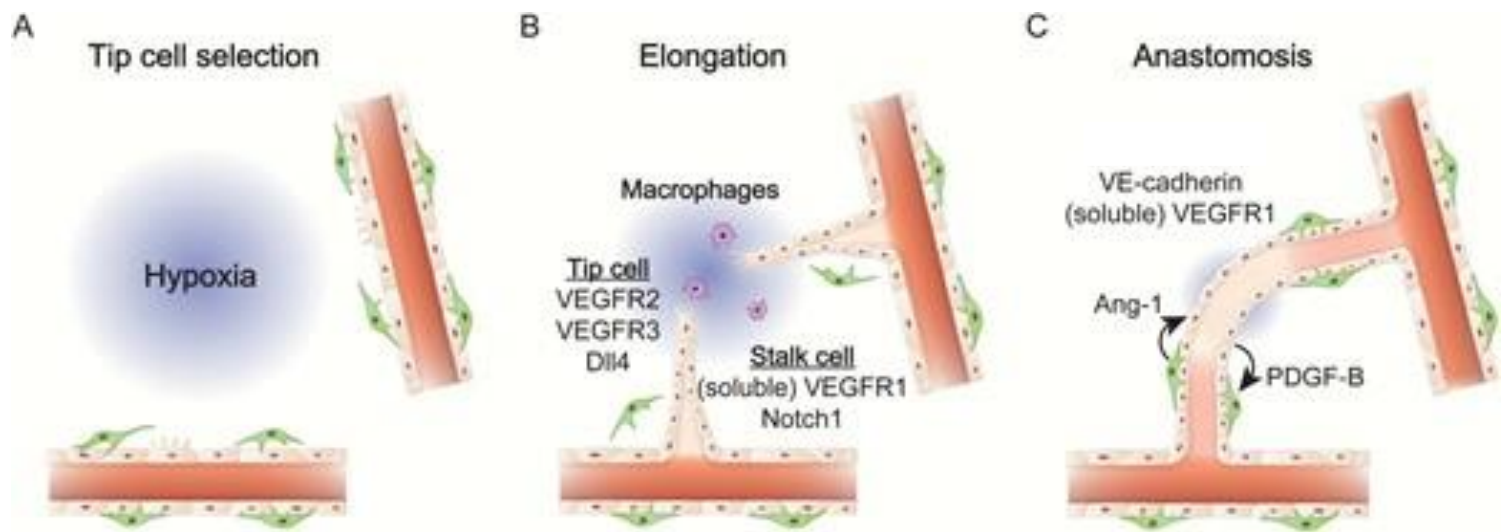


Figure 1.1: Macrophages and ECs are intimately involved in angiogenic processes.

Angiogenesis is a multiple stage process. (A) Angiogenic factors stimulate ECs. Signalling from VEGF-VEGFR and DLL4-Notch1 induces tip and stalk cells. (B) New sprouts extend towards hypoxic areas. Tip cells undergo anastomosis to form a network, which is facilitated by MΦs. (C) The increased blood flow and pericytes (green cells) help to stabilise the new blood vessel. *Image by Naito et al. (20)*

1.2 The ancestral link between macrophages and endothelial cells

1.2.1 Development of the embryonic haematopoietic system

The exact mechanisms underpinning the emergence of the haematopoietic system are yet to be fully elucidated. Haematopoiesis in prenatal development is complex and involves different stages that begin outside the embryo proper. It has long been accepted that extra-embryonic haematopoiesis precedes intra-embryonic haematopoiesis. Three major waves of blood cell development have been identified, classified as follows in the murine embryo: primitive, transient-definitive and definitive haematopoiesis (**Figure 1.2**) (21).

The primitive wave arises around embryonic day (E) 7 in mice. Proliferative embryonic progenitor cells from the lateral and posterior mesoderm arrange themselves to form “blood islands” along the endoderm of the YS (22). While the outermost cells give rise to angioblasts, which are precursors to ECs that later establish the primitive vascular plexus, the central cluster of cells provides the first source of primitive erythrocytes, as well as MΦs. Primitive erythrocytes are morphologically and functionally distinct from postnatal erythrocytes as they are large, nucleated cells that express β -globulin, prior to their release into the blood and function transiently for a narrow window between E7.25-8.75 (23).

Studies in mice have found early evidence for the presence of primitive MΦs in two distinct waves: (i) maternal MΦs that circulate to the extra-embryonic YS without seeding the embryo and (ii) primitive MΦs that arise from embryonic progenitors in YS around E7.5 without passing through a monocyte intermediate stage (20, 24, 25). Although it has long since been recognised that the primitive wave gives rise to early MΦ phenotypes, a clear ancestral and mechanistic understanding of how this occurs is still lacking.

Initial evidence for primitive MΦs first arose from studies using inducible *Runx1* promoter-driven GFP reporter mice that revealed that seeding of brain microglia directly originated from E7.5 YS-derived CD45⁺c-Kit⁺ progenitors (26). These c-Kit⁺ progenitors were also found to exclusively give rise to colonies of the MΦ subtype in culture (27). Moreover, a large proportion of tissue-resident MΦs in the embryonic and postnatal liver, brain, skin epidermis and lung have been shown to originate from a *Tie2* expressing cell in the YS before E10.5 (28, 29) (**Figure 1.3**). MΦs generated from these YS progenitors appear to have a high proliferative potential, which was thought to propagate their expansion and self-maintenance in different tissues during foetal development (28). Conversely, studies in Zebrafish reveal that the primitive MΦs originate from a mesodermal precursor that then migrates to form the blood islands following differentiation to vasculogenic cells (30). The emergence of both primitive haematopoietic cells and angioblasts at YS development lays early evidence for the familial relationship between haematopoietic and ECs via a shared a common bipotent ancestor “haemangioblast”.

The second major stage of developmental haematopoiesis *in utero* arises from YS erythromyeloid progenitor cells (EMPs) and is named the transient-definitive wave due to its overlapping timeline with both the primitive and definitive haematopoietic waves, as well as its short-term haematopoietic potential (31). EMPs emerge in YS around E7.5-8.5, then migrate to the embryo proper and seed the foetal liver between E10.5-11 (32). The foetal liver, derived from both the endoderm and the mesoderm, is the first intra-embryonic site of haematopoiesis. Following rapid differentiation, this wave gives rise to the first circulating definitive erythrocytes, bipotent granulocyte/MΦ progenitors and mast cells (31). In addition, cell lineages that contain both megakaryocyte and myeloid potential are also established (33) (**Figure 1.2**). From E12.5 onwards, EMP-derived MΦs gradually replace those produced during the primitive wave and are thought to comprise most tissue-resident MΦs

found at birth, apart from the microglia in the brain and Langerhans cells in the skin (34, 35) (**Figure 1.3**).

Some studies have suggested the existence of two distinct, “early” and “late” EMP populations (36). The differentiation of MΦs from early EMPs does not involve a monocyte intermediate but rather formation of CX₃CR1⁺ pre-MΦs which emerge in YS around E9.5 and thereafter produce mature F4/80^{Hi} MΦs (27). In contrast, late EMPs do transition through monocytes (36). Up until ~E16, most foetal liver myeloid cells are of EMP origin. While Hoeffel *et al.* concluded that late EMPs in the liver seed resident MΦs in kidney, gut, skin, liver and lung prenatally (36), results from Schulz *et al.* indicated that early EMPs seed resident MΦs in the brain, skin and liver (37). Another regulator of importance was found to be RUNX1, as deficiency was deemed embryonically lethal at E12.5 due to lack of foetal haematopoiesis (38). However, studies that activated the *Csf1r* or *Runx1* promoters at E13.5 proved to be exhaustive since they also label foetal MΦs, monocytes, granulocytes and adult foetal-derived MΦs (26, 38, 39).

It is still unclear whether early or late EMPs are ultimately responsible for the origin of different tissue-resident MΦs (28, 36). On the one hand, some lineage tracing and adoptive transfer irradiation studies have indicated that YS-derived late EMPs in the liver give rise to resident MΦs in adult tissues via monocyte intermediates (36), while others suggest robust seeding of residential MΦs from early CSF1R⁺ EMPs (E8.5) and/or CX₃CR1⁺ YS precursors (E9.5) (26, 40) (**Figure 1.3**). There is also evidence for the migration of CX₃CR1⁺ progenitors via the bloodstream at E9 and the relocation of all CX₃CR1⁺ cells in the liver as well as around the embryo by E12.5, with CX₃CR1 dependency for migration as seen in CX₃CR1^{-/-} mice (41, 42).

Overlapping with EMP production is the definitive wave of HSCs that emerge intra-embryonically from the ventral floor of the dorsal aorta gonad mesonephros (AGM) region and other haemogenic sites (placenta, vitelline and umbilical arteries) between E10 and E12 (43). This was first studied in chick-quail embryos and chimeras (33, 44). In the AGM, ECs that line the ventral wall, bend luminally and differentiate asymmetrically in a RUNX1-dependent fashion into HSCs (45). Along with evidence that AGM VE-cadherin⁺ (CDH5) ECs can generate HSCs in coculture with OP9 mesenchymal stromal or ECs *in vitro*, it is therefore hypothesised that HSCs are generated from haemogenic endothelium (45-47) (**Figure 1.2**).

Murine studies have shown that haemogenic endothelium in extra-embryonic YS also gives rise to EMPs at ~E8.25, T and B cell progenitors at ~E9.5 and AGM HSCs at ~E10.5 (31). Hence, it is now believed that haemogenic endothelium gives rise to both the YS EMP and AGM HSC definitive waves of haematopoiesis. In mice, EMPs are c-Kit⁺CD41⁺ and share markers with haemogenic ECs and developing definitive HSCs including CD31, CD45 and CD61 (48-50). However, Fcγ receptor (CD16/32) expression and the lack of stem cell antigen (Sca-1) are unique to EMPs, while only 15% of E9.5 EMPs express CD93 (AA4.1) which is otherwise highly expressed in HSCs (48, 51, 52). Interestingly, a proportion of CD93⁺ YS cells were found to be c-Kit⁻CDH5⁺ ECs (53).

Notably, one key difference between primitive MΦs and YS EMPs and definitive HSCs is the expression of c-Myb. Primitive MΦs are largely independent of c-Myb while foetal livers from Myb^{-/-} mice showed a lack of all c-Kit⁺ cells, noting the importance of c-Myb for the regulation of both EMP and HSCs (36). Indeed, late EMPs are c-Myb⁺ both in E9.5 YS and foetal liver at later gestational ages, while early EMPs are c-Myb⁻.

AGM-derived HSCs and YS-derived EMPs co-exist with each other in foetal liver between E11.5-12.5 in mice (54). Between E11.5-16.5, HSCs rapidly proliferate and expand in the foetal liver. After contributing largely to myeloid, megakaryocyte and mast cell progenitors at E16.5, they migrate to the spleen (E16.5-17.5) and later to the bone marrow (BM) (E17.5) (55, 56), which becomes the predominant site of haematopoiesis in extra-uterine life. Gradually, numbers of HSCs in the spleen and liver begin to decline following BM seeding (57) (**Figure 1.2**).

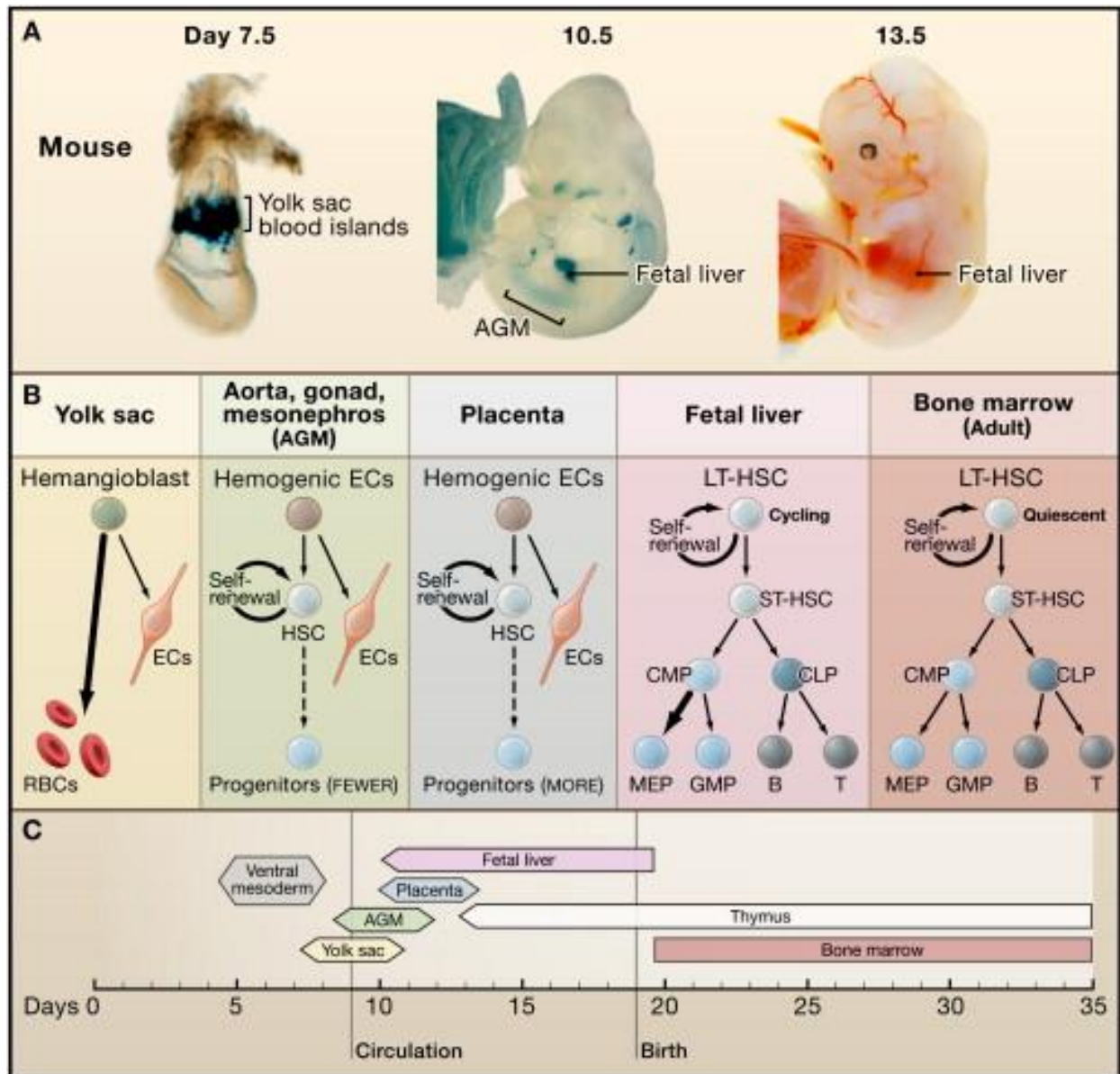


Figure 1.2: The successive waves of murine haematopoietic development.

(A) Haematopoiesis begins in the yolk sac (YS) blood islands and progresses to the aorta-gonad mesonephros (AGM), placenta, and foetal liver (FL). LacZ labelling of transgenic embryos expressing GATA-1-driven LacZ reveals YS blood islands. LacZ stained AGM and FL in Runx1-LacZ knockin mice. (B) Haematopoiesis encourages the formation of certain blood lineages in each place. Abbreviations: ECs, endothelial cells; RBCs, red blood cells; LT-HSC, long-term haematopoietic stem cell; ST-HSC, short-term haematopoietic stem cell; CMP, common myeloid progenitor; CLP, common lymphoid progenitor; MEP, megakaryocyte/erythroid progenitor; GMP, granulocyte/ M Φ progenitor. (C) Developmental time windows for shifting sites of haematopoiesis. *Image by Orkin et al. (33)*

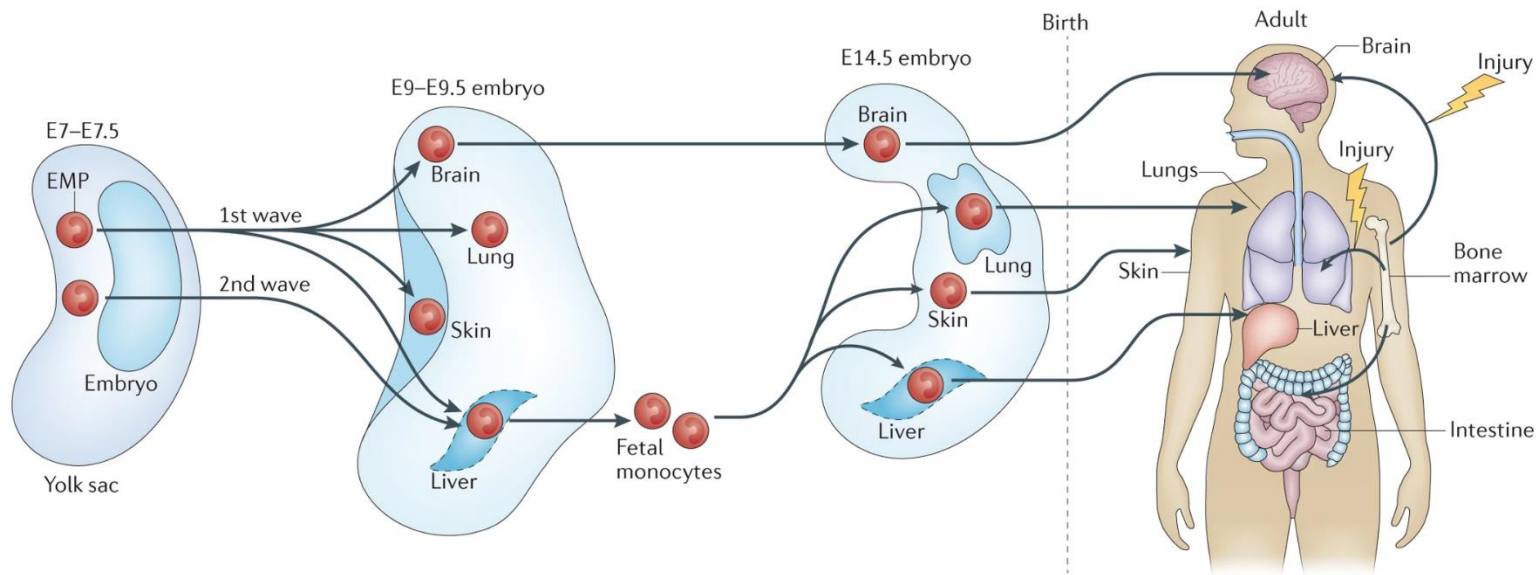


Figure 1.3: Origins of tissue-resident macrophages.

MΦs are maintained in most healthy tissues in mice by embryonic precursors (embryonic MΦs) independently of monocytes, with the exception of intestinal MΦs, dermal MΦs and a subset of cardiac MΦs. Two hypotheses exist about the origin of embryonic MΦs. The first hypothesis suggests that all embryonic MΦs derive from yolk sac-derived erythromyeloid precursors (EMPs) that develop around embryonic day 7.5 (E7.5). The second hypothesis suggests that yolk sac-derived EMPs arise in two waves that differentially contribute to adult microglia and other MΦs: an early wave of yolk sac-derived EMPs that appear around E7.5 in the yolk sac colonise the brain and other foetal tissues around E9 to give rise to all tissue MΦs, and a later wave of yolk sac-derived EMPs that colonise and expand in the foetal liver to differentiate into foetal liver monocytes, which subsequently replace foetal MΦs, with the exception of microglia, and maintain them in adulthood. *Image by Donath et al (58)*

1.2.2 Maintenance of postnatal tissue macrophages

The assumption that MΦs are derived from circulating monocytes was based on the classic observation that monocytes give rise to MΦs in pathological settings and constitute a precursor reservoir for tissue-resident mononuclear phagocytes (59). Monocytes and their progeny, on the other hand, have developed as a dynamic cellular system capable of supplementing the conventional tissue-resident mononuclear phagocyte compartment on demand (60, 61). Early studies established the existence of BM-derived monocyte subsets in human blood (62). Ly6C^{hi} monocytes (also known as CX₃CR1^{int}CCR2⁺CD62L⁺CD43^{low}) and Ly6C^{low} monocytes (CX₃CR1^{hi}CCR2⁻CD62L⁻CD43^{hi}) are the two subsets of CD115⁺ mouse monocytes (63). On one hand, Ly6C^{Lo} monocytes express MHCII while it is absent in the Ly6C^{hi} subset. Gene expression profiling results corroborate the alignment of the mouse Ly6C^{hi} and Ly6C^{low} populations with the two major CD14⁺ and CD14^{low}CD16⁺ human groups (63). Both monocyte subsets derive from MΦ/dendritic precursors (MDP) and common monocyte progenitors (cMoPs), although with different kinetics in the BM, indicating a precursor-product relationship of Ly6C^{hi} and Ly6C^{low} monocytes (64). Increasing evidence dictate that murine blood monocyte subsets constitute a steady-state developmental process, with Ly6C^{hi} monocytes developing into Ly6C^{low} cells, most likely in the circulation (65). In keeping with this, the primary role of Ly6C^{low} cells appears to be intravascular inspection of endothelium integrity rather than extravasation and tissue engraftment (66, 67). Ly6C^{hi} monocytes, on the other hand are recruited to sites of pathological changes, and act as precursors of monocyte-derived tissue MΦs.

Previously it was unclear as to whether embryonic MΦs survive into adulthood and, if so, whether these cells, and hence primitive haematopoiesis, contribute significantly to adult tissue MΦ populations. As discussed above, it is now well documented that the majority of tissue MΦs are of embryonic origin and are not dependent on monocyte input (28, 29). Multiple studies involving mutant mice which selectively impair definitive haematopoietic stage of development revealed

significant contribution from the YS to tissue-resident MΦ populations (37). As previously mentioned, definitive haematopoiesis is dependent on c-Myb expression and c-Myb deficient murine embryos still harboured normal tissue-resident MΦs in liver, epidermis and the brain (68). In addition to this, the persistence of embryonic MΦs into postnatal life was studied using Cre-Lox approaches and parabiosis studies, to show that most tissue MΦs are generated prenatally and are maintained in postnatal tissue via local self-renewal (69, 70). Although monocytes do produce adult tissue MΦs, they appear to provide only a little contribution to the replacement of embryonically implanted, YS-derived macrophages in healthy brain, liver, and skin epidermis (71). A growing body of research shows that YS- and HSC-derived MΦs coexist in other healthy tissues to maintain normal homeostasis. As demonstrated for the dermis (72), heart (73), aorta (74), and skeletal muscle (SkM) (75), distinct MΦs sources often correlate to diverse macrophage subtypes, each with its unique set of biological roles, transcriptomic and phenotypic characteristics.

1.2.3 Haemangioblasts and haemogenic endothelium: two possible candidates for bipotent progenitors for haematopoietic and endothelial cells.

1.2.3.1 Haemangioblasts

A century since the notion of the haemangioblast was first introduced by His *et al.* (76), its existence still remains controversial. Early studies identified a strong relationship between the first blood cells and vascular progenitor cells in blood islands inside the YS of chick embryos, which they attributed to a single bipotent ancestral progenitor, called the haemangioblast, which was thought to derive from primitive mesoderm (23). Although single-cell labelling and tracking of gastrula-stage zebrafish embryos has led to the conclusion that individual mesodermal cells can give rise to both blood and ECs, the bulk of these two lineages were discovered to be independently fated (77). Lineage-tracing data from mice have also suggested that the cellular composition of individual YS blood islands may be derived from distinct mesodermal progenitors (78) and that the VEGFR2⁺ mesodermal subpopulation is not only restricted to endothelial and haematopoietic lineages, but also gives rise to muscle cell progeny (79).

More recently, specific human embryonic stem cell (ESC) lines have been found that can generate blast colony forming cells (BL-CFC) and can be coaxed to develop into both haematopoietic and ECs at the single-cell level (77, 80, 81). These BL-CFCs were discovered to exhibit a mesoderm-specific marker, mesodermal gene T (*Brachyury*) and Foetal Liver Kinase 1 (Flk1). Differentiation and control of pluripotent model systems have been connected to multiple genes and signalling networks including Runt-related transcription factor [*Runx-1* (AML1)], (31), *Scl* (Tal1)(82), *Flk1* (77, 80, 81, 83-85), *brachyury* (86) and angiotensin converting enzyme (*Ace*, CD143) (86), markers consistent with haemangioblasts. Furthermore, fate-mapping research in Zebrafish gastrula revealed the presence of an analogous clonal population with both haematopoietic and endothelial bipotency, which was found in the ventral-lateral mesoderm during Zebrafish development (77, 87).

Furthermore, when subjected to endothelium and haematopoietic growth medium conditions, blast colonies from E7-7.5 mouse embryos have been demonstrated to give rise to adherent and non-adherent cells (80). These were shown to comprise primitive erythroid, MΦ, and immature haematopoietic cells based on expression of the haematopoietic markers, H1 and α -major globin, as well as the erythroid transcription factor, *Gata1*, *Csf1r*, and *Myb* in the non-adherent population. Flk1, Tie2, and platelet EC adhesion molecule (Pecam1 or Cd31) were expressed by adherent cells, as were smooth muscle actin (*Acta2*), smooth muscle protein 22 kDa (*Sm22*), and calponin (*Cnn1*), indicating endothelial and smooth muscle cell (SMC) growth, respectively (80).

Ex vivo experiments with mouse embryos have also shown that BL-CFCs can give rise to both haematopoietic cells and ECs, leading to speculation that the haemangioblast is a state of competence, and that experimental manipulations may reveal a dormant competency state, as opposed to an inherent bipotent progenitor state that is active *in vivo* (88). Indeed, the *in vivo* demonstration of haemangioblasts in postnatal tissues has so far proven to be notoriously elusive. Emerging tools, such as single-cell RNA sequencing (scRNA-seq) and multi-colour lineage-mapping systems (e.g., Confetti or the Rainbow-Cre mice), may help future studies to finally determine if haemangioblasts do exist after birth.

1.2.3.2 Haemogenic Endothelium

Although some have speculated that haemangioblasts give rise to the first haematopoietic cells, a contrary theory is that they instead arise from haemogenic endothelium (89). Haemogenic endothelium is a phenotypically differentiated EC subpopulation with the ability to develop into blood cells. This is currently thought to happen via endothelial-to-haematopoietic transition involving asymmetric cell division, rather than through a single cell giving rise to two daughter cells (90). The discovery of haemogenic endothelium was made by lineage-tracing studies in mice and zebrafish,

which used a CDH5-Cre system and time-lapse imaging to show that CDH5⁺ ECs create definitive HSCs in the AGM at E10.5 (91, 92). Subsequent mouse studies have also revealed that haemogenic ECs in extra-embryonic YS give birth to EMPs at E8.25 (93), T and B cell progenitors at E9.5 (94, 95), and AGM HSCs at E10.5 (96). As a result, it is now thought that haemogenic ECs are responsible for both the YS EMP and AGM HSC waves of haematopoiesis. Furthermore, utilising an endothelial "niche" population, some groups have successfully differentiated endothelial precursors into HSCs (97-99), lending further support to the concept of haemogenic endothelium.

There is also compelling evidence that primitive haematopoiesis develops from progenitors expressing EC markers, such as Tie2, CD144 (CDH5) and CD31 (81, 100-102). Surprisingly, these progenitors are found within a mass of endothelial-expressing cells rather than the wall of blood vessels in YS (100, 103). As a result, Lancrin *et al.* proposed that the haemangioblast may create haematopoietic cells via a haemogenic endothelium intermediate (100). This was based on experimental work, in which they differentiated mouse haemangioblasts/BL-CFCs into haematopoietic cells *in vitro* via a two-step process. The haemangioblasts first converted into a densely adherent cell layer, that displayed EC markers, which they called the transitory haemogenic endothelium stage, and then became non-adherent haematopoietic cells after 36-48 hours (h) of culture. Taken together, it is still not certain whether primitive haematopoiesis arises directly from mesoderm, haemangioblasts or haemogenic endothelium, or all of these different sources which themselves may be hierarchically linked.

1.2.4 Development of the embryonic vascular system

The emergence of an extra-embryonic vascular plexus begins as early as E7-7.25 in mice with the onset of the YS blood island giving rise to embryonic angioblasts. Growth and fusion of blood islands eventually give rise to the YS capillary network; this network then differentiates into the arteriovenous vascular system (104). Embryonic angioblasts express Flk-1, that responds to VEGF to promote EC differentiation, proliferation and migration. Studies in quail/chick chimeras show that fibroblast growth factor-2 (FGF-2) regulates the differentiation of angioblasts from the mesoderm, while PDGF regulates distinct differentiation of Flk-1⁺ angioblasts into mural cells (pericytes and vascular smooth muscle cells) (105). Flk-1 knockout is embryonically lethal with both haematopoietic and endothelial lineage development attenuated, indicating the critical importance of Flk-1 in regulating the differentiation of both lineages. However, the exact mechanism behind haematopoietic and EC lineage commitment has not yet been identified.

Intraembryonic vasculature soon follows via the rudimentary migration of the YS angioblasts to establish the dorsal aorta and the great vessels, endocardium, and the cardinal vein between E9.5-10.5. Subsequently, the generation of local angioblasts in tissues contributes to the expansion of the vascular network connections between major vessels, while the migration of angioblasts from mesodermal somites constructs the limb vessels. With the establishment of a stable dorsal aorta, mesoangioblasts from the posterior and lateral walls soon also appear in the system. While the definitive origin of these cells is unknown, they are thought to play a supportive role during organogenesis, especially to branching cells in the vasculature, allowing them to adapt to local tissue-specific properties (106). As such, embryonic mesoangioblasts may be homologous with postnatal mesenchymogenic pericytes. Notably, mesoangioblasts express endothelial, mesodermal and haematopoietic markers but do not show *in vivo* haematopoietic differentiation potential (107). This is an important point of difference from haemogenic endothelium.

Interestingly, a recent study used *Csf1r*-Cre and *Kit*-Cre lineage-mapping techniques to show that early YS EMPs also contribute to mature ECs, that line the blood vessels of YS, as well as other embryonic and postnatal tissues, such as liver, brain, heart and lung (108). However, this novel finding was subsequently contradicted by another group that used alternative lineage-mapping systems coupled with immunofluorescence confocal microscopy and could not find any evidence of EMP-derived ECs in different murine tissues (109). Although therefore contentious, the possibility that YS EMPs give rise to both MΦs and ECs, does align with the notion that these two distinct cell lineages are developmentally related, along with the historical evidence for the existence of bipotent haemangioblasts during early embryogenesis.

1.2.5 Origins of postnatal endothelial cells

In postnatal life, mature ECs were thought to be the main mediators of angiogenesis through their active proliferation, sprouting and migration (1). In most steady-state tissues, mature ECs are considered almost quiescent, showing limited turnover in the vasculature, except for when postnatal angiogenesis occurs during organ growth, the ovarian menstrual cycle and in different pathophysiological processes, such as wound healing, bone repair, post-ischaemic repair and tumorigenesis. Bone marrow (BM) -derived, circulating endothelial progenitor cells (EPCs) were first proposed as an ancestral source for postnatal ECs following seminal work by Asahara and colleagues more than 20 years ago. Since then, there has been an enormous amount of research dedicated to the study of these cells, both in peripheral blood and the discovery of other endothelial progenitor populations that are resident in different tissues (110-113). Circulating EPCs have been identified and studied through various isolation and cell culture techniques and based on their surface expression of different combinations of cell surface markers (e.g. CD34, Flk-1, CD133), which are largely non-specific as they are also found on haematopoietic cells (110, 114). This has led to considerable

inconsistency and controversy in the field, as well as confusion over correct nomenclature. Broadly speaking, circulating “EPCs” have been shown to mobilise from BM in response to certain exposures (e.g. remote tissue injury), migrate to different tissues in response to chemokine gradients and differentiate into mature ECs in response to angiogenic growth factors (e.g., VEGF) to help achieve neovascularisation and/or re-endothelialisation (110, 115). Certain pathologies, such as diabetes and hypertension attenuate the mobilisation and function of EPCs and thereby stunt these repair responses (116). A growing body of evidence has also revealed the existence of vascular- and tissue-resident EPCs, which also express CD34, Flk-1/KDR, and c-kit but potentially lower levels of CD133 (117, 118). Recent studies by Patel *et al* have helped elucidate a hierarchical of endothelial ancestry within different murine tissues, by identifying self-renewing resident EVPs that can differentiate into mature ECs via an intermediate population of transit amplifying (TA) cells (119). Here, three subpopulations were characterised among the VE-Cadherin⁺CD45[−] cells, comprising CD31^{−/Lo}VEGFR2^{Lo/intracellular} endovascular progenitors (EVPs), CD31^{int}VEGFR2^{Lo/intracellular} transit amplifying precursors and definitive differentiated CD31^{Hi}VEGFR2^{Hi/extracellular} ECs. Each population expressed Sca-1 and was identified only after excluding the CD45⁺ fraction (Sca-1⁺ CD45[−]).

Interim conclusion

- Traditional views contend that tissue MΦs are primarily derived from the recruitment and differentiation of circulating monocytes. However, evidence suggests that some postnatal tissue MΦ populations are seeded embryonically from either an extra-embryonic YS or foetal liver source and are self-maintained.
- ECs are derived from the proliferative renewal of resident, mature ECs, proliferation and differentiation of local progenitor cells, and recruitment and differentiation of circulating BM-derived EPCs. YS EMPs may also be a source of mature ECs that line the blood vessels, although this is controversial.

1.3 Diabetes mellitus

1.3.1 Epidemiology

Diabetes is a chronic metabolic disorder of inadequate blood glucose control. It is a fast-growing global problem with devastating social, economic and health consequences. In 2021, the International Diabetes Federation reported that ~537 million people suffer from diabetes globally, and this is predicted to rise to 630 million by 2030 and 783 million by 2045 (120). 2022 census data revealed that there are currently 1.2 million Australians living with diabetes. On the health economic front, diabetes was responsible for an estimated USD 966 billion in global health expenditure in 2021, which represents a 316% increase over the last 15 years (120). With the rise of industrialisation and staggering increase in obesity, diabetes has established itself as a global pandemic and is the sixth leading cause of morbidity and mortality worldwide. Complicating this problem further, is the alarming estimate that almost 50% of people suffering from diabetes currently remain undiagnosed. Over the years, exceptional progress has been made in our understanding of the pathogenesis and complications of diabetes, as well as in glucose monitoring and treatment strategies, although there is much work still needed to adequately tackle its enormous mortality, morbidity, and health economic burden.

1.3.2 Maintaining glucose homeostasis

The human body works in synchrony to maintain a constant internal state or homeostasis. The regulation of normal tissue and metabolic homeostasis requires a fine balance between negative and positive feedback loops. In the case of hyperglycaemia, a negative feedback loop sets out a cascade of events that aim to restore glucose levels back to healthy ranges via endocrine secretion of hormones. Initially, the β cells of the islets of Langerhans in the pancreas are triggered to release a 51-amino acid polypeptide, insulin. Insulin is composed of two chains (A and B) connected by disulphide bridges. The action of the enzymes pro-hormone convertases (PC1 and PC2) and exo-

protease carboxypeptidase brings about the synthesis of insulin and C-peptide from pro-insulin. Insulin binds to target cells via the extracellular alpha (α)-subunit of the tyrosine kinase insulin receptor, which leads to activation of intracellular substrate-1 (IRS-1) via autophosphorylation of the internal beta (β) subunit of the receptor (121) (**Figure 1.4**). As a result, phosphatidylinositol 3-kinase (PI3K) and Akt kinase are activated downstream. In mammalian cells, Akt kinase triggers the translocation of the glucose transporter, glucose transporter type 4 (GLUT4) to the cell surface thereby facilitating glucose uptake inside the cell. In the liver, insulin signals the conversion of excess glucose to glycogen for storage via increased expression of glucokinase and reduced expression of gluconeogenic and ketogenic enzymes (122). In the vasculature, insulin triggers EC nitric oxide synthase (NOS), which leads to the formation of nitric oxide (NO) to mediate vasodilation. In addition to these effects, insulin signalling also sets off protein-protein interactions that activate the mitogen-activated protein kinase (MAPK) pathway, promoting cell proliferation and mitogenesis (123).

In contrast, low blood glucose levels trigger the release of glucagon, a peptide hormone comprised of 29 amino acids, from islet- α cells. Activation of plasma membrane glucagon receptors in the hepatic cells results in adenylate cyclase activation and cyclic adenosine 3', 5'-monophosphate (cAMP) formation which in turn activates protein kinase A (PKA). The resultant signalling cascade induces the transcription of glucose 6-phosphatase and phosphoenolpyruvate carboxykinase (PEPCK), two enzymes that contribute to increased gluconeogenesis (118). More importantly, PKA initiates the glycogenolysis cascade increasing the conversion of stored glycogen into glucose which is then released to the blood to achieve glucose homeostasis (124). This balance of insulin and glucagon signalling is thus largely responsible for the maintenance of physiological euglycemia (**Figure 1.5**) (125). Aberration of this homeostatic process results in pathological states such as diabetes which is largely due to the (i) dysfunction in the synthesis or secretion of insulin in Type 1 diabetes (T1D) or (ii) resistance to insulin's actions coupled with its suboptimal production in Type 2 diabetes (T2D)

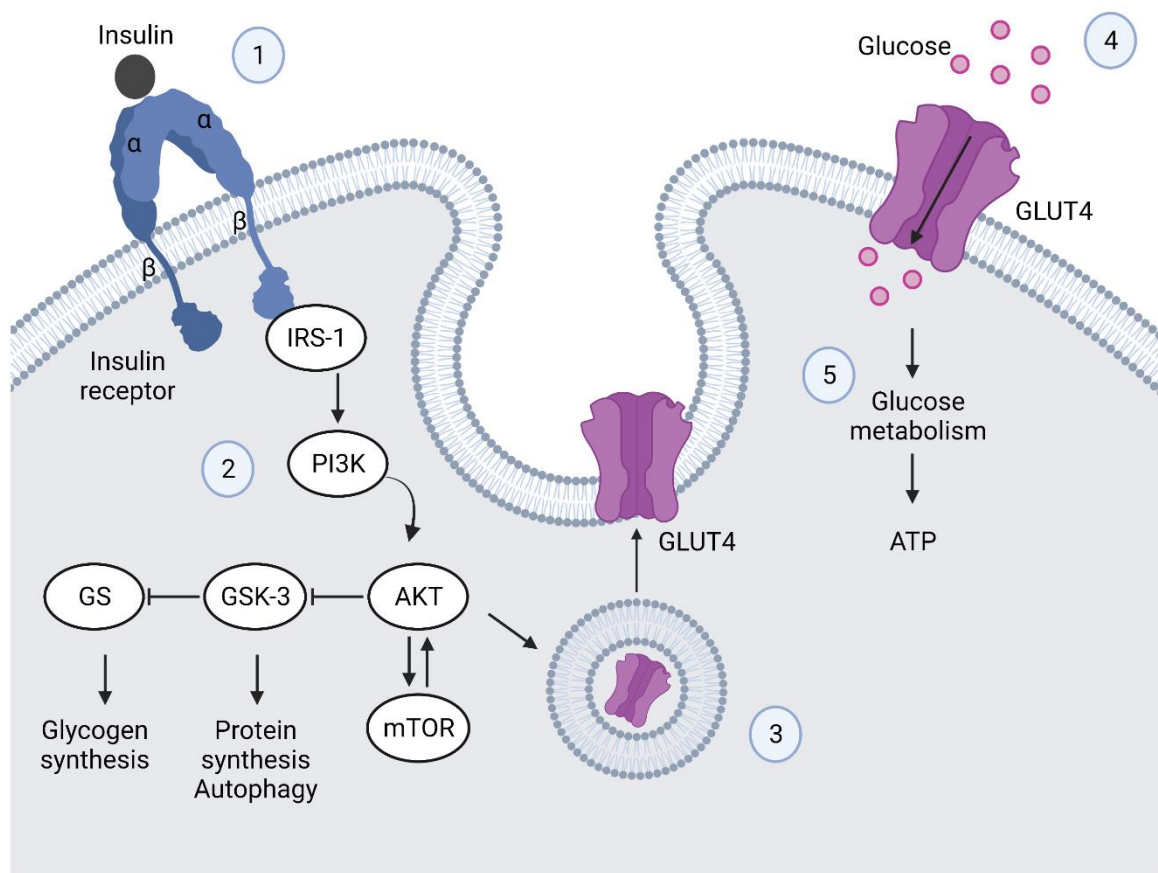


Figure 1.4: Insulin signalling pathway.

1. Insulin binds to insulin receptor which contains tyrosine-protein kinase activity. 2. Binding of insulin triggers downstream mediator insulin receptor substrate-1 (IRS-1) and phosphatidylinositol 3-kinase (PI3K). The insulin receptor stimulates phosphorylation and activation of AKT. Afterward, AKT phosphorylates the Serine-9 site of glycogen synthase kinase 3 (GSK-3) and inhibits its activity. The PI3K/AKT/GSK-3 signalling pathway is involved in the insulin signalling transduction, and GSK-3 is regulated and controlled by insulin in this signalling pathway, which is related to the glycogen synthesis regulation. 3. Akt phosphorylates key proteins leading to increased recruitment of glucose transporter type 4 (GLUT4). 4. GLUT4 mobilises movement of glucose into the cell for metabolic reactions. 5. Glucose metabolism in the form of cellular respiration reactions brings about the formation of adenosine triphosphate (ATP), the cells energy currency.

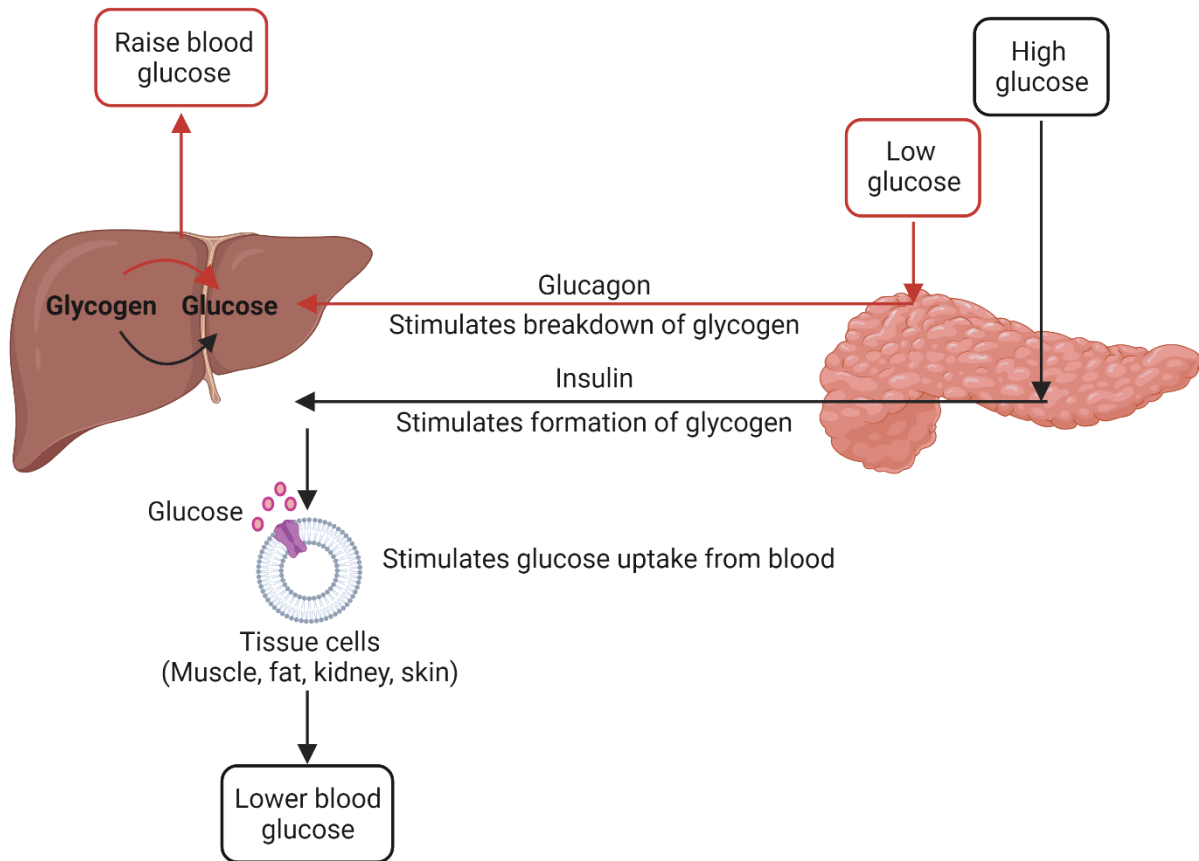


Figure 1.5: Glucose homeostasis in the human body.

In black arrows: High blood glucose triggers the production and release of insulin hormone from the β -cells of the pancreas. Insulin signalling upregulates translocation of glucose transporter type 4 (GLUT4) in tissue cells facilitating the uptake of glucose into cells for metabolic function. This, together with the stimulation of glycogen formation for excess glucose storage in the liver leads to lower blood glucose levels. In red arrows: Low blood glucose stimulates the release of glucagon from the α -cells of pancreas. Glucagon triggers the breakdown of glycogen stores to glucose in the liver and therefore raises blood glucose levels.

:

1.3.3 Classification of diabetes mellitus

Diabetes captures a range of heterogeneous diseases that lead to prolonged hyperglycaemia. The classification of diabetes is imperative for the determination of appropriate therapies, as clinical presentation and disease progression vary considerably. The two main types are insulin-dependent or T1D and insulin-independent or T2D. T1D is an autoimmune disorder that involves the progressive destruction of β cells by activated T-helper cell (Th1) ($CD4^+$) and cytotoxic T cell (T_c) ($CD8^+$), and MΦs infiltrating the pancreas, usually leading to absolute insulin deficiency (126). T2D is characterised by the insufficient insulin synthesis, secretion and insulin resistance (127). Other types include gestational diabetes and monogenic diabetes syndromes (such as neonatal diabetes and maturity-onset diabetes of the young). While traditionally it was thought that T2D occurs exclusively in adults and T1D only in children, this has since been proven as inaccurate, as all age groups are susceptible to both diseases (128).

1.3.3.1 Type 1 diabetes mellitus

Genetic as well as environmental factors contribute to the susceptibility of both T1- and T2D; however, characterisation of the pathophysiological demise or dysfunction of β -cell function is better defined in T1D than in T2D. In T1D, mutations in the human leucocyte antigen (*HLA*) loci, responsible for distinguishing foreign non-infectious and infectious agents, are closely associated with the autoimmune response against insulin producing β -cells (126). HLA contributes 50% of the inherited risk for T1D with HLA-class II haplotypes carrying the most intense susceptibility determinants (126). HLA-class II locus is responsible for the presentation of “diabetogenic peptide” in T-cell receptor protein on the surface of T cells inducing autoimmunity (129). An additional 60 non-HLA loci associated with insulin gene expression in the thymus, regulation of T-cell activation, and viral responses have also been linked to T1D (126). Studies show that identical twins have a higher likelihood to develop T1D than fraternal twins, showing a strong familial genetic

predisposition (130). In contrast, certain important environmental triggering agents including obesity, viral infection, low levels of vitamin D and cow 's milk proteins are also known to stimulate the onset of T1D (126, 131, 132).

It is also now clear from prospective studies that the persistent presence of two or more β -cell autoantibodies such as anti-glutamic acid decarboxylase (anti-GAD), Islet antigen-2, Islet antigen-2f3 and anti-insulin antibodies, produced by damaged β -cells, is a near certain predictor of T1D (133, 134). Early studies to confirm the autoimmune nature of T1D include animal models, involving biobreeding (BB) rats and nonobese diabetic (NOD) mice. The transfer of anti-islet specific T cells ($CD4^+$, $CD8^+$) but not autoantibodies, induces diabetes and insulinitis in immuno-incompetent NOD mice (135, 136). Interestingly, M Φ infiltrates have been detected in the islets of young NOD mice and inhibition of M Φ influx into the pancreas attenuated T1D development (137). The question of whether a trigger for the immune response against β -cells exists or whether the immune response is a stochastic event has been a subject of considerable speculation and controversy. It is clear that both adaptive and innate immune cells are both intrinsically involved in β -cell destruction, along with various mechanisms of cell damage/death.

The adaptive immune response includes the presentation of β -cell autoantigens to T-helper cells via classically activated M Φ s or antigen-presenting cells (APC) (138, 139). M Φ s expressing major histocompatibility complex II (MHCII) migrate to pancreatic lymph nodes where $CD8^+$ T-cell activation targets against β -cell auto-antigens, thereby killing β -cells via release of cytolytic granules containing granzyme B and perforins (140). $CD4^+$ T cells support both B cells and $CD8^+$ T cells by providing cytokines, such as interleukin-21 (IL-21), and a positive-feedback loop via CD40L–CD40

interactions to antigen-presenting cells, culminating in a proficient autoreactive CD8⁺ T cell response and B cell antibody production against β -cell antigens.

Furthermore, inflammatory M Φ s and T cells release cytokines, namely IL-12, IFN- α and TNF- β and express costimulatory molecules important in T cell activation (MHC, CD40, CD86), that launch inflammatory responses via NOS which induces the release of reactive oxygen species (ROS) (141, 142). ROS, such as superoxide and hydrogen peroxide, then triggers β -cell DNA double-stranded breaks leading to cell necrosis (143, 144). NO is associated with β cell death via activation of endoplasmic reticulum stress pathways. Here, increased stress lead to alterations in messenger RNA (mRNA) splicing and protein synthesis; the resultant proteins have been proposed as immunogenic neoantigens (145).

On the other hand, alternatively activated M Φ s decrease hyperglycaemia, insulinitis and inflammation in the pancreas. They express high levels of program-death ligands (PDL), such as PDL-1 and PDL-2 and inhibit the proliferative response of activated T cells (146). β -cells demise has also been attributed to apoptotic signalling. The expression of apoptosis-inducing Fas receptors via cytokine signalling in β -cells has shown to be a contributing factor (145, 147)

On the innate immunity front, gut-microbiota has been recognised to launch innate inflammatory responses via pattern-recognition receptors (PRR), such as toll-like receptors (TLR) 7, MyD88 and inflammasome protein NLPR3 to induce phagocytosis, autophagy and interferon activity that promote cell death (148).

As many as 50% of adults with T1D might be initially misclassified as having T2D (149). Diagnosis of T1D is based on a fasting blood glucose concentration above 7 mmol/L, abnormal oral glucose tolerance test or glycated haemoglobin concentration (HbA_{1c}) above 48 mmol/mol (6.5%) (128). The symptoms for T1D include polyuria, polyphagia and increased thirst, loss of weight, diabetic ketoacidosis, weakness and fatigue. In the absence of symptoms, abnormal glycaemia must be present on at least two different occasions. Management of T1D is crucial to avoid large fluctuations of glucose levels to prevent the development of microvascular and macrovascular complications. Hence, insulin administration via oral or novel delivery systems such as nanotechnology has remained the mainstay of therapy (150). Global efforts to manage T1D continue to improve with major breakthroughs in the last decade.

Despite advances in care and management, T1D poses substantial medical, psychological, and financial burden. Episodes of hypoglycaemia and ketoacidosis pose life-threatening risk. Recurrent hypoglycaemia results in subsequent severe hypoglycaemic events due to the impaired counter regulatory responses, that are launched to return to euglycemia. Cognitive function, macrovascular and microvascular disease, are major complications of T1D (140). Both chronic and acute neurocognitive decline including cognitive function, psychomotor speed, cognitive flexibility and attention have been linked to both macrovascular and microvascular changes. Macrovascular complications include ischaemic stroke, heart disease and peripheral vascular disease resulting from accelerated atherosclerosis, while microvascular complications involve damage to the small blood vessels and contribute to diabetic neuropathy, nephropathy, and retinopathy.

1.3.3.2 Type 2 diabetes mellitus

Insulin-independent or T2D is the most common form of diabetes, accounting for 90% of all diabetic patients and is characterised by loss of insulin sensitivity, abnormal pulsatility of basal insulin secretion, and increased glucagon secretion. It is widely recognised that both insulin resistance and β -cell dysfunction are important in the pathogenesis of glucose intolerance. T2D mostly results from the interaction among genetic, environmental and other risk factors. Evidence of a major genetic component to T2D arises from the higher concordance rates found among monozygotic (96%) than dizygotic twins (151). Genome-wide association studies have discovered a considerable number of susceptibility loci of T2D which have opened avenues as therapeutic targets for the extensively used pharmaceuticals of T2D (151).

T2D is also strongly attributed to obesity, caused by poor diet and lifestyle habits. Due to the substantially higher amounts of adipose tissue in obese individuals, the increased secretion of hormones (growth hormone, testosterone, oestrogen) and other substances may increase the fluctuation of insulin insensitivity. In animal studies, high fatty-acid environments with hyperglycaemic conditions resulted in reduced insulin gene expression with lipoprotein fractions and cholesterol contributing to β -cell failure (152). While high density lipoproteins have shown protective effects by increasing β -cell function and plasma glucose disposal, oxidated low density lipoproteins decreased pre-pro insulin expression in β -cells (153). Moreover, post-mortem studies revealed a marked loss in β -cell mass, which probably is due to increased apoptosis rather than decreased β -cell replication. The abnormally high demand of glucose induced by insulin resistance that increase β -cell workload might also contribute to this loss. Of note, *in vivo* studies of high fat exposure highlight the increased production of M Φ migration inhibitory factor (MIF) by islets, which leads to lipotoxic death of β -cells (154). Hyperglycaemia and hyperlipidaemia in the blood, increased amyloid deposits in the

pancreas, mitochondrial dysfunction as well as inflammatory cytokines released from adipose tissue trigger oxidative and ER stress, together leading to β -cell exhaustion and death (155-157).

In obese mice, a lack of TNF- α function resulted in improved insulin and glucose homeostasis, confirming that inflammation plays a critical role in regulating insulin's action (158). TNF- α is also overexpressed in the adipose and muscle tissues of obese humans, and when administered exogenously, leads to insulin resistance (159-161). The insulin signalling pathway has been described in detail above (**Figure 1.5**). Briefly, insulin receptor signalling utilises intracellular docking proteins (IRS1-6). Phosphorylation of IRS proteins via insulin stimulation is a crucial event in insulin action (162, 163). In both animal models and humans, this step is defective in most cases of insulin resistance. TNF- α also targets insulin signalling by inhibitory serine phosphorylation of IRS-1 by various kinases, that interfere with the ability of this protein to engage in insulin-receptor signalling and result in alterations in insulin action (164). Interestingly, this post translational modification of IRS-1 through serine phosphorylation has been detected in insulin resistant tissues in mice and humans (164). IRS-modifying kinases [c-Jun amino-terminal kinase (JNK), IKK- β , Protein Kinase C (PKC)] also exert powerful effects on inflammatory gene expression via NF- κ B activation, further exacerbating insulin resistance. Activation of JNK, PKC and IKK- β pathways are critical to the development of insulin resistance (165, 166). Deficiency of JNK, PKC and IKK- β protects mice from obesity-induced insulin resistance and interventions to block these kinases in established models of diabetes improved systemic glucose homeostasis and insulin sensitivity (167, 168), therefore, providing a promising therapeutic avenue for T2D (168, 169).

One question that has created some debate over the past decade is the cause of inflammatory response activation in obesity and T2D. Recent evidence sheds light onto ER stress as a critical factor to the

initiation and integration of inflammation in T2D (170). Proper folding, maturation, storage and transport of proteins take place in the ER. Under T2D conditions, increased adiposity produces an environment that challenges ER function owing to architectural constraints that limit ER expansion and energy availability. This leads to activation of a complex response system known as unfolded protein response (UPR) to restore its functional integrity (171). The downstream signalling mediators of UPR, inositol-requiring enzyme 1 (IRE-1), PKR-like ER kinase (PERK) and activating transcription factor 6 (ATF6), are all linked to JNK, and IKK- β activation as described above, leading to insulin resistance (172, 173). Therefore, ER is directly involved in metabolic stress sensing and the translation of that stress into inflammatory signalling and responses (174). In turn, inflammatory mediators can trigger ER stress and lead to stress responses. Importantly, ER is a major source of ROS and consequently oxidative stress in all cells (174). Oxidative stress is directly linked to diabetic complications through EC dysfunction (175). Recent evidence indicates that ROS and mitochondrial dysfunction together activate inflammatory pathways and insulin resistance in cells as well as impair β -cell functions (176). This is further elaborated in another section of this thesis.

Taken together, it is unclear as to whether T2D leads to inflammation or whether inflammation is proximal to disease. However, evaluating signalling pathways at a molecular and cellular levels reveal that this is indeed a vicious cycle. Lipids and cytokines can trigger inflammatory kinases (JNK and IKK) and ER stress. ER stress can also activate JNK and IKK together, then regulate production of cytokines, such as TNF- α . TNF- α in return also triggers further ER stress. Similarly, ROS production from mitochondria or ER activate JNK and IKK which also accentuate ER stress, block insulin action and produce more ROS, inducing further inflammatory responses.

T2D is diagnosed by elevated fasting blood glucose and an abnormal glucose tolerance test without evidence of autoimmune destruction of pancreatic islet β -cells. However, some studies do indicate an autoimmune component that initiates inflammation and damages β -cells to contribute to the pathogenesis of T2D (177, 178). Dietary and lifestyle modifications, including increased exercise and weight loss are the first line of defence in the prevention and management of T2D (179). Several pharmacological options are also available, including drugs that: 1) reduce gluconeogenesis in the liver (e.g. metformin); 2) increase insulin secretion (e.g. sulfonylureas); 3) sensitise peripheral tissues to the actions of insulin (e.g. thiazolidinediones); and 4) insulin analogues which provide exogenous insulin. In addition, people with T2D need to manage other metabolic and cardiovascular risk factors (e.g. dyslipidaemia, blood pressure, cigarette smoking) to mitigate the risk of micro- and macrovascular complications described earlier for T1D (180).

Interim conclusion

- The body launches a negative feedback loop to maintain glucose homeostasis. Failure to produce or respond to insulin leads to diabetic conditions.
- Two types of diabetes are type 1 and type 2 diabetes characterised by the autoimmune destruction of β -cells in the pancreas or the abnormal pulsatility of insulin and insulin insensitivity in cells, respectively.
- Genetic, environmental factors, the presence of autoantibodies against β -cells, abnormal inflammatory responses and oxidative stress all trigger the demise of pancreatic β -cells and trigger the onset of T1D
- Hyperglycaemia-induced inflammation, mitochondrial dysfunction and oxidative stress are among the different factors that underpin progression of T2D.

1.4 The effect of diabetes on mitochondrial biology

Mitochondria are intuitively of interest to the pathophysiology of diabetes, given their central role in cellular aerobic metabolism. They are highly dynamic organelles that regulate cellular processes in all cell types, including adenosine triphosphate (ATP) production, Ca^{2+} homeostasis, emission of radical species and cell death. Broadly, two main subtypes of mitochondria have been defined: i) larger, lamellar shaped subsarcolemmal mitochondria (SLM), that contribute energy for transport processes and ii) smaller intermyofibrillar mitochondria (IMFM), that contribute to contractile function (181, 182). Both T1D and T2D, as well as the less common forms of diabetes, are associated with similar long-term complications that, at least in part, appear to result from disturbances at the mitochondrial level. In rare cases, mutations in the mitochondrial encoded tRNA gene, *A3243G*, lead to impaired mitochondrial protein synthesis and overall islet cell dysfunction, resulting in “mitochondrial diabetes”, which is characterised by decreased glucose-induced insulin release (183).

1.4.1 Basic physiology of aerobic respiration in steady state

The generation of aerobic respiration includes a series of dynamic chemical reactions that yield energy in the form of ATP and are broadly classified as: i) glycolysis, ii) the citric acid (TCA) cycle and iii) oxidative phosphorylation.

1.4.1.1 Glycolysis

This is the first step of cellular respiration and is an anaerobic process which includes a series of ten cytoplasmic oxidation reactions that break down glucose into two pyruvate molecules, a three-carbon compound. Each step of the glycolytic pathway is catalysed by a separate enzyme. Overall, this is an exergonic reaction that yields four ATP molecules, two of which are reused for the initiation of glycolysis. In addition to this, it also yields two electron donors in the form of Nicotinamide adenine

dinucleotide (NADH) via the reduction of coenzyme NAD⁺ (184). In aerobic conditions, the final product of glycolysis, pyruvate, is then further oxidised into a two-carbon molecule, acetyl coenzyme A (acetyl-coA), in the mitochondrial matrix. Here, carbon dioxide is produced as a waste product and two more NADHs are generated (**Figure 1.6**). In the absence of oxygen, glycolysis continues to produce pyruvate from glucose as mentioned above. However, the NADH produced is now used to donate electrons directly to pyruvate itself to generate a biproduct- lactate, in a process called lactic acid fermentation. Here, the overall net output yields two ATP molecules (185).

1.4.1.2 The citric acid cycle

The TCA cycle occurs in the outer mitochondrial membrane. Here substrates, such as previously described acetyl-CoA, or others, such as succinate, pyruvate or glutamate, generate NADH and Flavin adenine dinucleotide (FADH₂) (186). These electron donors eventually oxidise to NAD⁺ and FAD⁺ and feed electrons into the various complexes in the electron transport chain (ETC). Overall, this process yields ATP, NADH, FADH₂ and CO₂ waste (186) (**Figure 1.6**).

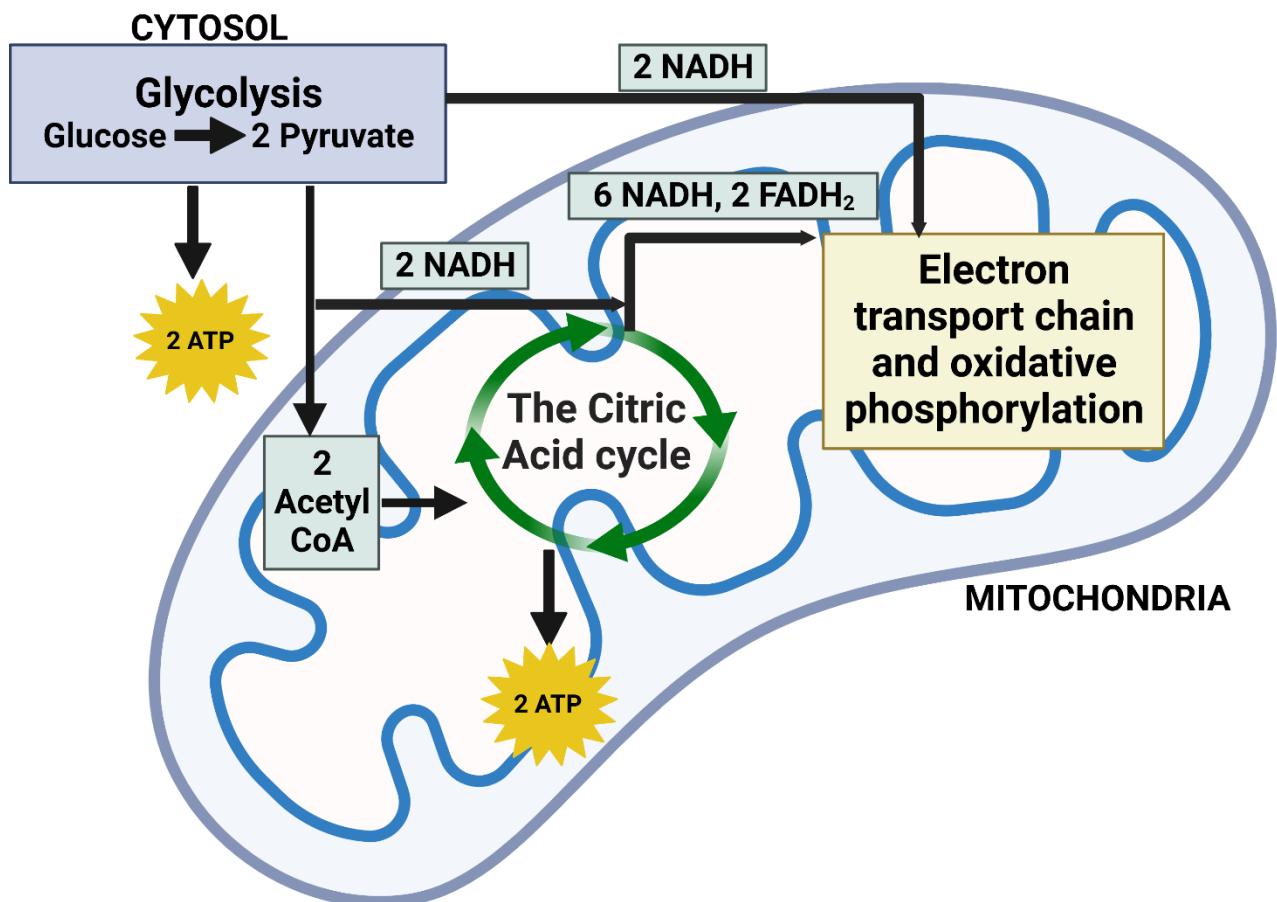


Figure 1.6: The stages of cellular aerobic respiration

The image summarises the stages of aerobic respiration. Glycolysis occurs in the cytoplasm where glucose is broken down to pyruvate through a series of enzyme driven reactions. This yields 2 net Adenosine triphosphate (ATP) molecules which is the cellular energy currency as well as 2 NADH molecules. Pyruvate is then converted to Acetyl CoA in the inner side of the mitochondrial matrix and yields 2 NADH molecules. Acetyl CoA feeds into the citric acid cycle that produces 2 ATP, 6 NADH and 2 FADH₂ molecules. The yielded electron donors NADH and FADH₂ then supplies electrons into the electron transport chain that initiates the movement of protons for the generation of a gradient. The movement of protons down the concentration gradient generates ATP.

1.4.1.3 Oxidative phosphorylation

The ETC is a series of membrane-embedded proteins located in the inner membrane of the mitochondria that consist of five protein complexes: Complex I (NADH ubiquinone reductase), II (Succinate dehydrogenase), III (ubiquinol–cytochrome c reductase), IV (cytochrome c oxidase) and V (ATP synthase). Electron donors such as NADH and FADH_2 oxidise to feed electrons to the complex I and complex II respectively. Here, electrons are passed from one member of the ETC to another in a series of redox reactions (187). The flow of electrons from each site is directed through an intermediate ubiquinone, via the oxidation of ubiquinone (Q) by complex III. The subsequent transfer of electrons occurs via another mobile intermediate, cytochrome c, which directs electron transport to complex IV. Finally, complex V which consists of a membrane bound ATP-synthase converts ADP into ATP via the coupling of the proton gradient in an intricate manner that remains to be understood (**Figure 1.7**) (188).

Energy is generated by the transport of electrons from donors to acceptors along a redox gradient potential through various protein complexes. This movement occurs in parallel with the movement of protons from the mitochondrial matrix outward, thus creating a potential difference or a proton gradient across the inner membrane. The subsequent leaking of protons back into the matrix through ATP synthase (complex V), results in the transfer of potential energy to ATP or the dissipation of energy as heat. Eventually, a majority of the mobilised electrons are passed along to molecular oxygen and respiratory biproduct, water, is formed (**Figure 1.7**). A small proportion of electrons leaks out of the matrix leading to one-electron reduction of oxygen to superoxide, a radical species (189). Mitochondrial membrane potential or proton motive force ($\Delta\Psi$) is generated as protons are pumped outward from the matrix, a process that depends on substrate utilisation and electron transport. The $\Delta\Psi$ is generated by proton pumping at complex I, III and IV out of the matrix and offset by proton transfer into the matrix referred to as a proton leak. Much of proton leak is a catalytic property of

specific molecules termed uncoupling proteins (UCPs), such as UCP1, UCP2 and UCP3. Functions of these UCPs are defined by their ability to generate heat via converting the $\Delta\Psi$ to heat production in brown adipose (UCP1), regulation of insulin release (UCP2) and the mitigation of ROS generation (UCP3) (190). Loss of $\Delta\Psi$ may also result from nonspecific leaks or general disruption of the inner membrane.

Overall, ETC has two distinct functions: i) To regenerate electron carriers by oxidising NADH and FADH_2 back to NAD^+ and FAD^+ , which are required to carry out glycolysis and citric acid cycle, and ii) Establish a proton gradient via the movement of protons out of the matrix. This gradient is used to make ATP. During aerobic respiration, the cell yields 32 ATP molecules per glucose molecule. A breakdown of this is shown in (**Table 1.1**).

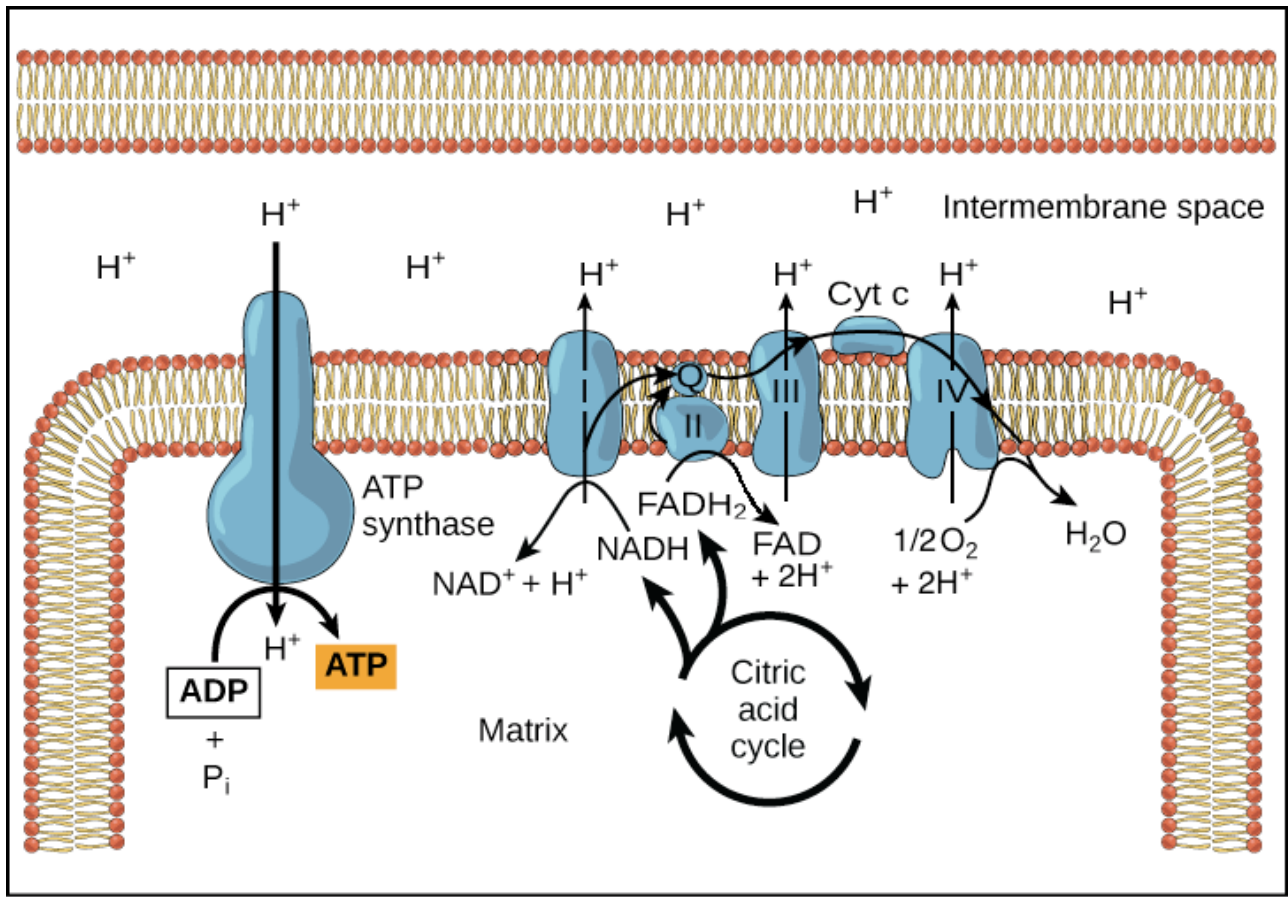


Figure 1.7: Oxidative phosphorylation- the electron transport chain

The electron transport chain is a collection of electron transporters located in the inner mitochondrial membrane that transfer electrons from $NADH$ and $FADH_2$ to oxygen. Protons are pumped from the mitochondrial matrix to the intermembranous space throughout the process, and oxygen is reduced to generate water. The proton gradient created by the electron transport chain is utilised by ATP synthase to form ATP in oxidative phosphorylation. *Image by Openstax college biology textbook. (191)*

Table 1.1: The breakdown of ATP yield during aerobic respiration.

The table summarises the net ATP yield during the stages of aerobic respiration utilising one glucose molecule. Apart from the 4 ATP molecules produced at glycolysis (2ATP) and later in the citric acid cycle (TCA) (2ATP), the rest is as a result of electron transport and therefore the proton gradient during oxidative phosphorylation. When electrons from NADH pass through the transport chain, approximately 10 H⁺ are pushed from the matrix to the intermembranous region, yielding approximately 2.5 ATP for each NADH. Electrons from FADH₂, which join the chain later, induce pumping of just 6 H⁺, resulting in the synthesis of about 1.5 ATP. Altogether this results in the formation of 32 ATP molecules.

Stage	Net product output	Ultimate net ATP yield
Glycolysis	2 ATP	2 ATP
	2 NADH	5 ATP
Pyruvate oxidation	2 NADH	5 ATP
TCA cycle	2 ATP	2 ATP
	6 NADH	15 ATP
	2FADH ₂	3 ATP
Total		32 ATP

1.4.2 Mitochondrial dysfunction in type 1 and type 2 diabetes

Perturbations in mitochondria have been demonstrated in both insulin-deficient and -resistant forms of diabetes (183). This includes defects in mitochondrial fusion and fission, along with biogenesis, number, morphology and excessive ROS production, with shifts in metabolic substrate utilisation (192). The term *mitochondrial dysfunction* is therefore non-specific and ill-defined, and it remains unclear whether mitochondrial irregularities and the resultant cellular dysfunction that accompany diseases, such as diabetes, are as a result of a pathological maladaptation or physiological adaptation of mitochondria.

1.4.2.1 Type 1 diabetes and mitochondrial dysfunction

The earliest reports from the 1950s of mitochondrial dysfunction in T1D rodents indicated that compromised substrates in complex I or II in isolated SkM mitochondria lead to decreased respiratory states (193-195). More recent studies describing mitochondrial bioenergetics from various tissues of T1D rats have provided conflicting insights. While some reveal that respiration is impaired in heart and brain mitochondria, others suggest that an increase in respiratory function in kidney on succinate or complex I substrates (196-198).

Alloxan-induced T1D rodent models display a decrease in mitochondrial number in the heart and SkM cells, along with swelling and damage to mitochondrial cristae and membranes (199, 200). SkM mitochondria in streptozotocin (STZ)-induced T1D models also show a marked loss of cristae and lipid accumulation around mitochondria (201). In contrast, other studies that have utilised isotope techniques to study mitochondria, showed no change in matrix volumes in STZ-diabetic rats in different tissues (202). Recent studies in cardiomyocytes of insulin-deficient Akita mice revealed reduced crista density but unchanged mitochondrial numbers compared to wild-type (WT) mice

(203). Meanwhile in some humans, T1D is associated with impairment in muscle mass, function and metabolism, which poses an increased risk of sarcopaenia, reduced mobility, physical disability and frailty especially with ageing (204-206). While the underlying mechanisms for this are undoubtedly multifactorial, mitochondrial irregularities in skeletal myocytes are associated with significant reduction in exercise capacity and metabolic health in T1D individuals (205).

Recent research on separated SkM mitochondria from people with T1D revealed that a brief interruption in insulin therapy caused the isolated organelles to produce less ATP (207). Despite considering that respiratory uncoupling would explain their findings, the authors were cautious to note that there is no evidence to support this. The authors hypothesised that their findings may be explained by documented higher oxygen consumption in T1D. Human studies are constrained by the scarcity of tissue and the difficulties of examining the untreated disease state, particularly in T1D, which would necessitate stopping insulin use.

Bugger *et al.* reported a marked decrease in muscle mitochondrial respiration on complex I substrates pyruvate and glutamate with reduction in ATP production on the complex I (203). While studies in STZ-diabetic mouse heart and SkM mitochondria manifested decreased respiration following uncoupling of protons, significantly decreased ATP production was not shown (202). These results were more obvious in 8-week diabetic animals compared to 2-week diabetic rats. These findings suggested that the proton conductance of the SkM mitochondria of diabetic rats was lower than that of nondiabetic controls based on the kinetic relationship between hydrogen transfer and membrane potential. Although it is not clear why an increased coupling without a change in ATP synthesis was observed, this could have been caused by a flaw in a protein involved in oxidative phosphorylation or ATP.

Even though the results of these investigations have not been consistent, when considered collectively, they tend to imply that, at least when mitochondria are separated and investigated *ex vivo*, insulin deprivation impairs ATP generation and respiration in SkM and heart mitochondria. It is possible that the proportionate decrease in respiration and ATP production accounts for the lack of respiratory uncoupling in these tissues in the diabetic state.

1.4.2.2 Type 2 diabetes and mitochondrial dysfunction

Similar mitochondrial abnormalities have also been observed in preclinical and clinical studies of T2D. Murine models of db/db mice revealed that mitochondrial size was significantly smaller in cardiomyocytes (208). In human subjects, the offspring of T2D parents have been found to have lower mitochondrial density together with mitochondrial morphologic alterations (209), reduced ECT activity and number of SLM type mitochondria, which has been linked to functional impairments in skeletal myocytes and cardiomyocytes (210). A key factor responsible for the biogenesis of mitochondria at the molecular level is the peroxisome proliferator-activated receptor gamma (PPAR γ) coactivator, PGC-1 α . PGC-1 α coactivates transcription factors responsible for the regulation of genes involved in energy homeostasis, mitochondrial replication and import machinery and oxidative phosphorylation (211, 212). In transgenic mouse models, increased expression of PGC-1 α was involved with increased expression of mitochondrial genes and enhanced mitochondrial function, along with improved insulin sensitivity and reduced oxidative damage in SkM (211). It has also been suggested that defective expression of PGC-1 α might be important in the pathogenesis of insulin-resistant states in clinical T2D (213).

For T2D the ineffective oxidation of fatty acids at the mitochondrial level by SkM contributes at least in part to the pathogenesis of insulin resistance (210). It makes sense to assume that mitochondria have a significant impact on insulin resistance. Uncertainty still exists over whether mitochondrial abnormalities are a primary or secondary cause of the process. In any event, it is crucial to understand that even if insulin resistance is the primary cause of mitochondrial dysfunction, mitochondrial deficiencies might exacerbate hyperglycaemia once it already exists and cause the diabetic condition to progressively deteriorate. There is evidence that insulin signalling in muscle cells may be impaired by mitochondrial malfunction (214). Impaired fatty acid oxidation from mitochondrial dysfunction should result in an increase of fatty acyl-CoA and diacylglycerol inside of cells, which will then activate protein kinase C (214). This in turn starts a serine kinase cascade, which eventually causes IRS-1 to be serine phosphorylated. As a result, the insulin signalling pathway is blocked by preventing the tyrosine kinase activity of the insulin receptor on IRS-1. In addition, the excess ROS that is produced may also exacerbate insulin resistance.

Clinical data suggests that insulin resistance may have its origins in abnormalities in mitochondrial activity. Family members of people with insulin-resistant T2D have been observed to have reduced expression of PGC-1a and PGC-1b, coactivators of NRF-1 and PPAR-dependent transcription involved in the expression of several genes related to oxidative phosphorylation(215). Additionally, those who have "prediabetes" or poor glucose tolerance exhibit evidence of decreased expression of oxidative phosphorylation genes (212).

1.4.3 Mitochondrial reactive oxygen species in steady state

Mitochondrial oxygen use is associated with a cost in terms of ROS generation and oxidative damage, in part derived from the electron leak as metabolism continues throughout the ETC. Biologically important ROS include the superoxide radical, $O_2^{\cdot-}$, hydrogen peroxide (H_2O_2), hydroxyl radical (OH^{\cdot}), hypochlorous acid ($HOCl$), NO , and peroxynitrite ($ONOO^-$) (216). Although mitochondria are considered a major intracellular superoxide production site, it must be noted that ROS derivatives also arise from outside this organelle, including via production of oxygen radicals from fatty acids, NADPH oxidase, the pro-oxidant heme molecule and arachidonic acid metabolism (217, 218).

The mitochondria invoke various adaptive mechanisms to protect against oxidative stress, launched by ROS production. This includes the adaptive response of physiological “uncoupling” of oxidative phosphorylation, in turn causing a reduction in superoxide production via reduced membrane potential (219, 220). In addition, various enzymatic processes, such as the conversion of superoxide to H_2O_2 by manganese superoxide dismutase (MnSOD) and the catalase activity of H_2O_2 scavenging glutathione peroxidase (GPX), are all efficient in protecting against oxidative stress. While catalase activity was deemed limiting as it has classically been considered a cytoplasmic protein than a mitochondrial one, recent evidence documents the presence of catalase in mitochondria of some organs, notably heart and liver (221-223).

Evidence of oxidative stress includes various markers of oxidative damage to DNA, lipids and proteins accompanied by chronic radical production. Gene mutations and cellular damage could result from oxidative damage to DNA via structural modifications of the nucleotide bases or by cross-linking. Lipid peroxidation as a result of self-sustained chain reactions is of great concern in

metabolic diseases such as diabetes, as it has been observed to accumulate near mitochondria causing cell-signalling interference (138). Moreover, this may lead to an amplification in oxygen radical insult. Unstable lipid peroxides such as isoprostanes have adverse vascular effects including vascular reactivity and mitogenesis. Protein denaturation, breakdown and cross-linking can also result from oxidative damage (224).

1.4.3.1 Site of ROS production in the mitochondria

Although the exact origins of the mitochondrial oxidative species are controversial, two major mitochondrial sites responsible for ROS are identified to be complex I and III in the ETC (225). Complex I superoxide is derived via the reduction of membrane bound flavin to flavin mononucleotide (FMNH₂) by NADH substrate. Consequently, the electrons that are passed along the ETC via ubiquinone may be passed by FMNH₂ to oxygen-generating superoxide (226). Complex III superoxide is highly dependent on membrane potential and includes a complex series of redox cycling of coenzyme Q (**Figure 1.8**) (220).

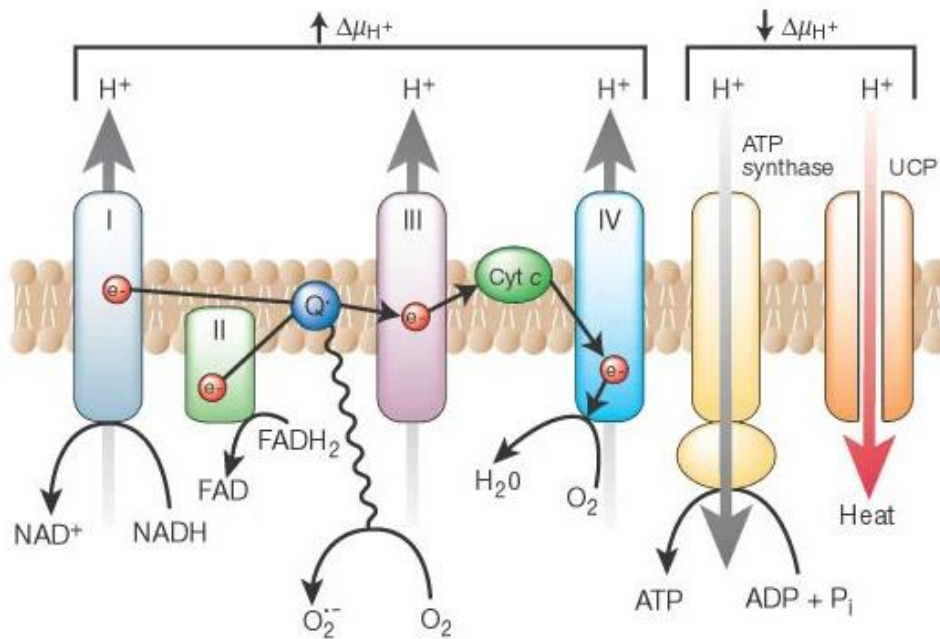


Figure 1.8: Reactive oxygen species production in the electron transport chain as a result of electron leak

Increased hyperglycaemia-derived electron donors from the TCA cycle (NADH and FADH₂) generate a high mitochondrial membrane potential ($\Delta\mu_{H^+}$) by pumping protons across the mitochondrial inner membrane. This inhibits electron transport at complex III, increasing the half-life of free-radical intermediates of coenzyme Q (ubiquinone), which reduce O₂ to superoxide.

1.4.3.2 ROS and diabetes

In the case of diabetes, the role of ROS is of major concern. While it would be an exaggeration to claim that the overarching cause of diabetes and its consequences are as a result of ROS, documentation does suggest a role for ROS in the onset and progression of the diabetes. Evidence to support this hypothesis lies within the agents used to induce T1D, including STZ and Alloxan, which impose the capacity for ROS to destroy islet cells via free radical damage (227, 228). In addition, a marked decrease in antioxidant protective enzymes, such as SOD, catalase and GPX in mouse islets in comparison with other tissues, account for β -cell sensitivity to cytotoxic damage by diabetogenic compounds (229). Emre *et al.* discovered that UCP2 defective mice were more vulnerable to diabetes brought on by repeated, low doses of STZ (230). This was found to be associated with increased intra-islet lymphocytic infiltration and damage from ROS and NO radicals (230). Therefore, it was assumed that these alterations were connected to a reduction in the UCP2-mediated mitochondrial oxidant defence. In contrast, Zang *et al.* found that UCP2-deficient mice had elevated islet ATP and insulin secretion. Based on these observations, any UCP2-mediated decrease in superoxide formation would be expected to also decrease ATP synthesis, which would have an adverse rather than beneficial impact on glucose-induced insulin secretion (231).

In muscle, myocyte mitochondria are not responsive to the ROS driving force of glycemia in the same manner as non-insulin-sensitive tissues like brain or EC since glucose transport depends on insulin. In the cardiac mitochondria of insulin-resistant obese, and leptin receptor-deficient db/db mice, a model of severe obesity associated with diabetes, Boudina *et al.* found an increase in ROS generation, a decrease in ATP production, and an increase in oxidative damage (208). The Akita mouse, an insulin-deficient animal that more closely reflects T1D in humans, on the other hand, showed a reduction in ROS generation from cardiac mitochondria (203), highlighting fundamental differences in ROS protection in both types of diabetes. In keeping with this, Herlein *et al.* also noted no increase

in ROS production measured as superoxide from heart, SkM and liver mitochondria of STZ-diabetic mice. However, a marked upregulation of MnSOD and UCP3 as well as cytoplasmic catalase in all tissues is of significance (202). The enhancement of antioxidant defence does imply that mitochondria extracted from animals lacking insulin have previously experienced *in vivo* oxidative stress.

One of the main causes of the problems of diabetes may be a high flux of fatty acids, glucose, or both to the mitochondria and the resulting formation of mitochondrial oxygen radicals (232). The mitochondria of numerous cell types, including those of ECs (233) , retinal ECs (234), renal mesangial cells (235), cardiomyocytes (236) and epineural blood arteries (237), have been implicated in such glycaemic effects. In addition, increased ROS have been associated with increased fatty acid oxidation and accumulation.(238).

Mechanisms by which ROS lead to diabetic complications include formation of ONOO⁻, as a result of NO and superoxide reaction, inducing lipid peroxidation which impairs endothelial vasodilation. Additionally, superoxide can damage iron-sulphur centres, lowering the catalysis of some enzymes like aconitase (239). The highly reactive hydroxyl molecule can be created when iron reacts with hydrogen peroxide, which MnSOD produces from superoxide. Consequently, mitochondrial superoxide produces additional radicals, causing protein, DNA, RNA, and lipids to sustain widespread damage (240). Additionally, damaged mitochondria and the resulting malfunction will impair calcium transport and may trigger a change in mitochondrial permeability that results in apoptosis(240).

Among this, the risk of vascular events increases by fourfold in diabetes, in part due to impaired vascular function. Mitochondrial function therefore is particularly of interest with respect to vascular

cells. Animal models of diabetes and humans with T1 and T2D are shown to have impaired endothelium-dependent vasodilation in a variety of arterial beds (241). Increased oxidative stress is one of the processes linked to diabetes-induced endothelial dysfunction. It has been proposed that the creation of superoxide by EC mitochondria in response to hyperglycaemia is a common factor in the pathways behind diabetes-related vascular dysfunction (242). Superoxide and ONOO⁻ production causes oxidative stress, which compromises vascular function and endothelium-dependent arterial relaxation, according to studies conducted on epineural arterioles of the sciatic nerve taken from T1D diabetic rats (243, 244). These findings suggested that the rise in superoxide production was caused by complex I of the mitochondrial electron-transport chain and NADH oxidase and was in part responsible for reduced vascular reactivity (237). It was also demonstrated that rotenone pre-treatment of diabetic rats' epineural arterioles decreased the production of superoxide.

Various studies have highlighted evidence to show antioxidant treatment to correct diabetes related vascular dysfunction. Administration of three types of antioxidants to diabetic rats prevented the development of superoxide and ONOO⁻ in diabetes-induced vascular and neural dysfunction, further suggesting that elevated oxidative stress is an important contributor to these complications in diabetes (237, 243). Cameron and colleagues showed that administering T1-diabetic rats -lipoic acid or the metal chelators hydroxyethyl starch deferoxamine or trientine reversed the diabetes-related reduction in vascular relaxation associated with hyperalgesia and neurovascular abnormalities (245-248). In another study, tempol, a stable mimic of SOD, was given to diabetic rats to successfully treat their elevated levels of vascular superoxide, malondialdehyde, and 8-epi-prostaglandin F, and corrected the impaired ability of their aortic rings to sprout after exposure to acetylcholine (249). In a recent study, antioxidant MitoQ was used to target myocardial infarcts of T2D rats to ameliorate ischaemic reperfusion injury and was deemed cardioprotective (250).

Interim conclusion

- Mitochondrial dysfunction underpins both T1D and T2D. In both cases, this involves alterations in mitochondrial biogenesis, density, mass, ATP production and ETC function. These disturbances in turn increase the production of ROS which leads to further oxidative and metabolic damage in different tissues and cells.

1.5 Wound regeneration in healthy and diabetic skin

1.5.1 Anatomy and functions of skin in steady state

Skin and its appendages make up the integumentary system. It is the body's largest organ, covering the whole exterior surface. It is composed of three layers: the epidermis, dermis, and hypodermis (or subcutaneous layer), each of which has a distinct architecture and function. The skin is composed of an extensive network that serves as the body's first line of defence against ultraviolet rays, toxins, and mechanical harm. The skin also plays a role in immunologic surveillance, sensory perception, control of insensible fluid loss, and homeostasis in general.

The epidermis, the outermost layer of skin, provides a waterproof barrier and contributes to skin tone. It is composed of five distinct layers depending on the region of skin being considered: *basale*, *spinosum*, *granulosum*, *lucidum*, and *corneum*. It contains a variety of different cell types, including Merkel cells, keratinocytes, melanocytes, Langerhans cells and other inflammatory cells. Blood capillaries that connect arterioles and venules are exclusively located beneath the epidermis. This means that the epidermis has no blood supply, but rather is fed by diffused oxygen from the surrounding air.

A basement membrane separates the epidermis from the dermis, which itself is divided into two layers, the papillary or upper layer and reticular or lower layer. Papillary dermis is found below the epidermal junction and is a thin layer made up of loose connective tissue comprising collagen proteins, elastic fibres, reticular fibres and capillaries. Meanwhile the reticular dermis is thicker and deeper and is located just above the subcutaneous layer. It is made up of a compact arrangement of connective tissue that contains collagen fibres, nerve endings, blood vessels and lymphatics. The cellular composition of the dermis includes fibroblasts, MΦs, adipocytes, mast cells, Schwann cells

and different populations of stem cells, among other cell types (251). Dermal MΦs are divided into many subsets, including resident MΦ subpopulation (165).

The third layer of the skin which is deep to the dermis, is the hypodermis or subcutaneous layer, which comprises fat and connective tissue and is also rich in fibroblasts, MΦs and adipocytes. This layer connects the skin to the underlying bone and muscle, supplies it with blood vessels and nerves, and also serves as the body's main insulation mechanism.

1.5.2 Cellular components of steady state skin

1.5.2.1 Stem cells in skin

Adult skin provides a unique microenvironment for a variety of distinct stem cell niches. Three types of epidermal stem cells have been identified in the basal layer of epidermis, the hair follicles and the base of the sebaceous glands (252, 253). Under steady-state conditions, each discrete niche maintains its respective lineage-specific compartment in a unipotent fashion, as shown by fate-mapping and live-imaging studies (254, 255). Various paradigms have been used to explain the maintenance of epidermal homeostasis. According to the standard hierarchical paradigm, slow cycling stem cells divide in the bottom layer and give rise to transit amplifying daughter cells, which increase the number of cells needed for tissue replenishment. As they move upwards toward the epidermal surface via the suprabasal layers, they undergo a limited number of cell divisions before becoming terminally differentiated (256, 257). However, this concept has recently been challenged by a novel stochastic model of homeostasis, whereby only one kind of progenitor cell can divide indefinitely to produce two terminally differentiating cells, two undifferentiated basal cells, or one of each type (258, 259).

There are two main subpopulations of stem cells in hair follicles, one within the hair germ just below the bulge that gives rise to the hair shaft and inner root sheath keratinocytes, and the other in the bulge region that gives rise to the basal outer root sheath keratinocytes. Although the bulge region is the most well-defined stem cell niche in skin (260) and is characterised by a slow cycling, quiescent nature (261), clonogenic capability (262) and expression of a specific subset of markers, recent studies have reported multiple partly overlapping stem cell populations outside of this anatomical region with varying abilities to contribute to the interfollicular epidermis, hair follicle and sebaceous gland (263, 264).

Hair follicle stem cells, as well as mesenchymal stem cells (MSCs) and skin-derived progenitor cells, are all present in the dermis. Dermal MSCs, like those found in other tissues, reside in perivascular niches and have the ability to self-renew and differentiate into different mesenchymal lineages, including adipocytes, smooth muscle cells (SMCs), osteocytes and chondrocytes (265-267). They also have major trophic effects on other cell types, both by direct cell-to-cell interactions and via production of paracrine mediators. These include pro-mitogenic actions on keratinocytes, immune cell response modulation (typically suppression), and pro-angiogenic effects, as occurs during wound healing and the growth of skin malignancies (268).

1.5.2.2 Macrophages in skin

For cell maintenance and function, the adult skin supplies spatially distinct microenvironments. Local skin niches contain immune and non-immune cell subgroups. MΦs play crucial roles in host defence and maintaining steady state homeostasis through the clearance of apoptotic cells, growth factor production, promotion and resolution of inflammation, and trophic support of cell proliferation, tissue restoration and neovascularisation following injury. Various populations of MΦs and dendritic cells

are present in the skin but, owing to their phenotypic overlap, the distinction between them is ambiguous (269, 270).

Aside from dendritic cells, the skin contains at least two types of tissue-resident MΦs: Langerhans cells are mostly found in the epidermis, whereas cutaneous (or dermal) MΦs are found in the dermis (271, 272). It is worth noting that Langerhans cells share traits with both MΦs and dendritic cells (for example, the ability to self-renew and activate T cells) (273). Langerhans cells and cutaneous MΦs are both highly diverse in terms of their developmental origins. Langerhans cells are produced from YS progenitors but are gradually supplanted by foetal liver haematopoietic precursors (40). Cutaneous MΦs, on the other hand, appear to originate in the foetal liver and are gradually replaced by circulating Ly6C⁺ monocytes after birth (274). Although Langerhans cells can self-renew, Ly6C⁺ monocytes can be recruited to replace them following injury (270). Tissue-resident MΦs (both Langerhans cells and cutaneous MΦs) are the only immune cells in skin before birth (270). The function of resident MΦs during skin development is currently not clear; however, it is believed that they are essential for extracellular matrix (ECM) synthesis and deposition, as well as skin layer differentiation (275).

Tamoutounour *et al.* published a seminal study that highlighted the profound heterogeneity of cutaneous MΦs (270). They discovered a large population of dermal CD11b⁺ non-DC MΦs in healthy skin, including CCR2⁻ and CCR2⁺ subgroups. CCR2⁻ MΦs were further subdivided into Ly6C^{Lo}MHCII⁻ and Ly6C^{Lo}MHCII⁺ subtypes, which were both CD64^{Hi}MerTK⁺ and exhibited features comparable to other tissue MΦs, such as a foamy cytoplasm, similar cell cycle kinetics and transcriptional profile (270). CCR2⁺ MΦs were divided into three subpopulations: Ly6C^{Hi}MHCII⁻, Ly6C^{Hi-to-Lo}MHCII⁺ and Ly6C^{Lo}MHCII⁺, with the latter two exhibiting intermediate morphology

between DCs and MΦs. Differentiation of these subtypes was discovered to occur via differential CSF1R signalling.

The content of these MΦs in skin changes during regular hair cycles, implying that they play a role in hair follicle growth. Because of MΦ apoptosis, the number of Langerhans cells and cutaneous MΦs increases in anagen (the active hair growth phase) and declines in telogen (the resting phase) (276, 277). Concurrently, there is a local increase in Wnt expression by MΦs which activates epithelial cells and initiates the anagen phase (278, 279). This indicates that MΦs influence the activity of hair follicle stem cells. It has been demonstrated that Ly6C^{hi} MΦs produce TGF1-β to stimulate follicular stem cells and consequently hair regeneration in the context of wound repair (280). Interestingly, this phenomenon is dependent on CX₃CR1 but not CCR2 (280), implying that blood derived, CCR2⁺ infiltrating monocytes are not involved. Furthermore, MΦs can influence the hair cycle and hair development by secreting TNFα (281).

1.5.2.3 Endothelial cells in skin

Healthy skin is a highly vascularised tissue with blood and lymphatic vessels and an elaborate microcirculation found in the dermis (282), which delivers oxygen and nutrients to assist maintain homeostasis and thermoregulation (283). Microvascular ECs are the primary constituents of dermal blood vessels and play an important role in cutaneous inflammatory reactions. In return, inflammatory cytokines such as TNF-α, IL-1β, and IFN-γ have all been found to influence microvascular endothelial function when produced locally (284). Canonical endothelial markers such as CD144, CD31, and CD34 are expressed by EC lining both cutaneous blood and lymphatic vessels (284). Other surface antigens include the HLA-DR (known as MHCII in mice) and modest expression of the CD36 cholesterol uptake receptor (284). The expression of LYVE-1 on lymphatic vessels is a differentiating

marker between vascular and lymphatic endothelium in healthy dermis. However, in chronic skin inflammatory conditions, dermal vascular ECs also exhibit low surface membrane expression of LYVE-1, along with podoplanin while expressing high levels of E-selectin, inter-cellular adhesion molecule-1 (ICAM-1) and vascular cell adhesion molecule-1 (VCAM-1) (285). In addition, there is evidence to support the prevalence of tissue-resident EVPs in skin that are quiescent in steady state skin which actively differentiate into mature ECs in response to injury.

1.5.3 Mechanisms of wound healing in steady state

In response to wound injury, the skin launches a complex but well-coordinated repair process that involves distinct overlapping stages: haemostasis, inflammation, proliferation, and remodelling (286).

1.5.3.1 Haemostasis

The first stage response, haemostasis initiates the inflammatory process and manages the recruitment of various cells (neutrophils and circulating monocytes) and clotting factors for healing (287). Clotting factors are triggered within the wound site to launch the extrinsic coagulation cascade, while exposed collagen induces platelet activation, adhesion and aggregation as part of the intrinsic coagulation cascade. Simultaneously, blood vessels within the wound environment undergo transient vasoconstriction induced by platelets in order to decrease blood loss and replace the tissue gap with a blood clot composed of cytokines and growth factors (288). Fibrin molecules, fibronectin, vitronectin, and thrombospondins that are present within this clot produce the provisional matrix, which acts as a scaffold structure for the migration of leukocytes, keratinocytes, fibroblasts, and ECs, as well as a reservoir of growth factors. This initial vasomotor and haemostatic response results in a local loss of perfusion within the wound, leading to oxygen deficiency, enhanced glycolysis and alterations in tissue pH (289). This is then followed by a vasodilation response, which allows platelets to penetrate the provisional wound matrix.

In addition, platelets help to regular the infiltration of leukocytes to the wound area by releasing chemotactic factors. Platelets and leukocytes both also release other cytokines and growth factors that activate the inflammatory process (IL-1 α , IL-1 β , IL-6, and TNF- α), stimulate collagen synthesis (FGF-2, insulin-like growth factor 1 (IGF-1), TGF- β), initiate angiogenesis (FGF-2, VEGF-A,

hypoxia-induced factor (HIF-1), TGF- β) and provide initial support to the re-epithelialisation process (EGF, FGF-2, IGF-1, TGF- β) (290).

1.5.3.2 Inflammatory phase

The inflammatory phase of the wound healing cascade can be separated into an early phase involving neutrophil recruitment and a late phase which is characterised by infiltration of monocytes and accumulation of M Φ s. Neutrophils are drawn to the site of skin damage as a result of the activated complement pathway, degranulated platelets, and by-products of bacterial breakdown, and remain there for 2-5 days (d) unless the lesion becomes infected (**Figure 1.9**). The capacity of neutrophils to phagocytose and secrete proteases kills local pathogens and aids in the degradation of necrotic tissue in the initial days following injury. They also serve as chemoattractant for other cells participating in the inflammatory phase. TNF- α , IL-1 β , and IL-6 are released by neutrophils, amplifying the inflammatory response and stimulating VEGF and IL-8 for a sufficient repair response. They also begin debridement by releasing extremely potent antimicrobial compounds (cationic peptides and eicosanoids) as well as proteinases (elastase, cathepsin G, proteinase 3, and a urokinase-type plasminogen activator) (291). *In vitro* investigations have revealed that neutrophils can alter the phenotype and cytokine profile of M Φ s, helping to coordinate the innate immune response during healing (292). After performing their antipathogenic role, neutrophils are either extruded with the eschar (the crust collecting dead cells and wound degradative products) or phagocytosed by M Φ s (293). Interestingly, depletion of neutrophils in preclinical models of wound healing (e.g. in mice, guinea pigs) did not result in decreased numbers of wound M Φ s (294), indicating that monocyte recruitment and M Φ infiltration can still proceed in the absence of a normal neutrophil response.

There are two lineages of skin MΦs: tissue-resident MΦs formed from embryonic progenitors and monocyte-derived MΦs derived from bone marrow (28, 34). The role of these various MΦ lineages in wound healing is unknown; nevertheless, tissue-resident MΦs are expected to be the earliest responders to wounds. They are known to express adhesion molecules that recruit and guide neutrophils into the early wound (295). On the other hand, monocytes undergo transendothelial migration across the vessel wall in response to chemotactic stimuli and interactions with EC that are mediated by selectin family adhesion molecules, their carbohydrate ligands and 4-integrins (296). This causes monocytes to attach weakly to the endothelium, triggering the adhesion cascade. Selectins, which are cell-surface proteins, then engage with glycoprotein ligands on monocytes, allowing them to connect to ECs (296). Cytokines and chemokines then drive the rolling monocyte to activate its surface integrins, which interact with additional receptors, such as ICAM and VCAM, which are expressed by ECs. This causes a strong adherence to the endothelium and transmigration into the wound site. After migrating to the ECM, monocytes are driven to differentiate into MΦs by cytokines such as IL-4, IL-10, IFN- γ , IL-13, bacterial products such as liposaccharides (LPS), and ECM components, which peaks 42 h after injury. Depending on the signals created in the surrounding tissue, monocytes moving into the wound often have an inflammatory or debriding character (297). Daley and colleagues recently reported that early (day 1) invading MΦs in the wound mostly (85%) exhibit an M1-like phenotype in a sponge mouse wound model (292).

MΦs are the most abundant cells in the healing tissue three to five days after damage. Lucas *et al.* found that MΦ reduction during the inflammatory phase resulted in a considerable delay in wound recovery (298). They play a vital role in the clearing of senescent cells and debris within the wound. In case of pathogen spreading in the wound bed, MΦs phagocytose these pathogens and present antigens to T-cells. MΦs involved in clearance of cells or dead tissue undergo apoptosis. They also display phenotypic plasticity and are able to transition from one phenotype to another as wound

healing progresses (e.g. from M1 to M2-like (299). As a result, MΦs play a critical role in the shift from the inflammatory to the proliferative phases of wound healing, where they coordinate and sustain wound healing activities (300).

1.5.3.3 Proliferation and neovascularisation phase of wound healing

Key features of the proliferative phase of wound healing include active fibroplasia, epidermal regeneration, wound contraction and angiogenesis. The crucial role of MΦs during this proliferative phase is highlighted by the fact that their experimental depletion results in dramatic disruption of the transition from the mid to late stages of repair response (298) (**Figure 1.9**). Using the now outdated M1/M2 classification system for MΦ heterogeneity, preclinical studies have suggested that M1 cells transform into M2 MΦs as wound healing progresses (301, 302). M2-like MΦs have been shown to decrease inflammatory responses and adaptive Th1-immunity, while scavenging debris and promoting angiogenesis, tissue remodelling and repair. Furthermore, they stimulate a Th2 response, which helps coordinate fibrinogenesis (303) and promote the release of TGF-β, which stimulates inflammation, chemotaxis, wound contraction, angiogenesis and ECM deposition (304). It is increasingly apparent that MΦ activation represents a spectrum of phenotypes dependent on the tissue microenvironment and cell lineage. An existing limitation of our understanding of the behaviour of MΦs in the wound environment is that studies of MΦ heterogeneity in wounds during different stages is limited to the old M1 vs M2 classification system, and our refined understanding on MΦ heterogeneity based on lineage mapping studies and scRNA-seq hasn't yet been applied to wounds.

Simultaneously, fibroblasts and ECs begin to move into the wound area via the transitional wound matrix, aided by matrix metalloproteinases (MMPs). ECs that has moved to the wound bed help to generate neovessels. The proliferation, motility and pro-angiogenic activity of ECs are promoted by

chemicals that are produced within the hypoxic wound environment. This endothelial reaction has four stages: 1) protease production for degradation of the basal lamina, 2) chemotaxis, 3) proliferation and 4) remodelling and differentiation, stimulated via VEGF, FGF, IL-1, Angiopoietins and TGF- β (305). Increased IL-1 levels occur if there is an excessive inflammatory state (e.g. with superimposed infection), and may result in ECM breakdown and delayed wound healing (306). The binding of growth factors to their receptors on the endothelium of existing blood vessels is the initial step in the creation of new vessels, triggering intracellular signalling cascades. Proteolytic enzymes are secreted by stimulated ECs, which disintegrate the basal lamina. As a result, ECs can now proliferate and migrate into the wound, by orientating themselves towards surface adhesion molecules, such as integrins (v3, v5, 51). Furthermore, at the front of their proliferative wave, they release MMPs, lysing the surrounding tissue for ongoing endothelial proliferation. Following this, the nascent vasculature differentiates into arterioles and venules and matures through further vessel wall stabilisation via the recruitment of pericytes and smooth muscle cells. Finally, the angiogenic process is completed by the beginning blood flow (307).

Since the discovery of BM-derived circulating EPCs by Asahara *et al*, there has been increasing evidence for its contribution to neovascularisation in wounds (115, 308). Following injury, EPCs are increasingly mobilised to respond to chemokine signalling (e.g.: IL-8, CSCR2, CXCR4) in tissues that are home to injury (309). Once EPCs initiate transendothelial migration into sites of vascular remodelling, they migrate to vascular basement membrane and interstitial ECM to exert their functions. This includes: i) direct incorporation into neovessels; ii) differentiation into mature ECs via growth factor induced proliferation; and iii) production of paracrine or juxtacrine signals (e.g.: VEGF, stromal derived factor 1 (SDF-1), IGF-1, monocyte chemotactic protein 1 (MCP-1), M Φ inflammatory protein 1a, and PDGF) (310, 311). In addition, recent evidence dictates that a population of tissue-resident endovascular progenitors (EVPs) (119) also proliferate and differentiate

into mature ECs in response to signals produced by perivascular cells, including MΦs, governing *de novo* blood vessels regeneration during cutaneous wound healing (312). EVPs remain quiescence during tissue homeostasis but retain the capacity to regenerate damaged blood vessels. A study by Sim *et al.* revealed that Wnt signalling by MΦs may help regulate EVP quiescence and reactivation during wound healing (313).

As mentioned above other cell types also provide crucial structural and paracrine support to stimulate angiogenesis, including MΦs, MSCs and pericytes (314, 315). It follows that MΦ depletion in the wound leads to decreased vascularisation, as well as significant haemorrhage, fibrin and serum exudates in the granulation tissue that is formed (298, 316, 317). Tissue-resident MΦs also serve as cellular chaperones, guiding and bridging endothelial tip cell sprouts, leading to fused anastomotic branch points via VEGF expression (9). Murine studies reveal that MSCs enhance vascularisation via the release of VEGF and through direct differentiation into vascular ECs (318). In another study, injection of BM MSCs reduced arteriolar vascular resistance and increased functional capillary density in murine wounds (319). It is evident that novel methods to amplify the delivery and efficacy of MSCs is an attractive therapeutic avenue for wound healing. This is in keeping with other stem cell therapies for wound healing (e.g., transplant or reprogramming), involving the use of induced pluripotent stem cells (iPSCs) (320) or EPCs (311). MΦs also stimulate the proliferation of fibroblasts and keratinocytes during the last step in the proliferation phase of wound healing, through the production of cytokines, including the pro-inflammatory mediators, IL-1 α , IL-1 β , IL-6 and TNF- α (290). This helps the development of the acute granulation tissue, which is characterised by a high density of fibroblasts, granulocytes, MΦs, capillaries, and loosely organised collagen bundles.

Subsequently, reepithelialisation begins via keratinocyte recruitment across granulation tissue, termed contact guidance, and continues until the epidermis over the newly formed scar tissue is re-established. This includes cytokine driven keratinocyte morphogenesis, elongation, and establishment of lamellipodia and filopodia (316, 321). Once the wound surface is covered by a monolayer of keratinocytes, epidermal migration ceases and a new stratified epidermis with underlying basal lamina is re-established from the margins of the wound inwards. In this phase, stem/progenitor cells also rapidly activate and differentiate into progeny that are required for re-epithelialisation (322, 323). When spatial confinement and lineage restriction are temporarily eliminated, stem/progenitor cells are activated and recruited from diverse skin locations, allowing them to contribute to the creation of various mature cells (324). At this moment, the defect is filled with granulation tissue and covered by a newly formed epidermal layer.

1.5.3.4 Remodelling phase

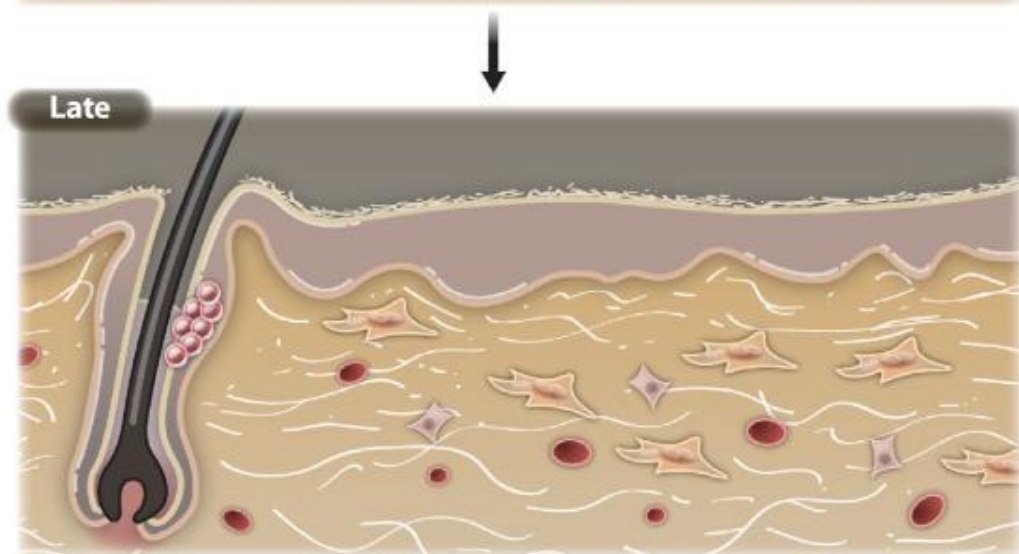
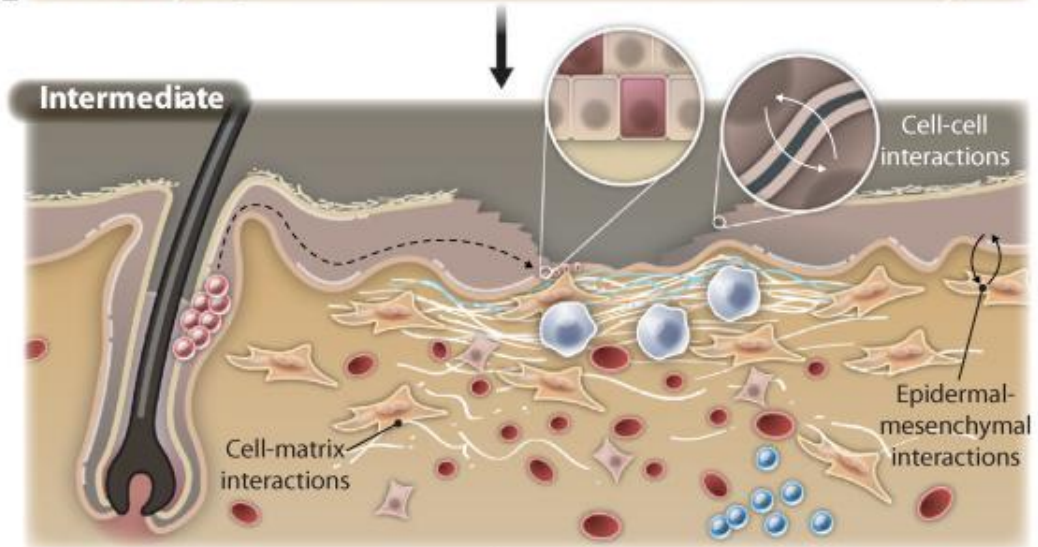
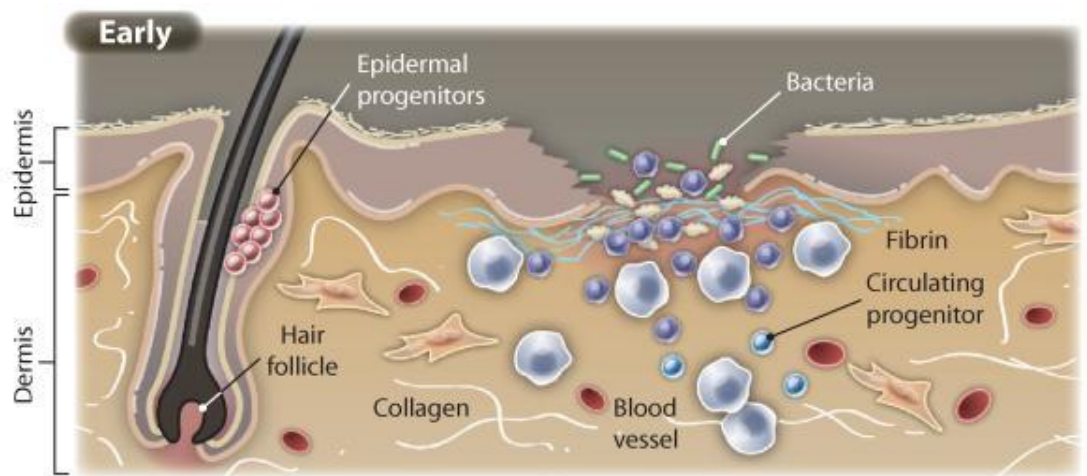
Finally, the long remodelling phase is initiated. During this time, cell proliferation and protein synthesis largely slow down and collagen remodelling ensues. Regression of capillaries to accommodate the decreased demand and MΦ and EC apoptosis follow suit (325). ECM breakdown and remodelling is balanced by means of Th1 and Th2 dominated environment. T-lymphocytes infiltrate the wound bed in the late inflammatory phase of wound repair and establish crosstalk with MΦ via cytokines for expansion and differentiation to Th1 and Th2 cells (326). It has been suggested that Th1 cells in turn trigger differentiation of M1-like MΦs and downregulate fibrous tissue growth while the Th2 response results in ECM production (327). The collagen fibres produced by myofibroblasts in the ECM are rearranged and crosslinked to strengthen the wound tissue. MΦs are a rich source of MMPs (MMP-2, MMP-12 and MMP-19) and serine proteases, that degrade virtually all ECM components aid during this remodelling process (328, 329). Finally, in the last phase of wound healing, both the number and functional activity of MΦs dampens down and this puts the

brakes on ECM production. These changes, together with contraction of the wound ultimately result in a decrease in wound size and volume (**Figure 1.9**).

Pathological conditions such as infection and diabetes as well as foreign objects and aging alter each of the above processes via prolonged inflammation and impaired healing that leads to devastating outcomes (330) (**Table 1.2**).

Table 1.2: The local and systemic factors that impair the wound healing process.

Local Factors	Systemic factors
Oxygenation (331)	Age and gender (332)
Infection (333)	Sex hormones (334)
Foreign body (335)	Stress (336)
Venous sufficiency (337)	Ischaemia (338)
	Diabetes, keloids, fibrosis, hereditary (339)
	Obesity (340)
	Medications: glucocorticoid steroids, non-steroidal anti-inflammatory drugs, chemotherapy (341-343)
	Alcoholism and smoking (344, 345)
	Nutrition (346)






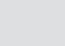


					
Platelets	Neutrophils	Fibroblasts and myofibroblasts	Keratinocytes	Endothelial cells	Macrophages
PDGF	IL-1 PDGFR		EGF EGFR	FGF FGFR	IL-1 PDGFR
TGFβ	IL-6 TGFβR		IL-1 IL-1R	VEGF VEGFR	IL-6 TGFβR
EGF	TNFα	KGF PDGFR	TGFβ TGFβR	PDGF HGFR	TNFα VEGFR
	VEGF	TNFβ TGFβR	TNFα KGFR	FGF-2	VEGF
		FGFs FGFRs	MCP-1 KGFRs		PDGF
		IGF IL-1R	SDF1 SDF1R		EGF
		VEGF TNFαR	HGF		
		EGF SDF1R			
		HGF			

Figure 1.9: The four phases of wound healing and the specific timelines in murine wound healing

The illustrations depict molecular and cellular systems important for wound healing development in murine skin. Haemostasis and activation of keratinocytes and inflammatory cells are early phases around 2-4 h (h) after wound injury. Immediately after, inflammatory responses are carried out and usually lasts for 2-5 d. Keratinocyte proliferation and migration, fibroblast proliferation, matrix deposition, and angiogenesis are all part of the intermediate proliferative stage (6-8 d after injury). Late-stage healing involves ECM remodelling, which results in scar formation and barrier repair (>10 d). Multiple cell types tightly control this spatiotemporal process by secreting numerous growth factors, cytokines, and chemokines (listed below) to achieve barrier closure and functional restoration. (286)

1.5.4 Mechanisms of impaired wound healing in diabetes

Diabetes impaired wound healing is a common cause of morbidity and mortality in patients. Diabetic skin ulcerations are characterised by the breakdown of many layers of epidermal, dermal and subcutaneous tissue. Ulcerations on the lower limbs affect 5-10% of patients with diabetes, with the feet being most affected. Of non-healing diabetic foot ulcers (DFUs), 25% of patients ultimately require lower limb amputation, a high-risk and life-altering treatment, which is associated with a five-year mortality rate approaching 50% (347, 348). The global prevalence of diabetic foot ulcers has been shown to be higher in T2D than T1D (349).

Due to the lack of peripheral sensory function that commonly occurs in diabetes, the diminished capacity of affected individuals to feel and therefore recognise superficial cuts, blisters or ulcers may lead to prolonged delays in seeking medical attention and receiving treatment. Dysregulated metabolic pathways and alterations in the host's immune and angiogenic response all contribute to abnormalities in each stage of the wound healing process, resulting in diabetes-related delayed wound healing (330). Changes in the quantity and phenotype of wound monocytes/MΦs, endothelial dysfunction, microbial invasion, epithelial breakdown, together with other variables, all compound the suboptimal nature of wound healing in diabetes (350, 351).

1.5.4.1 Impaired inflammatory responses in diabetic wounds.

Diabetes itself causes low-grade systemic inflammation, which has been linked to immune system dysfunction (352). Early after wounding, the number of invading monocytes has been shown to be greater in the wounds of leptin receptor mutant (*Lepr^{db}*) db/db T2D mice (353). Following such enhanced monocyte accumulation, MΦ subsets (Ly6C⁺F4/80⁺ and Ly6C⁻F4/80⁺) were found to be considerably increased in diabetic wounds at later timepoints, resulting in an unfavourable, persistent infiltration of both monocytes and their MΦ progeny (354-356). Of note, a recent study has also shown that in early wounds of db/db mice, the proportion of MΦs differentiated from infiltrating monocytes is enhanced, whereas the content of local tissue-resident MΦs is unchanged compared to WT controls (357). Prolonged infiltration of blood Ly6C^{Hi} monocytes and a failure for them to effectively transition into the Ly6C^{Lo} state, is thought to be the major driver for the sustained accumulation of pro-inflammatory monocytes and MΦs in the skin wounds of diet-induced obese (DIO) mice (356). Joshi *et al.* concluded that a major difference in healing-impaired diabetic mice was a much higher percentage of immune cells in late wounds, mainly as a result of neutrophil, MΦ, and monocyte persistence (358). Monocytes and MΦs in the wounds of diabetic mice and human ulcers show persistently high expression of M1 genes and markers, including NOS2, TNF-α, IL-1β, MMP9, and lower levels of M2 markers, such as Arginase 1, CD206, CD36 while also exhibiting decreased expression of pro-healing factors, such as IGF-1, TGF-β and VEGF (353-355, 359). It is worth noting that occasional studies have provided contrary findings, showing that diabetic wounds, at least in early stage, contain lower levels of GM-CSF and fewer monocytes and MΦs, along with impaired chemotaxis and defective phagocytic function (360, 361). The discrepancies between these studies could simply be due to technical differences and thus requires further investigation.

The enhanced recruitment of monocytes to diabetic wounds may be partly due to increased myelopoiesis in BM, which has been shown to occur in both STZ-induced and Akita (*Ins2Akita*) type

1 diabetic, DIO pre-diabetic mice, and db/db type 2 diabetic mice under steady state (362-365). Diabetes has been associated with numerous important changes in the BM haematopoietic stem and progenitor cell (HSPC) compartment (355, 366, 367). One such example shown in db/db mice was an increased capacity to produce monocytes *in vitro* upon IL-1 or M-CSF challenge (365). In addition, the diabetes-related effects on HSPC function are also likely to be caused by changes in the BM microenvironment, or stem cell niche, which governs the maintenance, mobilisation and differentiation of HSPCs *in vivo* (366, 368, 369).

The continuous pro-inflammatory nature of diabetic wound Mφs most likely contributes to a chronic pro-inflammatory microenvironment in diabetic wounds. Evidence suggests that hyperglycaemia and its associated increased oxidative stress induce changes in the epigenetic code of Mφs during diabetic wound healing (370). This may account for disruptions in their ability to undergo phenotypic transformation and underpin their reduced capacity to carry out certain functions, including phagocytosis and the clearance of apoptotic cells and other debris (371).

Alterations in the functional phenotype of MΦs in diabetic wounds may be imposed directly by molecular and cellular factors in the local wound microenvironment or through epigenetic modifications that occur in BM HSPCs and are ultimately passed down to MΦ progeny (355, 359). The impact of the local microenvironment on influencing MΦ biology is well documented. For example, conditioned media from diabetic wounds has been shown to promote M1-like phenotypes in BM-derived MΦs *in vitro* (359). Studies also show that local modification of diabetic wounds by blocking IL-1, RAGE or activation of the NLRP3 inflammasome, can shift wound MΦs towards pro-healing phenotypes (359, 372). Similarly, levels of MCP-1, have been shown to be higher the wounds of DIO mice, and antibody-mediated suppression of this chemokine during the inflammatory phase

of wound healing restores the number of inflammatory wound monocytes and MΦs toward the non-diabetic state and promotes more efficient wound healing (356).

Epigenetic alteration of BM HSPCs via reduced restrictive histone methylation mark H3K27me3 at the *IL-12* gene promoter has been shown to be transmitted down to wound MΦs in DIO animals, resulting in an increased pro-inflammatory state that is associated with impaired wound healing (355). Epigenetic modification of myeloid lineage associated genes, such as *Notch1*, *PU.1* and *Klf4* by DNA methyltransferase 1 (Dnmt1) mediated hypermethylation, may also induce delayed healing in combination with persistent accumulation of M1-like MΦs in wounds (361). In contrast, other studies have concluded that the dysregulation of diabetic wound MΦs is independent of any changes to the BM stem cell compartment, based on results from irradiation and transfer of HSCs from db/db donors into WT mice (361). Altered MΦ function in diabetic wounds is also accompanied by reduced production of angiogenic factors, such as VEGF-A, which has a profoundly negative effect on the neovascularisation and remodelling of wounds (373-376).

In summary, both sustained increases in the number of wound monocytes and MΦs and dysregulation of their phenotype, caused both by intrinsic alterations in BM progenitors and by a pro-inflammatory wound microenvironment, lead to impaired wound healing in diabetes (377).

1.5.4.2 Impairments in vascular function in diabetic wounds

Studies on vascular function in diabetic wounds have mostly focused on the impaired angiogenic phase of healing and localised endothelial dysfunction. Several processes, including impaired cell and growth factor responsiveness, contribute to decreased peripheral blood flow and EC proliferation, and therefore to the absence of healing in diabetes. Evidence suggests that NO generated during the healing process controls and augments wound repair (378). Frank *et al.* showed that lower endothelial-NOS (eNOS)- and iNOS -dependent NO generation significantly affects the expression of other growth factors and chemokines in wounds, and this inhibits angiogenesis and repair (379). This was reversed by enhancing eNOS expression via the topical application of a peptide that prevented CCR10-eNOS interaction and subsequent eNOS downregulation (380). In another recent study, elevated ROS was shown to impair neovascularisation by impacting EC proliferation and migration and inducing apoptosis, resulting in inefficient wound closure (381). This was rescued following MnSOD gene therapy techniques (**Figure 1.10**) (382).

Interestingly, there is also evidence that vascular ECs in diabetic wounds display a distinctive trait associated with cellular senescence (383). The functional impact of the chain of events from cell cycle arrest, increased cell cycle inhibitors (CKIs) p53, p21, and p16, to reduced cell cycle promoters including Cyclin D1 and CDK4/6 in these cells was demonstrated by a significant decrease in diabetic EC proliferation, migration, and tube formation (383). MicroCT analysis of the 3D architecture of the capillary bed in these wounds also revealed significantly increased capillary permeability and decreased pericyte coverage. As compared to WT mice, the surface area, branch junction number, total length and total branch number of blood vessels were all significantly decreased in diabetic wounds (384).

Disturbances to BM-derived EPCs may also mediate the impaired healing of diabetic wounds. Gallagher and colleagues showed that BM EPCs respond to VEGF and SDF-1 chemokine gradients, which leads to their homing to hypoxic areas where they assist in the development of new blood vessels (385). They found that STZ diabetic mice had reduced eNOS activation of EPCs in BM and diminished SDF-1 expression by epithelial cells and myofibroblasts in skin wounds, which resulted in lower EPC recruitment (385). Diabetes also affects the local expression of other angiogenic factors in wounds, including FGF, M Φ Migration Inhibitory Factor (MIF), PDGF-BB, Sprouty2, ANG-1 and ANG-2 (386). It has therefore been speculated that the simultaneous use of combined therapies, such as upregulation of angiogenic growth factors, targeting of eNOS activation and EPC recruitment, might hold the key to improving wound healing in diabetes (386).

In addition to angiogenic factors, diabetes also affects local expression of heat shock proteins (HSP90, HSP70, HSP47 and HSP27) along with their downstream molecules Toll like receptor 4 and p38-MAPK, which results in impaired recruitment of fibroblasts and proliferation and differentiation of keratinocytes, while also elevating oxidative stress (387). Other factors hinder the healing process in diabetes, such as particular metabolic inadequacies, altered physiological responses, such as hypoxia caused by glycation of haemoglobin, modification of red blood cell membranes, and constriction of blood vessels (381). Hypoxia is characterised by a reduction in oxygen delivery to wounds as a result of constricted blood vessels. Glycation of haemoglobin reduces the availability of nutrients and oxygen to tissue, further delaying recovery. Hypoxia/glucose deprivation, as well as malformed proteins, cause cells to respond to stress by accumulating unfolded proteins within the endoplasmic reticulum, known as UPR8. This UPR is triggered immediately upon tissue or skin damage and is associated with the generation of pro-inflammatory mediators, further inflammation (180).

Along with these, physiologic factors such as increased serum matrix metalloproteinase-9 (388), impaired collagen accumulation and variation in the ratio of collagen types, dysregulation of

neuropeptide expression in the skin along with a suppressed inflammatory response (389), a lack of thrombin-activatable fibrinolysis inhibitor (390), AGE11 modification of PDGF (391), accumulation of ECM components and their modification by matrix metalloproteinase contribute to healing impairments in diabetes.

In summary, the diabetes impaired healing involves prolonged inflammatory response following immune cell dysfunction, hypoxia, dysfunction in fibroblasts and epidermal cells, impaired angiogenesis and neovascularization, high levels of metalloproteases, damage from ROS and AGEs, decreased host immune resistance, and neuropathy.

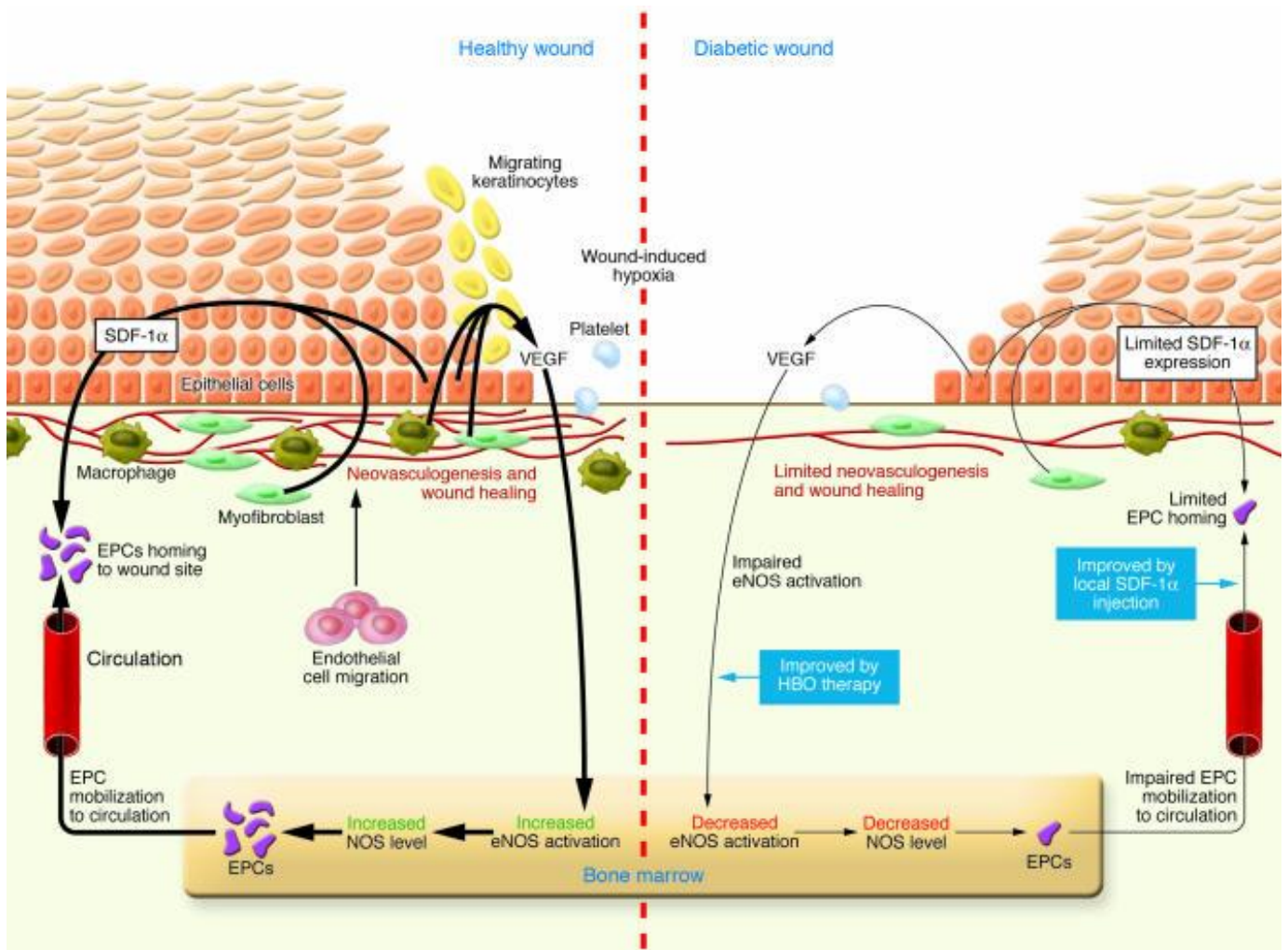


Figure 1.10: Mechanisms of wound healing in healthy versus diabetes.

The acute wound healing process in a healthy wound (left) is guided and sustained by the integration of various signals (cytokines and chemokines) generated by keratinocytes, fibroblasts, endothelial cells, MΦs, and platelets. During wound-induced hypoxia, VEGF generated by MΦs, fibroblasts, and epithelial cells activates eNOS in the bone marrow, resulting in an increase in NO levels and the mobilisation of bone marrow EPCs to the circulation. SDF-1, a chemokine, stimulates EPC homing to the site of damage, where they engage in neovascularization. In a diabetic mouse model (right), eNOS phosphorylation in the bone marrow is reduced, limiting EPC mobilisation from the bone marrow into the circulation. They also reveal that SDF-1 expression is reduced in diabetic wound epithelial cells and myofibroblasts, which hinders EPC homing to wounds and so impairs wound healing. The authors go on to show that inducing hyperoxia in wound tissue activated numerous NOS isoforms, raised NO levels, and boosted EPC mobilisation to the circulation. However, local

administration of SDF-1 was necessary to cause these cells to migrate to the wound site. These findings imply that hyperbaric oxygen treatment coupled with SDF-1 injection may be a viable therapeutic approach for accelerating diabetic wound healing, either alone or in conjunction with existing clinical protocols. *Image by Brem et al. (339)*

Interim conclusion

- Skin wound healing is a dynamic and complex process that is comprised of four overlapping stages involving a myriad of cell types and functions. MΦs and ECs play crucial roles in regulating inflammation and vascularisation of the wound leading to effective repair.
- Diabetic wound healing is characterised by the prolonged inflammatory phase and dysfunction in MΦ differentiation and EC function that lead to impaired wound closure and repair.

1.6 The response and adaptation of the skeletal muscle to diabetes

1.6.1 Skeletal muscle characteristics in physiological conditions

Mammalian adult SkM is a stable tissue with low turnover of cells under physiological conditions. The primary functions of SkM are locomotor activity, maintenance of posture and mechanical stability and to support breathing. From a metabolic perspective, SkM serves as storage for important substrates, such as amino acids and carbohydrates and contributes to basal energy metabolism, thermogenesis, oxygen consumption and fuel utilisation during physical activity and exercise (392). The role of SkM as a reserve of amino acids is of particular interest as it contributes to the maintenance of blood glucose levels during conditions of starvation (392).

The architecture of SkM is characterised by the well-described arrangement of muscle fibres (also called myofibers or muscle cells) and associated connective tissue. The individual bundles of fibres in a SkM are called fasciculi. The connective tissue surrounding each fasciculus is called the perimysium while the innermost sheath that surrounds individual muscle fibre is called the endomysium. Within each fibre is a collection of myofibrils containing multiple myofilaments. When bundled together, all the myofibrils get arranged in a unique striated pattern forming sarcomeres which are the fundamental contractile unit of a SkM. Actin and myosin are two significant myofilaments that arrange to form various bands on the SkM. Between the basement membrane and the sarcolemma (which is the cell membrane surrounding striated muscle fibre cells) are stem cells called satellite cells that differentiate into mature muscle fibres. The entire muscle itself is then surrounded by layer of outermost connective tissue called the epimysium (392, 393).

SkM is highly vascularised and rich in connective tissue, to provide vital nutrients for activity. As the myofiber matures, it is activated by a single neuron and exhibits contractile function-specific chemicals, primarily various myofibrillar protein isoforms and metabolic enzymes (392). Although the specific processes remain unknown, both the motor neuron and the myocyte origins have been implicated in determining myofiber contractile qualities.

Within sarcolemma, are regulatory proteins, such as the calcium-dependent troponin complex (including troponins C, I, and T), and tropomyosin that are associated with the actin filament and play very important roles in the activation process that leads to myofilament sliding and force generation. A transverse tubular system (T tubule), the sarcoplasmic reticulum, and a mitochondrial network are also found in the sarcoplasm of muscle fibres; the exact number of these components varies depending on the fibre type (393). Adult muscles fibres are classified into three types: type I (slow, oxidative, fatigue-resistant), type IIA (rapid, oxidative, intermediate metabolic characteristics), and type III (fastest, glycolytic, fatigable) (394).

The metabolic demand in SkM is met via the three basic energy pathways in the muscle fibre: stores of ATP, anaerobic glycolysis, and oxidative phosphorylation (392). Anaerobic glycolysis generates ATP fast, allowing muscular activities to be sustained for a few minutes, but the end products (hydrogen ions $[H^+]$, lactate) degrade muscle function and are linked to muscle exhaustion, while long durations of exercise are sustained via oxidative phosphorylation. It is important to emphasise that the use of these metabolic pathways is not an “all or nothing” situation. Pathways overlap and can be active at different times depending on the degree of use.

1.6.2 Skeletal muscle development

Except for the cranial muscles, all vertebrate SkM are produced from mesodermal precursor cells derived from the somites (epithelial spheres of paraxial mesoderm). Positive and negative signals from surrounding tissues influence the specification of mesodermal precursor cells to the myogenic lineage throughout embryonic development (395). Upregulation of *MyoD* and *Myf5*, basic helix-loop-helix transcriptional activators of the myogenic regulatory factor family (MRF), *WNT* and *Notch* genes are required for myogenic lineage selection (396, 397). This is evidenced by the absolute loss of SkM in *MyoD:Myf5* double knockout mice, as well as the finding that putative muscle progenitor cells remain multipotent and contribute to non-muscle tissues (398). Proliferative mesodermal myoblasts are myogenic cells that are *MyoD* and/or *Myf5* positive and are the lineage-committed precursors of mature SkM myocytes. Myoblasts exit the cell cycle to become terminally differentiated myocytes that express the "late" MRFs: Myogenin and MRF4, and then muscle-specific genes such as myosin heavy chain and muscle creatine kinase (*MCK*). Myogenin-deficient embryos perish perinatally due to a lack of myoblast development, as indicated by the nearly complete absence of myofibers in these mutants (399, 400). Similarly, MRF4-deficient animals exhibit a variety of abnormalities consistent with MRF4's late function in the myogenic process (401). Finally, mononucleated myocytes selectively combine to produce multinucleated syncytium, which matures into contracting muscle fibres. During muscle development, a unique subset of myoblasts fails to differentiate but stays attached to the growing myofiber's surface as quiescent muscular satellite cells (402). SkM is a stable tissue beyond sexual maturity, with multinucleated postmitotic muscle fibres (403, 404).

Muscle satellite cells are a population of undifferentiated mononuclear myogenic cells, that first appear as a distinct population of myoblasts during the 10th to 14th week of human limb development (405) and from around E17.5 in limbs of mouse embryos (406). When cultured *in vitro*, satellite cells

display specific characteristics allowing their distinction from embryonic and foetal myoblasts (407). Muscle satellite cells are easily identified by electron microscopy based on their specific placement inside the basal lamina surrounding individual myofibers, juxtaposed between the muscle fibre's plasma membrane and the basement membrane. The basal lamina serves as a scaffold for satellite cells and functions to limit and orient their migration during injury (408). Other distinguishing characteristics of satellite cells include a higher nuclear-to-cytoplasmic ratio, a lower organelle content and a smaller nucleus size with more heterochromatin than myocytes (409). These traits reflect that satellite cells are less transcriptionally and mitotically active than myocytes.

1.6.3 Cellular components of muscle regeneration

In response to injury, SkM has the unique capacity to launch a quick and thorough healing process, limiting muscle mass loss. SkM healing is a highly coordinated process that involves the activation of several cellular responses. The first stage of muscle healing is characterised by necrosis of the injured tissue and the initiation of an inflammatory response. This is quickly followed by the activation of myogenic cells, which enables them to proliferate, differentiate and fuse, resulting in the production of new myofibers and the reconstruction of a fully vascularised functioning contractile apparatus. The activation of adult muscle satellite cells is a critical step in this process. Muscle satellite cell activation is similar to embryonic myogenesis in various aspects, including the *de novo* production of myogenic regulatory factors. Although this regeneration process is known to involve several key signalling pathways, their specific roles remain poorly understood (410). However, the discovery of multipotent stem cells capable of myogenic differentiation has broadened our understanding of the regeneration process.

Skeletal muscle is a rich source of adult stem cells. As discussed above, satellite cells, which are SkM-specific stem cells derived from PAX3⁺/PAX7⁺ embryonic progenitors, contribute to the postnatal maintenance, development, repair and regeneration of the SkM (410). Satellite cells and their descendant myoblasts have been considered as strong prospects for cell-based therapies to treat muscular dystrophies and other neuromuscular conditions, due to their availability and exceptional ability to restore injured muscle (410).

Under normal physiological settings, satellite cells are in a quiescent state unless triggered in response to muscle damage or activity which leads to proliferation, self-renewal and differentiation into mature new fibres (411). Prior research on satellite cell-depleted mice in SkM revealed that the hypertrophic

response to injury, involving both muscle fibre hyperplasia and regeneration were significantly blunted (412). Both quiescent and activated satellite cells express Pax7, while only the latter express Myf5 and MyoD, which help regulate myogenic lineage differentiation (413). Although most activated satellite cells proliferate and differentiate due to Pax7 downregulation, others exit the cell cycle and return to dormancy. Pax7⁺ Myf5⁺ satellite cells upregulate MyoD which is thought to be the master regulator in the transcription of myogenesis (414, 415).

The basal laminar has a significant number of integrin7/integrin1 binding sites, which link the actin cytoskeleton of satellite cells to allow extracellular mechanical cues (from myofibers) to be relayed into intracellular chemical signals (inside the satellite cells) (416). The acellular and cellular components of the satellite cell niche include growth factors, ECM proteins, fibroadipogenic progenitors (FAPs), chemokines, and MMPs (417). Local muscle interstitial cells (MIC), motor neurones, vasculature, and secreted substances all have the capacity to influence their activity outside of the immediate niche (418).

The term MICs is given to a range of different cell types found in the interstitium of SkM. They are typically classified into two main groups: cells that support muscle regeneration and those that may directly contribute to myonuclei. Interestingly, one of the subtypes of MICs has also been uniquely shown to have haematopoietic potential. More than 20 years ago, Gussoni *et al.* discovered a subpopulation of cells among healthy murine SkM digests that can efflux Hoechst 33342 - a hallmark of haematopoietic side-population stem cells (419). These HSC-like cells also formed haematopoietic colonies on methylcellulose and expressed Sca-1 and CD45 but no other haematopoietic lineage markers, including CD4, CD5, CD8, CD11, or Gr-1 (419-421). Further analysis indicated that these

haematopoietic cells in SkM were recruited from the peripheral circulation, which was thought to account for their close proximity to blood vessels (422, 423).

Myo-endothelial cells (MyoECs) are another notable subgroup of MICs, that express both satellite (CD56) and EC (CD34, CD144) markers, but are negative for CD45 (419, 420). These are located between myofibers but outside the basal lamina. Clonal cultures of CD34⁺CD45⁻ sorted MyoECs demonstrated their capacity to differentiate *in vitro* into myogenic and endothelial lineages, as well as their osteogenic and chondrogenic plasticity (423, 424). Furthermore, they have been shown to efficiently rebuild damaged SkM following transplantation *in vivo* (425).

Myogenic and endothelial cells have a shared embryonic mesoangioblast origin in the form of the dermomyotome. This is a transitory epithelial structure of the somite developed in the mouse at gestational age E9 which gives rise to myoblasts, ECs, SMC and skin dermal cells (426). It also produces a subset of unique ECs found in SkM, known as somite-derived ECs (SDECs), as demonstrated in avian, mouse, and zebrafish studies (427). During embryogenesis, these SDECs function as a supplementary input to the progenitors that produce HSCs.

Although multiple immune cells are involved in the inflammatory response induced by acute muscle injury, neutrophils and MΦs are the predominant ones (428). In steady state, MΦs are located in the perimysium and the epimysium of muscle at steady-state (429). During muscle regeneration, ECs work intimately with MΦs and satellite cells. They control MΦ development and maturation via angiocrine Notch signalling (Dll1), which promotes arteriogenesis during recovery after muscle ischaemia (430). Active satellite cells are typically in close proximity to EC-lined blood arteries and

produce VEGF-A, which helps sustain Delta-like ligand 4 (DLL4), a ligand involved in endothelial sprouting (431).

Currently, there is relatively little known about the respective roles of tissue-resident and circulation-derived MΦs involved in SkM repair and regeneration. Following acute injury, there is recruitment of Ly6C^{hi}CCR2⁺Cx₃CR1^{lo} monocytes from peripheral blood to the injured tissue. Notably, pro-inflammatory Ly6C⁺ MΦs have been shown to predominate early after SkM injury but lose expression of Ly6C after 48-72 h (432). Inhibited revascularisation is shown in mice missing the chemokine receptor CCR2 (433) or its ligand CCL2 (434, 435), as well as a lack of monocyte/MΦ infiltration in ischaemic regions (436). Similar results have been shown following the depletion of CD11b⁺ myeloid cells using a transgenic mouse model (432). On the other hand, depletion of MΦs has only led to partial alteration of SkM recovery after injury, supporting the existence of alternative mechanisms to ensure the functions of MΦs (437), perhaps via tissue-resident sources (**Figure 1.11**).

The phenotypic shift for MΦs from Ly6C^{hi} to Ly6C^{lo} has also been observed in other tissues (e.g., heart, liver, or kidney) during the recovery process after injury, and is controlled at the DNA, RNA and protein levels (438-440). TNF-α (at high levels), IL-6 and IL-1β are all expressed by Ly6C⁺ monocyte-derived MΦs shortly after invasion. These substances, in addition to their well-known activities as pro-inflammatory mediators, serve as mitogens, encouraging the proliferation of myogenic cells, while preventing their differentiation and fusion into injured SkM fibres (429, 432). Subsequently, Ly6C^{lo}CCR2⁻CX₃CR1^{hi} monocytes patrol the vascular endothelial surface before being recruited to injured SkM via CX₃CR1/CX₃CL1 signalling at later stages of recovery (66). In one study, BM transplantation was employed to demonstrate resident MΦ (identified as CD11b⁺F4/80⁺CD11c⁻Ly-6C⁻CX₃CR1⁻) accumulate first in the epimysium 1–6 h after injury and to cytokine-driven recruitment of neutrophils and monocytes from the blood (441).

Until recently, all MΦs in SkM were thought to be derived from BM haematopoietic progenitors via the recruitment of circulating monocytes. However, as with other tissues, recent use of lineage mapping approaches has uncovered the presence of resident MΦs that are embryonically seeded from both YS and foetal liver origins. Using scRNA-seq, Wang *et al.* discovered five unique MΦ clusters in SkM: 1) a CCR2 cluster, 2) a proliferating cluster, 3) a *Cd209* cluster, 4) a *Klf2* cluster and 5) "cluster 0" (75). BM-derived MΦs that expressed a MHCII^{Hi}LYVE-1^{Lo} surface immunophenotype were detected in the CCR2 cluster, whereas resident YS-derived MΦs that were MHCII^{Lo}LYVE-1^{Hi} were located in the non-CCR2 clusters. Interestingly, the *Cd209* cluster was only found in the quadriceps muscle (and not diaphragm) and was associated with increased expression of M2-like genes such as *Mrc1*, *Fcgrt*, *Folr2*, *Cd163*, *Fcna*, *Timd4*, and *Tslp*, as well as C-type lectin receptor (*CLR*) genes. Meanwhile, the *Klf2* cluster was exclusively found in the diaphragm and showed elevated expression of stress-response genes (e.g. *Egr1*, *Fosb*, *Ier3*). The Ccr2 cluster was particularly enriched in antigen-expressing genes. A recent study implicated the rapid cloaking ability of microlesions by SkM-resident MΦs, which dampen infiltration of neutrophils and prevent them mediating inflammatory tissue damage under steady state conditions (442).

MΦs are also intimately involved in the neovascularisation response to SkM ischaemia. They produce matrix-remodelling enzymes, such as MMP2, 13 and 14, and promote the pro-angiogenic commitment of EPCs and mature ECs through release of factors, such as VEGF (443). Indeed, CCR2 deficient mice have been shown to have slowed VEGF production and angiogenesis during the repair of cardiotoxin-injured muscle via reduction in MΦ infiltration (444). It has also been demonstrated that MΦ depletion induced a considerable endothelial-to-mesenchymal shift of endothelial-derived progenitors, impaired blood vessel development and increased collagen deposition in the cardiotoxin injury model (443).

Angiogenic cells are drawn into the damaged tissue during ischaemia and revitalise the vascular network. Angiogenic cells with paracrine potential and stem/progenitor cells with vasculogenic potential are found in abundance in many complex organs and is particularly prevalent in the BM. Various cell types (including haematopoietic progenitor cells, EPCs, and numerous proangiogenic cells) are momentarily mobilised in mice and humans by acute ischaemia disorders (445). Proteases such neutrophil-produced elastase, cathepsins, and matrix metalloproteinase types 2 and 9 regulate the mobilisation process. Integrin 4 and VCAM-1 interact with certain receptors in significant ways. As with CXCL-chemokines (CXCL), gradients of chemokines are necessary for the mobilisation of BM-derived cells (446).

Skeletal muscle

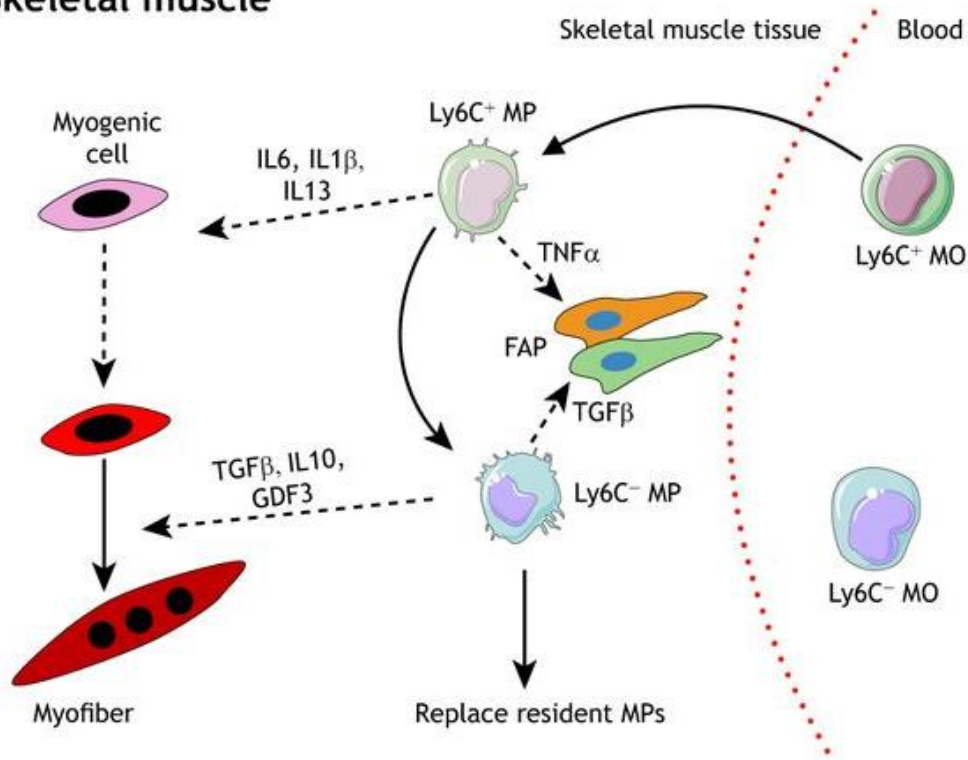


Figure 1.11: The role of macrophages in promoting myocyte recovery

Following injury, Ly6C⁺ monocytes (MO) invade SkM, develop into Ly6C⁺ MΦs (MP) and release cytokines such as IL-6, IL-1, IL-13, and TNF- α to promote myogenic cell proliferation and eliminate excess fibro/adipogenic progenitors (FAPs, orange cell). These Ly6C⁺ MΦs are then thought to transform into Ly6C⁻ MΦs, which initiate an anabolic programme via secretion of TGF- β , IL-10 and growth differentiation factor 3 (GDF3) which promotes the differentiation and maturation of myogenic cells and FAPs. *Image via Theret et al. (447)*

1.6.4 Skeletal muscle in diabetes

SkM is the most critical organ for the actions of insulin, meaning that it is highly vulnerable to the effects of both diabetic insulin deficiency and resistance and muscle atrophy is the most common structural alteration in SkM caused by diabetes (448). In STZ-induced diabetic rats, myofiber diameters of the soleus and extensor digitorum longus reduced by 30% compared to control animals (449). Other effects included reductions in skeletal myocyte metabolic control and switch to a glycolytic phenotype (450-452). Moreover, the SkM of diabetic rats showed increased protein breakdown and reduced protein synthesis (453), which may contribute to the loss of muscle tone.

SkM is made up of muscle fibres that are loosely categorised into three types as described above (454). In general, increasing SkM activity, such as electrostimulation and exercise, causes the muscle fibre type to move from fast to slow, while the converse occurs due to inactivity, such as casting and denervation (454). Diabetes induces a muscle fibre-type transition from slow to fast indicating a reduced oxidative capacity, as seen in the inactive state (454, 455). In addition, diabetes also effects SkM health and function through its effects on vascular perfusion and ischaemia (450, 456) and neuropathy (448).

SkM is the largest metabolic organ and is also well documented for altering energy metabolism in diabetes. Diet-induced thermogenesis, calculated as a percentage of calorie intake, has been shown to be lower in diabetic individuals (457), as is maximum oxygen consumption which is one of the earliest manifestations of diabetes-induced abnormalities in energy metabolism abnormalities (458). There are various causes of the impaired energy metabolism in diabetes, including the disturbed function of mitochondria, which create ATP through respiration and control myocyte metabolism. In diabetics, the rate of mitochondrial protein synthesis and enzyme activity are lowered (459).

Furthermore, it was observed that glycogen storage in diabetic SkM was considerably decreased compared to controls, which was driven by reduction of glycogen synthase activity (460).. Indeed, it has been reported that after insulin injection into the SkM of nondiabetic rats, glycogen synthase I activity and the content of glucose 6-phosphate, an intermediate metabolite produced by hexokinase in the first step of glucose uptake, were significantly increased, whereas a reduced reaction was observed in diabetic rats (461).

The negative effects of T1D on the regenerative capacity of SkM have been directly linked to satellite cell aberration (462). Satellite cells derived from STZ-induced diabetic mice failed to form myotubes and displayed reduced expression of myogenic regulatory factors and impaired differentiation following cardiotoxin-induced muscle injury (450, 463). MyoD and myogenin expression were markedly reduced in the gastrocnemius of STZ-induced diabetic rats (464). Furthermore, diabetic Akita mice showed impaired muscle regeneration after damage due to a decrease in MΦ infiltration and satellite cell recruitment into degenerative fibres following delayed ECM turnover (200). This was attributed to an elevation of IL-6 and plasminogen activator inhibitor-1 (PAI-1), a diurnally regulated hormone that is chronically increased in both types of diabetes (465). Other data also suggest that insulin's actions are critical for sustaining satellite cell function (466). Further improvement in our understanding of the changes to the satellite cell population and function in diabetes is required to allow the development of therapeutics to improve muscular health in this condition.

Similarly, reports on various T2D mouse models demonstrate insufficient muscle regeneration (467), along with deficiency of muscle satellite cells (468) and reductions in their capacity to proliferate, differentiate and undergo functional maturation (455). Interestingly, MyoD and myogenin protein

levels were markedly reduced in plantaris muscles of Zucker diabetic rats (455) and transgenic *ob/ob* and *db/db* mice (469). In addition to the blunting in their myogenic potential, satellite cells also display diabetic phenotypes, involving increased expression of inflammatory cytokines (470), reduced lipid oxidation (471), disturbed glucose uptake (472), and increased resistance to insulin (473). Satellite cell dysfunction in both T1D and T2D has also been linked to a redox imbalance, increased oxidative stress (474) and a decrease in the content of intermyofibrillar mitochondria (179, 464).

Taken together, steady state muscle in diabetic conditions launch structural, functional and metabolic abnormalities that lead to insufficient reparative responses.

1.6.5 Cellular mechanisms of diabetes impaired ischaemic repair

Cardiovascular complications are the leading cause of morbidity and mortality in persons with T1D and T2D. Microvascular disease such as retinopathy, nephropathy, and neuropathy are features of diabetes, as are macrovascular atherosclerotic complications, such as coronary heart disease (CHD), peripheral arterial disease (PAD), and cerebral artery involvement that increase morbidity and mortality (475). PAD is characterised by narrowing and restriction of blood flow in the peripheral arteries of the limbs and is accentuated in diabetes by the reduced capacity to undergo neovascularisation to promote collateral blood vessel growth (476). This can culminate in clinical manifestations ranging from intermittent claudication to the more severe consequences of critical limb ischaemia (CLI), which include rest pain and the development of ischaemic ulcers and gangrene, which may necessitate amputation (477). The current standard of therapy for CLI involves revascularisation via peripheral bypass grafting and percutaneous methods, but these often have limited success, and diabetic individuals experience even worse outcomes after vascular interventions. Additionally, many individuals are unsuitable for vascular procedures, necessitating the development of alternative treatment plans for diabetic patients with PAD, complicated by CLI (478, 479).

Recent research on diabetic ischaemic repair has demonstrated that endothelial damage and the emergence of vascular problems are also closely related to the effects of a heightened inflammatory state and metabolic imbalances (480). Endothelial dysfunction is defined by the transition in vascular homeostasis towards vasoconstrictive, proinflammatory, and prothrombotic-related pathways and occurs when the endothelium is unable to effectively control vascular tone, coagulation, and immunological responses (481, 482). The main endothelium-derived mediator is NO, and endothelial dysfunction is primarily linked to decrease NO bioavailability through a number of complementary processes, including decreased eNOS expression, eNOS uncoupling, and excessive ROS generation.

Reduced NO levels and endothelial dysfunction are caused by NADPH oxidase protein subunits (p22phox, p67phox, and p47phox), which are both dramatically elevated in diabetic veins and arteries (483). Induction of diabetes also results in oxidative loss of tetrahydrobiopterin (BH₄), a required cofactor for eNOS activity, by forming dihydrobiopterin (BH₂) and biopterin. In diabetic mice, endothelial-targeted overexpression of the guanosine triphosphate-cyclohydrolase I, the rate-limiting enzyme in BH₄ synthesis, lowers endothelial superoxide generation while maintaining NO-mediated vasodilation (484). Antioxidants such as SOD have also been shown to improve NO levels and endothelial function (485). Alternatively, this increases potent vasoconstrictors, such as angiotensin II and endothelin that foster vascular dysfunction in the diabetic milieu (486). The aetiology of vascular dysfunction in diabetes may also involve changes in the mechanical characteristics of big compliance arteries. Interestingly, long-term therapy with aminoguanidine reduces the build-up of advanced glycation end products (AGE) on collagen and has shown some success in improving arterial wall properties in experimental diabetic mice (487).

Chronic hyperglycaemia is a major contributor to elevated oxidative stress and endothelial dysfunction. Excess O₂⁻ has a strong affinity for NO, resulting not only in NO breakdown and inactivation, but also in the creation of ONOO⁻, that causes lipid peroxidation, DNA damage, and cell death. Furthermore, ONOO⁻ can oxidise the necessary BH₄ to the physiologically inert trihydrobiopterin (BH₃), resulting in BH₄ demise (488). In the absence of adequate BH₄, eNOS converts from a NO-producing enzyme to an O₂⁻ generating enzyme. In this scenario, inadequate endothelial function is compounded by a vicious cycle of increasing oxidative stress and eNOS uncoupling, resulting in increased O₂⁻ generation and decreased NO bioavailability.

In addition, hyperglycaemia causes endothelial dysfunction through diversion of glycolytic flux to alternative metabolic pathways (481). Overproduction of mitochondrial O₂⁻ inhibits the activity of the glycolytic enzyme glyceraldehyde-3-phosphate, which is required for glycolytic flux

maintenance, resulting in the accumulation of upstream glycolysis intermediates and increased flux of these metabolites into glucose overutilisation pathways such as the polyol pathway, hexosamine pathway, protein kinase C (PKC) pathway, and AGE pathway (175). Increased glucose flow into the polyol pathway depletes NADPH, essential for the regeneration of reduced antioxidant glutathione (GSH). As a result, intracellular concentrations of GSH decline, leading to an increase in intracellular oxidative stress (489). Excess intracellular glucose shunting into the hexosamine route enhances transcriptional factor modification via dysregulated protein glycosylation, resulting in altered protein expression (490). PKC activation caused by hyperglycaemia via increased diacylglycerol, has a number of pathogenic consequences, including decreased expression of eNOS, increased expression of endothelin-1 (ET-1), TGF- β and PAI-1, and activation of NF- κ B and NADPH oxidase, all of which impair endothelial function (491, 492).

Neovascularisation in response to ischaemia is regulated by hypoxia, at least in part through activation of hypoxia-inducible factor 1 (HIF-1)-related pathways. HIF-1 α instability is thought to be the most likely event that underpins the loss of the normal cellular response to hypoxia under increased glucose conditions (493). HIF-1 α levels were lower in biopsies from diabetic foot ulcers compared to non-diabetic venous ulcers that share a similar hypoxic environment but are not subjected to hyperglycaemia (494). It also follows that most HIF-1 α -targeted genes such as *VEGF-A* and its receptors VEGFR1 and VEGFR2 are diminished in preclinical models of diabetic ischaemia (495). Paradoxically, diabetic ischaemia increases the soluble form of VEGFR1 in SkM, which has anti-angiogenic properties and this presumably inhibits the ability of VEGF to promote an angiogenic response (496). VEGF-A may stimulate EC proliferation and survival via phosphatidylinositol 3' kinase/AKT/eNOS. The angiogenic response to VEGF-A in peripheral ischaemia is reliant on eNOS, and gene therapy delivery of eNOS has been shown to increase neovascularisation in the ischaemic

legs of control and diabetic animals, underlining the relevance of NO in this setting (**Figure 1.12**) (497).

T1D and T2D are also associated with reduced EPC numbers in circulation (498). In fact, the reduction in EPCs has also been shown to be related to the severity of PAD in diabetic patients (499). Moreover, EPCs from patients with diabetes exhibit activation of the Akt/p53/p21 signalling pathway and expedited senescence. This is important because depletion of endogenous p53 underpins the ability of EPCs to form angiogenic tube-like structures in culture, indicating that activation of the p53 pathway is likely to contribute to abnormal EPC function in the diabetic setting (500).

The macro- and microenvironment of diabetes may also affect the quantity, activation and differentiation states of different inflammatory cell populations, which also lead to adverse effects on neovascularisation and vascular remodelling in ischaemic tissue. In particular, diabetes has been characterised by an unbalanced M1/M2 MΦ ratio, and specifically a relative deficiency in the anti-inflammatory, pro-angiogenic M2 state. This has been observed in the tissues of diabetic subjects, even in the absence of any alterations to circulating classical (CD14⁺CD16⁻), intermediate (CD14⁺CD16⁺) and nonclassical (CD14⁻CD16⁺) monocytes (501). This alteration in the M1/M2 ratio has been linked to the incidence of microangiopathy and has a direct correlation with the glucose biomarker, HbA1c (501). An over-abundance of M1-like MΦs have been associated with increased myocardial injury in Zucker diabetic fatty rats, while administration of the heme oxygenase inducer, hemin, restores this state by preferentially polarising MΦs into the more anti-inflammatory M2-like phenotype (502). Additionally, diabetic mice exhibit higher levels of circulating neutrophils and Ly6C^{Hi}, which due to increased proliferation and expansion of myeloid progenitors in BM and accentuated release of monocytes from BM into the bloodstream (362). Diabetes also impacts the

recruitment of immune cells to ischaemic tissues. Patients with diabetes display a diminished monocyte chemotactic response to triggers, such as VEGF-A, due to a deficiency in downstream signal transduction (503). When compared to WT mice, db/db mice also show significantly lower levels of monocyte recruitment to the SkM of ischaemic hind limbs (504).

Diabetes also induces p21 and p27, which are targets of the transcription factor, FOXO3a, and leads to nuclear localisation of the proapoptotic factor FOXO3a in BM-derived CD34⁺ progenitor cells, which promotes apoptosis (kip1) (505). Diabetes-induced abrogation of BM-derived cell mobilisation may potentially be the reason for the decline in the number of angiogenic cells. Defective EPC mobilisation in T1D is associated with altered release of CXCL12 and VEGF and inability to upregulate muscle HIF-1a (506). Another factor that accentuates the impaired perfusion recovery of diabetic ischaemic tissues, is the presence of nerve dysfunction. Postganglionic sympathetic nerves regulate arterial tone by direct contact with arterial SMCs. Type 2 diabetic rats have been shown to have fewer nerve terminals innervating their BM, and this has been linked to the diminished release of pro-angiogenic EPCs into the circulation, which follows a strict circadian schedule (507). This relates, at least partly, to lower expression of the *clock* gene in both diabetic tissues and the EPCs themselves, and results in diminished repair of ischaemic tissue (508).

Murine models of T1 and T2D have also been shown to result in an autonomic neuropathy of BM, which is associated with impaired mobilisation of both Lin⁻Kit⁺Sca1⁺ HPSCs and EPCs, as well as delayed vascular recovery after ischaemia (499). Interestingly, proangiogenic growth factors, such as Desert Hedgehog, promote post-ischaemic neovascularisation by maintaining the pool of nerve-derived proangiogenic factors and the health and integrity of peripheral nerves in ischaemic SkM, instead of acting directly on vascular ECs (509). Signalling molecules, such as the secreted guidance

molecule, Netrin1, along with the Nrp1 and plexin D1 receptors for Semaphorins (Sema) govern the formation of both sympathetic nerve and vascular axons. These common guiding molecules may serve dual roles to promote neovascularisation by regulating both innervation of the vascular wall and the angiogenic process, itself (510). In one study, diabetic mice displayed higher levels of p53 and Sema3E expression than WT mice and consequently had inadequate neovascularisation in ischaemic regions after administration of VEGF treatment, whereas treatment with VEGF plus plexin D1-Fc restored neovascularisation (510). Similarly, netrins have been shown to speed up neovascularisation, while reversing neuropathy and vasculopathy in a diabetic mouse model of ischaemia (511). In ECs cultured under high glucose conditions, the neuropeptide secretoneurin increased proliferation and chemotaxis, while lowering apoptosis (512). This was associated with stimulated expression of extracellular regulated kinases, eNOS, AKT and the EGF receptor (512). In this same study, secretoneurin gene therapy promoted angiogenesis and arteriogenesis in diabetic mice leading to enhanced neovascularisation in ischaemic SkM (512). Finally, nerve growth factor has also been shown to promote reparative neovascularisation and protect ECs from T1D-induced cell death (513). Taken together, there are common signalling pathways for the neural and vascular systems and therefore the targeting of both is important to the recovery of neovascularisation and tissue repair under diabetic ischaemia.

Interestingly, a study by Yan *et al.* identified important differences between the ischaemic repair mechanisms between T1- and T2D (514). Following ischaemia, gastrocnemius eNOS expression was lower in T2D compared to T1D. In both cases mobilisation of EPC failed to increase, however, eNOS expression of EPC were significantly low in T1D. Additionally, EPC migration and integration into tubular structures were less efficient in T2D. Overall, T2D mice displayed significantly less reperfusion following ischaemia. The discrepancy in poor angiogenesis and arteriogenesis following prolonged ischaemia in experimental T2D may be explained by the tubule formation deficit in EPCs.

Rivard *et al.* have reported that exogenous VEGF rescues impaired blood flow in T1D NOD mice; however, some authors suggest that growth factor or gene therapy may be insufficient as a sole strategy to enhance T2D revascularisation (495, 515). This may be due to complexities in the aetiology of diabetes and due to different metabolic disturbances.

Interim conclusion

- SkM contains a rich source of stem cells, MICs, MΦ and ECs that maintain SkM integrity and repair processes. As in other tissues, MΦ and EC populations are heterogenous and originate from various sources.
- Diabetes directly influences myocyte and SkM cell function as SkM is the forebearer of energy production and therefore insulin use. During ischaemic repair, hyperglycaemia-driven impaired inflammatory repair responses as well as EC dysfunction lead to poor outcomes.

1.7 Discovery of yolk-sac derived Endothelial-Macrophage progenitors as a novel bipotent source of macrophages and endothelial cells

Over the past few years, our group has identified a novel population of YS-derived endothelial-MΦ (EndoMac) progenitor cells in different postnatal mouse tissues (115). The description of these resident progenitors adds a new perspective to the shared origins of tissue-resident MΦs and ECs in general. The following section will outline our preliminary, mostly unpublished findings, which serve as a foundation for this thesis.

1.7.1 EndoMac progenitors in adventitia of murine arteries.

Psaltis and Simari first identified the presence of adventitial Sca-1⁺CD45⁺ progenitor cells in the adventitia of postnatal mouse aorta, which selectively produce MΦ colony-forming units (CFU-M) when cultured in methylcellulose *in vitro* (517, 518). Cells contained within primary (1^o) aortic CFU-M formed secondary (2^o) colonies when re-cultured, and this was shown to occur from single cell origins. Separate studies showed that adventitial Sca-1⁺CD45⁺ cells could differentiate into MΦs and ECs under growth factor-induced conditions *in vitro* and following adoptive transfer into ischaemic hindlimbs and atherosclerotic carotid arteries *in vivo*, also forming intact endothelial-lined neovessels in the process (517, 518).

More recently, we have established that aortic CFU-M are made up of a homogeneous population of progenitors that express CD45, Sca-1, c-Kit, CX₃CR1 and CSF1R, but are negative for Lineage (Lin), mature MΦ (CD11b, F4/80) and EC (CD144) markers (64, 519). CFU-M progenitors also expressed the haematopoietic progenitor and EMP markers CD34, CD16/32, CD93 (AA4.1) and CD43, but not CD41 (very early-stage haematopoiesis), Flt3 (CD135) (definitive haematopoiesis), or Brachyury (haemangioblasts) (28, 520). The stem cell marker c-Myc, which regulates self-renewal, was

expressed on 15% of these permeabilised cells, although Sox2, Nanog, and Oct4 were much more lowly expressed. Other mature myeloid markers were negative or expressed at very low levels (CCR2, CD206, CD86, MerTK, MHCII, Ly6C, Gr1, CD64, CD24, LYVE-1). CFU-M progenitors were also negative for the erythroid marker, Ter119, and the endothelial markers, CD144, VEGFR2 and TIE2, albeit they did express CD31, which is already known to be found on other myeloid progenitors (27). Importantly, we also detected the presence of Lin⁻CD45^{+Lo}CD11b⁻F4/80⁻cKit⁺Sca-1⁺CX3CR1⁺CSF1R⁺ progenitors in freshly digested adult aorta, with a mean frequency of 0.3% or approximately 3,000 cells per whole aorta.

Lineage-mapping using *Flt3*^{Cre} x *Rosa26*^{mT/mG} mice was used to study the relationship between aortic CFU-M progenitors and definitive BM haematopoiesis. Cells derived from BM HSCs in these mice express GFP (*Flt3*-Cre⁺), whereas those that are not, are GFP⁻ and express tdTomato (tdTom⁺/*Flt3*-Cre⁻). In addition to aorta, we discovered that digests of postnatal heart, lung, skin, and SkM all selectively formed CFU-M in methylcellulose that were >90% *Flt3*-cre⁻ (GFP⁻tdTom⁺), whereas BM CFUs were >90% *Flt3*-cre⁺ (GFP⁺tdTom⁻), indicating likely independence from BM haematopoiesis. Postnatal age profiling then revealed that CFU-M yield from aorta, skin and SkM is highest for newborn mice and diminishes with ageing, suggesting probable prenatal seeding and progressive, age-related exhaustion of tissue reserves of these progenitors after birth. This led us to perform embryonic analysis, which revealed that CFU-M progenitors first appear in extra-embryonic YS around E8.5 of gestation, and in other tissues (e.g. aorta, heart, lung) from E10.5 onwards (**Figure 1.13**) (520).

These findings motivated us to investigate whether CFU-M progenitors are in fact derived from YS EMPs. We crossed *Csf1r*^{Mer-iCre-Mer} and *Rosa26*^{mT/mG} mice and administered tamoxifen (TAM) 75

µg/g i.p. at E8.5 to induce GFP expression in CSF1R⁺ YS EMPs and their progeny. We examined for GFP⁺ labelling of different cell populations (CFU-M progenitors, MΦs and ECs) in different tissues across different embryonic and postnatal ages. After normalising GFP⁺ labelling to brain microglia which are exclusively produced from YS, we discovered that tissue-resident CFU-M progenitors were almost exclusively YS-derived, in contrast to BM haematopoietic stem/progenitor cells. Focusing on the aorta, we also used flow cytometry and confocal microscopy to confirm that CSF1R⁺ YS EMPs give rise to progenitors in the adventitia, as well as ECs and MΦs. We therefore considered whether YS-derived progenitors produce ECs and MΦs to account for the local renewal of these two distinct lineages after birth. Progenitors from aortic CFU-M formed complex cord networks when cultured in MatrigelTM that contained new ECs and MΦs, suggesting bipotency. Injection of progenitors from ubiquitous GFP (ubi-GFP) donor aortas into the gastrocnemius and quadriceps of recipient C57BL/6 mice also improved perfusion in a model of hind limb ischaemia, as measured by laser Doppler imaging, and produced host-perfused GFP⁺ EC-lined neovessels and adjacent clusters of MΦs *in vivo*. As exemplified for aorta, these highly novel results show that YS EMPs not only give rise to MΦs and ECs, but also clonogenic, renewable progenitors that are bipotent for both these lineages and vasculogenic. This has led us to name tissue-resident CFU-M progenitors, “EndoMac progenitors”.

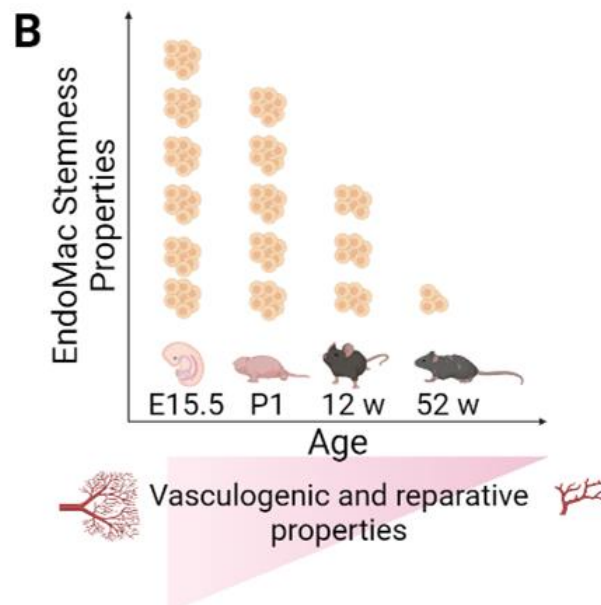
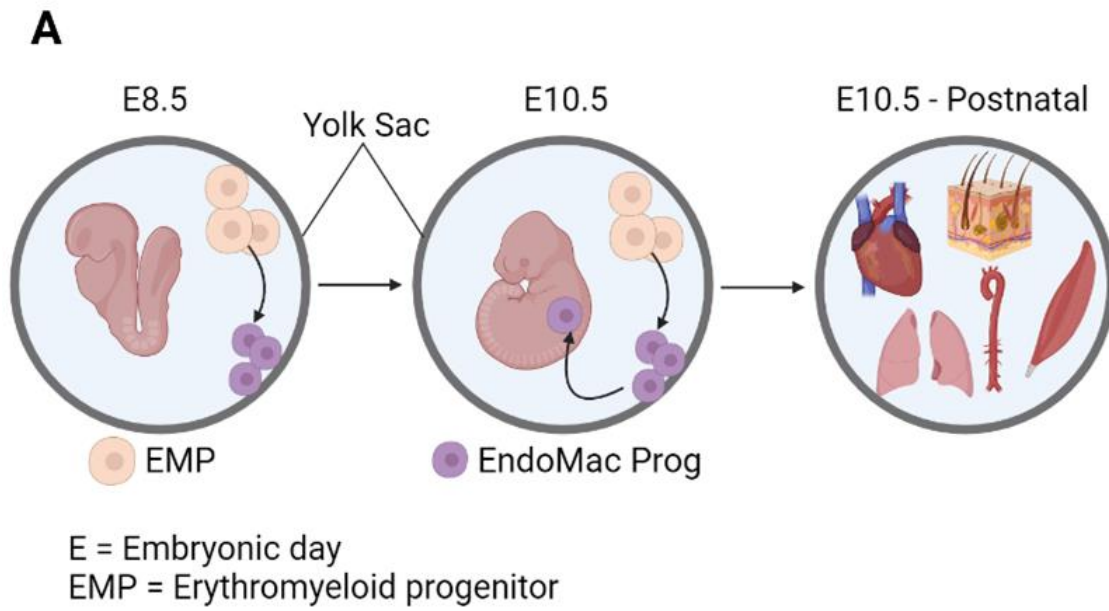


Figure 1.13: EndoMac progenitors in postnatal tissues

A. YS EMP-derived EndoMac progenitors are seeded in different embryonic tissues and persist after birth as a locally renewable source of ECs and Mφs. **B.** Their frequency and functional properties become diminished with steady state ageing.

1.7.2 EndoMac progenitors in murine skin and skeletal muscle

For homeostatic turnover and recovery after tissue damage, most mature cell types rely on stem cell self-renewal and the proliferation and differentiation of transitory amplifying progenitors. Although there has been debate regarding how embryonically derived MΦs are maintained after birth, the current consensus supports their ability to self-renew without losing functional or differentiated status (521). Investigations by our group have also uncovered that EndoMac progenitors are another potential source for the postnatal maintenance and expansion of YS-derived MΦs and ECs in both murine skin and SkM (522). We have found that skin and hind limb muscle of neonatal and postnatal mice contain CFU-M forming progenitors which have the same CX₃CR1⁺ and CSF1R⁺ YS ontogeny as EndoMac progenitors in aortic adventitia. In all cases, these progenitors are maintained independently of definitive haematopoiesis, as shown by Flt-3 Cre-Lox lineage mapping. Despite significant proliferative activity even in steady-state skin and SkM, their prevalence progressively decreases with postnatal ageing, coinciding with decreased clonogenic and self-renewal potential.

From a pathophysiological standpoint, we identified that the progenitors in skin locally increase after wound injury. The hypoxic environment of early wounds was found to increase their clonogenic, proliferative, endothelial-forming and vasculogenic potential (523). In line with this, surgical induction of wound injury resulted in a 2-fold increase in YS-derived EndoMac progenitors during the first 24 h, while YS-derived MΦs and ECs accumulated afterwards. TAM-induction of E8.5 CSF1R⁺ YS EMPs indicated that 35% of MΦs and 16% of ECs in steady state adult skin are YS-derived, which rises to 60% and 50% after 14 d of wound healing, respectively. This finding was consistent with previous research demonstrating the roles of resident MΦs (524-527) and EPCs (382, 528, 529) during the wound healing process. Importantly, injection of exogenous progenitors from ubi-GFP donor mice resulted in accelerated and more complete wound closure compared to injection of cell-free Matrigel as a vehicle control. In the wound environment, engrafted progenitors were

found to have differentiated into both ECs and MΦs, with the latter predominantly being of the LYVE-1⁺MHC-II⁻ local, resident subtype (**Figure 1.14**).

In a similar way, we also observed marked proliferative expansion of YS-derived EndoMac progenitors in SkM within the first 24-48 h of hind limb ischaemia (522). This was followed over subsequent days by accumulation of local, YS-derived MΦs which peaked on day 3 and then later on by YS-derived ECs, peaking on day 7. Using complementary techniques of adoptive transfer of GFP donor progenitors and bromodeoxyuridine (BrdU) pulse labelling followed by chase, we were able to demonstrate that this occurs by the sequential differentiation of SkM EndoMac progenitors into both these lineages, which in turn helps to vascularise the ischaemic muscle, thereby improving its perfusion recovery and enabling myocyte repair.

Based on these results, we propose that YS-derived EndoMac progenitors are a renewable, local source of MΦs and ECs that help mediate tissue inflammation and neovascularisation throughout different stages of development and postnatal life, and during repair after tissue injury or ischaemia.

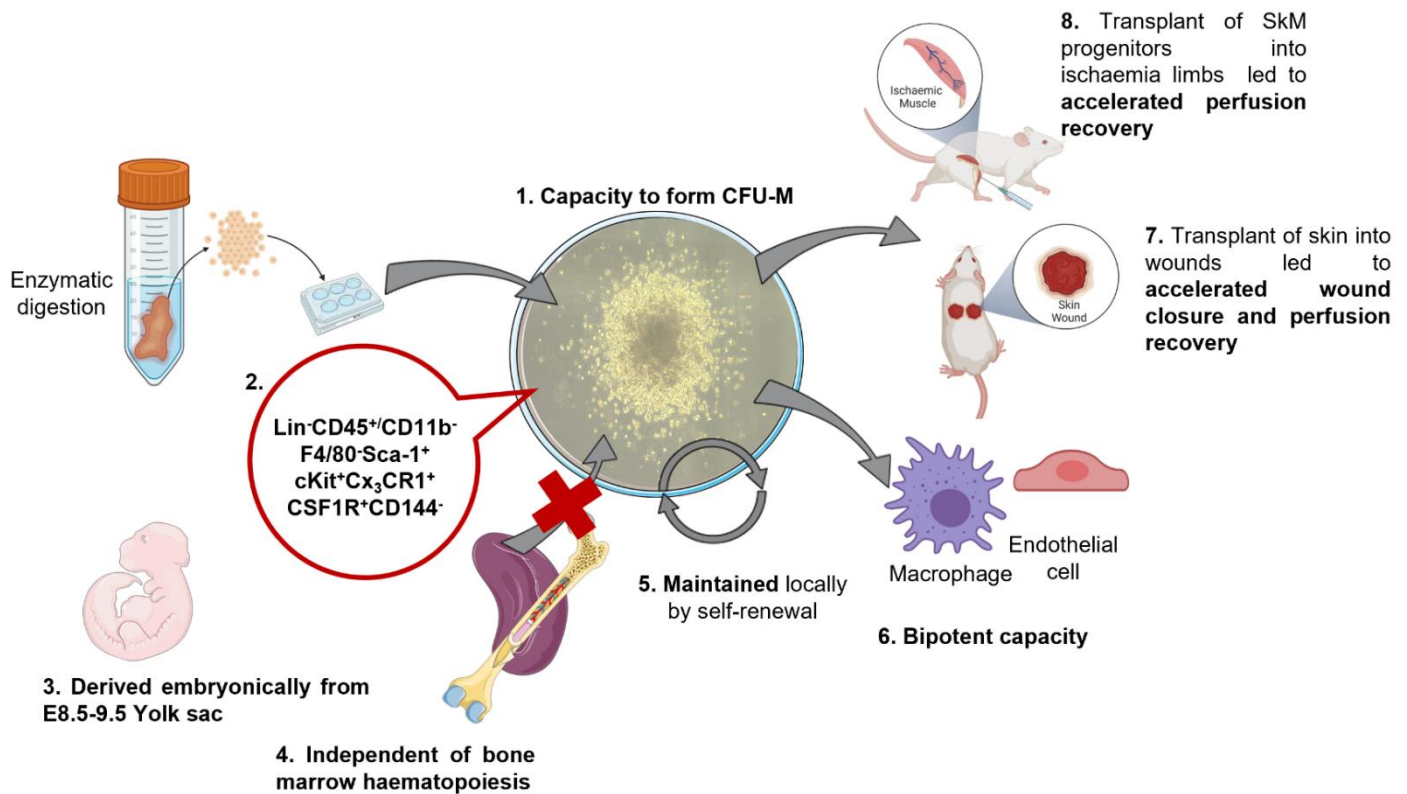


Figure 1.14: Summary of current findings on tissue-resident EndoMac progenitors.

1) EndoMac progenitors are identified by the capacity of single cell suspensions from tissue digests to selectively form CFU-M when cultured in methylcellulose for 14 d. 2) Flow cytometry analysis has revealed that EndoMac progenitors from different tissues are $\text{Lin}^-\text{CD45}^{+/Lo}\text{CD11b}^-\text{F4/80}^-\text{Sca-1}^+\text{cKit}^+\text{CX}_3\text{CR1}^+\text{CSF1R}^+\text{CD144}^-$. 3) They are embryonically derived from extraembryonic YS progenitors at around E 8.5-9.5 and are 4) then maintained independently of bone marrow (BM) haematopoiesis through a 5) finite process of local self-renewal. 6) EndoMac progenitors possess bipotent differentiation capacity for macrophages (MΦs) and endothelial cells (ECs). 7) Transplantation of skin progenitors into wounds led to accelerated wound closure and perfusion. Similarly, 8) Transplantation of SkM progenitors into ischaemic hind limbs resulted in increased reperfusion recovery and neovascularisation.

1.7.3 EndoMac progenitors in healthy and diabetic human vasculature

We have now also found the presence of analogous CFU-M forming progenitors in human vasculature by sampling undiseased saphenous vein (SV) and internal mammary artery (IMA) from patients undergoing coronary artery bypass grafting, and aortic aneurysm surgical samples (Long, Psaltis unpublished). Single cell digests of SV generated approximately 20 CFU-M per 10^5 cells in methylcellulose, approximating the recovery of CFU-M from adult mouse aorta. By comparison, CFU-M yield was much lower from IMA and several fold higher from aortic aneurysms. These results indicate that the presence of human vascular CFU-M progenitors varies by vessel type (e.g., artery vs vein), anatomical distribution and the presence or absence of disease. Like their murine counterparts, human progenitors were found to form complex cord networks when cultured for 7 d in MatrigelTM with endothelial growth media, and these contained newly formed CD45⁻CD31⁺ ECs and classical CD14⁺CD16⁻ MΦs (518, 530). This makes them a possible ancestral candidate for the local proliferation of MΦs and EC-lined vasa vasorum in the arterial wall during adventitial remodelling, which is associated with atherosclerosis and aneurysm formation (518, 530, 531). So far, we have established that human EndoMac progenitors have a distinct CD45⁺CD31⁻c-Kit⁺CD34⁺ surface marker phenotype, which to the best of our knowledge has not been described before for other types of vessel wall progenitors. Among numerous clinical factors studied, including age, gender, comorbid conditions, cardiovascular risk factors and medications, we have made the interesting discovery that diabetes mellitus is associated with lower recovery of EndoMac progenitors from human blood vessels, and marked inhibition of their angiogenic capacity *in vitro*.

1.8 Project Scope

An accurate understanding of how diabetes affects tissue inflammation and neovascularisation is essential to being able to develop new therapeutic strategies to address the unacceptable burden of diabetic wounds and ischaemic vascular complications. Our group's recent discovery of tissue-resident EndoMac progenitors provides a new paradigm to help explain the intimate relationships between MΦs and ECs, including a common pathway for their postnatal maintenance and renewal. This thesis is built around the observation that EndoMac progenitors proliferate and differentiate rapidly in response to wound injury in skin and peripheral ischaemia in SkM. In the process, they generate MΦs and ECs that stimulate neovascularisation and tissue repair (**Figure 1.15 left**). We hypothesise that diabetes dampens this response by inhibiting the key stem-like and metabolic properties of EndoMac progenitors in both these tissues (**Figure 1.15 right**).

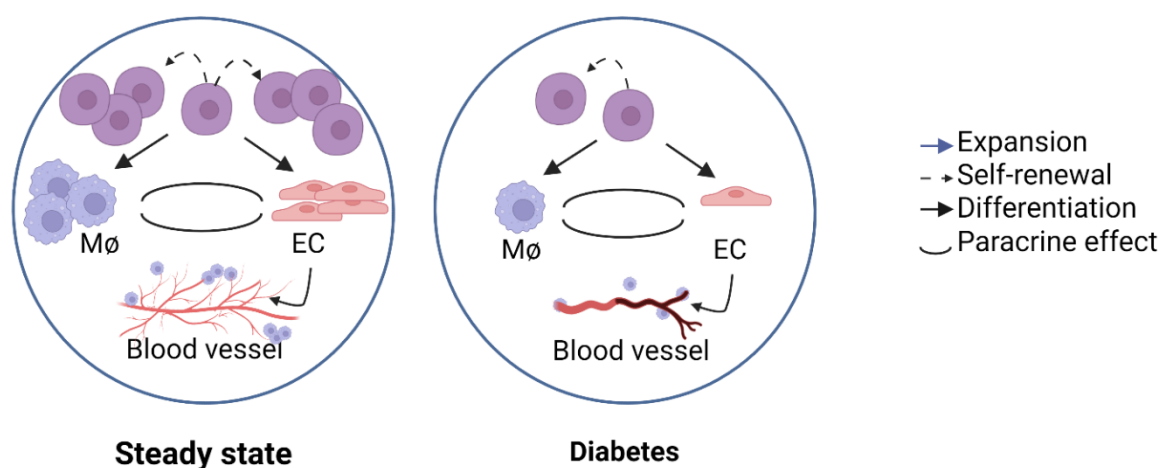


Figure 1.15: Central Hypothesis: Proposed inhibitory effects of diabetes on EndoMac progenitors.

Schematic illustrating the capacity of self-renewing EndoMac progenitors to generate both MΦs and ECs, which directly leads to formation of EC-lined neovessels, while also supporting neovascularisation indirectly through the paracrine and structural support provided by MΦs (left). This thesis investigates the hypothesis that diabetes inhibits these processes, which contributes to impaired tissue repair and neovascularisation (right).

To address this central hypothesis, we set out with the following aims:

Aim 1: To study the functional and transcriptional heterogeneity of EndoMac progenitors, with focus on how this is affected by different tissue types (Chapter 3).

Aim 2: To characterise the effects of high glucose *in vitro* and hyperglycaemia *in vivo* on EndoMac progenitors from adult murine skin under both steady state and wound injury conditions (Chapter 4).

Aim 3: To investigate how high glucose and hyperglycaemia affect EndoMac progenitors from adult murine SkM under both steady state and in response to ischaemia (Chapter 5).

Chapter 2

2. Materials and Methods

2.1 General materials

2.1.1 Equipment

Table 2.1: Equipment and software

Item name	Specifications and Supplier
<u>Electronic Equipment</u>	
Anaesthetic Machine	Stinger anaesthetic gas machine, DarvallVet, NSW, Australia
Bead steriliser	FST, Fine Science Tools, Vancouver, Canada
Centrifuges	Cell Culture/ Flow Cytometry – Eppendorf 5810R RNA – Eppendorf 5424R Giemsa stain-Thermo Shandon cytospin 4
CFX96 Touch Real-Time PCR Detection System	BIO-RAD Laboratories, CA, USA
Chemical Fume Hood	LabSystems, VIC, Australia
ChemiDoc™ MP Imaging system	#170-8280 BIO-RAD Laboratories, CA, USA
CO₂ asphyxiation machine	Quietek CO ₂ Induction System, Next Advance, NY, USA
Confocal microscopy	Leica TCS SP8, Leica, Wetzlar, Germany
Shandon Cytospin®4 Cytocentrifuge	Life Technologies, CA, US
Cryotome	Shandon Cryotome E, Thermo Scientific, MA, USA
Digital dry Bath	Corning LSE™, NY, USA
Extracellular flux analyser- Seahorse XFe-96	Agilent, Santa Clara, CA, USA
Embedder	HistoStar™ Embedding Workstation, ThermoFisher Scientific, MA, USA
Flow Cytometer	LSRFortessa™, BD Biosciences, CA, USA FACSCanto II™, BD Biosciences, CA, USA

	FACSAria™ Fusion Cell Sorter, BD Biosciences, CA, USA
Freezer	-20°C – Haier Biomedical, China -80°C – 89000 series, Thermo Scientific, MA, USA
Fridge	4°C – GPS series, Thermo Scientific, MA, USA
GloMax discover plate reader	Promega, WI, USA
IKAMAG™ multi-position magnetic stirrer	Sigma-Aldrich Inc., MO, USA
Incubator	Binder, LabFriend, Tuttlingen, Germany
Laser Doppler Imager	#MOORLDI2-IR, moor instruments, Devon, UK
Microscope Camera	AxioCam ERc 5s, Carl Zeiss Microscopy, Germany
Microscopes	<i>Dissecting</i> – Zeiss Stereo Discovery.V8, Carl Zeiss Microscopy, Germany <i>Inverted</i> – Olympus CKX31, Olympus Life Science, Tokyo, Japan <i>Light</i> – Zeiss Lab.A1, Carl Zeiss Microscopy, Germany
NanoDrop™ 8000 Spectrophotometer	Thermofisher Scientific, CA, USA
NanoZoomer HT Digital Scanner	Hamamatsu Photonics, Japan
pH meter	Metler Toledo, Vic, AU
Scales	#XS105, Mettler Toledo, OH, USA
T100 Thermal Cycler	BIO-RAD Laboratories, CA, USA
Tissue Culture Hood	CellGard™ ES (Energy Saver) NU-480 3ft Class II, Type A2 Biological Safety Cabinet, NuAire, MN, USA
Tissue Processor	Excelsior Tissue Processor™, Thermofisher Scientific, CA, USA
Vortex Mixer	Corning LSE™, NY, USA
Water bath	TW20 Julabo® Water bath, Sigma-Aldrich Inc., MO, USA
<u>Software</u>	

Adobe Photoshop	2019-2022, Creative Cloud, Adobe, CA, USA
Fiji (Image J)	Versions available in 2019-2022, NIH, MD, USA
FlowJo	Versions available between 2019-2022, BD Biosciences, CA, USA
Graph Pad Prism	Versions available in 2019-2022, GraphPad Software, LLC, CA, USA
Image Lab	BIO-RAD laboratories, CA, USA
moorLDL measurement	moorLD12-IR, Moor Instruments, Devon, UK
Microsoft Excel	Microsoft Excel® 2018 – 2021 versions, Microsoft Corporations, WA, USA
Microsoft Word	Microsoft Word® 2018 – 2021 versions, Microsoft Corporations, WA, USA
Wave	Versions available between 2019-2022, Agilent, CA, USA

2.2 Materials

Table 2.2: Materials and suppliers

Material	Catalog number (#) and Supplier
8-well Chamber Slides (removable)	#80841, ibidi, Gräfelfing, Germany
Biopsy punch (6mm)	#LIVBIOPUNCH06, Livingstone, NSW, Australia
Bottle-top vacuum filters polyethersulfone membrane, pore size 0.22 µm	#CLS431118-12EA, Sigma-Aldrich Inc., MO, USA
Brightline™ Haemocytometer	#Z359629, Sigma-Aldrich Inc., MO, USA
Castroviejo Callipers	#REF4050, Katalyst Surgical, MO, USA
Cautery Handle	#HIT1, Dalcross Medical Equipment, NSW, Australia
CellBIND® Surface Cell Culture	25cm ² - #CLS3289, Corning Incorporated, ME, USA
	75cm ² - #CLS3290, Corning Incorporated, ME, USA
CoolCell® Freezer Containers	#432000, Corning, NY, USA
Cell-strainer 40µm	#542040, Greiner Bio-One, Interpath Services, Victoria, Australia
Corning tissue-culture treated culture dishes 60mm x 15mm	#CLS430166, Invitro Technologies, VIC, Australia
Costar® Multiple well CellBIND® Cell Culture Plates	6 wells – #3516, Corning Incorporated, ME, USA
	12 wells – #3513, Corning Incorporated, ME, USA
	24 wells - #3738, Corning Incorporated, ME, USA
Costar® Ultra-Low Attachment Multiple Well Plates	6 wells – #3471, Corning Incorporated, ME, USA
	24 wells - #3473, Corning Incorporated, ME, USA
Countess cell counter chamber slides	#C10228, Life Technologies, CA, USA
Cryogenic vials	#431386, Corning, NY, USA

Easy strainer Green	#542040, Interpath, VIC, Australia
Embedding Cassette	#40634001, Techno Plas, SA, Australia
Ethylenediamine tetra acetic acid (EDTA) tubes	#22-040-035, Thermo Fisher Scientific, Australia
Eppendorf Tubes	1.5mL safe-lock tubes – #T9661, Sigma-Aldrich Inc., MO, USA 0.6mL tubes – # T5149, Sigma-Aldrich Inc., MO, USA 1.5mL tubes – #T6649, Sigma-Aldrich Inc., MO, USA 2.0mL tubes – #T3031, Sigma-Aldrich Inc., MO, USA
Falcon® Tubes	5mL Round bottom – #352003, Corning Incorporated, ME, USA 15mL – #352096, Corning Incorporated, ME, USA 50mL – #352070, Corning Incorporated, ME, USA
Filters	#SLGV033RS, 0.22µm, Millex® GV, Merk Millipore Ltd, Ireland
Fine surgical tools	Dumont Forceps #11254-20, FST, Vancouver, Canada Fine scissors 10.5cm #14094-11, FST, Vancouver, Canada Tough Cut Pattern Scissors #14054-13, FST, Vancouver, Canada Mini-perforated spoon #10370-19, FST, Vancouver, Canada Needle holder #12003-15, FST, Vancouver, Canada
Forceps	#14114, 15cm, 0.3mm tip, Coherent Scientific, SA, Australia
Glucometer	# 7400969032, Accu-Check, USA

Glucose strips	#497864, Accu-Check, USA
Hair removal cream	#2485516, Veet, Chemist Warehouse, SA, Australia
Iris scissors, 420SS. straight, 115mm	#TS0984, ProSci Tech, QLD, Australia
Needles	18G 1 1/2in - #302032, BD Biosciences, NJ, USA 19G 1 1/2in - #305187, BD Biosciences, NJ, USA 27 G x 1 1/2 in - #301629, BD Biosciences, NJ, USA
Opsite™	#4967, Smith & Nephew, London, UK
PAP pen for immunostaining, 2mm tip	#Z672548-1EA, Sigma-Aldrich Inc., MO, USA
Pipette Gun	Thermo Fisher Scientific, Australia
Pipettes 0.5-10 µl, 2-20 µl, 20-200 µl, 100-1000 µl	Eppendorf Research Plus Corning Lambda™ Plus, Corning Incorporated, ME, USA
Pointed tweezers, economy, style 5	#T05-811, ProSci Tech, QLD, Australia
Polyallomer Quick-Seal Centrifuge tubes	6.0mL - #58594, Beckman Coulter®, USA 40mL - #342414, Beckman Coulter®, USA
polypropylene round-bottom capped tubes	#14-959-11A, Thermofisher Scientific, CA, USA
Polystyrene Round-Bottom Tube with Cell-strainer cap	#FAL35225, Invitro Technologies, VIC, Australia
Polystyrene Test Tube without Cap, 12 x 75 mm	#FAL352008, Invitro Technologies, VIC, Australia
Seahorse XFe96 Fluxpak Mini 6 Assays	#SEA102601100, Agilent, USA
Scalpels	#0501, Swann-Morton®, Sheffield, England
Scintillation Vials	#Z376817, Sigma-Aldrich Inc., MO, USA

Shaver	#41590-0438, WAHL BravMini ⁺ , IL, USA
Silicone (0.5mm thick)	#P18178, Life technologies, CA, USA
Stripette® Serological Pipets	5mL – #4487, Corning Incorporated, ME, USA 10mL – #4488, Corning Incorporated, ME, USA 25mL – #4489, Corning Incorporated, ME, USA
Sutures	6-0 PROLENE™, 639G, Ethicon LLC, San Lorenzo, Puerto Rico 7-0 SILK, 768G, Ethicon LLC, San Lorenzo, Puerto Rico 8-0 PERMAHAND™, 818W, Ethicon LLC, San Lorenzo, Puerto Rico
Syringes	1mL - #SS+01T, Terumo, Tokyo, Japan 5mL - #SS05S, Terumo, Tokyo, Japan 10mL - #SS-10S, Terumo, Tokyo, Japan 20mL - #SS-20S2, Terumo, Tokyo, Japan 50mL – #SS*50ESE, Terumo, Tokyo, Japan
Tissue-tek® Cryomold	#4565, Sakura Finetek, C.A., USA
Transfer Pipets	#222, Samco Scientific, CA, USA
Vannas Scissors, delicate, straight, 3mm	#EMS72932-01, ProSci Tech, QLD, Australia

2.3 Reagents

Table 2.3: Reagents, chemicals and suppliers

Reagent	Catalog # and Supplier
Ammonium Chloride Solution	#07850, StemCell Technologies, Vancouver, Canada
Antibiotic Antimycotic Solution (100x)	#A5955, Sigma-Aldrich Inc., MO, USA
APC BrdU Flow Kit	#557892, BD Biosciences, NJ, USA
Antimycin	A8674-25MG, Sigma Aldrich Inc., MO, USA
Bovine Serum Albumin (BSA)	#A7906, Sigma Aldrich Inc., MO, USA
Brilliant Buffer Stain	#566349, BD Biosciences, NJ, USA
Buprenorphine	#TEMVET, Lyppard Australia Pty Ltd., Vic, Australia
Bupivacaine	#BUPIV1, Lyppard Australia Pty Ltd., Vic, Australia
Corn oil	#C8267-500ML, Sigma-Aldrich Inc., MO, USA
Citric acid	#C1909-500G, Sigma-Aldrich Inc., MO, USA
Carprofen	#ZENE, Lyppard Australia Pty Ltd., Vic, Australia
Chloroform	#AJA152-2.5L GL, Ajax Finechem, NSW, Australia
Cell recovery solution	#354253, Corning Incorporated, USA
Compensation Beads (Rat/Hamster)	#552843, BD Biosciences, NJ, USA

Cytofix Fixation Buffer	#554655, BD Biosciences, NJ, USA
Dimethyl sulphoxide (DMSO)	#D8418, Sigma Aldrich Inc., MO, USA
Dulbecco's Phosphate-buffered Saline 10x	#D1408, Sigma-Aldrich Inc., MO, USA
Dulbecco's Phosphate-buffered Saline 1x	#D8537, Sigma-Aldrich Inc., MO, USA
Dulbecco's Modified Eagle's Medium, High Modified (DMEM)	#D5030, Sigma Aldrich Inc., MO, USA
EGM-10	#CC-5035, Lonza, Basel, Switzerland
Enalapril	#E6888, Sigma-Aldrich, Inc., St Louis, MO, USA
Ethanol	#E7023, Sigma Aldrich Inc., MO, USA
Ethyl alcohol, Pure, for molecular biology	#E7023, Sigma Aldrich Inc., MO, USA
Fixable Viability Stain 700	#564997, BD Biosciences, NJ, USA
Foetal Bovine Serum (FBS)	#AU-FBS/PG, CellSera, NSW, Australia
Formaldehyde	#C004, ProSciTech, QLD, Australia
FCCP, mitochondrial oxidative phosphorylation uncoupler	#SEA103325100, Sigma-Aldrich Inc., MO, USA
Formalin	#HT501128, Sigma Aldrich Inc., MO, USA
Fractalkine	#F2302, Sigma-Aldrich Inc., MO, USA
Glycolysis assay substrate	#600451, Caymen chemical, MI, USA
Glycolysis assay enzyme mixture	#600452, Caymen chemical, MI, USA

Glycolysis assay cofactor	#600453, Caymen chemical, MI, USA
Glycolysis assay L-lactate standard	#600455, Caymen chemical, MI, USA
Glycolysis cell-based assay buffer	#10009322, Caymen chemical, MI, USA
Glucose-analog 2-NDBG glucose uptake kit	Ab235976, abcam, USA
Hanks' Balanced Salt Solution (HBSS)	#H9394, Sigma Aldrich Inc., MO, USA
Hydrogen peroxide solution	#216763, Sigma Aldrich Inc., MO, USA
Iscoe's Modified Dulbecco's Medium (IMDM)	Sigma Aldrich Inc., MO, USA
iScript cDNA Synthesis Kit	#1708841, Bio-Rad Laboratories, CA, USA
Isoprapanol	#I9516, Sigma-Aldrich Inc., MO, USA
L-glutamine	#G7513, Sigma-Aldrich Inc., MO, USA
Liberase™ Research Grade	#5401127001, Sigma-Aldrich Inc., MO, USA
Losartan	#61188, Sigma-Aldrich, Inc., St Louis, MO, USA
Matrigel™	#354234, Corning Inc, NY, USA
MethoCult GF M343, 100mL	#3434, StemCell Technologies, Vancouver, Canada
Mouse Inflammation CBA kit	#552364, BD Biosciences, NJ, USA
Mouse Inflammation Standards	#620290, BD Biosciences, NJ, USA
Murine M-CSF	#315-02-500, PeproTech, NJ, USA
Normal Horse Serum	#S2000, Vector Laboratories, CS, USA
Nuclease free water	#P1193, Promega, WI, USA

Opti-MEM™ I Serum Reduced Media	#31985070, Life technologies, CA, USA
Paraformaldehyde	#C004, ProSciTech, QLD, Australia
PBS control liposomes	clodronateliposomes.org, Vrije Universiteit, Netherlands
PD123,319	#PD186, Sigma Aldrich Inc., MO, USA
Penicillin-Streptomycin	#P433, Sigma-Aldrich Inc., MO, USA
Percoll	#P4937, Sigma-Aldrich Inc., MO, USA
Prolong Gold Antifade Mountant with DAPI	#P36935, Life Technologies, CA, USA
Propidium Iodide	#P4170, Sigma-Aldrich Inc., MO, USA
RNase A, DNase and protease-free	#G9545, Sigma-Aldrich Inc., MO, USA
Rotenone	R8875-1G, Sigma-Aldrich Inc., MO, USA
Sodium citrate tribasic dehydrate	#71402-250G, Sigma-Aldrich Inc., MO, USA
Sodium Azide	#SA189, Chem-supply, SA, Australia
Sodium Bicarbonate	#S5761, Sigma-Aldrich Inc., MO, USA
Sodium Hypochlorite 8-12.5%	#DT055-5L, ChemSupply, SA, Australia
Stain Buffer FBS	#554656, BD Biosciences, NJ, USA
Sucrose	#S0389, Sigma-Aldrich Inc., MO, USA
Tamoxifen	#T5648, Sigma-Aldrich Inc., MO, USA
Streptozotocin	#S0130-1G, Sigma-Aldrich Inc., MO, USA
TRI® Reagent	#T9424, Sigma-Aldrich Inc., MO, USA
Tris hydrochloride	#T3253, Sigma-Aldrich Inc., MO, USA

Triton X-100	#X100, Sigma-Aldrich Inc., MO, USA
Trypan Blue solution	#T8154, Sigma-Aldrich Inc., MO, USA
Trypsin-EDTA	#15400054, ThermoFisher Scientific, MA, USA
Tween®-20	#P9416, Sigma-Aldrich Inc., MO, USA
Type IV collagenase	#C4-BIOC, Sigma-Aldrich Inc., MO, USA
Oligomycin	#SEA103325100, Sigma-Aldrich Inc., MO, USA

2.4 Supplemented culture media

2.4.1 Dulbecco's Modified Eagle's Medium, High Modified (DMEM)

DMEM was supplemented with 10% FBS, 1% antimycotic/antibiotic solution. Stored at 4°C.

2.4.2 Endothelial Cell Growth Media (EGM)

EGM was supplemented with 10% FBS, 1% antimycotic/antibiotic solution to obtain EGM-10.

EGM-10 contains 20 ng/mL each of vascular endothelial growth factor (VEGF), platelet-derived growth factor (PDGF) and fibroblast growth factor (FGF). Stored at 4°C.

2.4.3 Freezing Media

Supplemented with FBS with 10% DMSO. Filtered and stored at 4°C.

2.4.4 Iscove's Modified Dulbecco's Medium (IMDM)

IMDM supplemented with 10% FBS and 1% antimycotic/antibiotic solution. Stored at 4°C.

2.5 Animal procedures

2.5.1 Animal ethics

All experimental procedures in animals and animal care were performed in accordance with the National Health and Medical Research Council (NHMRC) research guidelines and Australian Code for the Care and Use of Animals for Scientific Purposes.

Ethics approvals were obtained from South Australian Health and Medical Research Institute (SAHMRI) (ID SAM117, ID SAM20.032 and SAM432.19).

2.5.2 Mice

C57BL/6 (C57BL/6J) mice were available in the animal facility at SAHMRI. *Rosa*^{mTmG} (Gt(ROSA)26Sor^{tm4}(ACTB-tdTomato,-EGFP)Luo/J), *Csf1r*^{Mer-iCre-Mer} (FVB-Tg(Csf1r-cre/Esr1*)1Jwp/J) and UBI-GFP (C57BL/6-Tg(UBC-GFP)30Scha/J) strains, were purchased from The Jackson Laboratory (Bar Harbor, ME, USA). *Csf1r*^{Mer-iCre-Mer} mice were maintained on a mixed FVB and C57BL/6J background. *Csf1r*^{Mer-iCre-Mer} mice were crossed with *Rosa*^{mTmG} mice to obtain *Csf1r*^{Mer-iCre-Mer} x *Rosa*^{mT/mG} mice. Mice were housed in SAHMRI animal care facility and maintained on a standard chow diet.

For studies in Chapters 3-5, embryonic age of mice was defined based on the day of vaginal plug formation, which was set as E0.5. Plug was detected by examining the vaginal opening of female mice for a whitish mass (532). In Chapters 4 and 5, to achieve Cre-Lox recombination in *Csf1r*^{Mer-iCre-Mer} x *Rosa*^{mT/mG} mice, 75µg/g of 4-hydroxytamoxifen (TAM) dissolved in corn oil was intraperitoneally injected into pregnant dams at E8.5.

For analysing the cell cycle status of different cell populations in different tissues, 1 mg of bromodeoxyuridine (BrdU) was injected intraperitoneally before euthanasia and tissue harvested at times specified in Chapters 4 and 5.

In all instances, euthanasia was performed under isoflurane anaesthesia by cardiac puncture or CO₂ asphyxiation (following SAHMRI SOP-0491 and SOP-0501 for humane killing methods for mice). Death of an animal was determined by loss of breathing, changes in eye colour and toe-pinch tests. Blood was collected by cardiac puncture using a 100µL syringe with a 27G needle and aliquoted into ethylenediamine tetra acetic acid tubes (EDTA). The heart and aorta were flushed with cold phosphate buffer solution (PBS) before harvesting tissues.

2.6 Preparation of single cells

2.6.1 Preparation of aortic, skin, and skeletal muscle cells

Tissues were harvested from mice immediately after euthanasia to prepare single cell disaggregates of aorta (or aortic adventitia), skin comprising epidermis and dermis, but not subcutaneous fat and gastrocnemius, soleus, and quadriceps skeletal muscle (SkM). Aortas were dissected out intact, along their entire length from aortic valve to iliac bifurcation and flushed extensively with PBS, before dissection of surrounding perivascular fat and, where indicated, careful separation of the adventitia, under a dissecting microscope. Once all tissues were harvested, each was cut into smaller pieces with sterile surgical blades and digested with LiberaseTM (50 µg/ml) for up to 1.5 h at 37°C (vortexing every 30 min). Tissue digests were then passed through a 40 µm nylon mesh and neutralised in IMDM and washed before performing cell counts.

2.6.2 Preparation of brain cells

The brain was carefully removed from cephalic mesenchyme and meninges, dissected out, minced, and incubated in LiberaseTM (50 µg/ml) for 2 h (533). The suspension was then passed through a 40 µm nylon mesh. Digests of brain were resuspended in 37% isotonic Percoll and underlayered with 70% isotonic Percoll and centrifuged at room temperature at 600 *g* for 25 min. Cells in the interface were collected and cell counts were performed.

2.6.3 Preparation of blood

Blood was collected by cardiac puncture in EDTA coated blood collection tubes. For blood samples of less than 1 mL, PBS was added to make up the volume to 1 mL. Erythrocytes were lysed in a 1:10

dilution of ammonium chloride (0.15 M) at 4°C for 10 min and the resulting suspension was washed and resuspended in IMDM, before performing total white cell counts.

2.6.4 Preparation of bone marrow (BM)

Following euthanasia, BM cell suspensions were prepared by snipping femurs and tibias from mice at each end, then centrifuging at 800 g for 2 min at 22°C in a perforated (made with a 19 G needle) 2 mL microcentrifuge tube, containing 500 µL of PBS. The flow-through was collected and resuspended in an additional 500 µL of PBS to make a total volume of 1 mL. This BM cell suspension was incubated in a 1:10 dilution of ammonium chloride (0.15 M) at 4°C for 8 min, following which the cells were washed and resuspended in IMDM before performing cell counts.

2.6.5 Cell counts and viability

Cell viability was assessed by diluting samples with 0.1% trypan blue solution to stain dead cells followed by cell counting. For counting cells, 10 µL of cell suspension was transferred to a haemocytometer counting chamber. The average number of cells per square in the central large square were counted to calculate the concentration of cells as follows:

$$\text{Cell concentration (cells/mL)} = \text{average number of cells per square} \times \text{dilution factor} \times 10^4$$

2.7 In vivo techniques

2.7.1 Streptozotocin (STZ)-induced type 1 diabetes model

C57BL/J, UBI-GFP and *Csf1r*^{Mer-iCre-Mer} x *Rosa*^{mT/mG} mice ~8 w of age, were weighed and fasted for 4 h prior to STZ injection. Sodium citrate buffer was prepared by mixing 0.1 M citric acid and 0.1 M sodium citrate. pH was adjusted to 4.5 using a pH meter and buffer passed through a 0.22 µm Millipore™ filter to remove any debris. Immediately prior to injection, STZ was carefully weighed out in a fume hood, protected from light, and suspended in the pre-made buffer (25 mg/ml). Mice were then injected a dose of 165 µg/g per mouse i.p. and housed in cytotoxic cages for 72 h prior to cage change. A cohort of mice were injected with sodium citrate buffer as sham (STZ-) controls (534).

One-week post-injection, blood was drawn via tail-vein bleeds using sterile scalpels and blood glucose concentration (BGC) tested using a glucometer. A second STZ injection was administered if the BGC was <15 mM by repeating the above procedure. Mice were deemed diabetic if BGCs were >15 mM. Following induction of diabetes, mice were weighed every day for three weeks and BGCs were taken weekly. Both male and female mice were used in each strain of mice.

2.7.2 Hind limb ischaemia

Hind limb ischaemia surgeries were performed for studies in Chapters 5 using a well-established model (535). Surgeries were performed under general anaesthesia utilising 2-5% isoflurane. To induce hind limb ischaemia, the proximal portion of the left femoral artery and the distal saphenous artery were both suture ligated, as well as the popliteal artery and all branches in between, and an arterectomy performed to remove the intermediate segment of vessel. Blood flow through the ischaemic (left) and nonischaemic (right) limbs was immediately measured to determine perfusion

ratio and compared to pre-surgical baseline using laser Doppler perfusion imaging. Once adequate ischaemia was confirmed by the complete absence of blood perfusion, the surgical site was closed. Mice were recovered from anaesthesia and given 0.1 mg of Buprenorphine via subcutaneous injection on the day of surgery and 24 h later for analgesia.

For adoptive cell transfer studies, 12 w STZ+-diabetic male and female adult C57BL/6 mice were used as recipients and both non-diabetic (STZ-) and diabetic (STZ+) UBI-GFP mice as donors. EndoMac progenitors were obtained from CFU-M (section 2.9.1.1) after 14 d of culturing SkM digests from STZ- or STZ+ adult UBI-GFP mice in methycellulose. GFP⁺ progenitors (7.5×10^5 in 60 μ L MatrigelTM) were administered as a single intramuscular injection (27 G needle) into the gastrocnemius muscle in the ischaemic limb of diabetic 12 w C57BL/6 recipients immediately after surgery. In each experiment, a control group received injections of MatrigelTM without cells (60 μ L). Mice were recovered following closure of surgical site, and then Laser Doppler perfusion scans repeated at 0, 3, 7 and 14 d under general anaesthesia to determine the perfusion ratio between the ischaemic and non-ischaemic limbs. Euthanasia was performed after the final scan on day 14. Peripheral blood was taken by cardiac puncture, while muscle from both hind limbs was harvested and processed for, 1) haematopoietic colony forming unit (CFU) assays, 2) flow cytometry or 3) immunofluorescence staining and confocal microscopy, to detect engraftment of donor GFP⁺ cells, their cellular fate and vasculogenic capacity.

Additional experiments were performed without cell transfer, to study the prevalence, cell cycle status and developmental origins of EndoMac progenitors, macrophages (M Φ) and endothelial cells (EC) in hind limb muscles at different time-points after ischaemia. These experiments were performed in E8.5 TAM-induced adult (12 w) female and male *Csf1r*^{Mer-iCre-Mer} x *Rosa*^{mT/mG} mice in which diabetes

was induced three weeks prior to surgery as described above. BGCs were measured before surgery and on the day of euthanasia. Their non-diabetic counterparts were used as a comparator. Mice were sacrificed at 1, 3, 7 or 14 d after ischaemia surgery and different tissues (muscle from both limbs, brain, blood) were harvested and processed for CFU assays, flow cytometry or immunofluorescent staining and confocal microscopy. For the day 1 time-point, BrdU was administered 1 h prior to sacrifice to analyse the cell cycle status of different YS-derived GFP⁺ populations in ischaemic muscle.

2.7.3 Wound healing

For wound healing studies in Chapter 4, 12 w female and male C57BL/6 and *Csf1r*^{Mer-iCre-Mer} x *Rosa*^{mT/mG} mice underwent surgery to create a well validated model of skin wound injury (536). Mice were anaesthetised with isoflurane and hair removed from their upper dorsal skin using clippers and depilatory cream. Two full thickness excision wounds that included the *panniculus carnosus* were created on either side of the dorsal midline. A 0.5mm thick silicone splint was secured around the wound using an adhesive and interrupted 6-0 PROLENETM sutures to prevent healing via contraction. All wounds were covered with OpsiteTM dressings. Mice were recovered from anaesthesia and given 0.1 mg of Buprenorphine via subcutaneous injection on the day of surgery and 24 h later for analgesia. For adoptive cell transfer studies, STZ-injected, diabetic male and female adult C57BL/6 mice were used as recipients and non-diabetic (STZ-) and diabetic (STZ+) UBI-GFP mice as donors. EndoMac progenitors were obtained from CFU-M (section 2.8.1.1) after 14 d of culturing skin digests from STZ- or STZ+ adult GFP mice in methylcellulose. GFP⁺ progenitors (7.5x10⁵ in 60 µL MatrigelTM) were injected around the circumference of one of the two newly created wounds using a 27 G needle, with the other receiving MatrigelTM without cells (cell-free control), or a. BGCs were measured before surgery and on the day of euthanasia. Wound sizes were measured daily for 14 d using a standard Vernier calliper in two perpendicular dimensions. Mice were harvested at day 14 and skin from each

wound site harvested. Half of the wound was used to prepare skin digests for flow cytometry, and the remainder fixed in 30% sucrose and 10% formalin for embedding in optimal cutting temperature (O.C.T) compound and later sectioning and immunofluorescent staining.

Additional experiments were performed without cell transfer, to study the prevalence, cell cycle status and developmental origins of EndoMac progenitors, macrophages (MΦ) and endothelial cells (EC) in skin at different time-points after wound injury. These experiments used adult (12 w) female and male E8.5 TAM-induced *Csf1r*^{Mer-iCre-Mer} x *Rosa*^{mT/mG} mice that were i.p injected with sodium citrate buffer or STZ, three weeks prior to surgery as above. BGCs were checked before surgery and on the day of euthanasia. Mice were euthanised at 1, 3, 7 or 10 d and different tissues (both wounds, brain and blood) were harvested and processed for CFU assays, flow cytometry or immunofluorescent staining and confocal microscopy. For the day 1 time-point, BrdU was administered 1 h prior to sacrifice to analyse the cell cycle status of different YS-derived GFP⁺ populations in skin.

2.8 *In vitro* methods

2.8.1 Primary cultures

2.8.1.1 *Colony-forming unit (CFU) assay*

Clonogenicity of EndoMac progenitors was assessed by establishing primary (1°) CFU cultures, as described (517, 518, 530). Briefly, 2×10^5 freshly isolated cells from aorta, skin and SkM were plated in methylcellulose in 24 well plates. In glucose exposure studies, cells were cultured in the presence or absence of different concentrations of D-glucose (5 mM, 15 mM, 25 mM) or 25 mM mannitol as an osmolarity control. Cultures were replenished every three days with respective glucose/ mannitol concentrations. After 14 d, CFUs were counted by light microscopy and classified by colony subtype (e.g. CFU-M) and size, using published morphological criteria. By definition, CFUs comprised a minimum of 30 cells.

2.8.1.2 *CFU-M renewal assay*

CFU-M renewal assays were performed by carefully harvesting individual 1° CFU-M from methylcellulose under light microscopy with a 10 μ L pipette. The cells contained in each individual CFU-M were disaggregated by vortexing, and re-plated as single cells in methylcellulose in 96-well plates. In studies with glucose, cells were cultured as mentioned above. Wells were inspected the following day (1 d) to confirm their content of single cells and rule out cell couplets or clumps. They were subsequently imaged daily until 14 d to document and quantify the emergence of new 2° colonies from individual cells.

2.8.1.3 MatrigelTM-based cord formation assay

EndoMac progenitors were obtained by harvesting day 14 aortic, skin and SkM CFU-M from methylcellulose, and then disaggregating into single cell suspensions, with gentle vortexing. Progenitors were then resuspended in 200 μ L of EGM-10 and plated on 80 μ L of growth factor-reduced MatrigelTM at 3×10^4 cells per well in 96-well plates, to study their capacity to form angiogenic cord networks over time. For glucose exposure studies, cells were cultured in the presence of different concentrations of glucose or mannitol, as described above. From 24 h onward, wells were inspected daily and photographed by light microscopy until day 7 to detect the presence of cords, identified as cellular extensions linking cell masses or branch points. Images were captured at 10x magnification in five different regions (upper centre, centre, lower centre, left centre, right centre) to encompass the entire well. Total cord length, cord number and the number of branching points were quantified from each image using Image J software. For the purposes of flow cytometry analysis, MatrigelTM was liquidised by incubation with 1 mL of CorningTM cell recovery solution and was digested with collagenase in 4°C for 1.5 h. The cell suspension was stained for progenitor, M Φ and EC markers and analysed via flow cytometry (section 2.11.1) (520) .

2.8.1.4 Glycolysis assay

Progenitor cells were obtained from freshly harvested 1° CFU-M and made up as single cell suspensions in IMDM, which were then incubated overnight at 37°C at a density of 7×10^3 cells per well in a 96-well plate. L-lactate standards and the reaction solution were prepared according to the Glycolysis cell-based assay kit protocol. Following incubation, the plate was centrifuged at 1000 g for 5 min and 10 μ l of the supernatant transferred into a new 96-well plate with Assay buffer, as specified in the protocol. This was then incubated for 30 min at room temperature on an orbital shaker with the reaction solution prepared above. The absorbance was measured at 490 nm using the GloMax discover plate reader.

The average absorbance of each standard and sample was determined and corrected by subtracting it with the absorbance value of the blank standard. The corrected absorbance value of each standard was plotted as a function of the final concentration of lactate for a typical standard curve and the L-lactate concentration for each sample calculated using the corrected absorbance with the following equation:

$$L - \text{lactate (mM)} = \left[\frac{\text{Absorbance} - (y - \text{intercept})}{\text{Slope}} \right] \times 1$$

2.8.1.5 Glucose uptake assay

Primary CFU-M were freshly harvested, and progenitors incubated (in IMDM for 2 h with 2-NBDG (150 ug/mL) at 37°C at a density of 7 x10³ cells per well in a 96-well plate, in accordance with the 2-NBDG glucose uptake assay kit. The plate was centrifuged at 400 g at room temperature and the supernatant then aspirated. Cells were washed with Cell-based Assay buffer and immediately analysed for fluorescence (Ex/Em = 485/535 nm) using the GloMax discover plate reader.

2.8.1.6 Seahorse assay

Skin and SkM digests were cultured in methylcellulose from STZ (+) and STZ (-) C57BL/6 mice, and were exposed to different concentrations of glucose as specified above. 24 h prior to performing metabolic analysis using the Seahorse assay, EndoMac progenitor cells were isolated from day 14 1° CFU-M and replated in DMEM culture medium in XF24 cell culture plates (40,000 cells/well) and incubated in 5% CO₂ at 37°C overnight. Background temperature correction wells were left blank. The sensor cartridge was hydrated by addition of milliQ water to each well of the utility plate and

was incubated in a non-CO₂ incubator at 37°C overnight. Further, the Seahorse instrument and the XF24 software was turned on and pre-heated to 37°C.

On the day of assay run, XF media was prepared with supplementation of 1 M glucose. The culture plate was then washed and replaced with prewarmed XF media. Following confirmation of cell adhesion to the bottom of the wells by light microscopy, the plate was incubated in a non-CO₂ incubator at 37°C for 1 h. The utility plate of the hydrated sensor cartridge was replaced with calibrant and incubated in a non-CO₂ incubator at 37°C for 1 h. The XF Cell Mito Stress Test experimental design template was selected using the Wave software. The sensor cartridge ports were then injected with diluted inhibitors and run on the machine for cartridge calibration. Inhibitors and their respective ports are shown in **Table 2.4**. Finally, following completion of calibration, the culture plate was loaded into the machine and the assay was run.

Table 2.4: Mitochondrial Inhibitors

Compound	Injection port	Concentration (μM)	Injection Volume (μL)
Oligomycin	A	1.5	20
FCCP	B	0.5	22
Rotenone/Antimycin	C	0.5	20

2.9 Immunostaining

2.9.1 Immunofluorescence labelling and confocal microscopy

Tissue samples were harvested from mice and placed in 10% formalin for 24 h, followed by 30% sucrose overnight and then embedded in O.C.T. and stored at -80°C for later use. 5 µm thick frozen sections were cut, fixed in 10% formalin for 7 min and then washed under running water for 7 min. Endogenous peroxidase was blocked with 3% hydrogen peroxide in methanol for 30 min at room temperature. Slides were washed 3 times for 5 min each using 1x PBS and then antigen retrieval was performed in Citrate Buffer (10 mM sodium citrate, pH 6) at 37°C for 30 min followed by cooling before blocking. Sections were blocked with 3% normal horse serum for 30 min, and then incubated with primary antibodies overnight at 4°C. The following day, slides were incubated with fluorophore conjugated secondary antibodies (1:250, Invitrogen) for 1 h in dark at room temperature. Primary and secondary antibodies were diluted in 3% normal horse serum. Nuclei were stained with mounted with DAPI mounting medium (Invitrogen). and imaged on Leica TCS laser scanning confocal microscope system (Leica TCS SP8X/MP, Wetzlar, Germany) using 40-60x objective.

2.9.2 Cytoimmunofluorescence

Single cell suspensions were prepared from cultured CFU-M and cord-networks formed in Matrigel™. For cytopsin preparations, 100 µL of cell suspension was placed into Shandon single cytofunnels (EPKM5991040, EpreDia™) and centrifuged onto coated cytoslides (EPKM5991056, EpreDia™) at 1000 rcf for 5 min on Shandon Cytospin®4 Cytocentrifuge (Life Technologies, CA, US). Slides were fixed in 4% paraformaldehyde (PFA) for 10 min at room temperature. Blocking and permeabilisation were performed with 5% normal horse serum and 0.1% Triton for 30 min, and then hybridisation with primary (1°) antibody overnight at 4°C followed by secondary (2°) antibody for 45 min at 37°C. All antibodies were diluted in 3% normal horse serum. Nuclei were counterstained

with DAPI. Imaging was carried out by confocal microscopy with a TCS SP8X/MP laser scanning confocal microscope (Leica Microsystems). Images were analysed using ImageJ software.

Table 2.5: Reagents used for immunostaining

<i>Antibody</i>	<i>Concentration</i>	<i>Catalog # Manufacturer</i>
<u>Controls</u>		
<i>Goat IgG, polyclonal</i>	50 μ M	#026202, Invitrogen, MA, USA
<i>Rat IgG, polyclonal</i>	5 μ M	#NBP1-71666, Novus Biologicals, USA
<i>Rabbit IgG, polyclonal</i>	16 μ M	#ab172730, Abcam, Cambridge, UK
<i>Chicken IgY, polyclonal</i>	10 μ M	#AB-101-C, R&D system, MN, USA
<u>Primary antibodies</u>		
<i>Chicken anti-GFP</i>	2 μ M	#ab13970, Abcam, Cambridge, UK
<i>Rat anti-mouse CD68</i>	10 μ M	#MCA1957GA, Bio-Rad, Laboratories, CA, USA
<i>Goat anti-mouse Endomucin</i>	2 μ M	#AF4666, R&D Systems, MN, USA
<i>Rabbit anti-Ki67</i>	10 μ M	#ab16667, Abcam, Cambridge, UK
<i>Goat anti-mouse c-kit</i>	2 μ M	#AF1356, R&D Systems, MN, USA
<u>Secondary antibodies</u>		
<i>Donkey anti-Chicken AF488</i>	8 μ M	#SAB4600031-250UL, Sigma, USA

<i>Donkey anti-Rat AF594</i>	8 μ M	#A21209, Life Technologies, CA, USA
<i>Donkey anti-Goat AF488, AF647</i>	8 μ M	#A32814, #A32849, Life Technologies, CA, USA
<i>Donkey anti-Rat AF488</i>	8 μ M	#A21208, Life Technologies, CA, USA
<i>Donkey anti-Rabbit AF647</i>	8 μ M	#A32795 Life Technologies, CA, USA
<u>Other</u>		
<i>Horse serum</i>		#H1138, Sigma-Aldrich Inc., MO, USA
<i>DAPI</i>		#P3935, Life Technologies, CA, USA
<i>Mounting medium</i>		#S36920-5X2ML, ThermoFisher Scientific, CA, USA

2.10 Protein analysis

2.10.1 Flow cytometry

Single cell suspensions from tissues (aorta, skin and muscle) were resuspended in aliquots of $\leq 10 \times 10^6$ cells in 1 ml of 1 X PBS / 5% FBS / 0.2% sodium azide (FACS wash). 1 μ l of fixable viability stain 700 was added to each sample and incubated for 15 min on ice. After washing, samples were blocked for 5 min on ice with purified rat anti-mouse CD16/CD32 (BD Pharmingen, San Diego CA, USA) antibody. Cells were then incubated for 30 min with primary antibodies (1:10) (Table 2.10.1). Samples were washed and fixed in FACS fix (1x PBS containing 2% glucose (w/v), 1% formaldehyde (v/v), 0.02% sodium azide) for analysis with a BD LSRFortessa™ X-20 flow cytometer equipped with BD FACSDiva Software. Data were analysed using FlowJo version 9 software (Tree Star Inc., Ashland, OR, USA). For analysis, gating was performed based on FSC-A (to exclude cell debris), single cells and cells selected by viability stain, and fluorescence-minus-one (FMO) controls (≤ 1) to determine the positive percentage of cells with expression of different surface markers. FACSFusion™ cell sorter (BD Bioscience) was used to sort cells for primary cultures.

For mitochondrial evaluation, single cell suspensions were incubated with MitoTrackers™ (50 nM) and MitoSOX™ (50 nM) for 30 mins and fixed with FACS fix (1x PBS containing 2% glucose (w/v), 1% formaldehyde (v/v), 0.02% sodium azide) (537).

BD Pharmingen BrdU Flow Kit was used for cell cycle analysis. Briefly, after cells were stained with surface antigens, they were fixed and permeabilised with BD Cytofix Cytoperm Buffer and BD Cytoperm Permeabilization Buffer Plus as per manufacturer's instructions. Cells were then treated with DNase to expose incorporated BrdU that was stained. 7-aminoactinomycin (7-AAD) was added 15 min prior to data acquisition.

Table 2.6 :Reagents used for flow cytometry

<i>Reagents</i>	<i>Catalog # Manufacturer</i>
<u><i>Conjugated primary antibodies</i></u>	
<i>AF647 Mouse anti-mouse CX3CR1</i>	#149004, BioLegend, CA, USA
<i>APC Rat anti-mouse CD115</i>	#17-1152-82, eBioscience, CA, USA
<i>APC Anti-BrdU</i>	#555627, BD Pharmingen™, NJ, USA
<i>APC-Cy™7 Rat anti-CD11b</i>	#557657, BD Pharmingen™, NJ, USA
<i>BUV395 Mouse anti-mouse CD45.2</i>	#564616, BD Horizon™, CA, USA
<i>BUV395 Mouse anti-mouse CD45.2</i>	#564616, BD Horizon™, CA, USA
<i>BV421 Rat anti-mouse CD115 (CSF1R)</i>	#135513, BioLegend, CA, USA
<i>BV421 Rat anti-mouse CD31</i>	#563356, BD Horizon™, CA, USA
<i>BV421 Rat anti-mouse CD34</i>	#562608, BD Horizon™, CA, USA
<i>BV421 Rat anti-mouse CD115 (CSF1R)</i>	#135513, BioLegend, CA, USA
<i>BV421 Rat anti-mouse Ly-6A/E</i>	#562729, BD Horizon™, CA, USA
<i>BV421 Rat anti-mouse CD34</i>	#562608, BD Horizon™, CA, USA

<i>BV510 Rat anti-mouse Gr-1 (Ly6G/Ly6C)</i>	#108438, BioLegend, CA, USA
<i>BV421 Rat anti-mouse Ly- 6A/E</i>	#562729, BD Horizon™, CA, USA
<i>BV605 Rat anti-mouse Flt-1 (VEGFR2)</i>	#745220, BD OptiBuild™, CA, USA
<i>BV510 Rat anti-mouse Gr-1 (Ly6G/Ly6C)</i>	#108438, BioLegend, CA, USA
<i>BV785 Mouse anti-mouse CX₃CR1</i>	#149029, BioLegend, CA, USA
<i>BV785 Rat Anti-mouse Ly- 6A/E</i>	#563991, BD Horizon™, CA, USA #
<i>FITC Anti-mouse F4/80</i>	#123108, BioLegend, CA, USA
<i>BV785 Rat Anti-mouse Ly- 6A/E</i>	#563991, BD Horizon™, CA, USA
<i>FITC Rat anti-mouse CCR2</i>	#150608, BioLegend, CA, USA
<i>FITC Anti-mouse F4/80</i>	#123108, BioLegend, CA, USA
<i>FITC Rat anti-mouse CCR2</i>	#150608, BioLegend, CA, USA
<i>PE Rat anti-mouse CD115 (CSF1R)</i>	#12115281, eBioscience™, CA, USA
<i>Pe/Cy7 Anti-mouse F4/80</i>	#123141, BioLegend, CA, USA
<i>Pe/Cy7 Rat anti-mouse CD144 (Ve-Cadherin)</i>	#138016, BioLegend, CA, USA #
<i>Pe/Cy7 Anti-mouse F4/80</i>	123141, BioLegend, CA, USA

<i>PE-CF594 Hamster anti-mouse CD11cPe/Cy7 Rat anti-mouse CD43</i>	#562454, BD Pharmingen™, NJ, USA#562866, Rat Pharmingen™, NJ, USA
<i>PE-CF594 Rat anti-mouse CD117 (c-Kit)</i>	#562417, BD Horizon™, CA, USA
<i>PerCp-Cy™5.5 Rat anti-mouse CD31</i>	#562861, BD Pharmingen™, NJ, USA
<i>PerCp-Cy™5.5 Rat anti-mouse CD45R/B220</i>	#552771, BD Pharmingen™, NJ, USA
<i>PerCp-Cy™5.5 Rat anti-mouse CD3</i>	#560527, BD Pharmingen™, NJ, USA
<i>PerCp-Cy™5.5 Rat anti-mouse Ly-6G</i>	#560602, BD Pharmingen™, NJ, USA
<i>PerCp-Cy™5.5 Rat anti-mouse CD31</i>	#562861, BD Pharmingen™, NJ, USA
<i>PerCp-Cy™5.5 Rat anti-mouse Ter-119</i>	#560512, BD Pharmingen™, NJ, USA
<i>BV421 Rat anti-mouse H2AX</i>	#564720, BD Horizon™, CA, USA
<u>Others</u>	
<i>7-AAD</i>	#559925, BD Pharmingen™, NJ, USA
<i>BD™ Comp beads anti-mouse Ig,</i>	#51-90-9001229, BD Biosciences, CA, USA
<i>BD™ Comp beads anti-rat and anti-hamster Ig,</i>	#51-90-9000949, BD Biosciences, CA, USA

<i>BD™ Comp beads negative control</i>	#51-90-9001291, BD Biosciences, CA, USA
<i>Brilliant Stain BufferBD™</i>	#566349, BD Biosciences, CA, USA
<i>CytofixBD™</i>	#554655, BD Pharmingen™, NJ, USA
<i>Fixable Viability Stain 700</i>	#564997, BD Horizon™, CA, USA
<u>MitoSOX™ Red, APC</u>	#M36008, ThermoFisher Scientific, MA, USA
<u>MitoTracker™ Red</u> <u>CMXRos, PE</u>	#M7512, ThermoFisher Scientific, MA, USA
<u>MitoTracker™ Green, FITC</u>	#M7514, ThermoFisher Scientific, MA, USA
<i>Propidium Iodide (PI)</i>	#P4170, Sigma-Aldrich Inc., MO, USA
<i>Stain Buffer (FBS)</i>	#554656, BD Pharmingen™, NJ, USA

2.11 Molecular biology techniques

2.11.1 RNA isolation from cells and tissues

Following experimental treatments, cells were washed twice with cold 1 x PBS. Total RNA was extracted by scraping cells in 500 μ L of TRI reagent (per well in a 6-well plate) before transferring the lysates to autoclaved 1.5 mL Eppendorf tubes. Similarly, 500 μ L TRI reagent was added to homogenise tissues in an autoclaved 1.5 mL Eppendorf tubes. 50 μ L 1-bromo-3-chloropropane (BCP) was added to each sample and the tubes were vigorously vortex mixed for 15 sec to ensure complete mixing of both aqueous and organic phases. Samples were then centrifuged at 14,000 g for 15 min at 4°C. The topmost aqueous layer was carefully transferred to a fresh autoclaved 1.5 mL tube containing 250 μ L of isopropanol prior to precipitation at –80°C at least overnight. The samples were then briefly vortex mixed and centrifuged at 14,000 g for 15 min at 4°C. The supernatant was carefully removed, and the remaining cell pellet was washed with 250 μ L ice-cold 70% (v/v) molecular-grade ethanol. The samples were vortex mixed and centrifuged again at 14,000 g for 10 min at 4°C. The ethanol wash was removed, and the pellet allowed to air-dry in a fume hood for 5-10 min prior to dissolution in 20 μ L of nuclease-free water pre-warmed to 60°C. To facilitate complete dissolution, samples were further agitated in a Thermoshaker at 300 g for 5 min at 60°C. The extracted RNA was kept on ice or stored at –80°C prior to quantitation.

2.11.2 RNA quantification

The quantity of RNA in each sample was determined using a Agilent 2200 TapeStation System and Qubit. Samples with RNA Integrity Number (RIN) ≥ 7 , were considered suitable for RNASeq.

2.11.3 Bulk-RNA-sequencing

2.11.3.1 RNA extraction

Cell suspensions from aorta, muscle and skin from 12-week-old C57BL/6 mice were cultured in methylcellulose for 14 days for CFU-M formation. The resulting CFU-M cells from tissues from 3-4 mice (Male and Female) were harvested and pooled for RNA extraction. Total RNA was extracted from four independent pools of CFU-Ms from a tissue as mentioned above.

2.11.3.2 Library preparation and RNA Sequencing

mRNA sequencing libraries were prepared, and bulk RNA sequencing performed at the South Australia Genomics Centre (SAGC, SAHMRI, Adelaide, Australia). Briefly, poly-A RNA libraries were generated according to the Nugen Universal Plus mRNA-seq (Part No. 0508) protocol M01442 v2 (Illumina) and included 13 cycles of amplification. Equimolar pools of libraries were prepared and converted into MGI compatible libraries using MGIEasy Universal Library Conversion Kit (Part No. MGI1000004155, Cat. No.: 1000004155). Paired-end sequencing (98bp + 8 bp UMI (Unique Molecular Identifier)) was performed using the MGI DNBSEQ-G400 chemistry and MGI FCL (2 x 100) Flowcell (MGISEQ-2000RS FCL PE200).

2.11.3.3 Data analysis

Data analysis was performed using the R package (version 4.2.1) and standardised data processing pipeline at the SAGC. In brief, raw data was processed to obtain FASTQ data that was aligned to the mouse genome (version 1.4) for gene annotation and generation of gene count matrix; gene information was obtained from Ensembl (release 107). All genes with zero counts across all samples were removed and data normalised employing Trimmed Mean of M-values (TMM) method to

normalise counts according to library size differences between samples. Principal component analysis was performed to assess similarity of samples within a group and differences between groups. After filtering low-expressed genes, genes with at least 1 cpm in 3 samples (1 cpm ~ average around 35 reads aligned to a gene based on library size) were retained for differential gene expression analysis. *voom* transformation was applied to transform the discrete counts into log2-counts per million (log2 CPM) and differential gene expression analysis performed using *limma-voom* to determine significant differences. For each comparison, differentially expressed genes were defined by False Discovery Rate (FDR) of <0.05. Data visualisation was with volcano plots, venn diagrams and heat maps.

2.11.3.4 Bioinformatic analysis

Bioinformatic analysis of differentially expressed genes was performed using InnateDB (538). To identify gene ontology terms and molecular pathways associated with differentially expressed genes in a comparison, gene ontology and pathway over-representation analyses were undertaken considering differential expression with log2FC cut off 1.0 and associated adjusted p value cut off 0.05. Analyses were performed using hypergeometric algorithm and Benjaminin & Hochberg correction for multiple testing with FDR of 0.05.

2.12 Statistical analysis

Statistical analyses were performed with Excel (Microsoft) and Prism version 9 (GraphPad Software, Inc.). Data sets were tested for normality of distribution by Shapiro-Wilk test. Statistical comparisons were performed with parametric or non-parametric unpaired or paired two-sample *t*-tests or ANOVA (with post-test multiple comparisons), as specified. Non-parametric data between two groups was compared using the Mann-Whitney, or in the case of paired groups with the Wilcoxon signed-rank test. Comparison of non-parametric data between more than two groups was performed with the Kruskal-Wallis test or for repeated measures with the Friedman test. Results are expressed as mean \pm standard deviation of multiple experiments. In all cases, statistical significance was established at $p < 0.05$. The statistical parameters and the number of mice used per experiment are found in the figure legends.

Chapter 3

3. Understanding the heterogeneity of endothelial-macrophage progenitors

3.1 Introduction

Many physiological and pathological processes rely on the formation of neovessels via angiogenesis and/or vasculogenesis (1). Angiogenesis is defined as the coordinated involvement of endothelial cell (EC) migration, proliferation and tube formation to form new vessels as outgrowths from the endothelium of existing blood vessels. Vasculogenesis, on the other hand, occurs via the activity and differentiation of endothelial progenitor cells (EPCs) rather than established endothelium. Previously, it was thought that much of this was caused by the homing of circulating and/or bone marrow (BM)-derived EPCs to sites of tissue neovascularisation (9, 539); however, local tissue-resident progenitor cells that are not BM-derived have also been shown to contribute endothelial progeny to newly developing microvessels (28, 108, 540). Angiogenesis and vasculogenesis are also supported by the production of soluble cytokines and growth factors by non-endothelial myeloid cell populations, such as M2-like (alternately activated) macrophages (MΦs) (44, 71, 521). Although different subtypes of MΦs undergo phenotypic changes in response to their surrounding microenvironment, they are not known to have endothelial differentiation capacity, so their involvement in neovascularisation is considered paracrine (439). Understanding how MΦ-EC interactions arise is critical for targeting inflammation and neovascularisation in various pathophysiological conditions. MΦs play key supportive roles in the development of blood and lymphatic vessels during normal organogenesis and in response to tissue injury, ischaemia and other diseases (9, 376, 541). They proliferate and cluster around neovessels, producing angiogenic factors and promoting endothelial anastomosis and vascular remodelling (9). Endothelial cells, in turn, aid in the regulation of haematopoietic stem cell (HSC) self-renewal and their differentiation into MΦs (18).

Historically, tissue MΦs were thought to be derived primarily from the recruitment and differentiation of circulating monocytes, that in turn arise from definitive haematopoiesis. Although BM is the main

site of definitive haematopoiesis after birth, this process commences embryonically in the aorta-gonad-mesonephros (AGM) region. This begins in mice around embryonic day (E) 10.5 with the emergence of HSC clusters from haemogenic endothelium of the ventral floor of the dorsal aorta (47, 96, 542, 543). These multipotent HSCs soon seed the foetal liver and eventually colonise BM around the time of birth (543). Over the past decade, it has become well-established that HSC-monocyte ancestry does not account for all MΦs in different postnatal tissues. Instead, some MΦ populations are maintained postnatally without input from monocytes and independently of BM haematopoiesis (81). These self-maintained MΦs are believed to be seeded embryonically from either an extra-embryonic yolk sac (YS) (71, 73) or foetal liver source (40).

Between E7.0 and E8.25, YS is the first site of primitive MΦ precursors that emerge from early blood islands via distinct developmental mechanisms (27, 34). This is followed by the development of erythromyeloid progenitors (EMPs) from YS haemogenic endothelium (34, 112). From E7.5, c-Kit⁺CSF1R⁺ EMPs produce YS MΦs, megakaryocytes and erythrocytes in a process that is independent of the transcription factor, Myb, and involves sequential differentiation into CX₃CR1⁺ pre-MΦs and mature F4/80^{hi} MΦs, without forming monocyte intermediates (24, 27, 28, 37, 41). Both multipotent EMPs and pre-MΦs expand in YS, before entering the circulation from E10.5 and seeding embryonic tissues to complete MΦ maturation by E12.5 (42). A second subpopulation of Myb⁺c-Kit⁺CSF1R^{Lo} EMPs also arises in YS around E8.5, and then traffics to liver, where they expand and generate lineage-specific haematopoietic progenitor cells and foetal blood cells, including monocytes (34, 40, 53). Long-lived populations of YS and foetal liver derived MΦs persist in adult tissues, including brain, skin, muscle, heart, lung, liver and aortic adventitia (28, 29, 37, 71, 73, 270). Although the precise mechanisms for their maintenance remain unclear, it has been largely assumed that they are capable of proliferative self-renewal (28, 521).

Although controversial, recent evidence also indicates that YS EMPs are a source of mature ECs that line the blood vessels of brain, liver, lung and heart (108, 541). The notion that EMPs give rise to long-lived populations of haematopoietic and endothelial lineage aligns with long-standing speculation around the existence of bipotent haemangioblasts in early embryonic development (44). Although analogous progenitor cells have been shown to emerge during induced haemato-endothelial differentiation of pluripotent stem cells *in vitro*, proof of their existence in postnatal tissues has remained elusive (544). As a possible candidate for haemangioblast-like cells, we recently identified undifferentiated progenitor cells in postnatal mouse aorta, heart, lung, skin and skeletal muscle (SkM), that derive embryonically from a YS CX₃CR1⁺CSF1R⁺ source (517, 518, 520, 522). These progenitors are clonogenic, with high proliferative, but finite self-renewal capacity and are maintained independently of definitive haematopoiesis. They possess a bipotent differentiation capacity for MΦs and ECs and form vascular-like cords *in vitro* and neovessels *in vivo*. We previously demonstrated that these endothelial-macrophage (EndoMac) progenitors contribute to local inflammatory and vasculogenic responses by promoting the local expansion and maintenance of YS-derived MΦs and ECs in both steady-state and injured tissues (522). In this chapter, we address some important gaps in our understanding around EndoMac progenitors, including their transcriptional heterogeneity when freshly isolated and culture-derived, and their functional and transcriptional differences based on their tissue source. We also begin to explore the inhibitory effects of high glucose on the functional and metabolic properties of aortic progenitors, as a possible new mechanism to explain why diabetes has such a profound effect on the ability of tissues to undergo neovascularisation.

3.2 Methods in brief

3.2.1 Overview

All animal experiments and care were performed following the standards stated in the Guide for the Care and Use of Laboratory Animals (Institute of Laboratory Animal Resources, National Academy of Sciences, Bethesda, MD, USA) and in accordance with the National Health and Medical Research Council of Australia research guidelines and Australian Code for the Care and Use of Animals for Scientific Purposes. Ethics approval was obtained from the SAHMRI animal ethics committee (ID SAM20.032 and SAM432.19). Breeding pairs of C57BL/6 (C57BL/6J) and ubiquitous (UBI)-GFP (C57BL/6-Tg(UBC-GFP)30Scha/J) mouse strains were acquired from The Jackson Laboratory (Bar Harbor, ME, USA). Mice were housed in the animal care facility at SAHMRI on standard chow diet with a continuous water supply replaced every other day. In all cases, both genders were used. For the induction of diabetes, intraperitoneal (i.p) injections of streptozotocin (STZ) were administered to 8–12-week-old (w) mice, while controls received citrate buffer injection as sham. Blood glucose levels were monitored a week post injection and diabetes was confirmed by a level >15 mmol/L. An extra dose was administered if the levels were <15 mmol/L one week after the initial STZ injection.

Aorta with adventitia, skin (including dermis and epidermis) and hind limb SkM were enzymatically digested into single cell suspensions for use in different experiments, including fluorescence activated cell sorting (FACS), methylcellulose colony forming unit (CFU) and MatrigelTM-based angiogenesis assays, multi-colour flow cytometry and immunocytofluorescence staining. EndoMac progenitors were obtained either from FACS-based immunoselection of single cell tissue digests, or pipette isolation of colony forming units-MΦ (CFU-M) from methylcellulose cultures under microscopic guidance. Bulk RNA-sequencing was performed as described in Chapter 2.

3.2.2 Statistical analysis

Where relevant, analysis was performed blinded to study group. Statistical comparisons were performed using Prism (GraphPad version 10). Datasets were tested for normality of distribution by Shapiro-Wilk test. Statistical comparisons were performed with parametric or non-parametric unpaired or paired two sample *t*-tests or one-way ANOVA (with post-test multiple comparisons). Results are expressed as mean \pm standard deviation of multiple experiments or donor mouse replicates. In all cases, statistical significance was established at two-tailed $p < 0.05$. The statistical test and number of mice used for each experiment are found in the Figure Legends.

3.3 Results

3.3.1 Immunophenotypic characterisation of EndoMac progenitors

We first identified EndoMac progenitors in postnatal mouse aorta based on the ability of single cell aortic digests to selectively form CFU-M after 14 days (d) in methylcellulose (520, 522). CFU-M were found to contain cells that were immunophenotypically homogeneous for the markers CD45, c-Kit and Sca-1 but negative for mature lineage (Lin) antigens and the mature monocyte/MΦ markers, CD11b and F4/80 (520, 522). We subsequently used flow cytometry to identify the presence of Lin⁻CD45⁺CD11b⁻F4/80⁻Sca-1⁺c-Kit⁺ cells within the adventitia of intact adult aorta, with a frequency of approximately 3000 cells per aorta (520). However, a remaining gap in our knowledge was whether this population is in fact responsible for the growth of CFU-M from aorta. To address this, we used FACS to isolate CD45⁺CD11b⁻F4/80⁻Sca-1⁺c-Kit⁺ progenitors, CD45⁺CD11b⁺F4/80⁺ MΦs and CD45⁻CD31⁺ ECs from aorta at high purity (**Figure 3.1A, B**) and plated each population in Methylcellulose M3434, (StemCell Technologies) for 14 d. CFU-M were only produced by sorted progenitors with a yield of ~400 colonies per 10⁵ plated cells, while no colonies were produced by either mature MΦs or ECs (**Figure 3.1C**). These CFU-M were then individually isolated under microscopic guidance, disaggregated, labelled and analysed by flow cytometry. Importantly, this confirmed that they contained progenitor cells with the same surface phenotype as the founding population that had been FACS-isolated from aorta (**Figure 3.1D**). In addition, these colonies showed enriched expression for two other key markers, CSF1R/CD115 and CX₃CR1 and crucially, no contamination with differentiated CD144⁺ (VE-Cadherin⁺) ECs or CD11b⁺F4/80⁺ MΦs.

We further studied the phenotypic homogeneity of culture-derived progenitors from aortic CFU-M by immunofluorescence staining of cytopsin preparations and fluorescence microscopy. Progenitors were mostly c-Kit⁺ and showed no expression of either the MΦ marker, CD68, or the endothelial

marker, Endomucin (EMCN) (**Figure 3.1E, F**). In keeping with their high proliferative activity, ~85% of progenitors also displayed nuclear staining for Ki67 (**Figure 3.1E, F**).

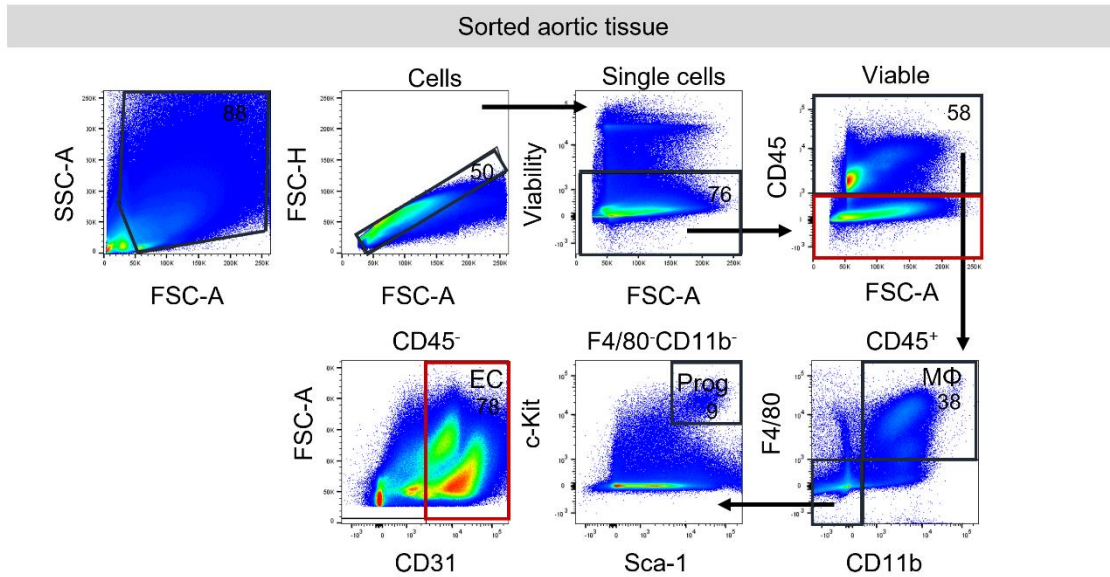
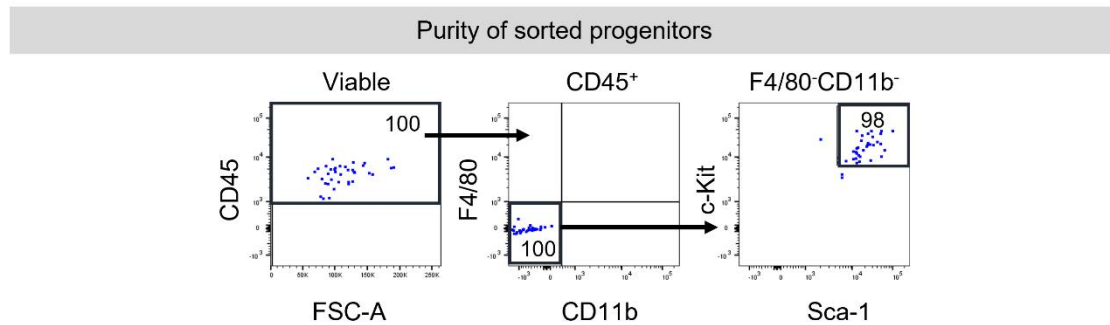
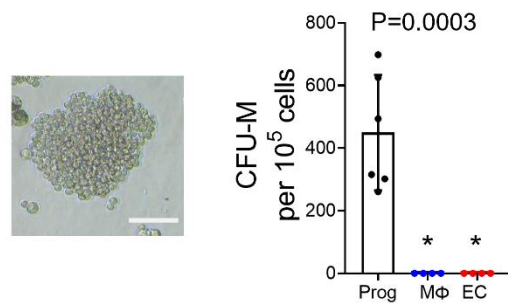
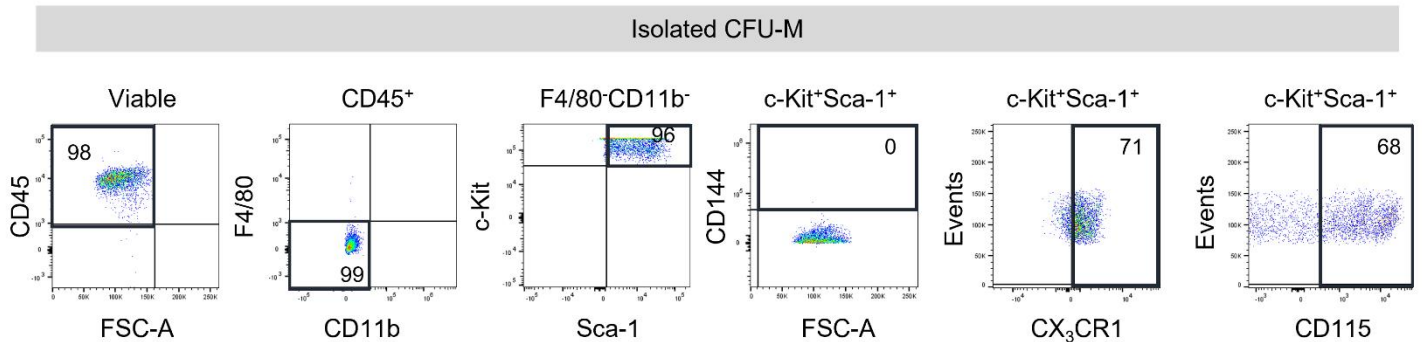
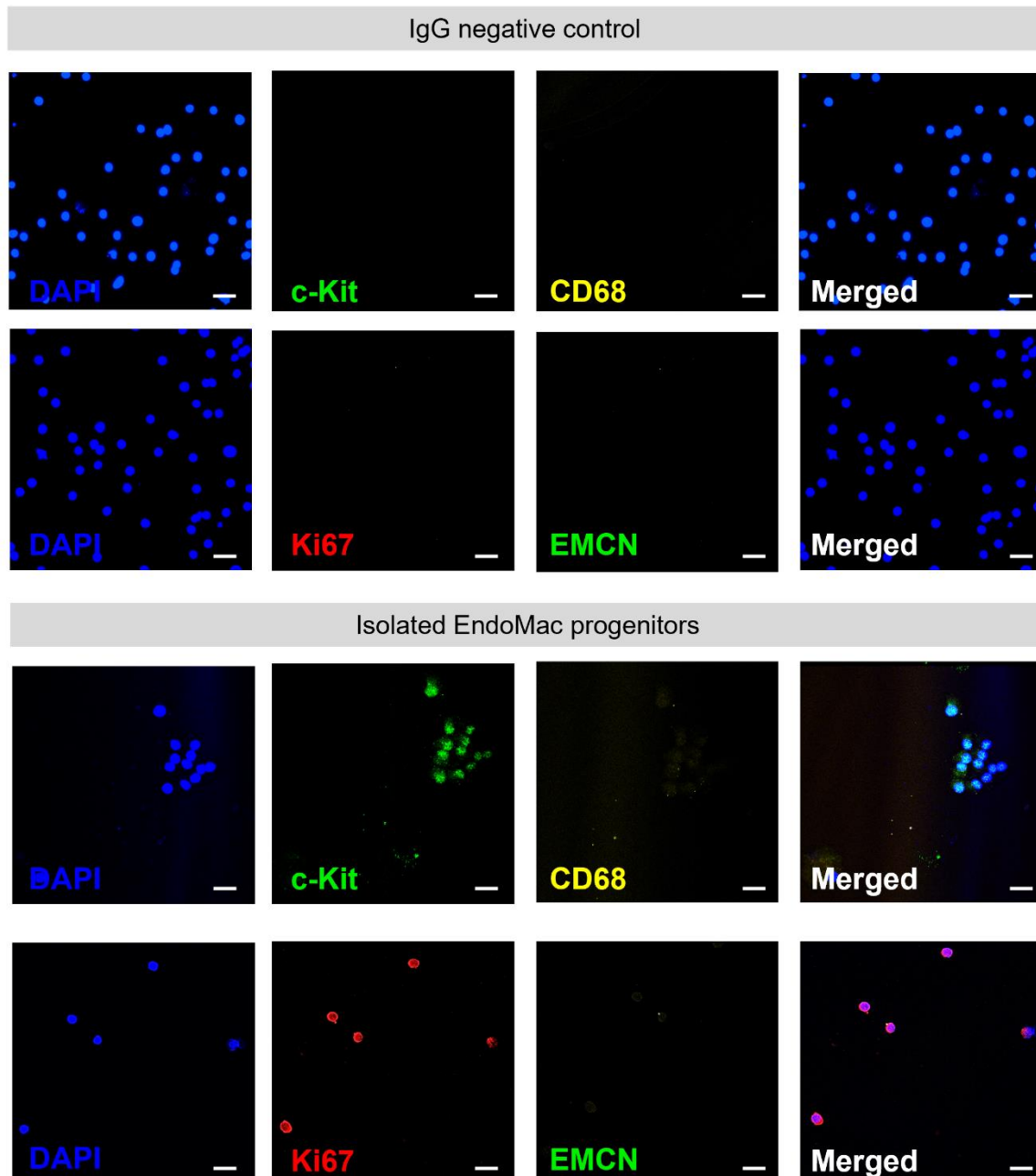
A**B****C****D**

Figure continued P.T.O.

E



F

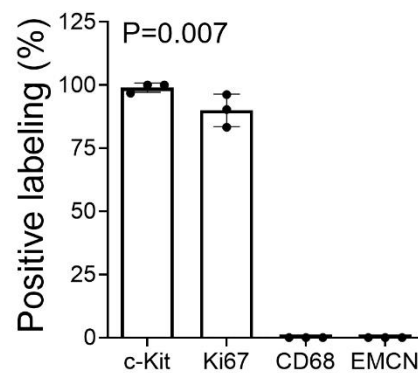


Figure continued P.T.O.

Figure 3.1: Aortic EndoMac progenitors give rise to CFU-M

- A)** FACS gating of single cell digests from adult C57BL/6 aorta. Numbers in black gated regions represent mean % expression from 6 different experiments, each using aortas from ≥ 6 mice.
- B)** Flow cytometry to confirm purity of progenitors immediately after FACS isolation. Mean % expression from 6 experiments is represented in black gated regions.
- C)** Light microscopy image shows a representative CFU-M. Scale bar, 100 μm . Graph shows comparison of CFU-M yield per 10^5 cells plated from FACS-isolated progenitors (Prog), macrophages ($\text{M}\Phi$) and endothelial cells (EC) after 14 d in methylcellulose. $n=4-6$, $P=0.0003$, Kruskal-Wallis test.
- D)** Flow cytometry of cells isolated from CFU-M formed from FACS-isolated aortic progenitors after 14 d in methylcellulose. Percentages in black gated regions represent mean % expression from 4 different experiments.
- E)** Immunocytofluorescence staining of single cells isolated from culture derived progenitors. IgG isotype negative controls shown for each primary antibody. Cells were co-labelled with primary antibodies against c-Kit and CD68 (top) or Ki67 and Endomucin (EMCN) (bottom). Images are at 40x magnification. 40 μm scale bar.
- F)** Graph shows frequency of cells expressing c-Kit, Ki67, CD68 and Endomucin (EMCN), $n=3$, $P=0.007$, Friedman test.
- .

3.3.2 Aortic EndoMac progenitors are angiogenic and possess bipotent differentiation capacity

Aortic EndoMac progenitors possess the ability to form complex sprouting networks and cord-like structures when cultured for 7 d in MatrigelTM with endothelial growth media (517, 520, 522) (**Figure 3.2A**). Angiogenic assays were carried out by isolating ~50 CFU-M under microscopic guidance and replating it in MatrigelTM medium. Enzymatic digestion of these cultures after 7 d allowed us to analyse their cellular composition by flow cytometry, as described previously (**Figure 3.2B**) (517, 520, 522). This revealed that progenitors produce new ECs and MΦs (**Figure 3.2C**). We also corroborated these results by immunostaining cytopsin preparations of the cells produced in MatrigelTM and imaging under confocal microscopy. This showed the presence of cells that expressed the endothelial surface marker, Endomucin, with a smaller number that expressed the MΦ marker, CD68 (**Figure 3.2D, E**). As shown in **Figure 3.1** above, it is important to re-emphasise that EndoMac progenitors did not express either of these markers in their undifferentiated state when freshly isolated from CFU-M.

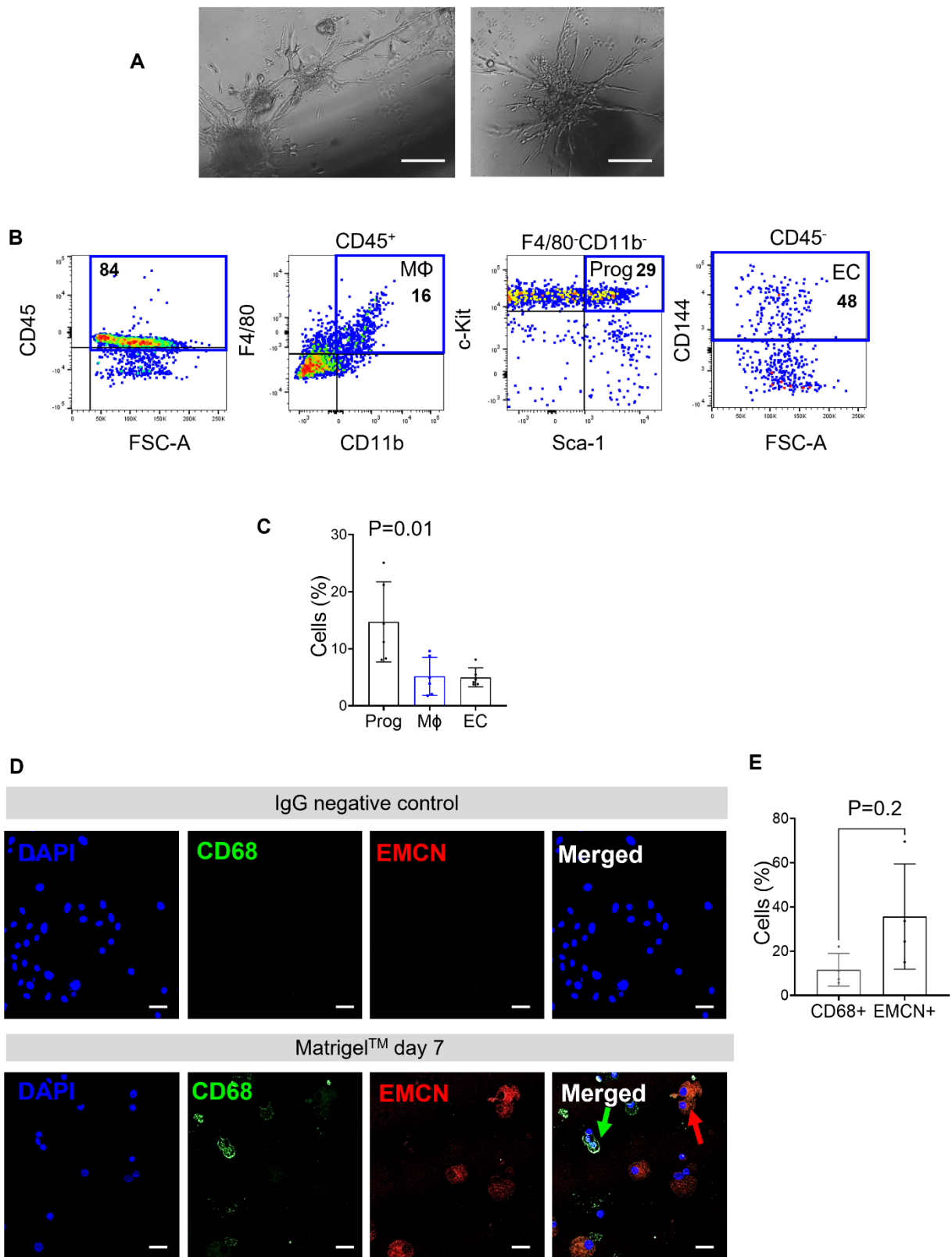


Figure 3.2: Aortic EndoMac progenitors form complex sprouts and cords in Matrigel™ containing new ECs and MΦs

A) Light microscopy images of Matrigel™ cord networks from EndoMac progenitors isolated from aortic CFU-M. Representative of n=6 donor experiments using adult C57BL/6 mice. Scale bar, 100 μm.

B) Flow cytometry plots show fate of CFU-M-derived EndoMac progenitors in Matrigel™. CD45⁺CD11b⁻F4/80⁻Sca-1⁺c-Kit⁺ progenitors, CD45⁺CD11b⁺F4/80⁺ macrophages (MΦ) and CD45⁻CD144⁺ endothelial cells (ECs). Percentages represent mean of n=6.

C) Frequency of progenitors, MΦs and ECs formed in Matrigel™ assays from aortic culture derived progenitors. n=6/gp, P=0.01, One-way repeated measures ANOVA.

D) Confocal microscopy images of immunolabelled cytopsin preparations of cells produced by EndoMac progenitors after 7d in Matrigel™. Cells stained with nuclear dye DAPI (blue), and immunolabelled against MΦ marker, CD68 (green) and EC marker, EMCN (red). 40x magnification. Green arrow indicates CD68⁺ and red arrow indicates EMCN⁺ cells. Representative of n=4 animals. Scale bar, 40 μm.

E) Frequency of CD68⁺ and EMCN⁺ cells formed in Matrigel™ assays from culture derived aortic progenitors of C57BL/6 mice. n=4/gp, P=0.2, Paired *t*-test.

3.3.3 EndoMac progenitors are bipotent at a clonal and single cell level

We further explored the differentiation capacity of EndoMac progenitors by isolating single CFU-M - which had each been generated by a single parent cell - and replating the cellular content of each colony in separate wells in MatrigelTM for 7 d. Progenitors from solitary CFU-M formed intricate cord-forming networks (**Figure 3.3A-B**), which again contained new MΦs and ECs, confirming that bipotency is contained at the clonal, and by extension single parent cell, level (**Figure 3.3C-D**).

We elaborated on this result by also performing single cell differentiation assays. To do this, we prepared CFU-M from adult UBI-GFP (GFP⁺) and C57BL/6 (GFP⁻) aortas. These colonies were individually isolated and disaggregated into single cell suspensions. We then performed co-culture experiments, whereby a single GFP⁺ progenitor cell was seeded in MatrigelTM together with pooled GFP⁻ progenitors (**Figure 3.3E**). We were able to track the formation of multicellular GFP⁺ sprouting networks from single cell origins in several replicate experiments (**Figure 3.3F**). Cytospin preparations were labelled with antibodies for GFP, CD68 and EMCN for fluorescence confocal microscopy and revealed the presence of both GFP⁺CD68⁺ MΦs and GFP⁺EMCN⁺ ECs in the same wells (**Figure 3.3G**). This crucial breakthrough proves that progenitors can differentiate into both lineages at a single cell level.

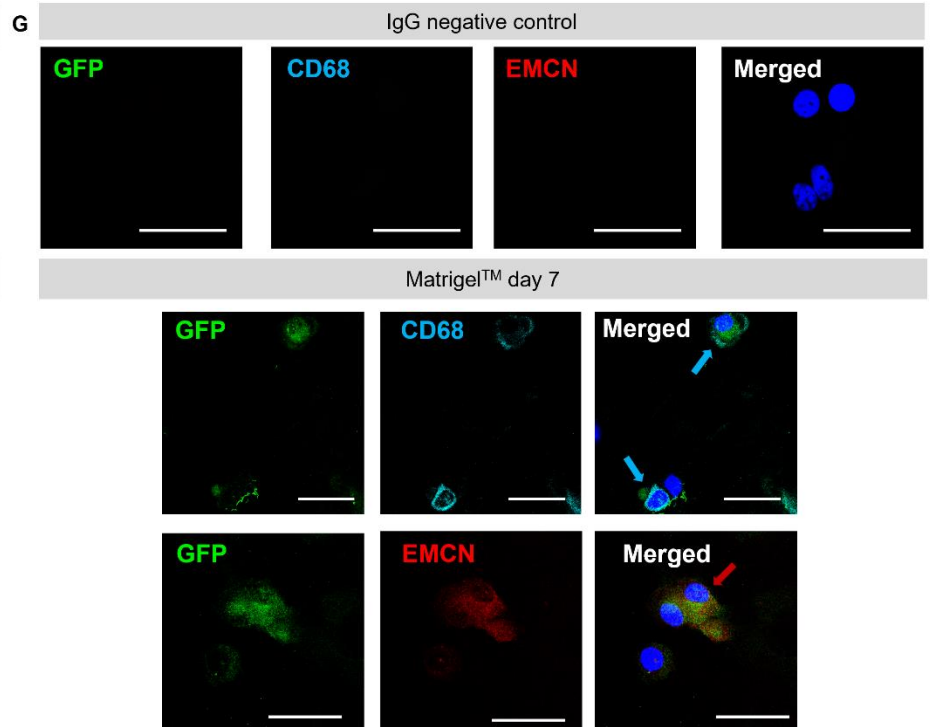
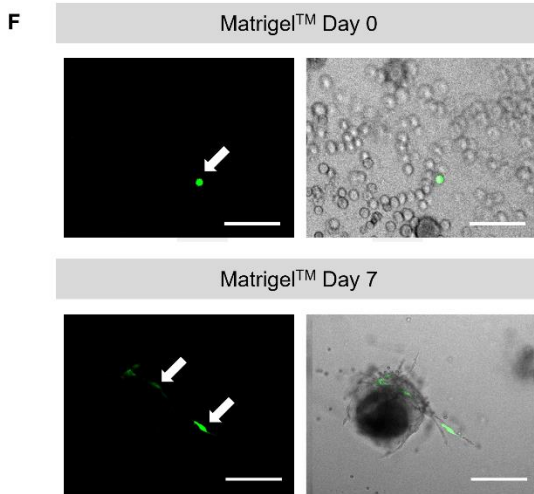
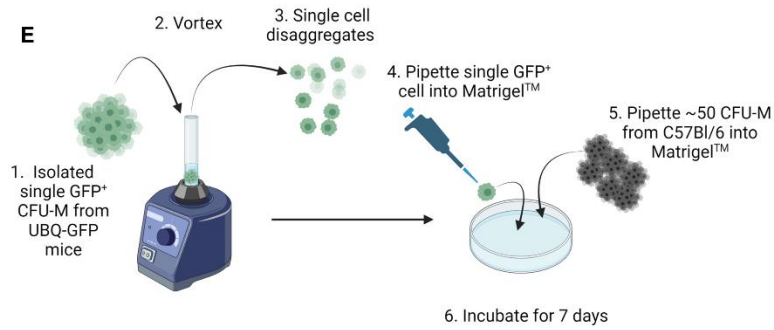
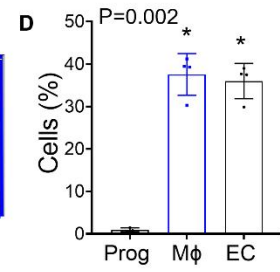
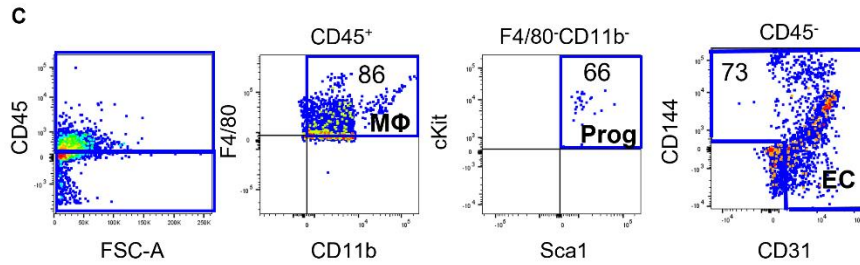
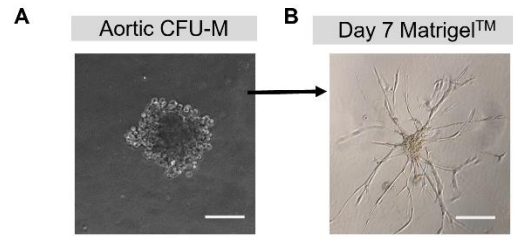


Figure 3.3: EndoMac progenitors are capable of bipotent differentiation at a clonal and single cell level

A) Light microscopy image shows a representative single aortic CFU-M from C57Bl/6 mouse. Representative image of n=4. Scale bar, 100 μ m.

B) Light microscopy images of branching sprout and cord networks produced from the progenitors contained within a single CFU-M after 7 d in MatrigelTM with endothelial growth medium. Scale bar, 100 μ m.

C) Flow cytometry plots show the presence of different cell populations in MatrigelTM 7 d after culturing one aortic CFU-M. CD45⁺CD11b⁺F4/80⁺Sca-1⁺c-Kit⁺ progenitors (Prog), CD45⁺CD11b⁺F4/80⁺ macrophages (M Φ) and CD45⁺CD31⁺ and/or CD144⁺ endothelial cells (ECs). Numbers in gated regions represent mean % expression for that gate from n=4.

D) Frequency of progenitors, M Φ s and ECs formed in MatrigelTM assays from single CFU-M. n=4 experiments. One-way repeated measures ANOVA. Multiple comparisons: *P<0.05 compared to Prog.

E) Schematic of single cell differentiation assay using a single GFP⁺ progenitor cell co-cultured with a pool of GFP⁻ progenitors in MatrigelTM.

F) Epifluorescence microscopy image showing single GFP⁺ cell at day 0 (top) and cord-network formed from that single cell at day 7 (bottom). Corresponding merged brightfield images shown in left. Representative of n=2. Scale bar, 100 μ m.

G) Confocal microscopy images showing presence of GFP⁺CD68⁺ M Φ s (blue arrow) and GFP⁺EMCN⁺ ECs (red arrow) within the same well arising from a single GFP⁺ progenitor.

3.3.4 Effect of different tissue source on the biology of EndoMac progenitors

Although they are distinct lineages, ECs and Mφs both display considerable heterogeneity, such that different tissue environments influence their functional and transcriptional properties (545, 546). Defining the source of this heterogeneity is important to unravelling the tissue-related differences in the way that blood vessels form pre- and postnatally. In addition to aortic adventitia, we have previously identified CFU-M forming EndoMac progenitors from murine heart, lung, skin and SkM. Here, we performed direct comparisons between progenitors from three of these tissue sources. Single cell disaggregates from adult C57BL/6 aorta, skin (including epidermis and dermis) and SkM from gastrocnemius and quadriceps were plated in methylcellulose for 14 d to study haematopoietic colony formation (**Figure 3.4A**). Each tissue showed a clear predilection for producing CFU-M (% of CFU-M from all CFUs grown were $89\pm2\%$ from aorta, $92\pm2\%$ from skin and $95\pm3\%$ from SkM). However, skin cells produced the most CFU-M, with a yield that was three-fold that of aorta and two-fold that of SkM (**Figure 3.4B**). CFU-M that were grown from aorta were predominantly small, containing 30-100 cells per colony, whereas those from skin and especially, SkM, included a larger proportion of medium (100-1000 cells) and large (>1000 cells) colonies (**Figure 3.4C**). This suggests that progenitors from these tissues have different proliferative and/or renewal capacity. We confirmed this in 2° culture assays, whereby 1° CFU-M were individually isolated from methylcellulose at day 14 under microscopic guidance and disaggregated. Replating of single cells from 1° CFU-M showed greater capacity for 2° colony renewal for both skin and SkM than for aorta (**Figure 3.4D**). In keeping with these results, Lin⁻CD45⁺CD11b⁻F4/80⁻Sca-1⁺c-Kit⁺ progenitors were more prevalent in digests of skin ($7,494\pm3,394$ cells/g of all viable cells) than SkM ($2,787\pm2,017$ cells/g) or aorta ($3,785\pm1,781$ cells/g) (n=9-10 adult C57BL/6 mice, repeated measures one-way ANOVA, P=0.002) (data not shown).

We next speculated whether the higher renewal capacity of SkM progenitors might be associated with higher metabolic activity, especially as mature skeletal myocytes and SkM satellite cells are known to be metabolically active (431). To do this we used the SeahorseTM assay which analyses oxygen consumption rate (OCR) as an indicator of cellular aerobic respiration that uses mitochondrial oxidative phosphorylation pathways, and extracellular acidification rate (ECAR), as an indicator of the anerobic glycolysis pathway for energy production. Metabolic profiling confirmed that SkM progenitors are indeed more metabolically active than progenitors from aorta or skin, displaying a seven-fold higher basal OCR and six-fold higher ECAR (**Figure 3.4E-F**).

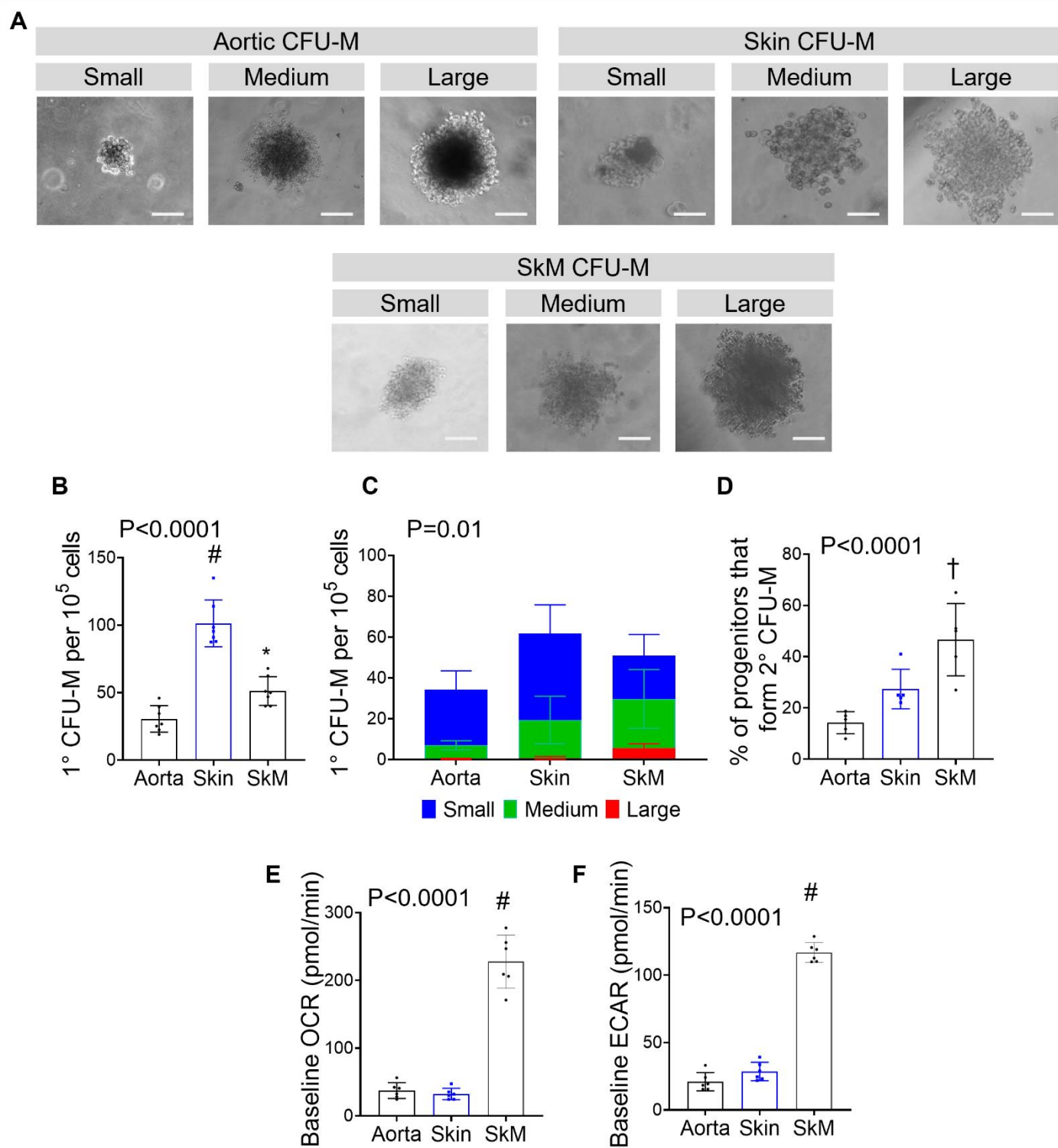


Figure 3.4: EndoMac progenitors display tissue-specific differences in their clonogenic, renewal and metabolic properties

- A)** Light microscopy images of aortic, skin and SkM CFU-M from adult C57BL/6 mice showing representative small, medium and large colonies. Scale bar, 100 μ m.
- B)** Comparison of 1° CFU-M yield from donor-matched C57BL/6 aortic, skin and SkM digests. n=7 mice/gp. One-way ANOVA. Multiple comparisons, *P<0.05 and #P<0.0001 versus aorta.
- C)** Bar graphs with CFU-M sizes overlaid from different tissues. n=7 mice/gp.
- D)** Comparison of 2° colony renewal from single cells obtained from 1° CFU-M. Experiment was performed using cells from n=5 mice/gp. Kruskal-Wallis test. Multiple comparison, †P<0.01 compared to aorta and skin.
- E, F)** Baseline **E)** oxygen consumption rate (OCR) and **F)** extracellular acidification rate (ECAR) of progenitors obtained from aortic, skin and SkM CFU-M. n=6, One-way ANOVA. Multiple comparisons, #P<0.0001 compared to aorta and skin.
- Data are shown as mean \pm SD.

3.3.5 Tissue-related effects on the angiogenic and differentiation capacity of EndoMac progenitors

Comparison between MatrigelTM cultures from aortic, skin and SkM progenitors revealed that all three tissue sources formed complex, branched networks of sprouts and cords over 7 d. Morphologically, SkM and aortic progenitors both produced clusters with numerous outgrowths of fine sprouts, whereas skin progenitors appeared to produce more robust, thicker inter-connecting cords (**Figure 3.5A**). SkM progenitors formed the highest number of cords and branch points especially when compared to aorta, although their cords were individually shorter in length (**Figure 3.5B-D**). Flow cytometry analysis of the cellular composition of these networks revealed similar levels of cell viability between the three tissue types (**Figure 3.5E, F**). Like aorta, skin and SkM progenitors also demonstrated bipotent differentiation capacity by producing new CD45⁺CD11b⁺F4/80⁺ MΦs and CD45⁻CD144⁺ ECs (**Figure 3.5E, G-I**). The most notable difference between tissue types was that SkM progenitors produced the highest proportion of ECs (**Figure 3.5I**), which was consistent with the higher number of cords formed in these wells. Approximately 15% of the viable cells present after 7 d of culturing SkM progenitors could not be classified as progenitor, MΦs or ECs. These “other” cells were much more frequent in the cultures arising from aortic (75%) and skin (54%) progenitors. More work is needed to determine their immunophenotypic nature so that we can better understand the full lineage potential of the progenitors.

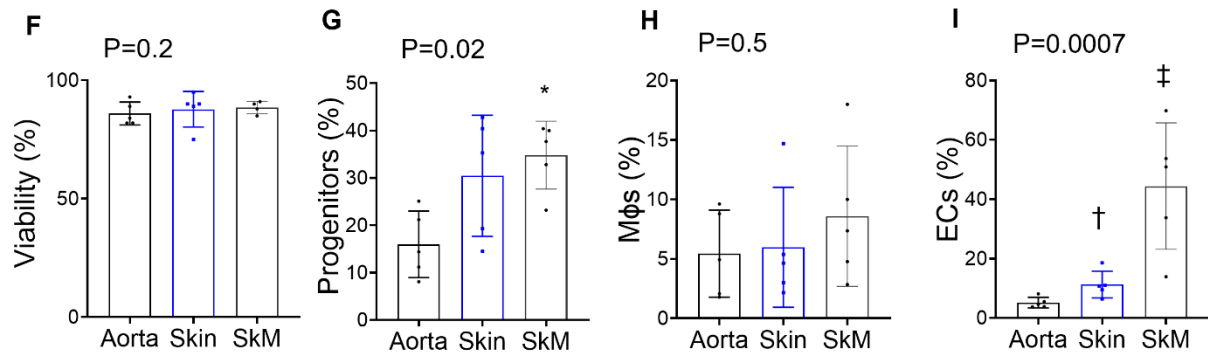


Figure 3.5: Tissue-related effects on the angiogenic and differentiation capacity of EndoMac progenitors

A) Light microscopy images of branching sprout and cord networks produced from aortic, skin and SkM progenitors after 7 d in MatrigelTM with endothelial growth medium. Scale bar, 100 μ m (top) and 1000 μ m (bottom). Sprouts/cords are denoted by blue arrows and branch points by red arrows.

B-D) Graphs display comparisons of **B)** total cord length, **C)** cord number and **D)** branch number produced by aortic, skin and SkM progenitors from adult C57Bl/6 mice. $n \geq 6$ donor mice/gp. **B-C)** Kruskal-Wallis. **D)** One-way ANOVA. Multiple comparisons, $\ddagger p < 0.001$ versus aorta.

E) Flow cytometry plots show the presence of different cell populations in MatrigelTM 7 d after culturing progenitors from different tissue sources. CD45⁺CD11b⁻F4/80⁻c-Kit⁺Sca-1⁺ progenitors (Prog), CD45⁺CD11b⁺F4/80⁺ macrophages (M Φ) and CD45⁻CD144⁺ endothelial cells (EC). Percentages in gated regions represent mean % expression for that gate from $n=8$ /gp.

F-I) Frequency of **F)** viable cells, **G)** progenitors, **H)** M Φ s and **I)** ECs in day 7 MatrigelTM assays arising from progenitors from different tissue sources. $n=5$ /gp. One-way ANOVA. Multiple comparisons, $*p < 0.05$, $\dagger p < 0.01$, and $\ddagger p < 0.001$ versus aorta.

Data are summarised as mean \pm SD.

3.3.6 Transcriptomic comparison of EndoMac progenitors from different tissue sources

Discovery of progenitors from different mouse tissues that exhibited self-renewing, angiogenic and reparative properties prompted the question as to whether these cells are similar across tissues or display tissue-specific differences. To address this, we performed comparative transcriptomics of CFU-M progenitors from mouse aorta, skin and SkM using RNA-seq. mRNA from three independent pools of progenitors from each tissue were analysed (see Chapter 2, section 2.11.4). Bioinformatic analysis was carried out in collaboration with Dr Shiwani Sharma, postdoctoral researcher in the Psaltis group (Complete gene list: **Appendix 7.1**).

The number of reads produced per sample were generally consistent across tissues except for one skin sample that yielded lower reads (23M reads), but they were still sufficient for further analysis (**Appendix 7.2 and 7.3**). Average quality score of 30 (Q30) was achieved for 91.51% of reads. More than 92% of the reads per sample aligned to the mouse reference genome. Principle component analysis showed segregation of samples by tissue type, indicating similarity of biological replicates from a tissue and differences between tissues (**Figure 3.6A**). After data processing, normalisation and filtering low-expressed genes (see Chapter 2, section 2.11.4), 13,890 genes were found to be expressed in CFU-M progenitors. Overall, 1,951 of the 13,890 genes (0.14%) were differentially expressed among cells from the three tissues, indicating that transcriptional profiles of CFU-M progenitors from these different sources are generally similar, albeit with some differences. The comparison between aortic and skin progenitors revealed 559 significantly differentially expressed genes (FDR <0.05), with 251 upregulated (Log2 fold change (FC) = 6.35 to 0.39) and 308 downregulated (Log2FC = -8.95 to -0.39) in aortic cells (**Figure 3.6B, D and Appendix 7.1**). Fewer genes, 237, were differentially expressed between aortic and muscle progenitors, of which 159 were upregulated and 78 downregulated in aortic progenitors (Log2FC = 7.65 to 0.42 and -7.89 to -0.49, respectively, FDR <0.05) (**Figure 3.6B, C and Appendix 7.1**). The comparison between SkM and

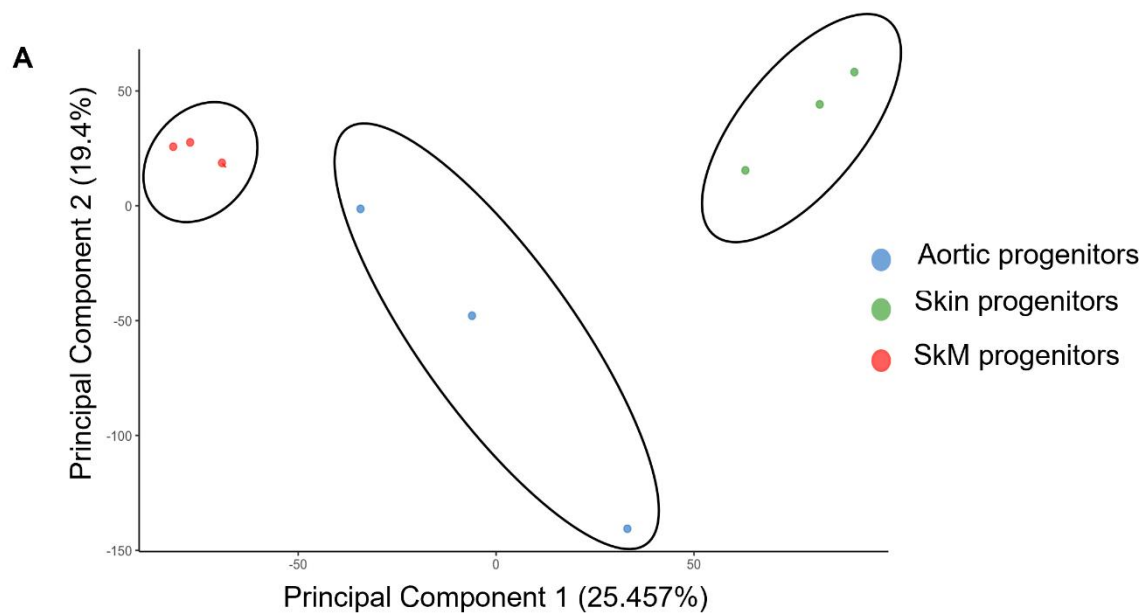
skin progenitors revealed the largest number of differentially expressed genes (1,785), with 962 upregulated ($\text{Log}_2\text{FC} = 9.04$ to 0.32) and 823 downregulated ($\text{Log}_2\text{FC} = 9.85$ to 0.31) in SkM cells (**Figure 3.6B, E** and **Appendix Figure 7.1**). The 20 most up- and down- regulated genes for each comparison are listed in **Tables 3.1-3.3**.

Interestingly, 22 genes were differentially expressed in all the three comparisons (**Figure 3.6F**), indicating that there are significant differences in the levels of expression of these genes in CFU-M progenitors from mouse aorta, skin and SkM (**Figure 3.6G**). For example, *Cx3cr1* was expressed in all three tissues, but with highest expression in SkM progenitors, followed by aortic and lowest expression in progenitors from skin. On the other hand, *Ism1* was expressed in aorta in a much higher expression capacity compared to skin and SkM.

To understand the functional significance of differential expression in progenitors between tissues, over-represented gene ontology terms and pathways in differentially expressed genes were determined using InnateDB (538). In aortic compared to skin progenitors, sequence-specific DNA binding transcription factor activity (molecular function) and cellular response to amino acid stimulus (biological process) were downregulated ($\text{FDR} < 0.05$), as were collagen degradation and extracellular matrix organisation and degradation pathways (**Table 3.4**). The differentially expressed genes driving these changes are also shown in **Table 3.4**. The analysis of differentially expressed genes between aortic and SkM progenitors did not reveal any significantly over-represented gene ontology terms or pathways. For the comparison of SkM versus skin progenitors, scavenger receptor and metallopeptidase activities (molecular functions) and biological processes, including collagen fibril organisation and catabolic process, receptor mediated endocytosis and axon guidance were significantly downregulated (**Table 3.5**). Interestingly, like aortic versus skin progenitors, cellular

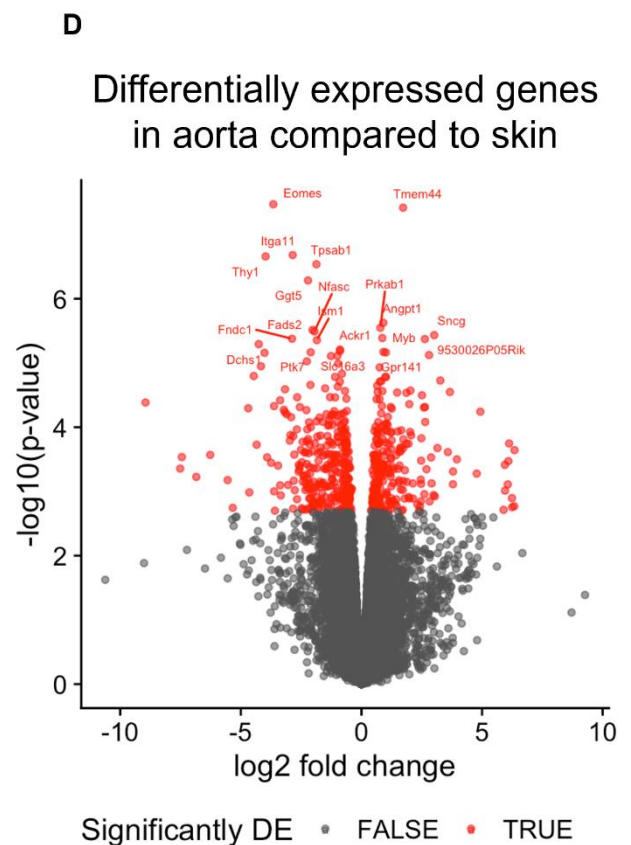
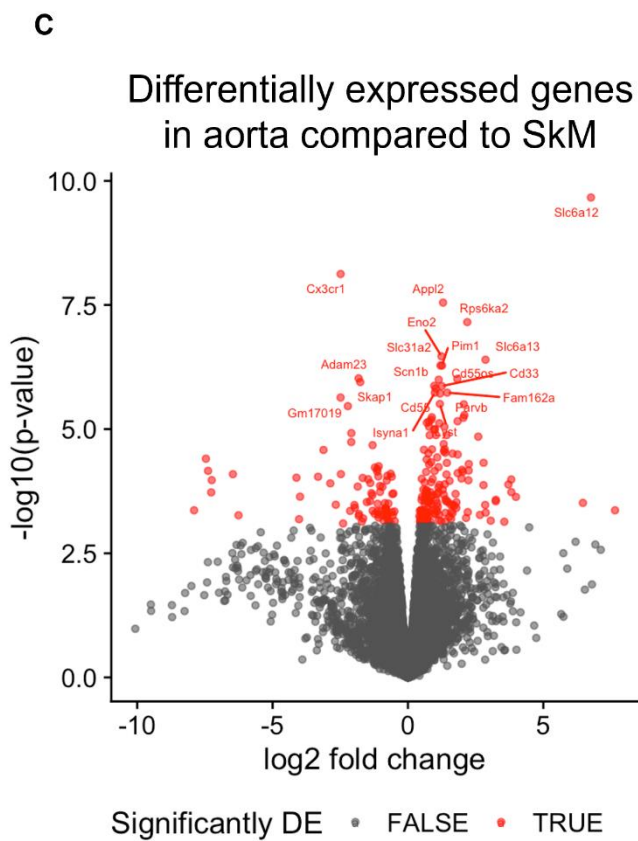
response to amino acid stimulus was also downregulated in SkM versus skin cells (**Table 3.5**). Hypertrophic cardiomyopathy was the only significantly over-represented biological pathway in SkM compared to skin progenitors and was downregulated in the former (**Table 3.5**).

Together, these results suggest that EndoMac progenitors from mouse aorta, skin and SkM share largely similar transcriptional profiles, with some molecular and biological differences.



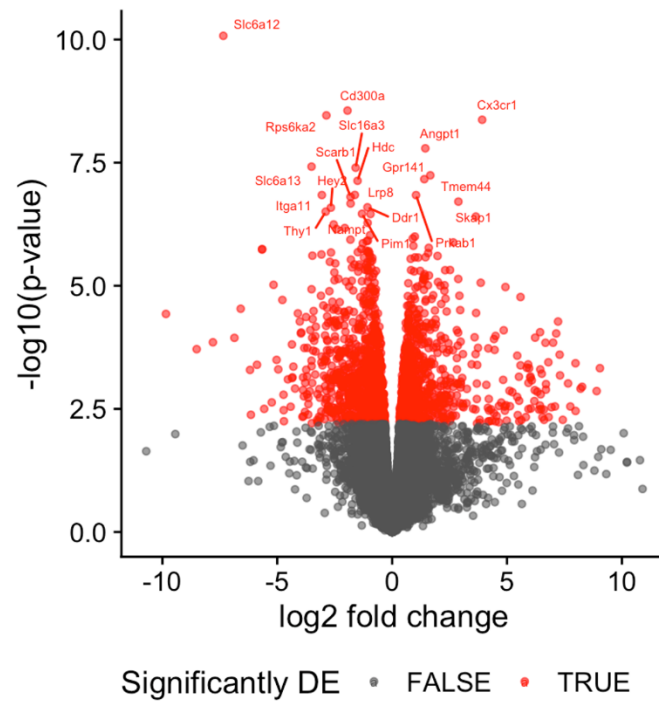
B

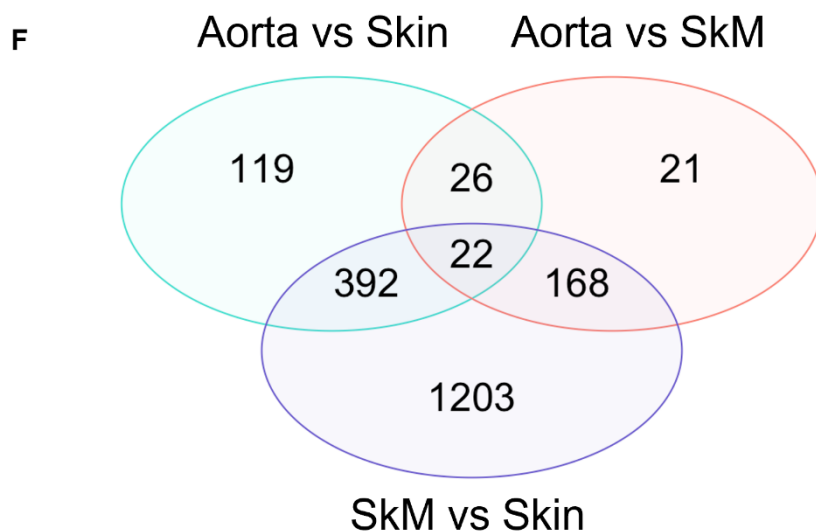
Direction	Aorta vs Skin	Aorta vs SkM	Muscle vs SkM
Down	308	78	962
Up	251	159	823
NotSig	13331	13653	12105



E

Differentially expressed genes in SkM compared to skin





G

GeneName	Log 2-fold change			Adjusted P value		
	Ao v SkM	Ao v Skin	SkM v Skin	Ao v SkM	Ao v Skin	SkM v Skin
<i>Slc6a12</i>				0.000003	0.014544	0.000001
<i>Gm14066</i>				0.023544	0.018372	0.001304
<i>Ism1</i>				0.016677	0.004081	0.000656
<i>Nfasc</i>				0.018837	0.004081	0.000656
<i>Npr3</i>				0.018837	0.017900	0.001353
<i>Slc6a13</i>				0.000910	0.037233	0.000079
<i>Rps6ka2</i>				0.000243	0.028084	0.000015
<i>Enc1</i>				0.030853	0.038070	0.000755
<i>Hey2</i>				0.017014	0.010851	0.000200
<i>Tbxas1</i>				0.039769	0.020768	0.000661
<i>Appl2</i>				0.000131	0.018372	0.000973
<i>Cd300a</i>				0.001275	0.006775	0.000015
<i>Hdc</i>				0.012066	0.013601	0.000103
<i>Slc16a3</i>				0.024001	0.004343	0.000079
<i>Ddr1</i>				0.044278	0.010851	0.000200
<i>Hexa</i>				0.046544	0.022452	0.000483
<i>Gpr141</i>				0.044278	0.004343	0.000103
<i>Angpt1</i>				0.024001	0.004081	0.000045
<i>Rbfox1</i>				0.038300	0.044294	0.000688
<i>Atp1b1</i>				0.034575	0.004343	0.000248
<i>Kcng5</i>				0.023544	0.017900	0.000553
<i>Cx3cr1</i>				0.000052	0.018372	0.000015



Figure 3.6: Differential gene expression signatures of aortic, skin and SkM EndoMac progenitors

A) Principle component analysis of aortic, skin and SkM EndoMac progenitors based on global gene expression analysis by RNA-seq showing segregation of samples. n=3 pools/gp.

B) Table summarises the number of genes upregulated and downregulated in EndoMac progenitors from aorta, SkM and skin in the indicated comparisons. The number of genes with non-significant difference in expression for each comparison are also shown.

C-E) Volcano plots show differentially expressed genes for **C)** aorta compared to SkM, **D)** aorta compared to skin, and **E)** SkM compared to skin.

F) Venn diagram showing the numbers of differentially expressed genes that are unique to a comparison and common between comparisons.

G) Heat map depicts the level of expression of the 22 differentially expressed genes that were identified in all three comparisons. Log₂-fold change in expression and adjusted p-values are shown. The key indicates level of expression from lowest (green) to greatest (red).

Table 3.1: Genes most differentially expressed in EndoMac progenitors between aorta and SkM

Differentially expressed genes in aorta v SkM EndoMac progenitors			
Upregulated in aorta compared to SkM			
Gene ID	Gene Name	Log2-fold change	Adjusted P value
ENSMUSG00000016458	<i>Wt1</i>	7.648571314	0.035847371
ENSMUSG00000030109	<i>Slc6a12</i>	6.759539473	3.00E-06
ENSMUSG00000020875	<i>Hoxb9</i>	6.462740229	0.030107741
ENSMUSG00000069270	<i>H2ac6</i>	3.989091609	0.025558253
ENSMUSG00000085071	<i>Gm14066</i>	3.818644032	0.023544328
ENSMUSG00000074766	<i>Ism1</i>	3.815547505	0.016676721
ENSMUSG00000026442	<i>Nfasc</i>	3.709707116	0.018837352
ENSMUSG00000022181	<i>C6</i>	3.55695727	0.044654824
ENSMUSG00000036446	<i>Lum</i>	3.247000215	0.0284441
ENSMUSG00000034463	<i>Scara3</i>	3.242688304	0.029214161
ENSMUSG00000027171	<i>Prrg4</i>	3.056966144	0.044059323
ENSMUSG00000029648	<i>Flt1</i>	2.872304213	0.036904023
ENSMUSG00000030108	<i>Slc6a13</i>	2.864664275	9.10E-04
ENSMUSG00000059412	<i>Fxyd2</i>	2.853487363	0.030853312
ENSMUSG00000036596	<i>Cpz</i>	2.793633928	0.011645501
ENSMUSG00000085601	<i>Meiosin</i>	2.790388065	0.019024671
ENSMUSG00000036655	<i>Colec11</i>	2.659071544	0.038025157
ENSMUSG00000058492	<i>Scp2-ps2</i>	2.596468493	0.005051616
ENSMUSG00000001249	<i>Hpn</i>	2.246636014	0.012065704
ENSMUSG00000022037	<i>Clu</i>	2.242541008	0.014395111
Downregulated in aorta compared to SkM			
Gene ID	Gene Name	Log2-fold change	Adjusted P value
ENSMUSG00000035835	<i>Plppr3</i>	-2.136864432	0.035847371
ENSMUSG00000072188	<i>Gm10354</i>	-2.219043161	0.002175728
ENSMUSG00000040035	<i>Disp2</i>	-2.396138554	0.047035351
ENSMUSG00000024427	<i>Spry4</i>	-2.476322438	0.015155677
ENSMUSG00000052336	<i>Cx3cr1</i>	-2.486616748	5.21E-05
ENSMUSG00000091897	<i>Gm17019</i>	-2.488326721	0.001689786
ENSMUSG00000027559	<i>Car3</i>	-2.664238715	0.030853312
ENSMUSG00000023092	<i>Fhl1</i>	-2.868020849	0.018256828
ENSMUSG00000031725	<i>Ces1f</i>	-3.119647944	0.007933238
ENSMUSG00000033219	<i>Gm9758</i>	-3.32017889	0.015989431
ENSMUSG00000027868	<i>Tbx15</i>	-3.985303067	0.025558253
ENSMUSG00000030730	<i>Atp2a1</i>	-4.021088358	0.042291245
ENSMUSG00000051985	<i>Igfn1</i>	-4.119599625	0.016478574
ENSMUSG00000044938	<i>Klhl31</i>	-6.259206957	0.038299928
ENSMUSG00000028396	<i>2310002L09Rik</i>	-6.46523781	0.015155677
ENSMUSG00000074001	<i>Klhl40</i>	-7.247294069	0.016867565
ENSMUSG00000001508	<i>Sgca</i>	-7.267475202	0.023544328
ENSMUSG00000028736	<i>Pax7</i>	-7.382315479	0.014395111
ENSMUSG00000042717	<i>Ppp1r3a</i>	-7.462748323	0.010323095
ENSMUSG00000090066	<i>1110002E22Rik</i>	-7.898747711	0.035847371

Table 3.2: Genes most differentially expressed in EndoMac progenitors between aorta and skin

Differentially expressed genes in aorta vs skin EndoMac progenitors

Upregulated in aorta compared to skin

Gene ID	Gene Name	Log2-fold change	Adjusted P value
ENSMUSG00000031849	<i>Comp</i>	6.346893409	0.017581785
ENSMUSG00000030249	<i>Abcc9</i>	6.332651415	0.046162082
ENSMUSG00000047230	<i>Cldn2</i>	6.248459795	0.047020892
ENSMUSG00000037492	<i>Zmat4</i>	6.241801666	0.039481235
ENSMUSG00000027748	<i>Trpc4</i>	6.120348768	0.015681937
ENSMUSG00000069515	<i>Lyz1</i>	6.090962377	0.020634889
ENSMUSG00000005952	<i>Trpv1</i>	6.067037176	0.031035149
ENSMUSG00000047592	<i>Nxpe5</i>	5.954689767	0.035116526
ENSMUSG00000041020	<i>Map7d2</i>	5.944058306	0.021547291
ENSMUSG00000016458	<i>Wtl</i>	5.894204967	0.049171129
ENSMUSG00000040314	<i>Ctsg</i>	4.929690313	0.01089738
ENSMUSG00000030218	<i>Mgp</i>	4.780156208	0.025015923
ENSMUSG00000022657	<i>Cd96</i>	3.957013283	0.019974554
ENSMUSG00000025150	<i>Cbr2</i>	3.797893321	0.023939325
ENSMUSG00000019577	<i>Pdk4</i>	3.793638274	0.031035149
ENSMUSG00000022037	<i>Clu</i>	3.667299225	0.008111073
ENSMUSG00000022206	<i>Npr3</i>	3.583607465	0.017899688
ENSMUSG00000043073	<i>Usp17le</i>	3.26919949	0.007125323
ENSMUSG00000069516	<i>Lyz2</i>	3.150668462	0.016766716
ENSMUSG00000040522	<i>Tlr8</i>	3.045052125	0.039186085

Downregulated in aorta compared to skin

Gene ID	Gene Name	Log2-fold change	Adjusted P value
ENSMUSG00000038305	<i>Spats2l</i>	-3.619170389	0.03548719
ENSMUSG00000032006	<i>Pdgfd</i>	-3.621203813	0.010380287
ENSMUSG00000032446	<i>Eomes</i>	-3.65381044	2.66E-04
ENSMUSG00000043969	<i>Emx2</i>	-3.743730061	0.021153271
ENSMUSG00000023885	<i>Thbs2</i>	-3.910072442	0.01900278
ENSMUSG00000032011	<i>Thy1</i>	-3.973371307	7.62E-04
ENSMUSG00000060572	<i>Mfap2</i>	-4.015981507	0.004342712
ENSMUSG00000039114	<i>Nrn1</i>	-4.163926888	0.005574488
ENSMUSG00000036862	<i>Dchs1</i>	-4.25641699	0.004342712
ENSMUSG00000054203	<i>Ifi205</i>	-4.34393685	0.015681937
ENSMUSG00000027996	<i>Sfrp2</i>	-4.463299917	0.006774565
ENSMUSG00000039109	<i>F13a1</i>	-4.648155534	0.036215226
ENSMUSG00000027868	<i>Tbx15</i>	-4.693548295	0.010482179
ENSMUSG00000049093	<i>Il23r</i>	-5.334533236	0.04768419
ENSMUSG00000102504	<i>Gm21955</i>	-5.547820827	0.028884794
ENSMUSG00000024064	<i>Galnt14</i>	-6.268799173	0.018371779
ENSMUSG00000031737	<i>Irx5</i>	-6.845100111	0.026915004
ENSMUSG00000055022	<i>Cntn1</i>	-7.445529235	0.018926551
ENSMUSG00000060969	<i>Irx1</i>	-7.513691452	0.022597987
ENSMUSG00000032368	<i>Zic1</i>	-8.950689788	0.009717562

Table 3.3: Genes most differentially expressed in EndoMac progenitors between SkM and skin

Differentially expressed genes in SkM vs skin EndoMac progenitors

Upregulated in SkM compared to skin

Gene ID	Gene Name	Log2-fold change	Adjusted P value
ENSMUSG00000030399	<i>Ckm</i>	9.042679067	0.011121153
ENSMUSG00000055489	<i>Ano5</i>	8.901095651	0.019943633
ENSMUSG00000042451	<i>Mybph</i>	8.267687679	0.017405377
ENSMUSG00000033196	<i>Myh2</i>	8.199920722	0.018530367
ENSMUSG00000019787	<i>Trdn</i>	7.98379532	0.034198383
ENSMUSG00000005716	<i>Pvalb</i>	7.980428875	0.010021755
ENSMUSG00000009214	<i>Mymk</i>	7.755006152	0.030170976
ENSMUSG00000027022	<i>Xirp2</i>	7.658102252	0.016221304
ENSMUSG00000026418	<i>Tnni1</i>	7.425784637	0.044282756
ENSMUSG00000026459	<i>Myog</i>	7.305941745	0.013527655
ENSMUSG000000110246	<i>C130073E24Rik</i>	7.290615165	0.008110446
ENSMUSG00000042717	<i>Ppp1r3a</i>	7.220213682	0.00350777
ENSMUSG00000028736	<i>Pax7</i>	7.139780838	0.004617644
ENSMUSG00000031962	<i>Cdh15</i>	7.087868593	0.030170976
ENSMUSG00000074001	<i>Klhl40</i>	7.004759428	0.005882607
ENSMUSG00000026253	<i>Chrng</i>	6.93220344	0.030738437
ENSMUSG00000027861	<i>Casq2</i>	6.811996716	0.040740735
ENSMUSG00000005320	<i>Fgfr4</i>	6.799581885	0.009788844
ENSMUSG00000020722	<i>Cacng1</i>	6.695870263	0.016354395
ENSMUSG00000041700	<i>Lhfp11</i>	6.691819516	0.019103844

Downregulated in SkM compared to skin

Gene ID	Gene Name	Log2-fold change	Adjusted P value
ENSMUSG00000026073	<i>Il1r2</i>	-4.711287876	0.046126779
ENSMUSG00000086447	<i>Gm13522</i>	-4.721492766	0.033449995
ENSMUSG00000036412	<i>Arsi</i>	-4.729165251	0.022082762
ENSMUSG00000027996	<i>Sfrp2</i>	-4.777672176	0.001940757
ENSMUSG00000078117	<i>Gm16485</i>	-4.956487296	0.011422068
ENSMUSG00000020646	<i>Mboat2</i>	-5.02955025	0.009213738
ENSMUSG00000085071	<i>Gm14066</i>	-5.162384918	0.001304302
ENSMUSG00000022015	<i>Tnfrsf11</i>	-5.240527819	0.02717114
ENSMUSG00000006014	<i>Prg4</i>	-5.571072206	0.0322493
ENSMUSG00000026442	<i>Nfasc</i>	-5.658656674	6.56E-04
ENSMUSG00000074766	<i>Ism1</i>	-5.663098141	6.56E-04
ENSMUSG00000037482	<i>Erv3</i>	-5.88219333	0.010333548
ENSMUSG00000042436	<i>Mfap4</i>	-6.147698279	0.038315196
ENSMUSG00000020875	<i>Hoxb9</i>	-6.186604903	0.011561089
ENSMUSG00000029322	<i>Plac8</i>	-6.592678906	0.002502903
ENSMUSG000000102504	<i>Gm21955</i>	-6.865601216	0.005186787
ENSMUSG00000030109	<i>Slc6a12</i>	-7.349027538	1.17E-06
ENSMUSG00000032368	<i>Zic1</i>	-7.801510364	0.005836538
ENSMUSG00000049093	<i>Il23r</i>	-8.50853278	0.007015791
ENSMUSG00000032446	<i>Eomes</i>	-9.845853208	0.002811177

Table 3.4: Gene ontology terms and pathways over-represented in aortic versus skin EndoMac progenitors

The significant (corrected) gene ontology terms and pathways represented by the differentially expressed genes between aortic and skin progenitors are listed. Red and green indicate significantly up- and down- regulated genes, respectively, in aortic compared to skin progenitors in a pathway. Genes in black indicate non-significantly regulated genes. #Log₂FC cut off +/- 1.0 and associated adjusted p <0.05. Pathway Ids that contain GO are the overrepresented gene ontology (GO) terms and the pathway Ids without GO are the overexpressed pathways.

Pathway Name	Pathway Id (Source name)	Pathway uploaded gene count	Genes in InnateDB for this entity	Pathway up- regulated genes count [#]	Pathway up- regulated p-value (corrected)	Pathway down- regulated genes count [#]	Pathway down- regulated p- value (corrected)	Gene Symbols
Sequence-specific DNA binding transcription factor activity	GO:0003700 molecular function	30	30	1	1	21	0.02	<i>A930001N09Rik</i> ; <i>Atf5</i> ; <i>Cebpb</i> ; <i>Emx2</i> ; <i>En1</i> ; <i>Eomes</i> ; <i>Etv5</i> ; <i>Gli2</i> ; <i>Hes1</i> ; <i>Hey2</i> ; <i>Hoxa7</i> ; <i>Irx1</i> ; <i>Irx2</i> ; <i>Irx5</i> ; <i>Lhx8</i> ; <i>Mmp14</i> ; <i>Myb</i> ; <i>Nfatc4</i> ; <i>Nfe2l1</i> ; <i>Nfkb1</i> ; <i>Nr1h3</i> ; <i>Prrx2</i> ; <i>Rorb</i> ; <i>Shox2</i> ; <i>Stat5a</i> ; <i>Tbx15</i> ; <i>Twist1</i> ; <i>Twist2</i> ; <i>Zfp191</i> ; <i>Zic1</i>
Cellular response to amino acid stimulus	GO:0071230 biological process	9	9	0	1	9	0.02	<i>Cebpb</i> ; <i>Col16a1</i> ; <i>Col1a1</i> ; <i>Col1a2</i> ; <i>Col3a1</i> ; <i>Col5a2</i> ; <i>Mmp2</i> ; <i>Pdgfd</i> ; <i>Sh3bp4</i>
Collagen trimer	GO:0005581 cellular component	12	12	0	1	12	0.003	<i>C1qtnf6</i> ; <i>Col12a1</i> ; <i>Col16a1</i> ; <i>Col1a1</i> ; <i>Col1a2</i> ; <i>Col23a1</i> ; <i>Col24a1</i> ; <i>Col3a1</i> ; <i>Col5a1</i> ; <i>Col5a2</i> ; <i>Col6a2</i> ; <i>Lox</i>
Proteinaceous extracellular matrix	GO:0005578 cellular component	23	23	1	1	18	0.009	<i>Adamts2</i> ; <i>Col12a1</i> ; <i>Col16a1</i> ; <i>Col1a1</i> ; <i>Col24a1</i> ; <i>Col6a2</i> ; <i>Comp</i> ; <i>Crtap</i> ; <i>Efemp2</i> ; <i>Fbln2</i> ; <i>Lamc1</i> ; <i>Lepre1</i> ; <i>Lgals3</i> ; <i>Lgals3bp</i> ; <i>Lox</i> ; <i>Mmp10</i> ; <i>Mmp11</i> ; <i>Mmp2</i> ; <i>Nid2</i> ; <i>Smoc2</i> ; <i>Sparc</i> ; <i>Tgfb3</i> ; <i>Wnt16</i>

Proteinaceous extracellular matrix	GO:0005578 cellular component	23	23	1	1	18	0.009	<i>Adamts2; Col12a1; Col16a1; Col1a1; Col24a1; Col6a2; Comp; Crtap; Efemp2; Fbln2; Lamc1; Lepre1; Lgals3; Lgals3bp; Lox; Mmp10; Mmp11; Mmp2; Nid2; Smoc2; Sparc; Tgfbr3; Wnt16</i>
Extracellular region	GO:0005576 cellular component	47	47	7	1	29	0.01	<i>4930503L19Rik; Abhd15; C1ra; C4b; Calu; Ccl11; Ccl8; Ccl9; Cd59a; Clstn1; Col23a1; Col6a2; Comp; Dhrrs11 Draxin; F13a1; Fam3c; Fbln1; Fbln2; Fibin; Figf; Fstl1; Gas6; Glipr2; Gpx7; Igfbp6; Igslf10; Il1rl1; Ism1; Lyz1; Lyz2; Mgp; Mif; Nid2; Olfrml2b; Pdgfrl; Pla1a; Plat; Ptch1; Rnase4; Serpinf1; Tfr; Thbs2; Tpsb2; Wfdc17; Wisp2; Wnt16</i>
Collagen degradation	19760 REACTOME	12	12	0	1	12	5.09E-04	<i>Col16a1; Col1a1; Col1a2; Col23a1; Col3a1; Col5a1; Col5a2; Col6a2; Mmp10; Mmp11; Mmp14; Mmp2;</i>
Extracellular matrix organization	17713 REACTOME	35	35	4	1	23	0.006	<i>Adamts2; Bmp7; Bsg; Col12a1; Col16a1; Col1a1; Col1a2; Col23a1; Col3a1; Col5a1; Col5a2; Col6a2; Comp; Crtap; Ctsg; Ctss; Ddr1; Efemp2; Fbln1; Fbln2; Lepre1; Leprel2; Lox; Mfap2; Mmp10; Mmp11; Mmp14; Mmp2; Nid2; P4hb; Pcolce; Plod1; Plod3; Serpinh1; Sparc;</i>
Degradation of the extracellular matrix	19757 REACTOME	15	15	2	1	12	0.02	<i>Bsg; Col16a1; Col1a1; Col1a2; Col23a1; Col3a1; Col5a1; Col5a2; Col6a2; Ctsg; Ctss; Mmp10; Mmp11; Mmp14; Mmp2;</i>

Table 3.5: Gene ontology terms and pathways over-represented in SkM versus skin EndoMac progenitors

The significant (corrected) gene ontology terms and pathways represented by the differentially expressed genes between SkM and skin progenitors are listed. Red and green indicate significantly up- and down- regulated genes, respectively, in SkM compared to skin progenitors in a pathway. Genes in black indicate non-significantly regulated genes. #Log₂FC cut off +/- 1.0 and associated adjusted p <0.05.

Pathway Name	Pathway Id (Source name)	Pathway uploaded gene count	Genes in InnateDB for this entity	Pathway up- regulated genes count#	Pathway up- regulated p- value (corrected)	Pathway down- regulated genes count#	Pathway down- regulated p-value (corrected)	Gene Symbols
Over-Represented Gene Ontology terms								
Scavenger receptor activity	GO:0005044 molecular function	11	11	1	1	10	0.01	<i>Cxcl16; Enpp2; Hhip1; Lgals3bp; Loxl2; Loxl4; Msr1; Prg4; Scara5; Scarf2; Susd2;</i>
Metallopeptidase activity	GO:0008237 Molecular function	17	17	1	1	13	0.01	<i>4833403I15Rik; Adam9; Adamts7; Adamts1; Bmp1; Folh1; Lta4h; Mmp10; Mmp11; Mmp14; Mmp2; Mmp23; Mmp27; Mmp3; Mmp8; Npepps; Pappa2;</i>
Collagen fibril organization	GO:0030199 Biological function	15	15	0	1	14	1.74E-04	<i>Adamts2; Col14a1; Col1a1; Col1a2; Col3a1; Col5a1; Col5a2; Cyp1b1; Lepre1; Loxl2; Lum; Mmp11; Plod3; Serpinh1; Sfrp2;</i>
Receptor-mediated endocytosis	GO:0006898 Biological function	21	21	4	1	16	0.003	<i>Cd300a; Cd36; Cxcl16; Enpp2; Hhip1; Ldlr; Lgals3bp; Loxl2; Loxl4; Lrp8; Mrc1; Msr1; Pla2r1; Pld2; Prg4; Repts1; Scara5; Scarb1; Scarf2; Susd2; Tfrc;</i>
Cellular response to amino acid stimulus	GO:0071230 Biological function	14	14	2	1	12	0.006	<i>0910001L09Rik; Cebpb; Col16a1; Col1a1; Col1a2; Col3a1; Col5a2; Egfr; Mmp2; Mmp3; Pdgd; Pdgra; Rragb; Sh3bp4;</i>
Collagen catabolic process	GO:0030574 Biological function	8	8	0	1	8	0.01	<i>Adamts2; Ctsk; Mmp10; Mmp11; Mmp14; Mmp2; Mmp3; Mmp8;</i>
Axon guidance	GO:0007411 Biological function	24	24	2	1	16	0.03	<i>Ablim1; Apbb1; Boc; Cdk5r1; Chl1; Draxin; Efna5; Enah; Eph4; Gas1; Gli2; Gli3; Nfasc; Ngfr; Nrp1; Ntn1; Plxna4; Pvr11; Scn1b; Sema3c; Sema4f; Sema5a; Slit3; Unc5b;</i>

Extracellular space	GO:0005615	141	141	21	1	83	2.30E-12	<p>1100001G20Rik; 9830001H06Rik; <i>Abi3bp</i>; <i>Adam9</i>; <i>Aebp1</i>; <i>Alox5</i>; <i>Alpl</i>; <i>Angpt1</i>; <i>App</i>; <i>Arsa</i>; <i>B4galt1</i>; <i>Bmp1</i>; <i>C1qtnf6</i>; <i>C1qtnf7</i>; <i>C4b</i>; <i>Car2</i>; <i>Cbr3</i>; <i>Ccl11</i>; <i>Ccl7</i>; <i>Ccl8</i>; <i>Ccl9</i>; <i>Cd36</i>; <i>Cfd</i>; <i>Cfl2</i>; <i>Cmtm3</i>; <i>Cmtm4</i>; <i>Col12a1</i>; <i>Col14a1</i>; <i>Col1a1</i>; <i>Col1a2</i>; <i>Col3a1</i>; <i>Comp</i>; <i>Cpxm1</i>; <i>Crtap</i>; <i>Ctsq</i>; <i>Ctsh</i>; <i>Ctsk</i>; <i>Cxcl16</i>; <i>Dcn</i>; <i>Ddr1</i>; <i>Dlg3</i>; <i>Eno2</i>; <i>Eno3</i>; <i>Enpp2</i>; <i>Ezr</i>; <i>F3</i>; <i>Fbln1</i>; <i>Fgf10</i>; <i>Figf</i>; <i>Frmd4b</i>; <i>Fstl1</i>; <i>Furin</i>; <i>Gas6</i>; <i>Gcnt1</i>; <i>Gdf11</i>; <i>Ghr</i>; <i>Golm1</i>; <i>Gpx3</i>; <i>Grem2</i>; <i>Gm</i>; <i>Hfe2</i>; <i>Icam1</i>; <i>Idc</i>; <i>Igf2r</i>; <i>Igfbp4</i>; <i>Igfbp6</i>; <i>Igfbp7</i>; <i>Il15</i>; <i>Il15ra</i>; <i>Il1b</i>; <i>Il4ra</i>; <i>Itm2b</i>; <i>Kcp</i>; <i>Lgals3</i>; <i>Lgals3bp</i>; <i>Loxl2</i>; <i>Loxl4</i>; <i>Lrp8</i>; <i>Ltp2</i>; <i>Lum</i>; <i>Mertk</i>; <i>Mif</i>; <i>Mmp2</i>; <i>Mmp8</i>; <i>Mov10</i>; <i>Mthfd2</i>; <i>Mtus1</i>; <i>Nampt</i>; <i>Nrp1</i>; <i>Otop1</i>; <i>Pcolce</i>; <i>Pcsk5</i>; <i>Pdgfa</i>; <i>Pdgfd</i>; <i>Pla2g7</i>; <i>Plat</i>; <i>Plau</i>; <i>Pltp</i>; <i>Podn</i>; <i>Prdx1</i>; <i>Prg4</i>; <i>Prkag2</i>; <i>Pros1</i>; <i>Prss34</i>; <i>Ptgis</i>; <i>Rab11fip4</i>; <i>Saa1</i>; <i>Scg2</i>; <i>Sema3c</i>; <i>Sema4c</i>; <i>Serpina3i</i>; <i>Serpinb1a</i>; <i>Serpinb9b</i>; <i>Serpinf1</i>; <i>Serping1</i>; <i>Serpinh1</i>; <i>Sfrp1</i>; <i>Sfrp2</i>; <i>Slit3</i>; <i>Sod3</i>; <i>Sorl1</i>; <i>Sparc</i>; <i>Spn</i>; <i>Srp2</i>; <i>Sulf2</i>; <i>Tfpi</i>; <i>Tfrc</i>; <i>Tg</i>; <i>Tgfb3</i>; <i>Timp2</i>; <i>Tnfrsf1a</i>; <i>Tnfsf11</i>; <i>Tnfsf9</i>; <i>Twsg1</i>; <i>Vash1</i>; <i>Vcan</i>; <i>Vegfa</i>; <i>Vegfb</i>; <i>Wdr60</i>; <i>Wisp2</i>; <i>Wnt16</i>;</p>
Extracellular matrix	GO:0031012	47	47	4	1	38	5.84E-11	<p><i>Abi3bp</i>; <i>Adamts10</i>; <i>Adamts15</i>; <i>Adamts2</i>; <i>Adamts6</i>; <i>Adamts7</i>; <i>Adamtsl1</i>; <i>Aebp1</i>; <i>Alpl</i>; <i>Col12a1</i>; <i>Col14a1</i>; <i>Col1a1</i>; <i>Col1a2</i>; <i>Col3a1</i>; <i>Col5a1</i>; <i>Comp</i>; <i>Ctsq</i>; <i>Dcn</i>; <i>Emilin1</i>; <i>F3</i>; <i>Fbln1</i>; <i>Fgf10</i>; <i>Igfbp7</i>; <i>Il1r1</i>; <i>Lgals3</i>; <i>Lgals3bp</i>; <i>Ltp2</i>; <i>Lum</i>; <i>Mmp10</i>; <i>Mmp11</i>; <i>Mmp14</i>; <i>Mmp2</i>; <i>Mmp23</i>; <i>Mmp27</i>; <i>Mmp3</i>; <i>Mmp8</i>; <i>Ndnf</i>; <i>Olfml2b</i>; <i>Pcolce</i>; <i>Prss34</i>; <i>Serpinf1</i>; <i>Sfrp1</i>; <i>Smoc2</i>; <i>Sod3</i>; <i>Sparc</i>; <i>Thbs2</i>; <i>Vcan</i>;</p>
Proteinaceous extracellular matrix	GO:0005578	39	39	3	1	32	2.42E-09	<p><i>Adamts15</i>; <i>Adamts2</i>; <i>Adamts6</i>; <i>Adamts7</i>; <i>Adamtsl1</i>; <i>Bmp1</i>; <i>Chl1</i>; <i>Col12a1</i>; <i>Col16a1</i>; <i>Col1a1</i>; <i>Col24a1</i>; <i>Comp</i>; <i>Cpz</i>; <i>Crtap</i>; <i>Dcn</i>; <i>Efemp2</i>; <i>Eln</i>; <i>Emilin1</i>; <i>Fbln2</i>; <i>Hapln4</i>; <i>Hpse</i>; <i>Lepre1</i>; <i>Lgals3</i>; <i>Lgals3bp</i>; <i>Lum</i>; <i>Mfap4</i>; <i>Mmp10</i>; <i>Mmp11</i>; <i>Mmp2</i>; <i>Mmp3</i>; <i>Mmp8</i>; <i>Podn</i>; <i>Sfrp1</i>; <i>Smoc1</i>; <i>Smoc2</i>; <i>Sparc</i>; <i>Tgfb3</i>; <i>Vcan</i>; <i>Wnt16</i>;</p>
Extracellular region	GO:0005576	109	109	20	1	61	1.73E-07	<p>1100001G20Rik; 4930503L19Rik; <i>Adam23</i>; <i>Adamts7</i>; <i>Adpgk</i>; <i>Apol6</i>; <i>Arsi</i>; <i>B4galt1</i>; <i>C1ra</i>; <i>C1s</i>; <i>C4b</i>; <i>Ccdc3</i>; <i>Ccl11</i>; <i>Ccl7</i>; <i>Ccl8</i>; <i>Ccl9</i>; <i>Cd34</i>; <i>Cd59a</i>; <i>Chrdl1</i>; <i>Col23a1</i>; <i>Colec11</i>; <i>Comp</i>; <i>Creg1</i>; <i>Cst7</i>; <i>Dhrs11</i>; <i>Dpp7</i>; <i>Draxin</i>; <i>Eln</i>; <i>Emc10</i>; <i>Emilin1</i>; <i>F13a1</i>; <i>Fbln1</i>; <i>Fbln2</i>; <i>Fgfbp3</i>; <i>Fibin</i>; <i>Figf</i>; <i>Fstl1</i>; <i>Fth1</i>; <i>Furin</i>; <i>Gas6</i>; <i>Ghr</i>; <i>Glb1l2</i>; <i>Glpr2</i>; <i>Gm885</i>; <i>Gnas</i>; <i>Gpr98</i>; <i>Hhpl1</i>; <i>Hmcn2</i>; <i>Hsd17b11</i>; <i>Igfbp4</i>; <i>Igfbp5</i>; <i>Igfbp6</i>; <i>Igfbp7</i>; <i>Iglon5</i>; <i>Igsf10</i>; <i>Il13ra2</i>; <i>Il15</i>; <i>Il1r1</i>; <i>Il1r2</i>; <i>Il1r11</i>; <i>Inhbb</i>; <i>Ism1</i>; <i>Itih5</i>; <i>Lama4</i>; <i>Lgi2</i>; <i>Lifr</i>; <i>Loxl4</i>; <i>Lyz1</i>; <i>Lyz2</i>; <i>Mif</i>; <i>Mmp3</i>; <i>Nbl1</i>; <i>Ndnf</i>; <i>Npc1</i>; <i>Ntn1</i>; <i>Olfml2b</i>; <i>Olfml3</i>; <i>Pdgfrl</i>; <i>Pla1a</i>; <i>Pla2g15</i>; <i>Pla2r1</i>; <i>Plat</i>; <i>Pltp</i>; <i>Pros1</i>; <i>Prrg4</i>; <i>Ptch1</i>; <i>Ptgfr</i>; <i>Rnase4</i>; <i>Saa1</i>; <i>Saa3</i>; <i>Scsep1</i>; <i>Serpinf1</i>; <i>Siglec1</i>; <i>St3gal1</i>; <i>St3gal2</i>; <i>Tek</i>; <i>Tfpi</i>; <i>Tfrc</i>; <i>Tg</i>; <i>Thbs2</i>; <i>Thsd7a</i>; <i>Tpsb2</i>; <i>Tulp3</i>; <i>Vcan</i>; <i>Vegfa</i>; <i>Vegfb</i>; <i>Wfdc17</i>; <i>Wisp2</i>; <i>Wnt16</i>;</p>

Collagen trimer	GO:0005581	16	16	1	1	14	8.70E-04	<i>C1qtnf6; C1qtnf7; Col12a1; Col14a1; Col16a1; Col1a1; Col1a2; Col23a1; Col24a1; Col3a1; Col5a1; Col5a2; Colec11; Emilin1; Msr1; Scara3;</i>
Over-Represented Pathways								
Collagen degradation	19760 REACTOME	12	12	0	1	12	5.09E-04	<i>Col16a1; Col1a1; Col1a2; Col23a1; Col3a1; Col5a1; Col5a2; Col6a2; Mmp10; Mmp11; Mmp14; Mmp2;</i>

3.3.7 STZ-induced hyperglycaemia is associated with fewer EndoMac progenitors with limited clonal renewal capacity in aorta

In addition to the functional and transcriptional differences observed between progenitors from different steady-state tissues, we have previously identified that different disease states also affect the properties of these cells. Recently, we identified CFU-M forming progenitors from digests of human saphenous vein (SV) and internal mammary artery (IMA) obtained from patients undergoing coronary artery bypass grafting surgery (A. Long, P. Psaltis, unpublished Honours Thesis). Among many different clinical factors recorded in almost 50 subjects enrolled in this study, a history of diabetes was associated with marked reductions in 1° CFU-M growth and 2° CFU-M renewal, as well as the ability of CFU-M progenitors to form cord networks in Matrigel™ and for SV “rings” to produce adventitial vascular sprouts in culture. These results strongly suggest that diabetes adversely affects the properties of these progenitors, which is consistent with its known inhibition of other stem/progenitor cell types (353, 499, 547). Here, we began to explore this further by using a murine model of STZ-induced type 1 diabetes (**Figure 3.7A**) (548). Three weeks after administering i.p. sodium citrate buffer or STZ (165 mg/kg), we confirmed significant differences in blood glucose concentrations (BGC) (sham/STZ- 9.1 ± 0.7 mmol/L vs diabetic/STZ+ 26.6 ± 6.9 mmol/L, $n=7$, $P<0.0001$) (**Figure 3.7B**) (548). We then harvested whole aortas intact, before carefully removing all surrounding fat and enzymatically digesting into single cell preparations.

We found a reduction in 1° CFU-M yield from STZ+ aortic cells (**Figure 3.7C**), while the progenitors isolated from these 1° CFU-M also had reduced capacity to form 2° CFU-M when compared to the sham group (**Figure 3.7D, E**). In keeping with these results, STZ+ aortas had a 2-fold lower prevalence of EndoMac progenitors, as quantified by flow cytometry (**Figure 3.7F, G**). This was

despite there being no significant difference in their content of MΦs, although they did have a non-significant trend toward fewer MΦs as well as ECs (**Figure 3.7H, I**).

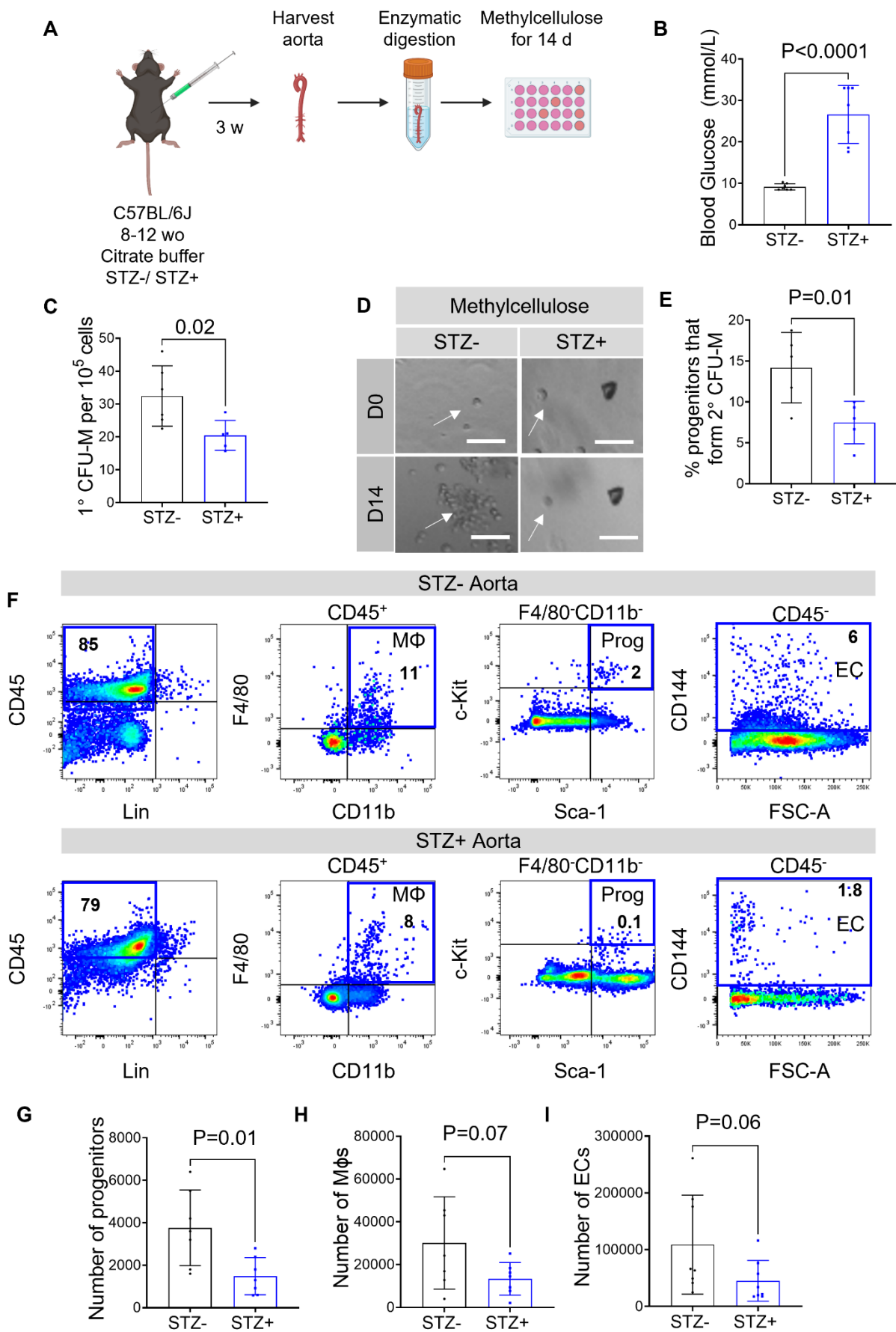


Figure 3.7: Hyperglycaemia is associated with fewer EndoMac progenitors in aorta

- A)** Schematic shows STZ induction of diabetes and enzymatic digestion of aortic tissue.
- B)** Blood glucose concentrations of STZ- and STZ+ C57Bl/6 mice 3 w after injection. n=7, unpaired *t*-test.
- C)** Comparison of 1° aortic CFU-M yield per 10⁵ cells plated from age-matched STZ- and STZ+ C57Bl/6 mice. n=5-6/gp, Unpaired *t*-test.
- D)** Light microscopy image of 2° CFU-M produced from single cell obtained from 1° CFU-M of STZ- aorta, whereas no 2° colony was formed from this example from STZ+ group. Scale bar, 100 µm.
- E)** Comparison of 2° colony renewal from single cells obtained from aortic 1° CFU-M of STZ- and STZ+ C57BL/6 mice. n=4-5/gp, Unpaired *t*-test.
- F)** Flow cytometry showing CD45⁺CD11b⁺F4/80⁺Sca-1⁺c-Kit⁺ EndoMac progenitors (Prog), CD45⁺CD11b⁺F4/80⁺ macrophages (MΦ) and CD45⁺CD144⁺ endothelial cells (ECs) in digests of STZ- and STZ+ aortas. Numerical values in dot plots represent mean percentages from n=7-8/gp.
- G-I)** Number of **G)** progenitors, **H)** MΦs and **I)** ECs per aorta of age-matched STZ- and STZ+ mice. n=7-8/gp, Unpaired *t*-test used in **G)** and **H)** and Mann-Whitney test in **I)**.

3.3.8 Aortic progenitors have diminished differentiation and angiogenic capacity from diabetic mice

We next examined the effect of hyperglycaemia on the *in vitro* capacity of aortic progenitors to form angiogenic cords in MatrigelTM. When compared to the STZ- sham group, progenitors from STZ+ mice had limited sprouting potential and formed less robust cords after 7 d of culture. (**Figure 3.8A**). Cumulative cord lengths were almost three-fold greater from STZ- aorta (**Figure 3.8B**), with significantly higher numbers of both cords (**Figure 3.8C**) and branch points (**Figure 3.8D**). Examination of the cellular composition of these branching cord networks in MatrigelTM by flow cytometry showed no significant differences between the STZ- and STZ+ progenitors for overall cell number (**Figure 3.8E, F**), although cell viability was significantly lower for the cultures from STZ+ progenitors (**Figure 3.8G**). The cord networks produced by STZ- progenitors contained more newly formed ECs (**Figure 3.8H**), along with a non-significant trend towards more MΦs compared to the STZ+ group (**Figure 3.8I**). Some retention of progenitors after 7 d in MatrigelTM was seen for both groups with no significant difference between the two (**Figure 3.8J**).

Taken together, our results show that diabetes attenuates the angiogenic capacity of aortic EndoMac progenitors, and this may be the result of decreased cell viability or decreased capacity for bipotent differentiation.

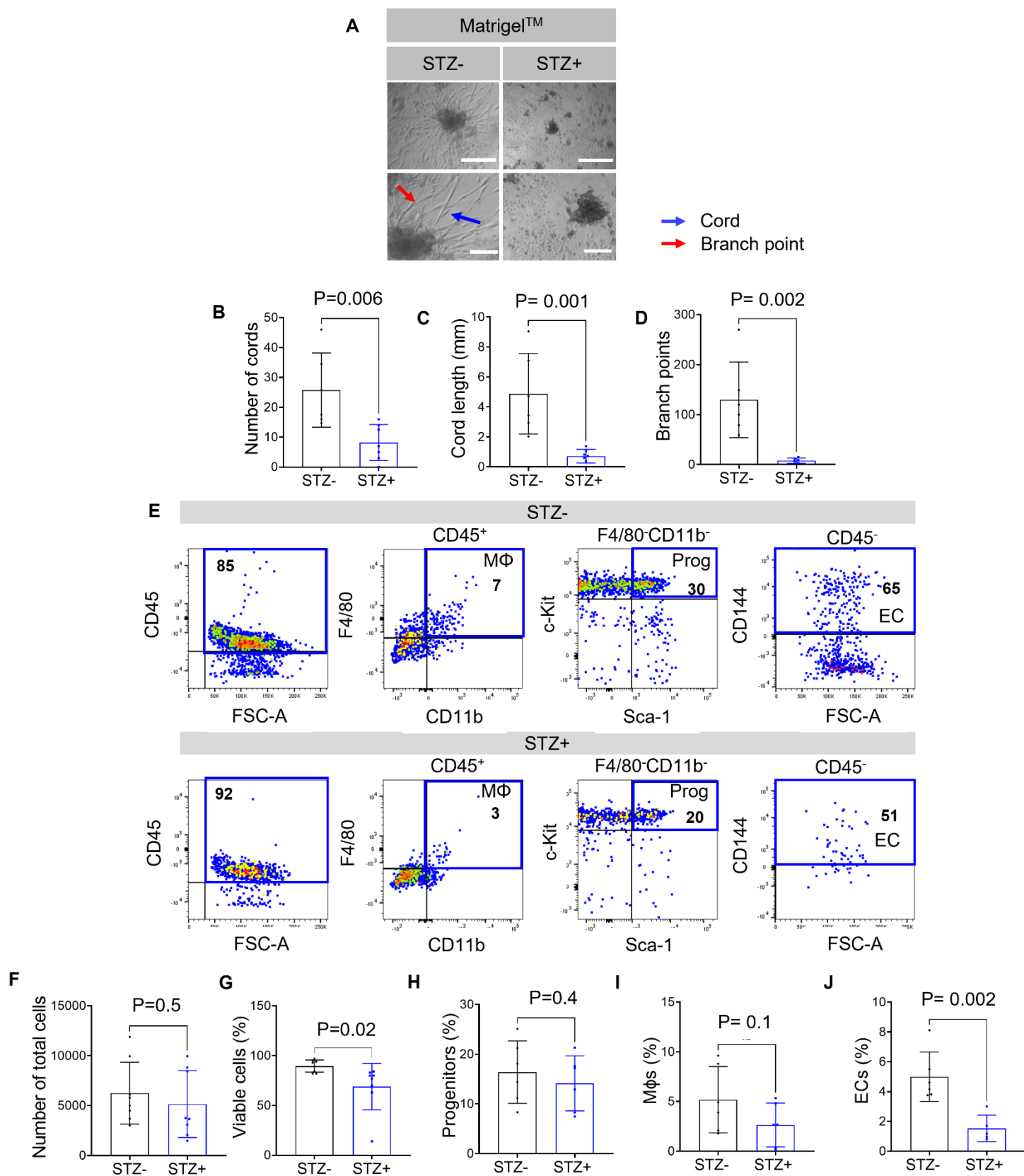


Figure 3.8: Diabetic aortic CFU-M progenitors have diminished differentiation and angiogenic capacity

A) Light microscopy images of cord networks produced by aortic progenitors from STZ- and STZ+ C57BL/6 mice. Cords denoted by blue arrows and branch points by red arrows. Scale bar, 100 μ m.

B-D) Graphs display comparisons of **B)** cord length, **C)** count and **D)** branch number. $n \geq 5$ /gp, Unpaired *t*-test.

E) Flow cytometry plots show cellular composition after progenitors were cultured in MatrigelTM for 7d, with evidence of residual CD45⁺CD11b⁻F4/80⁻Sca-1⁺c-Kit⁺ progenitors (Prog), CD45⁺CD11b⁺F4/80⁺ macrophages (M Φ) and CD45⁻CD144⁺ endothelial cells (ECs).

F-J) Graphs summarise the numbers of **F)** total cells and frequencies of **G)** viable cells, **H)** progenitors, **I)** M Φ s and **J)** ECs present in MatrigelTM after 7 d from the two groups. $n \geq 6$ /gp. Unpaired *t*-tests used in **F)**, **G)**, **H)** and **I)** and Mann-Whitney test for **J)**.

Data are summarised as mean \pm SD.

3.3.9 Diabetic aortic progenitors are prone to double-stranded DNA breaks

Having observed the inhibitory effects of hyperglycaemia on the key properties of aortic progenitors, we examined whether this was related to defects in their mitochondrial function and viability. Culture-derived aortic progenitors were isolated from CFU-M under microscopic guidance and stained with MitoTrackerTM green for mitochondrial viability and MitoTrackerTM red, which is taken up by the inner mitochondrial matrix and is dependent on membrane potential. Somewhat surprisingly, we did not find significant differences in either viable mitochondrial mass or membrane function between non-diabetic and diabetic cells (**Figure 3.9A, B**).

DNA damage may occur as a result of DNA replication in steady state, and largely due to oxidative stress in pathological conditions, resulting in double-stranded breaks, which are considered one of the most lethal forms of DNA damage (549). An early cellular response to these double-stranded breaks is the serine phosphorylation of H2AX, a histone variant, to produce γ H2AX (550). We therefore used flow cytometry to assess DNA integrity by measuring the H2AX expression percentage in aortic progenitors. This revealed that progenitors from STZ+ mice significantly higher levels of DNA damage (**Figure 3.9C**).

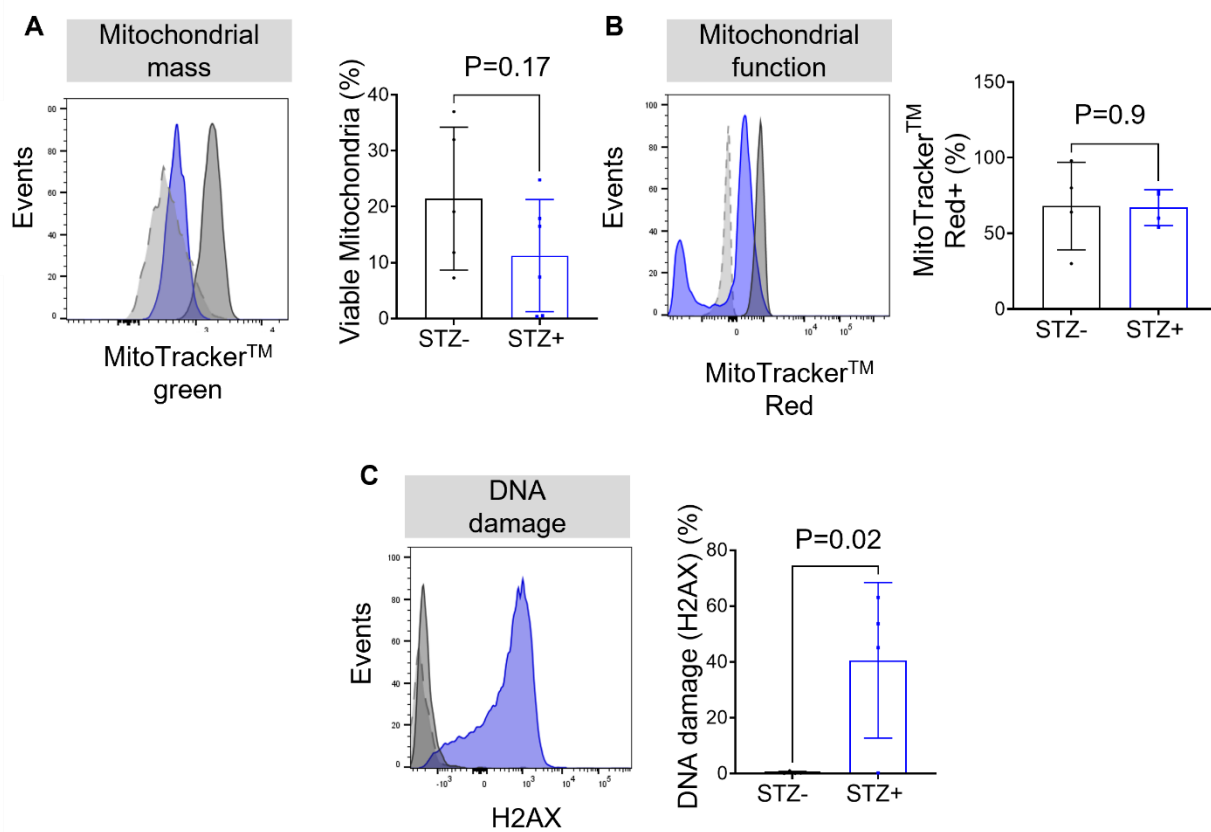


Figure 3.9: Diabetic aortic progenitors are prone to double-stranded DNA breaks

- A)** Flow cytometry histograms depict expression of MitotrackerTM green in progenitors isolated from aortic CFU-M from STZ+ (blue histogram) and STZ- (dark grey) mice. Graph summarises the percentage frequency of MitotrackerTM green expression from n=5-6/gp. Unpaired *t*-test.
- B)** Flow cytometry histograms show expression of MitoTrackerTM red in aortic progenitors from STZ+ (blue) and STZ- (dark grey) mice. Graph summarises the percentage frequency of MitotrackerTM red expression from n=4/gp. Unpaired *t*-test.
- C)** Flow cytometry histograms for expression of H2AX in aortic progenitors from the STZ+ (blue) and STZ- (dark grey) groups. Graph summarises the percentage frequency of H2AX expression from n=4/gp. Mann-Whitney test.

Data are summarised as mean±SD. used throughout. Light grey dotted lined histograms are negative controls.

3.3.10 Effects of *in vitro* exposure to high glucose on aortic progenitors

Finally, we also studied whether exposure to high glucose concentrations *in vitro* recapitulates similar inhibitory effects on progenitors, as that seen after STZ treatment and hyperglycaemia *in vivo*. Aortic cells from C57Bl/6 mice were cultured in methylcellulose. Replicate wells were exposed to two different concentrations of glucose (basal: 5 mM and high: 25 mM) or 25 mM mannitol as an osmolarity control, which were replenished every three days. Exposure to high glucose decreased aortic CFU-M yield by 4-fold compared to basal glucose (**Figure 3.10A**). Although we had previously observed that hyperglycaemia did not affect mitochondrial mass or function, addition of high glucose to culture medium substantially increased the production of lactate in the cell supernatant after 14 d (**Figure 3.10B**). Lactate/lactic acid is a by-product of anaerobic glycolysis, so this result could be an indication of progenitors using a non-mitochondrial pathway for ATP production under high glucose exposure. Alternatively, higher levels of lactate release may occur because of increased substrate utilisation, which was suggested by progenitors having a trend toward increased uptake of the glucose analogue, 2-(N-(7-Nitrobenz-2-oxa-1,3-diazol-4-yl)Amino)-2-Deoxyglucose (2-NBDG), when high glucose was added (**Figure 3.10C**). We also used the Seahorse™ assay to assess whether the increased glucose substrate presence led to heightened aerobic respiration. However, here we found that it significantly diminished cellular OCR (**Figure 3.10D**), which indicates attenuated mitochondrial respiration. Finally, despite being associated with higher lactate in the supernatant of cultured CFU-M, high glucose caused progenitors to have lower ECAR, indicating reduced anaerobic respiration (**Figure 3.10E**). These conflicting results (e.g., between higher supernatant lactate and lower cellular ECAR) are difficult to reconcile and will require further investigation.

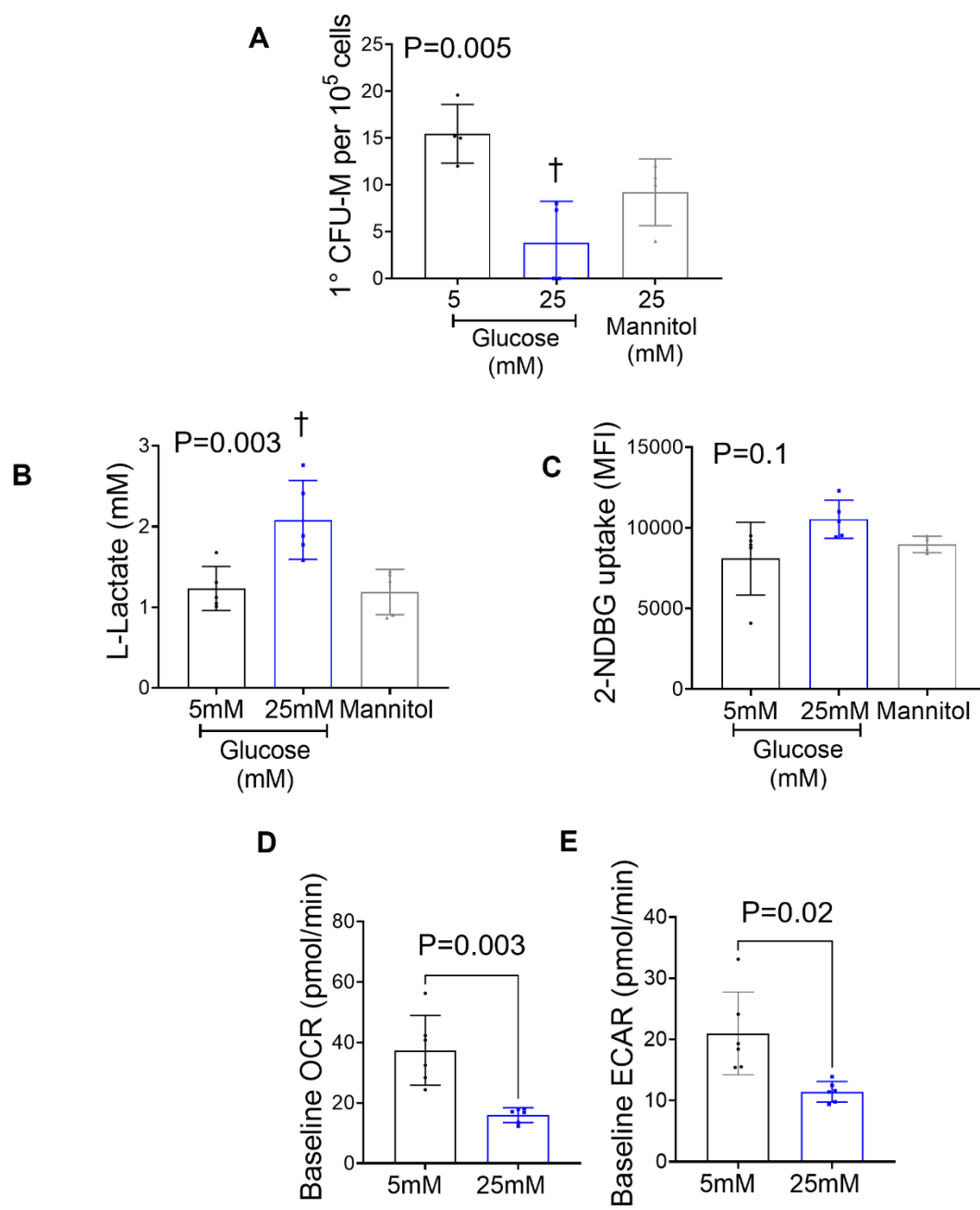


Figure 3.10: High glucose inhibits clonal expansion of EndoMac progenitors *in vitro* and alters their metabolic activity

A) Comparison of 1° CFU-M yield from C57BL/6 aortic cells under different concentrations of glucose (5 mM, 25 mM) and mannitol (25 mM). n=4/gp. One-way ANOVA. Multiple comparisons: † p<0.01 versus 5 mM glucose.

B) L-lactate concentrations in the supernatants of aortic CFU-M exposed to different glucose and mannitol concentrations. n=5/gp. One-way ANOVA. Multiple comparisons: † p<0.01 versus 5 mM glucose.

C) Comparison of mean fluorescent intensity (MFI) of uptake of 2-NDBG by aortic progenitors under different glucose conditions. n=5/gp. One-way ANOVA.

D-E) Comparison of baseline **D)** OCR and **E)** ECAR for progenitors isolated from aortic CFU-M following exposure to 5 mM and 25 mM glucose for 14 d in culture. n=6/gp. Paired *t*-test.

Data are summarised as mean±SD.

3.4 Discussion

Uncovering the mechanisms behind MΦ and EC crosstalk and the source of their tissue heterogeneity are key steps toward better understanding how inflammation and neovascularisation are regulated in different tissues. While both types of cells are thought to arise from multiple ontogeny pathways, YS EMPs have been identified as a common ancestral source during early embryogenesis. Our group's discovery of tissue EndoMac progenitors provides a plausible explanation for how embryonically derived MΦs and ECs can be maintained and replenished after birth in different tissue niches, without necessarily requiring circulatory input. To the best of our knowledge, these cells are the closest candidate yet described for the elusive, postnatal haemangioblast, which has intrigued scientists for almost a century (44, 76).

In this chapter, we have taken several key steps to better understanding the identity of EndoMac progenitors. Focusing on aorta, we have firstly confirmed that the cells responsible for the ability to produce CFU-M are indeed Lin⁻CD45⁺CD11b⁻F4/80⁻Sca-1⁺c-Kit⁺ progenitors. Just as importantly, we categorically show that CD11b⁺F4/80⁺ MΦs themselves have no clonogenic potential *in vitro*, which casts some doubt on the prevailing view that tissue MΦs can sustain themselves after birth by ongoing self-renewal (71, 73, 521). Indeed, previous studies that have propagated this claim have generally failed to provide direct proof that MΦs undergo self-renewal *in vivo*, except in the context of genetic knock-out models (521). The results of our analysis by flow cytometry and cytofluorescence microscopy all indicate that FACS-isolated and CFU-M derived progenitors both express several key surface antigens and genes, including c-Kit, Sca-1 (*Ly6a*) and CD45 (*Ptprc*), but in keeping with their undifferentiated status they do not yet exhibit mature endothelial (CDH5, EMCN) or macrophage (CD11b, F4/80, CD68) markers. This is of particular importance as other studies of progenitor cells, e.g., EPCs, show major phenotypic variations depending on method of

isolation and characterisation, which has hampered their investigation and potential use for regenerative, cell-based therapeutics (110, 424, 545, 551, 552).

Among the other findings from this study, we also demonstrate considerable overlap between EndoMac progenitors from adult mouse aorta, skin and SkM, while also beginning to uncover a degree of tissue-specific functional and transcriptional heterogeneity. MΦs and ECs are both well known for exhibiting heterogeneity across different tissue types, ages and pathophysiological settings (20, 75, 545, 553-555). In both instances, this is represented in the form of distinct sub-lineage populations that express different surface markers, functional repertoires, and genes (34, 75, 119, 555). Much of this seems to relate back to the varied pathways by which different subpopulations of MΦs and ECs are derived, including the influence of circulating versus embryonic ancestry, and systemic versus local renewal (28, 34, 36, 65, 70, 71, 112, 113, 556). In addition, the local tissue microenvironment is also thought to impart specific, niche-dependent regulatory cues on these cells shortly after they are seeded, including through epigenetic modifications (557, 558). Our results show that EndoMac progenitors are relatively consistent across the three tissues studied, which speaks to their common origin and shared fundamental properties (i.e., surface marker phenotype, capacity to form CFU-M, bipotency). However, we also identified that they possess some functional and gene expression differences, depending on the tissue milieu in which they are seeded. Presumably, this ensures that their properties are aligned to the specific needs of their host tissue across the spectrum of prenatal development, postnatal growth, homeostatic maintenance, and post-injury repair.

An exemplar of this, is the fact that EndoMac progenitors from SkM had upregulation of several muscle-related genes, including: *Ano5*, which is abundantly expressed in skeletal myocytes and regulates intracellular chloride ion movement essential for their contractile function (559); *Pax7*,

which drives the transition of SkM satellite cells from a quiescent to activated state (402, 413); and *Ckm*, which encodes for a pyruvate kinase involved in glycolysis that catalyses the transfer of a phosphoryl group from phosphoenolpyruvate to ADP, generating ATP and pyruvate (560). The latter was also corroborated by our *in vitro* metabolic assays that showed higher metabolic activity (both glycolysis and oxidative phosphorylation) for SkM progenitors compared to those from donor-matched aorta and skin. Conversely, aortic progenitors showed marked upregulation of *Wt1*, involved in cell proliferation and differentiation, as well as *Hoxb9* genes (561), that induce the expression of several angiogenic factors (e.g., VEGF, bFGF) (562). Pathway analysis revealed significant downregulation of genes involved in extracellular matrix organisation and degradation, as well as cellular response to amino acid stimulus when compared to skin progenitors. This may provide some insight as to why aortic progenitors also displayed lower clonogenic and self-renewal capacity.

In addition to the influence of tissue niche, we have also previously determined that the prevalence and stem-like properties of EndoMac progenitors become progressively attenuated due to postnatal ageing (520, 522). Based on our observations pertaining to CFU-M progenitors in human vasculature (563), we also focused here on the effect of high glucose on murine aortic progenitors. Using both the STZ-induced model of type 1 diabetes and addition of high glucose to culture medium, we elucidated wide-ranging inhibition of the key properties of these cells. Our results suggested adverse effects on both their proliferative expansion and renewal, as well as viability and DNA integrity. Each of these effects could contribute to the reduced prevalence of EndoMac progenitors in the diabetic aortic wall, which was detectable after just 3 w of hyperglycaemia. The glucose-induced suppression of the "stemness" and angiogenic characteristics of murine aortic progenitors aligns with the known inhibitory effects of diabetes on other types of BM and tissue-resident progenitor cells (547, 564). The underlying mechanisms for this are most likely complex. Here, we elected to explore for potential metabolic/mitochondrial disturbances, as these are known to help mediate the effects of diabetes on

other stem/progenitor cell populations in different tissues (197, 225, 565, 566). Limited by small sample size, we failed to elicit alterations in viable mitochondrial mass or function in progenitors cultured from STZ+ diabetic aortas but did find that exposure to a high glucose concentration *in vitro* diminished both aerobic and glycolytic respiration. However, the latter seemed at odds with the parallel finding of excess lactate accumulation in culture supernatant.

In the case of the vasculature, the effects of hyperglycaemia on aortic EndoMac progenitors may have important consequences for the way that arteries remodel in different disease states, such as atherosclerosis and aneurysm formation. Our preliminary studies have indicated that the progenitors, which are located within the *tunica adventitia*, contribute to adventitial inflammation and neovascularisation, and therefore the formation of *vasa vasorum* during development of atherosclerosis (517). This creates an intriguing paradox, as *vasa vasorum* feed and promote the growth and instability of atherosclerotic plaques (517, 544). It follows that impaired formation of *vasa vasorum* by glucose-induced dampening of adventitial EndoMac progenitors may be expected to have a beneficial, anti-atherosclerotic effect on diabetic vasculature. However, other studies have shown that although diabetic plaques do contain fewer *vasa vasorum*, their microvessels tend to be poorly developed and leaky (567). This increases the likelihood of haemorrhage and the exudation of inflammatory cells and molecular mediators into the plaque, making it more prone to rupture and thrombotic complications.

Limitations and future directions

Our RNA-bulk sequencing experiment showed considerable overlap in gene expression between progenitors from three different tissue sources, but with some variations. Factors that may have confounded these results are small group sizes and precision in age and gender matching of samples. Validation of differentially expressed genes from independent samples at the mRNA and protein

levels is required to confirm these findings. Going forward we will study transcriptomic variations in EndoMac progenitors from non-diabetic and diabetic tissues to identify specific mechanistic pathways that may be up- or downregulated to account for the inhibitory functional effects of hyperglycaemia. For this purpose, samples have already been collected and processed, which will allow transcriptomic pathway analysis in the future. In addition, we intend to study the effect of high glucose on the productions of reactive oxidative species (i.e., superoxide) of aortic EndoMac progenitors, which was attempted here unsuccessfully due to a methodological failure. We hypothesise that diabetic aortic progenitors will have increased superoxide production, which may explain the increased DNA double-stranded breaks and their diminished renewal and differentiation capacity.

Conclusion

In conclusion, this chapter describes the phenotypic uniformity of EndoMac progenitors from both tissue and culture-derived sources and demonstrates their unique angiogenic and bipotent differentiation capacity for MΦs and EC at both a clonal and a single-cell level. Further, progenitors isolated from various tissue sources possess some niche-specific transcriptional, functional, and metabolic variations and RNA bulk sequencing allow insight into various genes responsible for this heterogeneity. Finally, we address the effect of tissue state on these EndoMac progenitors and demonstrated the profound inhibitory effects of high glucose *in vitro* and hyperglycaemia *in vivo* on the prevalence, stemness, and function of aortic progenitors. Broadly, these findings provide critical scientific knowledge into the shared origins of MΦs and ECs.

Chapter 4

4. Inhibitory effects of diabetes on yolk-sac derived endothelial-macrophage progenitors in murine skin and wound healing

4.1 Introduction

Skin wounds and ulcers are among the most debilitating complications of diabetes mellitus. As the global burden of diabetes rapidly rises, the incidence of diabetic ulcers continues to advance (120). The lifetime chance of a person with diabetes developing a foot ulcer has been estimated to be 19-34%, while diabetes-related foot amputations have increased by more than 50% in the past 10 years (120). A significant percentage of diabetic ulcers are caused by mixed micro- and macrovascular dysfunction leading to impaired perfusion of tissue (347). Left untreated, chronic limb-threatening ischaemia has a poor prognosis and is correlated with limb loss and increased mortality. Despite intensive research and subsequent advances in diabetic wound care technology, current treatment options are still associated with clinical outcomes that are grossly suboptimal (347, 350).

Wound healing is a complicated process that involves both resident and invading immune cells in skin (286, 325, 568). The typical healing process is defined by three dynamic, overlapping phases: inflammation, proliferation, and tissue remodelling (325). Macrophages (MΦs) and endothelial cells (ECs) are two crucial cell types that are reciprocally involved in tissue inflammation and perfusion recovery, especially in the context of wound repair (19). While ECs are responsible for neovascularisation, MΦs play crucial paracrine roles via the secretion of pro-angiogenic cytokines (e.g., vascular endothelial growth factor A, VEGF-A) and coordinate vascular fusion of emerging endothelial sprouts (569). In turn, ECs are known to support the expansion and differentiation of pro-angiogenic MΦs from myeloid cells (10).

Skin wound MΦs originate both from tissue-resident MΦs and infiltrating monocytes from the peripheral circulation, with a larger contribution from the latter (275, 357, 525, 555). Tissue-resident MΦs are thought to be early responders to skin injury via their detection of damage-associated

molecular pattern (DAMP) or pathogen-associated molecular pattern (PAMP) molecules (555). These MΦs originate prenatally from extra-embryonic yolk sac (YS) but are replenished by foetal liver-derived monocytes in the embryo and by bone marrow (BM) derived monocytes after birth (8, 29, 270). In addition, epidermal dendritic cells, called Langerhans cells, which share MΦ markers (e.g. MHC-II, F4/80, CD14) also play important roles in wound healing (525, 555). Langerhans cells originate both from the YS during primitive haematopoiesis and foetal liver-derived monocytes during definitive haematopoiesis. They are maintained after birth by self-replication without replenishment from BM-derived cells (28, 29, 40). Recent studies have revealed that a subset of dermal MΦs also originate from YS erythromyeloid progenitors (EMPs) and these too are maintained via local renewal throughout postnatal life (28, 36, 37). Like MΦs, ECs in skin also display phenotypic, functional and transcriptomic heterogeneity and this is thought to be, at least in part, due to their complex origins (570). Cutaneous ECs may arise from proliferative renewal of resident, mature ECs (382, 528, 529), proliferation and differentiation of local progenitor cells (111, 114, 119, 551, 570-572) or recruitment and differentiation of circulating BM-derived endothelial progenitor cells (EPCs) (284). However, the respective contributions of these sources to ECs remains unknown, both under steady-state and pathophysiological conditions, such as wound injury. Interestingly, YS EMPs have been shown to give rise to ECs in some murine organs, including the brain, liver, lung, and heart (109), while our group has also demonstrated this for skin (522).

In diabetes, the wound repair process is delayed, at least in part, due to increased wound inflammation and changes in the number, phenotype, and function of MΦs, including decreased VEGF-A production (180, 330, 358, 375, 573). In addition, the hyperglycaemic conditions in diabetes cause EC dysfunction, which contributes to poor wound perfusion and recovery (574). In some studies, reduced number (575, 576), apoptosis (577) and dysfunction (116) of circulating EPCs have also been implicated in delayed diabetic wound healing. Although the mechanisms for MΦ and EC

dysfunction in diabetes are multifactorial, key roles have been attributed to mitochondrial dysfunction and the intracellular production of subsequent damaging reactive oxygen species (ROS) for both cell types (383, 578-580). Diabetes has also been shown to cause mitochondrial dysfunction, DNA damage and low expression of cyclin D1 in epidermal stem cells, which impairs their clonal renewal and reparative properties, and this may also contribute to impaired skin healing (564, 581).

As discussed in Chapter 3, we have identified that some adult mouse tissues, including skin, contain local, YS-derived progenitor cells that are capable of clonal self-renewal and bipotent differentiation into MΦs and EC (517, 518, 520). Notably, our unpublished studies have found that skin EndoMac progenitors expand rapidly in both wound injury and melanoma models in wildtype mice, before differentiating into MΦs and ECs and contributing to the formation of new blood vessels (520, 522). In the case of wound injury, this was associated with accelerated and improved wound closure, while in melanoma it resulted in larger tumour size. This chapter set out to build on this previous work by examining how skin EndoMac progenitor cells are affected by high glucose conditions, and whether this may help mediate impaired wound healing in diabetes.

4.2 Methods in brief

4.2.1 Overview

Breeding pairs of C57BL/6 (C57BL/6J), *Csf1r*^{Mer-iCre-Mer} (FVB-Tg(Csf1r-cre/Esr1*)1Jwp/J), *Rosa*^{mT/mG} (Gt(ROSA)26Sor^{tm4}(ACTB-tdTomato,-EGFP)Luo/J) and UBI-GFP (C57BL/6-Tg(UBC-GFP)30Scha/J) mouse strains were acquired from The Jackson Laboratory (Bar Harbor, ME, USA). *Csf1r*^{Mer-iCre-Mer} and *Rosa*^{mT/mG} mice were crossed to obtain *Csf1r*^{Mer-iCre-Mer} x *Rosa*^{mT/mG} pups. Mice were housed in the animal care facility at SAHMRI. In all cases, both genders were utilised. For the induction of type 1 diabetes, intraperitoneal injections of 165 µg/g streptozotocin (STZ) were administered while non-diabetic controls received citrate buffer injections. Blood glucose concentrations (BGC) were monitored beginning from a week post-injection and diabetes was confirmed by a BGC >15 mmol/L. An extra dose of STZ was administered if the levels were <15 mmol/L one-week post-injection.

Animals were housed on a standard chow diet with a continuous water supply replaced every other day or as needed for a period of three weeks. Skin from these mice comprising epidermis and dermis, but not subcutaneous fat, was enzymatically digested into single cell suspensions for use in different experiments, including methylcellulose colony forming unit (CFU), MatrigelTM-based angiogenesis assays and multi-colour flow cytometry. Several experiments also made use of a validated model of murine wound healing (582), either in combination with tamoxifen (TAM)-inducible *Csf1r*^{Mer-iCre-Mer} x *Rosa*^{mT/mG} fate-mapping or with adoptive transfer of GFP⁺ Skin EndoMac progenitors into C57BL/6 recipient mice. All animal experiments and care were performed following the standards stated in the Guide for the Care and Use of Laboratory Animals (Institute of Laboratory Animal Resources, National Academy of Sciences, Bethesda, MD, USA) and in accordance with the National Health and Medical Research Council of Australia research guidelines and Australian Code for the Care and Use

of Animals for Scientific Purposes. Ethics approval was obtained from the SAHMRI animal ethics committee (ID SAM20.032 and SAM432.19).

4.2.2 Statistical analysis

Where relevant, analysis was performed blinded to study group. Statistical comparisons were performed using Prism (GraphPad version 10). Data sets were tested for normality of distribution by Shapiro-Wilk test. Statistical comparisons were performed with parametric or non-parametric unpaired or paired two sample *t*-tests or ANOVA (with post-test multiple comparisons), as specified. Results are expressed as mean \pm standard deviation of multiple experiments. In all cases, statistical significance was established at two-tailed $p < 0.05$. The statistical parameters and the number of mice used per experiment are found in the figure legends.

4.3 Results

4.3.1 High glucose attenuates stem-like and angiogenic properties of skin EndoMac progenitors

As described in Chapter 3, skin cells showed a unique predilection for forming primary (1°) CFU-M when cultured in methylcellulose. To study the effect of glucose on haematopoietic colony formation, we digested dorsal skin from 8–12 w C57BL/6J mice and cultured the resulting single cell suspensions at a density of 2×10^5 cells per well in 24 well-plates in methylcellulose for 14 d (**Figure 4.1A**). Replicate wells were exposed to three different concentrations of glucose (basal: 5 mM, intermediate: 15 mM, high: 25 mM) and 25 mM mannitol as an osmolarity control. Exposure to basal glucose and mannitol produced no significant difference in CFU-M yield (59.8 ± 20.5 vs 36.0 ± 12.9 colonies/ 10^5 cells, $n=5/\text{gp}$). Intermediate and high glucose levels significantly decreased skin CFU-M yield by 3 and 5.4-fold, respectively compared to basal glucose (**Figure 4.1B**). CFU-M in basal glucose consisted of 69% small (30-100 cells), 29% medium (100-1000 cells) and 1% large (>1000 cells) colonies. By comparison, the high glucose condition was associated with the formation of only of small CFU-M (**Figure 4.1C**). This suggests that the progenitors responsible for CFU-M development *in vitro* may be inhibited by high glucose in terms of their proliferative and/or renewal capability.

This was confirmed by colony renewal assays where CFU-M were individually isolated from 1° methylcellulose cultures at day 14 under microscopic guidance and disaggregated to allow the seeding of single cells into different wells in 2° CFU-M assays. Skin CFU-M were observed to renew from single cell origins (**Figure 4.1D**), with 83% of cells from 1° CFU-M giving rise to at least one 2° colony under basal glucose conditions, compared to only 5.9% under exposure to intermediate and 2.7% under high glucose concentrations ($n=5/\text{gp}$, $P<0.0001$). In the presence of the 25 mM mannitol

osmolarity control, we found a more modest but still significant drop in 2° CFU-M renewal compared to the basal condition.

Progenitors isolated from 1° skin CFU-M also produce complex, vascular-like cord networks when cultured for 7 d in endothelial growth media on Matrigel™ (**Figure 4.1E**). This capacity was substantially reduced when cultured in 15 mM and 25 mM glucose (**Figure 4.1E**), with 78% and 81% mean reduction, respectively, in total cord length formed compared to 5 mM glucose (**Figure 4.1F**). Similarly, increased glucose exposure led to the formation of fewer cords (**Figure 4.1G**) and connecting branch points (**Figure 4.1H**).

These findings show that increased glucose concentrations significantly reduce the clonal, renewal and angiogenic potential of skin EndoMac progenitors *in vitro*.

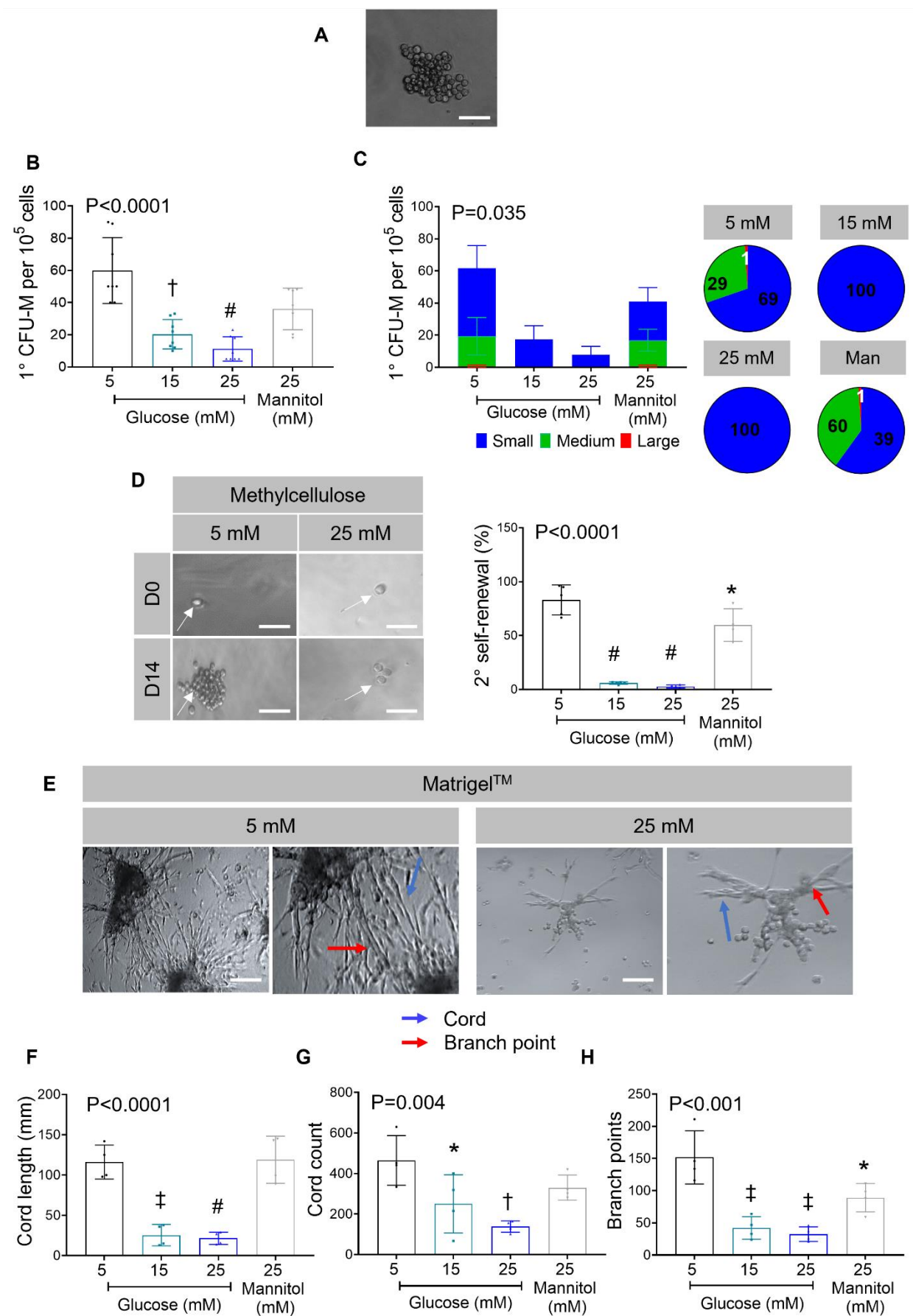


Figure 4.1: High glucose attenuates stem-like and angiogenic properties of skin EndoMac progenitors.

A) Light microscopy of a skin CFU-M of the small size (30-100 cells) from adult C57BL/6 mouse. Scale bar, 100 μ m.

B) Comparison of 1° CFU-M yield from donor-matched C57BL/6 skin cells cultured in different concentrations of glucose (5 mM, 15 mM, 25 mM) and mannitol (25 mM). n=7-8 mice/gp. Kruskal-Wallis. Multiple comparisons: †P<0.01, #P<0.0001, in comparison to 5 mM glucose.

C) Bar graph showing size distribution of 1° CFU-M from donor-matched C57BL/6 skin cells cultured in different concentrations of glucose (5 mM, 15 mM, 25 mM) and mannitol (25 mM). CFU-M size is classified as small (30-100 cells), medium (100-1000 cells) and large (>1000 cells). n=6 mice/gp. One-way ANOVA. Adjacent pie charts show the same data as a % of CFU-M based on colony size classification. Percentages represent mean of n=6 mice/gp. Man=mannitol

D) Light microscopy of 2° CFU-M produced from a single cell obtained from C57BL/6 skin 1° CFU-M exposed to 5 mM and 25 mM glucose. Scale bar, 100 μ m. Graphs shows comparison of 2° colony renewal from single cells obtained from 1° CFU-M. The experiment was performed using cells from n=5 mice. One-way ANOVA. Multiple comparisons: *P=0.05 and #P<0.0001 in comparison to 5 mM glucose.

E) Light microscopy images of branching cord networks produced from skin EndoMac progenitors in Matrigel™ cultured in the presence of 5 mM and 25 mM glucose. Scale bar, 100 μ m (left) and 1000 μ m (right). Scale bar, 100 μ m.

F-H) Graphs display comparisons of **F)** total cord length, **G)** cord number and **H)** branch number produced from skin EndoMac progenitors under different glucose concentrations. n=4 mice. One-way ANOVA. Multiple comparison: *p<0.05, †P<0.01 ‡P<0.001 and #P<0.0001 in comparison to 5 mM.

4.3.2 High glucose inhibits mitochondrial metabolic activity of skin EndoMac progenitors

Diabetes is known to alter mitochondrial and metabolic function of adult stem cells, as described for multiple tissues (192, 209, 583). Therefore, we examined whether mitochondrial function of skin EndoMac progenitors is altered in high glucose and accounts for the functional inhibition of these cells *in vitro*. We carried out a series of metabolic assays that investigate mitochondrial viability and function. Skin EndoMac progenitors were isolated from 1° CFU-M cultures in basal and high glucose conditions and stained for three mitochondrial markers (MitoTracker™ Green, MitoTracker™ Red, MitoSOX™) and analysed by flow cytometry. As we had limited n-values for some of these experiments, this may have precluded statistical significance. Nevertheless, the high glucose condition showed a strong trend for reduced viable mitochondria measured by expression of MitoTracker™ green (**Figure 4.2A**). This was accompanied by a 1.5-fold increase in mitochondrial ROS, as measured by uptake of the MitoSOX™ dye, indicating superoxide build-up (**Figure 4.2B**). Mitochondrial function was studied by the proportion of MitoTracker™ red expression which showed a trend for reduction in the 25 mM glucose condition. This is indicative of a potential defect in mitochondrial membrane potential in response to high glucose (**Figure 4.2C**).

Having established a high glucose related reduction in the number and function of mitochondria, we explored the glycolytic capacity of these cells by measuring the build-up of lactate in supernatants after culture. Glycolysis is an anaerobic process that does not require functional mitochondria to supply energy for cellular functions. We observed a 3-fold increase in extracellular lactate in cells exposed to high glucose levels. This suggests that in the presence of mitochondrial defects, skin EndoMac progenitors may predominantly utilise an alternative anaerobic pathway to supply cellular energy demand (**Figure 4.2D**). This corresponded with a 1.6-fold increase in uptake of the glucose analogue, 2-(N-(7-nitrobenzene-2-oxa-1,3-diazol-4-yl)amino)-2-deoxyglucose (2NDBG), under high compared to basal glucose conditions (**Figure 4.2E**). Based on this, we can speculate that the

increase in glucose uptake into the cells may be due to increased substrate utilisation to supply the energy demand that is being carried out by glycolytic means. Glycolysis itself yields only two ATP molecules per reaction and therefore would require fast uptake of substrates to meet the cellular energy demand. Increased substrate uptake may also be linked to the production of damaging ROS in response to high glucose. Taken together, the functional defects caused by high glucose on EndoMac progenitors might at least be partly due to mitochondrial dysfunction, with compensatory increased reliance on anaerobic glycolysis for energy production.

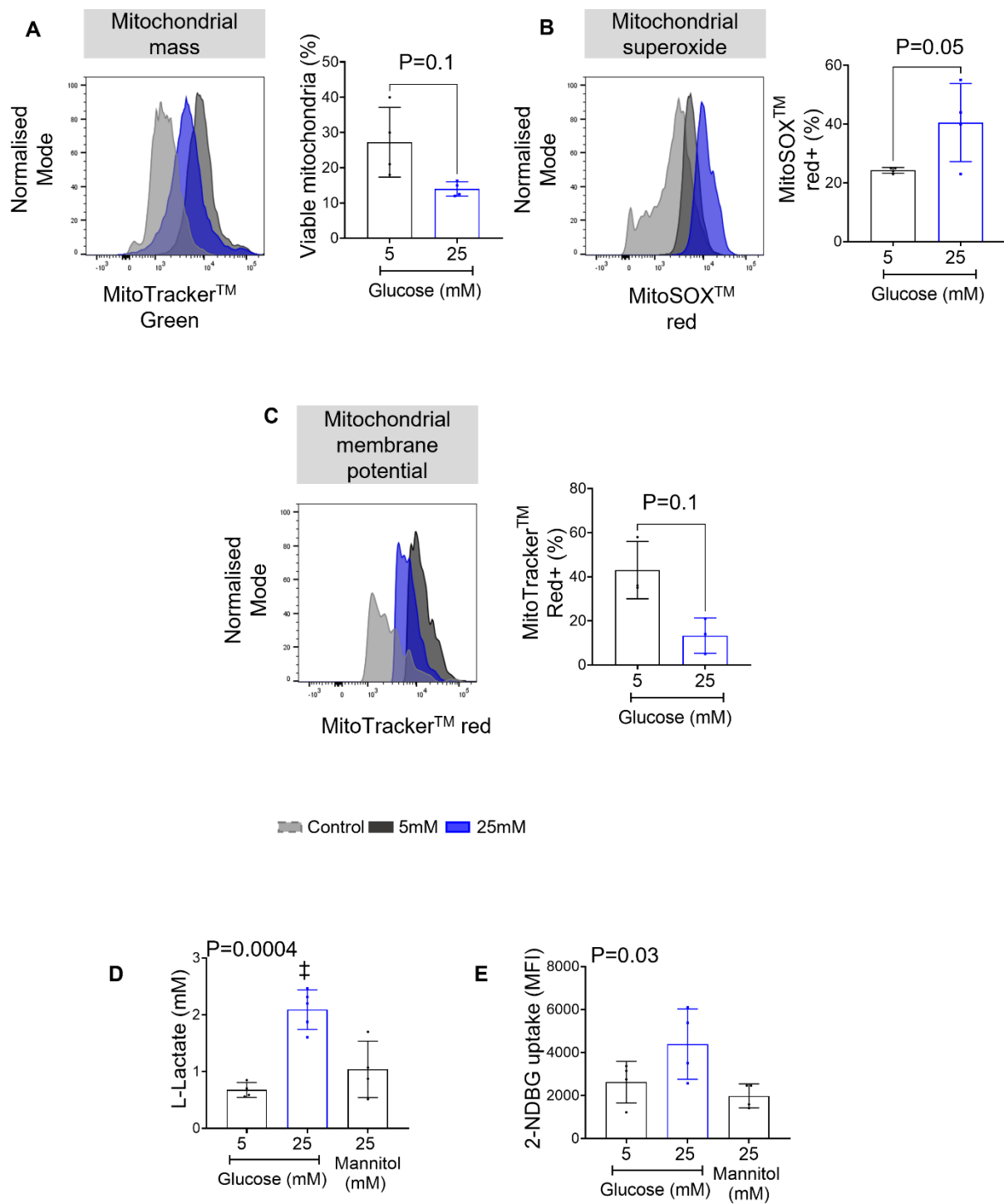


Figure 4.2: Exposure to high glucose levels dampen the mitochondrial function of skin progenitors

A) Flow cytometry histograms depict the expression of MitoTracker™ green as marker of viable mitochondrial mass. Light grey histograms are FMO controls. Representative of n=3 12 w C57BL/6 mice. The graph shows frequency of MitoTracker™ green expression from CFU-M derived EndoMac progenitors under exposure to 5 mM and 25 mM glucose. n=3, paired *t*-test.

B) Flow cytometry histograms show expression of MitoSOX™ red mitochondrial superoxide. Light grey histograms represent FMO controls. Representative of n=4 12 w C57BL/6 mice. The graph shows the frequency of MitoSOX™ Red expression in progenitors exposed to 5 mM and 25 mM glucose indicating mitochondrial superoxide. n=4, paired *t*-test.

C) Flow cytometry histograms depict the expression of MitoTracker™ red. Light grey histograms represent FMO controls. Representative of n=3 12 w C57BL/6 mice. The graph shows the frequency of MitoTracker™ red expression from progenitors exposed to 5 mM and 25 mM glucose. n=3, paired *t*-test.

D) Comparison of L-lactate concentrations in the supernatants of cultures with progenitors exposed to different glucose and mannitol concentrations. n=4, One-way ANOVA. Multiple comparison test: ‡p<0.001 for 25 mM vs 5 mM.

E) Comparison of mean fluorescent intensity indicating uptake of glucose analogue (2-NDBG) by progenitors under different glucose conditions. n=4, One-way ANOVA.

4.3.3 Skin EndoMac progenitors function at lower metabolic capacity when exposed to high glucose

Mitochondrial function can be further investigated by examining its oxygen consumption rate (OCR) and extracellular acidification rate (ECAR). While OCR corresponds to mitochondrial oxidative phosphorylation, ECAR is an indirect measure of anaerobic glycolysis. The gold standard in measuring this involves the Seahorse™ Assay that utilises three mitochondrial inhibitors: Oligomycin, carbonyl cyanide p-trifluoro methoxyphenylhydrazone (FCCP) and Rotenone/Antimycin-A at time points as specified in (**Figures 4.3A**). Skin CFU-M cultured in basal and high glucose were isolated to assess OCR and ECAR following exposure to these three mitochondrial inhibitors. Initially, baseline OCR was significantly lower in progenitors exposed to 25 mM glucose (5 mM: 32.3 ± 8.5 vs 25 mM: 13.9 ± 10.7 pmol/min, $n=6$, $P=0.03$) (**Figure 4.3B**). This finding reveals that high glucose exposure may directly attenuate aerobic respiration of mitochondria.

Oligomycin, which inhibits ATP synthase (complex V) was injected first in the assay 16 min after basal measurements. Targeting the ATP synthase complex of the electron transport chain (ETC) directly alters the electron flow and the membrane potential gradient of the ETC, leading to reduced mitochondrial respiration, or OCR (**Figure 4.3A**). Therefore, as expected, an OCR decrease was observed in both 5 mM and 25 mM groups as inhibition of ATP-synthase in the ETC would prevent phosphorylation of Adenosine diphosphate (ADP) into ATP during oxidative phosphorylation, a process that utilises O_2 . This decline in OCR was used to calculate mitochondrial ATP-linked respiration (ATP-linked respiration = average basal OCR - average OCR post oligomycin). Interestingly, the dependence on mitochondrial ATP-synthase for ATP production showed a higher trend in the basal glucose group, with an OCR of ~16 pmol/min for basal and ~8 pmol/min for high glucose concentrations, contributing to the production of ATP (difference of 8 pmol/min between the two groups, $n=6$, $P=0.1$) (**Figure 4.3C**).

The sudden increase in OCR beyond baseline was observed at 40 min following injection of the uncoupler FCCP to potentially supply the energy demand that was unmet during the ATP synthase inhibition stage. FCCP simulates a physiological energy requirement by driving the respiratory chain to work at full capacity, resulting in fast oxidation of substrates (sugars, lipids, and amino acids) to meet this metabolic challenge and boosting mitochondrial oxygen consumption. This rapid increase was used to calculate reserve capacity compared to basal respiration, which was 6-fold higher for basal glucose compared to high glucose (**Figure 4.3D**). This provided further information on the maximal respiration capacity of mitochondria, which demonstrated a mean OCR difference of ~23 pmol/min under basal compared to high glucose conditions (37.7 ± 8.5 vs 14.7 ± 10.8 , $n=6$, $P=0.01$) (**Figure 4.3E**). This indicates the cells' capacity to adapt to metabolic change and is a measure of their ability to restore the unmet energy demand. Taken together, our findings suggest that excessive glucose inhibits the metabolic activity of skin progenitors at both mitochondrial oxidative phosphorylation stages, as well as their ability to recover after metabolic stress.

The final inhibitors used were Rotenone/Antimycin A which target and inhibit the function of the mitochondrial ETC complex I and III. The inhibition of these complexes would prevent electron transport all together and therefore cause a reduction in OCR to a minimal value as mitochondrial oxidative function is paused. The fall in OCR following ETC complex inhibition for basal glucose compared to high glucose was significantly larger ($\Delta\text{OCR } 19.7 \pm 9.4$ pmol/L vs 7.3 ± 3.7 pmol/L, $n=6$, $P=0.01$). This further confirms the dependence on mitochondria for ATP synthesis in skin EndoMac progenitors.

To investigate whether high glucose launches a compensatory mechanism to meet the increasing energy demand following mitochondrial inhibitors, we next investigated anaerobic glycolysis activity

by measuring extracellular acidification rate (ECAR) (**Figure 4.3F**). Overall, cytoplasmic baseline glycolysis was significantly higher under basal compared to high glucose levels, as observed by a 1.6-fold higher ECAR (28.5 ± 6.7 vs 17.3 ± 3.4 , $n=6$, $P=0.01$) (**Figure 4.3G**). Following oligomycin injection, the glycolytic capacity of both basal and high glucose groups increased by 3.4 pmol/min and 3.9 pmol/min, respectively, compared to baseline ECAR ($n=6$, $P=0.6$) (**Figure 4.3H**). This indicates that inhibition of mitochondrial ATP synthesis may potentially result in the use of anaerobic glycolysis as the predominant source of energy for both groups. Maximum glycolytic capacity was observed following uncoupling via FCCP. This capacity once again showed a trend towards a higher for the basal glucose condition (42 ± 10.1 vs 28.6 ± 8.5 , $n=6$, $P=0.1$) (**Figure 4.3I**). ECAR continued to be maintained at a higher rate following inhibition of mitochondrial complexes with Rotenone and Antimycin A, further implying that glycolysis may also contribute to supplying the demand for energy within the cell.

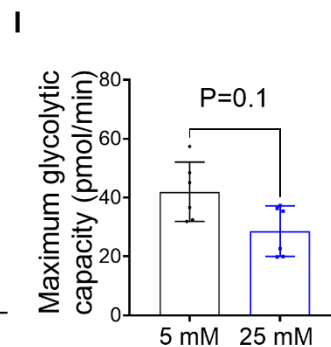
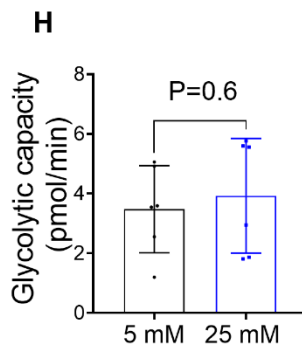
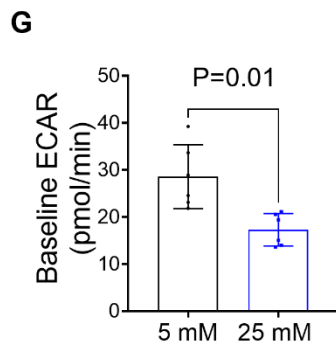
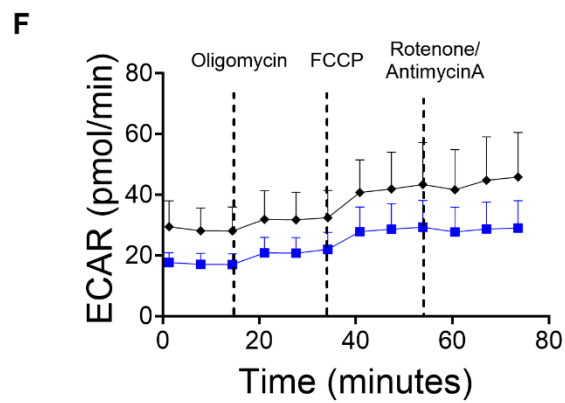
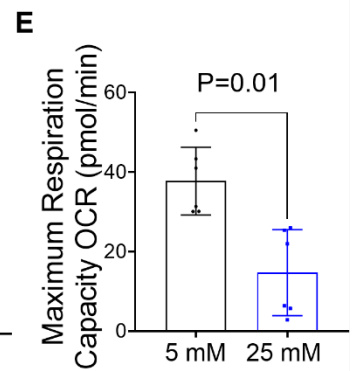
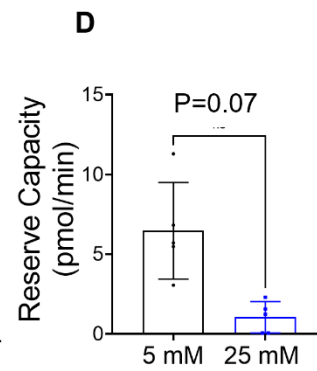
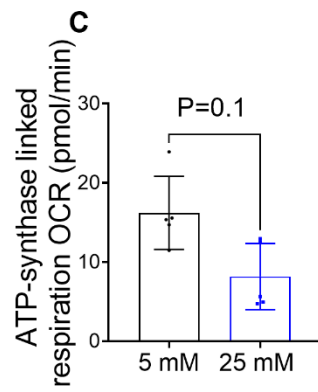
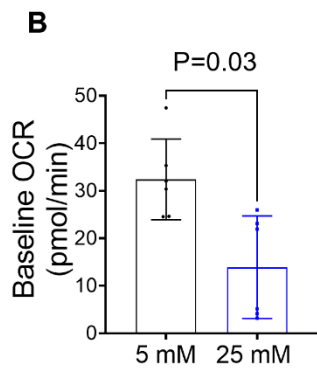
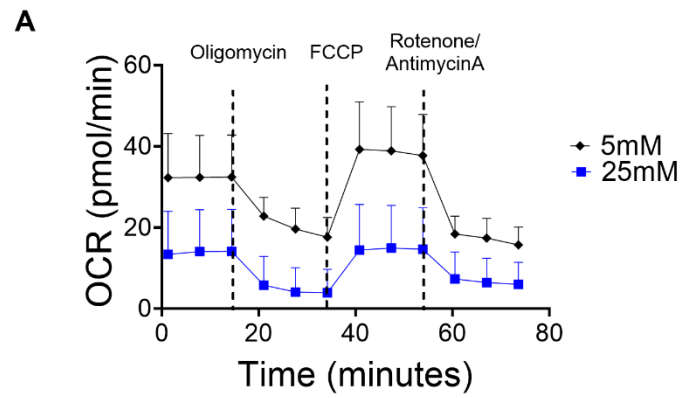


Figure 4.3: Skin EndoMac progenitor function at a lower metabolic capacity under high glucose.

A) Comparison of oxygen consumption rate (OCR) over a period of 73 min for skin CFU-M exposed to 5 mM and 25 mM glucose. Dotted lines indicate the time at which mitochondrial inhibitors: Oligomycin (Oligo), Carbonyl cyanide 4-(trifluoromethoxy)phenylhydrazone (FCCP), Rotenone and Antimycin-A was added. n=6. Skin CFU-M cultures were obtained from C57BL/6 skin digests.

B) Baseline OCR **C)** ATP-linked respiration **D)** Reserve capacity **E)** Maximal respiration capacity of skin progenitors exposed to 5 mM and 25 mM glucose. n=6, **B-C)** Wilcoxon test, **D-E)** Paired *t*-test.

F) Comparison of extracellular acidification rate (ECAR) over a period of 73 min for skin CFU-M exposed to 5 mM and 25 mM glucose. Dotted lines indicate the time at which mitochondrial inhibitors: Oligomycin (Oligo), Carbonyl cyanide 4-(trifluoromethoxy)phenylhydrazone (FCCP), Rotenone and Antimycin-A was added. n=6.

G) Baseline ECAR, **H)** Glycolytic capacity and **I)** Maximum glycolytic capacity for skin CFU-M/EndoMac progenitors exposed to 5 mM and 25 mM glucose. n=6, **G)** Paired *t*-test, **H-I)** Wilcoxon test

4.3.4 STZ-induced hyperglycaemia is associated with fewer EndoMac progenitors in skin

Inhibition of the properties of skin EndoMac progenitors by high glucose prompted us to investigate the effect of hyperglycaemia on these cells *in vivo*. For this, fresh tissue digests of adult skin from C57BL/6 non-diabetic (STZ)- and diabetic (STZ+) mice were examined for their content of EndoMac progenitors, MΦs and ECs by flow cytometry (**Figure 4.4A**). As per our previous studies (517, 518, 520), EndoMac progenitors were gated as CD45⁺CD11b⁻F4/80⁻ Sca-1⁺c-Kit⁺ cells, while MΦs were detected as CD45⁺CD11b⁺F4/80⁺ and ECs as CD45⁻CD144⁺ (**Figure 4.4B**). Diabetes led to a significant decrease in the prevalence of EndoMac progenitors compared to non-diabetic skin (STZ-: 7,494±3,394 vs STZ+ 4,040 ±2,875 cells/g, n=9-10/gp, P=0.02) (**Figure 4.4B, C**). On the other hand, the prevalence of MΦs was not significantly different between the two groups (STZ-: 43,180±34,708 vs STZ+: 26,177±21,927 cells/g, n=9-10, P=0.3) (**Figure 4.4D**). Similarly, we did not observe significant differences in the content of ECs between digests of STZ- and STZ+ skin (214,020±105,475 vs 133,286±121,373 cells/g, n=9-10/gp, P=0.1) (**Figure 4.4E**). However, for both cell types, results indicated a trend towards a lower prevalence in diabetic skin.

We further studied the relationship between BGCs and these three cells populations and found significant inverse relationships between BGCs and skin content of EndoMac progenitors (**Figure 4.4F**) but not MΦs (**Figure 4.4G**) or ECs (**Figure 4.4H**).

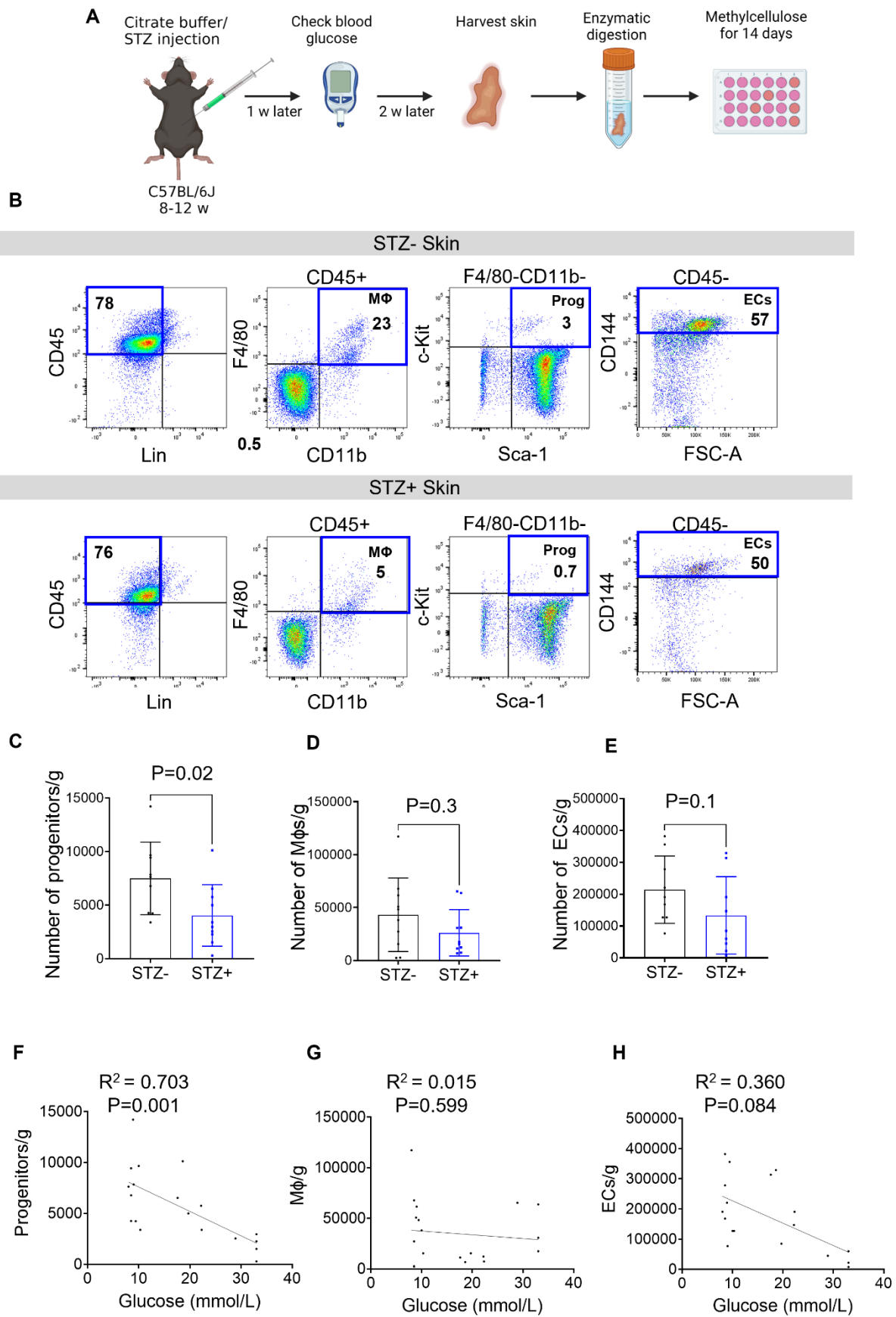


Figure 4.4: STZ-induced diabetes is associated with fewer EndoMac progenitors in skin

A) Schematic showing induction of diabetes in mice with STZ and the process of establishing CFU-M cultures from skin progenitors of diabetic and non-diabetic mice

B) Flow cytometry showing expression of skin $CD45^+CD11b-F4/80-Sca-1^+c-Kit^+$ EndoMac progenitors, $CD45^+CD11b^+F4/80^+$ macrophages (MΦ) and $CD45^-CD144^+$ endothelial cells (ECs) from STZ- and STZ+ C57Bl/6 mice. Numerical values in dot plots represent mean percentages from n=9-10/gp.

C-E) Graphs show **C)** number of progenitors, **D)** MΦs and **E)** ECs per gram (g) of skin from age-matched STZ- and STZ+ mice. N=9-10/gp. Unpaired *t*-test for **C)** and **E)**, Mann-Whitney test for **D)**.

F-H) Simple linear regression graphs showing relationships between the number of **F)** progenitors, **G)** MΦs and **H)** ECs per gram in skin and BGCs from all mice studied, n=9-10/gp.

(Refer to Appendix 7.4)

Consistent with the decreased prevalence of EndoMac progenitors in diabetic skin measured by flow cytometry, we also observed a marked reduction in 1° CFU-M yield from STZ+ skin cells (STZ-101±16.4 vs STZ+ 37.9±15.7 CFU-M per 105 cells plated, n=10/gp, P<0.0001). (**Figure 4.5A-C**). In addition, in keeping with the formation of exclusively small colonies under high glucose conditions *in vitro*, the colonies cultured from STZ+ mice showed a trend for similarly diminished clonal growth (**Figure 4.5D**) and much lower capacity to form 2° CFU-M when replated in methylcellulose (**Figure 4.5E-F**). These striking findings show that exposure to hyperglycaemia *in vivo* inhibits both the prevalence and clonal renewal capacity of skin EndoMac progenitors, even when these cells are subsequently cultured under basal glucose concentration for 14 d (1° CFU-M assay) and 28 d (2° CFU-M assay) after their removal from the diabetic environment.

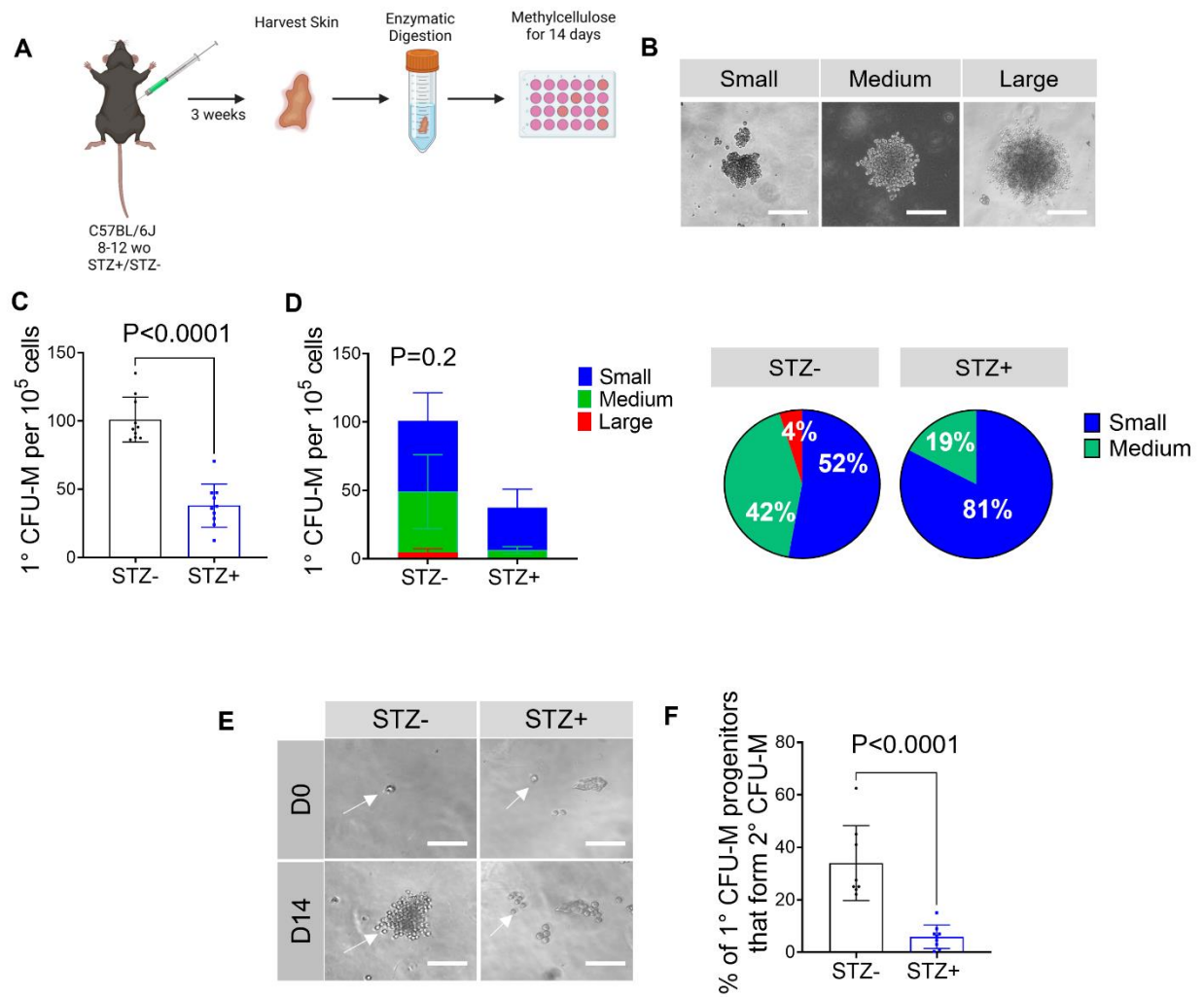


Figure 4.5: Diabetes attenuates the clonal renewal capacity of skin EndoMac progenitors.

- A)** Schematic showing enzymatic digestion of skin tissue from age-matched STZ- and STZ+ C57Bl/6 mice.
- B)** Light microscopy images show representative CFU-M from skin digests, classified according to size: small, medium, and large. Scale bar, 100 μ m.
- C)** Comparison of 1° skin CFU-M yield per 10⁵ cells plated from age-matched STZ- and STZ+ C57Bl/6 mice. n=10/gp. Mann-Whitney test.
- D)** Bar graphs with CFU-M sizes overlayed from the two groups. n=10 mice/gp. Two-way ANOVA results: p=<0.0001 for size; p=<0.0001 for group; p=0.004 for size x group.
- Pie charts show classification of CFU-M based on colony size from STZ- and STZ+ skin digests. Percentages represent mean of n=10 mice/gp.
- E)** Light microscopy images show a 2° CFU-M produced from single cell obtained from skin 1° CFU-M from a STZ- mouse, compared to only a small 2° cluster from STZ+ mouse. Scale bar, 100 μ m.
- F)** Graph shows comparison of 2° colony renewal from single cells obtained from skin 1° CFU-M of STZ- and STZ+ C57BL/6 mice. n=8-9/gp, Mann-Whitney test.

4.3.5 Diabetic skin EndoMac progenitors are more prone to DNA damage and mitochondrial abnormalities

Besides mitochondrial dysfunction, diabetes is also known to lead to DNA damage (584, 585). Hence, we investigated the presence of double-stranded DNA breaks in skin EndoMac progenitors as the possible basis for attenuation of their clonogenicity and renewal capacity by diabetes. We used expression of the fluorescent marker, anti-H2AX, which detects γ -H2AX at sites of nucleotide double-stranded breaks, to analyse for the proportion of DNA damage in cultured progenitors via flow cytometry. STZ+ progenitors showed more than doubling in the percentage of phosphorylated H2AX expression compared to STZ- cells (STZ- $0.9 \pm 0.4\%$ vs STZ+ 2.0 ± 1.5 , $n=5/\text{gp}$, $P=0.04$) (**Figure 4.6A**).

In keeping with the reduced mitochondrial viability observed under high glucose conditions *in vitro* (**Figure 4.2A**), progenitors from diabetic skin CFU-M showed a significant reduction in viable mitochondrial mass (**Figure 4.6B**). Further, they displayed higher expression of MitoSoxTM red consistent with increased accumulation of ROS and suggesting increased metabolic stress (**Figure 4.6C**). This may also explain the elevated proportion of DNA damage described above. STZ+ progenitors also showed significant dampening of mitochondrial membrane potential indicating dysfunction in oxidative phosphorylation (**Figure 4.6D**). Taken together, it can be speculated that the decline in mitochondrial oxidative function as seen by defective membrane potential, may have resulted in an alternative metabolic pathway to supply the energy demand or may be due to the significant loss in mitochondrial mass within cells. To further investigate this, we analysed the concentrations of lactate in the supernatants of progenitor cultures and found higher extracellular lactate concentrations in EndoMac progenitors from skin of STZ+ compared to STZ- mice (**Figure 4.6E**). STZ+ progenitors also displayed a significantly higher substrate utilisation that was evident by the higher uptake of 2-NDBG. This likely occurred to supply the energy demand by anaerobic

means that would otherwise be unmet by fewer functional mitochondria. (**Figure 4.6F**). This increased glucose utilisation may also contribute to the overall increase in mitochondrial oxidative stress in the diabetic cells.

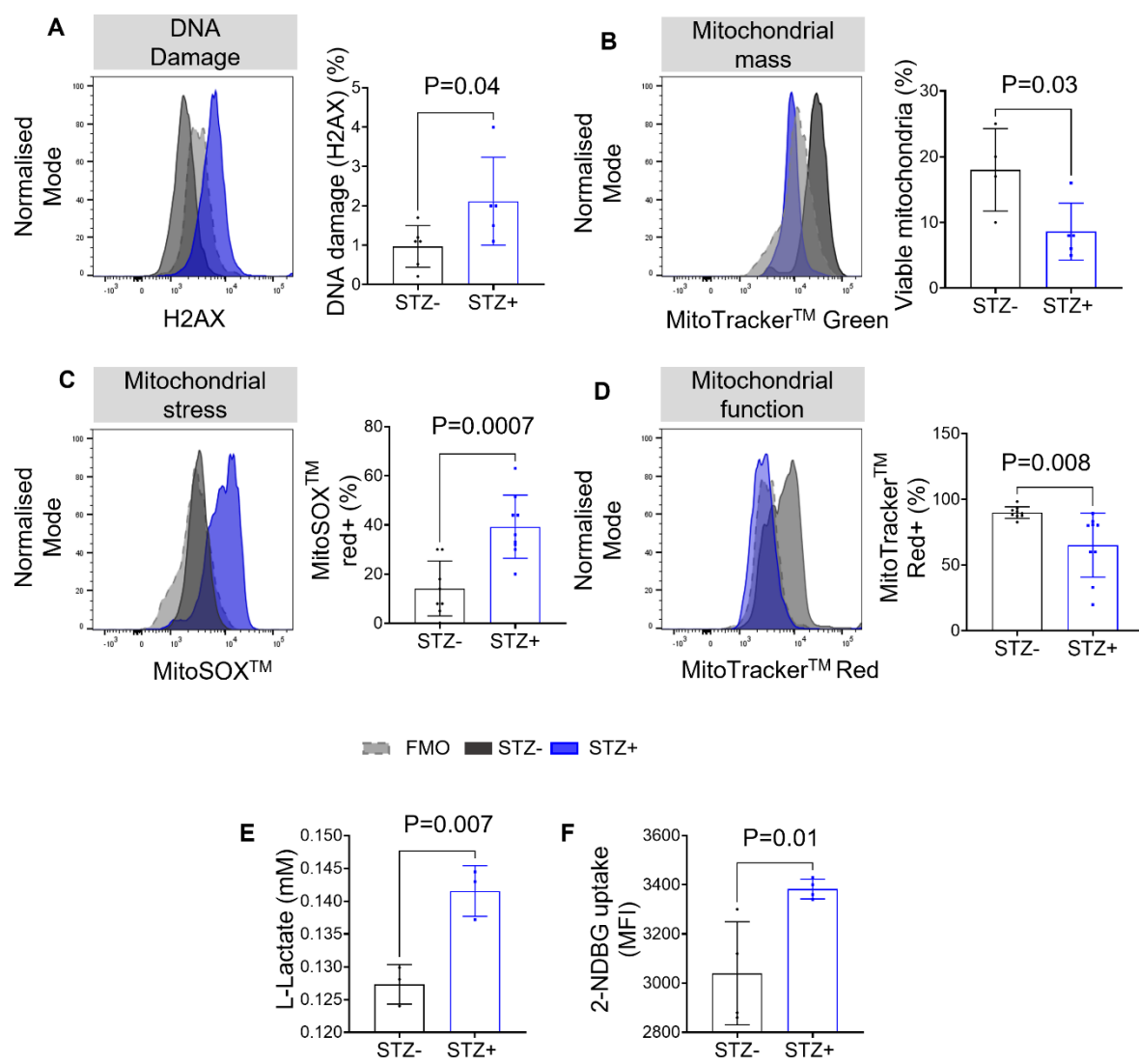


Figure 4.6: Diabetic skin EndoMac progenitors are more prone to DNA damage and mitochondrial abnormalities.

A) Flow cytometry histograms depicting levels of expression of γ -H2AX in progenitors isolated from skin CFU-M from STZ+ and STZ- C57BL/6 mice. Light grey histograms represent FMO controls. Graph summarises the percentage frequency of γ -H2AX expression from n=5-6 mice/gp. Unpaired *t*-test.

B) Flow cytometry histograms depicting MitoTracker™ green labelling of progenitors isolated from skin CFU-M from STZ+ and STZ- C57BL/6 mice (12 w, n=5-6). Light grey histograms represent FMO controls. Graph summarises the percentage frequency of MitoTracker™ green expression from n=5-6/gp. Unpaired *t*-test.

C) Flow cytometry histograms depicting MitoSOX™ red labelling of progenitors isolated from skin CFU-M from STZ+ and STZ- C57BL/6 mice (12 w, n=9). Light grey histograms represent FMO controls. Graph summarises the percentage frequency of MitoSOX™ red expression from n=9 per group. Unpaired *t*-test.

D) Flow cytometry histograms depicting MitotTacker™ red labelling of progenitors isolated from skin CFU-M from STZ+ and STZ- C57BL/6 mice (12 w, n=9). Light grey histograms represent FMO controls. Graph summarises the percentage frequency of MitoTracker™ red expression from n=9 per group. Unpaired *t*-test.

E) L-lactate concentrations in the supernatants of 1° EndoMac progenitors. from STZ- and STZ+ C57BL/6 mice. n=3, unpaired *t*-test.

F) Comparison of mean florescent intensity of glucose analogue (2-NDBG) indicating glucose uptake by 1° CFU-M from STZ- and STZ+ C57BL/6 mice. n=4, unpaired *t*-test.

4.3.6 Diabetic skin EndoMac progenitors have diminished differentiation and angiogenic capacity *in vitro*

Having established the functional decline of wildtype EndoMac progenitors when exposed to high glucose *in vitro*, we next examined the effect of hyperglycaemia on the capacity of diabetic skin progenitors to form angiogenic cords in MatrigelTM. Progenitors from STZ+ diabetic mice showed limited sprouting potential and formed less robust cords compared to the STZ- sham group (**Figure 4.7A**). Cumulative cord lengths were almost 6.4-fold greater from STZ- skin (**Figure 4.7B**), with significantly higher numbers of both cords (**Figure 4.7C**) and branch points (**Figure 4.7D**).

Examination of the cellular composition of MatrigelTM cords by flow cytometry revealed that the networks produced by STZ- skin progenitors contained newly formed ECs, along with fewer than expected MΦs based on our prior work, and some retained progenitor cells (**Figure 4.7E**). Comparing the results of culturing STZ+ and STZ- skin progenitors in MatrigelTM for 7 d, we found a borderline significant reduction in overall cell viability for the STZ+ group (**Figure 4.7F**). Whereas the proportion of remaining progenitor cells was similar between groups (**Figure 4.7G**), STZ+ cultures showed a trend toward containing more MΦs (**Figure 4.7H**) and a significant reduction in the percentage of new ECs (**Figure 4.7I**). Interestingly, in these assays we observed that most cells that were produced from both STZ+ and STZ- progenitors did not fall into the three specified populations of progenitors, MΦs, ECs. Based on these results we speculate that these “other” cells may represent alternative lineages that we have not yet considered (e.g., mesenchymal) or intermediate subpopulations that are yet to acquire “mature” surface markers for myeloid and endothelial fates (**Figure 4.7J**). This will require further evaluation but falls outside the scope of my PhD.

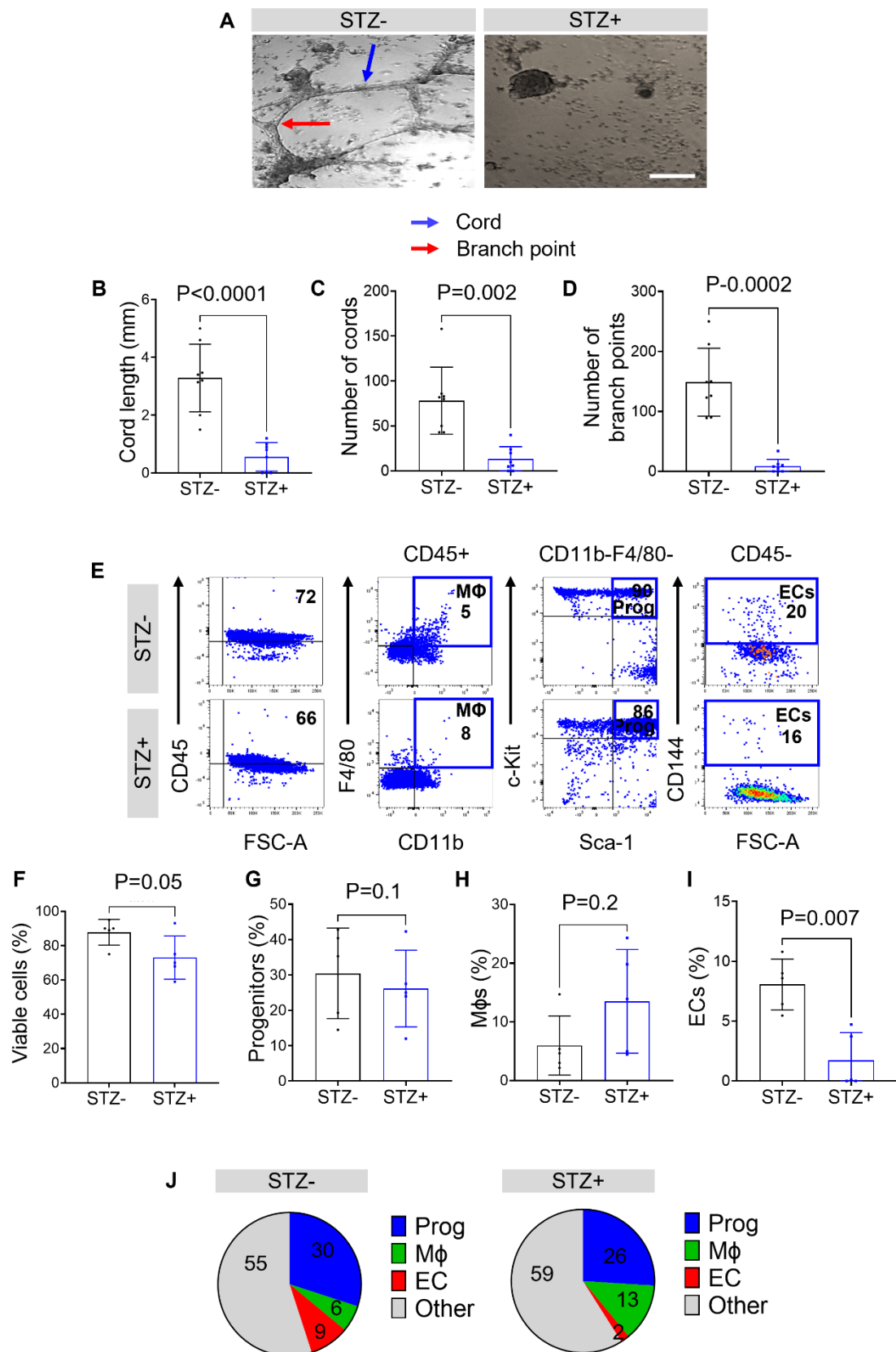


Figure 4.7: Diabetic skin progenitors have diminished cord-forming capacity.

A) Light microscopy images of representative cord networks from progenitors isolated from skin CFU-M of STZ- and STZ+ C57BL/6 mice in Matrigel™. Cords shown by blue arrows and branch points shown by red arrows. Scale bar, 100 μ m.

B-D) Graphs display comparisons of **B)** cord length, **C)** cord count and **D)** branch number. n=10/gp, unpaired *t*-test for **B)**. Mann-Whitney test for **C)** and **D)**

E) Flow cytometry plots showing the cellular composition of skin CFU-M progenitors from STZ- and STZ+ C57BL/6 mice after 7 d of culture in Matrigel™. Gating used was Single cells⁺AF700⁺ for viability, CD45⁺CD11b⁺F4/80⁻c-Kit⁺Sca-1⁺ for progenitors (Prog), CD45⁺CD11b⁺F4/80⁺ for macrophages (MΦ) and CD45⁻CD144⁺ for endothelial cells (ECs). Numbers represent the mean percentages in that respective gate from n=5/gp.

F-I) Graphs show frequency of **F)** total viable cells, **G)** progenitors, **H)** MΦ and **I)** ECs after 7 d in Matrigel™ assays from skin CFU-M progenitors from STZ- and STZ+ C57BL/6 mice after 7 d in culture. n=5/gp, unpaired *t*-tests for **F)** and **G)**, and Mann-Whitney for **I)**

Pie charts depict the frequency of different cell lineages produced after skin CFU-M progenitors from STZ- and STZ+ C57BL/6 mice were cultured in Matrigel™. n=5/gp.

(Refer to Appendix 7.4)

4.3.7 Diabetes impairs wound healing with diminished expansion of EndoMac progenitors after wound injury

We previously established that skin EndoMac progenitors derive from CSF1R⁺ YS EMPs (Williamson, Psaltis unpublished) (522). In the same study, we confirmed an adaptive role of bipotent EndoMac progenitors in promoting wound closure in healthy skin (522). Having now established the inhibitory effect of diabetes on these progenitors, we next studied the kinetics of YS-derived skin EndoMac progenitors during diabetic wound healing by using the TAM-inducible *Csf1r*^{Mer-iCre-Mer} x *Rosa*^{mT/mG} lineage-tracing model. We injected TAM into pregnant dams at E8.5 to induce GFP labelling in CSF1R⁺ YS EMPs and their progeny. The offspring were administered STZ (STZ+) or citrate buffer sham (STZ-) at 12 w of age. Three weeks after injection, surgery was performed to create two full thickness wounds on the dorsal side of each mouse, as described previously (Chapter 2 section 2.5) (582). Wounds were then harvested at four time points: day 1, 3, 7 and 10 (**Figure 4.8A**). Higher BGCs, consistent with diabetes, were maintained at all time points in the STZ+ mice (**Figure 4.8B**). The diabetic group also lost weight prior to surgery following STZ treatment (**Figure 4.8C-E**). As described previously in other studies of diabetic wound healing (356, 371), STZ+ mice showed impaired wound closure over 10 d (**Figure 4.8F**).

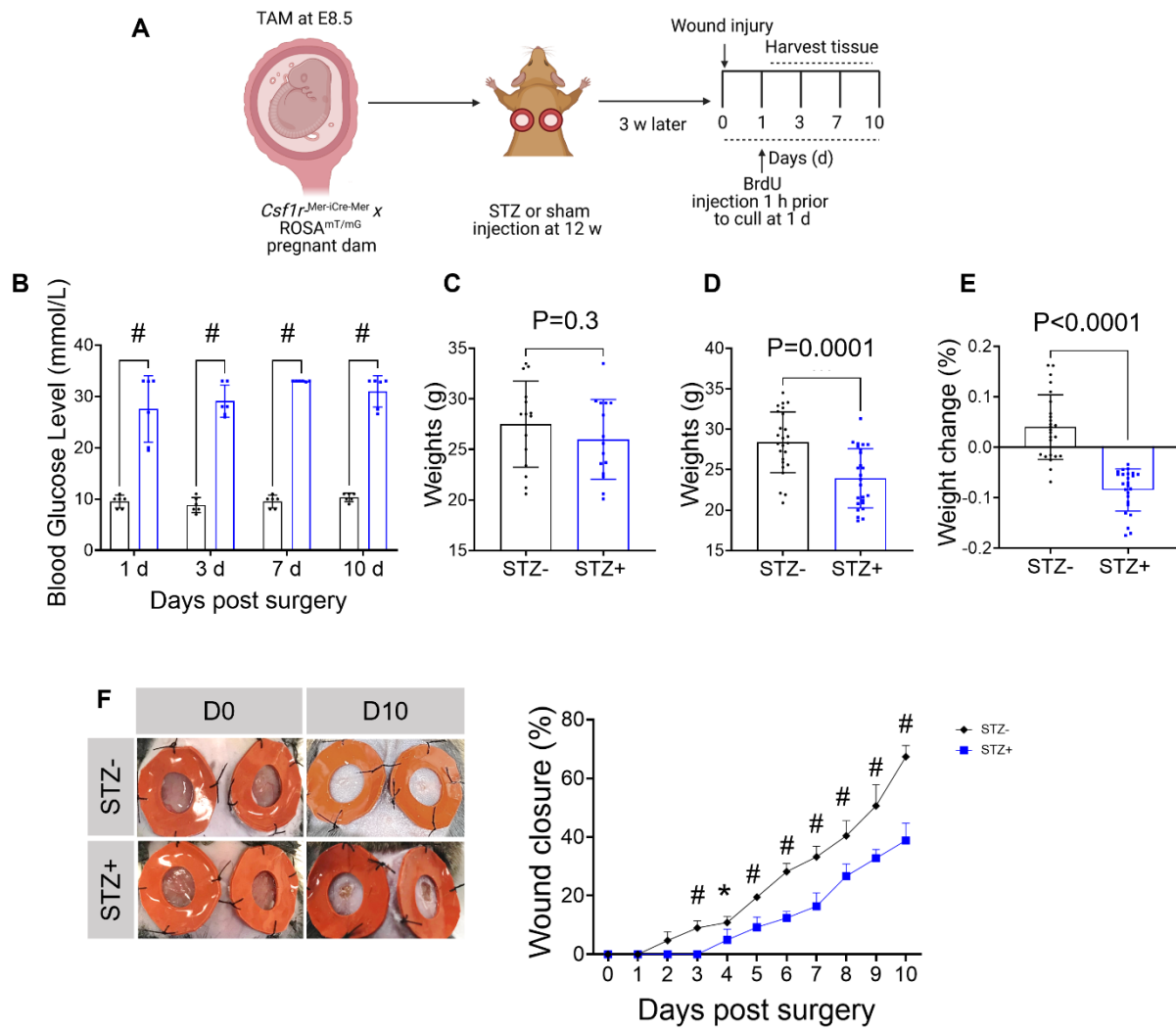
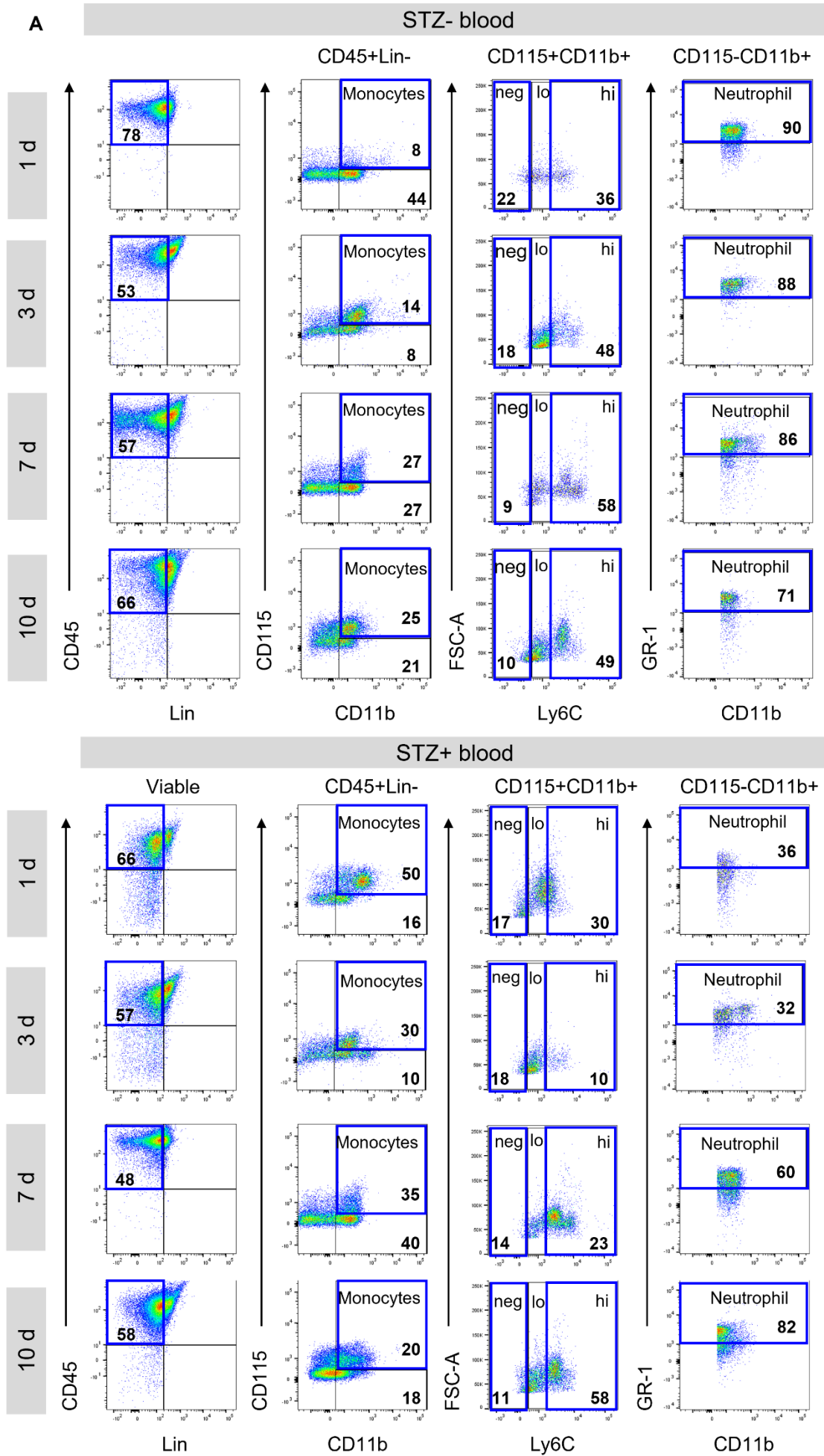


Figure 4.8: Diabetes impairs wound healing of injured skin.

- A)** Schematic showing the experimental design. Pregnant *Csf1r*^{Mer-iCre-Mer} or *Rosa*^{mT/mG} mice were injected with TAM at E8.5 to induce GFP expression in CSF1R⁺ YS EMPs and their progeny. Their adult offspring were subjected to wound healing surgery after induction of type 1 diabetes with i.p STZ or citrate buffer. Wound closure was monitored, and tissue harvested for analyses at the indicated time-points.
- B)** Blood glucose concentrations in STZ- (black) and STZ+ (blue) mice on the days of humane cull, post wound healing surgery. n=5/gp, One-way ANOVA, multiple comparisons: # P<0.0001
- C)** Baseline weights of *Csf1r*^{Mer-iCre-Mer} x *Rosa*^{mT/mG} mice pre-STZ injection. n=24/gp. unpaired *t*-test.
- D)** Body weight comparison of STZ- and STZ+ *Csf1r*^{Mer-iCre-Mer} x *Rosa*^{mT/mG} mice prior to wound injury surgeries. n=24/gp. unpaired *t*-test.
- E)** Change in body weight from baseline to pre-surgery in STZ+ and STZ- *Csf1r*^{Mer-iCre-Mer} x *Rosa*^{mT/mG} mice. n=24/gp. Unpaired *t*-test.
- F)** Representative images immediately post-surgery on day 0 and 14 after injury in the STZ- and STZ+ mice. Graph shows percentage of wound closure over 10 d. n=6 mice/gp/timepoint. Mixed effects two-way ANOVA: p<0.0001 for time; p<0.0001 for group; p<0.0001 for time x group. Multiple comparison test: *p<0.05 and # p<0.0001 for STZ- vs STZ+.
- Black bars: STZ-, Blue bars: STZ+.

Flow cytometry was used to analyse the blood from both STZ- and STZ+ mice at each time point post-surgery (**Figure 4.9A**). We first confirmed that there was no GFP expression in circulating neutrophils or monocytes, that served as internal controls, indicating that these cells do not originate at all from YS EMPs (data not shown). As expected, the frequency of Lin⁻CD45⁺CD11b⁺CD115⁻GR-1⁺ neutrophils peaked on day 1 after wound injury in STZ- mice, followed by a gradual decline (**Figure 4.9B**). On the other hand, STZ+ mice displayed a delayed increase in neutrophils peaking at day 10. STZ- blood had a 2.2-fold higher content of neutrophils at day 1 compared to the STZ+ group, while there were no significant differences between the two groups at the later time points: day 3, 7 and 10. Monocytes (Lin⁻CD45⁺CD11b⁺CD115⁺) displayed a more modest and decreased increase in STZ- blood, peaking at days 7 and 10 (**Figure 4.9C**). In contrast, we observed two distinct peaks in the STZ+ group, occurring at days 1 and 7. Although not significant, this suggests that STZ+ blood exhibited trends for higher total monocyte percentages at both these time points compared to STZ- blood. Surprisingly, the kinetics of Ly6C^{hi} “inflammatory” monocytes (Lin⁻CD45⁺CD11b⁺CD115⁺Ly6C^{hi}) showed a late peak in both groups at day 10, with significantly higher prevalence in the STZ+ mice compared to STZ- sham controls (**Figure 4.9D**). In contrast, STZ+ blood had a striking peak in its content of Ly6C^{lo} “patrolling” monocytes (Lin⁻CD45⁺CD11b⁺CD115⁺Ly6C^{lo}) at day 1 after wound injury, with a 4-fold higher frequency compared to the STZ- blood. This was followed by an immediate decline at day 3 with similar, plateaued frequencies of these cells in both groups at days 7 and 10 (**Figure 4.9E**). These results indicate that wound injury launches a different inflammatory response in the blood of diabetic compared to euglycaemic mice.



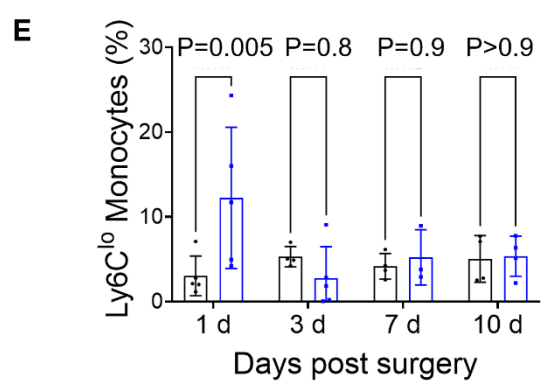
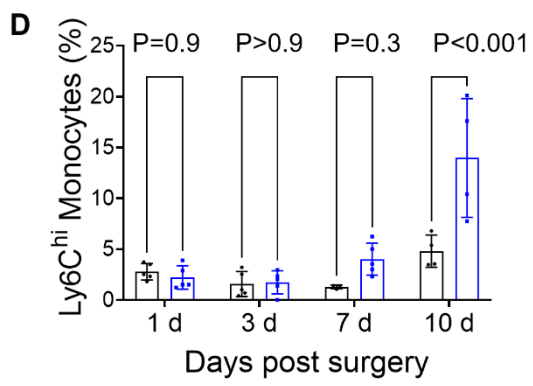
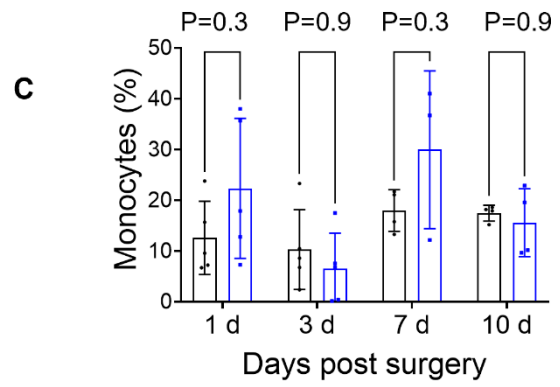
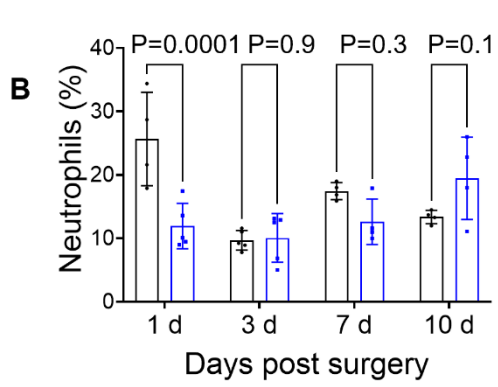


Figure 4.9: Diabetes launches a delayed inflammatory response following wound injury.

A) Flow cytometry plots showing the frequency of blood CD45⁺Lin⁻CD115⁺CD11b⁺ monocytes, Ly6C^{neg}, Ly6C^{lo}, Ly6C^{hi} monocytes and Lin⁻CD45⁺CD11b⁺CD115⁻GR-1⁺neutrophils from STZ- and STZ+ *Csf1r*^{Mer-iCre-Mer} *Rosa*^{mT/mG} post-wound injury at the indicated time points. Numerical values in plots represent the mean percentage from n=5/gp mice.

B-E) Graphs show comparisons of the frequency of blood **B)** neutrophils, **C)** total monocytes, **D)** Ly6C^{hi} and **E)** Ly6C^{lo} monocytes from STZ- and STZ+ *Csf1r*^{Mer-iCre-Mer} *Rosa*^{mT/mG} mice. n=5/gp, Percentages were calculated as the frequency of total live cells. Mixed effects two-way ANOVA results: **B)** p=0.0006 for time; p=0.03 for group; p=0.0003 for time x group; **C)** p=0.01 for time; p=0.1 for group; p=0.1 for time x group; **D)** p<0.0001 for time; p=0.0007 for group; p=0.0004 for time x group; **E)** p=0.2 for time; p=0.1 for group; p=0.02 for time x group. Multiple comparisons.

Black bars: STZ-, Blue bars: STZ+.

Flow cytometry analysis of skin wound digests from the STZ- and STZ+ mice demonstrated early increases in the overall number of progenitors at day 1 in both groups, with this diminishing by day 10; however, at all time-points, these cells were much more prevalent in the STZ- group (**Figure 4.10A-B**). MΦ numbers were highest at days 1 and 3 after wound injury in the STZ- group before progressively decreasing at days 7 and 10 (**Figure 4.10C**). Conversely, STZ+ wounds showed a steady increase in their overall content of MΦs with the peak occurring at day 7, before a marked drop-off at day 10. Finally, comparing MΦs between STZ- and STZ+ wounds showed a 2.7-fold and 2.2-fold higher number in the STZ- group at days 1 and 3, respectively, with a trend to a higher count in the STZ+ group at day 7 (**Figure 4.10C**). The kinetics for ECs showed a progressive increase in the STZ- group from lowest numbers at day 1 to a peak at day 7 (**Figure 4.10D**). Meanwhile, throughout the ten days studied, STZ+ wounds showed much lower numbers of ECs. These results reveal important discrepancies between diabetic and non-diabetic wounds during the healing process, with the former having: 1) fewer progenitors at all time intervals; 2) delayed expansion of MΦs, which somewhat mirrors the monocyte kinetics in blood; and 3) a profound deficiency of ECs which never recovers.

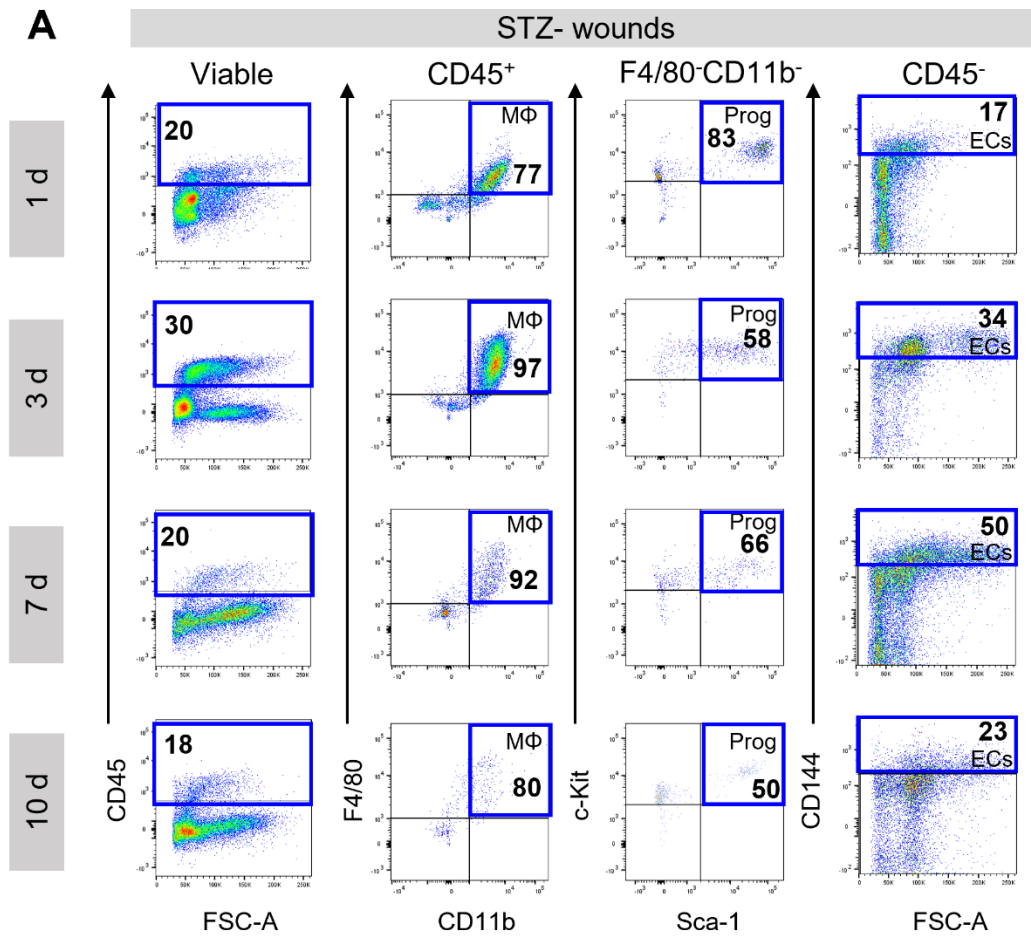


Figure continued P.T.O

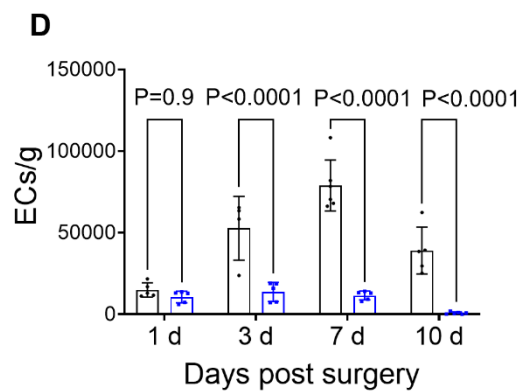
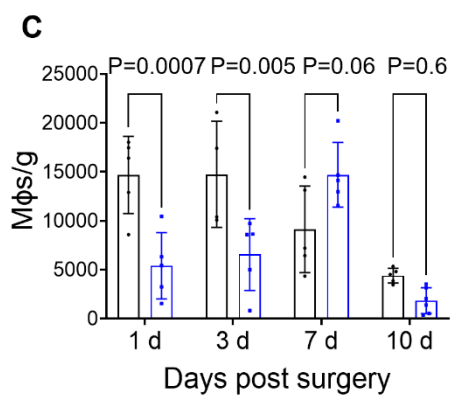
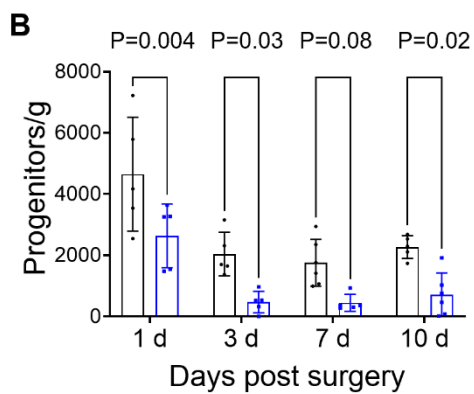
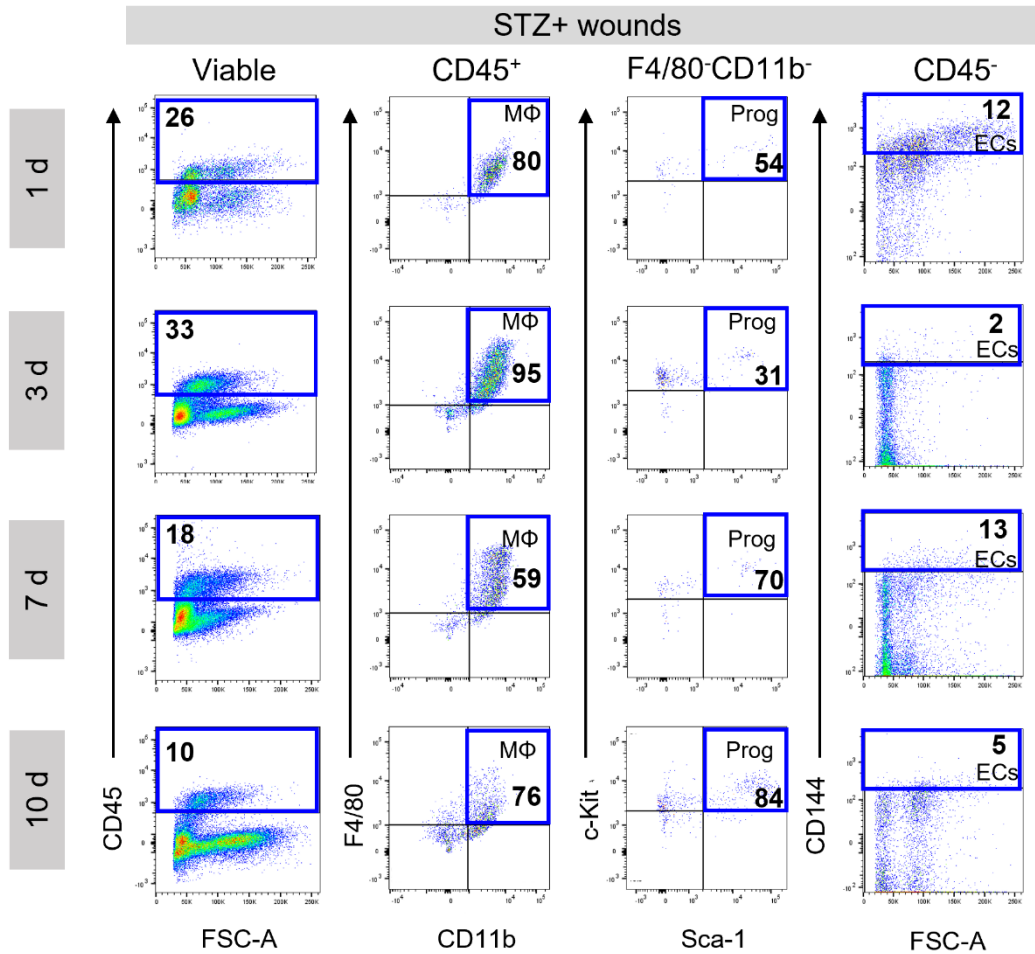


Figure 4.10: Diabetic skin has different content of progenitors, MΦs and ECs during wound healing.

A) Flow cytometry showing the gating for SkM CD45⁺ CD11b⁺ F4/80⁺ macrophages (MΦs), CD45⁺CD11b⁻ F4/80⁻c-Kit⁺Sca-1⁺ progenitors and CD45⁻CD144⁺ endothelial cells (EC) from STZ- and STZ+ *Csf1r*^{MerCreMer} x *Rosa*^{mT/mG} wound tissue across four time points (1 d, 3 d, 7 d, 10 d). Numerical values in plots represent the mean percentage. Representative of n=5-6/gp

B-D) Graphs showing comparison of numbers of **B)** progenitors/g, **C)** macrophages (MΦ)/g and **D)** endothelial cells (EC)/g, in skin wound of STZ- and STZ+ *Csf1r*^{Mer-iCre-Mer} x *Rosa*^{mT/mG} mice across four time points (1 d, 3 d, 7 d, 10 d). n=5-6/gp, two -way ANOVA results: **B)** p<0.0001 for time; p<0.0001 for group; p=0.8 for time x group; **C)** p<0.0001 for time; p=0.0025 for group; p=0.0001 for time x group; **D)** p<0.0001 for time; p<0.0001 for group; p<0.0001 for time x group. Black bars: STZ-, Blue bars: STZ+.

(Refer to Appendix 7.5)

In keeping with the diminished accumulation of progenitors in diabetic wounds, we also observed a reduction in the recovery of CFU-M from methylcellulose cultures of STZ+ wound digests (**Figure 4.11A**). CFU-M yield was highest from STZ- wounds at day 3 and from STZ+ wounds at day 7. However, at all-time points, STZ- wound digests produced more colonies, with fold comparisons compared to the STZ+ group: 2.8x at day 1, 2.8x at day 3, 1.5x at day 7 and 5x at day 10 (**Figure 4.11B**).

We also specifically investigated for the kinetics of YS-derived cells in skin wounds by studying for the expression of the GFP fluorescence reporter in *Csf1r*^{Mer-iCre-Mer} x *Rosa*^{mTmG} mice. Control *Csf1r*^{Mer-iCre-Mer} x *Rosa*^{mTmG} mice which had not received TAM *in utero* were used as GFP negative fluorescence controls (**Figure 4.11B**). GFP⁺ cells were gated for progenitors, MΦs and ECs as described above (**Figure 4.11B**). Flow cytometry revealed that the overall number of YS-derived GFP⁺ cells was significantly higher in the STZ- compared to STZ+ wounds throughout all four time-points (fold comparisons STZ- versus STZ+: 2.6x at day 1, 3.5x at day 3, 7.7x at day 7, 9.6x at day 10, n=5-6/gp and time point) (**Figure 4.11C**). GFP⁺ cells peaked at day 3 in diabetic wounds and day 7 in non-diabetic wounds, before markedly diminishing in number by day 10 in both groups (**Figure 4.11C**). GFP⁺ progenitors peaked at day 1 in STZ- wounds, at which point they were 6-fold more prevalent than in STZ+ wounds (**Figure 4.11D**). Although their numbers subsequently diminished, they remained much higher in STZ- wounds at all later time-points, with fold comparisons versus STZ+ 10x at day 3 and 18x at day 10. (**Figure 4.11D**)

We also observed that the number of YS-derived MΦs rose sharply in non-diabetic wounds between days 1 and 3, before becoming progressively sparser by day 10 (**Figure 4.11E**). A similar expansion of GFP⁺ MΦs was not seen in STZ+ wounds, which therefore were left with much fewer of these

cells at both day 3 and 7 compared to the STZ- group. Meanwhile, YS-derived GFP⁺ ECs increased steadily from day 1 to their peak numbers on day 7 in STZ- mice, with minimal expansion in the STZ+ setting (**Figure 4.11F**). This resulted in significantly more of these cells in non-diabetic compared to diabetic wounds at days 3 (2.7x higher), 7 (8.8x higher) and 10 (16x higher) (**Figure 4.11F**).

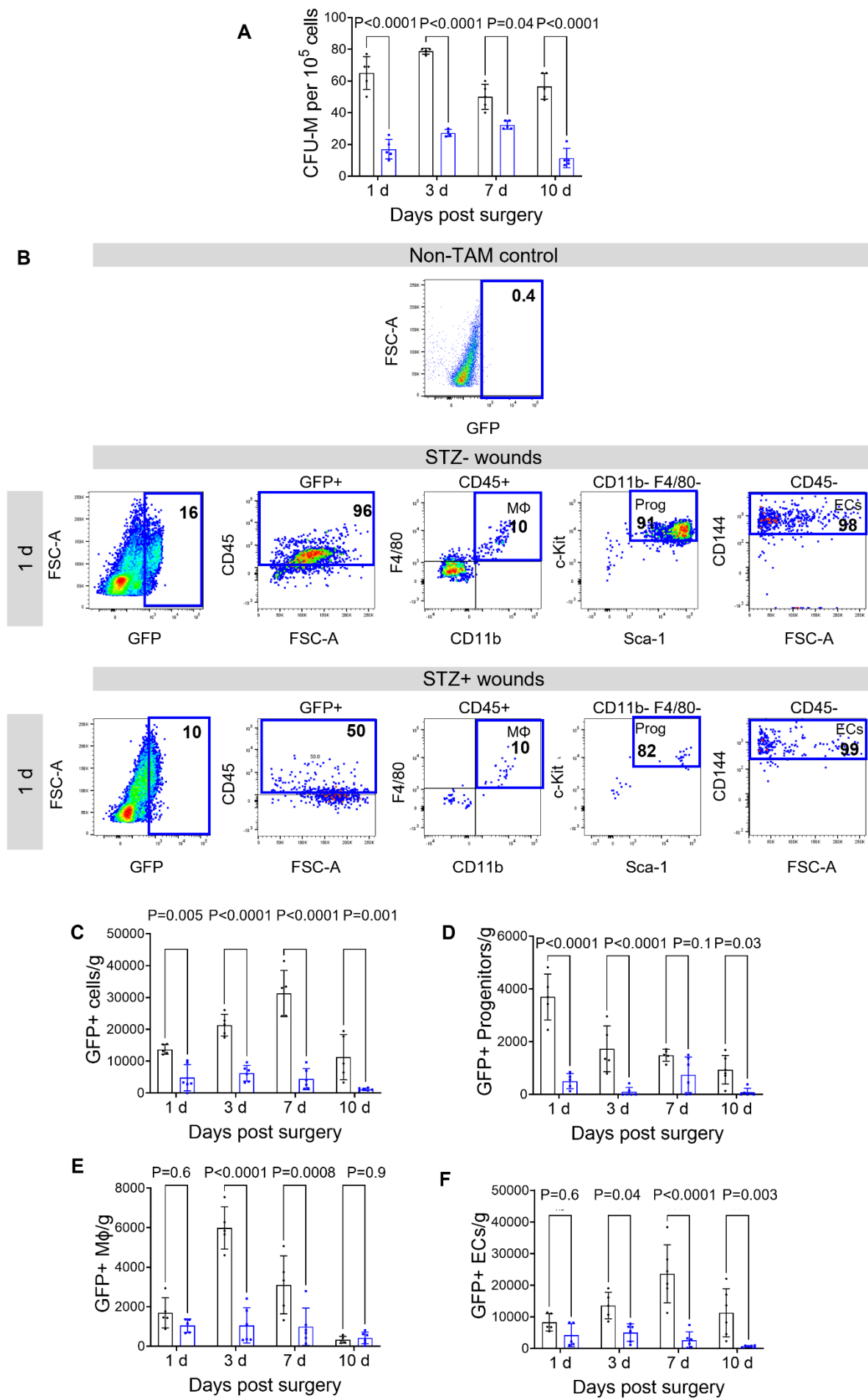


Figure 4.11: Kinetics of YS-derived cells in non-diabetic and diabetic wounds during healing.

A) Graph showing the comparison of 1° skin CFU-M yield from STZ- and STZ+ *Csf1r*^{Mer-iCre-Mer} x *Rosa*^{mT/mG} wounds across four time-points (pre-surg, 1 d, 3 d, 7 d, 10 d) after injury. n=5-6 mice/gp. Two-way ANOVA results: p<0.0001 for time; p<0.0001 for group; p<0.0001 for time x group

B) Representative flow cytometry gating for GFP expression in a no TAM Cre control (top) and flow cytometry profiling of YS-derived GFP⁺ cells in skin wounds of STZ- (middle) and STZ+ (bottom) of TAM-induced *Csf1r*^{Mer-iCre-Mer} x *Rosa*^{mT/mG} mice at 1 d after injury. Representative of n=5-6/gp.

C-F) Graph showing comparison of numbers of **C)** GFP⁺ cells/g, **D)** progenitors/g, **E)** macrophages (MΦ)/g and **F)** endothelial cells (EC)/g of STZ- and STZ+ *Csf1r*^{Mer-iCre-Mer} x *Rosa*^{mT/mG} wounds across four time-points (1 d, 3 d, 7 d, 10 d). n=5-6 mice/gp. Two-way ANOVA results: **C)** p=<0.0001 for time; p<0.0001 for group; p<0.0001 for time x group. **D)** p=<0.0001 for time; p<0.0001 for group; p<0.0001 for time x group. **E)** p=<0.0001 for time; p=0.0001 for group; p=0.0025 for time x group. **F)** p=0.0048 for time; p<0.0001 for group; p=0.0026 for time x group.

Black bars: STZ-, Blue bars: STZ+.

(Refer to Appendix 7.5)

Finally, we also studied the proliferative status of the different YS-derived populations in early skin wounds by administering bromodeoxyuridine (BrdU) 1 h prior to humane killing for the day 1 time-point and analysing cell cycle activity by flow cytometry (**Figure 4.12A**). Although limited by relatively small n-values, STZ- wounds showed a significantly higher proportion of GFP⁺ cells, GFP⁺ progenitors and GFP⁺ ECs that were in S-phase of cell cycle compared to STZ+ wounds with a similar trend seen for GFP⁺ MΦs (**Figure 4.12B-E**). We also identified a higher percentage of GFP⁺ ECs that were apoptotic in the STZ+ wounds, with non-significant trends for more apoptosis among the other populations in these mice also (**Figure 4.12F-I**).

A

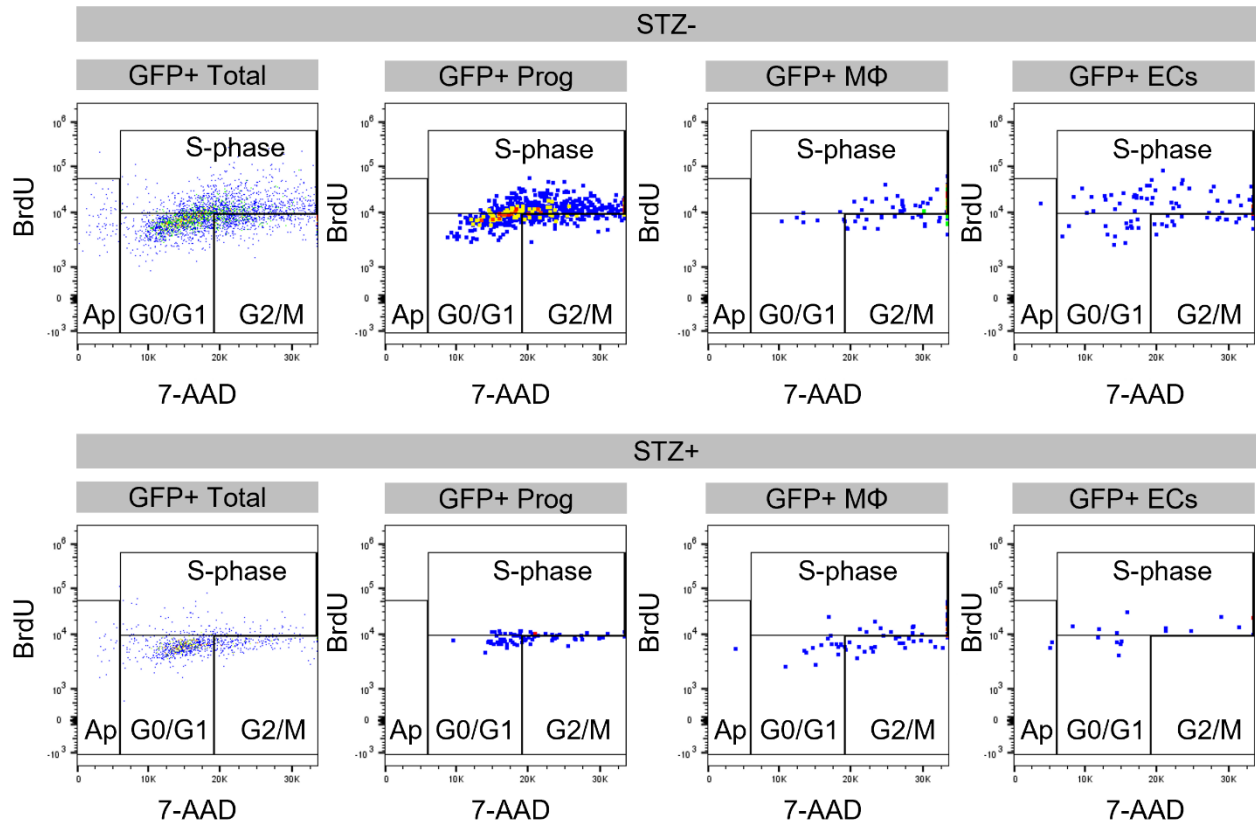


Figure continued P.T.O

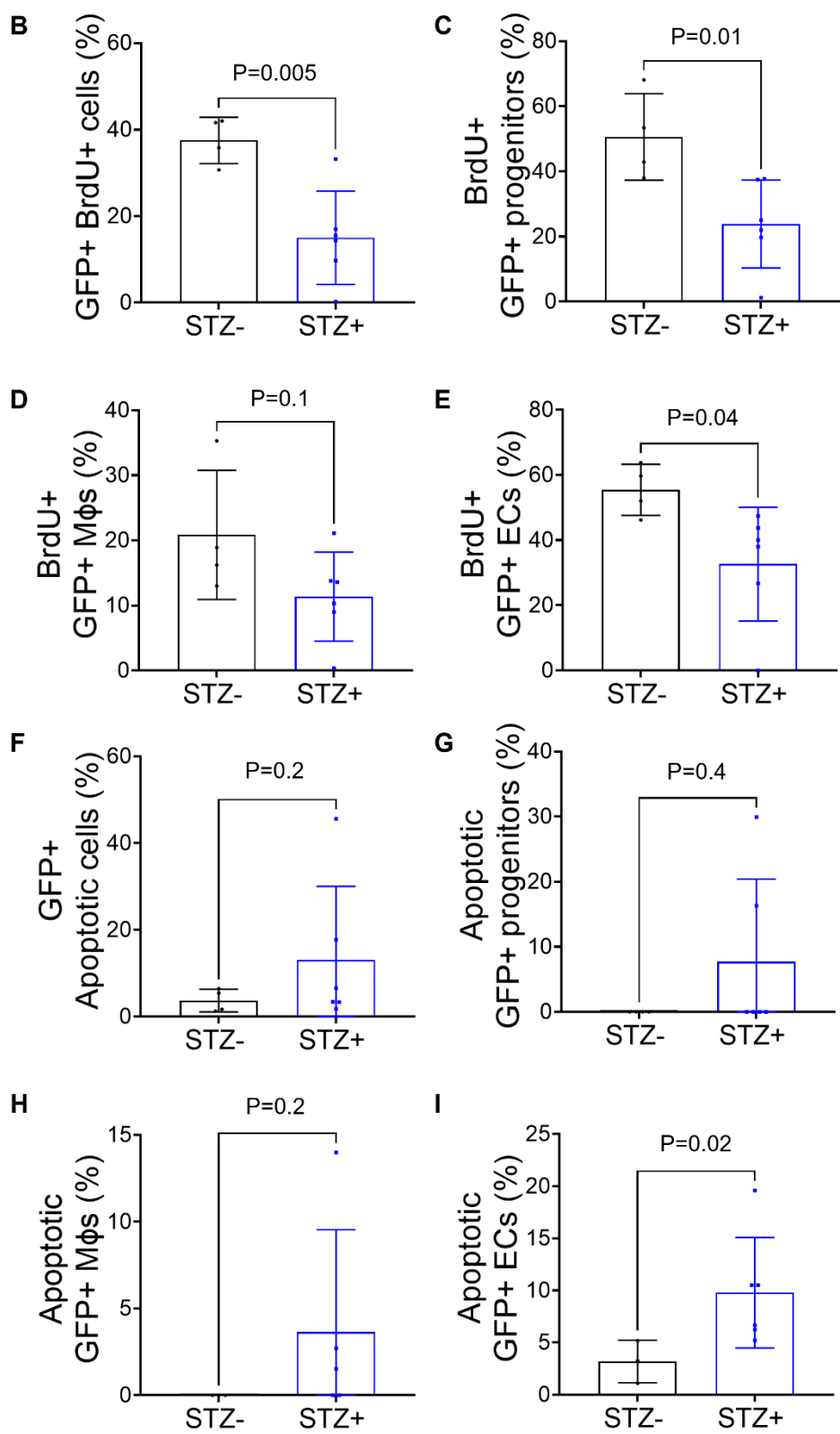


Figure 4.12: Reduced cell proliferation and increased apoptosis in diabetic wounds immediately post-injury.

A) Representative flow cytometry gating for BrdU expression of YS-derived total GFP⁺ cells, GFP⁺ progenitors, GFP⁺ macrophages (MΦ) and GFP⁺ endothelial cells (EC) in skin wounds of STZ- (top) and STZ+ (bottom). TAM-induced *Csf1r*^{Mer-iCre-Mer} x *Rosa*^{mT/mG} mice. Gating of cells in different phases of cell cycle and apoptotic cells has been shown. Representative of n=4-5/gp.

B-E) Graphs showing comparison of frequency of BrdU expression of GFP⁺ **B)** total cells **C)** progenitors **D)** MΦ and **E)** EC. n=4-5/gp. Unpaired *t*-test.

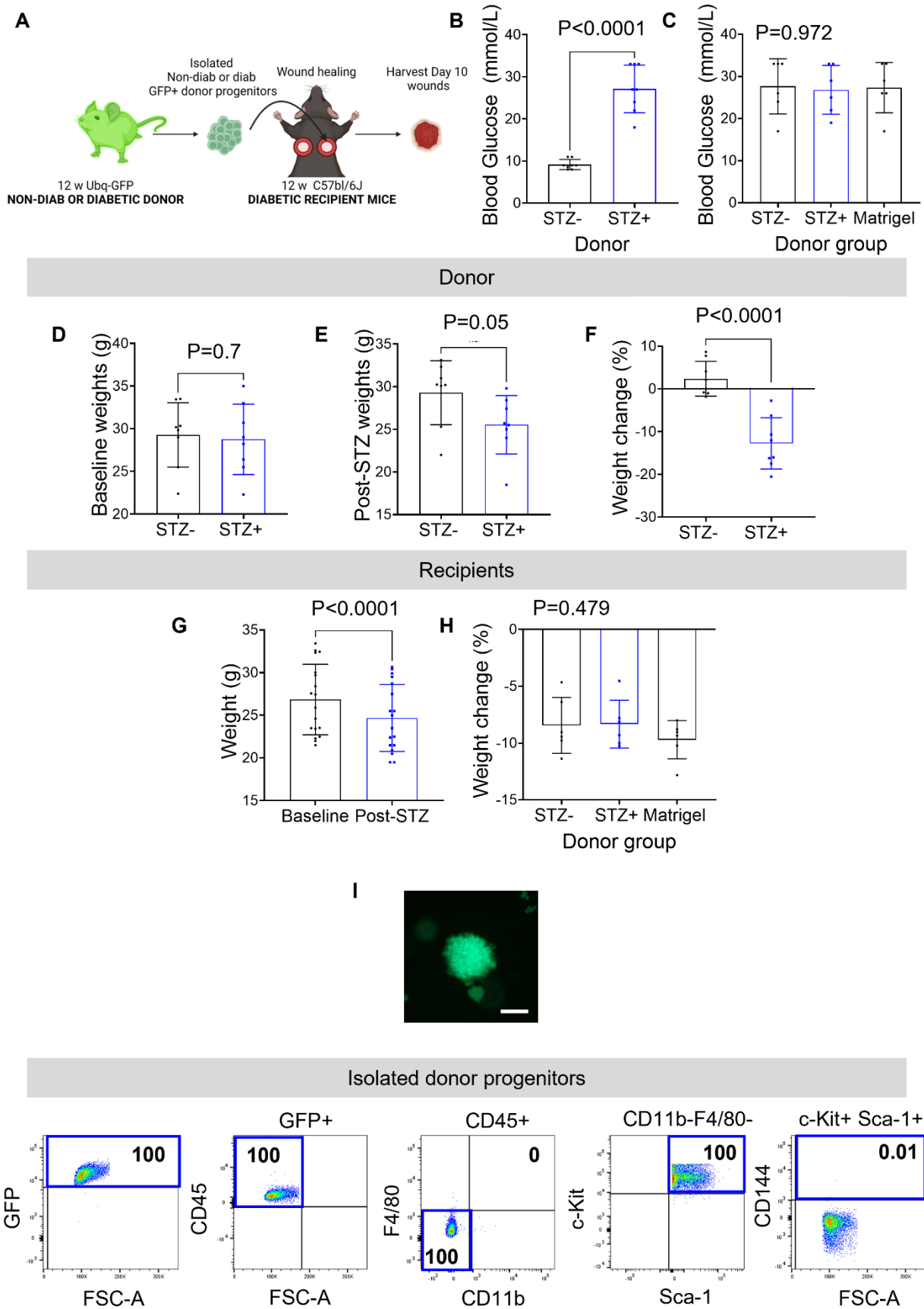
F-I) Graphs show frequency of apoptosis of GFP⁺ **F)** total cells **G)** progenitors **H)** MΦ and **I)** EC. n=4-5/gp. Mann-Whitney

4.3.8 Transfer of non-diabetic but not diabetic progenitors promotes wound healing in diabetic skin

We previously established the adaptive properties of EndoMac progenitors in the healing of non-diabetic skin wounds (522). With the impairments observed in diabetic skin healing above, we next investigated whether this could be rescued by transplanting non-diabetic progenitors into the diabetic wound environment. We used adult C57BL/6 mice that were induced by STZ to develop diabetes and subjected them to wound injury surgery two weeks later. Immediately after surgery, these mice were injected with equal volumes of either cell-free MatrigelTM (vehicle control) into one of the two wounds, or skin EndoMac progenitors from non-diabetic (STZ-) or diabetic (STZ+) UBI-GFP donor mice into the other (1.5×10^4 cells per recipient) (**Figure 4.13A**). Wound healing was then monitored for the next ten days. STZ+ donor mice had three-fold higher BGCs than STZ- donors (**Figure 4.13B**). Meanwhile, all three groups of STZ+ recipient mice had similar BGCs consistent with diabetes (Control 27.6 ± 6.5 ; STZ- 26.8 ± 5.8 ; STZ+ 27.3 ± 5.9 mmol/L, $n=6/\text{gp}$, $P=0.9$) (**Figure 4.13C**). STZ+ donors had similar body weight to their STZ- counterparts at baseline but showed significant weight loss following development of diabetes (**Figure 4.13D-F**), while all recipient mice showed significant weight loss after STZ injection and establishment of diabetes (**Figure 4.13G-H**).

Donor GFP⁺ progenitors were carefully isolated under microscopic guidance from CFU-M after 14 d of culture in methylcellulose. Flow cytometry confirmed that isolated GFP⁺ progenitors were homogeneous for expression of the previously described EndoMac progenitor phenotype (CD45⁺ CD11b⁻F4/80⁻Sca-1⁺c-Kit⁺CD144⁻), and therefore did not contain differentiated CD45⁺CD11b⁺F4/80⁺ MΦs or CD45⁺CD144⁺ ECs prior to transplant (**Figure 4.13I**).

Wound closure was accelerated and augmented in mice that received STZ- skin progenitors compared to those that received STZ+ progenitors or vehicle control, with wound closure curves diverging from day 3 onwards and remaining significantly higher in the STZ- group until day 10 (**Figure 4.13J**).



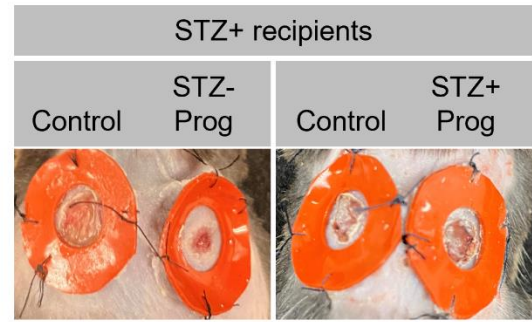
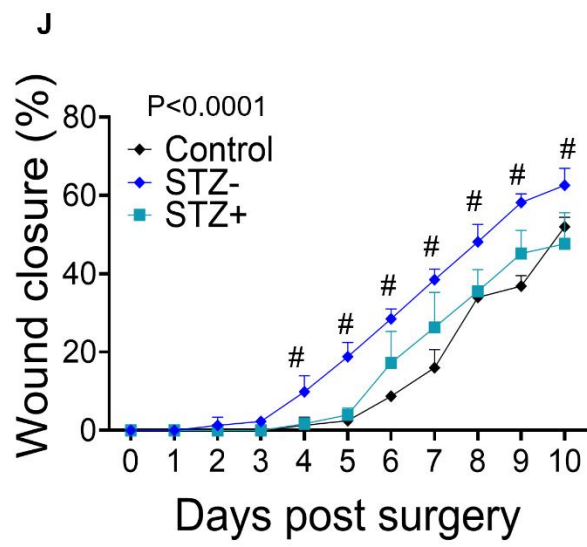


Figure 4.13: Non-diabetic EndoMac progenitors accelerate wound healing in diabetic skin.

- A)** Schematic of experimental design. Recipient groups were STZ+ diabetic C57BL/6 mice that underwent wound healing surgery immediately before receiving subcutaneous injections of cell-free MatrigelTM (vehicle control) or GFP⁺ non-diabetic (STZ-) or diabetic (STZ+) skin progenitors.
- B)** Blood glucose concentrations of donor UBI-GFP mice. n=8/gp. Unpaired *t*-test.
- C)** Blood glucose concentrations of recipient C57BL/6 mice: STZ-, STZ+ and control groups. n=6/gp, one-way ANOVA.
- D-F)** Weight comparison of **D)** baseline (8 w), **E)** post-STZ injection and **F)** frequency of weight change of donor STZ- and STZ+ 12 w UBI-GFP mice. n=8/gp. Unpaired *t*-test.
- G-H)** Comparison of **G)** baseline weights with post-STZ injection and **H)** Frequency of weight change among 12 w recipient C57BL/6 mice that received STZ- or STZ+ progenitors of cell-free control. n=6/gp. Paired *t*-test for **G)** and One-way ANOVA for **H)**.
- I)** Light microscopy (left) and fluorescent microscopy (right) of a representative 1° CFU-M from a 12 w STZ- donor UBI-GFP mouse. Flow cytometry showing cell surface marker expression of donor GFP⁺ progenitors that were used for transfer into wounds. Representative of n=2. Scale bar, 100 μ m.
- J)** Graph showing comparison of percentage wound closure over time among the three recipient groups that received: STZ-, STZ+ and cell-free control. n=6/gp. Two-way ANOVA results: $p < 0.0001$ for time; $p < 0.0001$ for group; $p < 0.0001$ for time x group. Multiple comparisons test: $\#p < 0.0001$. The representative images show wounds from STZ+ recipient mice that received STZ- (left) and STZ+ (right) progenitor cells.

We also harvested skin wounds at day 10 to confirm the engraftment of GFP⁺ progenitors and examine their differentiation into new CD45⁺CD11b⁺F4/80⁺ MΦs and CD45⁺CD144⁺ ECs (**Figure 4.14A**). Engraftment of GFP⁺ cells was much higher from STZ⁻ compared to STZ⁺ donors (**Figure 4.14B**). By comparison to the STZ⁺ donor group, transfer of STZ⁻ non-diabetic progenitors also resulted in significantly higher numbers of GFP⁺ progenitors (**Figure 4.14C**), MΦs (**Figure 4.14D**) and ECs (**Figure 4.14E**) in recipient wounds. Importantly, in each of these experiments we did not detect any GFP⁺ cells in the wounds that had only been injected with vehicle control (**Figure 4.14B-E**), which is consistent with the fact that EndoMac progenitors are tissue-resident and do not circulate via peripheral blood. As observed in our earlier *in vitro* MatrigelTM assays, we were somewhat surprised to find that a majority of GFP⁺ cells retained in day 10 wounds could not be classified as either EndoMac progenitors, MΦs or ECs based on their surface marker expression (**Figure 4.14F**). These “other” cells made up an average of 53% and 79% of donor-derived cells in the STZ⁻ and STZ⁺ groups, respectively. At this stage, the precise lineage identities of these cells are not clear and this will require further interrogation.

Overall, these results show that even when injected into a host environment that is diabetic, non-diabetic EndoMac progenitors retained a higher ability to 1) engraft, 2) accumulate and 3) differentiate into myeloid and endothelial progeny, and this was associated with augmentation of wound closure compared to diabetic progenitors.

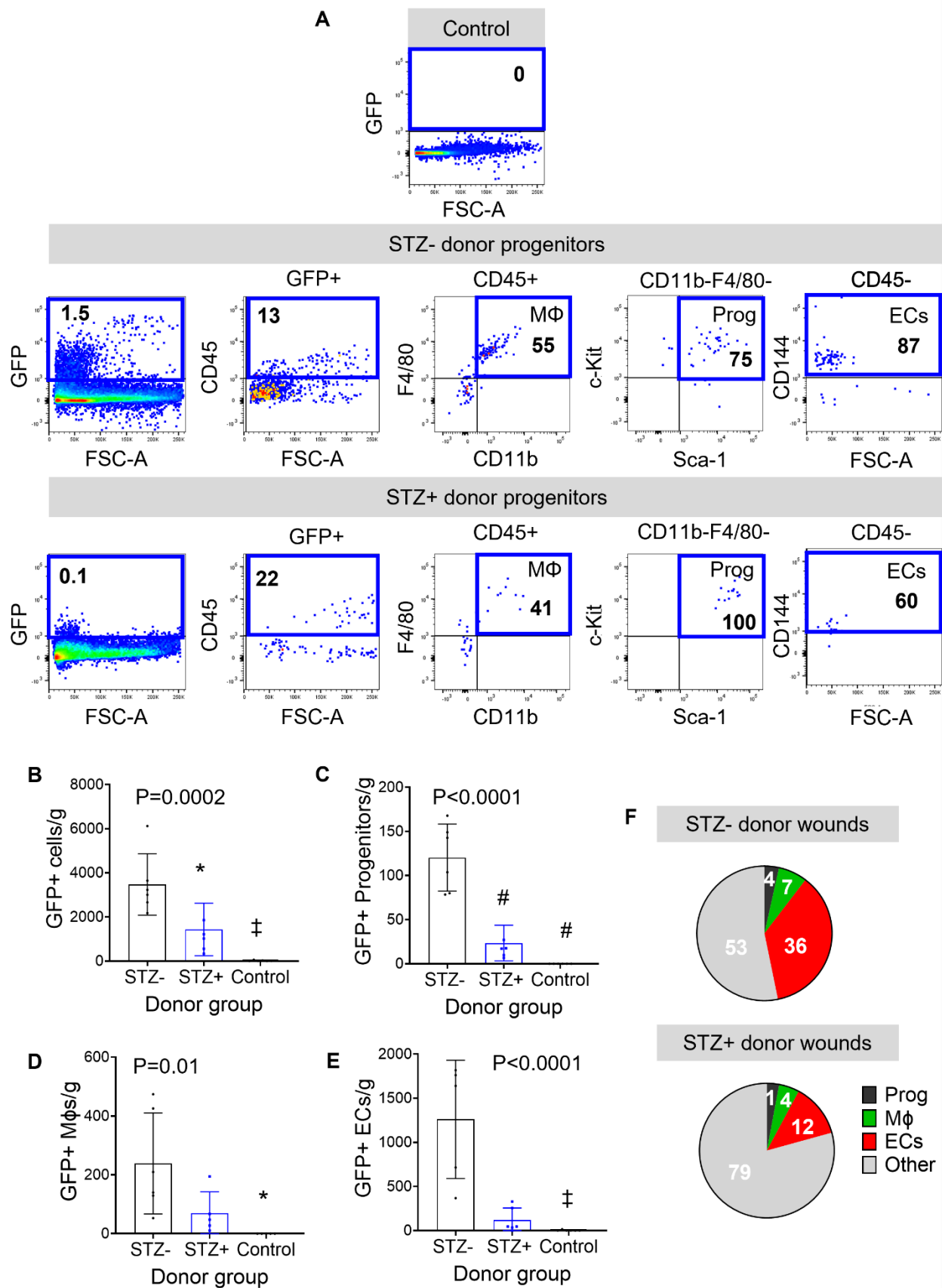


Figure 4.14: Transfer of non-diabetic but not diabetic Endo-Mac progenitors engraft, accumulate, and differentiate in diabetic wounds.

A) Flow cytometry plots showing the fate of GFP⁺ donor cells in wounds of recipient mice with cell numbers shown in boxes: CD45⁺CD11b⁺F4/80⁺ macrophages (MΦ), CD45⁺CD11b⁺F4/80⁻c-Kit⁺Sca-1⁺ progenitors (prog) and CD45⁺CD144⁺ endothelial cells (ECs). Representative flow plots are from wounds of STZ⁺ recipient C57BL/6 mice at day 10 that received cell-free MatrigelTM (top), STZ⁻ (middle) and STZ⁺ (bottom) donor UBI-GFP CFU-M progenitors.

B-E) Graphs showing the number of GFP⁺ **B)** total cells, **C)** progenitors, **D)** MΦs and **E)** ECs at day 10 from wounds of STZ⁺ recipient C57BL/6 mice that received GFP⁺ CFU-M cells from STZ⁻ and STZ⁺ UBI-GFP mice, and vehicle control. n=6/gp. **B-D)** One-way ANOVA, **E)** Kruskal-Wallis. Multiple comparisons: *P=0.05, ‡P<0.001, #P<0.0001

F) Pie charts show the frequency of progenitors (prog), MΦ and ECs that originated from transplanted GFP⁺ STZ⁻ (left) and STZ⁺ (right) donor-derived CFU-M into recipient wounds. n=6/gp.

Finally, we also assessed the effect of donor EndoMac progenitors on total (i.e., not just GFP⁺) cell populations within recipient wounds (**Figure 4.15A**). Ten days after cell transfer, we observed that wounds that received STZ⁻ progenitors contained higher overall numbers of progenitors (**Figure 4.15B**), MΦs (**Figure 4.15C**) and ECs (**Figure 4.15D**) than those that received STZ⁺ progenitors or no cells. We speculate that this means that in addition to their own trans-differentiation, non-diabetic donor progenitors may also have exerted paracrine effects to boost the accumulation of local, host-derived cell populations. However, this also will need further investigation.

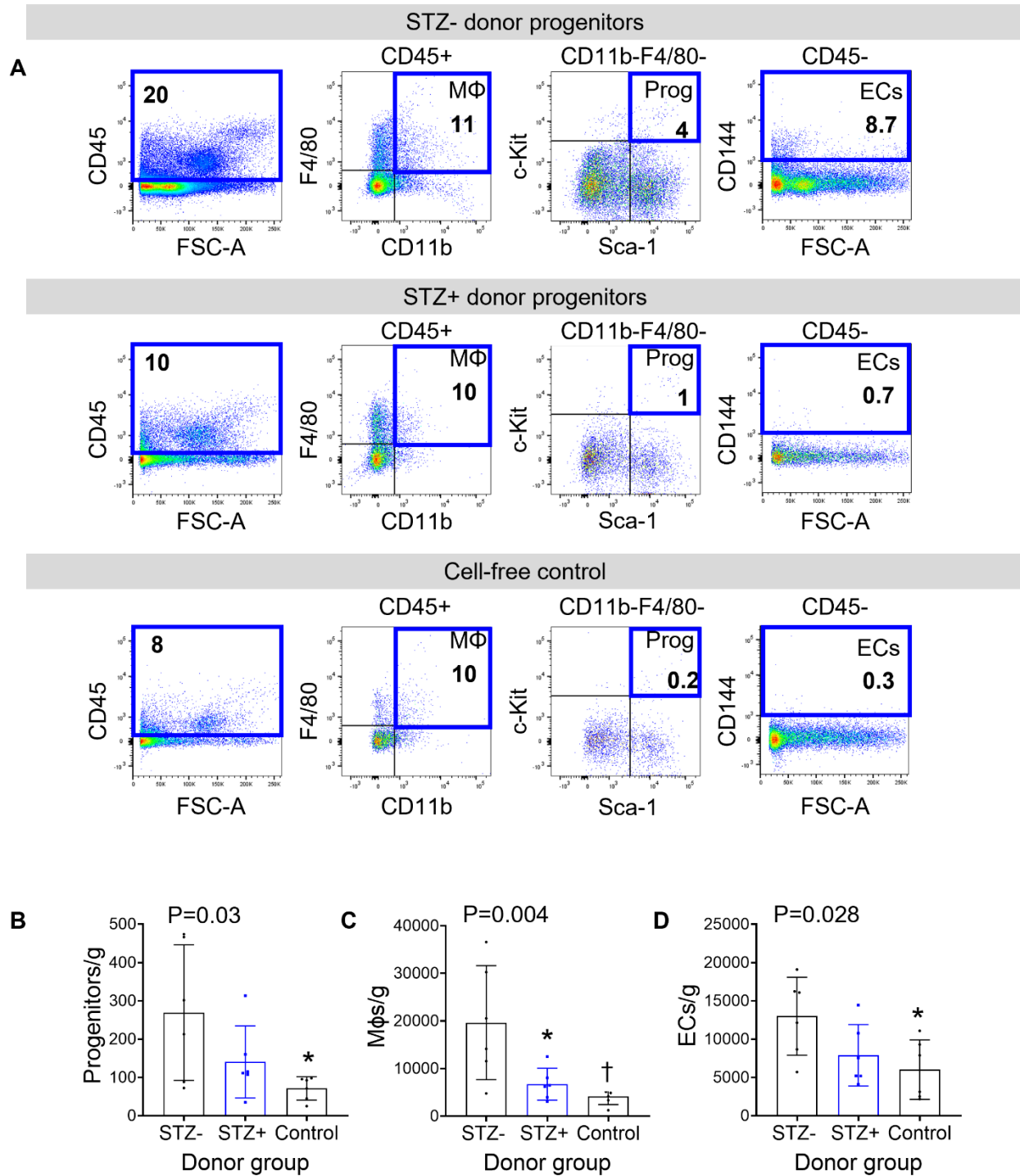


Figure 4.15: Transferred non-diabetic donor EndoMac progenitors increase overall numbers of progenitors, MΦs and ECs in recipient wounds.

A) Flow cytometry plots showing cells in recipient wound cells shown in boxes: CD45⁺CD11b⁺F4/80⁺ macrophages (MΦ), CD45⁺CD11b⁺F4/80⁻Sca-1⁺c-Kit⁺progenitors (prog) and CD45⁻CD144⁺ endothelial cells (ECs). Representative flow plots are from STZ⁺ recipient C57BL/6 wounds at day 10 that received GFP⁺ progenitors from STZ⁻ (top) or STZ⁺ (middle) donor UBI-GFP mice, or vehicle control (bottom). Representative of n=6/gp.

B-D) Graphs showing the comparison of the number of **B)** progenitors, **C)** MΦs and **D)** ECs from recipient STZ⁺ C57BL/6 wounds at day 10 after receiving GFP⁺ progenitors from STZ⁻ or STZ⁺ donor mice, or vehicle control. n=6/gp. One-way ANOVA, multiple comparisons: *P=0.05, †P<0.01

4.4 Discussion

Impaired wound healing is an important consequence of diabetes, accentuated by a prolonged inflammatory and abnormal neovascularisation response in injured skin (120). MΦs and ECs play intertwined roles during the normal wound healing process, each comprising heterogeneous subtypes that reflect their complex developmental ontogeny (28, 36, 108, 119, 546, 586). Here, we studied the origins of these two populations in diabetic wounds through the unique lens of embryonically derived EndoMac progenitors. Our results demonstrate marked inhibitory effects of high glucose on the properties of these progenitor cells. This includes marked reductions in their: 1) prevalence in diabetic mouse skin as shown by flow cytometry; 2) clonogenic renewal capacity *in vitro*; 3) ability to form vascular-like cords in MatrigelTM and endothelial culture medium; and 4) metabolic function. We also observed a deficiency of YS-derived progenitors in diabetic wounds *in vivo*, with relative failure of these cells to mount the early proliferative response and expansion seen after wound injury in the non-diabetic state. This was accompanied by a similar failure of YS-derived MΦs and ECs to accumulate in the mid and later stages of diabetic wound healing, respectively. Finally, we have demonstrated through adoptive transfer experiments that “healthy” progenitors are able to engraft in diabetic wounds, differentiate into new progeny (including MΦs and ECs) and promote wound closure, whereas these properties are substantially compromised in progenitors from diabetic donors.

Our previous work has shown that EndoMac progenitors emerge from YS EMPs around E8.5 and are seeded in different embryonic mouse tissues from E10.5, where they remain until after birth (517, 520). They are then maintained in their local tissue niches independently of definitive BM haematopoiesis. In adult skin, they are characterised by their capacity to preferentially generate CFU-M in methylcellulose-based culture and by their expression of a Lin⁻CD45⁺CD11b⁻F4/80⁻c-Kit⁺Sca-1⁺ surface marker phenotype, along with the fractalkine (CX₃CR1) and macrophage colony-stimulating factor (CSF1R/CD115) receptors (517, 520). They demonstrate a steady loss in their

proliferative and renewal capacity over time, as seen by high abundance in neonatal skin, with progressive diminution as mice age postnatally. Importantly, we have also demonstrated that EndoMac progenitors possess at least bipotent differentiation capacity and undergo rapid expansion immediately post-injury in healthy skin (520). In prior experiments, transplantation of these cells not only accelerated wound closure but also successfully promoted wound neovascularisation and perfusion (522). In the current chapter, we now demonstrate that there is high glucose-induced depletion of their prevalence and renewal, without significant changes to their viability, which may contribute to delayed and incomplete wound closure. The reduction in stem-like cells by diabetes has been extensively described for other populations, such as neural stem cells, satellite cells and epidermal stem cells (462, 564). In particular, the dysfunctional specification and differentiation of epidermal stem cells due to abnormal telomere function and/or absence of cyclin *DI* gene expression, have been directly linked to impaired diabetic wound healing (564, 581). Diabetes has also been shown to induce abnormal cellular senescence, mitochondrial and metabolic dysfunction in various stem and mature cell populations, although relatively little is known about its effects on other cell populations found in skin (383, 440, 587).

We found that exposure to high glucose had multifaceted effects on the metabolic activity of skin EndoMac progenitors, consisting of reduced mitochondrial viability and membrane function, oxygen consumption, ATP-synthase dependence, reserve capacity to recover following mitochondrial ETC stress, and glycolytic capacity. This was associated with increased levels of oxidative stress and DNA damage. Low functional metabolic activity has previously been identified in healthy adult stem cells, including epidermal stem cells and mesenchymal stromal cells, where it may serve as a compensatory mechanism to preserve their long-term renewal capacity by maintaining them in a state of quiescence (267, 421, 547). A potentially contradictory observation made here was the fact that both high glucose *in vitro* and hyperglycaemia *in vivo* resulted in higher lactate concentrations measured in the

supernatants of progenitors after their culture in methylcellulose for 14 d. On the surface, this would be expected if the cells were in a heightened state of glycolysis. However, this was not supported by the results of the Seahorse™ assay which showed that high glucose induced lower baseline ECAR. Instead, we speculate that the increased lactate build-up may have been due to increased glucose substrate utilisation from the culture medium to supply the cells with energy via anaerobic means, in the setting of impaired mitochondrial activity. Further assays will be needed to confirm this. In contrast, under normal glucose conditions EndoMac progenitors displayed a marked dependence on mitochondrial oxidative phosphorylation for ATP synthesis. This metabolic switch to more aerobic activity tends to be a hallmark of stem/progenitor cells that are more actively proliferating, such as myeloid progenitors in BM (409, 588, 589). Indeed, this is consistent with the actively cycling status of tissue-resident EndoMac progenitors, which we have observed in this chapter as well as in our previous work (520).

We found that the kinetics of circulating myeloid cells in diabetic mice showed a surprising trend towards a higher percentage of Ly6C^{Lo} monocytes early after wound injury, with a more delayed increase in inflammatory Ly6C^{Hi} monocytes and a similar trend for neutrophils at day 10 of wound healing. In contrast, as expected, non-diabetic wounds were accompanied by a sharp peak in peripheral blood neutrophils immediately after injury, with a relatively even presence of Ly6C^{Lo} and Ly6C^{Hi} monocytes throughout the ten days of observation. These data suggest that there is an altered systemic inflammatory response for diabetic wounds, that may be characterised by a delayed and/or prolonged pro-inflammatory state in circulating blood. In another study, Joshi *et al.* recently identified that MΦs and neutrophils were less abundant at early stages of healing in diabetic wounds compared to non-diabetic wounds, but this pattern was reversed in later stages (356, 358). Similarly, we also observed that the overall expansion of MΦs in wounds peaked at days 1 and 3 under euglycaemic conditions, but at day 7 for diabetic mice. Based on the absence of GFP expression in our *Csf1r* CRE-

LOX fate-mapping study, most of this delayed accumulation of MΦs in STZ-induced diabetes was from a non-YS-derived source, which we expect involved the recruitment and differentiation of circulating monocytes. Notably, diabetes resulted in marked attenuation of the local expansion of GFP⁺ YS-derived MΦs, as opposed to in non-diabetic wounds where these cells accumulated sharply from day 3 to 7 of the healing process. Along with our previous unpublished work (522), the current chapter also reaffirms that YS EMPs are an important source of ECs in steady-state mouse skin, with clear expansion of this population as wounds repair. This finding aligns with the seminal study by Plein *et al.* who first reported the presence of EMP-derived EC-lining blood vessels in mouse brain, heart, lungs and liver (108). Our results also show a profound failure of diabetic wounds to “endothelialise” and this seems to apply to ECs from both YS and non-YS origins.

Based on our previous and current findings, we propose that EndoMac progenitors are a renewable, local source for the postnatal maintenance and production of YS-derived MΦs and ECs in skin, with the ability for this to be rapidly upscaled after wound injury. Exposure to high glucose not only dampens the capacity for these cells to undergo proliferative renewal, but also strongly inhibits their ability to form “angiogenic” cords *in vitro*. It also affects their differentiation capacity, with our results indicating very strong abrogation of their potential to form new ECs and possible skewing toward alternative lineages instead, including MΦs and other progeny that we are yet to define. This was evident in both the cord-forming MatrigelTM assay and also our adoptive transfer experiment, in which almost 80% of donor-derived cells were classified as “other” (i.e. not progenitor, MΦ or EC) after transplanting STZ+ progenitors, as compared to ~50% from STZ- progenitors. Importantly, diabetic wounds displayed accelerated wound closure following local injection of non-diabetic progenitors, which still retained their ability to engraft and differentiate into new ECs and MΦs even in a diabetic host milieu. A crucial next step will be for us to elucidate the signalling and growth factors present in the wound microenvironment that support these processes and unravel how these

vary between diabetic and non-diabetic wounds across different stages of repair. In addition, our findings show that STZ- EndoMac progenitors mediated the accumulation of host-derived cells in wounds, which implies that they may also possess paracrine properties that also need further evaluation.

Limitations and future directions

Another lingering question relates to the precise localisation of EndoMac progenitors (i.e., their specific niche) within the different layers of skin. This is especially relevant as epidermal Langerhans cells, which are also known to clonally expand (91), originate primarily from YS, as do a substantial minority of different MΦ subpopulations in the dermis (555). I have recently found that single cell digests of dermis and epidermis from adult mouse skin both give rise to CFU-M in culture, although clonal efficiency is higher from the dermis (epidermis: 8.3 ± 4.1 vs dermis: 50.7 ± 9.7 per 10^5 cells, $n=3$, $p=0.03$). Similarly, by flow cytometry analysis I observed a trend towards a higher content of EndoMac progenitors in dermis (epidermis: 0.5 ± 0.2 vs dermis: 3.2 ± 1.7 %, $n=3$, $p=0.1$) (**Appendix 7.6**). In very preliminary studies, our group has also identified analogous CFU-M progenitors from skin digests from amputated limbs of patients with peripheral artery disease (Hassanshahi, Psaltis unpublished). This will provide important impetus for us to characterise the phenotypic, functional, metabolic and transcriptional properties of these human cells to better understand their relevance to healthy and impaired skin healing in the clinic.

The therapeutic use of stem cells to treat diabetic wounds has been examined in several clinical studies with promising results (590-592). Intramuscular injections of autologous peripheral blood mononuclear cells (PBMNCs) (593), bone marrow mesenchymal stem cells (BM MSCs) (594) or bone marrow-derived mononuclear cells (BMMNCs) (595) into the wounds and ischaemic lower

limbs of patients with diabetes have been shown to promote neovascularisation and assist repair. The ability to deliver skin EndoMac progenitors into human wounds would depend firstly on identifying their presence in human skin, and secondly, on demonstrating the safety of transplanting these cells allogeneically from healthy, non-diabetic donors to ensure their capacity to engraft, proliferate and differentiate in recipient diabetic tissue. This will therefore require a detailed understanding of their immune properties, and specifically their susceptibility to immune rejection. An alternative strategy may be to target endogenous progenitors in the skin of affected individuals with diabetes, with molecular, pharmacological or genetic engineering techniques that rescue or upregulate their salutary properties. Based on the data in this chapter, one such approach may be to metabolically reprogram these cells with treatments that restore their mitochondrial alterations in the diabetic setting. Potential candidates for this may include riboflavin (B2) (596) and antioxidants, such as L-Carnosine (597). Although we have demonstrated glucose-induced reduction in the mitochondrial health and function of skin EndoMac progenitors, the specific mechanisms by which this occurs also requires further study. This could involve comparing the transcriptomic and/or epigenetic profiles of progenitors from diabetic and non-diabetic mouse and human skin. It will also be important to extend all of these questions to the setting of type 2 diabetes, which can be modelled in mice using different strains (e.g. genetic models, (e.g., B6.Cg-Lep ob/J, BKS.Cg-Dock7 m +/+ Lepr db/J) and diet responsive models (DIO-C57BL/6J, B6D2F1/J) (127).

Using specimens already processed from the mice used in this chapter, we now intend to stain and label wound sections to determine the effects of progenitors on epithelial closure, collagen deposition, capillary and arteriolar neovascularisation, and to corroborate our results from flow cytometry with immunofluorescence microscopy. The latter will also help identify the proximity of different YS-derived cell populations with each other and with other important structures, such as the different cutaneous layers, wound margins and microvasculature. Of note, the heterogeneity of MΦ and EC

subtypes have been well described for murine skin (555), but less so in the settings of either wound injury or diabetes. Reports by Malissen *et al.*, and later by Williamson *et al.* on the composition, ontogeny and functional specialisation of skin myeloid cells have revealed distinct immunophenotypic subtypes, annotated as CD11b⁺CD11c⁺ dendritic cells and dermal CD11b⁺ P1-P5 monocyte/macrophages (520, 522, 555). A tissue-resident YS-derived source was previously shown to make the biggest contribution to dendritic cells (days 1-3), pro-inflammatory “P1” MΦs (days 1-7) and anti-inflammatory “P4” MΦs (day 7) during wound healing in the non-diabetic state (522). Although not yet analysed, the wound specimens collected here have already been labelled with relevant surface markers before performing flow cytometry, and this will allow us to delineate these subpopulations and their YS origins in the diabetic versus non-diabetic settings.

Conclusion

Skin EndoMac progenitors are highly susceptible to the inhibitory effects of high glucose, as evidenced by a range of mitochondrial abnormalities and profound attenuation of their ability to proliferate, expand, and differentiate. Our findings also introduce EndoMac progenitors as a potential cell therapy candidate or treatment target to help promote wound closure that is severely impaired in diabetes.

Chapter 5

5. Inhibitory effects of diabetes on yolk-sac derived endothelial-macrophage progenitors in murine skeletal muscle and ischaemia

5.1 Introduction

Peripheral artery disease (PAD) is usually characterised by the atherosclerotic narrowing of peripheral arteries that restricts blood flow to the lower limbs, resulting in tissue ischaemia, including to skeletal muscle (SkM). It affects up to 15% of adult Australians (598). Diabetes is a major risk factor for PAD, conferring a four-fold increased risk compared to patients without diabetes (599, 600). Despite breakthroughs in risk factor management and arterial revascularisation therapies, the morbidity, mortality, and health-care costs associated with diabetes-related PAD remain unacceptably high (599). Atherosclerosis in diabetes-related PAD is often more diffuse with increased involvement of the distal vasculature (e.g., tibial arteries) (601). Furthermore, diabetes impairs neovascularisation, the body's natural response to ischaemia, and is associated with metabolic disturbances to endothelial cells (ECs) (e.g., mitochondrial dysfunction) and an exaggerated and prolonged inflammatory response in ischaemic tissue (534). Together, these factors result in a higher rate of PAD complications in diabetes, including increased risk of distal ischaemic ulcers, extensive tissue loss and increased risk of amputation (602, 603).

The mechanisms linking diabetes to poorer outcomes in PAD are complex and multifactorial. Mitochondrial dysfunction of skeletal myocytes appears to play a central role (192, 604, 605). Interestingly, even in the absence of vascular problems, the SkM in type 1 diabetes (T1D) exhibits impaired mitochondrial oxidative phosphorylation (207), while mitochondrial impairment may precede the onset of hyperglycaemia in patients who go on to develop type 2 diabetes (T2D) (606). These abnormalities also include increased oxidative stress and are accentuated both in the presence of chronic PAD and after acute ischaemia-reperfusion injury (607-612). Similarly, diabetes has been shown to impair the mitochondrial function of macrophages (MΦs) and ECs. Diabetes promotes polarisation of MΦs into a more prolonged “inflammatory” subset by activation of hypoxia-inducible

factor (HIF), that shifts cellular fuel consumption from mitochondrial oxidative phosphorylation (typical of “patrolling” MΦs) towards glycolysis (typical of inflammatory MΦs) (613-616). Furthermore, external lipid ligand activation of CD36 activates nuclear factor-κB to downregulate electron transport chain (ETC) function and enhances the generation of mitochondrial reactive oxygen species (ROS), which further boosts the expression of inflammatory MΦ-related genes (613, 617, 618). This may lead to the development of diabetes-associated inflammation and consequent vascular complications. The high glucose state also results in increased mitochondrial dysfunction and ROS overproduction in ECs and their EPC ancestors (481, 619, 620). This results in an activated state, whereby ECs release pro-inflammatory cytokines and increase their expression of adhesion molecules, that promote monocyte recruitment and transmigration into diabetic tissues, which exacerbates and maintains tissue inflammation in the setting of diabetic ischaemia (621, 622).

MΦs and ECs share an intimate bidirectional relationship to mediate inflammation and neovascularisation during the repair of tissues post-ischaemia (623). MΦs perform the following pleiotropic functions: i) secretion of pro-inflammatory cytokines and chemokines to maintain initial leukocyte infiltration; (ii) phagocytosis to remove invading pathogens and necrotic cell debris; (iii) release of matrix metalloproteinases for extracellular matrix remodelling (624); and (iv) pro-angiogenic effects by guiding the sprouting of new blood vessels and the proliferation of ECs and smooth muscle cells (623). This functional diversity reflects the tremendous heterogeneity and plasticity that is characteristic of tissue MΦs more broadly, and has been linked to their different ontogeny, as well as the local regulatory effects of different tissue and disease settings (73, 625, 626). Previous studies highlight that MΦs arise from various sources. On the one hand, this involves the recruitment and differentiation of bone marrow (BM) derived monocytes from blood (627), and on the other, the local proliferative renewal of embryonically derived tissue MΦs, including those from yolk sac (YS) erythromyeloid progenitor cells (EMPs) (28, 34, 546, 586), that persist into postnatal

life. Recently, Wang *et al.* studied the diversity and developmental origins of MΦs in adult steady-state SkM and identified distinct subsets with unique surface marker and transcriptomic signatures, that were derived from different circulatory and local sources (75).

With paracrine support from MΦs, ECs proliferate, migrate, and coalesce to form intricate vascular labyrinths. Neovascularisation thereby restores the delivery of oxygen and nutrients to ischaemic tissue that promote muscle repair and regeneration. Like MΦs, ECs are also known to arise from heterogeneous sources. This includes the clonal expansion of local ECs (21, 628), recruitment of circulatory, BM-derived EPCs (115), and differentiation of local tissue-resident hierarchies of proliferative endovascular progenitors (119, 570-572). Recent data has emerged to indicate that YS EMPs also give rise to ECs in some murine tissues, including brain, liver, lung and heart (108), although this has since been disputed (109). The possibility that YS EMPs can generate progeny of both haematopoietic (e.g. MΦ) and endothelial lineages aligns with the discovery of bipotent haemangioblasts during early embryogenesis, nearly a century ago (629). Until now, evidence that haemangioblasts also persist after birth has remained elusive (630).

As discussed in Chapters 3 and 4, we have identified that some adult mouse tissues, including SkM, contain local Lin⁻CD45⁺CD11b⁻F4/80⁻ Sca-1⁺c-Kit⁺ (CX₃CR1⁺CSF1R⁺) progenitor cells that self-renew, differentiate into both MΦs and ECs and promote neovascularisation (517, 518, 520). We have established that these bipotent endothelial-macrophage (EndoMac) progenitors are seeded during prenatal development from YS EMPs (522). SkM EndoMac progenitors expand rapidly in response to hind limb ischaemia in wildtype mice, differentiate into MΦs and ECs and contribute to the formation of new blood vessels, resulting in perfusion recovery of ischaemic muscle (520, 522). In this chapter, we investigated whether high glucose also affects the functional and metabolic

properties of embryonically derived SkM EndoMac progenitors and explored whether this in turn is associated with the impaired perfusion recovery of diabetic ischaemic SkM.

5.2 Methods in brief

5.2.1 Overview

Breeding pairs of C57BL/6 (C57BL/6J), *Csf1r*^{Mer-iCre-Mer} (FVB-Tg(Csf1r-cre/Esr1*)1Jwp/J), *Rosa*^{mT/mG} (Gt(ROSA)26Sor^{tm4}(ACTB-tdTomato,-EGFP)Luo/J) and UBI-GFP (C57BL/6-Tg(UBC-GFP)30Scha/J) mouse strains were acquired from The Jackson Laboratory (Bar Harbor, ME, USA). *Csf1r*^{Mer-iCre-Mer} and *Rosa*^{mT/mG} mice were crossed to obtain *Csf1r*^{Mer-iCre-Mer} x *Rosa*^{mT/mG} pups. Mice were housed in the animal care facility at SAHMRI and were maintained on standard chow diet. In all cases, both genders were utilised. For the induction of T1D, intraperitoneal (i.p) injections of 165 µg/g streptozotocin (STZ) were administered to 8–12-week-old (w) mice, while controls received citrate buffer injection as sham. Blood glucose concentrations (BCG) were monitored a week after injection and diabetes was confirmed by a level >15 mmol/L. An extra dose was administered if the levels were <15 mmol/L one week post initial injection.

Animals were housed on a standard chow diet with a continuous water supply replaced every other day or as needed for a period of three weeks. Gastrocnemius, soleus, and quadriceps SkM from the hind limbs of these mice was enzymatically digested into single cell suspensions for use in different experiments, including methylcellulose colony forming unit (CFU) and MatrigelTM-based angiogenesis assays and multi-colour flow cytometry. Several experiments also made use of a validated model of hind limb ischaemia surgery (535) in combination with gestation stage (E) 8.5 tamoxifen (TAM)-inducible *Csf1r*^{Mer-iCre-Mer} x *Rosa*^{mT/mG} fate-mapping strains or with adoptive transfer of GFP⁺ SkM EndoMac progenitors into C57BL/6 recipients. All animal experiments and care were performed following the standards stated in the Guide for the Care and Use of Laboratory Animals (Institute of Laboratory Animal Resources, National Academy of Sciences, Bethesda, MD, USA) and in accordance with the National Health and Medical Research Council of Australia

research guidelines and Australian Code for the Care and Use of Animals for Scientific Purposes. Ethics approval was obtained from the SAHMRI animal ethics committee (ID SAM20.032 and SAM432.19)

5.2.2 Statistical analysis

Where relevant, analysis was performed blinded to study group. Statistical comparisons were performed using Prism (GraphPad version 10). Datasets were tested for normality of distribution by Shapiro-Wilk test. Statistical comparisons were performed with parametric or non-parametric unpaired or paired two sample *t*-tests or ANOVA (with post-test multiple comparisons), as specified. Results are expressed as mean \pm standard deviation of multiple experiments. In all cases, statistical significance was established at two-tailed $p < 0.05$. The statistical parameters and the number of mice used per experiment are found in the figure legends.

5.3 Results

5.3.1 High glucose attenuates stem-like and angiogenic properties of SkM EndoMac progenitors.

Hind limb SkM from 8–12 w C57BL/6 mice was digested into single cell suspensions and cultured at a density of 2×10^5 cells per well in a 24 well-plate in methylcellulose for 14 d to study haematopoietic colony formation. Replicate wells were exposed to three different concentrations of glucose (basal: 5 mM, intermediate: 15 mM, high: 25 mM) and 25 mM mannitol as an osmolarity control. As described in Chapter 3, SkM cells showed a unique predilection for forming primary (1°) CFU-M (**Figure 5.1A**). Exposure to basal glucose (5 mM) and mannitol (25 mM) produced no significant difference in CFU-M yield (48.4 ± 15.9 vs 36.0 ± 10.4 colonies/ 10^5 cells, $n=5/\text{gp}$). In keeping with results from aortic and skin CFU-M described in Chapter 3 and 4, high glucose (25 mM) levels significantly decreased SkM CFU-M yield by 4.4-fold (**Figure 5.1B**). CFU-M in basal glucose consisted of 68% small (30-100 cells), 27% medium (100-1000 cells) and 3% large (>1000 cells) colonies. By comparison, the high glucose condition was associated with a higher proportion (90%) of small CFU-M and a complete absence of large CFU-M (**Figure 5.1C**). This indicates a potential inhibitory effect of high glucose on the proliferative and/or renewal capacity of the EndoMac progenitors responsible for CFU-M growth *in vitro*.

We therefore next examined the effect of glucose on colony renewal. CFU-M were individually isolated from 1° methylcellulose cultures at day 14 under microscopic guidance and disaggregated to allow seeding of single cells into different wells in 2° CFU-M assays. SkM CFU-M were observed to renew from single cell origins (**Figure 5.1D**), with 81% of cells from 1° CFU-M giving rise to at least one 2° colony under basal glucose conditions, compared to only 6.3% under exposure to high glucose

(n=5/gp, $P<0.0001$). Notably, we also observed a smaller but still significant decrease in CFU-M renewal in the presence of the 25 mM mannitol osmolarity control.

As for aortic and skin progenitors (Chapters 3 and 4), SkM EndoMac progenitors also produce vascular-like cord networks when cultured for 7 d in endothelial growth media on MatrigelTM (**Figure 5.1E**). This capacity was substantially reduced when cultured in 15 mM and 25 mM glucose (**Figure 5.1E**), with a 72% and 80% reduction, respectively, in total cord length formed compared to 5 mM glucose (**Figure 5.1F**). Similarly, higher glucose exposure also resulted in the formation of fewer cords (**Figure 5.1G**) and fewer connecting branch points (**Figure 5.1H**). Taken together, these data demonstrate that exposure to high glucose severely dampen the clonal, renewal and angiogenic capacity of SkM EndoMac progenitors *in vitro*.

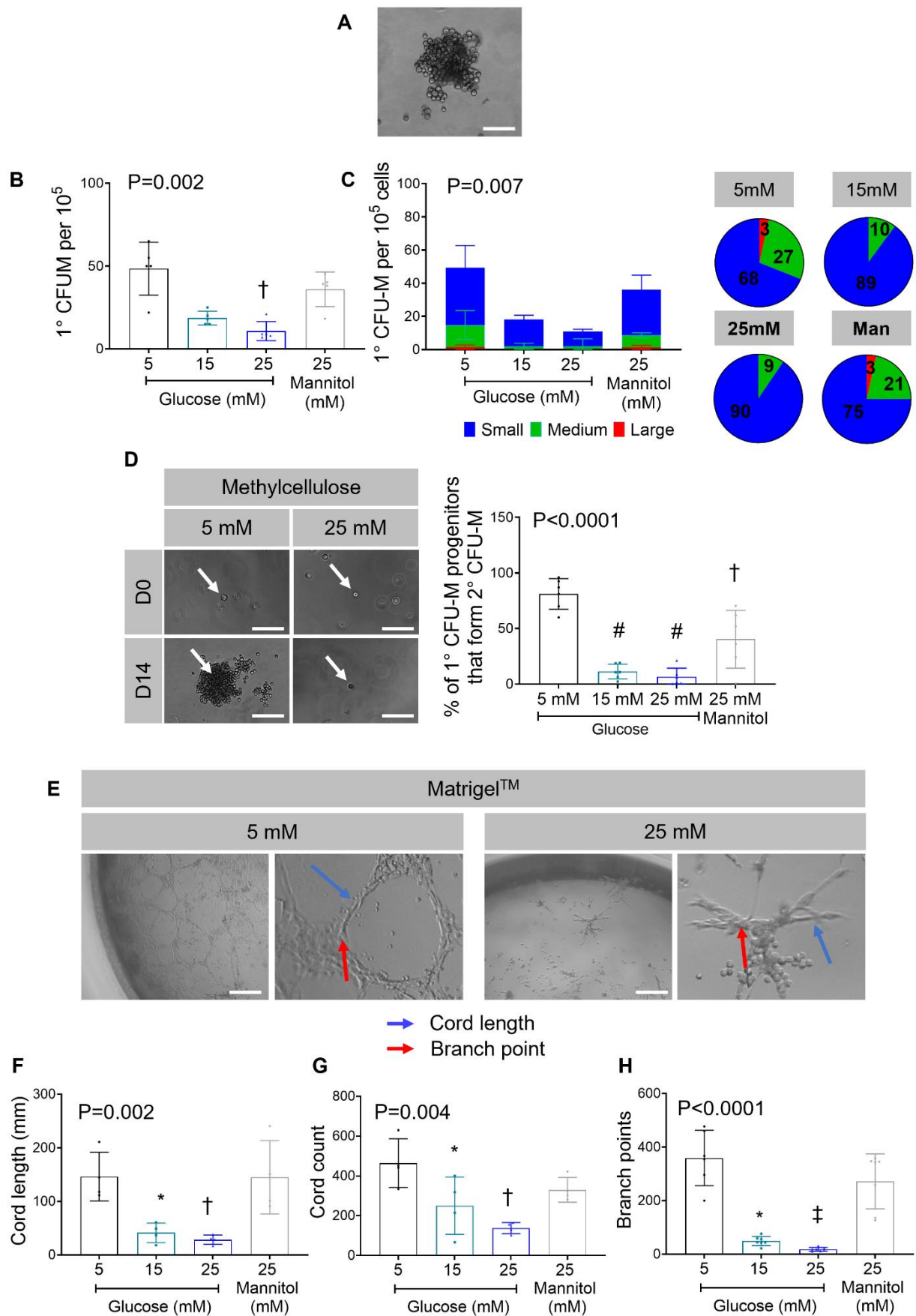


Figure 5.1: High glucose attenuates clonal, renewal and angiogenic properties of SkM progenitors.

- A)** Light microscopy of a representative SkM CFU-M from adult C57BL/6 mouse. Scale bar, 100 μ m.
- B)** Comparison of 1° CFU-M yield from donor-matched SkM digests from C57BL/6 mice following exposure to glucose (5 mM, 15 mM, 25 mM) and mannitol (25 mM) osmolarity control. n=5 mice/gp. Kruskal-Wallis. Multiple comparison: †P<0.01 ‡P<0.001 in comparison to 5 mM glucose.
- C)** Bar graphs showing comparison of 1° CFU-M yield by size from donor matched SkM digests from C57BL/6 mice following exposure to glucose (5 mM, 15 mM, 25 mM) and mannitol (25 mM). CFU-M sizes classified as small (30-100 cells), medium (100-1000 cells) and large (>1000 cells). n=5 mice/gp. One-way ANOVA. Adjacent pie charts showing percentage of those 1° CFU-M. Percentages represent mean of n=6 mice/gp.
- D)** Representative light microscopy image of 2° colonies produced from single cell obtained from SkM 1° CFU-M from C57BL/6 mice at day 0 (D0) and 14 (D14). exposed to 5 mM and 25 mM glucose. Scale bar, 100 μ m. Bar graph showing comparison of 2° colony renewal from single cells obtained from 1° CFU-M upon exposure to glucose (5 mM, 15 mM, 25 mM) and mannitol (25 mM). n=5/gp. One-way ANOVA. Multiple comparison: †P<0.01 and #P<0.0001 in comparison to 5 mM.
- E)** Representative light microscopy images of branching cord networks produced from SkM EndoMac progenitors in Matrigel™ when cultured under 5 mM and 25 mM glucose conditions. n=4/gp. Scale bar, 100 μ m (left) and 1000 μ m (right). Cords are denoted by blue arrows and branch points by red arrows.
- F-H)** Graphs display comparisons of **F)** total cord length, **G)** cord number and **H)** branch points produced under different glucose concentrations. n=4/gp mice. One-way ANOVA for **F-G)** and Kruskal-Wallis for **H)**. Multiple comparison: *p<0.05, †P<0.01 and #P<0.0001 in comparison to 5 mM.

5.3.2 Effects of high glucose on the mitochondrial and metabolic activity of SkM progenitors.

To examine for possible mechanistic alterations responsible for the inhibitory effects of high glucose on SkM progenitors *in vitro*, we carried out a series of metabolic assays that investigate mitochondrial viability and function. EndoMac progenitors were isolated from 1° CFU-M cultured from SkM cells in basal and higher glucose conditions and stained for three mitochondrial markers (MitoTracker™ green, MitoTracker™ red, MitoSOX™ red) before analysis by flow cytometry. 25 mM glucose was associated with almost a 25% relative reduction in expression of MitoTracker™ green, indicating the presence of fewer viable mitochondria (**Figure 5.2A**). This was accompanied by a 2.8-fold increase in mitochondrial reactive oxygen species as measured by superoxide build-up using uptake of the MitoSOX™ red dye (**Figure 5.2B**). Furthermore, the proportion of cells that expressed MitoTracker™ red was significantly lower for the 25 mM glucose condition, indicating defective mitochondrial membrane potential (**Figure 5.2C**).

As high glucose seemingly alters mitochondrial membrane potential and thereby the ETC function, we investigated alternative metabolic pathways by examining the by-product of anaerobic glycolysis: lactate. Supernatant from progenitors exposed to high glucose did not show significant differences in lactate concentration, suggesting that energy production might still be predominantly driven by aerobic means, albeit at a lower capacity due to the mitochondrial defects described above (**Figure 5.2D**). However, we did observe a 1.4-fold increase in uptake of the glucose analogue, 2-(N-(7-nitrobenz-2-oxa-1,3-diazol-4-yl)amino)-2-deoxyglucose (2NDBG) under the higher glucose condition, which would be consistent with other studies of stem cells (631) (**Figure 5.2E**). Based on these results, EndoMac progenitors exposed to high glucose demonstrated a higher glucose uptake ability, which may be explained as a compensatory mechanism to meet the high energy demand in the setting of defective mitochondrial oxidative membrane potential and a diminished number of

viable mitochondria. Similar lactate concentrations across the two groups indicate that the unmet energy demand in the high glucose group has not shifted the metabolic pathway into a more glycolytic one but is rather driven by mitochondrial respiration. Increased substrate uptake may also be linked to the production of damaging ROS following oxidative phosphorylation. As glucose is the dominant substrate for all cellular metabolic function, the functional defects caused by high glucose on EndoMac progenitors might at least be partly due to mitochondrial dysfunction.

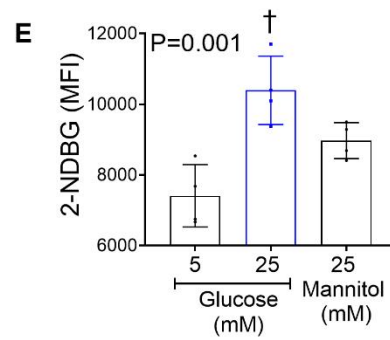
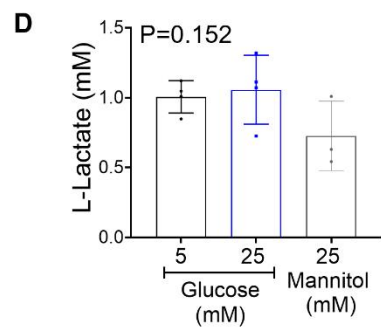
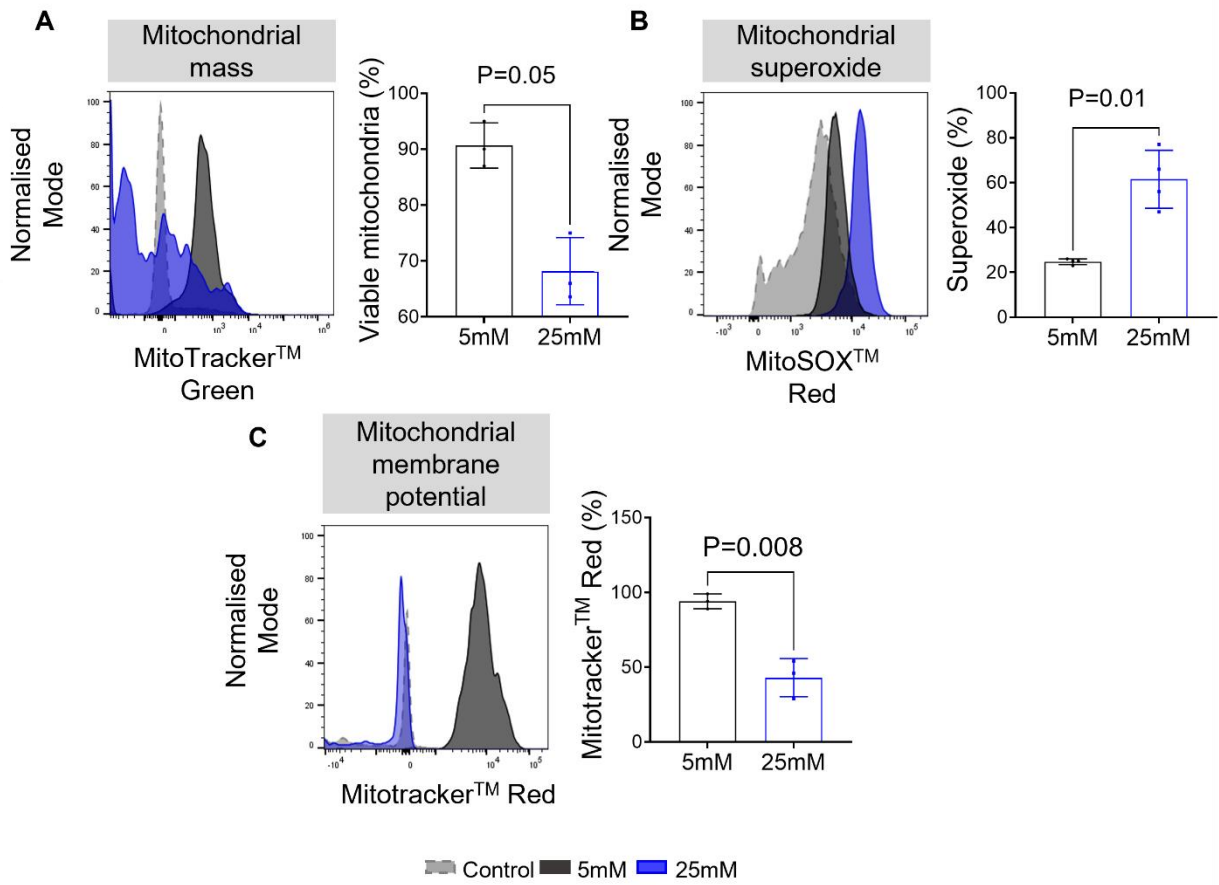


Figure 5.2: Exposure to high glucose levels dampen the mitochondrial function of SkM progenitors

A) Flow cytometry histogram depicting staining with Mitotracker™ green as marker of viable mitochondrial mass of CFU-M derived EndoMac progenitors after exposure to 5 mM and 25 mM glucose. Data is representative of n=3, 12 w C57BL/6 mice. Light grey dotted lined histogram indicates FMO control. P=0.05, paired *t*-test.

B) Flow cytometry histogram showing uptake of MitoSOX™ Red as marker of mitochondrial superoxide levels by the progenitors exposed to 5 mM and 25 mM glucose. Data is representative of n=4, 12 w C57BL/6 mice. Light grey dotted lined histogram indicates FMO control. P=0.01, Paired *t*-test.

C) Flow cytometry histogram depicting labelling with Mitotracker™ deep red as marker of mitochondrial membrane potential of the progenitors exposed to 5 mM and 25 mM glucose. Data is representative of n=3, 12 w C57BL/6 mice. Light grey dotted lined histogram indicates FMO control. P=0.008, Paired *t*-test.

D) Comparison of mean L-lactate concentrations in the supernatants of progenitors exposed to the indicated glucose and mannitol concentrations. Data is representative of n=4 12 w C57BL/6 mice. P=0.1, One-way repeated-measures ANOVA.

E) Comparison of mean florescent intensity of uptake of glucose analogue (2-NDBG) by progenitors exposed to the indicated glucose and mannitol concentrations. Data is representative of n=4, 12 w C57BL/6 mice. P=0.001, One-way Anova.

Data in graphs are presented as mean \pm SD.

5.3.3 SkM EndoMac progenitors' function at a lower metabolic capacity when exposed to high glucose

Mitochondrial alterations observed in section 5.3.2 were further investigated by carrying out the Seahorse assay, which is the current gold standard to assess cellular metabolic health and function (632). Briefly, SkM progenitors cultured in basal and high glucose were isolated to assess oxygen consumption rate (OCR) and extracellular acidification rate (ECAR) following exposure to three mitochondrial inhibitors: Oligomycin, carbonyl cyanide p-trifluoro methoxyphenylhydrazone (FCCP) and Rotenone/Antimycin-A at different time-points (**Figures 5.3A, F**) OCR is proportional to mitochondrial respiration, while ECAR is proportional to glycolysis. Initially, baseline OCR was significantly lower in progenitors exposed to 25 mM glucose (5 mM: 227.8 ± 39.1 vs 25 mM: 103.4 ± 29.3 pmol/min, n=6, P=0.0002) (**Figure 5.3B**).

Next, Oligomycin, which inhibits ATP synthase (complex V) was injected first in the assay following basal measurements. It impacts or decreases electron flow through the ETC, resulting in a reduction in mitochondrial respiration or OCR (**Figure 5.3A**). This OCR decrease is expected as inhibition of ATP-synthase in the ETC would prevent phosphorylation of Adenosine diphosphate (ADP) into Adenosine triphosphate (ATP) during oxidative phosphorylation. This decline in OCR was utilised to calculate mitochondrial ATP-linked respiration (ATP-linked respiration=average basal OCR-average OCR post oligomycin). Interestingly, the dependence on mitochondria for ATP synthesis was stronger for the basal glucose condition with an OCR of ~30 pmol/min compared to ~18 pmol/min for high glucose concentrations, contributing to the production of ATP (difference of 11.6 pmol/min between the two groups, n=6, P=0.03) (**Figure 5.3C**).

The second agent introduced was an uncoupler: FCCP. FCCP mimics a physiological energy demand by stimulating the respiratory chain to operate at maximum capacity, which causes rapid oxidation of substrates (sugars, fats, and amino acids) to meet this metabolic challenge and stimulates mitochondrial oxygen consumption. A sudden increase in OCR beyond baseline OCR is therefore also expected to supply the energy demand that was unmet during the ATP synthase inhibition stage. This rapid increase was used to calculate reserve capacity compared to basal respiration, which was 4.7-fold higher for basal glucose compared to high glucose (**Figure 5.3D**). This provided further information on the maximal respiration capacity of mitochondria, which demonstrated a mean OCR difference of ~ 290 pmol/min under basal compared to high glucose conditions (437.2 ± 72.3 vs 147.5 ± 42.2 , $n=6$, $P=0.0001$) (**Figure 5.3E**). This reflects the capability of the cells to respond to changes in energetic demand and is an indication of the “fitness” of the cells. Taken together, these results indicate that high glucose impairs the metabolic function of SkM progenitors at both mitochondrial oxidative phosphorylation stages, as well as its ability to recover following metabolic stress.

The final inhibitor used was Rotenone/Antimycin A that targets and inhibits function of the mitochondrial ETC complex I and III. This would once again be expected to cause a reduction in OCR to a minimal value as mitochondrial oxidative function is paused. The fall in OCR following ETC complex inhibition for basal glucose compared to high glucose was significantly larger (ΔOCR -255.7 ± 70.6 pmol/L vs -40.5 ± 29.2 pmol/L, $n=6$, $P<0.0001$). This further confirms the dependence on mitochondria for ATP synthesis in SkM EndoMac progenitors.

To investigate whether high glucose launches a compensatory mechanism to meet the increasing energy demand following mitochondrial inhibitors, we next investigated anaerobic glycolysis activity

by measuring ECAR. Overall, cytoplasmic baseline glycolysis was significantly higher under basal compared to high glucose levels, as observed by a 1.4-fold higher ECAR (116.8 ± 7.3 vs 79.4 ± 11.0 , $n=6$, $P=0.0005$) (**Figure 5.3G**). Following oligomycin injection, glycolytic capacity of both basal and high glucose groups increased by 13.5 mpH/min and 9.4 mpH/min, respectively, compared to baseline ECAR ($n=6$, $P=0.1$) (**Figure 5.3H**). This indicates that inhibition of mitochondrial ATP synthesis may use anaerobic glycolysis as the predominant source of energy for both groups. Maximum glycolytic capacity was observed following uncoupling via FCCP. This capacity was once again significantly higher for the basal glucose condition (182.4 ± 8 vs 113.4 ± 13.6 mpH/min, $n=6$, $P<0.0001$) (**Figure 5.3I**). ECAR continued to be maintained at a higher rate following inhibition of mitochondrial complexes with Rotenone and Antimycin A, further implying that glycolysis may contribute to supply the demand of energy within the cell.

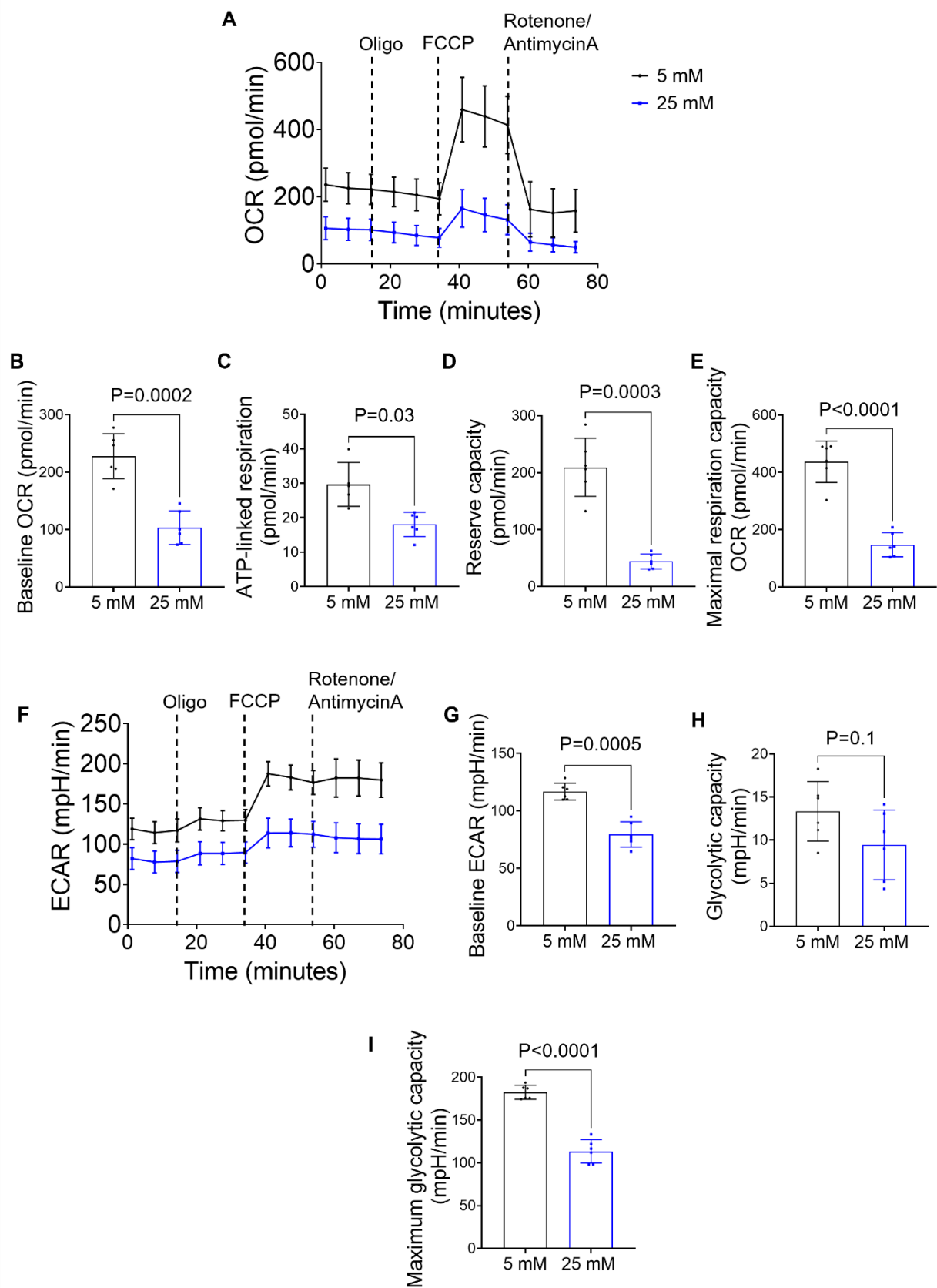


Figure 5.3: SkM EndoMac progenitors function at a lower metabolic capacity under high glucose.

A) Comparison of oxygen consumption rate (OCR) by progenitors exposed to 5 mM and 25 mM glucose. Dotted lines indicate the time at which mitochondrial inhibitors: Oligomycin (Oligo), Carbonyl cyanide 4-(trifluoromethoxy)phenylhydrazone (FCCP), Rotenone and Antimycin-A was added. n=6.

B) Baseline OCR **C)** ATP-linked respiration **D)** Reserve capacity **E)** Maximal respiration capacity of progenitors exposed to 5 mM and 25 mM glucose. n=6, Paired *t*-test.

F) Comparison of extracellular acidification rate (ECAR) over a period of 73 min for progenitors exposed to 5 mM and 25 mM glucose. Dotted lines indicate the time at which mitochondrial inhibitors: Oligomycin (Oligo), Carbonyl cyanide 4-(trifluoromethoxy)phenylhydrazone (FCCP), Rotenone and Antimycin-A was added. n=6.

G-H) Comparison of **G)** Baseline ECAR **H)** Glycolytic capacity for progenitors exposed to 5 mM and 25 mM glucose. n=6, Paired *t*-test.

I) Maximum glycolytic capacity of progenitors exposed to 5 mM and 25 mM glucose following FCCP injection, n=6, Paired *t*-test.

5.3.4 Streptozotocin-induced hyperglycaemia induces a systemic inflammatory state

The inhibitory effects of high glucose on SkM EndoMac progenitors *in vitro* led us to investigate how they are affected by hyperglycaemia *in vivo*. We used a murine model of T1D induced by STZ i.p. injection (548). Sham control (STZ-) and diabetic (STZ+) mice showed significant differences in blood glucose concentrations (BGC) (8.9 ± 0.7 vs 26.1 ± 6.6 mmol/L, $n=10$, $P<0.0001$) (**Figure 5.4B**), as well as body weight (28.2 ± 3.0 vs 21.0 ± 4.4 g, $n=8$, $P=0.001$) (**Figure 5.4C**) (548). Three weeks after STZ or sham injection, we collected and prepared blood and BM cells for analysis (**Figure 5.4A**).

We found no significant difference between groups in the percentage of BM cells that were $CD45^+Lin^-Kit^+ Sca-1^+$ haematopoietic stem/progenitor cells (HSPCs) (**Figure 5.4D**). However, STZ+ mice showed a trend toward a higher frequency of $CD45^+Lin^-CD115^+CD11b^+$ circulating monocytes (**Figure 5.4E, F**), consisting of a significant increase in “inflammatory” $Ly6C^{hi}$ monocytes (**Figure 5.4G**) but not “patrolling” $Ly6C^{lo}$ monocytes (**Figure 5.4H**). Similarly, circulating neutrophils were also increased by 3.5-fold after STZ-induced hyperglycaemia (**Figure 5.4I**). These results speak to a more inflammatory state in the peripheral blood of diabetic mice under otherwise steady state conditions.

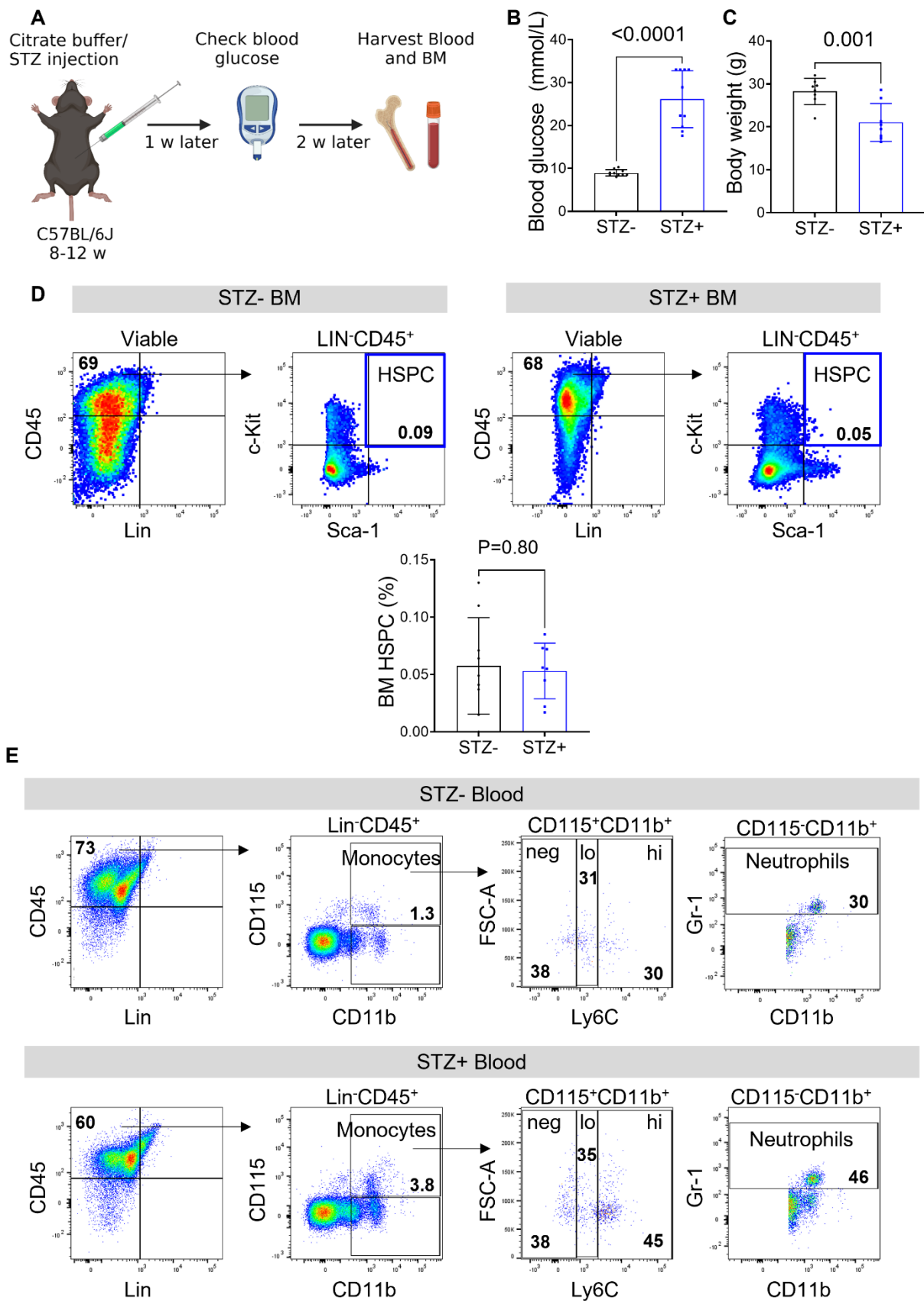


Figure continued P.T.O

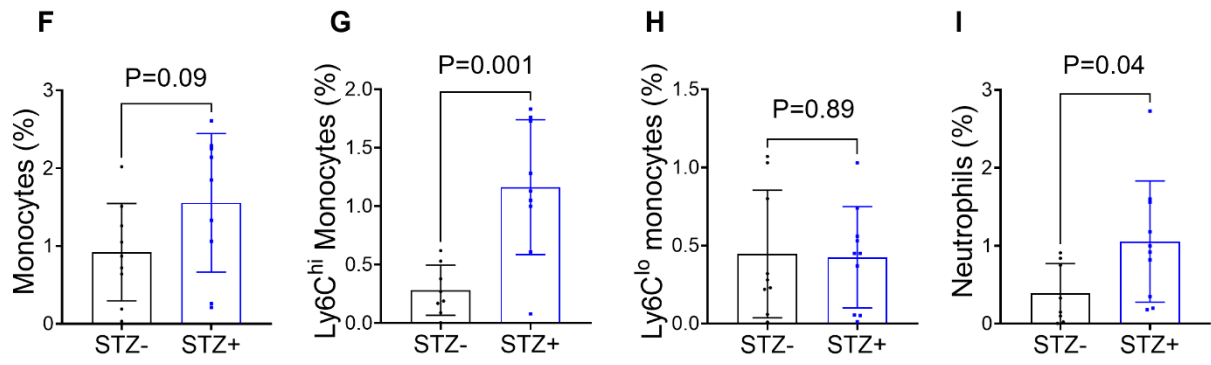


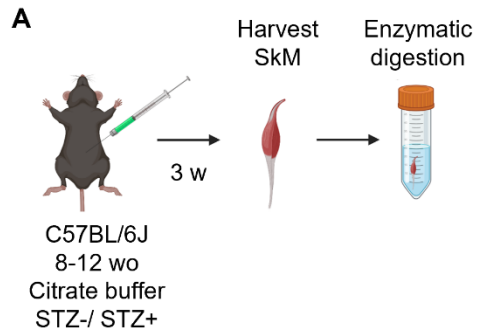
Figure 5.4: STZ-induced hyperglycaemia induces a more inflammatory state in peripheral blood.

- A)** Schematic shows STZ induction of hyperglycaemia in adult C57BL/6 mice.
- B)** Blood glucose concentrations of STZ- and STZ+ C57BL/6 mice 3 w after injection. n=10, Mann-Whitney test.
- C)** Body weight comparison of STZ- and STZ+ C57BL/6 mice 3 w after injection. n=10, unpaired *t*-test.
- D)** Flow cytometry of STZ- (left) and STZ+ (right) bone marrow (BM) HSPCs. Percentages in blue gated region represent mean % of HSPCs and graph shows quantitative results from n=9-10 mice per group. Unpaired *t*-test.
- E)** Flow cytometry plots showing expression of blood CD45⁺Lin⁻CD115⁺CD11b⁺ monocytes, Ly6C^{neg}, Ly6C^{lo}, Ly6C^{hi} monocytes and neutrophils from STZ- and STZ+ C57BL/6 mice. Numerical values shown represent the mean percentage from n=9-10 mice.
- F-I)** Frequency graphs show comparisons of the frequency of blood **F)** total monocytes, **G)** Ly6C^{hi} and **H)** Ly6C^{lo} monocytes and **I)** neutrophils from STZ- and STZ+ C57BL/6 mice. n=9-10 per group. Unpaired *t*-test.

5.3.5 STZ-induced hyperglycaemia is associated with fewer EndoMac progenitors in SkM

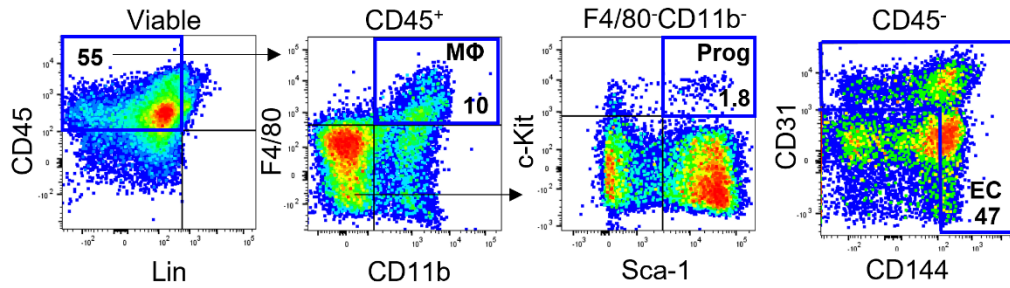
We next used flow cytometry to assess fresh tissue digests of hind limb SkM from adult C57BL/6 STZ- and STZ+ mice for their content of EndoMac progenitors, MΦs and ECs (**Figure 5.5A**). Based on our prior work (517, 518, 520), EndoMac progenitors were gated as CD45⁺CD11b⁻F4/80⁻c-Kit⁺Sca-1⁺ cells, while MΦs were CD45⁺CD11b⁺F4/80⁺ and ECs were CD45⁻CD31⁺ and/or CD45⁻CD144⁺ (**Figure 5.5B**).

STZ+ diabetic SkM showed a 50% reduction in the prevalence of EndoMac progenitors compared to STZ- sham (STZ- 2,787±2,017 vs STZ+ 1,309±690 cells/g, n=9-10/gp, P=0.04) (**Figure 5.5B, C**). Meanwhile, although the content of MΦs in SkM digests was not significantly different between the two groups (12,063±10,265 vs 9,102±7,784 cells/g, n=9-10, P=0.60) (**Figure 5.5D**), the density of ECs was markedly lower in the presence of hyperglycaemia (300,755±131,539 vs 125,436±63,659 cells/g, n=9-10/gp, P=0.002) (**Figure 5.5E**). We further studied the relationship between BGC and these three cell populations, finding significant inverse relationships between BGC and SkM content of EndoMac progenitors (**Figure 5.5F**) and ECs (**Figure 5.5H**), but not MΦs (**Figure 5.5G**).

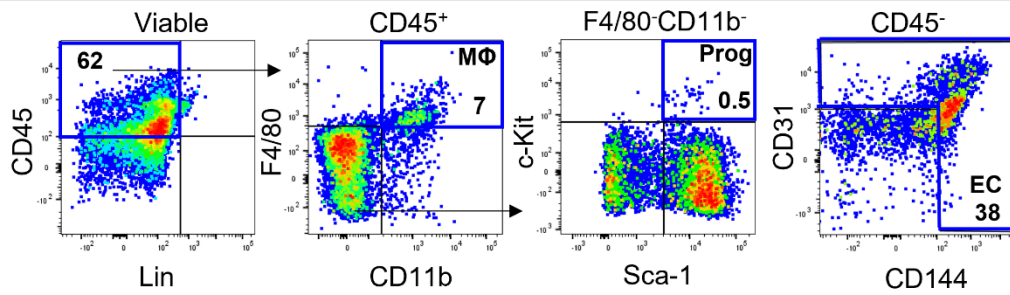


B

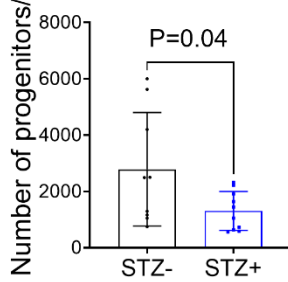
STZ- Muscle



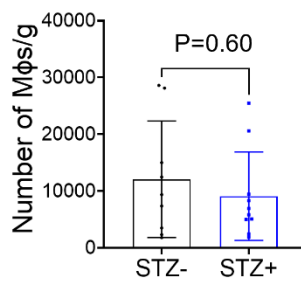
STZ+ Muscle



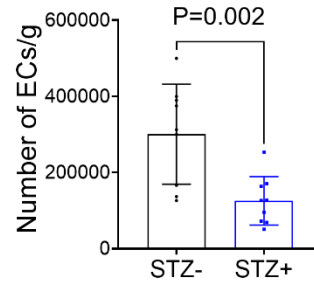
C



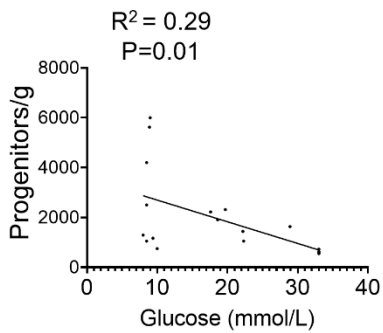
D



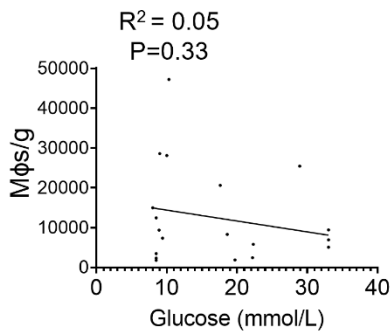
E



F



G



H

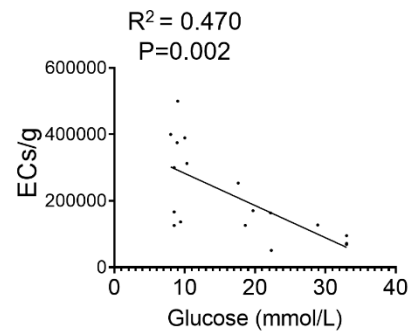


Figure 5.5: Hyperglycaemia is associated with fewer EndoMac progenitors in SkM.

A) Schematic shows STZ induction of T1D and enzymatic digestion of SkM.

B) Flow cytometry showing expression of SkM CD45⁺CD11b⁺F4/80⁺c-Kit⁺Sca-1⁺ EndoMac progenitors, CD45⁺CD11b⁺F4/80⁺ macrophages (MΦs) and CD45⁺CD31⁺ and/or CD144⁺ endothelial cells (ECs) from STZ- and STZ+ C57BL/6 mice. Numerical values in dot plots represent mean percentages from n=9-10/gp.

C-E) Number of **C)** progenitors, **D)** MΦs and **E)** ECs per g of age-matched STZ- and STZ+ mice. n=9-10/gp, unpaired *t*-test for **C)** and **E)**. Mann-Whitney test for **D)**

F-H) Simple linear regression graphs showing relationships between the content of **F)** progenitors, **G)** MΦs and **H)** ECs in SkM and blood glucose levels from all 20 mice studied (n=9-10/gp).

(Refer to Appendix 7.4)

In keeping with the decreased prevalence of EndoMac progenitors in diabetic SkM as measured by flow cytometry, we also observed a marked reduction in 1° CFU-M yield from STZ+ SkM cells (STZ- 53.0±9.3 vs STZ+ 20.7±8.6 CFU-M formed per 10⁵ cells plated, n=10/gp, P<0.0001). (**Figure 5.6A-C**). Moreover, as was the case for high glucose exposure *in vitro*, the colonies cultured from STZ+ mice were smaller, indicating diminished clonal growth and/or progenitor renewal (**Figure 5.6D, E**). This was examined further by performing CFU-M renewal assays as described above. As expected, progenitors isolated from 1° CFU-M showed much lower capacity to form 2° CFU-M when replated in methylcellulose (**Figure 5.6F, G**). These results corroborate the inhibitory effect of high glucose exposure *in vivo* on the stem-like properties of EndoMac progenitors from SkM.

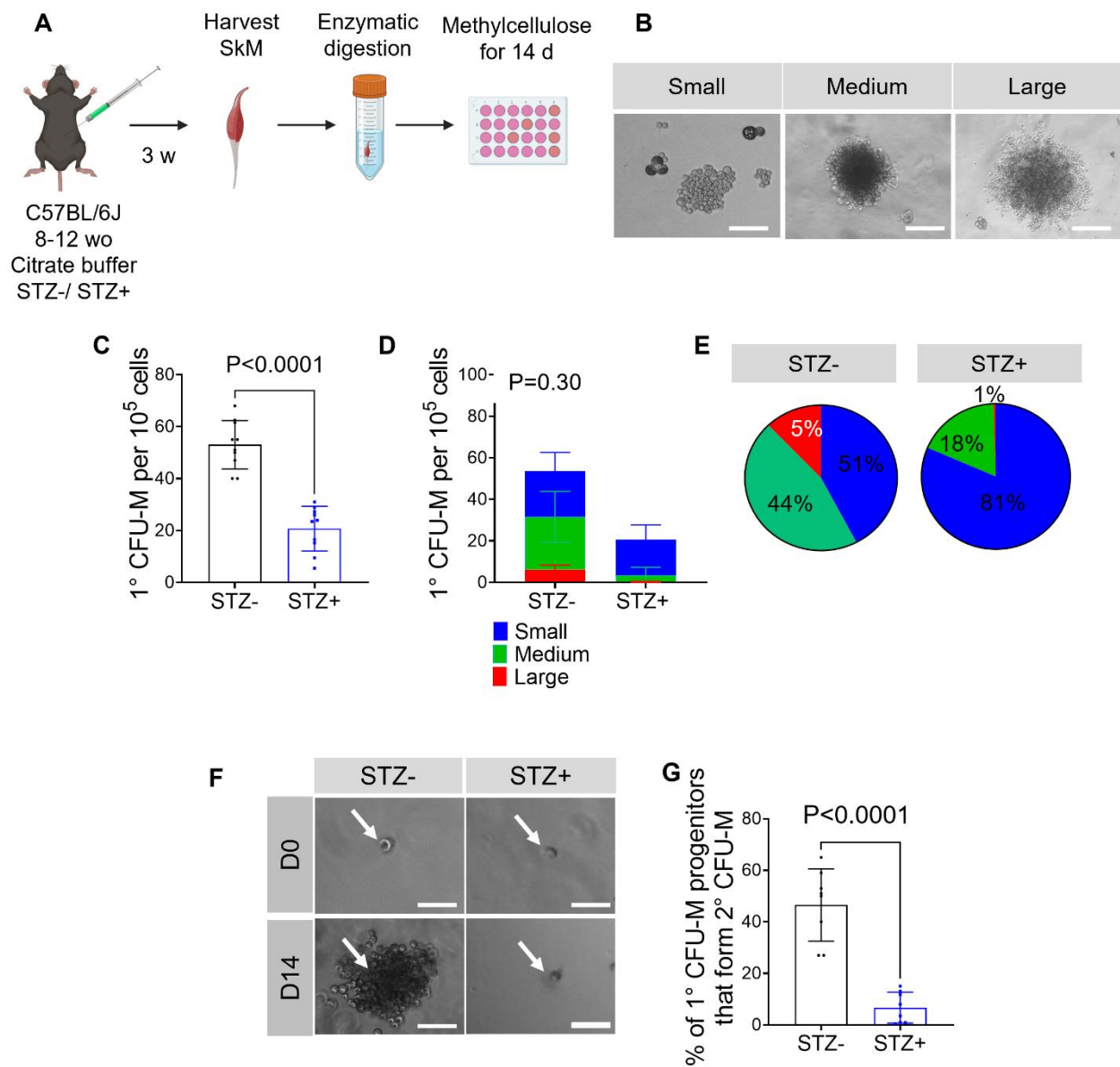


Figure 5.6: Diabetic SkM EndoMac progenitors have limited clonogenic renewal capacity

- A)** Schematic showing enzymatic digestion of SkM tissue from age matched STZ- and STZ+ C57BL/6 mice.
- B)** Light microscopy images show representative EndoMac progenitors classified according to size: small, medium, and large. Scale bar, 100 μ m.
- C)** Comparison of 1° SkM CFU-M yield per 10^5 cells plated of age matched STZ- and STZ+ C57BL/6 mice. n=10/gp, Unpaired *t*-test.
- D)** Bar graphs with CFU-M sizes overlaid from SkM digests. CFU-M sizes classified as small (30-100 cells/CFU-M) medium (100-1000 cells/CFU-M) and large (>1000 cells/CFU-M). n=10 mice/gp. Two-way ANOVA results: $p < 0.0001$ for size; $p < 0.0001$ for group; $p = 0.0004$ for size x group.
- E)** Pie charts show classification of CFU-M based on colony size from STZ- and STZ+ SkM digests. Percentages represent mean of n=10 mice/gp.
- F)** Light microscopy of 2° CFU-M produced from single cell obtained from SkM 1° CFU-M of STZ- and STZ+ C57BL/6 SkM 1° CFU-M. Scale bar, 100 μ m.
- G)** Comparison of 2° colony renewal from single cells obtained from SkM 1° CFU-M of STZ- and STZ+ C57BL/6 mice. n=8/gp, Unpaired *t*-test.

5.3.6 Diabetic SkM progenitors are more prone to DNA damage and possess mitochondrial abnormalities.

We next isolated EndoMac progenitors from SkM 1° CFU-M and analysed them for DNA damage to obtain insight into how STZ-induced hyperglycaemia affects their clonogenic and renewal properties. In the presence of double-stranded DNA breaks, the H2AX becomes serine-phosphorylated and therefore can be used as an indicator for nucleotide damage. Flow cytometry analysis showed that STZ+ progenitors had more than a three-fold increase in the percentage of H2AX expression compared to STZ- control, indicating increased DNA damage (STZ- $0.7 \pm 0.4\%$ vs STZ+ 2.3 ± 1.5 , $n=5/\text{gp}$, $P=0.03$) (**Figure 5.7A**).

In contrast to the results for mitochondrial viability when high glucose concentrations were used *in vitro*, progenitors from STZ+ SkM CFU-M showed no significant difference in mitochondrial viability (**Figure 5.7B**), although they did display higher expression of MitoSoxTM consistent with increased accumulation of ROS (**Figure 5.7C**). This was corroborated by significant dampening of their mitochondrial membrane potential indicating dysfunction in energy transduction (**Figure 5.7D**) and an overall heightened state of oxidative injury.

We also found higher lactate concentrations in the supernatants of EndoMac progenitors from STZ+ SkM CFU-M compared to STZ- progenitors (**Figure 5.7E**). Lactate build-up is an indirect indicator of anaerobic glycolysis. Therefore, the decline in mitochondrial oxidative function (as seen by defective membrane potential) may have resulted in an alternative metabolic pathway to supply the energy demand. As further support for this, an increase in energy demand in STZ+ progenitors was also evident by higher uptake of 2-NDBG (**Figure 5.7F**). However, it should be noted that because glycolysis results in a net output of two ATP molecules compared to mitochondrial aerobic

metabolism (which yields ~38 ATP), the 1-fold increase in substrates may be to power the glycolytic pathway. Further investigation is required to confirm this.

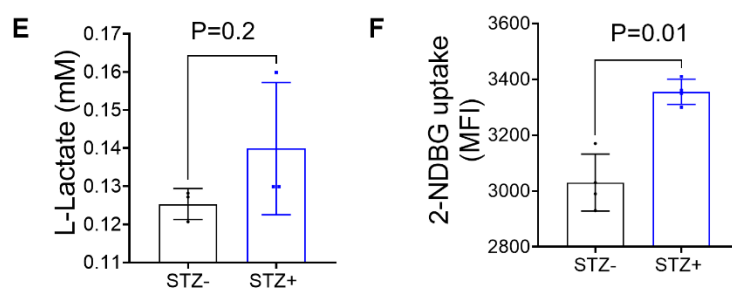
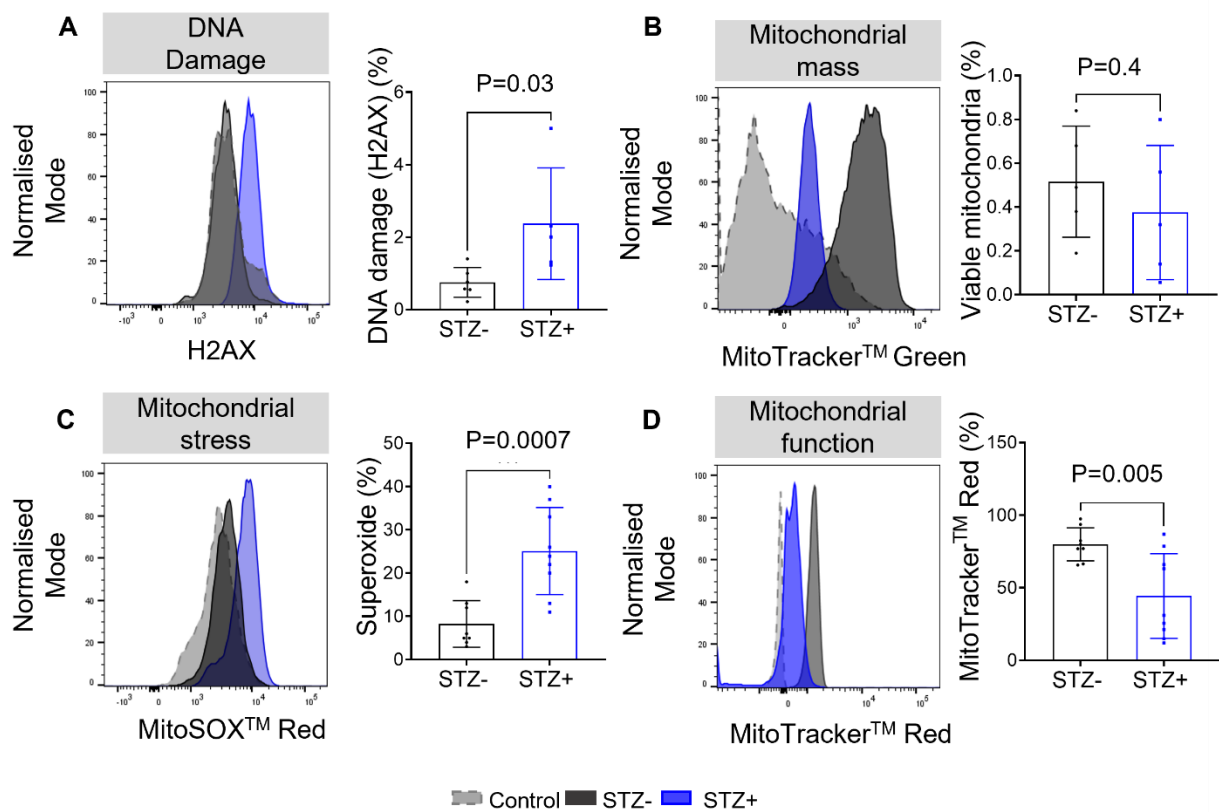


Figure 5.7: Diabetic SkM progenitors are more prone to DNA damage and possess mitochondrial abnormalities

- A)** Flow cytometry histograms depict expression of H2AX in progenitors isolated from SkM CFU-M from STZ+ and STZ- C57BL/6 mice. Light grey dotted lined histograms are FMO controls. Graph summarises the percentage frequency of H2AX expression from n=6/gp. Unpaired *t*-test.
- B)** Flow cytometry histograms depict expression of MitotrackerTM green in progenitors isolated from SkM CFU-M from STZ+ and STZ- C57BL/6 mice. Light grey dotted lined histograms are FMO controls. Representative of n=5 12 w C57BL/6 mice. Graph summarises the percentage frequency of MitotrackerTM green expression from n=9/gp. Unpaired *t*-test.
- C)** Flow cytometry histograms depict expression of MitoSOXTM red in progenitors isolated from SkM CFU-M from STZ+ and STZ- C57BL/6 mice. Light grey dotted lined histograms are FMO controls. Representative of n=8-9. 12 w C57BL/6 mice. Graph summarises the percentage frequency of MitoSOXTM red expression from n=9/gp. Unpaired *t*-test.
- D)** Flow cytometry histograms depict expression of MitotrackerTM red in progenitors isolated from SkM CFU-M from STZ+ and STZ- C57BL/6 mice. Light grey dotted lined histograms are FMO controls. Representative of n=8-9 12 w C57BL/6 mice. Graph summarises the percentage frequency of MitotrackerTM red expression from n=9/gp. Unpaired *t*-test.
- E)** L-lactate concentrations in the supernatants of 1° EndoMac progenitors. from STZ- and STZ+ C57BL/6 mice. n=3. Unpaired *t*-test.
- F)** Comparison of mean florescent intensity of glucose analogue (2-NDBG) of 1° CFU-M from STZ- and STZ+ C57BL/6 mice. n=4. Unpaired *t*-test.

5.3.7 Diabetic SkM EndoMac progenitors have diminished differentiation and angiogenic capacity

We next examined the effect of exposure to hyperglycaemia on the *in vitro* capacity of SkM progenitors to form angiogenic cords in MatrigelTM. Progenitors from STZ+ diabetic mice showed limited sprouting potential and formed less robust cords compared to the STZ- sham group (**Figure 5.8A**). Cumulative cord lengths were almost three-fold greater from STZ- SkM (**Figure 5.8B**), with significantly higher numbers of both cords (**Figure 5.8C**) and branch points (**Figure 5.8D**). We also examined the cellular composition of these branching cord networks in MatrigelTM by using flow cytometry as described previously (522). As expected, the networks produced by STZ- SkM progenitors contained a predominance of newly formed ECs, along with smaller numbers of MΦs and some retained progenitors (**Figure 5.8E**). Comparing the results of culturing STZ+ and STZ- SkM progenitors in MatrigelTM for 7 d, we found no significant differences in overall cell viability (**Figure 5.8F**) or the proportion of remaining cells that expressed the progenitor surface phenotype (**Figure 5.8G**). However, STZ+ cultures resulted in lower formation of new MΦs (**Figure 5.8H**) and especially new ECs, which were almost absent (**Figure 5.8I**). This was accounted for by a much higher proportion of “other” cells (STZ+ 60% vs STZ- 21%) that did not fall into the three specified populations of progenitors, MΦs, ECs. Pending further evaluation, we speculate that these cells may represent intermediate cell subpopulations that are yet to acquire “mature” surface markers for myeloid and endothelial fates. Overall, these results suggest that, as for aorta and skin (Chapters 3 and 4), SkM EndoMac progenitors display reduced and/or delayed bipotent differentiation capacity towards these lineages after exposure to hyperglycaemia *in vivo* (**Figure 5.8J**).

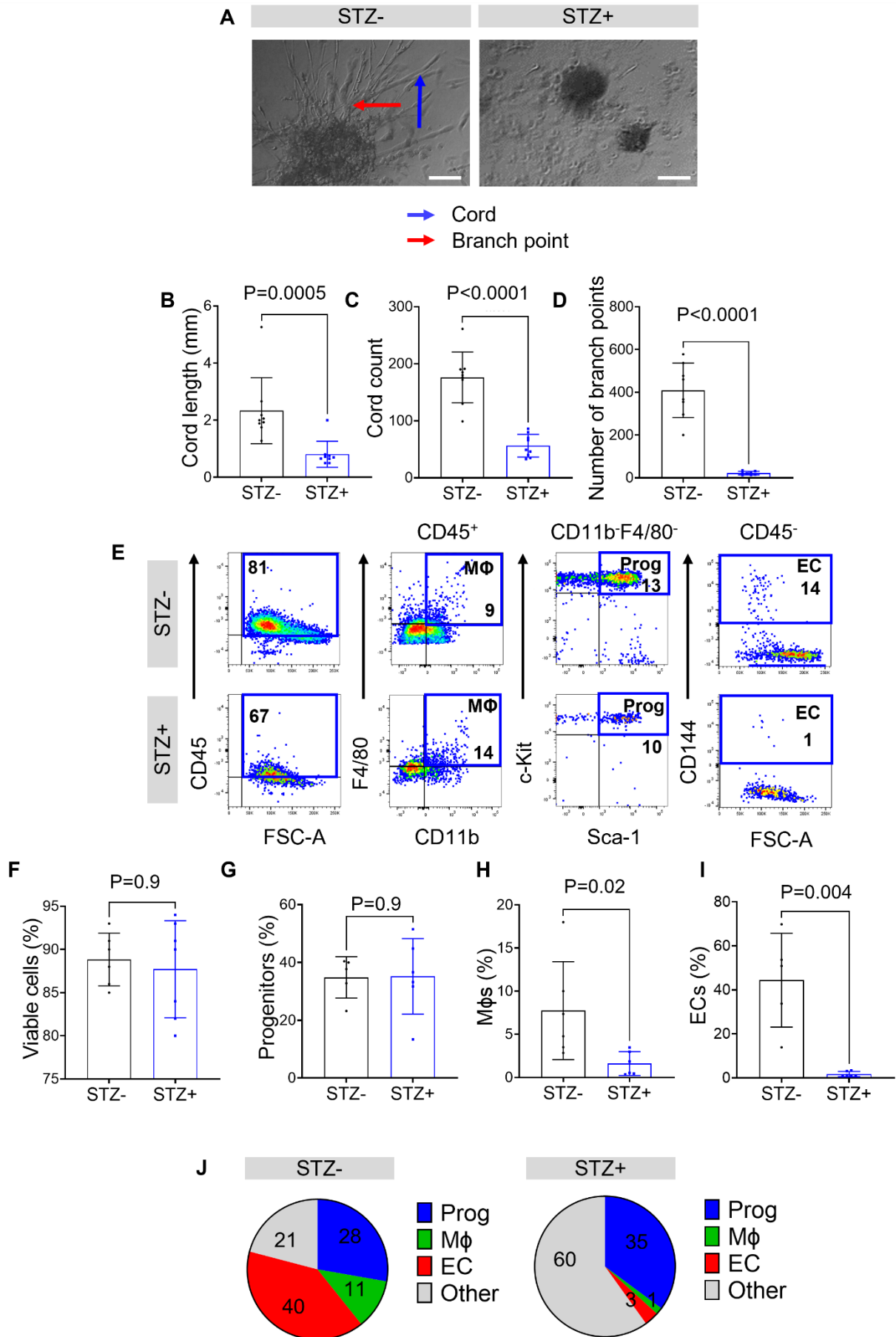


Figure 5.8: Diabetic SkM CFU-M progenitors have diminished differentiation and angiogenic capacity

A) Light microscopy images of Matrigel™ cord networks from SkM 1° CFU-M of STZ- and STZ+ C57BL/6 mice. Cord length shown by blue arrows. Branch points shown by red arrows. n=9 mice. Scale bar, 100 µm.

B) Graphs display comparisons of cord length, **C)** count and **D)** branch number. n=9/gp, Mann-Whitney for **B)** and Unpaired *t*-test for **C)** and **D)**.

E) Flow cytometry plots show fate of CFU-M derived progenitors in Matrigel from STZ- and STZ+ C57BL/6 mice. CD45⁺CD11b⁺F4/80⁻c-Kit⁺Sca-1⁺ progenitors, CD45⁺CD11b⁺F4/80⁺ macrophages (MΦs) and CD45⁺CD144⁺ endothelial cells (ECs). Percentages represent mean of n=8/gp.

F-I) Frequency of **F)** viable cells **G)** progenitors, **H)** MΦ and **I)** ECs in Matrigel™ assays from STZ- and STZ+ C57BL/6 mice. n=5-7/gp. Unpaired *t*-test for **F-H)** and Mann-Whitney test for **I)**

J) Pie charts depicts frequency of cell fate in Matrigel™ assays of STZ- and STZ+ C57BL/6 mice. n=8/gp, two-way ANOVA results: p=<0.0001 for cells; p=0.1 for group; p=<0.0001 for cells x group. Pie chart summarises results.

(Refer to Appendix 7.4)

5.3.8 Diabetic SkM has reduced capacity for ischaemic repair with delayed expansion of EndoMac progenitors

MΦs and ECs share an intimate relationship in two key processes crucial for ischaemic repair: inflammation and neovascularisation. Diabetes impairs the capacity of ischaemic tissue to coordinate the molecular and cellular mechanisms that contribute to the restoration of tissue perfusion in response to damage (496, 506, 619). As a result, the amount of ischaemic damage and unfavourable tissue remodelling are exacerbated in diabetes, leading to increased morbidity and death (516). Previously, we established adaptive roles of bipotent EndoMac progenitors in promoting reperfusion following ischaemia in healthy SkM (Williamson, Psaltis unpublished). Having now established that hyperglycaemia inhibits the properties of EndoMac progenitors in steady state muscle, we went on to examine of its effects on these cells in response to ischaemia. to confirm whether diabetic vascular repair is at least in part due to dysfunction in bipotent progenitors and its limited contribution to the population of tissue resident MΦs and ECs.

We recently confirmed that SkM EndoMac progenitors originate from a CSF1R⁺ YS source (Williamson, Psaltis unpublished). This study was performed following a recent report of a subset of resident MΦs in postnatal SkM that also originate from a similar YS source (75). We therefore used a 4-hydroxytamoxifen (TAM)-induced lineage-tracking system to examine on the kinetics of YS-derived EndoMac progenitors during different time points after hind limb ischaemia. TAM was administered *in utero* to *Csf1r*^{Mer-iCre-Mer} x *Rosa*^{mT/mG} mice at E8.5 (E=gestation stage) to induce expression of GFP labelling in YS CSF1R⁺ cells, including primitive MΦs, EMPs, and their progeny. 12 w offspring were induced with T1D using a single i.p STZ injection while controls received citrate buffer injections, as described above. Ischaemic surgeries were performed two weeks after injection, by permanent ligation of the left iliac artery and distal vessels to induce peripheral ischaemia and tissues were harvested at 1 d, 3 d, 7 d and 14 d (**Figure 5.9A**). T1D was confirmed via BGC checks

which were significantly higher in STZ+ mice across all four of these time points (**Figure 5.9B**). In keeping with type 1 diabetes characteristics, *Csf1r*^{Mer-iCre-Mer} x *Rosa*^{mT/mG} STZ+ mice also had lower body weights immediately prior to ischaemic surgeries (**Figure 5.9C-E**).

Following surgery, all mice underwent laser Doppler perfusion imaging until sacrifice, with STZ+ diabetic mice showing marked impairment of perfusion recovery in the ischaemic limb at day 14, but not at earlier time points (**Figure 5.9F**).

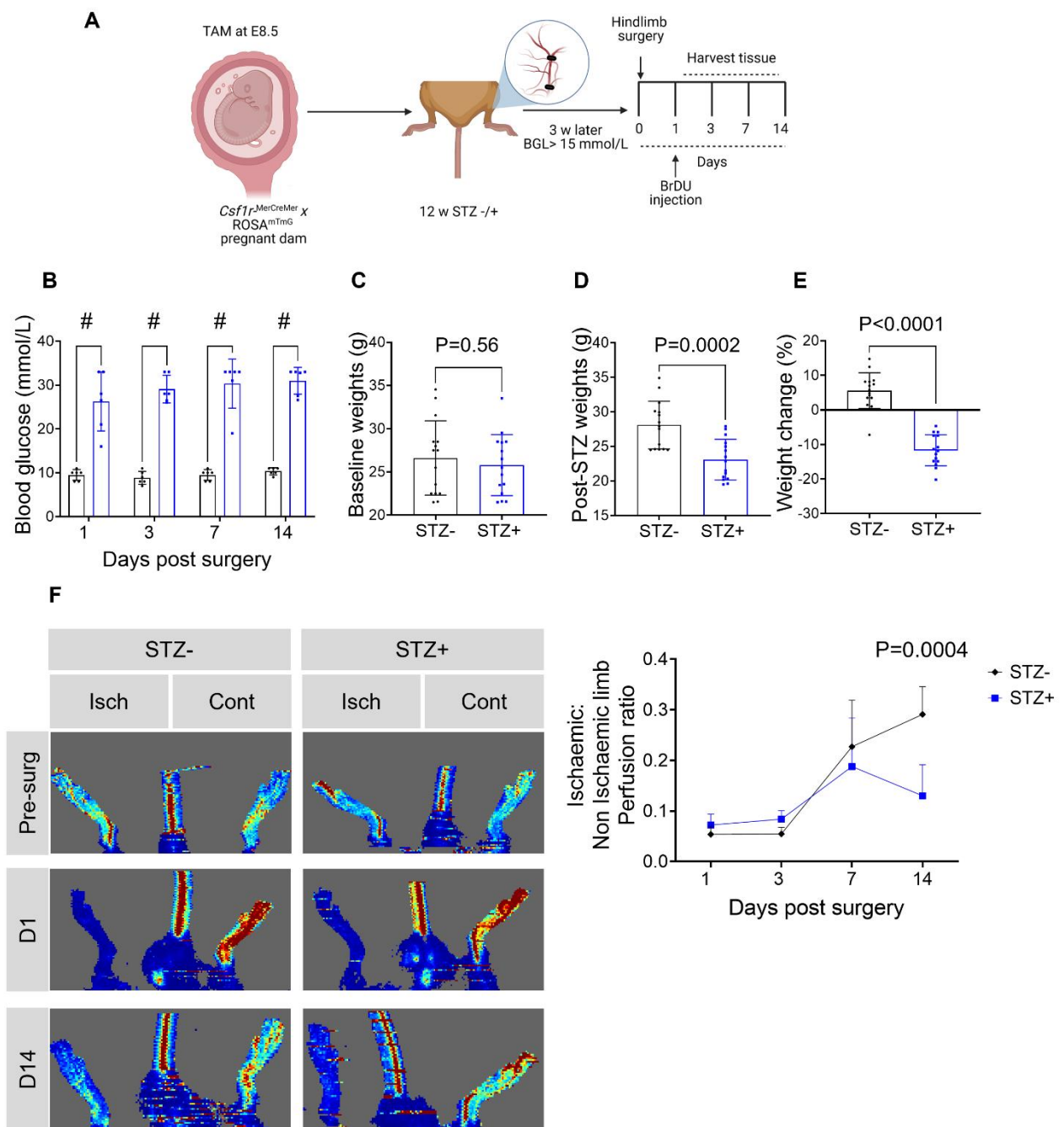


Figure 5.9: Diabetic mice display reduced perfusion recovery after hind limb ischaemia

- A)** Schematic shows the experimental design. Pregnant $Csf1r^{Mer-iCre-Mer}$ or $Rosa^{mT/mG}$ mice were induced with TAM at E8.5, with adult $Csf1r^{Mer-iCre-Mer} \times Rosa^{mT/mG}$ offspring subjected to hind limb ischaemia surgery after receiving STZ or citrate buffer i.p. injections.
- B)** Blood glucose concentrations on day of cull, across four time points post hind limb ischaemia surgery. n=5/gp, One-way ANOVA, multiple comparisons: # $P < 0.0001$
- C)** Baseline weights of $Csf1r^{Mer-iCre-Mer} \times Rosa^{mT/mG}$ mice pre-STZ injection. n=24/gp. unpaired t -test.
- D)** Body weight comparison of STZ- and STZ+ $Csf1r^{Mer-iCre-Mer} \times Rosa^{mT/mG}$ mice prior to ischaemic surgeries. n=24/gp. unpaired t -test.
- E)** Change in body weight from baseline to pre-surgery in STZ+ and STZ- groups. n=24/gp. unpaired t -test.
- F)** Representative laser Doppler perfusion images immediately before surgery and at days 0 and 14 after ischaemia in the two groups. Graph shows perfusion ratio results. n=6 mice/gp. Mixed effects two-way ANOVA: $p < 0.0001$ for time; $p = 0.02$ for group; $p = 0.01$ for time \times group. Multiple comparison test: † $p < 0.01$ for prog vs control

Flow cytometry analysis of STZ- and STZ+ SkM digests across the four time points after surgery demonstrated early increases in the overall number of progenitors from the ischaemic compared to non-ischaemic limb (**Figure 5.10A-B**). This peaked at day 1 for the STZ- group and then diminished but still remained higher in the ischaemic limb up until day 7 (fold comparisons versus non-ischaemic limb: 5.9x at 1 d, 6.3x at 3 d, 4.1x at 7 d, 0.9x at 14 d). By comparison, progenitors peaked in the ischaemic limb of STZ+ mice at day 3 and remained higher than in the non-ischaemic limb up until day 14 (fold comparisons versus non-ischaemic limb: 4x at 1 d, 14.7x at 3 d, 7x at 7 d, 2x at 14 d) (**Figure 5.10C-D**). Comparison between STZ- and STZ+ ischaemic limbs showed 3-fold more progenitors in the STZ- group at day 1, without significant differences at the later time points (**Figure 5.10E**). These data indicate that while progenitors expand after ischaemia in diabetic SkM, this response is somewhat delayed compared to the non-diabetic state.

The overall number of MΦs in SkM began increasing from around day 3 after ischaemia in the STZ- group and peaked at day 7 (fold comparison versus 1 d: 6.3x) but was still much higher than for the non-ischaemic limb at day 14 (**Figure 5.10F**). The diabetic STZ+ group showed a similar trend for MΦ expansion post-ischaemia, although MΦ numbers fell more sharply between days 7 and 14, almost reaching non-ischaemic levels (**Figure 5.10G**). This meant that the only significant difference between the overall MΦ count in SkM between STZ- and STZ+ mice was seen at day 14, with a 4.4-fold higher number in the STZ- group (**Figure 5.10H**). time point.

In contrast to progenitors and MΦs, we observed a depletion in the total pool of EC in SkM beginning at day 1 after ischaemia in the STZ- group, with progressive recovery of their numbers over 14 d back toward those measured in the non-ischaemic limb (**Figure 5.10I**). A similar kinetic profile was seen for ECs in the STZ+ group, although without such striking depletion at day 1 after ischaemia (**Figure**

5.10J). Comparing the ischaemic limbs between the STZ- and STZ+ groups, there were no significant differences in the number of ECs at either day 1 or 3, but the subsequent expansion of ECs was greater in the non-diabetic setting, leading to higher numbers in STZ- SkM at both days 7 (2-fold vs STZ+) and 14 (1.6-fold vs STZ+) (**Figure 5.10K**). Furthermore, by comparison to day 1, day 14 results showed a 3-fold increase in total EC numbers in STZ- SkM compared to a more modest 1.4-fold increase in the STZ+ group. These patterns indicate that endothelial recovery following ischaemia begins around day 7 for both non-diabetic and diabetic SkM, albeit to a lower extent in the latter.

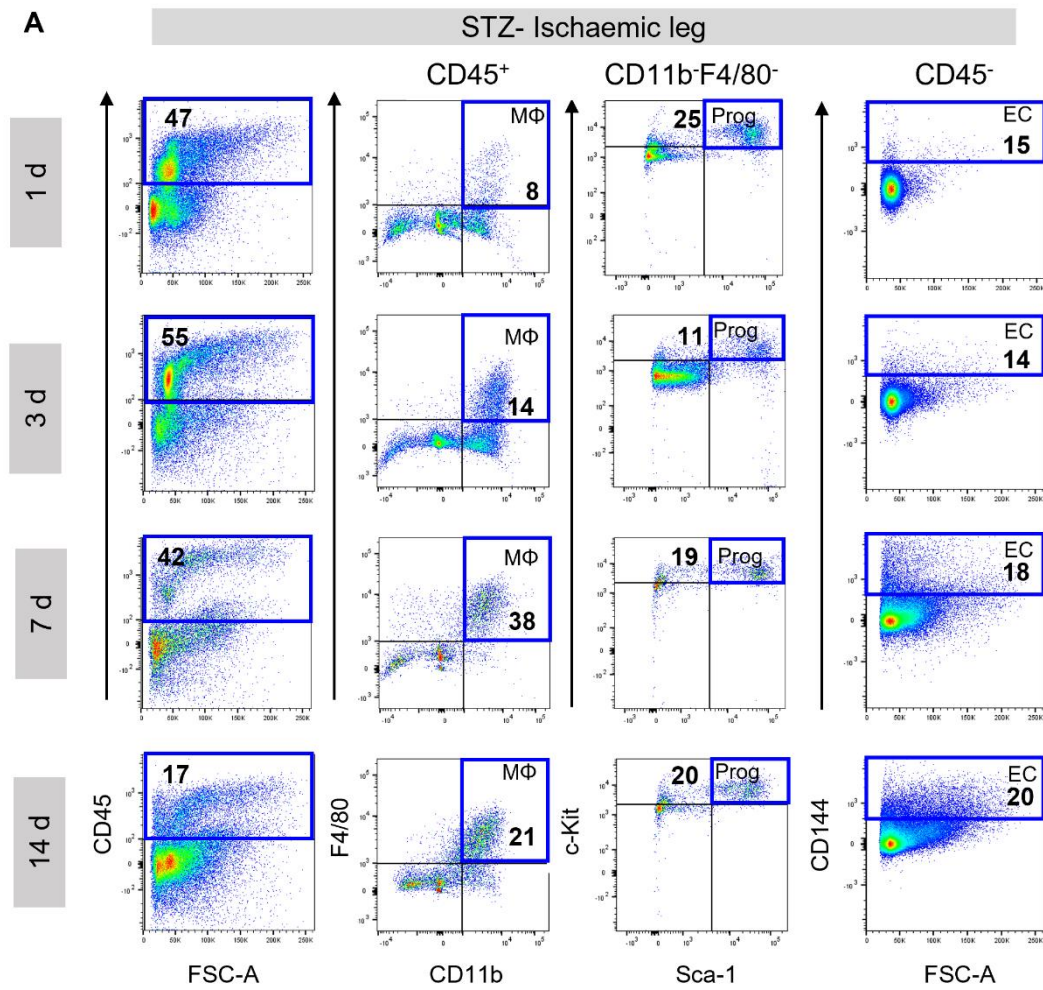


Figure continued P.T.O

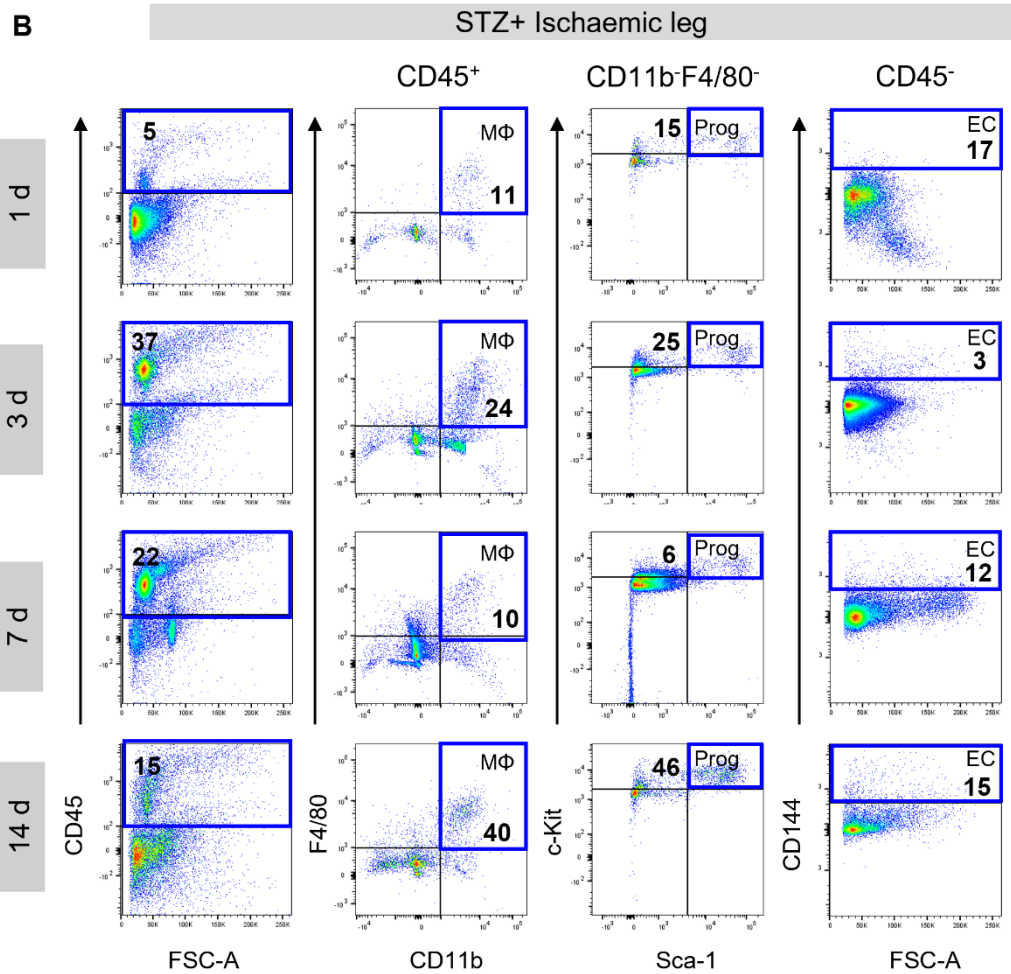


Figure continued P.T.O

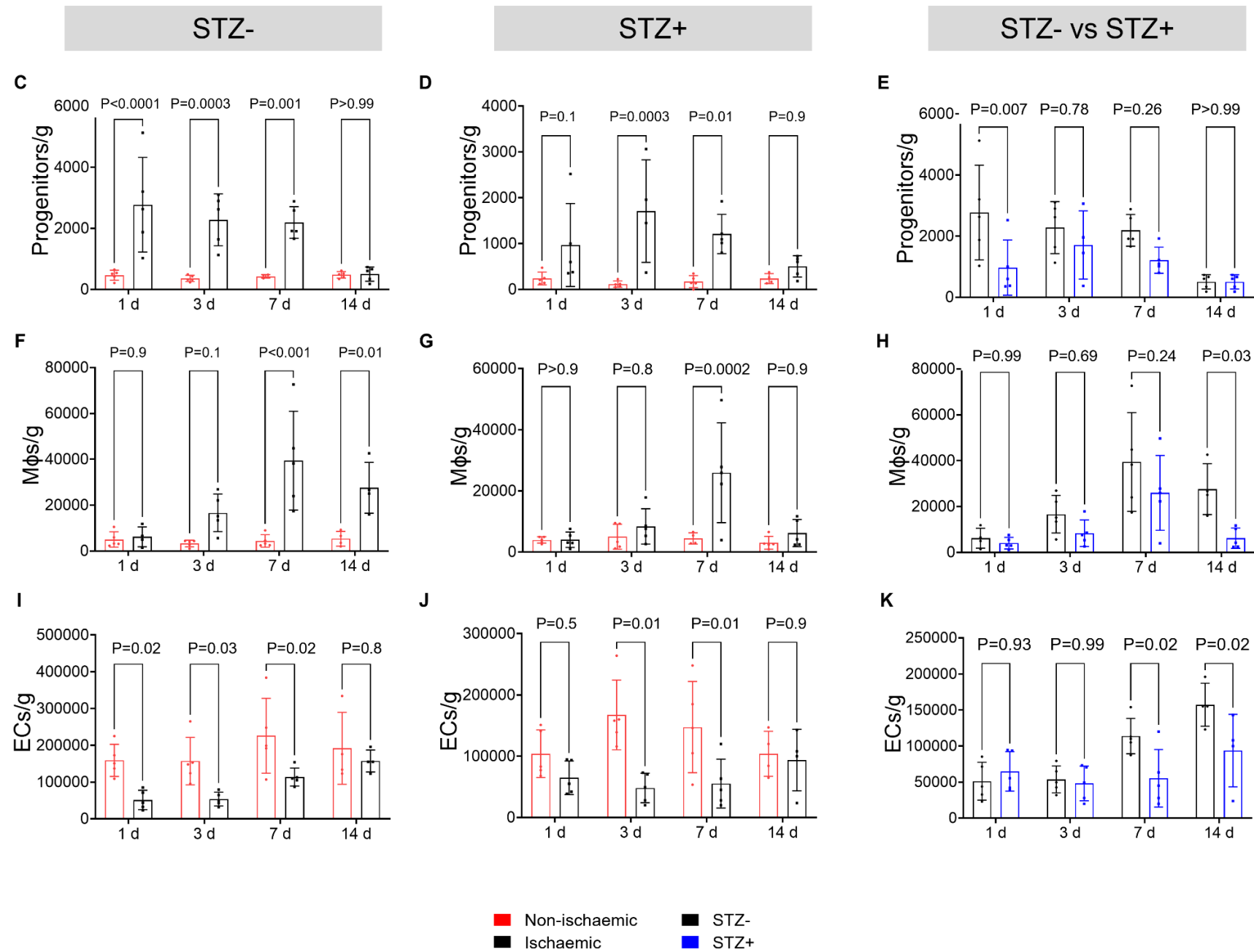


Figure 5.10: Kinetics of progenitors, MΦs and ECs in non-diabetic and diabetic ischaemic SkM.

A-B) Flow cytometry showing gating of SkM CD45⁺ CD11b⁺ F4/80⁺ macrophages (MΦs), CD45⁺CD11b⁻ F4/80⁻c-Kit⁺Sca-1⁺ progenitors and CD45⁻CD144⁺ endothelial cells (ECs) from **A)** STZ- and **B)** STZ+ *Csf1r*^{Mer-iCre-Mer} x *Rosa*^{mT/mG} ischaemic legs across four time points (1 d, 3 d, 7 d, 14 d). Representative of n=5/gp.

C-D) Graphs showing progenitors/g in non-ischaemic and ischaemic limbs of **C)** STZ- and **D)** STZ+ *Csf1r*^{Mer-iCre-Mer} x *Rosa*^{mT/mG} mice across four time points (1 d, 3 d, 7 d, 14 d). n=5/gp, two -way ANOVA results: **C)** p=0.005 for time; p<0.0001 for group; p=0.003 for time x group; **D)** p=0.2 for time; p<0.0001 for group; p=0.07 for time x group. (Red bars: control leg. Black bars: ischaemic leg)

E) Graphs showing progenitors/g in STZ- and STZ+ *Csf1r*^{Mer-iCre-Mer} x *Rosa*^{mT/mG} ischaemic legs across four time points (1 d, 3 d, 7 d, 14 d). n=5/gp, two -way ANOVA results: p=0.004 for time; p<0.0001 for group; p=0.3 for time x group. (Black bars: STZ-. Blue bars: STZ+).

F-G) Graphs showing MΦs/g in non-ischaemic and ischaemic limbs of **F)** STZ- and **G)** STZ+ *Csf1r*^{Mer-iCre-Mer} x *Rosa*^{mT/mG} mice across four time points (1 d, 3 d, 7 d, 14 d). n=5/gp, two -way ANOVA results: **F)** p=0.005 for time; p<0.0001 for group; p=0.005 for time x group; **G)** p=0.4 for time; p=0.002 for group; p=0.07 for time x group. (Red bars: non-ischaemic leg. Black bars: ischaemic leg).

H) Graphs showing MΦs/g in STZ- and STZ+ *Csf1r*^{Mer-iCre-Mer} x *Rosa*^{mT/mG} ischaemic legs across four time points (1 d, 3 d, 7 d, 14 d). n=5/gp, two -way ANOVA results: p<0.0001 for time; p=0.004 for group; p=0.3 for time x group. (Black bars: STZ-. Blue bars: STZ+).

I-J) Graphs showing endothelial cells (ECs)/g in non-ischaemic and ischaemic limbs of **I)** STZ- and **J)** STZ+ *Csf1r*^{MerCreMer} x *Rosa*^{mT/mG} mice across four time points (1 d, 3 d, 7 d, 14 d). n=5/gp, two -

way ANOVA results: **I**) $p=0.001$ for time; $p<0.0001$ for group; $p=0.4$ for time x group; **J**) $p=0.7$ for time; $p=0.002$ for group; $p=0.07$ for time x group. (Red bars: non-ischaemic leg. Black bars: ischaemic leg)

K) Graphs showing endothelial cells (ECs)/g in STZ- and STZ+ *Csf1r*^{MerCreMer} x *Rosa*^{mT/mG} surgical legs across four time points (1 d, 3 d, 7 d, 14 d). $n=5$ /gp, two -way ANOVA results: $p=0.001$ for time; $p<0.0001$ for group; $p=0.08$ for time x group. (Black bars: STZ-. Blue bars: STZ+).

(Refer to Appendix 7.5)

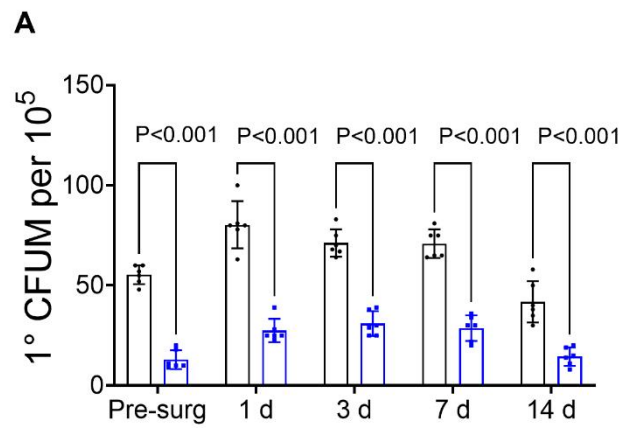
5.3.9 SkM progenitors arise from YS EMPS and show reduced expansion early post-ischaemia in diabetes.

In keeping with the expansion of progenitors early after ischaemia, we also observed higher CFU-M recovery from ischaemic limbs compared to pre-ischaemia in both the STZ- and STZ+ groups, although at each time point the CFU-M yield was higher from STZ- SkM (fold comparisons STZ- versus STZ+: 4.2x before ischaemia, 2.8x at 1 d post-ischaemia, 2.3x at 3 d, 2.5x at 7 d, 2.9x at 14 d) (**Figure 5.11A**). We next examined the degree to which progenitors, MΦs and ECs are derived from embryonic YS EMPs in non-diabetic and diabetic ischaemic SkM. *Csf1r*^{Mer-iCre-Mer} x *Rosa*^{mT/mG} mice which had not received TAM *in utero* were used as GFP negative fluorescence controls (**Figure 5.11B**). GFP⁺ cells were gated for progenitors, MΦs and ECs from flow cytometry plots, as described above (**Figure 5.11B**). Comparing ischaemic and non-ischaemic limbs at each time point, we only found a significant difference in the overall number of YS-derived GFP⁺ cells at day 7 post-surgery in the STZ- group ((**Figure 5.11C-D**). Meanwhile, comparison of ischaemic SkM between the STZ- and STZ+ groups, showed significantly higher numbers of YS-derived cells in the non-diabetic mice at days 1 and 7 (**Figure 5.11E**).

GFP⁺ progenitors showed marked expansion in ischaemic SkM of STZ- mice at day 1, with their numbers diminishing thereafter (**Figure 5.11F**). The kinetics of GFP⁺ progenitors were also similar after ischaemia, although the expansion at day 1 was more modest (9.3-fold compared to non-ischaemic limb) time point (**Figure 5.11G**). This meant that there were significantly more GFP⁺ progenitors in day 1 ischaemic limbs from STZ- mice than their STZ- counterparts, but not at the later time points (**Figure 5.11H**).

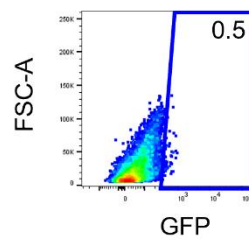
YS-derived GFP⁺ MΦs showed a similar pattern of expansion in ischaemic muscle for STZ- and STZ+ mice, beginning at day 3 and peaking at day 7, before returning back toward non-ischaemic levels by day 14 ((**Figure 5.11I-J**). Once again this was more striking in the STZ- group, meaning that these mice had two-fold higher counts of GFP⁺ MΦs in ischaemic SkM at day 7 compared to the STZ+ group (**Figure 5.11K**). Meanwhile, GFP⁺ ECs showed a more gradual expansion after ischaemia than GFP⁺ MΦs, with their numbers peaking at day 14 in both STZ- and STZ+ mice, although diabetic ischaemic SkM still had fewer of these cells at days 7 and 14 (fold comparisons for STZ- vs STZ+ ischaemic limb: 4-fold at 7 d, 2-fold at 14 d) (**Figure 5.11L-N**). time point

Collectively, these results confirm that YS EMPs contribute to the pool of progenitors, MΦs and ECs in adult SkM. Each of these embryonically derived populations expands after ischaemia, albeit with distinct kinetic profiles, such that EndoMac progenitors expand first, followed by MΦs and finally ECs. Within the timeframe studied here, progenitors and MΦs both peak before returning toward non-ischaemic levels by day 14. Although hyperglycaemia does dampen the extent to which each population expands in ischaemic SkM, it does not seem to alter the pattern of these responses.



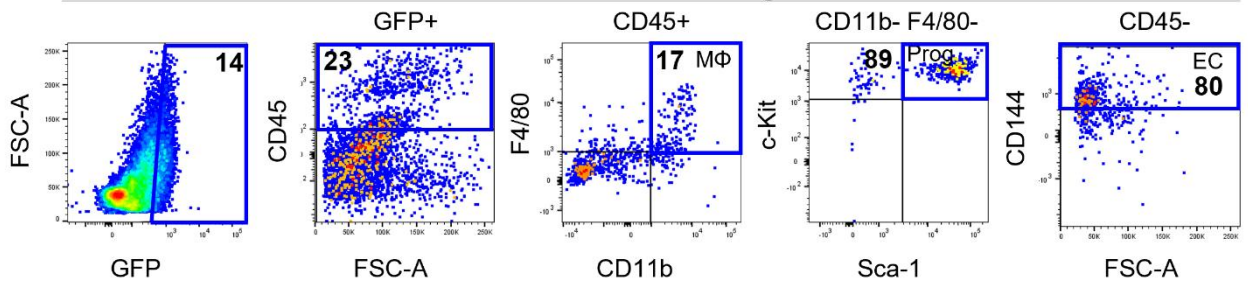
B

Non-TAM control



STZ- ischaemic leg

1 d



STZ+ ischaemic leg

1 d

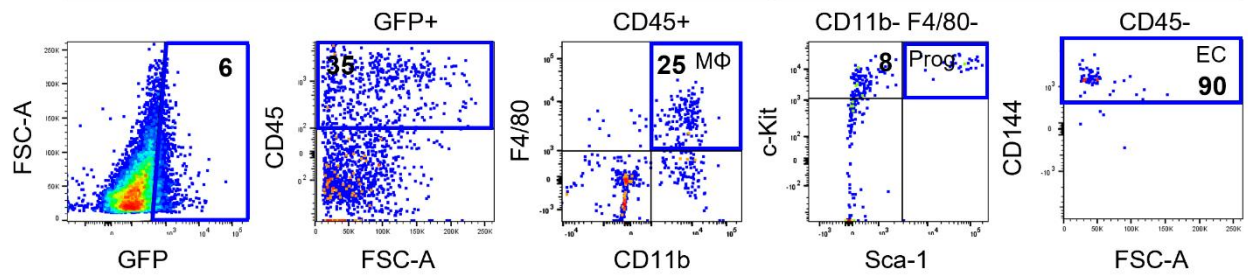


Figure continued P.T.O

STZ-

STZ+

STZ- vs STZ+

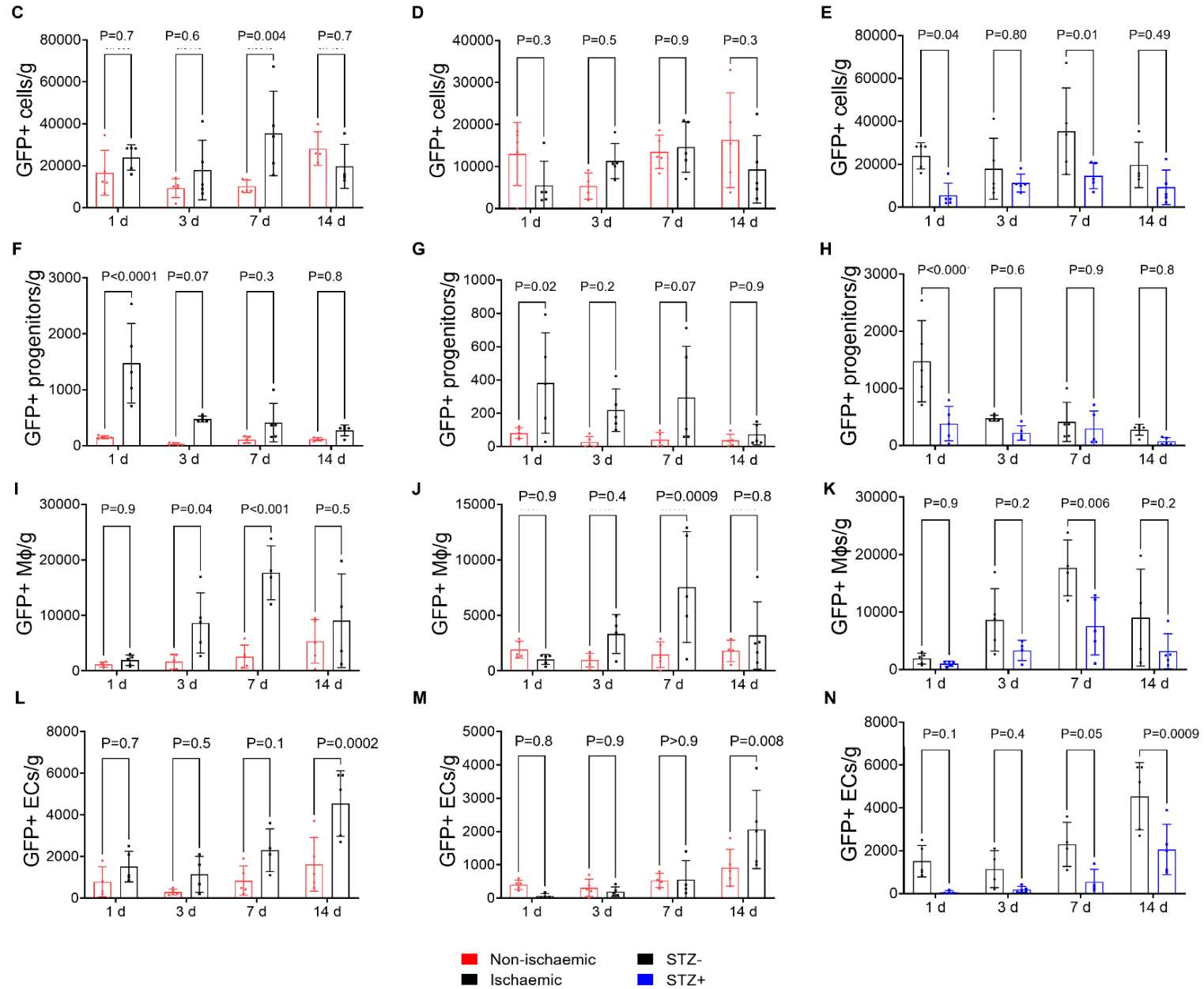


Figure 5.11: SkM progenitors arise from embryonic YS and show delayed expansion post-ischaemia in diabetes.

A) Graph shows 1° SkM CFU-M yield of STZ- (black) and STZ+ (blue) *Csf1r*^{Mer-iCre-Mer} x *Rosa*^{mT/mG} surgical legs across four time points (pre-surg, 1 d, 3 d, 7 d, 14 d). n=5 mice/gp. Two-way ANOVA results: p=<0.0001 for time; p=0.0001 for group; p=0.0025 for time x group.

B) Representative flow cytometry gating for GFP expression in a no TAM Cre control (top) and flow cytometry profiling of YS-derived GFP⁺ cells in SkM of STZ- (middle) and STZ+ (bottom) surgical legs at 1 d time point of TAM-induced *Csf1r*^{Mer-iCre-Mer} x *Rosa*^{mT/mG} mice. Representative of n=5/gp.

C-E) Graphical quantifications of all GFP⁺ cells in **C)** STZ- , **D)** STZ+ ischaemic and nonischaemic limbs and **E)** the comparison between STZ- and STZ+ ischaemic limbs. . n=5 mice/gp. Two-way ANOVA results: **C)** p=0.19 for time; p=0.03 for group; p=0.02 for time x group; **D)** p=0.2 for time; p=0.4 for group; p=0.1 for time x group; **E)** p=0.4 for time; p=0.1 for group; p=0.006 for time x group.

F-H) Graphical quantifications of all GFP⁺ progenitors in **F)** STZ-, **G)** STZ+ ischaemic and nonischaemic limbs and **H)** the comparison between STZ- and STZ+ ischaemic limbs. . n=5 mice/gp. Two-way ANOVA results: **F)** p=<0.0001 for time; p=<0.0001 for group; p=0.0004 for time x group; **G)** p=0.1 for time; p=0.0006 for group; p=0.3 for time x group; **H)** p=<0.0001 for time; p=0.0003 for group; p=0.006 for time x group.

I-K) Graphical quantifications of all GFP⁺ macrophages (MΦs) in **I)** STZ-, **J)** STZ+ ischaemic and nonischaemic limbs and **K)** the comparison between STZ- and STZ+ ischaemic limbs. . n=5 mice/gp. Two-way ANOVA results: **I)** p=0.0013 for time; p=<0.0001 for group; p=0.006 for time x group; **J)** p=0.0015 for time; p=0.09 for group; p=0.18 for time x group; **K)** p=<0.0001 for time; p=0.0003 for group; p=0.006 for time x group.

L-N) Graphical quantifications of all GFP⁺ endothelial cells (ECs) in **L)** STZ-, **M)** STZ+ ischaemic and nonischaemic limbs and **N)** the comparison between STZ- and STZ+ ischaemic limbs. n=5 mice/gp. Two-way ANOVA results: **L)** p=0.09 for time; p=0.0003 for group; p=0.42 for time x group; **M)** p=0.0015 for time; p=0.09 for group; p=0.18 for time x group; **N)** p=<0.0001 for time; p=0.0003 for group; p=0.006 for time x group.

(Refer to Appendix 7.5)

In order to determine the percentage contribution of YS EMPs to each cell population, we normalised their % GFP expression to that of brain microglia (gated as CD45⁺ CD11b⁺ F4/80⁺) from each mouse studied. Approximately 20-30% of microglia were labelled GFP⁺ with no significant differences between the STZ- and STZ+ groups at any of the time points time (Figure 5.12A). In both STZ- and STZ+ non-ischaemic limbs, ~50% progenitors were YS-derived compared to ~20% of MΦs and 10% of ECs (data not shown). In ischaemic limbs, the proportion of progenitors that were from YS EMPs ranged between 50-80% time point without significant differences between time points post-ischaemia or between STZ- and STZ+ groups (Figure 5.12B). Meanwhile, the proportion of YS-derived MΦs was highest at day 1 post-ischaemia, reaching ~55% in STZ- and ~40% in STZ+ mice, before diminishing to ~30% and ~25%, respectively at the later time points time point ANOVA (Figure 5.12C). Finally, the contribution of CSF1R⁺ YS EMPs to ECs showed a progressive and striking increase from ≤20% at day 1 post-ischaemia to ~80% at day 14 in the STZ- group and ~50% (Figure 5.12D). This reveals a major role for the local expansion of embryonically derived ECs in the post-ischaemia setting, especially in the non-diabetic state.

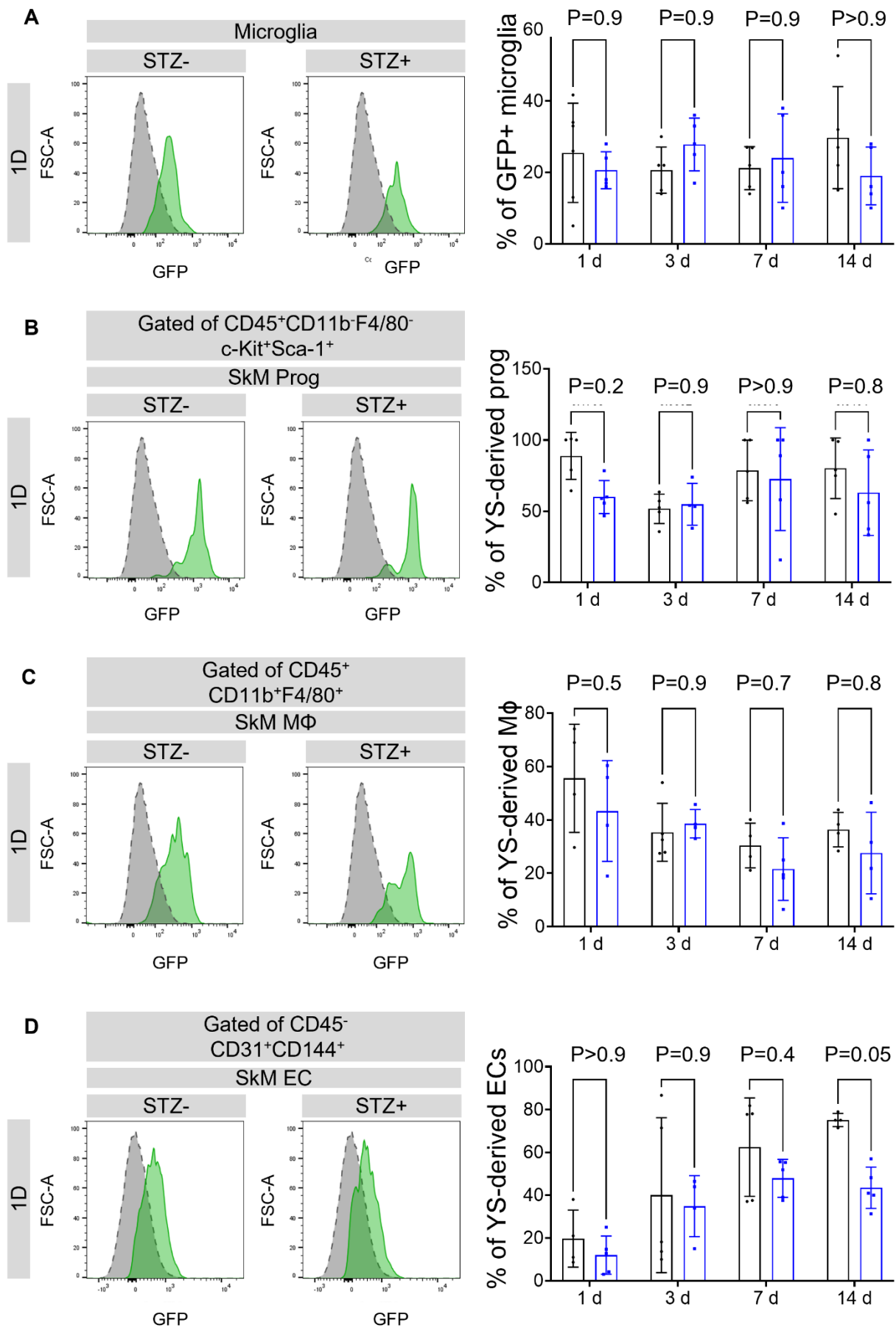


Figure 5.12: YS EMPs make a major contribution to EC recovery and expansion after ischaemia.

- A)** Flow cytometry histograms depict GFP expression in brain microglia from STZ- and STZ+ 12 w *Csf1r*^{Mer-iCre-Mer} x *Rosa*^{mT/mG} mice administered TAM at E8.5 *in utero*. Grey histograms are GFP expression from TAM negative controls. Graph shows frequency of GFP⁺ microglia at different time points post-ischaemia. n=5. Two-way ANOVA results: p=0.9 for time; p=0.9 for group; p=0.2 for time x group. Multiple comparisons between time points.
- B)** Flow cytometry histograms depict GFP⁺ progenitor cells in STZ- and STZ+ ischaemic legs. Grey histograms are FMO controls. Representative of n=5, 12 w *Csf1r*^{Mer-iCre-Mer} x *Rosa*^{mT/mG} mice. Graph shows frequency of YS-derived GFP⁺ progenitors. n=5, Two-way ANOVA results: p=0.1 for time; p=0.09 for group; p=0.4 for time x group. Multiple comparisons between time points.
- C)** Flow cytometry histograms depict GFP⁺ macrophages (MΦs) in STZ- and STZ+ ischaemic legs. Grey histograms are FMO controls. Representative of n=5, 12 w *Csf1r*^{Mer-iCre-Mer} x *Rosa*^{mT/mG} mice. Graph shows frequency of YS-derived GFP⁺ MΦs. n=5, Two-way ANOVA results: p=0.008 for time; p=0.01 for group; p=0.6 for time x group. Multiple comparisons between time points.
- D)** Flow cytometry histograms depict GFP⁺ endothelial cells (ECs) in STZ- and STZ+ ischaemic legs. Grey histograms are FMO controls. Representative of n=5, 12 w *Csf1r*^{Mer-iCre-Mer} x *Rosa*^{mT/mG} mice. Graph shows frequency of YS-derived GFP⁺ ECs. n=5, Two-way ANOVA results: p<0.0001 for time; p=0.01 for group; p=0.4 for time x group. Multiple comparisons between time points.

Finally, we also studied the proliferative status of the different YS-derived populations in SkM after hind limb ischaemia by administering BrdU 1 h prior to sacrifice for 1 d time point post-ischaemia and analysing cell cycle activity by flow cytometry (**Figure 5.13A**).

Overall, non-diabetic YS-derived cells showed a trend towards a higher proportion of proliferative activity in ischaemic legs (**Figure 5.13B**). In keeping with their early expansion after ischaemic surgery in STZ- mice, we also detected a trend for a higher proportion of proliferation of YS-derived progenitors in comparison with STZ+ ischaemic limbs (**Figure 5.13C**). Meanwhile, we found no significant difference in proliferative activity of YS-derived MΦs and ECs at this early time point (**Figure 5.13D-E**). Taken together, diabetes likely attenuates the early proliferative response of YS-derived EndoMac progenitors to ischaemia. This in turn may explain their reduced expansion, along with the dampened accumulation of YS-derived MΦs and ECs that are seen in ischaemic muscle at later time points.

Interestingly, diabetes launched a trend towards a higher proportion of apoptotic activity of YS-derived cells (**Figure 5.13F**). Non-diabetic YS-derived progenitors and MΦs showed no apoptotic activity while YS-derived ECs showed no differences in apoptosis compared to diabetics (**Figure 5.13G-I**).

A

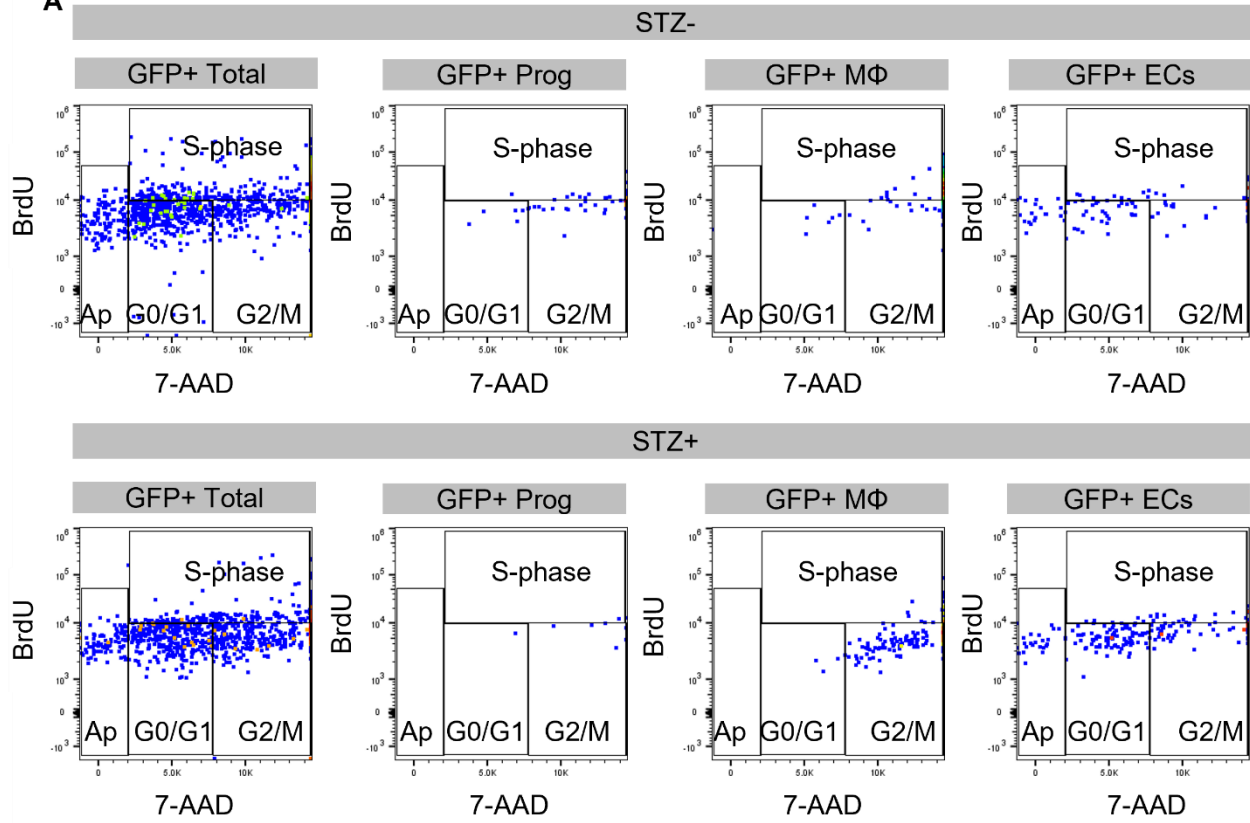


Figure continued P.T.O

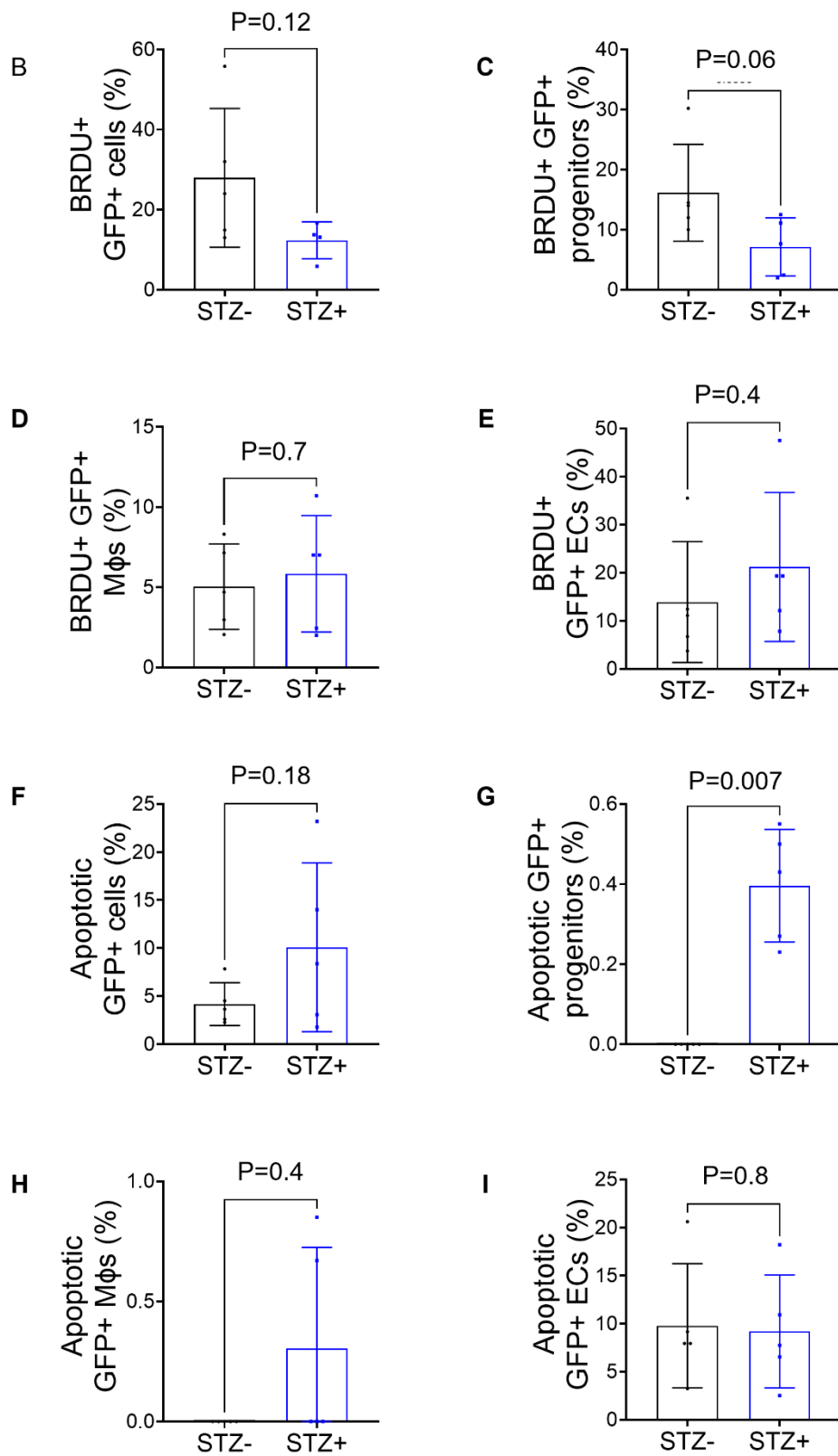


Figure 5.13: Proliferative status of YS-derived populations.

A) Flow cytometry gating for BrdU expression of YS-derived GFP⁺ cells in SkM of STZ- (top) and STZ+ (bottom) ischaemic legs at 1 d time point of TAM-induced *Csf1r*^{Mer-iCre-Mer} x *Rosa*^{mT/mG} mice, Representative of n=5/gp.

B-E) Graph shows percentage of BRDU expression in GFP+ **B)** total cells, **C)** progenitors, **D)** MΦs, and **E)** ECs. Ischaemic legs at 1 d time point of TAM-induced *Csf1r*^{Mer-iCre-Mer} x *Rosa*^{mT/mG} mice, n=5/gp. Unpaired *t*-test for **B)**, **D)** and **E)**. Mann-Whitney test for **C)**

F-I) Graph shows percentage of apoptotic GFP+ **F)** total cells, **G)** progenitors, **H)** MΦ, and **I)** EC. Ischaemic legs at 1 d time point of TAM-induced *Csf1r*^{Mer-iCre-Mer} x *Rosa*^{mT/mG} mice, n=5/gp, unpaired *t*-test for **F)** and **I)**. Mann-Whitney test for **G)** and **H)**

5.3.10 Transfer of non-diabetic but not diabetic progenitors promotes perfusion recovery after ischaemia in diabetic SkM.

Based on our existing knowledge of tissue-resident EndoMac progenitors from non-diabetic (520, 522), we speculated that transfer of non-diabetic SkM progenitors could promote perfusion recovery after hind limb ischaemia in diabetic recipients owing to their ability to engraft, differentiate and produce neovessels. To test this hypothesis, we used adult C57BL/6 mice that were induced with T1D by STZ and then subjected them to hind limb ischaemia surgery two weeks later. Immediately after surgery, these mice received injections of equal volumes of either cell-free MatrigelTM (vehicle control) or SkM EndoMac progenitors from non-diabetic (STZ-) or diabetic (STZ+) UBI-GFP donor mice into the ischaemic quadriceps and gastrocnemius muscle (1.5×10^4 cells per recipient) (**Figure 5.14A**). All STZ+ recipient mice had similar BGCs across the three donor groups (Control: 27.6 ± 6.5 , STZ-: 26.8 ± 5.8 vs STZ+: 27.3 ± 5.9 mmol/L, $n=6/\text{gp}$, $P=0.9$) (**Figure 5.14B**), while STZ+ donors had three-fold higher BGCs than STZ- donors (**Figure 5.14C**). Recipient mice showed significant weight loss after STZ injection (baseline: 25.7 ± 3.4 vs post STZ: 23.4 ± 3.1 g, $n=6$, $P<0.0001$) (**Figure 5.14D-E**). Similarly, STZ+ donors weighed less than their STZ- counterparts (**Figure 5.14F-H**). Laser Doppler imaging demonstrated that perfusion recovery more than doubled (2.6-fold) by day 14 in the ischaemic limb of mice that received STZ- SkM progenitors compared to the groups receiving STZ+ progenitors or vehicle control (**Figure 5.14I**). Most of this augmented perfusion occurred between days 7 and 14 after injection of STZ- progenitors.

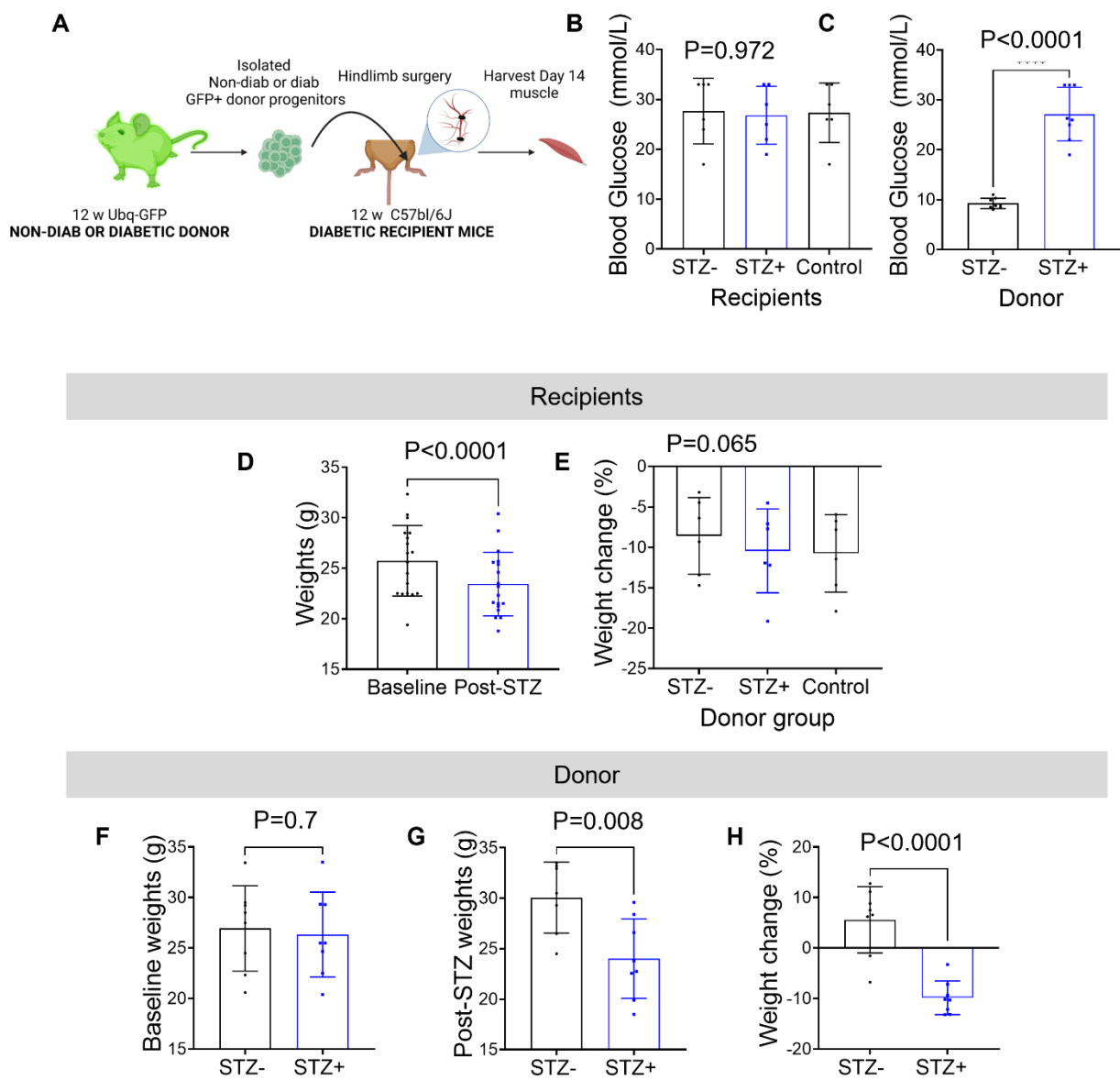


Figure continued P.T. O

I

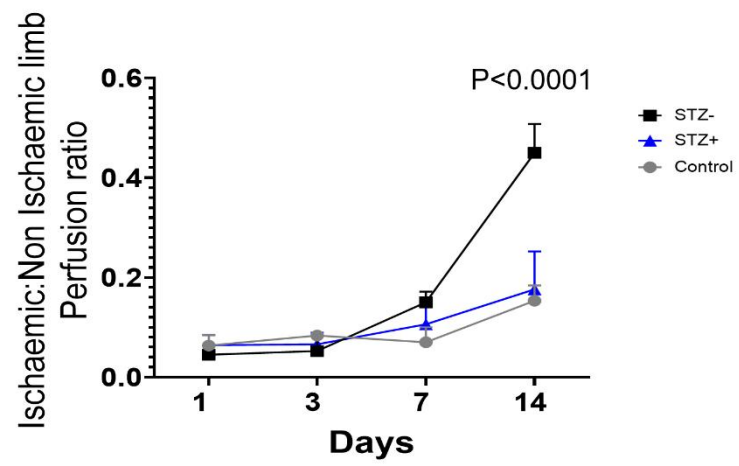
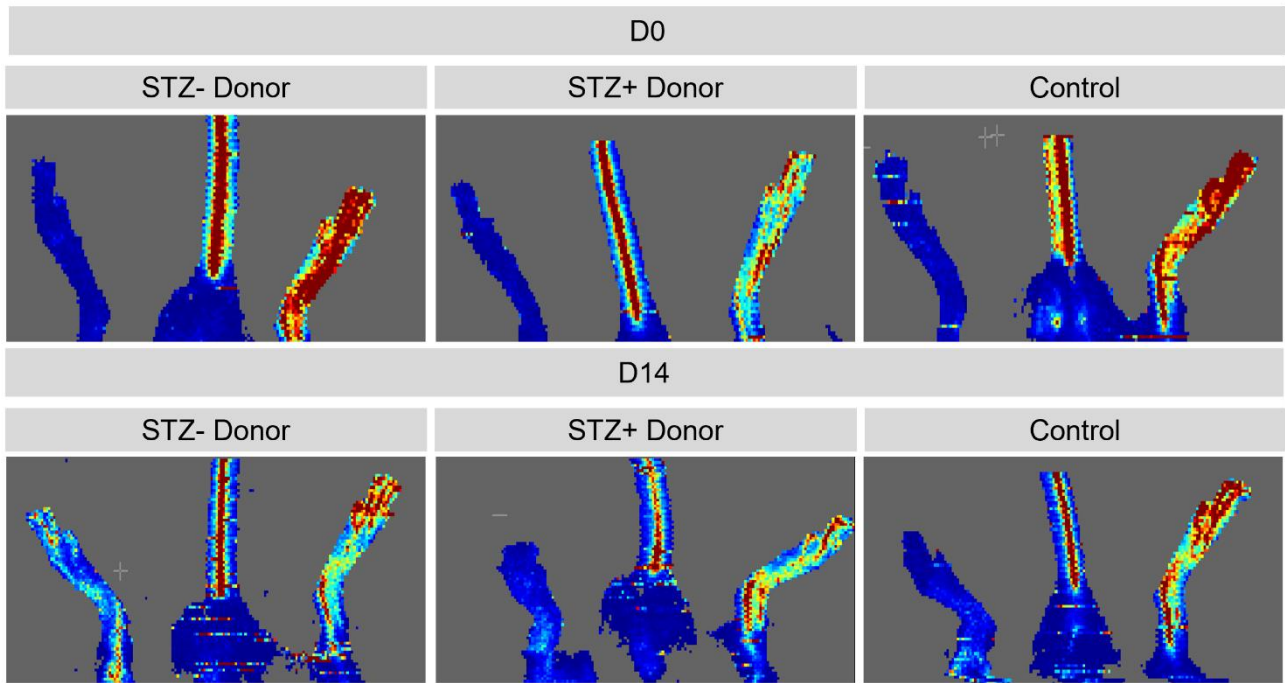


Figure 5.14: Non-diabetic EndoMac progenitors rescue perfusion recovery in diabetic ischaemic muscle.

- A)** Schematic of experimental design. Recipient groups were STZ+ diabetic C57BL/6 mice that underwent hind limb ischaemia surgery immediately before receiving intramuscular injections of MatrigelTM vehicle control or GFP⁺ non-diabetic (STZ-) or diabetic (STZ+) SkM progenitors.
- B)** Blood glucose concentrations of recipient C57BL/6 mice: STZ-, STZ+ and control groups. n=6, One-way ANOVA.
- C)** Blood glucose concentrations of donor UBI-GFP mice. n=8, Unpaired *t*-test.
- D)** Weight comparison of baseline (8 w) and post-STZ injection of recipient 12 w C57BL/6 mice. n=18/gp. Paired *t*-test.
- E)** Frequency of weight change between three recipient groups of 12 w STZ+ C57BL/6 mice. n=6/gp, One-way ANOVA.
- F-H)** **F)** Baseline weights of 8 w donor UBI-GFP mice pre-STZ injection. **G)** Body weight comparison of 12 w STZ- and STZ+ donor UBI-GFP mice. **H)** Frequency of weight change. n=8/gp. Unpaired *t*-test.
- I)** Laser doppler perfusion images on day 0 and day 14 after ischaemia in mice. Graph shows perfusion ratio results. n=6 mice/gp. Mixed effects two-way ANOVA.

We also studied the engraftment and differentiation of GFP⁺ EndoMac progenitors 14 d after injection into ischaemic diabetic SkM. Prior to transplantation, we used flow cytometry to confirm the purity of donor cells and importantly, showed that they were uniformly GFP⁺ and CD45⁺CD11b⁻F4/80⁻c-Kit⁺Sca-1⁺, consistent with the surface marker phenotype of EndoMac progenitors (**Figure 5.15A, B**). Fourteen days after injection, we observed that some GFP⁺ donor cells had engrafted and transitioned into new CD45⁺CD11b⁺F4/80⁺ MΦs or CD45⁻CD31⁺ and/or CD45⁻CD144⁺ ECs, confirming the bipotent differentiation capacity of SkM EndoMac progenitors *in vivo* (**Figure 5.15C**).

Notably, engraftment of GFP⁺ cells was much higher from STZ⁻ compared to STZ⁺ donors (**Figure 5.15D**). We observed that ~12% of engrafted GFP⁺ STZ⁻ cells retained a progenitor surface phenotype compared to ~5% of STZ⁺ donor cells (**Figure 5.15E**). This resulted in a 13-fold higher density of GFP⁺ progenitors from the non-diabetic source (**Figure 5.15F**). Non-diabetic donor progenitors also produced a 6-fold higher density of GFP⁺ MΦs (**Figure 5.15G**) and a 26-fold higher density of GFP⁺ ECs (**Figure 5.15H**). Importantly, in each of these experiments we did not detect any GFP⁺ cells in the uninjected, nonischaemic hind limb (**Figure 5.15I-L**), which is consistent with the fact that EndoMac progenitors are tissue-resident and do not circulate via peripheral blood.

Therefore, even when injected into a host environment that is diabetic and ischaemic, non-diabetic EndoMac progenitors retained a higher ability to 1) engraft, 2) accumulate and 3) differentiate into myeloid and endothelial progeny, and this was associated with augmentation of perfusion recovery that was not achieved by diabetic progenitors.

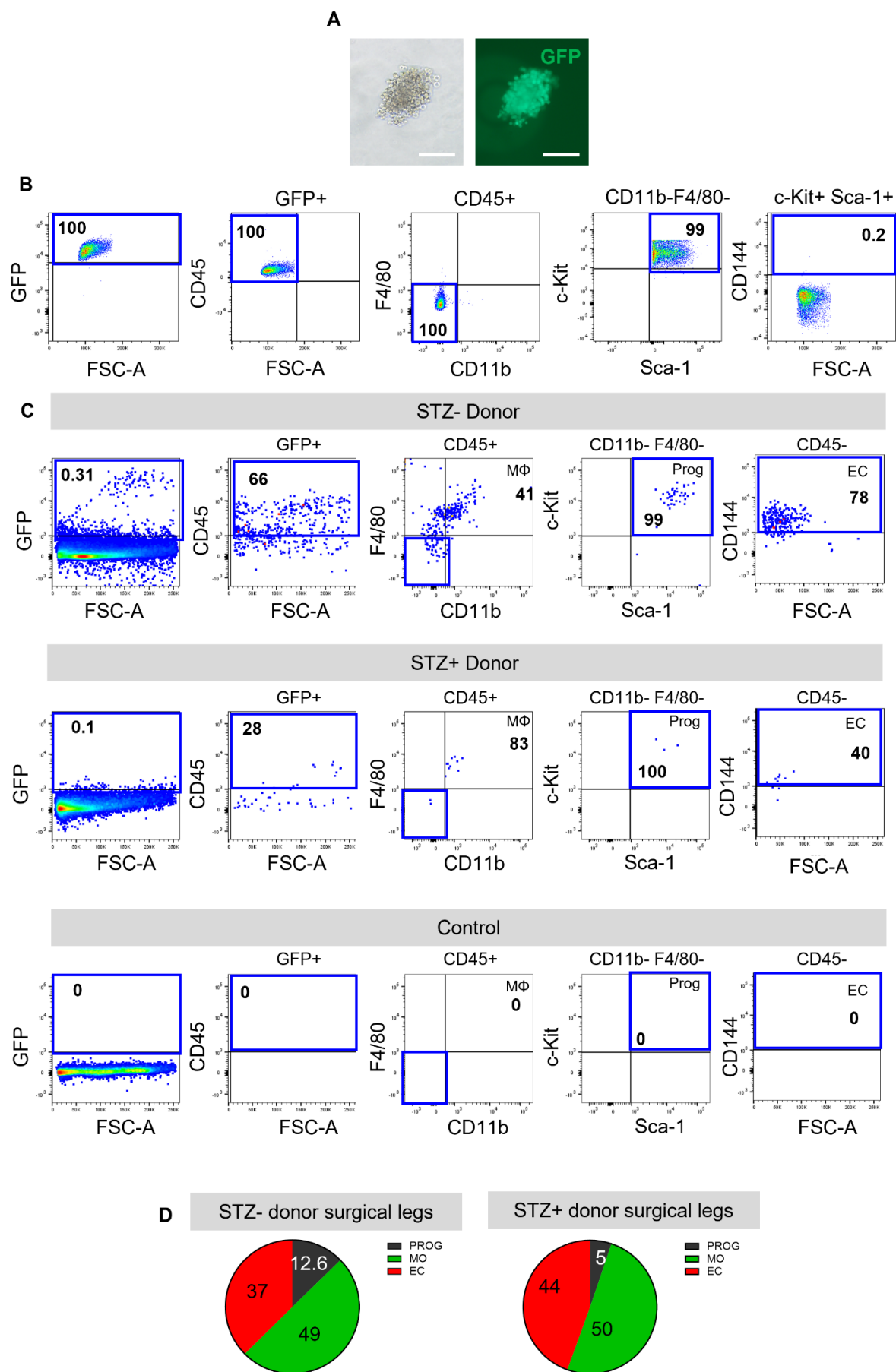


Figure continued P.T. O

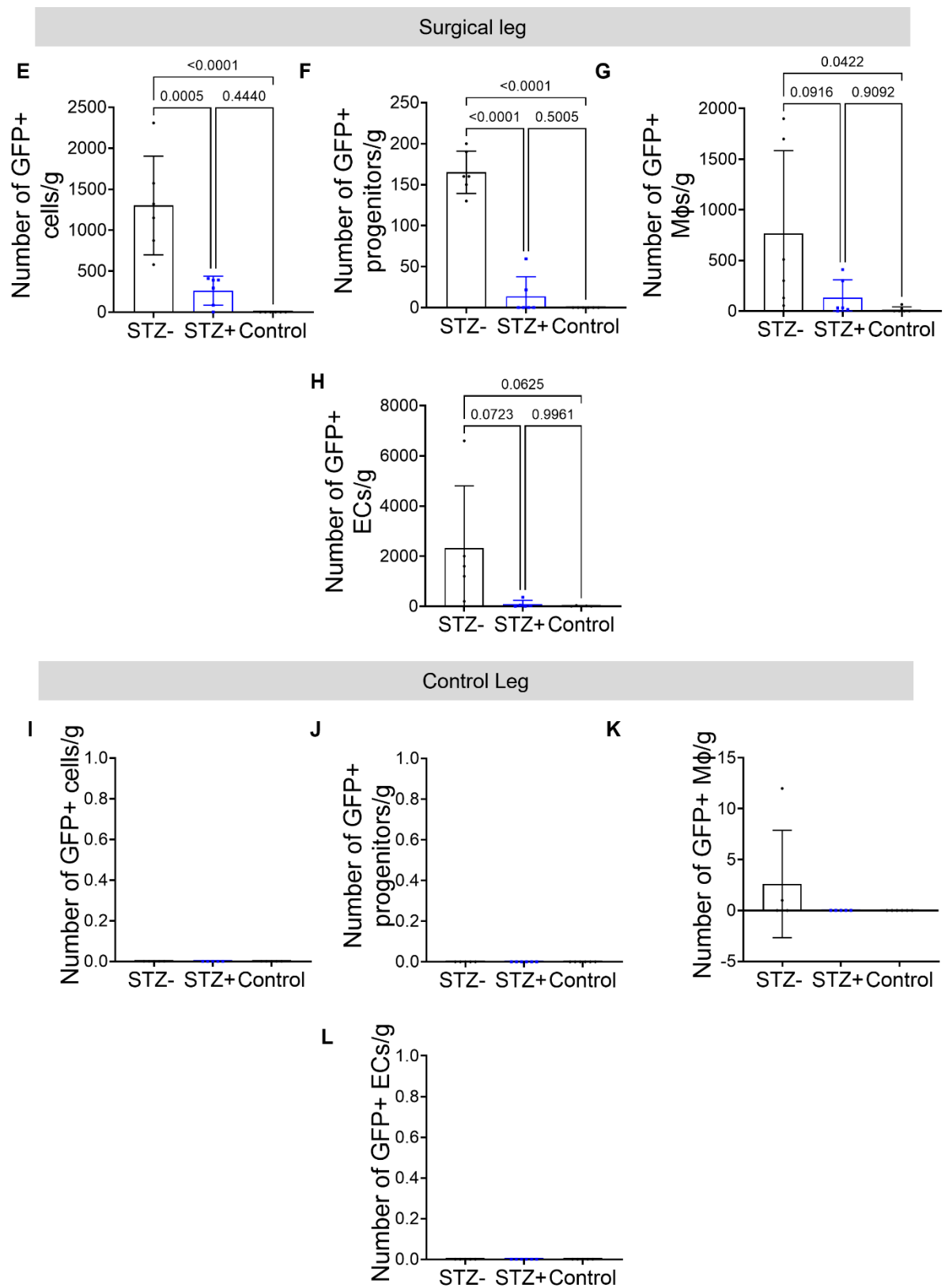


Figure 5.15: Non-diabetic progenitors engraft and differentiate in diabetic ischaemic muscle.

A) Light microscopy (left) and fluorescent microscopy (right) of 1° CFU-M from a 12 w STZ- donor UBI-GFP mouse. Representative of n=8.

B) Flow cytometry showing phenotypic profile of donor GFP⁺ 1° CFU-M from UBI-GFP mice. Isolated progenitors are CD45⁺CD11b⁻F4/80⁻c-Kit⁺Sca-1⁺.

C) Flow cytometry plots show fate of GFP⁺ donor cells in recipient gastrocnemius shown in boxes: CD45⁺ CD11b⁺ F4/80⁺ macrophages (MΦs), CD45⁺CD11b⁻F4/80⁻c-Kit⁺Sca-1⁺ progenitors and CD45⁻CD144⁺ endothelial cells (ECs). Representative flow plots are from STZ+ recipient C57BL/6 surgical legs at D14 that received GFP⁺ CFU-M from STZ- (top), STZ+ (middle) donor UBI-GFP mice and control (bottom). Representative of n=6/gp.

D) Pie charts show the frequency of progenitors, MΦs and ECs that originate from transplanted GFP⁺ STZ- (left) and STZ+ (right) donor-derived CFU-M in recipient gastrocnemius. n=6/gp.

E-G) Graphs show number of **E)** GFP⁺ **F)** progenitors, **G)** MΦs and **H)** ECs from STZ+ recipient C57BL/6 surgical legs at D14 that received GFP⁺ CFU-M from STZ-, STZ+ and control. n=6/gp. One-way ANOVA, multiple comparisons.

I-L) Graphs show number of **I)** GFP⁺ **J)** progenitors, **K)** MΦs and **L)** ECs from STZ+ recipient C57BL/6 control legs at D14. n=6/gp. One-way ANOVA, multiple comparisons.

Finally, we also found that transfer of non-diabetic progenitors resulted in higher overall numbers (i.e., not GFP⁺) of progenitors, MΦs and ECs in injected, but not contralateral uninjected limbs compared to the other two groups (**Figure 5.16**). This may indicate that non-diabetic donor EndoMac progenitors launched a stronger paracrine effect on host progenitors, MΦs and ECs which may have also helped to mediate the enhanced perfusion recovery seen in these recipient mice.

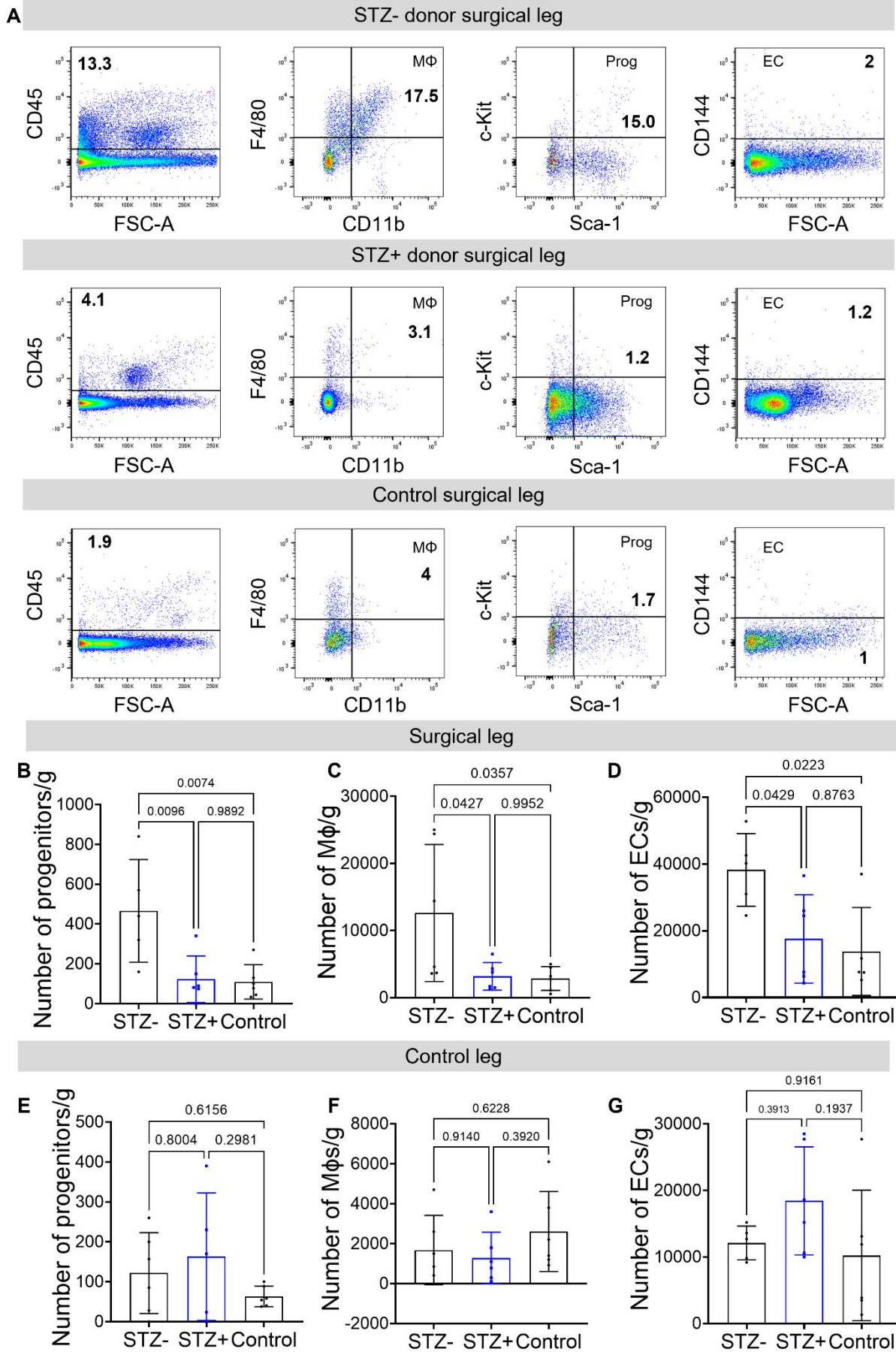


Figure 5.16: Effect of non-diabetic donor progenitors on overall numbers of progenitors, MΦs and ECs in recipient SkM.

A) Flow cytometry plots show recipient SkM cells 14 d after injection of STZ-. STZ+ progenitors or vehicle control. Gating strategy shown for: CD45⁺ CD11b⁺ F4/80⁺ macrophages (MΦs), CD45⁺CD11b⁻F4/80⁻c-Kit⁺Sca-1⁺ progenitors and CD45⁻CD144⁺ endothelial cells (ECs). Representative of n=5-6/gp.

B-D) Graphs show number of **B)** progenitors, **C)** MΦs and **D)** ECs from STZ+ recipient C57BL/6 surgical legs at D14 that received injection of STZ-. STZ+ progenitors or vehicle control. n=5-6/gp. One-way ANOVA, multiple comparisons

E-F) Graphs show number of **E)** progenitors, **F)** MΦs and **G)** ECs from STZ+ recipient C57BL/6 control legs at D14 that received injection of STZ-. STZ+ progenitors or vehicle control. n=5-6/gp. One-way ANOVA, multiple comparisons

5.4 Discussion

Diabetes impairs the body's natural mechanisms to vascularise and repair ischaemic tissue. A large component of this is mediated by metabolic disturbances to the key functions of ECs that are responsible for new blood vessel formation with support of inflammatory cells, such as MΦs (534). Recent studies have shed light on the complex ontogeny of both ECs and MΦs in postnatal SkM, highlighting the presence of locally derived MΦ and EC populations, as well as those that are renewed from circulating sources (28, 36, 108, 119, 546, 586). Here we investigated the recently discovered population of embryonically derived EndoMac progenitors in steady-state and ischaemic murine SkM in the context of diabetes. Our main findings are that high glucose tested *in vitro* and hyperglycaemia induced by STZ *in vivo* both had consistent inhibitory effects on the key functional properties of EndoMac progenitors, including their ability to form renewable colonies in culture and angiogenic structures *in vitro*, which contain newly formed MΦs and ECs. This was associated with disturbances in metabolic function, demonstrated by reduced mitochondrial membrane function and viability, increased oxidative stress, as well as reduced OCR and ECAR. As shown by fate-mapping studies, the early proliferative response of these progenitors to ischaemia was dampened in the setting of diabetes and this was associated with attenuated expansion of YS-derived MΦs and ECs at later time-points and reduced perfusion recovery. We have also demonstrated the bipotent capacity and reparative potential of non-diabetic progenitors transplanted into a diabetic ischaemic environment and showed that progenitors from a diabetic source no longer have these properties.

Our prior work has identified that EndoMac progenitors arise from YS EMPs and are then seeded in different embryonic mouse tissues around E10.5, where they persist until after birth (520). They are thereafter maintained in their local tissue niches without circulatory input and independently of definitive BM haematopoiesis. Notably, they are most prevalent around the time of birth and steadily decrease in number as mice age, at least part because of a progressive decline in their ability to

proliferate and renew (520). Within adult mouse SkM, as in other tissues, they can be identified by their ability to selectively form CFU-M in methylcellulose-based culture and their expression of a Lin⁻CD45⁺CD11b⁻F4/80⁻Sca-1⁺c-Kit⁺ surface marker phenotype, along with high levels of the receptors for fractalkine (CX₃CR1) and macrophage colony-stimulating factor (CSF1R/CD115) (520). Previously, we also observed that these progenitors undergo rapid proliferative expansion in SkM within the first day after acute ischaemia (522). Extending on this, the present study shows for the first time that these progenitors are substantially depleted in the hind limb SkM of diabetic mice under both steady-state and ischaemic conditions. As an explanation for this deficiency, we found that the effects of high glucose *in vitro* and hyperglycaemia *in vivo* were to reduce the clonal expansion and renewal of EndoMac progenitors, without significantly impairing their viability. This in turn would be expected to affect the local maintenance and self-renewal of these cells in the diabetic setting.

The inhibitory effects of diabetes on SkM EndoMac progenitors are consistent with those observed in Chapters 3 and 4 for the analogous cells in mouse aorta and skin, respectively. They are also in keeping with similar effects of high glucose on other adult stem cell populations, including BM HSPCs (633) and mesenchymal stromal/stem cells (547). Diabetes has previously been shown to attenuate the mobilisation of HSPCs from their BM niche into the peripheral blood, resulting in depletion of circulating HSPCs which contributes to an aberrant immune response (633, 634). This is mediated at least in part by diabetes-induced metabolic reprogramming and epigenetic changes (635), and has been linked to adverse outcomes in other tissues, including diabetic vascular complications (63). Other studies have demonstrated the negative effects of diabetes on tissue-resident stem cells, including adipose stromal cells (636) and satellite cells in SkM, with the latter resulting in poor muscle regeneration following injury in diabetic mouse models (462-464, 466, 637). Although we did not find significant changes in the overall prevalence of Lin⁻Sca-1⁺c-Kit⁺ BM

HSPCs in STZ-treated C57BL/6 mice, we did not examine the effect of hyperglycaemia on specific HSPC subsets (e.g., long-term HSCs vs multipotent progenitors), nor on the mobilisation of HSPCs into peripheral blood. However, we did find that diabetes resulted in ~3.3-fold and ~1.6-fold increases in circulating neutrophils and monocytes, respectively, with the latter mostly comprised of a 6-fold increase in pro-inflammatory Ly6C^{hi} monocytes. Although this suggests a heightened inflammatory state in peripheral blood, this was not associated with a significant increase in the total number of macrophages in steady-state, diabetic SkM.

Recently, both experimental and clinical studies have demonstrated that hyperglycaemia can induce alterations to differentiation and function of circulating exogenous EPCs, as well as mature ECs (480, 499). In addition, diabetes has been shown to attenuated myelopoiesis and affect the polarisation of MΦs (501). Aligned with this, our results demonstrate a diabetes-dependent attenuation of the angiogenic and differentiation capacity of SkM progenitors *in vitro* and *in vivo*. The mechanisms underlying this attenuation were explored by investigating mitochondrial and metabolic health given that diabetes is already known to cause metabolic dysfunction SkM satellite cells, circulating and BM myeloid precursor cells (366, 462, 466).

Adult stem cells, such as long-term HSCs, mesenchymal stromal cells, and SkM satellite cells have been shown to be metabolically quiescent to allow them to avoid cellular damage and ensure their capacity for life-long renewal (427, 499, 506, 635-637). A key property of maturation of adult stem/progenitor cells is the metabolic switch from anerobic respiration to aerobic glycolysis and oxidative phosphorylation for proliferative adult stem/progenitors ((578, 638). To this end, healthy SkM EndoMac progenitors showed a significant reliance on aerobic respiration, as evident by their overall increased oxygen consumption, mitochondrial membrane potential, mitochondrial mass, and

lower DNA double-stranded breaks. This is consistent with the fact that these progenitors are actively proliferative. In contrast, the higher ECAR (related to glycolysis) in basal glucose conditions may be as a result of aerobic glycolysis (also known as Warburg effect) rather than quiescence or low activity state (639).

In the present chapter, we found that high glucose significantly impaired mitochondrial membrane function, oxygen consumption, ATP-synthase dependence and reserve capacity to recover following mitochondrial ETC inhibition/stress. We also observed high glucose-induced downregulation of both glycolysis and oxidative phosphorylation, perhaps as an adaptive mechanism for increased substrate availability. One of the most frequently proposed mechanisms for mitochondrial dysfunction in diabetes is disruption of normal mitochondrial dynamics. We saw a marked reduction in the viable mitochondrial content of SkM progenitors under high glucose exposure. As in other studies, ROS production was markedly increased under high glucose and in diabetic progenitors, which may further exacerbate disturbances in their other functional properties (192, 200, 469, 604). Although multiple hypotheses have been put forward for the reduction in mitochondrial content in diabetic SkM, the exact mechanisms responsible are not known (192, 640).

The MΦ and EC pools in SkM are known to be derived from heterogenous sources, although these have not been well characterised in the ischaemic or diabetic settings. Previous studies by Wang *et al.* and Williamson *et al.* have suggested that in steady state, ~30% of quadriceps MΦs derive embryonically from a YS source and are maintained after birth independently of BM haematopoiesis (75, 520). Up until recently it was unclear if the YS also contributes to endothelium in SkM, although this has been suggested for other tissues (21, 35, 89, 93), while the use of confetti multi-colour reporter mice has demonstrated that local ECs expand clonally in SkM after ischaemia (641). Our

own fate-mapping results indicate that in non-ischaemic hind limb SkM, CSF1R⁺ YS EMPs contributed to ~30 % and ~10% of MΦs in STZ- and STZ+ mice, respectively. Importantly, early after ischaemia, this “local” contribution to the SkM MΦ pool was up to ~55% in the non-diabetic and ~40% in the diabetic state. Although YS-derived MΦs numerically expanded up until day 7 after ischaemia, their relative contribution to the overall MΦ pool diminished over time, indicating that there was also recruitment of MΦs from an alternative source(s). This most likely was from the recruitment and differentiation of peripheral blood monocytes, which would align with other studies that show that circulating monocytes accumulate in SkM between days 3 and 7 post-ischaemia (520). By comparison to MΦs, we found that a much lower proportion of ECs (~10-20%) were embryonically derived in the non-ischaemic SkM of both STZ- and STZ+ mice. However, these cells expanded considerably in the two weeks after ischaemia, ultimately making up ~80% of the total EC pool by day 14 in the non-diabetic setting, and ~40% in diabetic mice. These novel results highlight the importance of local rather than circulatory EC renewal, which presumably helps to facilitate perfusion recovery in ischaemic SkM. They also demonstrate that this process is impaired in diabetes.

Our experimental design in this chapter did not allow us to calculate the extent to which new MΦs and ECs are produced in ischaemic SkM from the proliferation and differentiation of YS-derived progenitors versus the self-renewal of these two cell types in their mature, differentiated states. Previously, we have used BrdU pulse-chase labelling after hind limb ischaemia to show that proliferative expansion of progenitors occurs much earlier than for the other two populations, with subsequent redistribution of the BrdU label from proliferating progenitors to YS-derived MΦs and finally ECs (522). These results suggest that at least a substantial proportion of locally produced MΦs and ECs are derived from EndoMac progenitors. Similarly, using a *Csf1r* Cre-Lox fate-mapping strategy with GFP reporter, we observed here that GFP⁺ progenitors expanded earliest after ischaemia, followed over 3-7 d by GFP⁺ MΦs and finally over 7-14 d by GFP⁺ ECs. In keeping with

our *in vitro* results, hyperglycaemia dampened the early expansion of progenitors in ischaemic SkM, with a trend toward fewer of these cells being in active cell cycle. Importantly, our adoptive transfer experiment confirmed the bipotent ability of non-diabetic progenitors to transdifferentiate into MΦs and ECs *in vivo* and promote perfusion recovery, even within a diabetic host environment. Our data also show their ability to mediate the accumulation of host-derived cells in ischaemic tissue, which may indicate additional paracrine effects that require dedicated investigation. The fact that all these salutary properties were absent from STZ+ donor progenitors even after culture for 14 d under normal glucose conditions, emphasises that hyperglycaemia's inhibitory effects on progenitors are both profound and long-lasting.

Limitations and future directions

Although the experiments in this chapter exclusively used mice, we have identified analogous CFU-M progenitors from SkM digests from amputated limbs of patients with PAD and critical limb ischaemia (Hassanshahi, Psaltis unpublished). This indicates the potential clinical relevance and translatability of our preclinical discoveries. Given that type 2 diabetes is far more prevalent than type 1 diabetes in humans, another major directive moving forward will be to see if our findings extend to appropriate mouse models of obesity, insulin resistance, pre-diabetes and type 2 diabetes (358, 642). The precise mechanisms by which high glucose inhibits SkM EndoMac progenitors will also require further evaluation, such as through transcriptomic and epigenetic profiling. Although we suspect that the metabolic abnormalities shown here may be responsible, it will be important to test the extent to which metabolic reprogramming of progenitors can restore their other salient properties (e.g. clonal renewal, proliferation, differentiation, angiogenesis/vasculogenesis). Possible candidates for this include the mitochondrial antioxidant, MitoQ (643), and nicotinamide riboside (644). The latter is a form of vitamin B3, that was recently found to restore youthful metabolic capacity to aged BM HSCs, by modifying mitochondrial function and dampening mitochondrial stress (645). If shown to rescue and/or promote the metabolic activity and stem-like actions of EndoMac progenitors *in vitro*, these

agents could then be examined for their ability to repair diabetic ischaemic tissues *in vivo*. This could be done by pre-treating donor progenitors prior to their transplantation, or by administering the metabolic agent to ischaemic mice systemically or locally to boost the actions of endogenous progenitors, MΦs and ECs.

Current treatments for diabetic PAD are limited. Since the discovery of circulating and BM-derived EPCs by Asahara *et al.* (115), many preclinical and clinical studies have attempted to administer pro-angiogenic progenitors to treat peripheral ischaemia ((590, 646, 647). However, most regenerative medicine and tissue engineering strategies have been hampered by inadequate vascularisation, leading to graft failure and suboptimal results (648). There is potential for EndoMac progenitors to be used as a new type of adult stem cell therapy, either in isolation or in combination with vascular scaffolds to perfuse ischaemic tissues. This could be an advance on existing approaches, which use unipotent endothelial progenitors without the supportive benefits of MΦs. Although our study shows in principle the ability to transplant these cells into diabetic, ischaemic tissue, the use of donor cells from an autologous diabetic source would almost certainly be ineffective, at least without some degree of pharmacological, metabolic, or genetic pre-conditioning to bolster their properties. The alternative of using allogeneic progenitors (e.g., from a young, healthy, non-diabetic source) will depend on showing that this population is immuno-privileged and able to avoid and/or suppress immune rejection, as is the case for mesenchymal stromal cells (518, 544). To this end, we have previously established that in their undifferentiated state, EndoMac progenitors from mouse aorta express very low levels of MHCII, while their differentiation into MΦs strongly favours those that are LYVE-1^{Hi}MHCII^{Lo} (520). Interestingly, this is consistent with the surface marker phenotype ascribed to tissue-resident, YS-derived MΦs, including those found in SkM (36, 73, 75, 520). Although we have yet to elucidate the subtype heterogeneity of ECs and MΦs produced by EndoMac progenitors *in vivo*, all SkM specimens studied by flow cytometry in this chapter were labelled with

appropriate surface markers to enable us to do this in the future. In addition, specimens have been processed from the mice used in this chapter, for the purpose of staining SkM sections to determine the localisation of progenitors and its effects on capillary and arteriolar neovascularisation, and to corroborate our results from flow cytometry with immunofluorescence microscopy.

Conclusion

Extending on previous work from our group which identified embryonically derived EndoMac progenitors in steady-state and ischaemic mouse SkM, here we have established that these cells are highly susceptible to the inhibitory effects of high glucose. This is associated with a range of metabolic and mitochondrial disturbances and a profound attenuation of their ability to expand, differentiate, and promote perfusion recovery of ischaemic SkM *in vivo*.

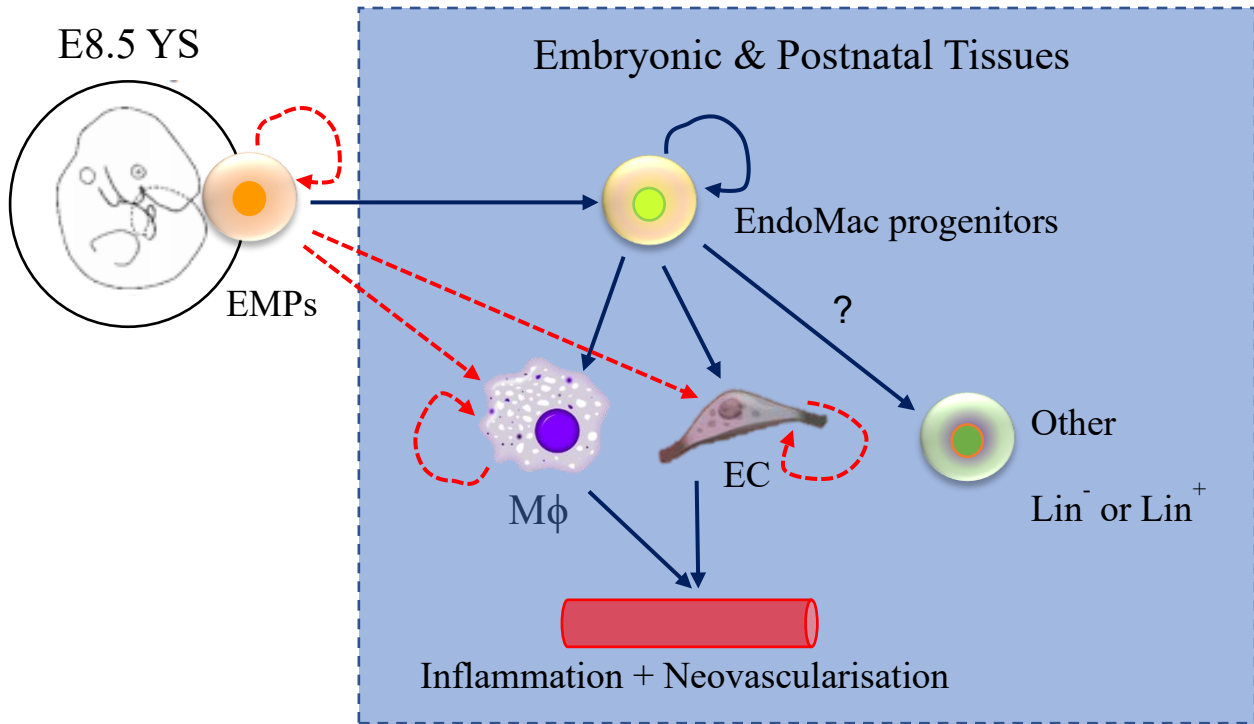
Chapter 6

6. General Discussion

6.1 General overview and key findings

Diabetes impairs wound healing and neovascularisation of ischaemic tissues, leading to devastating limb- and life-threatening consequences in people with peripheral artery disease. Diabetes-related amputations account for an ever-increasing global healthcare cost burden and impose debilitating effects on personal quality of life. Ineffective repair responses in diabetes are a result of abnormal angiogenic responses, characterised by endothelial dysfunction and uncontrolled inflammation, amongst a host of impaired signalling responses. Until now, research into new therapies that directly vascularise diabetic tissue has resulted in limited success and translation to the clinic despite early preclinical promise (330). This underscores the importance of acquiring a deeper, more sophisticated understanding of the complex cellular and molecular players that help mediate effective wound healing and tissue neovascularisation and how these are adversely affected by the diabetic state. To this end, the studies in thesis focused on two intimately associated cells, macrophages (MΦs) and endothelial cells (ECs), which play vital functions in injured tissues. MΦs accumulate at sites of injury to launch inflammatory responses, as well as aid ECs in the process of new vessel formation via chemokine release and direct contact support (19). In turn, ECs guide MΦs to switch to pro-angiogenic phenotypes at tissue sites that require reperfusion (19). Therefore, studying this intertwined relationship in the context of diabetic wounds and tissue ischaemia may open up new therapeutic avenues that help promote more effective neovascularisation and tissue repair.

Tissue MΦs and ECs are not only functionally related, but they also share an overlapping ontogeny that dates to a common ancestor from erythromyeloid progenitors (EMP) in extra-embryonic yolk sac (YS). Previous studies have claimed that YS-derived MΦs and ECs are seeded in prenatal tissues and maintained in their mature states after birth through local proliferative, self-renewal (28, 112). Here we expand our knowledge on YS-derived EndoMac progenitors, as an alternative source for the postnatal maintenance and turnover of these two distinct, tissue-resident lineages (**Figure 6.1**).



- > Current paradigm: YS EMPs seed tissue Mφs and ECs that self-renew
- > New paradigm: YS EMPs seed tissue EndoMac progenitors that self-renew and differentiate locally to maintain Mφs and ECs

Figure 6.1: EndoMac progenitors as a newly identified source for the renewal of YS-derived tissue macrophages and endothelial cells.

Converging evidence indicates a common ancestral origin for Mφs and ECs from E8.5 YS EMPs. The prevailing expert view is that EMP-derived Mφs and ECs are seeded in embryonic tissues and are then maintained in their mature, differentiated states by local self-renewal postnatally (red dotted arrows). We propose an alternative paradigm for the maintenance and renewal of some tissue-resident Mφs and ECs (black solid arrows), whereby undifferentiated EndoMac progenitors seed tissues during embryonic development and are locally maintained via self-renewal in postnatal life. These progenitor cells actively differentiate into tissue-resident Mφs and ECs and contribute to inflammatory and neovascularisation processes in different tissues. Based on very preliminary observations, we suspect that EndoMac progenitors also possess additional potency for “other” cell lineages which will require further research.

As described in the preceding chapters, EndoMac progenitors were first identified through the capacity of some adult mouse tissues – specifically aorta, skin and skeletal muscle (SkM) - to selectively produce colony-forming units of the macrophage subtype (CFU-M). Careful phenotyping of the cells responsible for these CFU-M, and indeed contained within them, has revealed a immunophenotypic fingerprint based on at 6-8 surface markers: LIN⁻CD45^{+Lo}CD11b⁻F4/80⁻Sca-1⁺c-Kit⁺(CX₃CR1⁺CSF1R⁺), consistent across multiple tissues. Fate mapping studies performed by our group previously (522) and herein, have established that these progenitors originate *in utero* from E8.5 CSF1R⁺ YS EMPs. After birth, they are maintained via local renewal in their tissue niches, independently of bone marrow (BM) haematopoiesis, albeit in declining numbers as mice get older. We have confirmed their bipotency and vasculogenic capacity both *in vitro* via MatrigelTM assays and *in vivo* by means of adoptive transfer into both wounds and ischaemic tissue of non-diabetic (522) and now, diabetic mice, where they help to promote tissue perfusion and repair.

In this thesis, our specific aims were to fill in some of the existing knowledge gaps on EndoMac progenitors in steady state tissue (Chapter 3), and to study impaired healing of diabetic skin and SkM through the unique lens of EndoMac progenitors (Chapters 4 and 5). In Chapter 3 we first confirmed that EndoMac progenitors FACS isolated from digested aortas are indeed responsible for producing CFU-M, whereas mature MΦs and ECs do not contain this clonogenic potential. Importantly, “freshly sorted” and “CFU-M culture-derived” progenitors not only exhibit the same core surface marker expression, but they also each have a homogeneous transcriptomic signature, with considerable overlap of key genes and biological pathways. We were also able to demonstrate the bipotency of aortic EndoMac progenitors into the myeloid and endothelial lineages, by using immunocytofluorescence. Not only did these experiments complement and corroborate our previous flow cytometry results, but crucially they established that this bipotency is contained at a clonal, and even single cell, level. In our comparative studies, we observed tissue-specific similarities and

differences in the function, gene expression and metabolic activity of progenitors from adult murine aorta, skin and SkM. Of note, the largest number of genes that were differentially expressed were between skin and SkM progenitors. We also identified that while EndoMac progenitors were most prevalent in skin, the capacity for secondary clonal renewal in methylcellulose and angiogenesis and differentiation in MatrigelTM was greatest for SkM progenitors, and this corresponded with greater metabolic activity, as measured by higher oxygen consumption and higher extracellular pH levels. This was not surprising given that SkM is a primary site for energy production in the body.

We next extended our study of EndoMac progenitors into the setting of hyperglycaemia, as modelled by streptozotocin (STZ)-induced type 1 diabetes (T1D). Beginning with aorta, we found a diabetes-related attenuation of their prevalence, stem-like properties and differentiation and angiogenic capacity. Although aortic EndoMac progenitors did not specifically exhibit variations in mitochondrial mass nor membrane function in hyperglycaemia, they did possess a significant loss in DNA integrity and marked depletions in metabolic function that may explain this inhibitory effect. Building on these very preliminary findings for aorta, we were prompted to also study the effect of diabetes on EndoMac progenitors in skin and SkM, in the contexts of wound healing and ischaemic repair, respectively.

In Chapters 4 and 5, we identified similar glucose and diabetes-related inhibition of the clonogenic, renewal and angiogenic capacity of skin and SkM EndoMac progenitors. These profound inhibitory effects led us to also analyse the effects of high glucose on their metabolic function and mitochondrial health. For both skin and SkM, exposure to high glucose significantly lowered the progenitors' capacity for oxygen consumption and mitochondrial ATP-synthase dependant respiration. It further compromised the mitochondrial ability to launch an effective compensatory response following

inhibition of mitochondrial electron transport chain (ETC) function and in turn, supply the unmet energy demand. We further observed a significant decline in the extracellular pH levels of progenitors cultured under high glucose conditions, suggesting attenuated anaerobic respiration. However, somewhat contradictory to this was the increased lactate concentrations shown in the supernatant of skin and SkM progenitors following *in vitro* exposure to high glucose, indicating upregulated anaerobic activity. Future metabolic pathway studies are now needed to provide further insight into this. In both cases, exposure to high glucose *in vitro* and hyperglycaemia *in vivo*, launched an increased capacity for skin and SkM progenitors to take up glucose, suggesting a potential alternative pathway to utilise substrate to meet their energy demand. Experiments that specifically tracked mitochondrial function revealed consistent reductions in mitochondrial mass, compromised inner membrane potential and increased mitochondrial stress. Taken together, these results highlight that high glucose and/or hyperglycaemia impose extensive metabolic and mitochondrial changes in EndoMac progenitors from both tissue types. Pending further experiments, we speculate that this may help to explain the accompanying alterations in their stemness and functionality.

In Chapters 4 and 5, we also explored the expansion and fate of YS-derived EndoMac progenitors, MΦs and ECs in models of wound injury and hind limb ischaemia in non-diabetic and diabetic mice. We identified a robust proliferative expansion of progenitors immediately after tissue insult in both models in the non-diabetic state (**Figure 6.2**). This subsequently abated over the following days, in parallel with sequential accumulation of YS-derived MΦs and then ECs. This kinetic pattern relating to the expansion of different types of YS-derived cells was profoundly dampened in the setting of STZ-induced diabetes. In both diabetic skin wounds and ischaemic SkM, we found a profound failure of EndoMac progenitors to launch their early response to tissue insult. This aligned with our earlier results, whereby high glucose dampened the clonal growth and renewal of these cells *in vitro* and hyperglycaemia markedly reduced their prevalence in steady state skin and SkM. Notably, we also

identified important contributions of YS-derived cells to the MΦ pool during the early/mid-inflammatory phases of non-diabetic wound and ischaemic repair, and similarly to ECs during the late angiogenic phases of tissue healing. In contrast, diabetic wounds and ischaemic SkM showed significantly diminished proportions and delayed expansions of YS-derived progenitor, MΦ and EC populations.

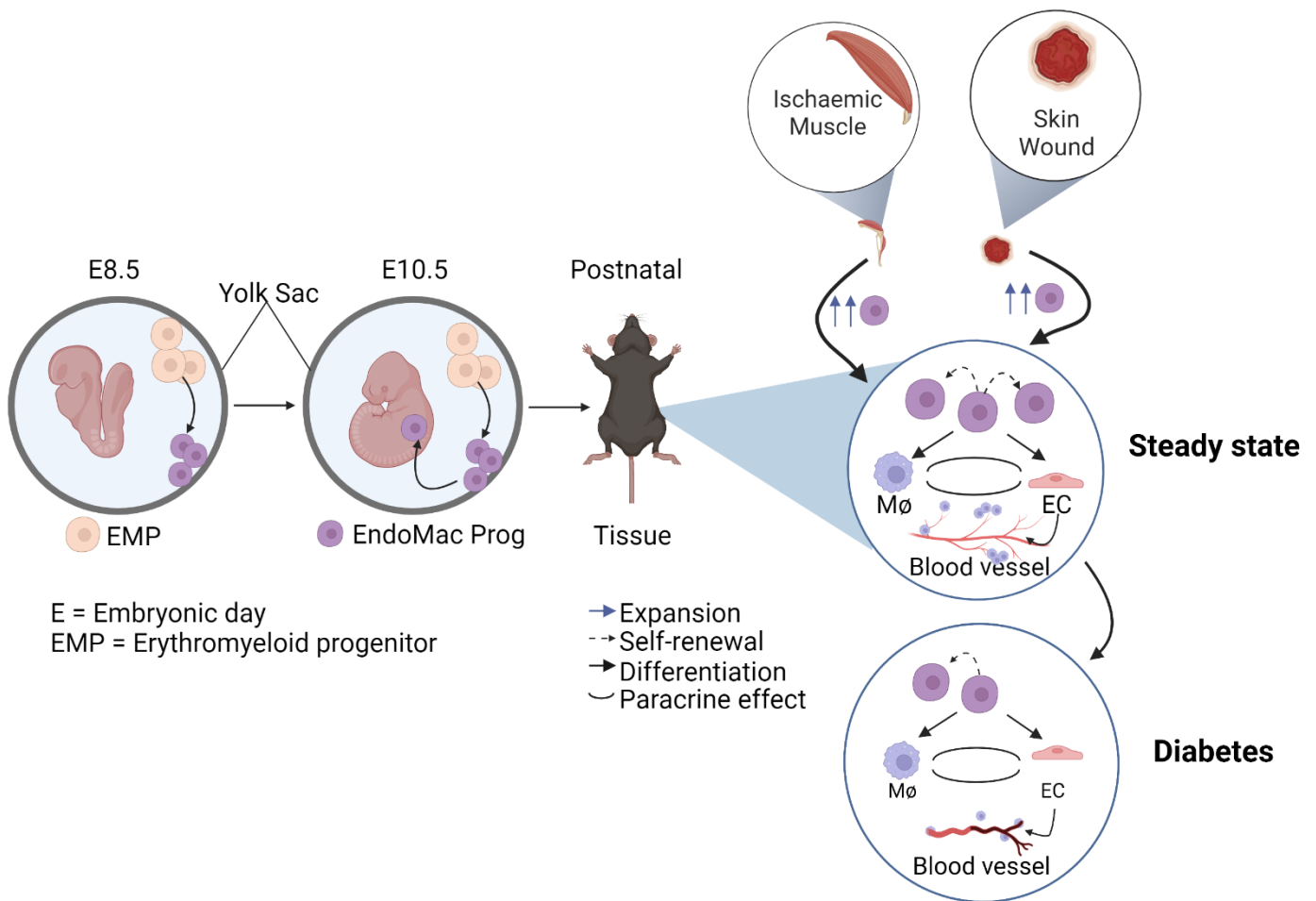


Figure 6.2: The role of EndoMac progenitors in tissue repair in steady state and pathological disease.

From the left: EndoMac progenitors arise from yolk-sac erythromyeloid progenitors (EMP) at embryonic day (E) 8.5 and subsequently seed foetal tissues by E10.5. They persist in tissues postnatally and are maintained locally via self-renewal. EndoMac progenitors are bipotent for macrophage (MΦ) and endothelial cells (EC) and collectively contribute to blood vessel formation in tissue. In both skeletal muscle ischaemia and skin wounds, EndoMac progenitors exhibit profound proliferation and differentiation that contribute to efficient

tissue repair. Diabetes attenuates the prevalence, stemness and differentiation capacity of EndoMac progenitors. In turn these attributes to the abnormal angiogenesis seen in diabetic tissue.

Having studied the cellular kinetics of diabetic skin and SkM following insult, we speculated that impaired wound healing and ischaemic repair in diabetes may be in part due to the attenuated properties of EndoMac progenitors. Therefore, as a means of rescuing this impairment, we carried out cell transplant studies in which non-diabetic or diabetic progenitors were injected into diabetic skin wounds and ischaemic SkM. This confirmed the salutary properties of non-diabetic progenitors, which were able to successfully engraft in the diabetic host environment, differentiate (at least bipotently) and promote repair of wounds and perfusion of ischaemic hind limbs. Notably, these reparative effects were almost completely absent for progenitors from diabetic donor mice.

It must be noted that YS-derived EndoMac progenitors are not the dominant source of MΦs and ECs in postnatal tissues. However, our discovery of these renewable, bipotent cells does provide a plausible explanation for the local turnover and renewal of YS-derived, tissue-resident MΦs and ECs in different tissues after birth. It also aligns with century-old evidence for the existence of bipotent haemangioblasts, that have been identified in different species during embryogenesis and *in vitro* culture (44, 71, 73, 76), but not in postnatal mammalian tissues. Our results show that EndoMac progenitors that are seeded in different tissues share many similarities, but also likely possess tissue-specific adaptations, that may reflect their function throughout postnatal life. Moreover, the hyperglycaemia-imposed attenuation in their prevalence, metabolism and function may contribute to the aberrant inflammatory and vasculogenic responses that underpin the impaired recovery of diabetic tissues. Future studies are now needed to determine whether the unique properties of EndoMac progenitors can be harnessed as a new therapeutic tool or target in the battle against diabetic micro- and macrovascular complications.

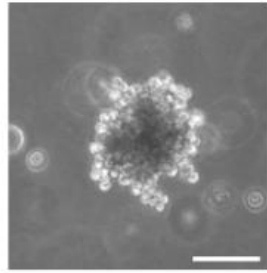
6.2 Bridging existing knowledge gaps

Our findings demonstrate a common ancestry that connects three YS-derived populations in different tissue niches postnatally, without continuous renewal from definitive BM HSCs or circulating progenitors (522). This is in line with previous studies that also utilised fate-mapping models to confirm a YS origin for tissue MΦs (28, 34, 36), vascular and lymphatic ECs (108, 649), as well as some tissue mast cells (650, 651), osteoclasts and foetal erythrocytes (652, 653). There is ample evidence for the intertwined relationship between MΦs and ECs in both prenatal (31, 100, 654) and postnatal development (6, 19) and in pathological conditions (11, 655). Their overlapping developmental origins were first speculated on nearly a century ago by His *et al.*, who described a bipotent haemangioblast progenitor in extraembryonic YS that tied together primitive haematopoiesis and vasculogenesis during early embryonic life (76). Despite much effort, it has proven extremely difficult to prove the *in vivo* existence of haemangioblasts in postnatal tissues, although elegant *in vitro* studies have shown that analogous cells arise during the induced haemato-endothelial differentiation of human embryonic stem cells and induced pluripotent stem cells (44, 656).

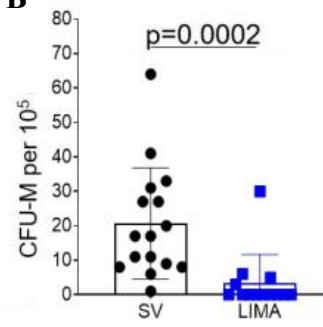
The presence of YS-derived EndoMac progenitors in various postnatal tissues was studied extensively by Dr Anna Williamson from our group during her recently completed PhD candidature (517, 518, 520, 522). However, their function and contribution to diabetic tissue repair is a novel avenue explored by this thesis for the first time. Reperfusion of ischaemic diabetic tissues is difficult to achieve and ongoing research on diabetic wound healing and peripheral vascular disease has focused on pathways that manipulate tissue neovascularisation (496, 516, 657). Converging lines of evidence also demonstrate the onset of metabolic dysfunction and inhibition of the properties of local and systemic stem/progenitor cell populations following the onset of diabetes, as exemplified for BM haematopoietic stem/progenitor cells (HSPC) (658), circulating endothelial progenitor cells (385, 499), mesenchymal stem cells (547), epidermal stem cells in skin (564, 581), and satellite cells in

SkM (462). Our current studies were carried out following unpublished data collected by an Honours student in our group, Dr Aaron Long, who firstly confirmed the existence of EndoMac progenitor-like cells in human saphenous vein (SV) and left internal mammary artery (LIMA). Samples were collected from patients following coronary artery bypass grafting. Like their counterparts in murine aorta, these progenitors have the selective capacity to form CFU-M in methylcellulose-based culture (~20 CFU-M per 10^5 cells plated) (**Figure 6.3A, B**), and possess angiogenic cord forming ability in MatrigelTM, with these cord networks containing newly formed ECs and MΦs (data not shown). As Sca-1 is not expressed in human cells, they express a different surface marker phenotype to murine progenitors and are CD45⁺CD31⁻c-Kit⁺CD34⁺ (data not shown). Another key finding from this work that prompted my own line of investigation in this thesis, was that CFU-M forming progenitors were significantly depleted in patients with diabetes (**Figure 6.3C**).

A



B



C

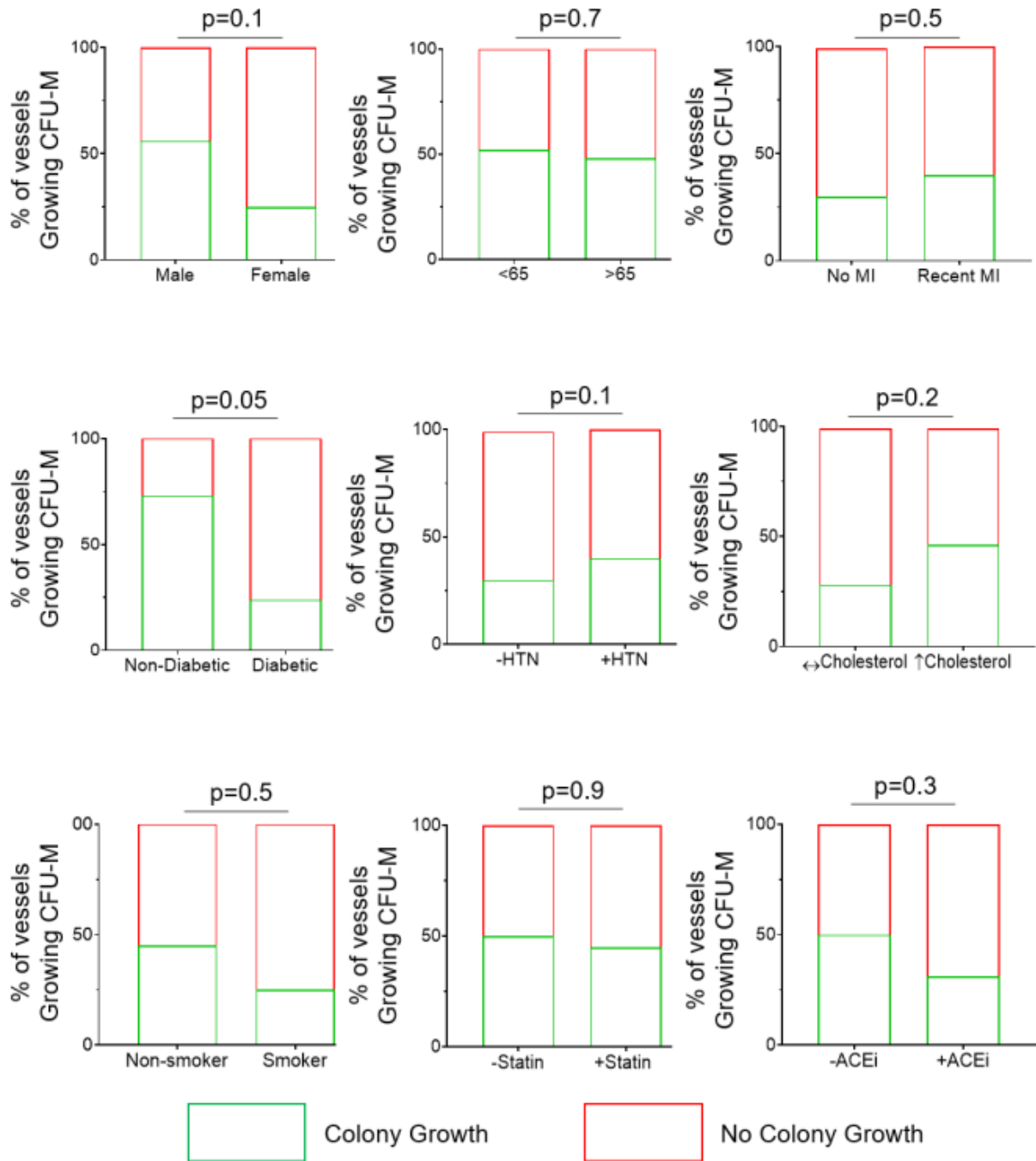


Figure 6.3: Discovery of CFU-M forming progenitors in human blood vessels.

- A)** Light microscopy image of CFU-M grown after plating single cell disaggregates from human saphenous vein (SV) in methylcellulose for 14 d. Scale bar 100 μm
- B)** CFU-M yield from single cell digests of human SV and left internal mammary artery (LIMA) digests. n=13-16 samples. Wilcoxon signed rank test.
- C)** Graphs showing percentage of SV specimens that grew CFU-M, according to the presence or absence of selected clinical characteristics. n=33, Chi-squared tests

Data by Dr Aaron Long, 2019.

6.2.1 Why defining the function of EndoMac progenitor cells in diabetes is important?

Diabetes profoundly affects vascular biology, and its associated complications are related to impairment of macro- and microvascular beds. The reasons for the aggressiveness of diabetic vasculopathy are incompletely understood, but it has long been established that glucose-induced dysfunction of vascular endothelium and circulating vascular regenerative progenitors plays a central role (115). This thesis unequivocally shows a significant reduction in the prevalence, clonal renewal and differentiation of EndoMac progenitors into MΦs and ECs, as well as their angiogenic potential and metabolic function in three diabetic tissues. CFU-M from diabetic aorta, skin and SkM were smaller in size and less capable of generating secondary colonies when re-plated in methylcellulose and vascular-like cords in MatrigelTM. These profound inhibitory effects do not necessarily mean that downregulation of EndoMac progenitors is the main reason for diabetic tissue complications, but they are consistent with the hyperglycaemia-related dampening of other progenitor populations in diabetes (659).

Over the past two decades, a major focus of angiogenesis research has revolved around the study of BM, circulating and tissue-resident EPCs (115, 119, 571). Unfortunately, this literature has been littered by inconsistencies in the methods used to isolate, culture and characterise these cells, leading to conflicting results and interpretations (660). Nevertheless, across multiple different preclinical and clinical studies, diabetes has consistently been shown to associate with EPC depletion and dysfunction, which in turn is thought to contribute to both impaired neovascularisation and endothelial repair. (552). In one notable study a systematic evaluation of multiple putative EPC subtypes in the peripheral blood of diabetic subjects found extensive reductions in CD133⁺, CD117⁺, CD133⁺ KDR⁺, CD34⁺ CD133⁺ KDR⁺, CD117⁺ KDR⁺ and CD34⁺ CD31⁺ cells (661). Meanwhile, Egan *et al.* reported that the decline in circulating EPC numbers correlates directly with the severity of diabetic complications (662). Others have demonstrated adverse effects of high glucose on EPC

function *in vitro* (663). In rodent models, diabetes-impaired mobilisation of progenitors from BM has been linked to impaired perfusion recovery and neovascularisation in ischaemic tissue (506). Reductions in both cardiac⁺ (664) and circulating c-Kit⁺ progenitors (665) have similarly been related to increased disease severity of diabetic cardiomyopathy. In contrast, not all stem/progenitor populations deplete in diabetic conditions. Some studies have shown that myofibroblast progenitor numbers increased in diabetic patients compared with controls (666), highlighting that such a dysfunction may be selective for cardio- and vasculoprotective progenitors, while there may be a concomitant expansion of circulating cells with pro-remodelling activities (667). To date, no new therapies exist to improve vasculogenic function via stem cells in diabetes and therefore an accurate understanding of EndoMac progenitor function in diabetes is imperative.

6.2.2 EndoMac progenitor origins and tissue heterogeneity

Multiple prior studies have established that tissue MΦs and ECs are both derived from multiple developmental sources and exhibit tissue-specific phenotypic, transcriptomic and functional heterogeneity (73, 74, 108, 668). Traditional views of angiogenesis primarily contended that mature ECs give rise to new blood vessels after birth via sprouting angiogenesis (1). This view has long since shifted to accommodate the involvement of EPCs in postnatal vasculogenesis. EPC-like cells have been identified in blood (30), BM (115) and numerous other tissues (113, 592). Recently, work by Patel, *et al.* has identified a hierarchy of tissue-resident ancestral and mature ECs, including endovascular progenitor cells (EVPs) in heart (551, 669), aorta (113, 670) and skin (119, 312). EVPs display a hierarchical differentiation capacity whereby they form transiently active (TA) ECs (CD45⁻CD144⁺CD34⁺CD31^{lo}VEGF^{lo}) and then mature differentiated ECs (CD45⁻CD144⁺CD34⁺CD31^{hi}VEGF^{hi}). Interestingly, these cells have also been shown to have fibroblastic potential, mediated by transforming growth factor-β, Notch signalling and this may underpin some of the mechanisms by which tissues undergo endothelial-to-mesenchymal transformation under

different pathophysiological states (671). However, to the best of our knowledge EVPs are not yet known to possess haematopoietic potential, nor has their precise ontogeny been elucidated.

As described above, YS EMPs recently were proposed by Plein *et al.* as a rather surprising candidate for the origins of tissue-resident ECs (108). Although disputed by a subsequent study by Feng and colleagues (109), our own lineage-mapping data across numerous experiments in different tissues also supports CSF1R⁺ (and CX₃CR1⁺) YS progenitors as a source of both embryonic and postnatal ECs (522). Adding to this, here we observed a substantial contribution from YS EMPs to tissue ECs in both skin wounds and ischaemic SkM, especially during the later angiogenic and remodelling phases of repair (day 7 and beyond) in non-diabetic mice. Similarly, in both skin and SkM, we confirmed that CSF1R⁺ YS EMPs also contribute to the pool of tissue MΦs, in keeping with numerous previous studies (28, 37, 41, 52).

Our previous and current findings (see Chapter 3) show that the selective generation of CFU-M from "non-haematopoietic" tissues arises from undifferentiated progenitors rather than proliferating monocytes or MΦs (522). We have demonstrated that these progenitors can renew themselves clonally *in vitro* without changing their immunophenotype, while after *in vitro* and *in vivo* differentiation, a fraction of progenitors also retain their "undifferentiated" surface phenotype. This suggests that these cells have the requisite capacity for self-maintenance and amplification, as well as the ability to phenotypically convert into mature daughter cells. The depletion of EndoMac progenitors in different diabetic tissues may be through increased apoptosis (not studied here) or loss of their proliferative and self-renewal properties as a result of hyperglycaemia. The latter was observed in each of our studies for aorta, skin and SkM. Whether it relates to the metabolic and mitochondrial changes we also observed still needs to be determined.

Although Chapter 3 demonstrated surface marker uniformity for EndoMac progenitors across three different tissues, this was not the case for all their properties (**Table 6.1**). Bulk RNA sequencing indicated that despite considerable transcriptional homogeneity, around 0.14% of the genes identified showed varied expression levels between culture-derived progenitors from different tissue sources. Of note, SkM and skin progenitors exhibited the greatest number of genes that were differentially expressed with one another. In particular, genes involved in scavenger receptor and metallopeptidase activities, including collagen fibril organisation and catabolic process, receptor mediated endocytosis and axon guidance were downregulated in SkM compared to skin cells.

We speculate that these tissue-related variations in progenitor function and gene expression, may in turn contribute to the tissue-specific heterogeneity that is well described for both MΦs and ECs (75, 545, 555). Although not studied in this thesis, we have previously established that EndoMac progenitors selectively contribute to the subpopulation of tissue-resident LYVE-1⁺MHCII^{-Lo} MΦs in both skin and SkM. Importantly, this subset has been consistently linked to YS/embryonic ontogeny in other studies (71, 73, 75). In each experiment carried out here, I incorporated a panel of surface markers that captures the heterogenous subpopulations of MΦs for the three tissues studied. These will be analysed in the future to see if diabetes also alters the commitment of YS EMPs and EndoMac progenitors into different MΦ subtypes.

Similarly, our previous work has indicated that EndoMac progenitors produce both vascular and lymphatic ECs, that not only express CD31 and CD144, but also VEGFR2, TIE2 and in the case of lymphatics, LYVE-1 (522). The effects of diabetes on the differentiation of progenitors into different EC subtypes also now needs close examination. We are especially interested in potential overlaps

between EndoMac progenitors and the hierarchy of locally resident EVPs, TA ECs and mature differentiated ECs, elucidated by Patel and co-workers (119, 312). We have begun to explore this for the experiments performed in this thesis, including the transfer of GFP⁺ SkM progenitors into diabetic ischaemic hind limbs. Preliminary analysis supports the existence of these three endothelial subpopulations in recovering SkM at day 14 post-ischaemia (**Figure 6.4A-D**). However, so far have only found that transplanted EndoMac progenitors produced differentiated ECs and not EVPs nor TA ECs (**Figure 6.4E**), suggesting that they are not related.

Table 6.1: Summary of EndoMac progenitor prevalence, stemness and function across three tissues.

Data shown as mean±SD from multiple donor mice

	Aorta	Skin	SkM
Phenotype	LIN ⁻ CD45 ^{+/Lo} CD11b ⁻ F4/80 ⁻ Sca-1 ⁺ c- Kit ⁺ CX ₃ CR1 ⁺ CSF1R ⁺	LIN ⁻ CD45 ^{+/Lo} CD11b ⁻ F4/80 ⁻ Sca-1 ⁺ c- Kit ⁺ CX ₃ CR1 ⁺ CSF1R ⁺	LIN ⁻ CD45 ^{+/Lo} CD11b ⁻ F4/80 ⁻ Sca-1 ⁺ c- Kit ⁺ CX ₃ CR1 ⁺ CSF1R ⁺
Prevalence %	0.3	0.7	0.3
CFU-M yield (x 10 ⁵)	32.4±9.1	101±16.4	53±9.3
2° renewal (%)	14.2±4.3	34±14.2	46.5±14
Number of cords	Least	Some	Most
Cord length (mm)	Most	Some	Least
Branch points	Least	Some	Most
Oxygen consumption	Low	Low	High

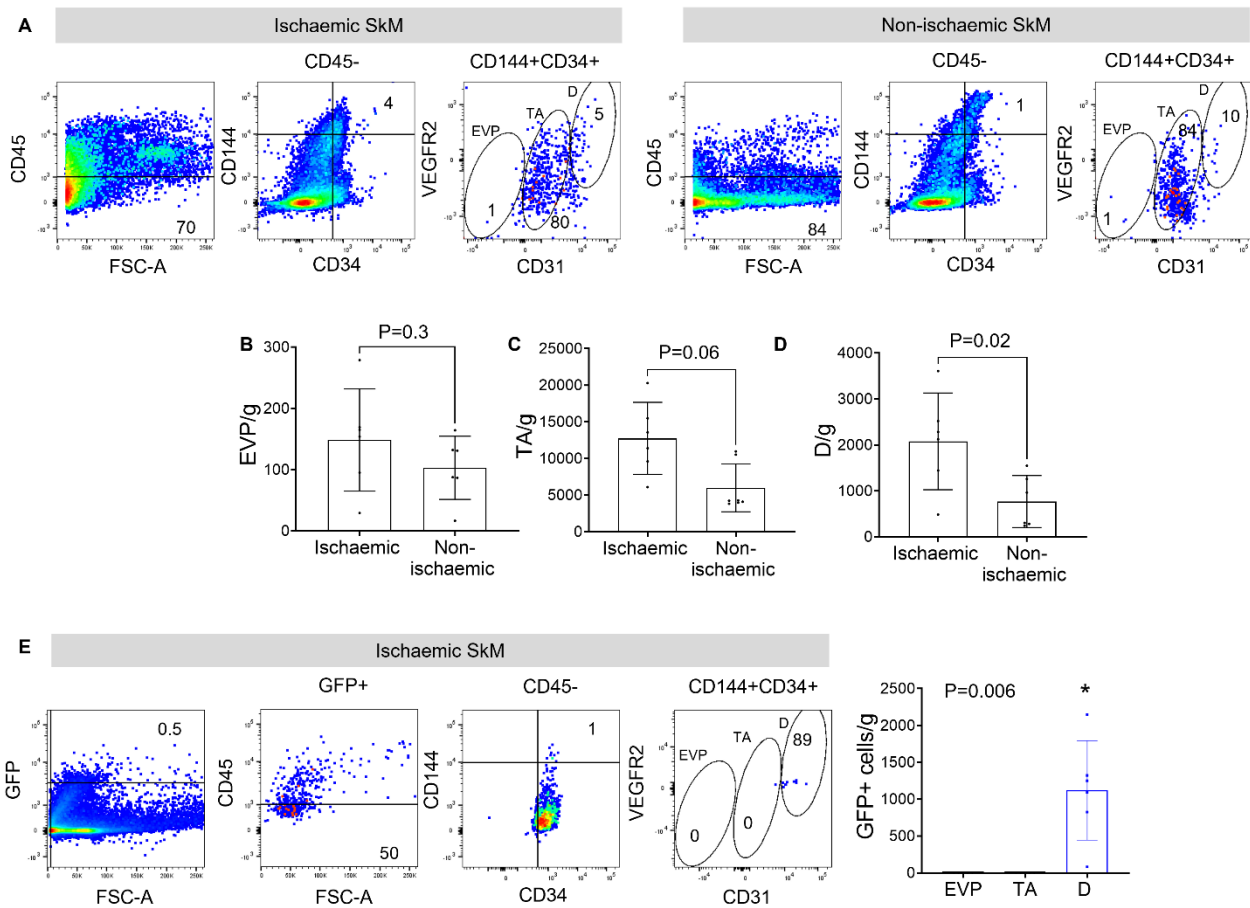


Figure 6.4: EndoMac progenitors produced differentiated ECs but not EVPs at Day 14 post-ischaemia.

A) Flow cytometry plots show endothelial cell hierarchy in ischaemic (left) and non-ischaemic SkM (right): Endovascular progenitors (EVP) ($CD45^-CD144^+CD34^+CD31^{neg}VEGF^{neg}$), transiently active (TA) ($CD45^-CD144^+CD34^+CD31^{lo}VEGF^{lo}$), mature differentiated (D) ECs ($CD45^-CD144^+CD34^+CD31^{hi}VEGF^{hi}$). Representative flow plots are from STZ+ recipient C57BL/6 ischaemic SkM at D14 that received GFP⁺ CFU-M from STZ- donor UBI-GFP mice and non-ischaemic SkM. Representative of n=6/gp.

B-D) Graphs show number of **B)** EVP **C)** TA and **D)** D ECs per gram of SkM from STZ+ recipient C57BL/6 ischaemic and non-ischaemic SkM at D14. Paired t-test, n=6/gp

E) Flow cytometry plots show gating for GFP⁺ cells that are Endovascular progenitors (EVP), transiently active (TA) and differentiated (D) ECs. Ischaemic SkM from STZ+ recipient C57BL/6 at D14 that received GFP⁺ CFU-M from STZ- donor UBI-GFP mice. Representative of n=6/gp. Graph shows number of GFP⁺ cells that are Endovascular progenitors (EVP), transiently active (TA) and differentiated (D) ECs per gram of ischaemic SkM. P=0.006, One-way repeated measures ANOVA, n=6.

6.2.3 Mitochondrial and metabolic function of EndoMac progenitors

Aside from inherited mitochondrial diseases, alterations in mitochondrial function and/or ultrastructure occur in many other conditions, ranging from “normal” ageing to cancer and various systemic and organ-specific chronic diseases (585, 672, 673). Oxidative stress and mitochondrial dysfunction are hallmarks of diabetes and its complications (224, 584, 607, 620). This results in excess oxidation of proteins, lipids, and DNA, as evidenced by increased levels of 15-F2t-iso-prostaglandin and 4-Hydroxynonenal (4-HNE) as lipid oxidation products, and advanced oxidation protein products, advanced glycation end products (AGEs), excess oxidative DNA damage (8-OHdG) and upregulated NADPH oxidase (566, 584, 674). In keeping with this, we found that exposure to high glucose caused significant changes in DNA integrity (double-stranded breaks) in EndoMac progenitors from all tissue sources studied.

Except for aortic progenitors, exposure to high glucose *in vitro* and hyperglycaemia *in vivo* also led to a significant decline in mitochondrial mass for skin and SkM progenitors (**Table 6.2**). Previous studies have reported a similar effect for other types of stem/progenitor and mature cells, although the exact mechanism underlying this is not clearly understood (192, 640). It is also unclear whether mitochondrial dysfunction in diabetic cells occurs primarily due to lower biogenesis of mitochondria, impaired mitochondrial viability or reduced intrinsic function. In the case of EndoMac progenitors, inner membrane potential was significantly disturbed, as seen by a decline in Mitotracker™ red uptake. Impaired membrane potential halts electron transport chain (ETC) activity and movement of H⁺ ions through ATP synthase (also called complex V) into the mitochondrial matrix that triggers ATP production (187). Hence this may be an indirect indicator of an impaired oxidative phosphorylation process occurring in diabetic progenitors. The lack of significant mitochondrial impairment for aortic progenitors could simply be due to the small sample size used in those experiments in Chapter 3. Alternatively, it may hint at important tissue-specific differences in the

metabolic susceptibility of progenitors to the high glucose environment. Conversely, oxygen consumption was decreased for progenitors from all three tissue sources, indicating that high glucose does disturb aerobic respiration and oxidative phosphorylation consistently.

Further investigations are now required to delve deeper into the metabolic differences between diabetic and non-diabetic EndoMac progenitors, including their mechanistic basis and how they are influenced by tissue niche, disease setting, age and even gender. Previous research has shown that diabetes disrupts the traditional pathways of cellular energy production, specifically the production of mitochondrial superoxide (233, 234, 483). Excess glucose is oxidised rapidly in the Krebs cycle in cells exposed to chronic hyperglycaemia, increasing the quantity of accessible electron donors (NADH and FADH₂) to the ETC. As a result, a voltage gradient across the mitochondrial membrane occurs, preventing electron transport inside the mitochondria. Electrons are sent to coenzyme Q, which then donates extra electrons to oxygen, resulting in superoxide. Superoxide is harmful to mitochondria and promotes the build-up of upstream glycolytic byproducts, reducing the cell's normal glycolytic capability (192, 200, 469, 604). This excessive production of superoxide was detected in both skin and SkM EndoMac progenitors in our studies, which may in turn exacerbate mitochondrial dysfunction (**Table 6.2**). Due to experimental and technical error, the results for superoxide production from aortic progenitors were excluded from this thesis and will require re-staining and analysis in the future.

The results of the Seahorse assay indicated that high glucose attenuates both aerobic and glycolytic respiration for aortic, skin and SkM progenitors. For skin and SkM progenitors, we also investigated their dependence on mitochondrial ATP-synthase activity for energy production by inhibiting complex V activity. Our data show that exposure to hyperglycaemia caused a significant decline in

this dependence suggesting that the cells were either in a perpetually low energy state due to a lack of mitochondrial oxidative phosphorylation or that alternative ATP production pathways were being utilised. Another indicator of mitochondrial dysfunction was the finding of decreased maximal respiration capacity for cells from diabetic mice. Uncoupling of the mitochondria following a period of ATP synthase inhibition would be expected to trigger a rapid use of oxygen to overcome the loss of energy and to supply the demand (675), which was the case for non-diabetic EndoMac progenitors. However, the inability of diabetic progenitors to replicate this maximal respiration may also indicate intrinsic electron transport dysfunction.

Taken together, EndoMac progenitors experience substantial mitochondrial dysfunction and oxidative stress under high glucose conditions. While we cannot definitively conclude that this is the primary cause for the diabetes-induced inhibition of the “stemness” properties of these cells, we believe that at the very least it is an important contributor. A greater mechanistic understanding will also require transcriptomic, epigenetic, proteomic and metabolomic profiling of progenitors from diabetic and non-diabetic tissues, which we have begun to prepare samples for.

Table 6.2: Summary of mitochondrial assay results for progenitors from different tissues for non-diabetic (STZ-) and diabetic (STZ+) mice.

All data shown as mean±SD from multiple donor mice. * denotes P<0.05 for comparison between STZ- and STZ+ groups.

	Aorta		SkM		Skin	
	STZ-	STZ+	STZ-	STZ+	STZ-	STZ+
Mitochondrial mass (%)	21.4±12.7	11.2±10.0	0.5±0.2	0.3±0.3	18±6.2	8.6±4.3*
Mitochondrial membrane potential (%)	68±28.8	67.0±11.8	79.9±11.3	44.3±29.1*	89.8±4.3	65.1±24.3*
DNA damage (%)	0.2±0.4	40.5±27.8*	0.7±0.4	2.3±1.5*	0.9±0.5	2.1±1.1*
Superoxide (%)	N/A	N/A	8.2±5.3	25.1±10.0*	14.1±11.1	39.2±12.8*

6.3 Future directions and research areas of interest

6.3.1 Type 2 diabetes

A limitation of this thesis was that the STZ model used to study hyperglycaemia does not recapitulate the complex biology of type 2 diabetes (T2D), which also involves insulin resistance or insensitivity and accounts for 90% of clinical diabetes cases (120). Patients with T2D are often older, more comorbid and more likely to develop diabetic foot ulcers and peripheral arterial disease (350, 514). To study EndoMac progenitors in murine models of T2D will require using other strains, such as genetically obese B6.Cg-*Lep^{ob}*/J or BKS.Cg-*Dock7^m* +/+ *Lepr^{db}*/J mice, or diet induced obese (DIO) mice (676). The latter would involve feeding AKR/J, DBA/2J, BTBR T+ tf/J or C57BL/6 mice a high fat diet for an extended time (676, 677). However, a shortcoming of this model is that diet alone is not sufficient to model all salient features of human T2D, and therefore it often needs to be combined with a series of low-dose STZ injections to cause pancreatic islet cell damage (678). Confirmation of the depletion, functional attenuation and/or metabolic dysfunction of EndoMac progenitors in T2D tissues could pave the way to developing and testing therapeutic “rescue” strategies which would provide an important stepping-stone to further human translational studies.

6.3.2 Studying EndoMac progenitors in human skin and muscle

As described above, we have identified EndoMac-like progenitors in human blood vessels and have shown their depletion in diabetes. We have speculated that human skin and SkM may also contain these cells (**Figure 6.5**), and this has been supported by initial experiments in which we have been able to grow CFU-M from single cell digests of skin and SkM from patients with lower limb amputations. Further work is now needed to better characterise the distribution, phenotypic, functional, and transcriptional properties of these human progenitors before examining whether they are subject to similar inhibitory effects of diabetes. This in turn could open new therapeutic avenues

to rescue or enhance the properties of these progenitors to improve tissue perfusion and repair that is otherwise impaired in diabetic patients.

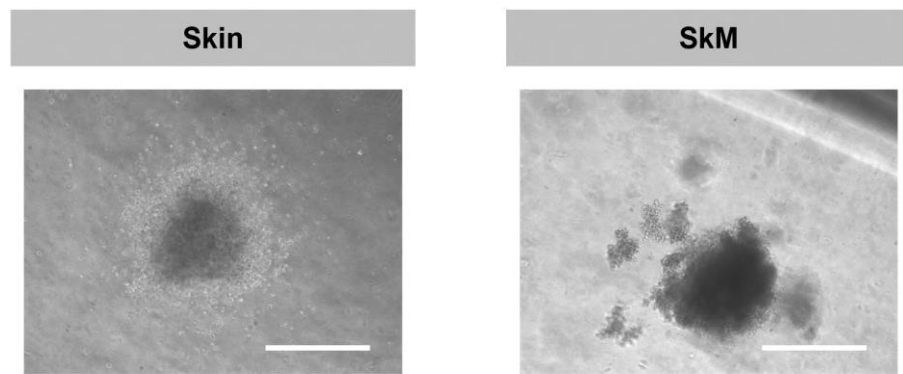


Figure 6.5: Macrophage colony forming units in human skin and skeletal muscle.

The light microscopy shows CFU-M from human skin and skeletal muscle (SkM) digests after 14 d in methylcellulose media. Scale bar 100 μ m, n=1.

6.3.3 EndoMac progenitors as a potential therapy for diabetic tissue repair

Without the support of Mφs, tissue vascularisation is rendered inadequate (679). Therefore, it is not surprising that the field of regenerative medicine has fallen short of its lofty objectives, as attempts to vascularise damaged tissues with EPCs or vascular scaffolds have neglected to target Mφs or exploit their supportive properties (648). The ability to isolate and transplant EndoMac progenitors or promote their endogenous vasculogenic potential could provide new therapeutic options for many prenatal, paediatric and adult health conditions. An important knowledge advance from this thesis is to highlight the reparative function of these cells when obtained from a “healthy”, non-diabetic source and transplanted into the hostile environment of diabetic recipient tissue. Our data firstly demonstrate the ability of healthy progenitors to engraft and differentiate successfully in diabetic tissue, and in the process promote closure of wounds and perfusion recovery of ischaemic muscle. As described in Chapters 4 and 5, we also suspect that some of their benefit may be mediated by indirect or paracrine effects on host cells. Further work is still needed to comprehensively define the scope of benefit and mechanism of action from transplanted progenitors. Ongoing histological and immunofluorescence analysis will help determine how the progenitors affected capillary and arteriolar density and collagen deposition in both models, skin epithelialisation in wounds, and the proliferation of satellite cells and viability of skeletal myocytes in ischaemic hind limbs.

On the other hand, our results also emphasise that the adaptive or salutary properties of EndoMac progenitors are virtually eliminated when isolated from diabetic donor tissues. With an eye to the potential of using these progenitors as a cellular therapy in human studies, we will therefore need to establish whether they can be given allogeneically from healthy, young donors into older, comorbid diabetic recipients without safety concerns or immune rejection. This will depend on being able to show that they are immunoprivileged and able to avoid and/or suppress host immune responses, as is the case for mesenchymal stromal cells (518, 544). Finally, as we obtain data from scRNA-seq

analysis, we also hope to elucidate the genes and signalling pathways that underpin the activity of EndoMac progenitors, including those that become dysregulated in diabetes. This could help identify new molecules that can be targeted pharmacologically or by other approaches to restore or augment endogenous progenitors as a strategy for promoting more efficient tissue repair.

6.3.4 Rescuing EndoMac progenitors by targeting mitochondrial dysfunction

Our results show that dysfunction of murine EndoMac progenitors in diabetes is associated with extensive inhibition of their mitochondrial function, including reductions in mitochondrial mass, membrane function, proton gradients and aerobic respiration, combined with increased oxidative stress. There is much work still to be done on accurately pinpointing metabolic and mitochondrial pathways that underscore these inhibitory effects to help identify how they can be therapeutically reversed. This will also require us to profile the transcriptional and epigenetic changes that occur when EndoMac progenitors are subjected to hyperglycaemia in different tissue and disease environments. Genes involved in cell cycle, self-renewal, angiogenesis, senescence, differentiation plasticity, and mitochondrial and glycolytic pathways of cellular metabolism are all of interest. Identification of dysregulated metabolic genes (e.g., *Pdk4* which encodes the mitochondrial enzyme Pyruvate dehydrogenase lipoamide kinase isozyme 4, a key player in cellular metabolism under altered glucose conditions (680), or metabolic sensors, such as Histone modifying enzymes (681)) could lead to finding specific pathways that can be targeted to restore mitochondrial respiration and progenitor "stemness".

There are already several pharmacological candidates that could be repurposed to restore the metabolic dysfunction of EndoMac progenitors under high glucose conditions. This includes antioxidants to decrease superoxide damage and other drugs known to enhance mitochondrial

biogenesis and/or ETC function, “buffer” cellular energy or cellular restore nitric oxide production (**Table 6.3**). These agents could be tested on progenitors *in vitro* for their effects on clonal expansion and renewal, angiogenesis, differentiation, metabolic function, and mitochondrial health, before investigating those with the most promising results in diabetic wound injury and ischaemia models *in vivo*.

Table 6.3: Table summarises different classes of potential drug candidates to address metabolic and mitochondrial dysfunction.

Target	Drug	Function	References
Electron transport chain function	Thiamine	Vitamin B. Increases the activity of pyruvate dehydrogenase, thus enhances the oxidative decomposition of pyruvate.	Sato <i>et al.</i> (682)
	Idebenone	Analogue of ubiquinone that restores electron flow and facilitates oxidative phosphorylation.	Klopstock <i>et al.</i> (683)
Energy buffering	Creatine monohydrate	Improves aerobic and anaerobic cellular metabolism.	Tarnopolsky <i>et al.</i> (684)
Antioxidants	Vitamin E	Reduces the toxicity of excessive reactive oxygen species (ROS).	Enns <i>et al.</i> (685)
	Vitamin C	Reduces the toxicity of excessive ROS.	Enns <i>et al.</i> (685)
	MitoQ	Prevents mitochondrial oxidative damage.	Ji <i>et al.</i> (250)
	Lipoic acid	Reduces plasma lactic acid content and oxidative stress markers.	Marangon <i>et al.</i> (686)
	Cysteamine	Eliminates excessive ROS production by restoring the level of glutathione.	Besouw <i>et al.</i> (687)
	Synthetic analogue of vitamin E- EPI-743	Prevents excessive ROS production by affecting the redox state of intracellular glutathione.	Enns <i>et al.</i> (688)
	Citrulline and Arginine	Restores NO deficiency in mitochondria and restore energy production.	Koga <i>et al.</i> (689)
Enhancing mitochondrial biogenesis	RTA 408	Increases the activity of the nuclear respiratory factor 2 (Nrf 2), a downstream effector of PGC-1 α . PGC-1 α a transcriptional co-activator known as the master regulator of mitochondrial biogenesis. In turn increases energy production	Rai <i>et al.</i> (690)

6.4 Conclusion

Mitigating the devastating burden of diabetic ulcers and limb-threatening ischaemia requires new therapeutic strategies that target the key mediators of inflammation and angiogenesis for more effective tissue repair and vascularisation. This thesis provides insights into the profound inhibitory effects of high glucose on the prevalence, functional and metabolic properties of YS-derived, tissue-resident EndoMac progenitor cells. Their diminished contribution to local MΦ and EC populations during the repair of diabetic skin wounds and ischaemic SkM may help explain the ineffective neovascularisation that is a hallmark of injured diabetic tissues. Importantly, we have also demonstrated the salutary properties of non-diabetic EndoMac progenitors which could be harnessed in the future as a therapeutic strategy for promoting diabetic wound healing and ischaemic reperfusion.

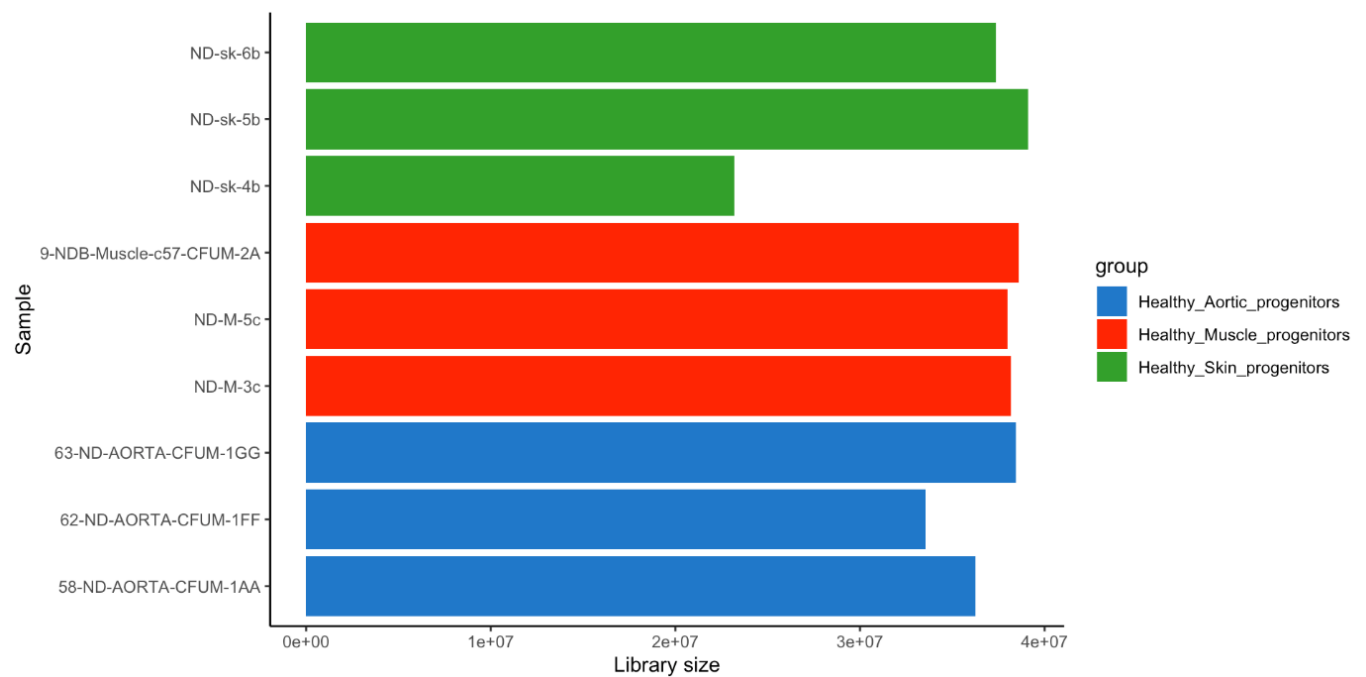
7. Appendices

A. <https://universityofadelaide.box.com/s/eci9s3glb1u6cbpudn8227v7syo2vw2d>

B. <https://universityofadelaide.box.com/s/u3onlx07tezu0xxlexk9e7h8k5tz6qj1>

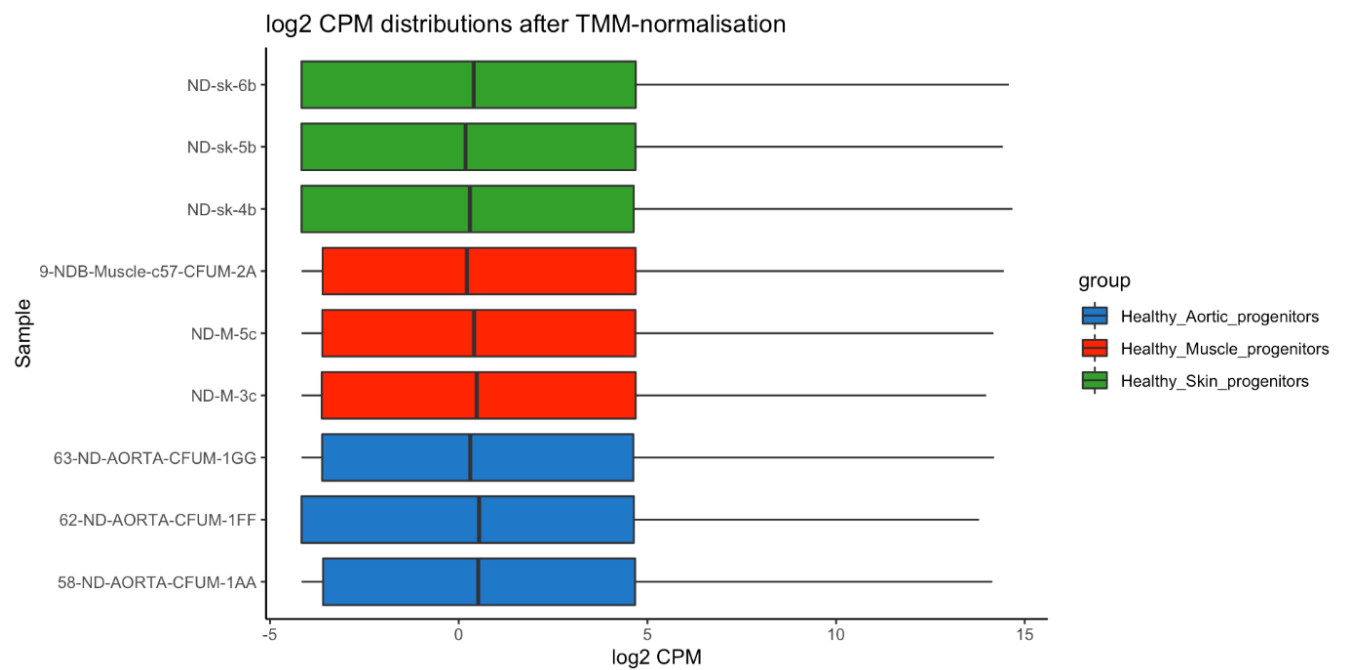
Appendix 7.1: Raw data files for bulk-sequencing analysis

A) The raw data files containing the list of genes analysed from RNA bulk sequencing. Transcriptomic data are separated into three comparison groups of cultured EndoMac progenitors: aorta vs SkM, aorta vs skin and SkM vs skin. **B)** The link contains the data files with differential gene expression analysis and bioinformatic analysis. *For Chapter 3- figure 3.7*



Appendix 7.2: Library sizes of samples analysed by RNASeq.

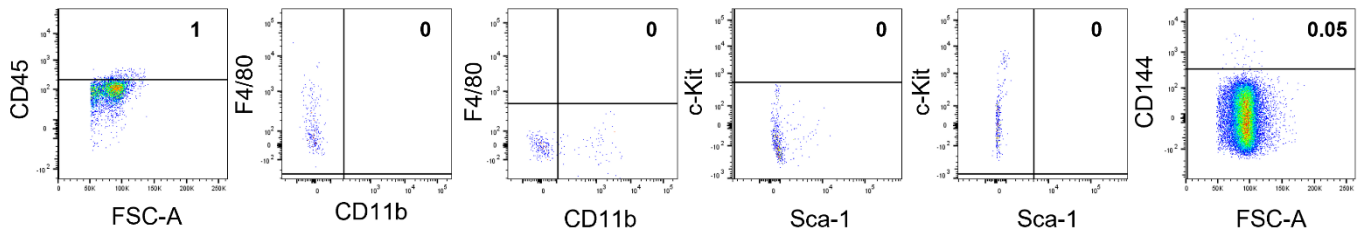
The bar graph shows mostly consistent library sizes across samples except one sample (ND-Sk-4b) generated lower reads (23M). *For Chapter 3- figure 3.5 and 3.6*



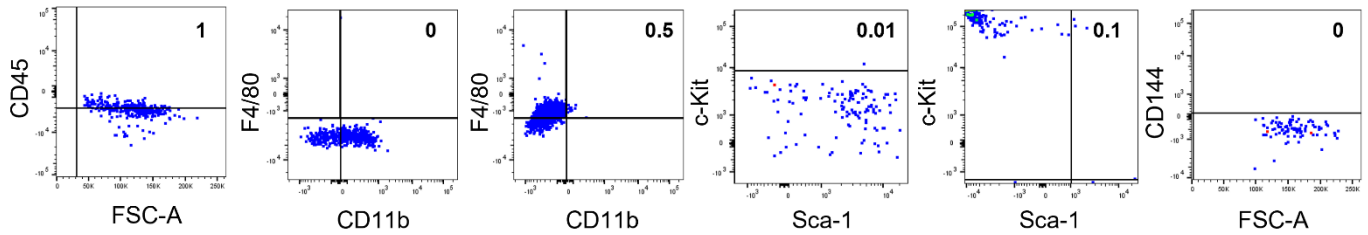
Appendix 7.3: Normalised counts distribution.

Bar graph shows consistent log transformed counts per million (Log_2 CPM) across samples after normalisation for variation in library sizes. *For Chapter 3- figure 3.5 and 3.6,*

FMO for STZ- and STZ+ skin and SkM tissue



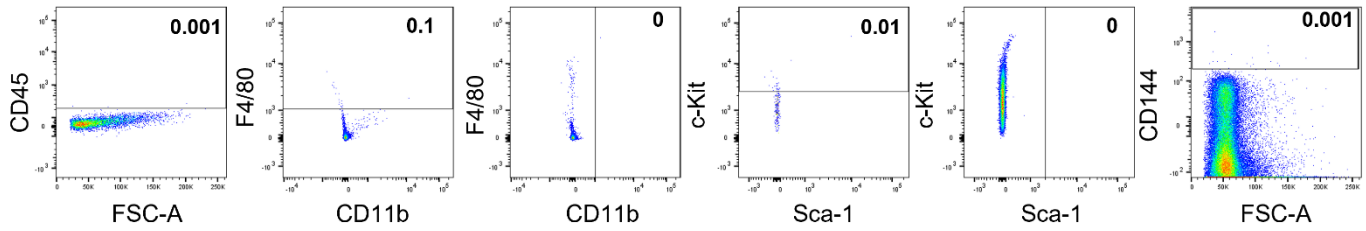
FMO for STZ- and STZ+ skin and SkM Matrigel



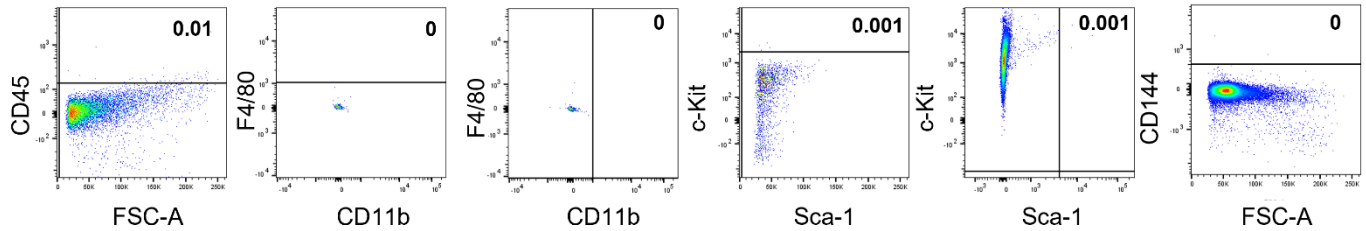
Appendix 7.4: Fluorescence minus one control for STZ- and STZ+ skin and SkM fresh tissue and Matrigel

The flow cytometry plots showing gating strategy of fluorescence minus one (FMO) controls of each marker for C57BL/6 STZ- and STZ+ skin and SkM fresh tissue (top) and Matrigel (bottom). Numbers on plots show frequency (%), n=1. For Chapter 4, 5 – figure 4.4, 4.7, 5.5 and 5.8

FMO for STZ- and STZ+ *Csf1r*^{Mer-iCre-Mer} x *Rosa*^{mT/mG} wounds

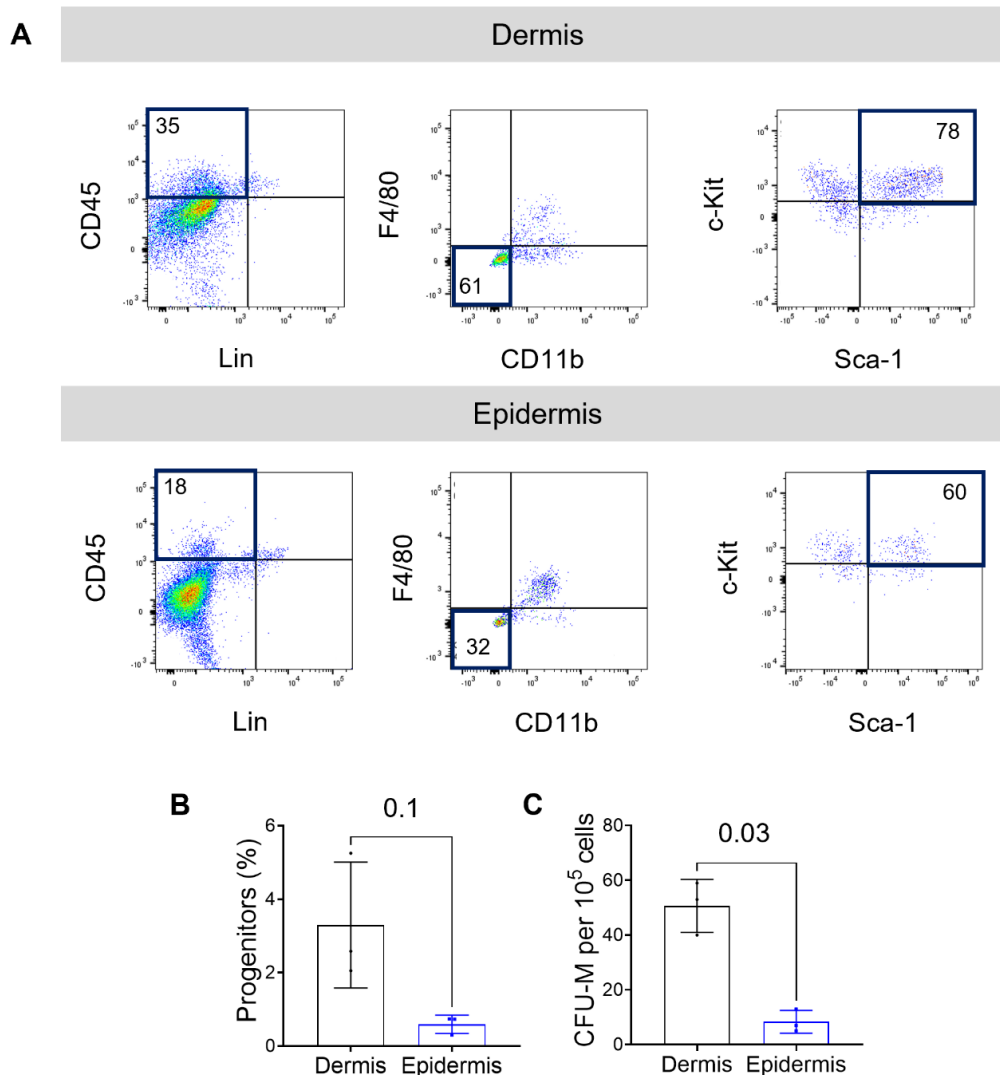


FMO for STZ- and STZ+ *Csf1r*^{Mer-iCre-Mer} x *Rosa*^{mT/mG} hindlimb ischaemic SkM



Appendix 7.5: Fluorescence minus one control for STZ- and STZ+ wounds and hind limb ischaemia SkM

The flow cytometry plots showing gating strategy of fluorescence minus one (FMO) controls of each marker for STZ- and STZ+ wounds (top) and hind limb ischaemia SkM tissue (bottom) from TAM induced *Csf1r*^{Mer-iCre-Mer} x *Rosa*^{mT/mG} mice. Numbers on plots show frequency (%), n=1. For Chapter 4, 5 – figure 4.10, 4.11, 5.10 and 5.11



Appendix 7.6: EndoMac progenitors are largely prevalent in skins dermis than the epidermis.

A) Flow cytometry showing expression of dermal (top) and epidermal (bottom) CD45⁺CD11b⁺F4/80⁻c-Kit⁺Sca-1⁺ EndoMac progenitors from C57BL/6 mice. Numerical values in dot plots represent mean percentages from n=3/gp.

B) Frequency graphs show comparisons of progenitor cells in dermis and epidermis in skin of C57BL/6 mice. n=3, paired t-test

C) Graph shows CFU-M yield per 10⁵ cells plated from dermis and epidermis isolated from C57BL/6 mice skin. n=3, paired t test

Data for chapter 4 discussion

8. References

1. Carmeliet P. Angiogenesis in health and disease. *Nat Med.* 2003;9(6):653-60.
2. Goldie LC, Nix MK, Hirschi KK. Embryonic vasculogenesis and hematopoietic specification. *Organogenesis.* 2008;4(4):257-63.
3. Heil M, Eitenmuller I, Schmitz-Rixen T, Schaper W. Arteriogenesis versus angiogenesis: similarities and differences. *J Cell Mol Med.* 2006;10(1):45-55.
4. del Toro R, Prahst C, Mathivet T, Siegfried G, Kaminker JS, Larrivee B, et al. Identification and functional analysis of endothelial tip cell-enriched genes. *Blood.* 2010;116(19):4025-33.
5. Gerhardt H, Betsholtz C. Endothelial-pericyte interactions in angiogenesis. *Cell Tissue Res.* 2003;314(1):15-23.
6. Corliss BA, Azimi MS, Munson JM, Peirce SM, Murfee WL. Macrophages: An Inflammatory Link Between Angiogenesis and Lymphangiogenesis. *Microcirculation.* 2016;23(2):95-121.
7. Elhelu MA. The role of macrophages in immunology. *J Natl Med Assoc.* 1983;75(3):314-7.
8. Yanez DA, Lacher RK, Vidyarthi A, Colegio OR. The role of macrophages in skin homeostasis. *Pflugers Arch.* 2017;469(3-4):455-63.
9. Fantin A, Vieira JM, Gestri G, Denti L, Schwarz Q, Prykhodzhiy S, et al. Tissue macrophages act as cellular chaperones for vascular anastomosis downstream of VEGF-mediated endothelial tip cell induction. *Blood.* 2010;116(5):829-40.
10. Squadrito ML, De Palma M. Macrophage regulation of tumor angiogenesis: implications for cancer therapy. *Mol Aspects Med.* 2011;32(2):123-45.
11. Kalucka J, Bierhansl L, Wielockx B, Carmeliet P, Eelen G. Interaction of endothelial cells with macrophages-linking molecular and metabolic signaling. *Pflugers Arch.* 2017;469(3-4):473-83.
12. Sierra JR, Corso S, Caione L, Cepero V, Conrotto P, Cignetti A, et al. Tumor angiogenesis and progression are enhanced by Sema4D produced by tumor-associated macrophages. *J Exp Med.* 2008;205(7):1673-85.
13. Tamagnone L. Emerging role of semaphorins as major regulatory signals and potential therapeutic targets in cancer. *Cancer Cell.* 2012;22(2):145-52.
14. Kubota Y, Takubo K, Shimizu T, Ohno H, Kishi K, Shibuya M, et al. M-CSF inhibition selectively targets pathological angiogenesis and lymphangiogenesis. *J Exp Med.* 2009;206(5):1089-102.
15. Tusavitz S, Keonela S, Kalkstein M, McCormick S, Gasser B, Arrigale M, et al. Macrophage-derived Wnt signaling increases endothelial permeability during skeletal muscle injury. *Inflamm Res.* 2020;69(12):1235-44.
16. Lobov IB, Rao S, Carroll TJ, Vallance JE, Ito M, Ondr JK, et al. WNT7b mediates macrophage-induced programmed cell death in patterning of the vasculature. *Nature.* 2005;437(7057):417-21.
17. Kishore A, Petrek M. Roles of Macrophage Polarization and Macrophage-Derived miRNAs in Pulmonary Fibrosis. *Front Immunol.* 2021;12:678457.
18. He H, Xu J, Warren CM, Duan D, Li X, Wu L, et al. Endothelial cells provide an instructive niche for the differentiation and functional polarization of M2-like macrophages. *Blood.* 2012;120(15):3152-62.
19. Baer C, Squadrito ML, Iruela-Arispe ML, De Palma M. Reciprocal interactions between endothelial cells and macrophages in angiogenic vascular niches. *Exp Cell Res.* 2013;319(11):1626-34.
20. Naito H, Iba T, Takakura N. Mechanisms of new blood-vessel formation and proliferative heterogeneity of endothelial cells. *Int Immunol.* 2020;32(5):295-305.
21. Canu G, Ruhrberg C. First blood: the endothelial origins of hematopoietic progenitors. *Angiogenesis.* 2021;24(2):199-211.
22. Cohen J. Embryology. Embryo development at the click of a mouse. *Science.* 2002;297(5587):1629.
23. Sabin FR. Preliminary note on the differentiation of angioblasts and the method by which they produce blood-vessels, blood-plasma and red blood-cells as seen in the living chick. 1917. *J Hematother Stem Cell Res.* 2002;11(1):5-7.
24. Palis J, Robertson S, Kennedy M, Wall C, Keller G. Development of erythroid and myeloid progenitors in the yolk sac and embryo proper of the mouse. *Development.* 1999;126(22):5073-84.
25. Takahashi K, Yamamura F, Naito M. Differentiation, maturation, and proliferation of macrophages in the mouse yolk sac: a light-microscopic, enzyme-cytochemical, immunohistochemical, and ultrastructural study. *J Leukoc Biol.* 1989;45(2):87-96.

26. Ginhoux F, Greter M, Leboeuf M, Nandi S, See P, Gokhan S, et al. Fate mapping analysis reveals that adult microglia derive from primitive macrophages. *Science*. 2010;330(6005):841-5.
27. Bertrand JY, Jalil A, Klaine M, Jung S, Cumano A, Godin I. Three pathways to mature macrophages in the early mouse yolk sac. *Blood*. 2005;106(9):3004-11.
28. Gomez Perdiguero E, Klapproth K, Schulz C, Busch K, Azzoni E, Crozet L, et al. Tissue-resident macrophages originate from yolk-sac-derived erythro-myeloid progenitors. *Nature*. 2015;518(7540):547-51.
29. Ginhoux F, Williams M. Tissue-Resident Macrophage Ontogeny and Homeostasis. *Immunity*. 2016;44(3):439-49.
30. Pardanaud L, Luton D, Prigent M, Bourcheix LM, Catala M, Dieterlen-Lievre F. Two distinct endothelial lineages in ontogeny, one of them related to hemopoiesis. *Development*. 1996;122(5):1363-71.
31. Lacaud G, Kouskoff V. Hemangioblast, hemogenic endothelium, and primitive versus definitive hematopoiesis. *Exp Hematol*. 2017;49:19-24.
32. de Bruijn MF, Speck NA, Peeters MC, Dzierzak E. Definitive hematopoietic stem cells first develop within the major arterial regions of the mouse embryo. *EMBO J*. 2000;19(11):2465-74.
33. Orkin SH, Zon LI. Hematopoiesis: an evolving paradigm for stem cell biology. *Cell*. 2008;132(4):631-44.
34. Hoeffel G, Ginhoux F. Fetal monocytes and the origins of tissue-resident macrophages. *Cell Immunol*. 2018;330:5-15.
35. Frame JM, McGrath KE, Palis J. Erythro-myeloid progenitors: "definitive" hematopoiesis in the conceptus prior to the emergence of hematopoietic stem cells. *Blood Cells Mol Dis*. 2013;51(4):220-5.
36. Hoeffel G, Chen J, Lavin Y, Low D, Almeida FF, See P, et al. C-Myb(+) erythro-myeloid progenitor-derived fetal monocytes give rise to adult tissue-resident macrophages. *Immunity*. 2015;42(4):665-78.
37. Schulz C, Gomez Perdiguero E, Chorro L, Szabo-Rogers H, Cagnard N, Kierdorf K, et al. A lineage of myeloid cells independent of Myb and hematopoietic stem cells. *Science*. 2012;336(6077):86-90.
38. Samokhvalov IM, Samokhvalova NI, Nishikawa S. Cell tracing shows the contribution of the yolk sac to adult haematopoiesis. *Nature*. 2007;446(7139):1056-61.
39. Fantin A, Tacconi C, Villa E, Ceccacci E, Denti L, Ruhrberg C. KIT Is Required for Fetal Liver Hematopoiesis. *Front Cell Dev Biol*. 2021;9:648630.
40. Hoeffel G, Wang Y, Greter M, See P, Teo P, Malleret B, et al. Adult Langerhans cells derive predominantly from embryonic fetal liver monocytes with a minor contribution of yolk sac-derived macrophages. *J Exp Med*. 2012;209(6):1167-81.
41. Mass E, Ballesteros I, Farlik M, Halbritter F, Gunther P, Crozet L, et al. Specification of tissue-resident macrophages during organogenesis. *Science*. 2016;353(6304).
42. Stremmel C, Schuchert R, Wagner F, Thaler R, Weinberger T, Pick R, et al. Yolk sac macrophage progenitors traffic to the embryo during defined stages of development. *Nat Commun*. 2018;9(1):75.
43. Ciau-Uitz A, Walmsley M, Patient R. Distinct origins of adult and embryonic blood in *Xenopus*. *Cell*. 2000;102(6):787-96.
44. PDF. M. The development in vitro of blood of early chick embryo. . *Proc R Soc Lond Biol Sci*. 1932;111:497-521.
45. Hadland BK, Varnum-Finney B, Poulos MG, Moon RT, Butler JM, Rafii S, et al. Endothelium and NOTCH specify and amplify aorta-gonad-mesonephros-derived hematopoietic stem cells. *J Clin Invest*. 2015;125(5):2032-45.
46. Kumar A, D'Souza SS, Thakur AS. Understanding the Journey of Human Hematopoietic Stem Cell Development. *Stem Cells Int*. 2019;2019:2141475.
47. Rybtsov S, Sobiesiak M, Taoudi S, Souilhol C, Senserrich J, Liakhovitskaia A, et al. Hierarchical organization and early hematopoietic specification of the developing HSC lineage in the AGM region. *J Exp Med*. 2011;208(6):1305-15.
48. Wu Y, Hirschi KK. Tissue-Resident Macrophage Development and Function. *Front Cell Dev Biol*. 2020;8:617879.
49. Mikkola HK, Fujiwara Y, Schlaeger TM, Traver D, Orkin SH. Expression of CD41 marks the initiation of definitive hematopoiesis in the mouse embryo. *Blood*. 2003;101(2):508-16.

50. Cortegano I, Serrano N, Ruiz C, Rodriguez M, Prado C, Alia M, et al. CD45 expression discriminates waves of embryonic megakaryocytes in the mouse. *Haematologica*. 2019;104(9):1853-65.
51. McGrath KE, Frame JM, Fromm GJ, Koniski AD, Kingsley PD, Little J, et al. A transient definitive erythroid lineage with unique regulation of the beta-globin locus in the mammalian embryo. *Blood*. 2011;117(17):4600-8.
52. Perdiguero EG, Geissmann F. The development and maintenance of resident macrophages. *Nat Immunol*. 2016;17(1):2-8.
53. McGrath KE, Frame JM, Fegan KH, Bowen JR, Conway SJ, Catherman SC, et al. Distinct Sources of Hematopoietic Progenitors Emerge before HSCs and Provide Functional Blood Cells in the Mammalian Embryo. *Cell Rep*. 2015;11(12):1892-904.
54. Bowie MB, McKnight KD, Kent DG, McCaffrey L, Hoodless PA, Eaves CJ. Hematopoietic stem cells proliferate until after birth and show a reversible phase-specific engraftment defect. *J Clin Invest*. 2006;116(10):2808-16.
55. Morrison SJ, Hemmati HD, Wandycz AM, Weissman IL. The purification and characterization of fetal liver hematopoietic stem cells. *Proc Natl Acad Sci U S A*. 1995;92(22):10302-6.
56. Wolber FM, Leonard E, Michael S, Orschell-Traycoff CM, Yoder MC, Srouf EF. Roles of spleen and liver in development of the murine hematopoietic system. *Exp Hematol*. 2002;30(9):1010-9.
57. Freyer L IL, Biton A, Perdiguero EG. Overlapping Definitive Progenitor Waves Divide and Conquer to Build a Layered Hematopoietic System. 2020.
58. Lavin Y, Mortha A, Rahman A, Merad M. Regulation of macrophage development and function in peripheral tissues. *Nat Rev Immunol*. 2015;15(12):731-44.
59. van Furth R, Cohn ZA, Hirsch JG, Humphrey JH, Spector WG, Langevoort HL. The mononuclear phagocyte system: a new classification of macrophages, monocytes, and their precursor cells. *Bull World Health Organ*. 1972;46(6):845-52.
60. Merad M, Sathe P, Helft J, Miller J, Mortha A. The dendritic cell lineage: ontogeny and function of dendritic cells and their subsets in the steady state and the inflamed setting. *Annu Rev Immunol*. 2013;31:563-604.
61. Mildner A, Yona S, Jung S. A close encounter of the third kind: monocyte-derived cells. *Adv Immunol*. 2013;120:69-103.
62. Passlick B, Flieger D, Ziegler-Heitbrock HW. Identification and characterization of a novel monocyte subpopulation in human peripheral blood. *Blood*. 1989;74(7):2527-34.
63. Ingersoll MA, Spanbroek R, Lottaz C, Gautier EL, Frankenberger M, Hoffmann R, et al. Comparison of gene expression profiles between human and mouse monocyte subsets. *Blood*. 2010;115(3):e10-9.
64. Hettinger J, Richards DM, Hansson J, Barra MM, Joschko AC, Krijgsvelde J, et al. Origin of monocytes and macrophages in a committed progenitor. *Nat Immunol*. 2013;14(8):821-30.
65. Ginhoux F, Jung S. Monocytes and macrophages: developmental pathways and tissue homeostasis. *Nat Rev Immunol*. 2014;14(6):392-404.
66. Auffray C, Fogg D, Garfa M, Elain G, Join-Lambert O, Kayal S, et al. Monitoring of blood vessels and tissues by a population of monocytes with patrolling behavior. *Science*. 2007;317(5838):666-70.
67. Carlin LM, Stamatiades EG, Auffray C, Hanna RN, Glover L, Vizcay-Barrena G, et al. Nr4a1-dependent Ly6C(low) monocytes monitor endothelial cells and orchestrate their disposal. *Cell*. 2013;153(2):362-75.
68. Sumner R, Crawford A, Mucenski M, Frampton J. Initiation of adult myelopoiesis can occur in the absence of c-Myb whereas subsequent development is strictly dependent on the transcription factor. *Oncogene*. 2000;19(30):3335-42.
69. Jung S, Aliberti J, Graemmel P, Sunshine MJ, Kreutzberg GW, Sher A, et al. Analysis of fractalkine receptor CX(3)CR1 function by targeted deletion and green fluorescent protein reporter gene insertion. *Mol Cell Biol*. 2000;20(11):4106-14.
70. Hashimoto D, Chow A, Noizat C, Teo P, Beasley MB, Leboeuf M, et al. Tissue-resident macrophages self-maintain locally throughout adult life with minimal contribution from circulating monocytes. *Immunity*. 2013;38(4):792-804.

71. Ensan S, Li A, Besla R, Degousee N, Cosme J, Roufaiel M, et al. Self-renewing resident arterial macrophages arise from embryonic CX3CR1(+) precursors and circulating monocytes immediately after birth. *Nat Immunol.* 2016;17(2):159-68.
72. Kolter J, Feuerstein R, Zeis P, Hagemeyer N, Paterson N, d'Errico P, et al. A Subset of Skin Macrophages Contributes to the Surveillance and Regeneration of Local Nerves. *Immunity.* 2019;50(6):1482-97 e7.
73. Epelman S, Lavine KJ, Beaudin AE, Sojka DK, Carrero JA, Calderon B, et al. Embryonic and adult-derived resident cardiac macrophages are maintained through distinct mechanisms at steady state and during inflammation. *Immunity.* 2014;40(1):91-104.
74. Wong NR, Mohan J, Kopecky BJ, Guo S, Du L, Leid J, et al. Resident cardiac macrophages mediate adaptive myocardial remodeling. *Immunity.* 2021;54(9):2072-88 e7.
75. Wang X, Sathe AA, Smith GR, Ruf-Zamojski F, Nair V, Lavine KJ, et al. Heterogeneous origins and functions of mouse skeletal muscle-resident macrophages. *Proc Natl Acad Sci U S A.* 2020;117(34):20729-40.
76. W. H. Die Häute und Höhlen des Körpers. Akademisches Programm: The British Library. 1865.
77. Vogeli KM, Jin SW, Martin GR, Stainier DY. A common progenitor for haematopoietic and endothelial lineages in the zebrafish gastrula. *Nature.* 2006;443(7109):337-9.
78. Kinder SJ, Tsang TE, Quinlan GA, Hadjantonakis AK, Nagy A, Tam PP. The orderly allocation of mesodermal cells to the extraembryonic structures and the anteroposterior axis during gastrulation of the mouse embryo. *Development.* 1999;126(21):4691-701.
79. Motoike T, Markham DW, Rossant J, Sato TN. Evidence for novel fate of Flk1+ progenitor: contribution to muscle lineage. *Genesis.* 2003;35(3):153-9.
80. Huber TL, Kouskoff V, Fehling HJ, Palis J, Keller G. Haemangioblast commitment is initiated in the primitive streak of the mouse embryo. *Nature.* 2004;432(7017):625-30.
81. Kennedy M, Firpo M, Choi K, Wall C, Robertson S, Kabrun N, et al. A common precursor for primitive erythropoiesis and definitive haematopoiesis. *Nature.* 1997;386(6624):488-93.
82. Robertson SM, Kennedy M, Shannon JM, Keller G. A transitional stage in the commitment of mesoderm to hematopoiesis requiring the transcription factor SCL/tal-1. *Development.* 2000;127(11):2447-59.
83. Kennedy M, D'Souza SL, Lynch-Kattman M, Schwantz S, Keller G. Development of the hemangioblast defines the onset of hematopoiesis in human ES cell differentiation cultures. *Blood.* 2007;109(7):2679-87.
84. Ueno H, Weissman IL. Clonal analysis of mouse development reveals a polyclonal origin for yolk sac blood islands. *Dev Cell.* 2006;11(4):519-33.
85. Choi YS, Gumbiner B. Expression of cell adhesion molecule E-cadherin in *Xenopus* embryos begins at gastrulation and predominates in the ectoderm. *J Cell Biol.* 1989;108(6):2449-58.
86. Fehling HJ, Lacaud G, Kubo A, Kennedy M, Robertson S, Keller G, et al. Tracking mesoderm induction and its specification to the hemangioblast during embryonic stem cell differentiation. *Development.* 2003;130(17):4217-27.
87. Henninger J, Santoso B, Hans S, Durand E, Moore J, Mosimann C, et al. Clonal fate mapping quantifies the number of haematopoietic stem cells that arise during development. *Nat Cell Biol.* 2017;19(1):17-27.
88. Amaya E. The hemangioblast: a state of competence. *Blood.* 2013;122(24):3853-4.
89. Choi K. The hemangioblast: a common progenitor of hematopoietic and endothelial cells. *J Hematother Stem Cell Res.* 2002;11(1):91-101.
90. Eilken HM, Nishikawa S, Schroeder T. Continuous single-cell imaging of blood generation from haemogenic endothelium. *Nature.* 2009;457(7231):896-900.
91. Gentek R, Ghigo C, Hoeffel G, Bulle MJ, Msallam R, Gautier G, et al. Hemogenic Endothelial Fate Mapping Reveals Dual Developmental Origin of Mast Cells. *Immunity.* 2018;48(6):1160-71 e5.
92. Anderson H, Patch TC, Reddy PN, Hagedorn EJ, Kim PG, Soltis KA, et al. Hematopoietic stem cells develop in the absence of endothelial cadherin 5 expression. *Blood.* 2015;126(26):2811-20.
93. Frame JM, Fegan KH, Conway SJ, McGrath KE, Palis J. Definitive Hematopoiesis in the Yolk Sac Emerges from Wnt-Responsive Hemogenic Endothelium Independently of Circulation and Arterial Identity. *Stem Cells.* 2016;34(2):431-44.

94. Yoshimoto M, Porayette P, Glosson NL, Conway SJ, Carlesso N, Cardoso AA, et al. Autonomous murine T-cell progenitor production in the extra-embryonic yolk sac before HSC emergence. *Blood*. 2012;119(24):5706-14.
95. Yoshimoto M, Montecino-Rodriguez E, Ferkowicz MJ, Porayette P, Shelley WC, Conway SJ, et al. Embryonic day 9 yolk sac and intra-embryonic hemogenic endothelium independently generate a B-1 and marginal zone progenitor lacking B-2 potential. *Proc Natl Acad Sci U S A*. 2011;108(4):1468-73.
96. Boisset JC, van Cappellen W, Andrieu-Soler C, Galjart N, Dzierzak E, Robin C. In vivo imaging of haematopoietic cells emerging from the mouse aortic endothelium. *Nature*. 2010;464(7285):116-20.
97. Bertrand JY, Cisson JL, Stachura DL, Traver D. Notch signaling distinguishes 2 waves of definitive hematopoiesis in the zebrafish embryo. *Blood*. 2010;115(14):2777-83.
98. Butko E, Pouget C, Traver D. Complex regulation of HSC emergence by the Notch signaling pathway. *Dev Biol*. 2016;409(1):129-38.
99. Butler JM, Nolan DJ, Vertes EL, Varnum-Finney B, Kobayashi H, Hooper AT, et al. Endothelial cells are essential for the self-renewal and repopulation of Notch-dependent hematopoietic stem cells. *Cell Stem Cell*. 2010;6(3):251-64.
100. Lancrin C, Sroczynska P, Stephenson C, Allen T, Kouskoff V, Lacaud G. The haemangioblast generates haematopoietic cells through a haemogenic endothelium stage. *Nature*. 2009;457(7231):892-5.
101. Fraser ST, Ogawa M, Yu RT, Nishikawa S, Yoder MC, Nishikawa S. Definitive hematopoietic commitment within the embryonic vascular endothelial-cadherin(+) population. *Exp Hematol*. 2002;30(9):1070-8.
102. Ema M, Yokomizo T, Wakamatsu A, Terunuma T, Yamamoto M, Takahashi S. Primitive erythropoiesis from mesodermal precursors expressing VE-cadherin, PECAM-1, Tie2, endoglin, and CD34 in the mouse embryo. *Blood*. 2006;108(13):4018-24.
103. Pearson S, Lancrin C, Lacaud G, Kouskoff V. The sequential expression of CD40 and Icam2 defines progressive steps in the formation of blood precursors from the mesoderm germ layer. *Stem Cells*. 2010;28(6):1089-98.
104. Risau W. Differentiation of endothelium. *FASEB J*. 1995;9(10):926-33.
105. Yamashita J, Itoh H, Hirashima M, Ogawa M, Nishikawa S, Yurugi T, et al. Flk1-positive cells derived from embryonic stem cells serve as vascular progenitors. *Nature*. 2000;408(6808):92-6.
106. Galli D, Innocenzi A, Staszewsky L, Zanetta L, Sampaolesi M, Bai A, et al. Mesoangioblasts, vessel-associated multipotent stem cells, repair the infarcted heart by multiple cellular mechanisms: a comparison with bone marrow progenitors, fibroblasts, and endothelial cells. *Arterioscler Thromb Vasc Biol*. 2005;25(4):692-7.
107. Giacomazzi G, Giovannelli G, Rotini A, Costamagna D, Quattrocchi M, Sampaolesi M. Isolation of Mammalian Mesoangioblasts: A Subset of Pericytes with Myogenic Potential. *Methods Mol Biol*. 2021;2235:155-67.
108. Plein A, Fantin A, Denti L, Pollard JW, Ruhrberg C. Erythro-myeloid progenitors contribute endothelial cells to blood vessels. *Nature*. 2018;562(7726):223-8.
109. Feng T, Gao Z, Kou S, Huang X, Jiang Z, Lu Z, et al. No Evidence for Erythro-Myeloid Progenitor-Derived Vascular Endothelial Cells in Multiple Organs. *Circ Res*. 2020;127(10):1221-32.
110. Urbich C, Dimmeler S. Endothelial progenitor cells: characterization and role in vascular biology. *Circ Res*. 2004;95(4):343-53.
111. Nolan DJ, Ciarrocchi A, Mellick AS, Jaggi JS, Bambino K, Gupta S, et al. Bone marrow-derived endothelial progenitor cells are a major determinant of nascent tumor neovascularization. *Genes Dev*. 2007;21(12):1546-58.
112. Kasaai B, Caolo V, Peacock HM, Lehoux S, Gomez-Perdiguero E, Luttun A, et al. Erythro-myeloid progenitors can differentiate from endothelial cells and modulate embryonic vascular remodeling. *Sci Rep*. 2017;7:43817.
113. Hatzopoulos AK, Folkman J, Vasile E, Eiselen GK, Rosenberg RD. Isolation and characterization of endothelial progenitor cells from mouse embryos. *Development*. 1998;125(8):1457-68.
114. Ishida Y, Kimura A, Nosaka M, Kuninaka Y, Shimada E, Yamamoto H, et al. Detection of endothelial progenitor cells in human skin wounds and its application for wound age determination. *Int J Legal Med*. 2015;129(5):1049-54.

115. Asahara T, Masuda H, Takahashi T, Kalka C, Pastore C, Silver M, et al. Bone marrow origin of endothelial progenitor cells responsible for postnatal vasculogenesis in physiological and pathological neovascularization. *Circ Res*. 1999;85(3):221-8.
116. Kim KA, Shin YJ, Kim JH, Lee H, Noh SY, Jang SH, et al. Dysfunction of endothelial progenitor cells under diabetic conditions and its underlying mechanisms. *Arch Pharm Res*. 2012;35(2):223-34.
117. Kawasaki T, Nishiwaki T, Sekine A, Nishimura R, Suda R, Urushibara T, et al. Vascular Repair by Tissue-Resident Endothelial Progenitor Cells in Endotoxin-Induced Lung Injury. *Am J Respir Cell Mol Biol*. 2015;53(4):500-12.
118. Mao SZ, Ye X, Liu G, Song D, Liu SF. Resident Endothelial Cells and Endothelial Progenitor Cells Restore Endothelial Barrier Function After Inflammatory Lung Injury. *Arterioscler Thromb Vasc Biol*. 2015;35(7):1635-44.
119. Patel J, Seppanen EJ, Rodero MP, Wong HY, Donovan P, Neufeld Z, et al. Functional Definition of Progenitors Versus Mature Endothelial Cells Reveals Key SoxF-Dependent Differentiation Process. *Circulation*. 2017;135(8):786-805.
120. International Diabetes Federation 2021.
121. Menting JG, Whittaker J, Margetts MB, Whittaker LJ, Kong GK, Smith BJ, et al. How insulin engages its primary binding site on the insulin receptor. *Nature*. 2013;493(7431):241-5.
122. Lee J, Pilch PF. The insulin receptor: structure, function, and signaling. *Am J Physiol*. 1994;266(2 Pt 1):C319-34.
123. Muniyappa R, Montagnani M, Koh KK, Quon MJ. Cardiovascular actions of insulin. *Endocr Rev*. 2007;28(5):463-91.
124. Janah L, Kjeldsen S, Galsgaard KD, Winther-Sorensen M, Stojanovska E, Pedersen J, et al. Glucagon Receptor Signaling and Glucagon Resistance. *Int J Mol Sci*. 2019;20(13).
125. Gerich JE. Physiology of glucose homeostasis. *Diabetes Obes Metab*. 2000;2(6):345-50.
126. Dahlquist G. The aetiology of type 1 diabetes: an epidemiological perspective. *Acta Paediatr Suppl*. 1998;425:5-10.
127. Baribault H. Mouse Models of Type 2 Diabetes Mellitus in Drug Discovery. *Methods Mol Biol*. 2016;1438:153-75.
128. American Diabetes A. 2. Classification and Diagnosis of Diabetes: Standards of Medical Care in Diabetes-2021. *Diabetes Care*. 2021;44(Suppl 1):S15-S33.
129. Thorsby E, Ronningen KS. Particular HLA-DQ molecules play a dominant role in determining susceptibility or resistance to type 1 (insulin-dependent) diabetes mellitus. *Diabetologia*. 1993;36(5):371-7.
130. Steck AK, Rewers MJ. Genetics of type 1 diabetes. *Clin Chem*. 2011;57(2):176-85.
131. King ML, Shaikh A, Bidwell D, Voller A, Banatvala JE. Coxsackie-B-virus-specific IgM responses in children with insulin-dependent (juvenile-onset; type I) diabetes mellitus. *Lancet*. 1983;1(8339):1397-9.
132. Forrest JM, Menser MA, Burgess JA. High frequency of diabetes mellitus in young adults with congenital rubella. *Lancet*. 1971;2(7720):332-4.
133. Ziegler AG, Rewers M, Simell O, Simell T, Lempainen J, Steck A, et al. Seroconversion to multiple islet autoantibodies and risk of progression to diabetes in children. *JAMA*. 2013;309(23):2473-9.
134. McLaughlin KA, Richardson CC, Ravishankar A, Brigatti C, Liberati D, Lampasona V, et al. Identification of Tetraspanin-7 as a Target of Autoantibodies in Type 1 Diabetes. *Diabetes*. 2016;65(6):1690-8.
135. Peterson JD, Pike B, McDuffie M, Haskins K. Islet-specific T cell clones transfer diabetes to nonobese diabetic (NOD) F1 mice. *J Immunol*. 1994;153(6):2800-6.
136. Christianson SW, Shultz LD, Leiter EH. Adoptive transfer of diabetes into immunodeficient NOD-scid/scid mice. Relative contributions of CD4+ and CD8+ T-cells from diabetic versus prediabetic NOD.NON-Thy-1a donors. *Diabetes*. 1993;42(1):44-55.
137. Hutchings PR, Cooke A. The transfer of autoimmune diabetes in NOD mice can be inhibited or accelerated by distinct cell populations present in normal splenocytes taken from young males. *J Autoimmun*. 1990;3(2):175-85.
138. Sharma RB, Alonso LC. Lipotoxicity in the pancreatic beta cell: not just survival and function, but proliferation as well? *Curr Diab Rep*. 2014;14(6):492.

139. Roep BO, Peakman M. Antigen targets of type 1 diabetes autoimmunity. *Cold Spring Harb Perspect Med.* 2012;2(4):a007781.
140. van Belle TL, Coppieters KT, von Herrath MG. Type 1 diabetes: etiology, immunology, and therapeutic strategies. *Physiol Rev.* 2011;91(1):79-118.
141. Nikolic T, Geutskens SB, van Rooijen N, Drexhage HA, Leenen PJ. Dendritic cells and macrophages are essential for the retention of lymphocytes in (peri)-insulitis of the nonobese diabetic mouse: a phagocyte depletion study. *Lab Invest.* 2005;85(4):487-501.
142. Jun HS, Yoon CS, Zbytnuik L, van Rooijen N, Yoon JW. The role of macrophages in T cell-mediated autoimmune diabetes in nonobese diabetic mice. *J Exp Med.* 1999;189(2):347-58.
143. Cernea S, Dobreanu M. Diabetes and beta cell function: from mechanisms to evaluation and clinical implications. *Biochem Med (Zagreb).* 2013;23(3):266-80.
144. Burkart V, Wang ZQ, Radons J, Heller B, Herceg Z, Stingl L, et al. Mice lacking the poly(ADP-ribose) polymerase gene are resistant to pancreatic beta-cell destruction and diabetes development induced by streptozocin. *Nat Med.* 1999;5(3):314-9.
145. Szablewski L. Role of immune system in type 1 diabetes mellitus pathogenesis. *Int Immunopharmacol.* 2014;22(1):182-91.
146. Terrazas LI, Montero D, Terrazas CA, Reyes JL, Rodriguez-Sosa M. Role of the programmed Death-1 pathway in the suppressive activity of alternatively activated macrophages in experimental cysticercosis. *Int J Parasitol.* 2005;35(13):1349-58.
147. Storling J, Binzer J, Andersson AK, Zullig RA, Tonnesen M, Lehmann R, et al. Nitric oxide contributes to cytokine-induced apoptosis in pancreatic beta cells via potentiation of JNK activity and inhibition of Akt. *Diabetologia.* 2005;48(10):2039-50.
148. Mas A, Montane J, Anguela XM, Munoz S, Douar AM, Riu E, et al. Reversal of type 1 diabetes by engineering a glucose sensor in skeletal muscle. *Diabetes.* 2006;55(6):1546-53.
149. Hope SV, Wienand-Barnett S, Shepherd M, King SM, Fox C, Khunti K, et al. Practical Classification Guidelines for Diabetes in patients treated with insulin: a cross-sectional study of the accuracy of diabetes diagnosis. *Br J Gen Pract.* 2016;66(646):e315-22.
150. Nathan DM, Group DER. The diabetes control and complications trial/epidemiology of diabetes interventions and complications study at 30 years: overview. *Diabetes Care.* 2014;37(1):9-16.
151. Sladek R, Rocheleau G, Rung J, Dina C, Shen L, Serre D, et al. A genome-wide association study identifies novel risk loci for type 2 diabetes. *Nature.* 2007;445(7130):881-5.
152. Amery CM, Nattrass M. Fatty acids and insulin secretion. *Diabetes Obes Metab.* 2000;2(4):213-21.
153. Roder PV, Wu B, Liu Y, Han W. Pancreatic regulation of glucose homeostasis. *Exp Mol Med.* 2016;48:e219.
154. Xu X, Ren J. Macrophage migration inhibitory factor (MIF) knockout preserves cardiac homeostasis through alleviating Akt-mediated myocardial autophagy suppression in high-fat diet-induced obesity. *Int J Obes (Lond).* 2015;39(3):387-96.
155. Harding HP, Ron D. Endoplasmic reticulum stress and the development of diabetes: a review. *Diabetes.* 2002;51 Suppl 3:S455-61.
156. Gasa R, Gomis R, Casamitjana R, Novials A. High glucose concentration favors the selective secretion of islet amyloid polypeptide through a constitutive secretory pathway in human pancreatic islets. *Pancreas.* 2001;22(3):307-10.
157. Gasa R, Gomis R, Casamitjana R, Rivera F, Novials A. Glucose regulation of islet amyloid polypeptide gene expression in rat pancreatic islets. *Am J Physiol.* 1997;272(4 Pt 1):E543-9.
158. Ventre J, Doebber T, Wu M, MacNaul K, Stevens K, Pasparakis M, et al. Targeted disruption of the tumor necrosis factor-alpha gene: metabolic consequences in obese and nonobese mice. *Diabetes.* 1997;46(9):1526-31.
159. Krogh-Madsen R, Plomgaard P, Moller K, Mittendorfer B, Pedersen BK. Influence of TNF-alpha and IL-6 infusions on insulin sensitivity and expression of IL-18 in humans. *Am J Physiol Endocrinol Metab.* 2006;291(1):E108-14.
160. Ofei F, Hurel S, Newkirk J, Sopwith M, Taylor R. Effects of an engineered human anti-TNF-alpha antibody (CDP571) on insulin sensitivity and glycemic control in patients with NIDDM. *Diabetes.* 1996;45(7):881-5.

161. Gonzalez-Gay MA, De Matias JM, Gonzalez-Juanatey C, Garcia-Porrúa C, Sanchez-Andrade A, Martin J, et al. Anti-tumor necrosis factor- α blockade improves insulin resistance in patients with rheumatoid arthritis. *Clin Exp Rheumatol*. 2006;24(1):83-6.
162. Hotamisligil GS, Peraldi P, Budavari A, Ellis R, White MF, Spiegelman BM. IRS-1-mediated inhibition of insulin receptor tyrosine kinase activity in TNF- α - and obesity-induced insulin resistance. *Science*. 1996;271(5249):665-8.
163. Paz K, Hemi R, LeRoith D, Karasik A, Elhanany E, Kanety H, et al. A molecular basis for insulin resistance. Elevated serine/threonine phosphorylation of IRS-1 and IRS-2 inhibits their binding to the juxtamembrane region of the insulin receptor and impairs their ability to undergo insulin-induced tyrosine phosphorylation. *J Biol Chem*. 1997;272(47):29911-8.
164. Baud V, Karin M. Signal transduction by tumor necrosis factor and its relatives. *Trends Cell Biol*. 2001;11(9):372-7.
165. Tuncman G, Hirosumi J, Solinas G, Chang L, Karin M, Hotamisligil GS. Functional in vivo interactions between JNK1 and JNK2 isoforms in obesity and insulin resistance. *Proc Natl Acad Sci U S A*. 2006;103(28):10741-6.
166. Hirosumi J, Tuncman G, Chang L, Gorgun CZ, Uysal KT, Maeda K, et al. A central role for JNK in obesity and insulin resistance. *Nature*. 2002;420(6913):333-6.
167. Liu G, Rondinone CM. JNK: bridging the insulin signaling and inflammatory pathway. *Curr Opin Investig Drugs*. 2005;6(10):979-87.
168. Yuan M, Konstantopoulos N, Lee J, Hansen L, Li ZW, Karin M, et al. Reversal of obesity- and diet-induced insulin resistance with salicylates or targeted disruption of Ikk β . *Science*. 2001;293(5535):1673-7.
169. Kaneto H, Nakatani Y, Miyatsuka T, Kawamori D, Matsuoka TA, Matsuhisa M, et al. Possible novel therapy for diabetes with cell-permeable JNK-inhibitory peptide. *Nat Med*. 2004;10(10):1128-32.
170. Marciniak SJ, Ron D. Endoplasmic reticulum stress signaling in disease. *Physiol Rev*. 2006;86(4):1133-49.
171. Schroder M, Kaufman RJ. The mammalian unfolded protein response. *Annu Rev Biochem*. 2005;74:739-89.
172. Harding HP, Zhang Y, Ron D. Protein translation and folding are coupled by an endoplasmic-reticulum-resident kinase. *Nature*. 1999;397(6716):271-4.
173. Nakatani Y, Kaneto H, Kawamori D, Yoshiuchi K, Hatazaki M, Matsuoka TA, et al. Involvement of endoplasmic reticulum stress in insulin resistance and diabetes. *J Biol Chem*. 2005;280(1):847-51.
174. Cullinan SB, Diehl JA. Coordination of ER and oxidative stress signaling: the PERK/Nrf2 signaling pathway. *Int J Biochem Cell Biol*. 2006;38(3):317-32.
175. Brownlee M. Biochemistry and molecular cell biology of diabetic complications. *Nature*. 2001;414(6865):813-20.
176. Houstis N, Rosen ED, Lander ES. Reactive oxygen species have a causal role in multiple forms of insulin resistance. *Nature*. 2006;440(7086):944-8.
177. Brooks-Worrell BM, Reichow JL, Goel A, Ismail H, Palmer JP. Identification of autoantibody-negative autoimmune type 2 diabetic patients. *Diabetes Care*. 2011;34(1):168-73.
178. Naik RG, Palmer JP. Latent autoimmune diabetes in adults (LADA). *Rev Endocr Metab Disord*. 2003;4(3):233-41.
179. Henriksen EJ, Diamond-Stanic MK, Marchionne EM. Oxidative stress and the etiology of insulin resistance and type 2 diabetes. *Free Radic Biol Med*. 2011;51(5):993-9.
180. Effect of intensive diabetes treatment on the development and progression of long-term complications in adolescents with insulin-dependent diabetes mellitus: Diabetes Control and Complications Trial. Diabetes Control and Complications Trial Research Group. *J Pediatr*. 1994;125(2):177-88.
181. Koves TR, Noland RC, Bates AL, Henes ST, Muoio DM, Cortright RN. Subsarcolemmal and intermyofibrillar mitochondria play distinct roles in regulating skeletal muscle fatty acid metabolism. *Am J Physiol Cell Physiol*. 2005;288(5):C1074-82.
182. Kalkhoran SB, Munro P, Qiao F, Ong SB, Hall AR, Cabrera-Fuentes H, et al. Unique morphological characteristics of mitochondrial subtypes in the heart: the effect of ischemia and ischemic preconditioning. *Discoveries (Craiova)*. 2017;5(1).

183. Maassen JA, LM TH, Van Essen E, Heine RJ, Nijpels G, Jahangir Tafrechi RS, et al. Mitochondrial diabetes: molecular mechanisms and clinical presentation. *Diabetes*. 2004;53 Suppl 1:S103-9.
184. Hofhaus G, Weiss H, Leonard K. Electron microscopic analysis of the peripheral and membrane parts of mitochondrial NADH dehydrogenase (complex I). *J Mol Biol*. 1991;221(3):1027-43.
185. Juturu V, Wu JC. Microbial production of lactic acid: the latest development. *Crit Rev Biotechnol*. 2016;36(6):967-77.
186. Akram M. Citric acid cycle and role of its intermediates in metabolism. *Cell Biochem Biophys*. 2014;68(3):475-8.
187. Sharma LK, Lu J, Bai Y. Mitochondrial respiratory complex I: structure, function and implication in human diseases. *Curr Med Chem*. 2009;16(10):1266-77.
188. Mitchell P. Coupling of phosphorylation to electron and hydrogen transfer by a chemi-osmotic type of mechanism. *Nature*. 1961;191:144-8.
189. Guo R, Gu J, Zong S, Wu M, Yang M. Structure and mechanism of mitochondrial electron transport chain. *Biomed J*. 2018;41(1):9-20.
190. Demine S, Renard P, Arnould T. Mitochondrial Uncoupling: A Key Controller of Biological Processes in Physiology and Diseases. *Cells*. 2019;8(8).
191. Openstax College, Biology
192. Bonnard C, Durand A, Peyrol S, Chanseaux E, Chauvin MA, Morio B, et al. Mitochondrial dysfunction results from oxidative stress in the skeletal muscle of diet-induced insulin-resistant mice. *J Clin Invest*. 2008;118(2):789-800.
193. Vester JW, Stadie WC. Studies of oxidative phosphorylation by hepatic mitochondria from the diabetic cat. *J Biol Chem*. 1957;227(2):669-76.
194. Hall JC, Sordahl LA, Steffen PL. The effect of insulin on oxidative phosphorylation in normal and diabetic mitochondria. *J Biol Chem*. 1960;235:1536-9.
195. Gross MD, Harris S, Beyer RE. The effect of streptozotocin-induced diabetes on oxidative phosphorylation and related reactions in skeletal muscle mitochondria. *Horm Metab Res*. 1972;4(1):1-7.
196. Ferko M, Gvozjakova A, Kucharska J, Mujkova J, Waczulikova I, Styk J, et al. Functional remodeling of heart mitochondria in acute diabetes: interrelationships between damage, endogenous protection and adaptation. *Gen Physiol Biophys*. 2006;25(4):397-413.
197. Moreira PI, Rolo AP, Sena C, Seica R, Oliveira CR, Santos MS. Insulin attenuates diabetes-related mitochondrial alterations: a comparative study. *Med Chem*. 2006;2(3):299-308.
198. Katyare SS, Satav JG. Effect of streptozotocin-induced diabetes on oxidative energy metabolism in rat kidney mitochondria. A comparative study of early and late effects. *Diabetes Obes Metab*. 2005;7(5):555-62.
199. Marinari UM, Monacelli R, Cottalasso D, Novelli A. Effects of alloxan diabetes and insulin on morphology and certain functional activities of mitochondria of the rat liver and heart. *Acta Diabetol Lat*. 1974;11(4):296-314.
200. Krause MP, Riddell MC, Hawke TJ. Effects of type 1 diabetes mellitus on skeletal muscle: clinical observations and physiological mechanisms. *Pediatr Diabetes*. 2011;12(4 Pt 1):345-64.
201. Goranson ES, Erulkar SD. The effect of insulin on the aerobic phosphorylation of creatine in tissues from alloxan-diabetic rats. *Arch Biochem*. 1949;24(1):40-8.
202. Herlein JA, Fink BD, O'Malley Y, Sivitz WI. Superoxide and respiratory coupling in mitochondria of insulin-deficient diabetic rats. *Endocrinology*. 2009;150(1):46-55.
203. Bugger H, Boudina S, Hu XX, Tuinei J, Zaha VG, Theobald HA, et al. Type 1 diabetic akita mouse hearts are insulin sensitive but manifest structurally abnormal mitochondria that remain coupled despite increased uncoupling protein 3. *Diabetes*. 2008;57(11):2924-32.
204. Brownlee M. The pathobiology of diabetic complications: a unifying mechanism. *Diabetes*. 2005;54(6):1615-25.
205. Monaco CMF, Gingrich MA, Hawke TJ. Considering Type 1 Diabetes as a Form of Accelerated Muscle Aging. *Exerc Sport Sci Rev*. 2019;47(2):98-107.
206. Yanase T, Yanagita I, Muta K, Nawata H. Frailty in elderly diabetes patients. *Endocr J*. 2018;65(1):1-11.

207. Karakelides H, Asmann YW, Bigelow ML, Short KR, Dhatariya K, Coenen-Schimke J, et al. Effect of insulin deprivation on muscle mitochondrial ATP production and gene transcript levels in type 1 diabetic subjects. *Diabetes*. 2007;56(11):2683-9.
208. Boudina S, Sena S, Theobald H, Sheng X, Wright JJ, Hu XX, et al. Mitochondrial energetics in the heart in obesity-related diabetes: direct evidence for increased uncoupled respiration and activation of uncoupling proteins. *Diabetes*. 2007;56(10):2457-66.
209. Morino K, Petersen KF, Dufour S, Befroy D, Frattini J, Shatzkes N, et al. Reduced mitochondrial density and increased IRS-1 serine phosphorylation in muscle of insulin-resistant offspring of type 2 diabetic parents. *J Clin Invest*. 2005;115(12):3587-93.
210. Ritov VB, Menshikova EV, He J, Ferrell RE, Goodpaster BH, Kelley DE. Deficiency of subsarcolemmal mitochondria in obesity and type 2 diabetes. *Diabetes*. 2005;54(1):8-14.
211. Wu Z, Puigserver P, Andersson U, Zhang C, Adelmant G, Mootha V, et al. Mechanisms controlling mitochondrial biogenesis and respiration through the thermogenic coactivator PGC-1. *Cell*. 1999;98(1):115-24.
212. Mootha VK, Lindgren CM, Eriksson KF, Subramanian A, Sihag S, Lehar J, et al. PGC-1alpha-responsive genes involved in oxidative phosphorylation are coordinately downregulated in human diabetes. *Nat Genet*. 2003;34(3):267-73.
213. Mensink M, Hesselink MK, Russell AP, Schaart G, Sels JP, Schrauwen P. Improved skeletal muscle oxidative enzyme activity and restoration of PGC-1 alpha and PPAR beta/delta gene expression upon rosiglitazone treatment in obese patients with type 2 diabetes mellitus. *Int J Obes (Lond)*. 2007;31(8):1302-10.
214. Krebs M, Roden M. Molecular mechanisms of lipid-induced insulin resistance in muscle, liver and vasculature. *Diabetes Obes Metab*. 2005;7(6):621-32.
215. Patti ME, Butte AJ, Crunkhorn S, Cusi K, Berria R, Kashyap S, et al. Coordinated reduction of genes of oxidative metabolism in humans with insulin resistance and diabetes: Potential role of PGC1 and NRF1. *Proc Natl Acad Sci U S A*. 2003;100(14):8466-71.
216. Fridovich I. Superoxide anion radical (O₂⁻), superoxide dismutases, and related matters. *J Biol Chem*. 1997;272(30):18515-7.
217. Morita T. Heme oxygenase and atherosclerosis. *Arterioscler Thromb Vasc Biol*. 2005;25(9):1786-95.
218. Beckman KB, Ames BN. The free radical theory of aging matures. *Physiol Rev*. 1998;78(2):547-81.
219. Green K, Brand MD, Murphy MP. Prevention of mitochondrial oxidative damage as a therapeutic strategy in diabetes. *Diabetes*. 2004;53 Suppl 1:S110-8.
220. Skulachev VP. Uncoupling: new approaches to an old problem of bioenergetics. *Biochim Biophys Acta*. 1998;1363(2):100-24.
221. Li X, May JM. Catalase-dependent measurement of H₂O₂ in intact mitochondria. *Mitochondrion*. 2002;1(5):447-53.
222. Radi R, Turrens JF, Chang LY, Bush KM, Crapo JD, Freeman BA. Detection of catalase in rat heart mitochondria. *J Biol Chem*. 1991;266(32):22028-34.
223. Salvi M, Battaglia V, Brunati AM, La Rocca N, Tibaldi E, Pietrangeli P, et al. Catalase takes part in rat liver mitochondria oxidative stress defense. *J Biol Chem*. 2007;282(33):24407-15.
224. Piconi L, Quagliario L, Ceriello A. Oxidative stress in diabetes. *Clin Chem Lab Med*. 2003;41(9):1144-9.
225. Raha S, Robinson BH. Mitochondria, oxygen free radicals, disease and ageing. *Trends Biochem Sci*. 2000;25(10):502-8.
226. Sazanov LA. Respiratory complex I: mechanistic and structural insights provided by the crystal structure of the hydrophilic domain. *Biochemistry*. 2007;46(9):2275-88.
227. Sakurai K, Katoh M, Someno K, Fujimoto Y. Apoptosis and mitochondrial damage in INS-1 cells treated with alloxan. *Biol Pharm Bull*. 2001;24(8):876-82.
228. Turk J, Corbett JA, Ramanadham S, Bohrer A, McDaniel ML. Biochemical evidence for nitric oxide formation from streptozotocin in isolated pancreatic islets. *Biochem Biophys Res Commun*. 1993;197(3):1458-64.
229. Lenzen S, Drinkgern J, Tiedge M. Low antioxidant enzyme gene expression in pancreatic islets compared with various other mouse tissues. *Free Radic Biol Med*. 1996;20(3):463-6.

230. Emre Y, Hurtaud C, Karaca M, Nubel T, Zavala F, Ricquier D. Role of uncoupling protein UCP2 in cell-mediated immunity: how macrophage-mediated insulinitis is accelerated in a model of autoimmune diabetes. *Proc Natl Acad Sci U S A*. 2007;104(48):19085-90.
231. Zhang CY, Baffy G, Perret P, Krauss S, Peroni O, Grujic D, et al. Uncoupling protein-2 negatively regulates insulin secretion and is a major link between obesity, beta cell dysfunction, and type 2 diabetes. *Cell*. 2001;105(6):745-55.
232. Nishikawa T, Edelstein D, Du XL, Yamagishi S, Matsumura T, Kaneda Y, et al. Normalizing mitochondrial superoxide production blocks three pathways of hyperglycaemic damage. *Nature*. 2000;404(6779):787-90.
233. Du XL, Edelstein D, Rossetti L, Fantus IG, Goldberg H, Ziyadeh F, et al. Hyperglycemia-induced mitochondrial superoxide overproduction activates the hexosamine pathway and induces plasminogen activator inhibitor-1 expression by increasing Sp1 glycosylation. *Proc Natl Acad Sci U S A*. 2000;97(22):12222-6.
234. Du Y, Miller CM, Kern TS. Hyperglycemia increases mitochondrial superoxide in retina and retinal cells. *Free Radic Biol Med*. 2003;35(11):1491-9.
235. Kiritoshi S, Nishikawa T, Sonoda K, Kukidome D, Senokuchi T, Matsuo T, et al. Reactive oxygen species from mitochondria induce cyclooxygenase-2 gene expression in human mesangial cells: potential role in diabetic nephropathy. *Diabetes*. 2003;52(10):2570-7.
236. Ye G, Metreveli NS, Donthi RV, Xia S, Xu M, Carlson EC, et al. Catalase protects cardiomyocyte function in models of type 1 and type 2 diabetes. *Diabetes*. 2004;53(5):1336-43.
237. Coppey LJ, Gellett JS, Davidson EP, Yorek MA. Preventing superoxide formation in epineurial arterioles of the sciatic nerve from diabetic rats restores endothelium-dependent vasodilation. *Free Radic Res*. 2003;37(1):33-40.
238. Yamagishi SI, Edelstein D, Du XL, Kaneda Y, Guzman M, Brownlee M. Leptin induces mitochondrial superoxide production and monocyte chemoattractant protein-1 expression in aortic endothelial cells by increasing fatty acid oxidation via protein kinase A. *J Biol Chem*. 2001;276(27):25096-100.
239. Vasquez-Vivar J, Kalyanaraman B, Kennedy MC. Mitochondrial aconitase is a source of hydroxyl radical. An electron spin resonance investigation. *J Biol Chem*. 2000;275(19):14064-9.
240. James AM, Murphy MP. How mitochondrial damage affects cell function. *J Biomed Sci*. 2002;9(6 Pt 1):475-87.
241. De Vriese AS, Verbeuren TJ, Van de Voorde J, Lameire NH, Vanhoutte PM. Endothelial dysfunction in diabetes. *Br J Pharmacol*. 2000;130(5):963-74.
242. Piconi L, Quagliaro L, Assaloni R, Da Ros R, Maier A, Zuodar G, et al. Constant and intermittent high glucose enhances endothelial cell apoptosis through mitochondrial superoxide overproduction. *Diabetes Metab Res Rev*. 2006;22(3):198-203.
243. Coppey LJ, Gellett JS, Davidson EP, Dunlap JA, Yorek MA. Effect of treating streptozotocin-induced diabetic rats with sorbinil, myo-inositol or aminoguanidine on endoneurial blood flow, motor nerve conduction velocity and vascular function of epineurial arterioles of the sciatic nerve. *Int J Exp Diabetes Res*. 2002;3(1):21-36.
244. Yorek MA, Coppey LJ, Gellett JS, Davidson EP, Bing X, Lund DD, et al. Effect of treatment of diabetic rats with dehydroepiandrosterone on vascular and neural function. *Am J Physiol Endocrinol Metab*. 2002;283(5):E1067-75.
245. Cameron NE, Cotter MA. Effects of an extracellular metal chelator on neurovascular function in diabetic rats. *Diabetologia*. 2001;44(5):621-8.
246. Cameron NE, Cotter MA. Neurovascular dysfunction in diabetic rats. Potential contribution of autooxidation and free radicals examined using transition metal chelating agents. *J Clin Invest*. 1995;96(2):1159-63.
247. Cameron NE, Jack AM, Cotter MA. Effect of alpha-lipoic acid on vascular responses and nociception in diabetic rats. *Free Radic Biol Med*. 2001;31(1):125-35.
248. Inkster ME, Cotter MA, Cameron NE. Effects of trientine, a metal chelator, on defective endothelium-dependent relaxation in the mesenteric vasculature of diabetic rats. *Free Radic Res*. 2002;36(10):1091-9.

249. Nassar T, Kadery B, Lotan C, Da'as N, Kleinman Y, Haj-Yehia A. Effects of the superoxide dismutase-mimetic compound tempol on endothelial dysfunction in streptozotocin-induced diabetic rats. *Eur J Pharmacol.* 2002;436(1-2):111-8.
250. Ji Y, Leng Y, Lei S, Qiu Z, Ming H, Zhang Y, et al. The mitochondria-targeted antioxidant MitoQ ameliorates myocardial ischemia-reperfusion injury by enhancing PINK1/Parkin-mediated mitophagy in type 2 diabetic rats. *Cell Stress Chaperones.* 2022;27(4):353-67.
251. Nguyen AV, Soulika AM. The Dynamics of the Skin's Immune System. *Int J Mol Sci.* 2019;20(8).
252. Watt FM, Lo Celso C, Silva-Vargas V. Epidermal stem cells: an update. *Curr Opin Genet Dev.* 2006;16(5):518-24.
253. Fuchs E. Skin stem cells: rising to the surface. *J Cell Biol.* 2008;180(2):273-84.
254. Schepeler T, Page ME, Jensen KB. Heterogeneity and plasticity of epidermal stem cells. *Development.* 2014;141(13):2559-67.
255. Fuchs E, Horsley V. Ferreting out stem cells from their niches. *Nat Cell Biol.* 2011;13(5):513-8.
256. Potten CS. Cell replacement in epidermis (keratopoiesis) via discrete units of proliferation. *Int Rev Cytol.* 1981;69:271-318.
257. Allen TD, Potten CS. Fine-structural identification and organization of the epidermal proliferative unit. *J Cell Sci.* 1974;15(2):291-319.
258. Hsu YC, Li L, Fuchs E. Emerging interactions between skin stem cells and their niches. *Nat Med.* 2014;20(8):847-56.
259. Clayton E, Doupe DP, Klein AM, Winton DJ, Simons BD, Jones PH. A single type of progenitor cell maintains normal epidermis. *Nature.* 2007;446(7132):185-9.
260. Blanpain C, Fuchs E. Epidermal stem cells of the skin. *Annu Rev Cell Dev Biol.* 2006;22:339-73.
261. Cotsarelis G, Sun TT, Lavker RM. Label-retaining cells reside in the bulge area of pilosebaceous unit: implications for follicular stem cells, hair cycle, and skin carcinogenesis. *Cell.* 1990;61(7):1329-37.
262. Oshima H, Rochat A, Kedzia C, Kobayashi K, Barrandon Y. Morphogenesis and renewal of hair follicles from adult multipotent stem cells. *Cell.* 2001;104(2):233-45.
263. Goldstein J, Horsley V. Home sweet home: skin stem cell niches. *Cell Mol Life Sci.* 2012;69(15):2573-82.
264. Fuchs E, Horsley V. More than one way to skin. *Genes Dev.* 2008;22(8):976-85.
265. Sellheyer K, Krahl D. Skin mesenchymal stem cells: prospects for clinical dermatology. *J Am Acad Dermatol.* 2010;63(5):859-65.
266. Zhao Z, Liao L, Cao Y, Jiang X, Zhao RC. Establishment and properties of fetal dermis-derived mesenchymal stem cell lines: plasticity in vitro and hematopoietic protection in vivo. *Bone Marrow Transplant.* 2005;36(4):355-65.
267. Castro-Manreza ME, Bonifaz L, Castro-Escamilla O, Monroy-Garcia A, Cortes-Morales A, Hernandez-Estevez E, et al. Mesenchymal Stromal Cells from the Epidermis and Dermis of Psoriasis Patients: Morphology, Immunophenotype, Differentiation Patterns, and Regulation of T Cell Proliferation. *Stem Cells Int.* 2019;2019:4541797.
268. Yamanishi H, Fujiwara S, Soma T. Perivascular localization of dermal stem cells in human scalp. *Exp Dermatol.* 2012;21(1):78-80.
269. Henri S, Poulin LF, Tamoutounour S, Ardouin L, Guillems M, de Bovis B, et al. CD207+ CD103+ dermal dendritic cells cross-present keratinocyte-derived antigens irrespective of the presence of Langerhans cells. *J Exp Med.* 2010;207(1):189-206.
270. Tamoutounour S, Guillems M, Montanana Sanchis F, Liu H, Terhorst D, Malosse C, et al. Origins and functional specialization of macrophages and of conventional and monocyte-derived dendritic cells in mouse skin. *Immunity.* 2013;39(5):925-38.
271. Di Meglio P, Perera GK, Nestle FO. The multitasking organ: recent insights into skin immune function. *Immunity.* 2011;35(6):857-69.
272. Mojumdar K, Liang F, Giordano C, Lemaire C, Danialou G, Okazaki T, et al. Inflammatory monocytes promote progression of Duchenne muscular dystrophy and can be therapeutically targeted via CCR2. *EMBO Mol Med.* 2014;6(11):1476-92.
273. Doebel T, Voisin B, Nagao K. Langerhans Cells - The Macrophage in Dendritic Cell Clothing. *Trends Immunol.* 2017;38(11):817-28.

274. Varol C, Vallon-Eberhard A, Elinav E, Aychek T, Shapira Y, Luche H, et al. Intestinal lamina propria dendritic cell subsets have different origin and functions. *Immunity*. 2009;31(3):502-12.
275. Davies LC, Jenkins SJ, Allen JE, Taylor PR. Tissue-resident macrophages. *Nat Immunol*. 2013;14(10):986-95.
276. Osaka N, Takahashi T, Murakami S, Matsuzawa A, Noguchi T, Fujiwara T, et al. ASK1-dependent recruitment and activation of macrophages induce hair growth in skin wounds. *J Cell Biol*. 2007;176(7):903-9.
277. Wang X, Chen H, Tian R, Zhang Y, Drutskaya MS, Wang C, et al. Macrophages induce AKT/beta-catenin-dependent Lgr5(+) stem cell activation and hair follicle regeneration through TNF. *Nat Commun*. 2017;8:14091.
278. Paus R. Principles of hair cycle control. *J Dermatol*. 1998;25(12):793-802.
279. Castellana D, Paus R, Perez-Moreno M. Macrophages contribute to the cyclic activation of adult hair follicle stem cells. *PLoS Biol*. 2014;12(12):e1002002.
280. Rahmani W, Liu Y, Rosin NL, Kline A, Raharjo E, Yoon J, et al. Macrophages Promote Wound-Induced Hair Follicle Regeneration in a CX3CR1- and TGF-beta1-Dependent Manner. *J Invest Dermatol*. 2018;138(10):2111-22.
281. Chen CC, Wang L, Plikus MV, Jiang TX, Murray PJ, Ramos R, et al. Organ-level quorum sensing directs regeneration in hair stem cell populations. *Cell*. 2015;161(2):277-90.
282. Gutterman DD, Chabowski DS, Kadlec AO, Durand MJ, Freed JK, Ait-Aissa K, et al. The Human Microcirculation: Regulation of Flow and Beyond. *Circ Res*. 2016;118(1):157-72.
283. Charkoudian N. Skin blood flow in adult human thermoregulation: how it works, when it does not, and why. *Mayo Clin Proc*. 2003;78(5):603-12.
284. Schuster C, Mildner M, Botta A, Nemec L, Rogojanu R, Beer L, et al. Development of Blood and Lymphatic Endothelial Cells in Embryonic and Fetal Human Skin. *Am J Pathol*. 2015;185(9):2563-74.
285. Groger M, Niederleithner H, Kerjaschki D, Petzelbauer P. A previously unknown dermal blood vessel phenotype in skin inflammation. *J Invest Dermatol*. 2007;127(12):2893-900.
286. Eming SA, Martin P, Tomic-Canic M. Wound repair and regeneration: mechanisms, signaling, and translation. *Sci Transl Med*. 2014;6(265):265sr6.
287. Robson MC, Steed DL, Franz MG. Wound healing: biologic features and approaches to maximize healing trajectories. *Curr Probl Surg*. 2001;38(2):72-140.
288. Martin P. Wound healing--aiming for perfect skin regeneration. *Science*. 1997;276(5309):75-81.
289. Woo YC, Park SS, Subieta AR, Brennan TJ. Changes in tissue pH and temperature after incision indicate acidosis may contribute to postoperative pain. *Anesthesiology*. 2004;101(2):468-75.
290. Werner S, Grose R. Regulation of wound healing by growth factors and cytokines. *Physiol Rev*. 2003;83(3):835-70.
291. Eming SA, Krieg T, Davidson JM. Inflammation in wound repair: molecular and cellular mechanisms. *J Invest Dermatol*. 2007;127(3):514-25.
292. Daley JM, Brancato SK, Thomay AA, Reichner JS, Albina JE. The phenotype of murine wound macrophages. *J Leukoc Biol*. 2010;87(1):59-67.
293. Simpson DM, Ross R. The neutrophilic leukocyte in wound repair a study with antineutrophil serum. *J Clin Invest*. 1972;51(8):2009-23.
294. Dovi JV, He LK, DiPietro LA. Accelerated wound closure in neutrophil-depleted mice. *J Leukoc Biol*. 2003;73(4):448-55.
295. Kim ND, Luster AD. The role of tissue resident cells in neutrophil recruitment. *Trends Immunol*. 2015;36(9):547-55.
296. Imhof BA, Aurrand-Lions M. Adhesion mechanisms regulating the migration of monocytes. *Nat Rev Immunol*. 2004;4(6):432-44.
297. Stout RD, Watkins SK, Suttles J. Functional plasticity of macrophages: in situ reprogramming of tumor-associated macrophages. *J Leukoc Biol*. 2009;86(5):1105-9.
298. Lucas T, Waisman A, Ranjan R, Roes J, Krieg T, Muller W, et al. Differential roles of macrophages in diverse phases of skin repair. *J Immunol*. 2010;184(7):3964-77.
299. Khallou-Laschet J, Varthaman A, Fornasa G, Compain C, Gaston AT, Clement M, et al. Macrophage plasticity in experimental atherosclerosis. *PLoS One*. 2010;5(1):e8852.
300. Singer AJ, Clark RA. Cutaneous wound healing. *N Engl J Med*. 1999;341(10):738-46.

301. Goerdts S, Orfanos CE. Other functions, other genes: alternative activation of antigen-presenting cells. *Immunity*. 1999;10(2):137-42.
302. Porcheray F, Viaud S, Rimaniol AC, Leone C, Samah B, Dereuddre-Bosquet N, et al. Macrophage activation switching: an asset for the resolution of inflammation. *Clin Exp Immunol*. 2005;142(3):481-9.
303. Wynn TA. Cellular and molecular mechanisms of fibrosis. *J Pathol*. 2008;214(2):199-210.
304. Martin P, Leibovich SJ. Inflammatory cells during wound repair: the good, the bad and the ugly. *Trends Cell Biol*. 2005;15(11):599-607.
305. Velmar T, Gradisnik L. Tissue Augmentation in Wound Healing: the Role of Endothelial and Epithelial Cells. *Med Arch*. 2018;72(6):444-8.
306. Niessen FB, Andriessen MP, Schalkwijk J, Visser L, Timens W. Keratinocyte-derived growth factors play a role in the formation of hypertrophic scars. *J Pathol*. 2001;194(2):207-16.
307. Sorg H, Krueger C, Vollmar B. Intravital insights in skin wound healing using the mouse dorsal skin fold chamber. *J Anat*. 2007;211(6):810-8.
308. Kalka C, Masuda H, Takahashi T, Kalka-Moll WM, Silver M, Kearney M, et al. Transplantation of ex vivo expanded endothelial progenitor cells for therapeutic neovascularization. *Proc Natl Acad Sci U S A*. 2000;97(7):3422-7.
309. Heissig B, Hattori K, Dias S, Friedrich M, Ferris B, Hackett NR, et al. Recruitment of stem and progenitor cells from the bone marrow niche requires MMP-9 mediated release of kit-ligand. *Cell*. 2002;109(5):625-37.
310. De Falco E, Porcelli D, Torella AR, Straino S, Iachininoto MG, Orlandi A, et al. SDF-1 involvement in endothelial phenotype and ischemia-induced recruitment of bone marrow progenitor cells. *Blood*. 2004;104(12):3472-82.
311. Balaji S, King A, Crombleholme TM, Keswani SG. The Role of Endothelial Progenitor Cells in Postnatal Vasculogenesis: Implications for Therapeutic Neovascularization and Wound Healing. *Adv Wound Care (New Rochelle)*. 2013;2(6):283-95.
312. Donovan P, Patel J, Dight J, Wong HY, Sim SL, Murigneux V, et al. Endovascular progenitors infiltrate melanomas and differentiate towards a variety of vascular beds promoting tumor metastasis. *Nat Commun*. 2019;10(1):18.
313. Sim SL, Blumenthal A, Kaur S, Khosrotehrani K. Myeloid Wls expression is dispensable for skin wound healing and blood vessel regeneration. *Front Endocrinol (Lausanne)*. 2022;13:957833.
314. Frank S, Hubner G, Breier G, Longaker MT, Greenhalgh DG, Werner S. Regulation of vascular endothelial growth factor expression in cultured keratinocytes. Implications for normal and impaired wound healing. *J Biol Chem*. 1995;270(21):12607-13.
315. Lee DE, Ayoub N, Agrawal DK. Mesenchymal stem cells and cutaneous wound healing: novel methods to increase cell delivery and therapeutic efficacy. *Stem Cell Res Ther*. 2016;7:37.
316. Mirza R, DiPietro LA, Koh TJ. Selective and specific macrophage ablation is detrimental to wound healing in mice. *Am J Pathol*. 2009;175(6):2454-62.
317. Knighton DR, Hunt TK, Scheuenstuhl H, Halliday BJ, Werb Z, Banda MJ. Oxygen tension regulates the expression of angiogenesis factor by macrophages. *Science*. 1983;221(4617):1283-5.
318. Nie C, Yang D, Xu J, Si Z, Jin X, Zhang J. Locally administered adipose-derived stem cells accelerate wound healing through differentiation and vasculogenesis. *Cell Transplant*. 2011;20(2):205-16.
319. Schlosser S, Dennler C, Schweizer R, Eberli D, Stein JV, Enzmann V, et al. Paracrine effects of mesenchymal stem cells enhance vascular regeneration in ischemic murine skin. *Microvasc Res*. 2012;83(3):267-75.
320. Gorecka J, Gao X, Fereydooni A, Dash BC, Luo J, Lee SR, et al. Induced pluripotent stem cell-derived smooth muscle cells increase angiogenesis and accelerate diabetic wound healing. *Regen Med*. 2020;15(2):1277-93.
321. Santoro MM, Gaudino G. Cellular and molecular facets of keratinocyte reepithelization during wound healing. *Exp Cell Res*. 2005;304(1):274-86.
322. Dekoninck S, Blanpain C. Stem cell dynamics, migration and plasticity during wound healing. *Nat Cell Biol*. 2019;21(1):18-24.
323. Arwert EN, Hoste E, Watt FM. Epithelial stem cells, wound healing and cancer. *Nat Rev Cancer*. 2012;12(3):170-80.

324. Yang R, Liu F, Wang J, Chen X, Xie J, Xiong K. Epidermal stem cells in wound healing and their clinical applications. *Stem Cell Res Ther.* 2019;10(1):229.
325. Gurtner GC, Werner S, Barrandon Y, Longaker MT. Wound repair and regeneration. *Nature.* 2008;453(7193):314-21.
326. Tredget EE, Yang L, Delehanty M, Shankowsky H, Scott PG. Polarized Th2 cytokine production in patients with hypertrophic scar following thermal injury. *J Interferon Cytokine Res.* 2006;26(3):179-89.
327. Doherty TM. T-cell regulation of macrophage function. *Curr Opin Immunol.* 1995;7(3):400-4.
328. Shapiro SD, Kobayashi DK, Ley TJ. Cloning and characterization of a unique elastolytic metalloproteinase produced by human alveolar macrophages. *J Biol Chem.* 1993;268(32):23824-9.
329. Madlener M, Parks WC, Werner S. Matrix metalloproteinases (MMPs) and their physiological inhibitors (TIMPs) are differentially expressed during excisional skin wound repair. *Exp Cell Res.* 1998;242(1):201-10.
330. Patel S, Srivastava S, Singh MR, Singh D. Mechanistic insight into diabetic wounds: Pathogenesis, molecular targets and treatment strategies to pace wound healing. *Biomed Pharmacother.* 2019;112:108615.
331. Bishop A. Role of oxygen in wound healing. *J Wound Care.* 2008;17(9):399-402.
332. Gosain A, DiPietro LA. Aging and wound healing. *World J Surg.* 2004;28(3):321-6.
333. Edwards R, Harding KG. Bacteria and wound healing. *Curr Opin Infect Dis.* 2004;17(2):91-6.
334. Gilliver SC, Ashworth JJ, Ashcroft GS. The hormonal regulation of cutaneous wound healing. *Clin Dermatol.* 2007;25(1):56-62.
335. Rupert J, Honeycutt JD, Odom MR. Foreign Bodies in the Skin: Evaluation and Management. *Am Fam Physician.* 2020;101(12):740-7.
336. Vileikyte L. Stress and wound healing. *Clin Dermatol.* 2007;25(1):49-55.
337. Raffetto JD, Ligi D, Maniscalco R, Khalil RA, Mannello F. Why Venous Leg Ulcers Have Difficulty Healing: Overview on Pathophysiology, Clinical Consequences, and Treatment. *J Clin Med.* 2020;10(1).
338. Kamler M, Lehr HA, Saetzler RK, Galla TJ, Messmer K. Impact of ischemia on tissue oxygenation and wound healing: improvement by vasoactive medication. *Adv Exp Med Biol.* 1992;316:419-24.
339. Brem H, Tomic-Canic M. Cellular and molecular basis of wound healing in diabetes. *J Clin Invest.* 2007;117(5):1219-22.
340. Wilson JA, Clark JJ. Obesity: impediment to postsurgical wound healing. *Adv Skin Wound Care.* 2004;17(8):426-35.
341. Wagner AE, Huck G, Stiehl DP, Jelkmann W, Hellwig-Burgel T. Dexamethasone impairs hypoxia-inducible factor-1 function. *Biochem Biophys Res Commun.* 2008;372(2):336-40.
342. Dong YL, Fleming RY, Yan TZ, Herndon DN, Waymack JP. Effect of ibuprofen on the inflammatory response to surgical wounds. *J Trauma.* 1993;35(3):340-3.
343. Franz MG, Steed DL, Robson MC. Optimizing healing of the acute wound by minimizing complications. *Curr Probl Surg.* 2007;44(11):691-763.
344. Choudhry MA, Chaudry IH. Alcohol intoxication and post-burn complications. *Front Biosci.* 2006;11:998-1005.
345. Siana JE, Rex S, Gottrup F. The effect of cigarette smoking on wound healing. *Scand J Plast Reconstr Surg Hand Surg.* 1989;23(3):207-9.
346. Arnold M, Barbul A. Nutrition and wound healing. *Plast Reconstr Surg.* 2006;117(7 Suppl):42S-58S.
347. Wu SC, Driver VR, Wrobel JS, Armstrong DG. Foot ulcers in the diabetic patient, prevention and treatment. *Vasc Health Risk Manag.* 2007;3(1):65-76.
348. Pemayun TG, Naibaho RM, Novitasari D, Amin N, Minuljo TT. Risk factors for lower extremity amputation in patients with diabetic foot ulcers: a hospital-based case-control study. *Diabet Foot Ankle.* 2015;6:29629.
349. Zhang P, Lu J, Jing Y, Tang S, Zhu D, Bi Y. Global epidemiology of diabetic foot ulceration: a systematic review and meta-analysis (dagger). *Ann Med.* 2017;49(2):106-16.
350. Noor S, Zubair M, Ahmad J. Diabetic foot ulcer--A review on pathophysiology, classification and microbial etiology. *Diabetes Metab Syndr.* 2015;9(3):192-9.

351. Loots MA, Lamme EN, Zeegelaar J, Mekkes JR, Bos JD, Middelkoop E. Differences in cellular infiltrate and extracellular matrix of chronic diabetic and venous ulcers versus acute wounds. *J Invest Dermatol.* 1998;111(5):850-7.
352. Esser N, Legrand-Poels S, Piette J, Scheen AJ, Paquot N. Inflammation as a link between obesity, metabolic syndrome and type 2 diabetes. *Diabetes Res Clin Pract.* 2014;105(2):141-50.
353. Bannon P, Wood S, Restivo T, Campbell L, Hardman MJ, Mace KA. Diabetes induces stable intrinsic changes to myeloid cells that contribute to chronic inflammation during wound healing in mice. *Dis Model Mech.* 2013;6(6):1434-47.
354. Mirza R, Koh TJ. Dysregulation of monocyte/macrophage phenotype in wounds of diabetic mice. *Cytokine.* 2011;56(2):256-64.
355. Gallagher KA, Joshi A, Carson WF, Schaller M, Allen R, Mukerjee S, et al. Epigenetic changes in bone marrow progenitor cells influence the inflammatory phenotype and alter wound healing in type 2 diabetes. *Diabetes.* 2015;64(4):1420-30.
356. Kimball A, Schaller M, Joshi A, Davis FM, denDekker A, Boniakowski A, et al. Ly6C(Hi) Blood Monocyte/Macrophage Drive Chronic Inflammation and Impair Wound Healing in Diabetes Mellitus. *Arterioscler Thromb Vasc Biol.* 2018;38(5):1102-14.
357. Burgess M, Wicks K, Gardasevic M, Mace KA. Cx3CR1 Expression Identifies Distinct Macrophage Populations That Contribute Differentially to Inflammation and Repair. *Immunohorizons.* 2019;3(7):262-73.
358. Joshi N, Pohlmeier L, Ben-Yehuda Greenwald M, Haertel E, Hiebert P, Kopf M, et al. Comprehensive characterization of myeloid cells during wound healing in healthy and healing-impaired diabetic mice. *Eur J Immunol.* 2020;50(9):1335-49.
359. Mirza RE, Fang MM, Ennis WJ, Koh TJ. Blocking interleukin-1beta induces a healing-associated wound macrophage phenotype and improves healing in type 2 diabetes. *Diabetes.* 2013;62(7):2579-87.
360. Wood S, Jayaraman V, Huelsmann EJ, Bonish B, Burgad D, Sivaramakrishnan G, et al. Pro-inflammatory chemokine CCL2 (MCP-1) promotes healing in diabetic wounds by restoring the macrophage response. *PLoS One.* 2014;9(3):e91574.
361. Yan J, Tie G, Wang S, Tutto A, DeMarco N, Khair L, et al. Diabetes impairs wound healing by Dnmt1-dependent dysregulation of hematopoietic stem cells differentiation towards macrophages. *Nat Commun.* 2018;9(1):33.
362. Nagareddy PR, Murphy AJ, Stirzaker RA, Hu Y, Yu S, Miller RG, et al. Hyperglycemia promotes myelopoiesis and impairs the resolution of atherosclerosis. *Cell Metab.* 2013;17(5):695-708.
363. Singer K, DelProposto J, Morris DL, Zamarron B, Mergian T, Maley N, et al. Diet-induced obesity promotes myelopoiesis in hematopoietic stem cells. *Mol Metab.* 2014;3(6):664-75.
364. Nagareddy PR, Kraakman M, Masters SL, Stirzaker RA, Gorman DJ, Grant RW, et al. Adipose tissue macrophages promote myelopoiesis and monocytosis in obesity. *Cell Metab.* 2014;19(5):821-35.
365. Barman PK, Urao N, Koh TJ. Diabetes induces myeloid bias in bone marrow progenitors associated with enhanced wound macrophage accumulation and impaired healing. *J Pathol.* 2019;249(4):435-46.
366. Ferraro F, Lymperi S, Mendez-Ferrer S, Saez B, Spencer JA, Yeap BY, et al. Diabetes impairs hematopoietic stem cell mobilization by altering niche function. *Sci Transl Med.* 2011;3(104):104ra1.
367. Lee JM, Govindarajah V, Goddard B, Hinge A, Muench DE, Filippi MD, et al. Obesity alters the long-term fitness of the hematopoietic stem cell compartment through modulation of Gfi1 expression. *J Exp Med.* 2018;215(2):627-44.
368. Lucas D, Scheiermann C, Chow A, Kunisaki Y, Bruns I, Barrick C, et al. Chemotherapy-induced bone marrow nerve injury impairs hematopoietic regeneration. *Nat Med.* 2013;19(6):695-703.
369. Morrison SJ, Scadden DT. The bone marrow niche for haematopoietic stem cells. *Nature.* 2014;505(7483):327-34.
370. Basu Mallik S, Jayashree BS, Shenoy RR. Epigenetic modulation of macrophage polarization-perspectives in diabetic wounds. *J Diabetes Complications.* 2018;32(5):524-30.
371. Khanna S, Biswas S, Shang Y, Collard E, Azad A, Kauh C, et al. Macrophage dysfunction impairs resolution of inflammation in the wounds of diabetic mice. *PLoS One.* 2010;5(3):e9539.
372. Wang Q, Zhu G, Cao X, Dong J, Song F, Niu Y. Blocking AGE-RAGE Signaling Improved Functional Disorders of Macrophages in Diabetic Wound. *J Diabetes Res.* 2017;2017:1428537.

373. Stockmann C, Kirmse S, Helfrich I, Weidemann A, Takeda N, Doedens A, et al. A wound size-dependent effect of myeloid cell-derived vascular endothelial growth factor on wound healing. *J Invest Dermatol.* 2011;131(3):797-801.
374. Willenborg S, Lucas T, van Loo G, Knipper JA, Krieg T, Haase I, et al. CCR2 recruits an inflammatory macrophage subpopulation critical for angiogenesis in tissue repair. *Blood.* 2012;120(3):613-25.
375. Okizaki S, Ito Y, Hosono K, Oba K, Ohkubo H, Kojo K, et al. Vascular Endothelial Growth Factor Receptor Type 1 Signaling Prevents Delayed Wound Healing in Diabetes by Attenuating the Production of IL-1 β by Recruited Macrophages. *Am J Pathol.* 2016;186(6):1481-98.
376. Gurevich DB, Severn CE, Twomey C, Greenhough A, Cash J, Tøye AM, et al. Live imaging of wound angiogenesis reveals macrophage orchestrated vessel sprouting and regression. *EMBO J.* 2018;37(13).
377. Maruyama K, Asai J, Ii M, Thorne T, Losordo DW, D'Amore PA. Decreased macrophage number and activation lead to reduced lymphatic vessel formation and contribute to impaired diabetic wound healing. *Am J Pathol.* 2007;170(4):1178-91.
378. Efron DT, Most D, Barbul A. Role of nitric oxide in wound healing. *Curr Opin Clin Nutr Metab Care.* 2000;3(3):197-204.
379. Frank S, Stallmeyer B, Kampfer H, Kolb N, Pfeilschifter J. Nitric oxide triggers enhanced induction of vascular endothelial growth factor expression in cultured keratinocytes (HaCaT) and during cutaneous wound repair. *FASEB J.* 1999;13(14):2002-14.
380. Chen Z, Haus JM, Chen L, Jiang Y, Sverdllov M, DiPietro LA, et al. Inhibition of CCL28/CCR10-Mediated eNOS Downregulation Improves Skin Wound Healing in the Obesity-Induced Mouse Model of Type 2 Diabetes. *Diabetes.* 2022;71(10):2166-80.
381. Deng L, Du C, Song P, Chen T, Rui S, Armstrong DG, et al. The Role of Oxidative Stress and Antioxidants in Diabetic Wound Healing. *Oxid Med Cell Longev.* 2021;2021:8852759.
382. Marrotte EJ, Chen DD, Hakim JS, Chen AF. Manganese superoxide dismutase expression in endothelial progenitor cells accelerates wound healing in diabetic mice. *J Clin Invest.* 2010;120(12):4207-19.
383. Bitar MS. Diabetes Impairs Angiogenesis and Induces Endothelial Cell Senescence by Up-Regulating Thrombospondin-CD47-Dependent Signaling. *Int J Mol Sci.* 2019;20(3).
384. Okonkwo UA, Chen L, Ma D, Haywood VA, Barakat M, Urao N, et al. Compromised angiogenesis and vascular Integrity in impaired diabetic wound healing. *PLoS One.* 2020;15(4):e0231962.
385. Gallagher KA, Liu ZJ, Xiao M, Chen H, Goldstein LJ, Buerk DG, et al. Diabetic impairments in NO-mediated endothelial progenitor cell mobilization and homing are reversed by hyperoxia and SDF-1 α . *J Clin Invest.* 2007;117(5):1249-59.
386. Galiano RD, Tepper OM, Pelo CR, Bhatt KA, Callaghan M, Bastidas N, et al. Topical vascular endothelial growth factor accelerates diabetic wound healing through increased angiogenesis and by mobilizing and recruiting bone marrow-derived cells. *Am J Pathol.* 2004;164(6):1935-47.
387. Atalay M, Oksala N, Lappalainen J, Laaksonen DE, Sen CK, Roy S. Heat shock proteins in diabetes and wound healing. *Curr Protein Pept Sci.* 2009;10(1):85-95.
388. Li Z, Guo S, Yao F, Zhang Y, Li T. Increased ratio of serum matrix metalloproteinase-9 against TIMP-1 predicts poor wound healing in diabetic foot ulcers. *J Diabetes Complications.* 2013;27(4):380-2.
389. Pradhan L, Cai X, Wu S, Andersen ND, Martin M, Malek J, et al. Gene expression of pro-inflammatory cytokines and neuropeptides in diabetic wound healing. *J Surg Res.* 2011;167(2):336-42.
390. Verkleij CJ, Roelofs JJ, Havik SR, Meijers JC, Marx PF. The role of thrombin-activatable fibrinolysis inhibitor in diabetic wound healing. *Thromb Res.* 2010;126(5):442-6.
391. Nass N, Vogel K, Hofmann B, Presek P, Silber RE, Simm A. Glycation of PDGF results in decreased biological activity. *Int J Biochem Cell Biol.* 2010;42(5):749-54.
392. Westerblad H, Bruton JD, Katz A. Skeletal muscle: energy metabolism, fiber types, fatigue and adaptability. *Exp Cell Res.* 2010;316(18):3093-9.
393. Frontera WR, Ochala J. Skeletal muscle: a brief review of structure and function. *Calcif Tissue Int.* 2015;96(3):183-95.

394. Zierath JR, Hawley JA. Skeletal muscle fiber type: influence on contractile and metabolic properties. *PLoS Biol.* 2004;2(10):e348.
395. Zembron-Lacny A, Krzywanski J, Ostapiuk-Karolczuk J, Kasperska A. Cell and molecular mechanisms of regeneration and reorganization of skeletal muscles. *Ortop Traumatol Rehabil.* 2012;14(1):1-11.
396. Hernandez-Hernandez JM, Garcia-Gonzalez EG, Brun CE, Rudnicki MA. The myogenic regulatory factors, determinants of muscle development, cell identity and regeneration. *Semin Cell Dev Biol.* 2017;72:10-8.
397. Buas MF, Kadesch T. Regulation of skeletal myogenesis by Notch. *Exp Cell Res.* 2010;316(18):3028-33.
398. Rudnicki MA, Schnegelsberg PN, Stead RH, Braun T, Arnold HH, Jaenisch R. MyoD or Myf-5 is required for the formation of skeletal muscle. *Cell.* 1993;75(7):1351-9.
399. Hasty P, Bradley A, Morris JH, Edmondson DG, Venuti JM, Olson EN, et al. Muscle deficiency and neonatal death in mice with a targeted mutation in the myogenin gene. *Nature.* 1993;364(6437):501-6.
400. Nabeshima Y, Hanaoka K, Hayasaka M, Esumi E, Li S, Nonaka I, et al. Myogenin gene disruption results in perinatal lethality because of severe muscle defect. *Nature.* 1993;364(6437):532-5.
401. Yoon JK, Olson EN, Arnold HH, Wold BJ. Different MRF4 knockout alleles differentially disrupt Myf-5 expression: cis-regulatory interactions at the MRF4/Myf-5 locus. *Dev Biol.* 1997;188(2):349-62.
402. Lepper C, Fan CM. Inducible lineage tracing of Pax7-descendant cells reveals embryonic origin of adult satellite cells. *Genesis.* 2010;48(7):424-36.
403. Decary S, Mouly V, Hamida CB, Sautet A, Barbet JP, Butler-Browne GS. Replicative potential and telomere length in human skeletal muscle: implications for satellite cell-mediated gene therapy. *Hum Gene Ther.* 1997;8(12):1429-38.
404. Schmalbruch H, Lewis DM. Dynamics of nuclei of muscle fibers and connective tissue cells in normal and denervated rat muscles. *Muscle Nerve.* 2000;23(4):617-26.
405. Cossu G, Cicinelli P, Fieri C, Coletta M, Molinaro M. Emergence of TPA-resistant 'satellite' cells during muscle histogenesis of human limb. *Exp Cell Res.* 1985;160(2):403-11.
406. Cossu G, Molinaro M. Cell heterogeneity in the myogenic lineage. *Curr Top Dev Biol.* 1987;23:185-208.
407. Cossu G, Molinaro M, Pacifici M. Differential response of satellite cells and embryonic myoblasts to a tumor promoter. *Dev Biol.* 1983;98(2):520-4.
408. Sanes JR. The basement membrane/basal lamina of skeletal muscle. *J Biol Chem.* 2003;278(15):12601-4.
409. Schultz E, Gibson MC, Champion T. Satellite cells are mitotically quiescent in mature mouse muscle: an EM and radioautographic study. *J Exp Zool.* 1978;206(3):451-6.
410. Kuang S, Rudnicki MA. The emerging biology of satellite cells and their therapeutic potential. *Trends Mol Med.* 2008;14(2):82-91.
411. Charge SB, Rudnicki MA. Cellular and molecular regulation of muscle regeneration. *Physiol Rev.* 2004;84(1):209-38.
412. McCarthy JJ, Mula J, Miyazaki M, Erfani R, Garrison K, Farooqui AB, et al. Effective fiber hypertrophy in satellite cell-depleted skeletal muscle. *Development.* 2011;138(17):3657-66.
413. Zammit PS, Relaix F, Nagata Y, Ruiz AP, Collins CA, Partridge TA, et al. Pax7 and myogenic progression in skeletal muscle satellite cells. *J Cell Sci.* 2006;119(Pt 9):1824-32.
414. Rampalli S, Li L, Mak E, Ge K, Brand M, Tapscott SJ, et al. p38 MAPK signaling regulates recruitment of Ash2L-containing methyltransferase complexes to specific genes during differentiation. *Nat Struct Mol Biol.* 2007;14(12):1150-6.
415. Olguin HC, Olwin BB. Pax-7 up-regulation inhibits myogenesis and cell cycle progression in satellite cells: a potential mechanism for self-renewal. *Dev Biol.* 2004;275(2):375-88.
416. Blanco-Bose WE, Yao CC, Kramer RH, Blau HM. Purification of mouse primary myoblasts based on alpha 7 integrin expression. *Exp Cell Res.* 2001;265(2):212-20.
417. Boppart MD, Burkin DJ, Kaufman SJ. Alpha7beta1-integrin regulates mechanotransduction and prevents skeletal muscle injury. *Am J Physiol Cell Physiol.* 2006;290(6):C1660-5.

418. Dumont NA, Wang YX, Rudnicki MA. Intrinsic and extrinsic mechanisms regulating satellite cell function. *Development*. 2015;142(9):1572-81.
419. Gussoni E, Soneoka Y, Strickland CD, Buzney EA, Khan MK, Flint AF, et al. Dystrophin expression in the mdx mouse restored by stem cell transplantation. *Nature*. 1999;401(6751):390-4.
420. Jackson KA, Mi T, Goodell MA. Hematopoietic potential of stem cells isolated from murine skeletal muscle. *Proc Natl Acad Sci U S A*. 1999;96(25):14482-6.
421. Aqmasheh S, Shamsasanjan K, Akbarzadehlaleh P, Pashoutan Sarvar D, Timari H. Effects of Mesenchymal Stem Cell Derivatives on Hematopoiesis and Hematopoietic Stem Cells. *Adv Pharm Bull*. 2017;7(2):165-77.
422. Asakura A, Seale P, Girgis-Gabardo A, Rudnicki MA. Myogenic specification of side population cells in skeletal muscle. *J Cell Biol*. 2002;159(1):123-34.
423. Tamaki T, Akatsuka A, Okada Y, Matsuzaki Y, Okano H, Kimura M. Growth and differentiation potential of main- and side-population cells derived from murine skeletal muscle. *Exp Cell Res*. 2003;291(1):83-90.
424. Tamaki T, Akatsuka A, Ando K, Nakamura Y, Matsuzawa H, Hotta T, et al. Identification of myogenic-endothelial progenitor cells in the interstitial spaces of skeletal muscle. *J Cell Biol*. 2002;157(4):571-7.
425. Zheng B, Cao B, Crisan M, Sun B, Li G, Logar A, et al. Prospective identification of myogenic endothelial cells in human skeletal muscle. *Nat Biotechnol*. 2007;25(9):1025-34.
426. Grimaldi A, Banfi S, Gerosa L, Tettamanti G, Noonan DM, Valvassori R, et al. Identification, isolation and expansion of myoendothelial cells involved in leech muscle regeneration. *PLoS One*. 2009;4(10):e7652.
427. Nguyen PD, Hollway GE, Sonntag C, Miles LB, Hall TE, Berger S, et al. Haematopoietic stem cell induction by somite-derived endothelial cells controlled by meox1. *Nature*. 2014;512(7514):314-8.
428. Tidball JG, Villalta SA. Regulatory interactions between muscle and the immune system during muscle regeneration. *Am J Physiol Regul Integr Comp Physiol*. 2010;298(5):R1173-87.
429. Saclier M, Theret M, Mounier R, Chazaud B. Effects of Macrophage Conditioned-Medium on Murine and Human Muscle Cells: Analysis of Proliferation, Differentiation, and Fusion. *Methods Mol Biol*. 2017;1556:317-27.
430. Zhang J, Muri J, Fitzgerald G, Gorski T, Gianni-Barrera R, Masschelein E, et al. Endothelial Lactate Controls Muscle Regeneration from Ischemia by Inducing M2-like Macrophage Polarization. *Cell Metab*. 2020;31(6):1136-53 e7.
431. Bhattacharya D, Scime A. Mitochondrial Function in Muscle Stem Cell Fates. *Front Cell Dev Biol*. 2020;8:480.
432. Arnold L, Henry A, Poron F, Baba-Amer Y, van Rooijen N, Plonquet A, et al. Inflammatory monocytes recruited after skeletal muscle injury switch into antiinflammatory macrophages to support myogenesis. *J Exp Med*. 2007;204(5):1057-69.
433. Heil M, Ziegelhoeffer T, Wagner S, Fernandez B, Helisch A, Martin S, et al. Collateral artery growth (arteriogenesis) after experimental arterial occlusion is impaired in mice lacking CC-chemokine receptor-2. *Circ Res*. 2004;94(5):671-7.
434. Waeckel L, Bignon J, Liu JM, Markovits D, Ebrahimian TG, Vilar J, et al. Tetrapeptide AcSDKP induces postischemic neovascularization through monocyte chemoattractant protein-1 signaling. *Arterioscler Thromb Vasc Biol*. 2006;26(4):773-9.
435. Cochain C, Rodero MP, Vilar J, Recalde A, Richart AL, Loinard C, et al. Regulation of monocyte subset systemic levels by distinct chemokine receptors controls post-ischaemic neovascularization. *Cardiovasc Res*. 2010;88(1):186-95.
436. Warren GL, Hulderman T, Mishra D, Gao X, Millecchia L, O'Farrell L, et al. Chemokine receptor CCR2 involvement in skeletal muscle regeneration. *FASEB J*. 2005;19(3):413-5.
437. Summan M, Warren GL, Mercer RR, Chapman R, Hulderman T, Van Rooijen N, et al. Macrophages and skeletal muscle regeneration: a clodronate-containing liposome depletion study. *Am J Physiol Regul Integr Comp Physiol*. 2006;290(6):R1488-95.
438. Barros MH, Hauck F, Dreyer JH, Kempkes B, Niedobitek G. Macrophage polarisation: an immunohistochemical approach for identifying M1 and M2 macrophages. *PLoS One*. 2013;8(11):e80908.

439. Sica A, Erreni M, Allavena P, Porta C. Macrophage polarization in pathology. *Cell Mol Life Sci*. 2015;72(21):4111-26.
440. Varga T, Mounier R, Horvath A, Cuvellier S, Dumont F, Poliska S, et al. Highly Dynamic Transcriptional Signature of Distinct Macrophage Subsets during Sterile Inflammation, Resolution, and Tissue Repair. *J Immunol*. 2016;196(11):4771-82.
441. Brigitte M, Schilte C, Plonquet A, Baba-Amer Y, Henri A, Charlier C, et al. Muscle resident macrophages control the immune cell reaction in a mouse model of notexin-induced myoinjury. *Arthritis Rheum*. 2010;62(1):268-79.
442. Uderhardt S, Martins AJ, Tsang JS, Lammermann T, Germain RN. Resident Macrophages Cloak Tissue Microlesions to Prevent Neutrophil-Driven Inflammatory Damage. *Cell*. 2019;177(3):541-55 e17.
443. Zordan P, Rigamonti E, Freudenberg K, Conti V, Azzoni E, Rovere-Querini P, et al. Macrophages commit postnatal endothelium-derived progenitors to angiogenesis and restrict endothelial to mesenchymal transition during muscle regeneration. *Cell Death Dis*. 2014;5:e1031.
444. Ochoa O, Sun D, Reyes-Reyna SM, Waite LL, Michalek JE, McManus LM, et al. Delayed angiogenesis and VEGF production in CCR2^{-/-} mice during impaired skeletal muscle regeneration. *Am J Physiol Regul Integr Comp Physiol*. 2007;293(2):R651-61.
445. Dimmeler S. Regulation of bone marrow-derived vascular progenitor cell mobilization and maintenance. *Arterioscler Thromb Vasc Biol*. 2010;30(6):1088-93.
446. Silvestre JS, Smadja DM, Levy BI. Postischemic revascularization: from cellular and molecular mechanisms to clinical applications. *Physiol Rev*. 2013;93(4):1743-802.
447. Theret M, Mounier R, Rossi F. The origins and non-canonical functions of macrophages in development and regeneration. *Development*. 2019;146(9).
448. Lesniewski LA, Miller TA, Armstrong RB. Mechanisms of force loss in diabetic mouse skeletal muscle. *Muscle Nerve*. 2003;28(4):493-500.
449. Punkt K, Psinia I, Welt K, Barth W, Asmussen G. Effects on skeletal muscle fibres of diabetes and Ginkgo biloba extract treatment. *Acta Histochem*. 1999;101(1):53-69.
450. Krause MP, Riddell MC, Gordon CS, Imam SA, Cafarelli E, Hawke TJ. Diabetic myopathy differs between Ins2Akita^{+/-} and streptozotocin-induced Type 1 diabetic models. *J Appl Physiol* (1985). 2009;106(5):1650-9.
451. Sexton WL, Poole DC, Mathieu-Costello O. Microcirculatory structure-function relationships in skeletal muscle of diabetic rats. *Am J Physiol*. 1994;266(4 Pt 2):H1502-11.
452. Kamei Y, Miura S, Suzuki M, Kai Y, Mizukami J, Taniguchi T, et al. Skeletal muscle FOXO1 (FKHR) transgenic mice have less skeletal muscle mass, down-regulated Type I (slow twitch/red muscle) fiber genes, and impaired glycemic control. *J Biol Chem*. 2004;279(39):41114-23.
453. Rodriguez T, Alvarez B, Busquets S, Carbo N, Lopez-Soriano FJ, Argiles JM. The increased skeletal muscle protein turnover of the streptozotocin diabetic rat is associated with high concentrations of branched-chain amino acids. *Biochem Mol Med*. 1997;61(1):87-94.
454. Pette D, Staron RS. Mammalian skeletal muscle fiber type transitions. *Int Rev Cytol*. 1997;170:143-223.
455. Peterson JM, Bryner RW, Alway SE. Satellite cell proliferation is reduced in muscles of obese Zucker rats but restored with loading. *Am J Physiol Cell Physiol*. 2008;295(2):C521-8.
456. McMillan DE. Diabetic angiopathy--its lessons in vascular physiology. *Am Heart J*. 1978;96(3):401-6.
457. Greco AV, Tataranni PA, Mingrone G, De Gaetano A, Manto A, Cotroneo P, et al. Daily energy metabolism in patients with type 1 diabetes mellitus. *J Am Coll Nutr*. 1995;14(3):286-91.
458. Thamer C, Stumvoll M, Niess A, Tschritter O, Haap M, Becker R, et al. Reduced skeletal muscle oxygen uptake and reduced beta-cell function: two early abnormalities in normal glucose-tolerant offspring of patients with type 2 diabetes. *Diabetes Care*. 2003;26(7):2126-32.
459. Halvatsiotis P, Short KR, Bigelow M, Nair KS. Synthesis rate of muscle proteins, muscle functions, and amino acid kinetics in type 2 diabetes. *Diabetes*. 2002;51(8):2395-404.
460. Bak JF, Jacobsen UK, Jorgensen FS, Pedersen O. Insulin receptor function and glycogen synthase activity in skeletal muscle biopsies from patients with insulin-dependent diabetes mellitus: effects of physical training. *J Clin Endocrinol Metab*. 1989;69(1):158-64.

461. Kruszynska YT, Mulford MI, Baloga J, Yu JG, Olefsky JM. Regulation of skeletal muscle hexokinase II by insulin in nondiabetic and NIDDM subjects. *Diabetes*. 1998;47(7):1107-13.
462. D'Souza DM, Zhou S, Rebalka IA, MacDonald B, Moradi J, Krause MP, et al. Decreased Satellite Cell Number and Function in Humans and Mice With Type 1 Diabetes Is the Result of Altered Notch Signaling. *Diabetes*. 2016;65(10):3053-61.
463. Jeong J, Conboy MJ, Conboy IM. Pharmacological inhibition of myostatin/TGF-beta receptor/pSmad3 signaling rescues muscle regenerative responses in mouse model of type 1 diabetes. *Acta Pharmacol Sin*. 2013;34(8):1052-60.
464. Aragno M, Mastrocola R, Catalano MG, Brignardello E, Danni O, Boccuzzi G. Oxidative stress impairs skeletal muscle repair in diabetic rats. *Diabetes*. 2004;53(4):1082-8.
465. Reis JS, Amaral CA, Volpe CM, Fernandes JS, Borges EA, Isoni CA, et al. Oxidative stress and interleukin-6 secretion during the progression of type 1 diabetes. *Arq Bras Endocrinol Metabol*. 2012;56(7):441-8.
466. Krause MP, Al-Sajee D, D'Souza DM, Rebalka IA, Moradi J, Riddell MC, et al. Impaired macrophage and satellite cell infiltration occurs in a muscle-specific fashion following injury in diabetic skeletal muscle. *PLoS One*. 2013;8(8):e70971.
467. Hu Z, Wang H, Lee IH, Modi S, Wang X, Du J, et al. PTEN inhibition improves muscle regeneration in mice fed a high-fat diet. *Diabetes*. 2010;59(6):1312-20.
468. Woo M, Isganaitis E, Cerletti M, Fitzpatrick C, Wagers AJ, Jimenez-Chillaron J, et al. Early life nutrition modulates muscle stem cell number: implications for muscle mass and repair. *Stem Cells Dev*. 2011;20(10):1763-9.
469. Nguyen MH, Cheng M, Koh TJ. Impaired muscle regeneration in ob/ob and db/db mice. *ScientificWorldJournal*. 2011;11:1525-35.
470. Green CJ, Pedersen M, Pedersen BK, Scheele C. Elevated NF-kappaB activation is conserved in human myocytes cultured from obese type 2 diabetic patients and attenuated by AMP-activated protein kinase. *Diabetes*. 2011;60(11):2810-9.
471. Gaster M, Rustan AC, Aas V, Beck-Nielsen H. Reduced lipid oxidation in skeletal muscle from type 2 diabetic subjects may be of genetic origin: evidence from cultured myotubes. *Diabetes*. 2004;53(3):542-8.
472. Gaster M, Petersen I, Hojlund K, Poulsen P, Beck-Nielsen H. The diabetic phenotype is conserved in myotubes established from diabetic subjects: evidence for primary defects in glucose transport and glycogen synthase activity. *Diabetes*. 2002;51(4):921-7.
473. Scarda A, Franzin C, Milan G, Sanna M, Dal Pra C, Pagano C, et al. Increased adipogenic conversion of muscle satellite cells in obese Zucker rats. *Int J Obes (Lond)*. 2010;34(8):1319-27.
474. Evans JL, Goldfine ID, Maddux BA, Grodsky GM. Oxidative stress and stress-activated signaling pathways: a unifying hypothesis of type 2 diabetes. *Endocr Rev*. 2002;23(5):599-622.
475. Beckman JA, Creager MA, Libby P. Diabetes and atherosclerosis: epidemiology, pathophysiology, and management. *JAMA*. 2002;287(19):2570-81.
476. Luan J, Xu J, Zhong W, Zhou Y, Liu H, Qian K. Adverse Prognosis of Peripheral Artery Disease Treatments Associated With Diabetes: A Comprehensive Meta-Analysis. *Angiology*. 2022;73(4):318-30.
477. Waltenberger J. Impaired collateral vessel development in diabetes: potential cellular mechanisms and therapeutic implications. *Cardiovasc Res*. 2001;49(3):554-60.
478. Ahari A, Bergqvist D, Troeng T, Elfstrom J, Hedberg B, Ljungstrom K, et al. Diabetes mellitus as a risk factor for early outcome after carotid endarterectomy--a population-based study. *Eur J Vasc Endovasc Surg*. 1999;18(2):122-6.
479. Mathew V, Gersh BJ, Williams BA, Laskey WK, Willerson JT, Tilbury RT, et al. Outcomes in patients with diabetes mellitus undergoing percutaneous coronary intervention in the current era: a report from the Prevention of REStenosis with Tranilast and its Outcomes (PRESTO) trial. *Circulation*. 2004;109(4):476-80.
480. Goldberg RB. Cytokine and cytokine-like inflammation markers, endothelial dysfunction, and imbalanced coagulation in development of diabetes and its complications. *J Clin Endocrinol Metab*. 2009;94(9):3171-82.
481. Roberts AC, Porter KE. Cellular and molecular mechanisms of endothelial dysfunction in diabetes. *Diab Vasc Dis Res*. 2013;10(6):472-82.

482. Tousoulis D, Papageorgiou N, Androulakis E, Siasos G, Latsios G, Tentolouris K, et al. Diabetes mellitus-associated vascular impairment: novel circulating biomarkers and therapeutic approaches. *J Am Coll Cardiol*. 2013;62(8):667-76.
483. Guzik TJ, Mussa S, Gastaldi D, Sadowski J, Ratnatunga C, Pillai R, et al. Mechanisms of increased vascular superoxide production in human diabetes mellitus: role of NAD(P)H oxidase and endothelial nitric oxide synthase. *Circulation*. 2002;105(14):1656-62.
484. Alp NJ, Mussa S, Khoo J, Cai S, Guzik T, Jefferson A, et al. Tetrahydrobiopterin-dependent preservation of nitric oxide-mediated endothelial function in diabetes by targeted transgenic GTP-cyclohydrolase I overexpression. *J Clin Invest*. 2003;112(5):725-35.
485. Voinea M, Georgescu A, Manea A, Dragomir E, Manduteanu I, Popov D, et al. Superoxide dismutase entrapped-liposomes restore the impaired endothelium-dependent relaxation of resistance arteries in experimental diabetes. *Eur J Pharmacol*. 2004;484(1):111-8.
486. Wenzel P, Schulz E, Oelze M, Muller J, Schuhmacher S, Alhamdani MS, et al. AT1-receptor blockade by telmisartan upregulates GTP-cyclohydrolase I and protects eNOS in diabetic rats. *Free Radic Biol Med*. 2008;45(5):619-26.
487. Huijberts MS, Wolffenbuttel BH, Boudier HA, Crijns FR, Kruseman AC, Poitevin P, et al. Aminoguanidine treatment increases elasticity and decreases fluid filtration of large arteries from diabetic rats. *J Clin Invest*. 1993;92(3):1407-11.
488. Forstermann U, Sessa WC. Nitric oxide synthases: regulation and function. *Eur Heart J*. 2012;33(7):829-37, 37a-37d.
489. Wilson DK, Bohren KM, Gabbay KH, Quijcho FA. An unlikely sugar substrate site in the 1.65 Å structure of the human aldose reductase holoenzyme implicated in diabetic complications. *Science*. 1992;257(5066):81-4.
490. Kolm-Litty V, Sauer U, Nerlich A, Lehmann R, Schleicher ED. High glucose-induced transforming growth factor beta1 production is mediated by the hexosamine pathway in porcine glomerular mesangial cells. *J Clin Invest*. 1998;101(1):160-9.
491. Xia P, Kramer RM, King GL. Identification of the mechanism for the inhibition of Na⁺,K⁺-adenosine triphosphatase by hyperglycemia involving activation of protein kinase C and cytosolic phospholipase A2. *J Clin Invest*. 1995;96(2):733-40.
492. Ganz MB, Seftel A. Glucose-induced changes in protein kinase C and nitric oxide are prevented by vitamin E. *Am J Physiol Endocrinol Metab*. 2000;278(1):E146-52.
493. Bento CF, Pereira P. Regulation of hypoxia-inducible factor 1 and the loss of the cellular response to hypoxia in diabetes. *Diabetologia*. 2011;54(8):1946-56.
494. Catrina SB, Okamoto K, Pereira T, Brismar K, Poellinger L. Hyperglycemia regulates hypoxia-inducible factor-1alpha protein stability and function. *Diabetes*. 2004;53(12):3226-32.
495. Rivard A, Silver M, Chen D, Kearney M, Magner M, Annex B, et al. Rescue of diabetes-related impairment of angiogenesis by intramuscular gene therapy with adeno-VEGF. *Am J Pathol*. 1999;154(2):355-63.
496. Hazarika S, Dokun AO, Li Y, Popel AS, Kontos CD, Annex BH. Impaired angiogenesis after hindlimb ischemia in type 2 diabetes mellitus: differential regulation of vascular endothelial growth factor receptor 1 and soluble vascular endothelial growth factor receptor 1. *Circ Res*. 2007;101(9):948-56.
497. Murohara T, Asahara T, Silver M, Bauters C, Masuda H, Kalka C, et al. Nitric oxide synthase modulates angiogenesis in response to tissue ischemia. *J Clin Invest*. 1998;101(11):2567-78.
498. Tamarat R, Silvestre JS, Le Ricousse-Roussanne S, Barateau V, Lecomte-Raclet L, Clergue M, et al. Impairment in ischemia-induced neovascularization in diabetes: bone marrow mononuclear cell dysfunction and therapeutic potential of placenta growth factor treatment. *Am J Pathol*. 2004;164(2):457-66.
499. Fadini GP, Sartore S, Albiero M, Baesso I, Murphy E, Menegolo M, et al. Number and function of endothelial progenitor cells as a marker of severity for diabetic vasculopathy. *Arterioscler Thromb Vasc Biol*. 2006;26(9):2140-6.
500. Rosso A, Balsamo A, Gambino R, Dentelli P, Falcioni R, Cassader M, et al. p53 Mediates the accelerated onset of senescence of endothelial progenitor cells in diabetes. *J Biol Chem*. 2006;281(7):4339-47.

501. Fadini GP, de Kreutzenberg SV, Boscaro E, Albiero M, Cappellari R, Krankel N, et al. An unbalanced monocyte polarisation in peripheral blood and bone marrow of patients with type 2 diabetes has an impact on microangiopathy. *Diabetologia*. 2013;56(8):1856-66.
502. Jadhav A, Tiwari S, Lee P, Ndisang JF. The heme oxygenase system selectively enhances the anti-inflammatory macrophage-M2 phenotype, reduces pericardial adiposity, and ameliorated cardiac injury in diabetic cardiomyopathy in Zucker diabetic fatty rats. *J Pharmacol Exp Ther*. 2013;345(2):239-49.
503. Waltenberger J, Lange J, Kranz A. Vascular endothelial growth factor-A-induced chemotaxis of monocytes is attenuated in patients with diabetes mellitus: A potential predictor for the individual capacity to develop collaterals. *Circulation*. 2000;102(2):185-90.
504. Carr CL, Qi Y, Davidson B, Chadderdon S, Jayaweera AR, Belcik JT, et al. Dysregulated selectin expression and monocyte recruitment during ischemia-related vascular remodeling in diabetes mellitus. *Arterioscler Thromb Vasc Biol*. 2011;31(11):2526-33.
505. Spinetti G, Cordella D, Fortunato O, Sangalli E, Losa S, Gotti A, et al. Global remodeling of the vascular stem cell niche in bone marrow of diabetic patients: implication of the microRNA-155/FOXO3a signaling pathway. *Circ Res*. 2013;112(3):510-22.
506. Fadini GP, Sartore S, Schiavon M, Albiero M, Baesso I, Cabrelle A, et al. Diabetes impairs progenitor cell mobilisation after hindlimb ischaemia-reperfusion injury in rats. *Diabetologia*. 2006;49(12):3075-84.
507. Otamas A, Grant PJ, Ajjan RA. Diabetes and atherothrombosis: The circadian rhythm and role of melatonin in vascular protection. *Diab Vasc Dis Res*. 2020;17(3):1479164120920582.
508. Busik JV, Tikhonenko M, Bhatwadekar A, Opreanu M, Yakubova N, Caballero S, et al. Diabetic retinopathy is associated with bone marrow neuropathy and a depressed peripheral clock. *J Exp Med*. 2009;206(13):2897-906.
509. Renault MA, Chapouly C, Yao Q, Larrieu-Lahargue F, Vandierdonck S, Reynaud A, et al. Desert hedgehog promotes ischemia-induced angiogenesis by ensuring peripheral nerve survival. *Circ Res*. 2013;112(5):762-70.
510. Moriya J, Minamino T, Tateno K, Okada S, Uemura A, Shimizu I, et al. Inhibition of semaphorin as a novel strategy for therapeutic angiogenesis. *Circ Res*. 2010;106(2):391-8.
511. Wilson BD, Li M, Park KW, Suli A, Sorensen LK, Larrieu-Lahargue F, et al. Netrins promote developmental and therapeutic angiogenesis. *Science*. 2006;313(5787):640-4.
512. Schgoer W, Theurl M, Albrecht-Schgoer K, Jonach V, Koller B, Lener D, et al. Secretoneurin gene therapy improves blood flow in an ischemia model in type 1 diabetic mice by enhancing therapeutic neovascularization. *PLoS One*. 2013;8(9):e74029.
513. Salis MB, Graiani G, Desortes E, Caldwell RB, Madeddu P, Emanuelli C. Nerve growth factor supplementation reverses the impairment, induced by Type 1 diabetes, of hindlimb post-ischaemic recovery in mice. *Diabetologia*. 2004;47(6):1055-63.
514. Yan J, Tie G, Park B, Yan Y, Nowicki PT, Messina LM. Recovery from hind limb ischemia is less effective in type 2 than in type 1 diabetic mice: roles of endothelial nitric oxide synthase and endothelial progenitor cells. *J Vasc Surg*. 2009;50(6):1412-22.
515. Simons M. Angiogenesis, arteriogenesis, and diabetes: paradigm reassessed? *J Am Coll Cardiol*. 2005;46(5):835-7.
516. Howangyin KY, Silvestre JS. Diabetes mellitus and ischemic diseases: molecular mechanisms of vascular repair dysfunction. *Arterioscler Thromb Vasc Biol*. 2014;34(6):1126-35.
517. Toledo-Flores D, Williamson A, Schwarz N, Fernando S, Dimasi C, Witt TA, et al. Vasculogenic properties of adventitial Sca-1(+)CD45(+) progenitor cells in mice: a potential source of vasa vasorum in atherosclerosis. *Sci Rep*. 2019;9(1):7286.
518. Psaltis PJ, Puranik AS, Spoon DB, Chue CD, Hoffman SJ, Witt TA, et al. Characterization of a resident population of adventitial macrophage progenitor cells in postnatal vasculature. *Circ Res*. 2014;115(3):364-75.
519. Auffray C, Fogg DK, Narni-Mancinelli E, Senechal B, Trouillet C, Saederup N, et al. CX3CR1+ CD115+ CD135+ common macrophage/DC precursors and the role of CX3CR1 in their response to inflammation. *J Exp Med*. 2009;206(3):595-606.
520. A. Williamson DT-F, S. Liyanage, M. Hassanshahi, C. Dimasi, N. Schwarz, S. Fernando, T. Salagaras, Aaron Long, B. D. Di Bartolo, J. Kazenwadel, N. Harvey, G. Drummond, Antony Vinh, V.

- Chandrasekaran, A. Misra, Joanne T. M. Tan, C. Bonder, S. Nicholls, C. Bursill, P. Psaltis. Self-renewing tissue-resident endothelial-macrophage progenitor cells originate from yolk sac and are a local source of inflammation and neovascularization in postnatal aorta. *bioRxiv*. 2022.
521. Sieweke MH, Allen JE. Beyond stem cells: self-renewal of differentiated macrophages. *Science*. 2013;342(6161):1242974.
522. Williamson A. Discovery and characterisation of yolk-sac derived Endothelial-Macrophage progenitor cells in postnatal murine tissues [Traditional]: University of Adelaide; 2022.
523. Henn D, Chen K, Fehlmann T, Trotsyuk AA, Sivaraj D, Maan ZN, et al. Xenogeneic skin transplantation promotes angiogenesis and tissue regeneration through activated Trem2(+) macrophages. *Sci Adv*. 2021;7(49):eabi4528.
524. Rodero MP, Khosrotehrani K. Skin wound healing modulation by macrophages. *Int J Clin Exp Pathol*. 2010;3(7):643-53.
525. Minutti CM, Knipper JA, Allen JE, Zaiss DM. Tissue-specific contribution of macrophages to wound healing. *Semin Cell Dev Biol*. 2017;61:3-11.
526. Ellis S, Lin EJ, Tartar D. Immunology of Wound Healing. *Curr Dermatol Rep*. 2018;7(4):350-8.
527. Krzyszczyk P, Schloss R, Palmer A, Berthiaume F. The Role of Macrophages in Acute and Chronic Wound Healing and Interventions to Promote Pro-wound Healing Phenotypes. *Front Physiol*. 2018;9:419.
528. Banyard DA, Adnani BO, Melkumyan S, Araniego CA, Widgerow AD. Endothelial progenitor cells and burn injury - exploring the relationship. *Burns Trauma*. 2016;4:4.
529. Wang C, Wang Q, Gao W, Zhang Z, Lou Y, Jin H, et al. Highly efficient local delivery of endothelial progenitor cells significantly potentiates angiogenesis and full-thickness wound healing. *Acta Biomater*. 2018;69:156-69.
530. Psaltis PJ, Harbuzariu A, Delacroix S, Witt TA, Holroyd EW, Spoon DB, et al. Identification of a monocyte-predisposed hierarchy of hematopoietic progenitor cells in the adventitia of postnatal murine aorta. *Circulation*. 2012;125(4):592-603.
531. Mulligan-Kehoe MJ, Simons M. Vasa vasorum in normal and diseased arteries. *Circulation*. 2014;129(24):2557-66.
532. Mader SL, Libal NL, Pritchett-Corning K, Yang R, Murphy SJ. Refining timed pregnancies in two strains of genetically engineered mice. *Lab Animal*. 2009;38(9):305-10.
533. Bordt EA, Block CL, Petrozziello T, Sadri-Vakili G, Smith CJ, Edlow AG, et al. Isolation of Microglia from Mouse or Human Tissue. *STAR Protoc*. 2020;1(1).
534. Tan JT, Prosser HC, Dunn LL, Vanags LZ, Ridiandries A, Tsatralis T, et al. High-Density Lipoproteins Rescue Diabetes-Impaired Angiogenesis via Scavenger Receptor Class B Type I. *Diabetes*. 2016;65(10):3091-103.
535. Niiyama H, Huang NF, Rollins MD, Cooke JP. Murine model of hindlimb ischemia. *J Vis Exp*. 2009(23).
536. Dunn L, Prosser HCG, Tan JTM, Vanags LZ, Ng MKC, Bursill CA. Murine Model of Wound Healing. *Journal of Visualized Experiments*. 2013(75).
537. Kauffman ME, Kauffman MK, Traore K, Zhu H, Trush MA, Jia Z, et al. MitoSOX-Based Flow Cytometry for Detecting Mitochondrial ROS. *React Oxyg Species (Apex)*. 2016;2(5):361-70.
538. Breuer K, Foroushani AK, Laird MR, Chen C, Sribnaia A, Lo R, et al. InnateDB: systems biology of innate immunity and beyond--recent updates and continuing curation. *Nucleic Acids Res*. 2013;41(Database issue):D1228-33.
539. Chambers SE, O'Neill CL, O'Doherty TM, Medina RJ, Stitt AW. The role of immune-related myeloid cells in angiogenesis. *Immunobiology*. 2013;218(11):1370-5.
540. Zorzi P, Aplin AC, Smith KD, Nicosia RF. Technical Advance: The rat aorta contains resident mononuclear phagocytes with proliferative capacity and proangiogenic properties. *J Leukoc Biol*. 2010;88(5):1051-9.
541. Cahill TJ, Sun X, Ravaud C, Villa Del Campo C, Klaourakis K, Lupu IE, et al. Tissue-resident macrophages regulate lymphatic vessel growth and patterning in the developing heart. *Development*. 2021;148(3).
542. van Furth R, Cohn ZA. The origin and kinetics of mononuclear phagocytes. *J Exp Med*. 1968;128(3):415-35.

543. Medvinsky A, Rybtsov S, Taoudi S. Embryonic origin of the adult hematopoietic system: advances and questions. *Development*. 2011;138(6):1017-31.
544. Psaltis PJ, Simari RD. Vascular wall progenitor cells in health and disease. *Circ Res*. 2015;116(8):1392-412.
545. Gurevich DB, David DT, Sundararaman A, Patel J. Endothelial Heterogeneity in Development and Wound Healing. *Cells*. 2021;10(9).
546. Bleriot C, Chakarov S, Ginhoux F. Determinants of Resident Tissue Macrophage Identity and Function. *Immunity*. 2020;52(6):957-70.
547. Fijany A, Sayadi LR, Khoshab N, Banyard DA, Shaterian A, Alexander M, et al. Mesenchymal stem cell dysfunction in diabetes. *Mol Biol Rep*. 2019;46(1):1459-75.
548. Yin D, Tao J, Lee DD, Shen J, Hara M, Lopez J, et al. Recovery of islet beta-cell function in streptozotocin- induced diabetic mice: an indirect role for the spleen. *Diabetes*. 2006;55(12):3256-63.
549. Karagiannis TC, El-Osta A. Double-strand breaks: signaling pathways and repair mechanisms. *Cell Mol Life Sci*. 2004;61(17):2137-47.
550. Redon C, Pilch D, Rogakou E, Sedelnikova O, Newrock K, Bonner W. Histone H2A variants H2AX and H2AZ. *Curr Opin Genet Dev*. 2002;12(2):162-9.
551. Yoder MC. Is endothelium the origin of endothelial progenitor cells? *Arterioscler Thromb Vasc Biol*. 2010;30(6):1094-103.
552. Fadini GP, Agostini C, Sartore S, Avogaro A. Endothelial progenitor cells in the natural history of atherosclerosis. *Atherosclerosis*. 2007;194(1):46-54.
553. Evren E, Ringqvist E, Willinger T. Origin and ontogeny of lung macrophages: from mice to humans. *Immunology*. 2020;160(2):126-38.
554. Bajpai G, Schneider C, Wong N, Bredemeyer A, Hulsmans M, Nahrendorf M, et al. The human heart contains distinct macrophage subsets with divergent origins and functions. *Nat Med*. 2018;24(8):1234-45.
555. Malissen B, Tamoutounour S, Henri S. The origins and functions of dendritic cells and macrophages in the skin. *Nat Rev Immunol*. 2014;14(6):417-28.
556. Crosby JR, Kaminski WE, Schatteman G, Martin PJ, Raines EW, Seifert RA, et al. Endothelial cells of hematopoietic origin make a significant contribution to adult blood vessel formation. *Circ Res*. 2000;87(9):728-30.
557. Chen S, Yang J, Wei Y, Wei X. Epigenetic regulation of macrophages: from homeostasis maintenance to host defense. *Cell Mol Immunol*. 2020;17(1):36-49.
558. Panara V, Monteiro R, Koltowska K. Epigenetic Regulation of Endothelial Cell Lineages During Zebrafish Development-New Insights From Technical Advances. *Front Cell Dev Biol*. 2022;10:891538.
559. Penttila S, Vihola A, Palmio J, Udd B. ANO5 Muscle Disease. In: Adam MP, Everman DB, Mirzaa GM, Pagon RA, Wallace SE, Bean LJH, et al., editors. *GeneReviews*((R)). Seattle (WA)1993.
560. Xiong Y, Zhuang R, Zhao G, Liu Y, Su Y, Wang W, et al. Identification of the CKM Gene as a Potential Muscle-Specific Safe Harbor Locus in Pig Genome. *Genes (Basel)*. 2022;13(5).
561. Hayashida T, Takahashi F, Chiba N, Brachtel E, Takahashi M, Godin-Heymann N, et al. HOXB9, a gene overexpressed in breast cancer, promotes tumorigenicity and lung metastasis. *Proc Natl Acad Sci U S A*. 2010;107(3):1100-5.
562. Sugiyama H. WT1 (Wilms' tumor gene 1): biology and cancer immunotherapy. *Jpn J Clin Oncol*. 2010;40(5):377-87.
563. Long A. Identification & Characterisation of Haemangioblasts in Adult Human Vasculature 2019.
564. Zhu FB, Liu DW, Zhang HY, Xu JC, Peng Y, Zhong QL, et al. [Effect of substance P combined with epidermal stem cells on wound healing and nerve regeneration in rats with diabetes mellitus]. *Zhonghua Shao Shang Za Zhi*. 2012;28(1):25-31.
565. Schrauwen P, Hesselink MK. Oxidative capacity, lipotoxicity, and mitochondrial damage in type 2 diabetes. *Diabetes*. 2004;53(6):1412-7.
566. Noriega-Cisneros R, Cortes-Rojas C, Manzo-Avalos S, Clemente-Guerrero M, Calderon-Cortes E, Salgado-Garciglia R, et al. Mitochondrial response to oxidative and nitrosative stress in early stages of diabetes. *Mitochondrion*. 2013;13(6):835-40.
567. Gerstein HC, Nair V, Chaube R, Stoute H, Werstuck G. Dysglycemia and the Density of the Coronary Vasa Vasorum. *Diabetes Care*. 2019;42(5):980-2.

568. Haertel E, Werner S, Schafer M. Transcriptional regulation of wound inflammation. *Semin Immunol.* 2014;26(4):321-8.
569. Tammela T, Zarkada G, Nurmi H, Jakobsson L, Heinolainen K, Tvorogov D, et al. VEGFR-3 controls tip to stalk conversion at vessel fusion sites by reinforcing Notch signalling. *Nat Cell Biol.* 2011;13(10):1202-13.
570. Dight J, Zhao J, Styke C, Khosrotehrani K, Patel J. Resident vascular endothelial progenitor definition and function: the age of reckoning. *Angiogenesis.* 2022;25(1):15-33.
571. Aird WC. Endothelial cell heterogeneity. *Cold Spring Harb Perspect Med.* 2012;2(1):a006429.
572. Wakabayashi T, Naito H, Suehiro JI, Lin Y, Kawaji H, Iba T, et al. CD157 Marks Tissue-Resident Endothelial Stem Cells with Homeostatic and Regenerative Properties. *Cell Stem Cell.* 2018;22(3):384-97 e6.
573. Barman PK, Koh TJ. Macrophage Dysregulation and Impaired Skin Wound Healing in Diabetes. *Front Cell Dev Biol.* 2020;8:528.
574. Laing T, Hanson R, Chan F, Bouchier-Hayes D. The role of endothelial dysfunction in the pathogenesis of impaired diabetic wound healing: a novel therapeutic target? *Med Hypotheses.* 2007;69(5):1029-31.
575. Dai X, Yan X, Zeng J, Chen J, Wang Y, Chen J, et al. Elevating CXCR7 Improves Angiogenic Function of EPCs via Akt/GSK-3beta/Fyn-Mediated Nrf2 Activation in Diabetic Limb Ischemia. *Circ Res.* 2017;120(5):e7-e23.
576. Balaji S, Han N, Moles C, Shaaban AF, Bollyky PL, Crombleholme TM, et al. Angiopoietin-1 improves endothelial progenitor cell-dependent neovascularization in diabetic wounds. *Surgery.* 2015;158(3):846-56.
577. Jin H, Zhang Z, Wang C, Tang Q, Wang J, Bai X, et al. Melatonin protects endothelial progenitor cells against AGE-induced apoptosis via autophagy flux stimulation and promotes wound healing in diabetic mice. *Exp Mol Med.* 2018;50(11):1-15.
578. Filippini A, Tamagnone L, D'Alessio A. Endothelial Cell Metabolism in Vascular Functions. *Cancers (Basel).* 2022;14(8).
579. Shenouda SM, Widlansky ME, Chen K, Xu G, Holbrook M, Tabit CE, et al. Altered mitochondrial dynamics contributes to endothelial dysfunction in diabetes mellitus. *Circulation.* 2011;124(4):444-53.
580. Wang L, Hu J, Zhou H. Macrophage and Adipocyte Mitochondrial Dysfunction in Obesity-Induced Metabolic Diseases. *World J Mens Health.* 2021;39(4):606-14.
581. Zhong QL, Liu FR, Liu DW, Peng Y, Zhang XR. Expression of beta-catenin and cyclin D1 in epidermal stem cells of diabetic rats. *Mol Med Rep.* 2011;4(2):377-81.
582. Dunn L, Prosser HC, Tan JT, Vanags LZ, Ng MK, Bursill CA. Murine model of wound healing. *J Vis Exp.* 2013(75):e50265.
583. Oliveira PJ, Rolo AP, Seica R, Palmeira CM, Santos MS, Moreno AJ. Decreased susceptibility of heart mitochondria from diabetic GK rats to mitochondrial permeability transition induced by calcium phosphate. *Biosci Rep.* 2001;21(1):45-53.
584. Tabak O, Gelisgen R, Erman H, Erdenen F, Muderrisoglu C, Aral H, et al. Oxidative lipid, protein, and DNA damage as oxidative stress markers in vascular complications of diabetes mellitus. *Clin Invest Med.* 2011;34(3):E163-71.
585. Piccolo G, Banfi P, Azan G, Rizzuto R, Bisson R, Sandona D, et al. Biological markers of oxidative stress in mitochondrial myopathies with progressive external ophthalmoplegia. *J Neurol Sci.* 1991;105(1):57-60.
586. Soucie EL, Weng Z, Geirsdottir L, Molawi K, Maurizio J, Fenouil R, et al. Lineage-specific enhancers activate self-renewal genes in macrophages and embryonic stem cells. *Science.* 2016;351(6274):aad5510.
587. Suda T, Takubo K, Semenza GL. Metabolic regulation of hematopoietic stem cells in the hypoxic niche. *Cell Stem Cell.* 2011;9(4):298-310.
588. Klimmeck D, Hansson J, Raffel S, Vakhrushev SY, Trumpp A, Krijgsveld J. Proteomic cornerstones of hematopoietic stem cell differentiation: distinct signatures of multipotent progenitors and myeloid committed cells. *Mol Cell Proteomics.* 2012;11(8):286-302.
589. Guillet-Deniau I, Leturque A, Girard J. Expression and cellular localization of glucose transporters (GLUT1, GLUT3, GLUT4) during differentiation of myogenic cells isolated from rat foetuses. *J Cell Sci.* 1994;107 (Pt 3):487-96.

590. Yang C, Zhang ZH, Lu SH, Yang RC, Qian GQ, Han ZC. [Transplantation of cord blood endothelial progenitor cells ameliorates limb ischemia]. *Zhonghua Yi Xue Za Zhi*. 2003;83(16):1437-41.
591. Leng M, Peng Y, Pan M, Wang H. Experimental Study on the Effect of Allogeneic Endothelial Progenitor Cells on Wound Healing in Diabetic Mice. *J Diabetes Res*. 2021;2021:9962877.
592. Kaushik K, Das A. Endothelial progenitor cell therapy for chronic wound tissue regeneration. *Cytotherapy*. 2019;21(11):1137-50.
593. Tanaka R, Ito-Hirano R, Fujimura S, Arita K, Hagiwara H, Mita T, et al. Ex vivo conditioning of peripheral blood mononuclear cells of diabetic patients promotes vasculogenic wound healing. *Stem Cells Transl Med*. 2021;10(6):895-909.
594. Li M, Zhao Y, Hao H, Han W, Fu X. Mesenchymal stem cell-based therapy for nonhealing wounds: today and tomorrow. *Wound Repair Regen*. 2015;23(4):465-82.
595. Humpert PM, Bartsch U, Konrade I, Hammes HP, Morcos M, Kasper M, et al. Locally applied mononuclear bone marrow cells restore angiogenesis and promote wound healing in a type 2 diabetic patient. *Exp Clin Endocrinol Diabetes*. 2005;113(9):538-40.
596. Udhayabanu T, Manole A, Rajeshwari M, Varalakshmi P, Houlden H, Ashokkumar B. Riboflavin Responsive Mitochondrial Dysfunction in Neurodegenerative Diseases. *J Clin Med*. 2017;6(5).
597. Virmani MA, Cirulli M. The Role of L-Carnitine in Mitochondria, Prevention of Metabolic Inflexibility and Disease Initiation. *Int J Mol Sci*. 2022;23(5).
598. Sigvant B, Lundin F, Wahlberg E. The Risk of Disease Progression in Peripheral Arterial Disease is Higher than Expected: A Meta-Analysis of Mortality and Disease Progression in Peripheral Arterial Disease. *Eur J Vasc Endovasc Surg*. 2016;51(3):395-403.
599. Norgren L, Hiatt WR, Dormandy JA, Nehler MR, Harris KA, Fowkes FG, et al. Inter-Society Consensus for the Management of Peripheral Arterial Disease (TASC II). *J Vasc Surg*. 2007;45 Suppl S:S5-67.
600. Takahara M. Diabetes Mellitus and Lower Extremity Peripheral Artery Disease. *JMA J*. 2021;4(3):225-31.
601. Aerden D, Massaad D, von Kemp K, van Tussenbroek F, Debing E, Keymeulen B, et al. The ankle-brachial index and the diabetic foot: a troublesome marriage. *Ann Vasc Surg*. 2011;25(6):770-7.
602. Jude EB, Oyibo SO, Chalmers N, Boulton AJ. Peripheral arterial disease in diabetic and nondiabetic patients: a comparison of severity and outcome. *Diabetes Care*. 2001;24(8):1433-7.
603. DeRubertis BG, Pierce M, Ryer EJ, Trocciola S, Kent KC, Faries PL. Reduced primary patency rate in diabetic patients after percutaneous intervention results from more frequent presentation with limb-threatening ischemia. *J Vasc Surg*. 2008;47(1):101-8.
604. Kelley DE, He J, Menshikova EV, Ritov VB. Dysfunction of mitochondria in human skeletal muscle in type 2 diabetes. *Diabetes*. 2002;51(10):2944-50.
605. Anderson EJ, Lustig ME, Boyle KE, Woodlief TL, Kane DA, Lin CT, et al. Mitochondrial H₂O₂ emission and cellular redox state link excess fat intake to insulin resistance in both rodents and humans. *J Clin Invest*. 2009;119(3):573-81.
606. Petersen KF, Dufour S, Befroy D, Garcia R, Shulman GI. Impaired mitochondrial activity in the insulin-resistant offspring of patients with type 2 diabetes. *N Engl J Med*. 2004;350(7):664-71.
607. Pipinos II, Judge AR, Zhu Z, Selsby JT, Swanson SA, Johanning JM, et al. Mitochondrial defects and oxidative damage in patients with peripheral arterial disease. *Free Radic Biol Med*. 2006;41(2):262-9.
608. Makris KI, Nella AA, Zhu Z, Swanson SA, Casale GP, Gutti TL, et al. Mitochondriopathy of peripheral arterial disease. *Vascular*. 2007;15(6):336-43.
609. Tran TP, Tu H, Liu J, Muellemann RL, Li YL. Mitochondria-derived superoxide links to tourniquet-induced apoptosis in mouse skeletal muscle. *PLoS One*. 2012;7(8):e43410.
610. Lejay A, Meyer A, Schlagowski AI, Charles AL, Singh F, Bouitbir J, et al. Mitochondria: mitochondrial participation in ischemia-reperfusion injury in skeletal muscle. *Int J Biochem Cell Biol*. 2014;50:101-5.
611. Lejay A, Laverny G, Paradis S, Schlagowski AI, Charles AL, Singh F, et al. Moderate Exercise Allows for shorter Recovery Time in Critical Limb Ischemia. *Front Physiol*. 2017;8:523.

612. Paradis S, Charles AL, Meyer A, Lejay A, Scholey JW, Chakfe N, et al. Chronology of mitochondrial and cellular events during skeletal muscle ischemia-reperfusion. *Am J Physiol Cell Physiol.* 2016;310(11):C968-82.
613. Mouton AJ, Li X, Hall ME, Hall JE. Obesity, Hypertension, and Cardiac Dysfunction: Novel Roles of Immunometabolism in Macrophage Activation and Inflammation. *Circ Res.* 2020;126(6):789-806.
614. Catrysse L, van Loo G. Adipose tissue macrophages and their polarization in health and obesity. *Cell Immunol.* 2018;330:114-9.
615. Bosca L, Gonzalez-Ramos S, Prieto P, Fernandez-Velasco M, Mojena M, Martin-Sanz P, et al. Metabolic signatures linked to macrophage polarization: from glucose metabolism to oxidative phosphorylation. *Biochem Soc Trans.* 2015;43(4):740-4.
616. O'Neill LA, Pearce EJ. Immunometabolism governs dendritic cell and macrophage function. *J Exp Med.* 2016;213(1):15-23.
617. Kohchi C, Inagawa H, Nishizawa T, Soma G. ROS and innate immunity. *Anticancer Res.* 2009;29(3):817-21.
618. Padgett LE, Burg AR, Lei W, Tse HM. Loss of NADPH oxidase-derived superoxide skews macrophage phenotypes to delay type 1 diabetes. *Diabetes.* 2015;64(3):937-46.
619. Madonna R, De Caterina R. Cellular and molecular mechanisms of vascular injury in diabetes--part II: cellular mechanisms and therapeutic targets. *Vascul Pharmacol.* 2011;54(3-6):75-9.
620. Giacco F, Brownlee M. Oxidative stress and diabetic complications. *Circ Res.* 2010;107(9):1058-70.
621. Miao H, Ou J, Ma Y, Guo F, Yang Z, Wiggins M, et al. Macrophage CGI-58 deficiency activates ROS-inflammasome pathway to promote insulin resistance in mice. *Cell Rep.* 2014;7(1):223-35.
622. Tabit CE, Chung WB, Hamburg NM, Vita JA. Endothelial dysfunction in diabetes mellitus: molecular mechanisms and clinical implications. *Rev Endocr Metab Disord.* 2010;11(1):61-74.
623. Hong H, Tian XY. The Role of Macrophages in Vascular Repair and Regeneration after Ischemic Injury. *Int J Mol Sci.* 2020;21(17).
624. Rigamonti E, Zordan P, Sciorati C, Rovere-Querini P, Brunelli S. Macrophage plasticity in skeletal muscle repair. *Biomed Res Int.* 2014;2014:560629.
625. Gautier EL, Shay T, Miller J, Greter M, Jakubzick C, Ivanov S, et al. Gene-expression profiles and transcriptional regulatory pathways that underlie the identity and diversity of mouse tissue macrophages. *Nat Immunol.* 2012;13(11):1118-28.
626. Gosselin D, Link VM, Romanoski CE, Fonseca GJ, Eichenfield DZ, Spann NJ, et al. Environment drives selection and function of enhancers controlling tissue-specific macrophage identities. *Cell.* 2014;159(6):1327-40.
627. Krishnasamy K, Limbourg A, Kapanadze T, Gamrekelashvili J, Beger C, Hager C, et al. Blood vessel control of macrophage maturation promotes arteriogenesis in ischemia. *Nat Commun.* 2017;8(1):952.
628. Li Z, Solomonidis EG, Meloni M, Taylor RS, Duffin R, Dobie R, et al. Single-cell transcriptome analyses reveal novel targets modulating cardiac neovascularization by resident endothelial cells following myocardial infarction. *Eur Heart J.* 2019;40(30):2507-20.
629. Bailey AS, Jiang S, Afentoulis M, Baumann CI, Schroeder DA, Olson SB, et al. Transplanted adult hematopoietic stem cells differentiate into functional endothelial cells. *Blood.* 2004;103(1):13-9.
630. Park C, Ma YD, Choi K. Evidence for the hemangioblast. *Exp Hematol.* 2005;33(9):965-70.
631. Shi J, Kandror KV. Study of glucose uptake in adipose cells. *Methods Mol Biol.* 2008;456:307-15.
632. Stork BA, Dean A, York B. Methodology for measuring oxidative capacity of isolated peroxisomes in the Seahorse assay. *J Biol Methods.* 2022;9(2):e160.
633. Fadini GP, DiPersio JF. Diabetes mellitus as a poor mobilizer condition. *Blood Rev.* 2018;32(3):184-91.
634. Fadini GP, Ciciliot S, Albiero M. Concise Review: Perspectives and Clinical Implications of Bone Marrow and Circulating Stem Cell Defects in Diabetes. *Stem Cells.* 2017;35(1):106-16.

635. Fadini GP, Rigato M, Cappellari R, Bonora BM, Avogaro A. Long-term Prediction of Cardiovascular Outcomes by Circulating CD34+ and CD34+CD133+ Stem Cells in Patients With Type 2 Diabetes. *Diabetes Care*. 2017;40(1):125-31.
636. Rennert RC, Sorkin M, Januszyk M, Duscher D, Kosaraju R, Chung MT, et al. Diabetes impairs the angiogenic potential of adipose-derived stem cells by selectively depleting cellular subpopulations. *Stem Cell Res Ther*. 2014;5(3):79.
637. Fujimaki S, Wakabayashi T, Asashima M, Takemasa T, Kuwabara T. Treadmill running induces satellite cell activation in diabetic mice. *Biochem Biophys Rep*. 2016;8:6-13.
638. Rossi DJ, Jamieson CH, Weissman IL. Stems cells and the pathways to aging and cancer. *Cell*. 2008;132(4):681-96.
639. Shyh-Chang N, Daley GQ, Cantley LC. Stem cell metabolism in tissue development and aging. *Development*. 2013;140(12):2535-47.
640. Asmann YW, Stump CS, Short KR, Coenen-Schimke JM, Guo Z, Bigelow ML, et al. Skeletal muscle mitochondrial functions, mitochondrial DNA copy numbers, and gene transcript profiles in type 2 diabetic and nondiabetic subjects at equal levels of low or high insulin and euglycemia. *Diabetes*. 2006;55(12):3309-19.
641. Livet J, Weissman TA, Kang H, Draft RW, Lu J, Bennis RA, et al. Transgenic strategies for combinatorial expression of fluorescent proteins in the nervous system. *Nature*. 2007;450(7166):56-62.
642. Katakam PV, Jordan JE, Snipes JA, Tulbert CD, Miller AW, Busija DW. Myocardial preconditioning against ischemia-reperfusion injury is abolished in Zucker obese rats with insulin resistance. *Am J Physiol Regul Integr Comp Physiol*. 2007;292(2):R920-6.
643. O'Malley Y, Fink BD, Ross NC, Prinszano TE, Sivitz WI. Reactive oxygen and targeted antioxidant administration in endothelial cell mitochondria. *J Biol Chem*. 2006;281(52):39766-75.
644. Mehmehl M, Jovanovic N, Spitz U. Nicotinamide Riboside-The Current State of Research and Therapeutic Uses. *Nutrients*. 2020;12(6).
645. Sun X, Cao B, Naval-Sanchez M, Pham T, Sun YBY, Williams B, et al. Nicotinamide riboside attenuates age-associated metabolic and functional changes in hematopoietic stem cells. *Nat Commun*. 2021;12(1):2665.
646. Fang J, Guo Y, Tan S, Li Z, Xie H, Chen P, et al. Autologous Endothelial Progenitor Cells Transplantation for Acute Ischemic Stroke: A 4-Year Follow-Up Study. *Stem Cells Transl Med*. 2019;8(1):14-21.
647. Geng J, Wang L, Qu M, Song Y, Lin X, Chen Y, et al. Endothelial progenitor cells transplantation attenuated blood-brain barrier damage after ischemia in diabetic mice via HIF-1alpha. *Stem Cell Res Ther*. 2017;8(1):163.
648. Masson-Meyers DS, Tayebi L. Vascularization strategies in tissue engineering approaches for soft tissue repair. *J Tissue Eng Regen Med*. 2021;15(9):747-62.
649. Schmeisser A, Garlich CD, Zhang H, Eskafi S, Graffy C, Ludwig J, et al. Monocytes coexpress endothelial and macrophagocytic lineage markers and form cord-like structures in Matrigel under angiogenic conditions. *Cardiovasc Res*. 2001;49(3):671-80.
650. Hirschi KK. Hemogenic endothelium during development and beyond. *Blood*. 2012;119(21):4823-7.
651. Li Z, Liu S, Xu J, Zhang X, Han D, Liu J, et al. Adult Connective Tissue-Resident Mast Cells Originate from Late Erythro-Myeloid Progenitors. *Immunity*. 2018;49(4):640-53 e5.
652. Soares-da-Silva F, Freyer L, Elsaid R, Burlen-Defranoux O, Iturri L, Sismeiro O, et al. Yolk sac, but not hematopoietic stem cell-derived progenitors, sustain erythropoiesis throughout murine embryonic life. *J Exp Med*. 2021;218(4).
653. Yahara Y, Barrientos T, Tang YJ, Puviindran V, Nadesan P, Zhang H, et al. Erythromyeloid progenitors give rise to a population of osteoclasts that contribute to bone homeostasis and repair. *Nat Cell Biol*. 2020;22(1):49-59.
654. MA. H. *Embryology Mouse Development*. 2021.
655. Kwon HM, Sangiorgi G, Ritman EL, McKenna C, Holmes DR, Jr., Schwartz RS, et al. Enhanced coronary vasa vasorum neovascularization in experimental hypercholesterolemia. *J Clin Invest*. 1998;101(8):1551-6.

656. Zambidis ET, Park TS, Yu W, Tam A, Levine M, Yuan X, et al. Expression of angiotensin-converting enzyme (CD143) identifies and regulates primitive hemangioblasts derived from human pluripotent stem cells. *Blood*. 2008;112(9):3601-14.
657. Solly EL, Psaltis PJ, Bursill CA, Tan JTM. The Role of miR-181c in Mechanisms of Diabetes-Impaired Angiogenesis: An Emerging Therapeutic Target for Diabetic Vascular Complications. *Front Pharmacol*. 2021;12:718679.
658. Hosang C, Saliba RM, Ahlawat S, Korbliing M, Kebriaei P, Alousi A, et al. Poor hematopoietic stem cell mobilizers: a single institution study of incidence and risk factors in patients with recurrent or relapsed lymphoma. *Am J Hematol*. 2009;84(6):335-7.
659. Chiba H, Ataka K, Iba K, Nagaishi K, Yamashita T, Fujimiya M. Diabetes impairs the interactions between long-term hematopoietic stem cells and osteopontin-positive cells in the endosteal niche of mouse bone marrow. *Am J Physiol Cell Physiol*. 2013;305(7):C693-703.
660. Fadini GP, Losordo D, Dimmeler S. Critical reevaluation of endothelial progenitor cell phenotypes for therapeutic and diagnostic use. *Circ Res*. 2012;110(4):624-37.
661. Fadini GP, Miorin M, Facco M, Bonamico S, Baesso I, Grego F, et al. Circulating endothelial progenitor cells are reduced in peripheral vascular complications of type 2 diabetes mellitus. *J Am Coll Cardiol*. 2005;45(9):1449-57.
662. Egan CG, Lavery R, Caporali F, Fondelli C, Laghi-Pasini F, Dotta F, et al. Generalised reduction of putative endothelial progenitors and CXCR4-positive peripheral blood cells in type 2 diabetes. *Diabetologia*. 2008;51(7):1296-305.
663. Ingram DA, Lien IZ, Mead LE, Estes M, Prater DN, Derr-Yellin E, et al. In vitro hyperglycemia or a diabetic intrauterine environment reduces neonatal endothelial colony-forming cell numbers and function. *Diabetes*. 2008;57(3):724-31.
664. Rota M, LeCapitaine N, Hosoda T, Boni A, De Angelis A, Padin-Iruegas ME, et al. Diabetes promotes cardiac stem cell aging and heart failure, which are prevented by deletion of the p66shc gene. *Circ Res*. 2006;99(1):42-52.
665. Wojakowski W, Tendera M, Michalowska A, Majka M, Kucia M, Maslankiewicz K, et al. Mobilization of CD34/CXCR4+, CD34/CD117+, c-met+ stem cells, and mononuclear cells expressing early cardiac, muscle, and endothelial markers into peripheral blood in patients with acute myocardial infarction. *Circulation*. 2004;110(20):3213-20.
666. Nguyen TQ, Chon H, van Nieuwenhoven FA, Braam B, Verhaar MC, Goldschmeding R. Myofibroblast progenitor cells are increased in number in patients with type 1 diabetes and express less bone morphogenetic protein 6: a novel clue to adverse tissue remodelling? *Diabetologia*. 2006;49(5):1039-48.
667. Sata M. Circulating vascular progenitor cells contribute to vascular repair, remodeling, and lesion formation. *Trends Cardiovasc Med*. 2003;13(6):249-53.
668. Lomeli H, Castillo-Castellanos F. Notch signaling and the emergence of hematopoietic stem cells. *Dev Dyn*. 2020;249(11):1302-17.
669. Beltrami AP, Barlucchi L, Torella D, Baker M, Limana F, Chimenti S, et al. Adult cardiac stem cells are multipotent and support myocardial regeneration. *Cell*. 2003;114(6):763-76.
670. Gehling UM, Ergun S, Schumacher U, Wagener C, Pantel K, Otte M, et al. In vitro differentiation of endothelial cells from AC133-positive progenitor cells. *Blood*. 2000;95(10):3106-12.
671. Lin F, Wang N, Zhang TC. The role of endothelial-mesenchymal transition in development and pathological process. *IUBMB Life*. 2012;64(9):717-23.
672. Di Monte DA, Chan P, Sandy MS. Glutathione in Parkinson's disease: a link between oxidative stress and mitochondrial damage? *Ann Neurol*. 1992;32 Suppl:S111-5.
673. Ma J, Zhang Q, Chen S, Fang B, Yang Q, Chen C, et al. Mitochondrial dysfunction promotes breast cancer cell migration and invasion through HIF1alpha accumulation via increased production of reactive oxygen species. *PLoS One*. 2013;8(7):e69485.
674. Bansal S, Siddarth M, Chawla D, Banerjee BD, Madhu SV, Tripathi AK. Advanced glycation end products enhance reactive oxygen and nitrogen species generation in neutrophils in vitro. *Mol Cell Biochem*. 2012;361(1-2):289-96.
675. Gu X, Ma Y, Liu Y, Wan Q. Measurement of mitochondrial respiration in adherent cells by Seahorse XF96 Cell Mito Stress Test. *STAR Protoc*. 2021;2(1):100245.

676. Tam CS, Lecoultre V, Ravussin E. Novel strategy for the use of leptin for obesity therapy. *Expert Opin Biol Ther.* 2011;11(12):1677-85.
677. Clee SM, Attie AD. The genetic landscape of type 2 diabetes in mice. *Endocr Rev.* 2007;28(1):48-83.
678. Luo J, Quan J, Tsai J, Hobensack CK, Sullivan C, Hector R, et al. Nongenetic mouse models of non-insulin-dependent diabetes mellitus. *Metabolism.* 1998;47(6):663-8.
679. Hadrian K, Willenborg S, Bock F, Cursiefen C, Eming SA, Hos D. Macrophage-Mediated Tissue Vascularization: Similarities and Differences Between Cornea and Skin. *Front Immunol.* 2021;12:667830.
680. Kim YI, Lee FN, Choi WS, Lee S, Youn JH. Insulin regulation of skeletal muscle PDK4 mRNA expression is impaired in acute insulin-resistant states. *Diabetes.* 2006;55(8):2311-7.
681. Yang Y, Luan Y, Feng Q, Chen X, Qin B, Ren KD, et al. Epigenetics and Beyond: Targeting Histone Methylation to Treat Type 2 Diabetes Mellitus. *Front Pharmacol.* 2021;12:807413.
682. Sato Y, Nakagawa M, Higuchi I, Osame M, Naito E, Oizumi K. Mitochondrial myopathy and familial thiamine deficiency. *Muscle Nerve.* 2000;23(7):1069-75.
683. Klopstock T, Metz G, Yu-Wai-Man P, Buchner B, Gallenmuller C, Bailie M, et al. Persistence of the treatment effect of idebenone in Leber's hereditary optic neuropathy. *Brain.* 2013;136(Pt 2):e230.
684. Tarnopolsky MA. Creatine as a therapeutic strategy for myopathies. *Amino Acids.* 2011;40(5):1397-407.
685. Enns GM. Treatment of mitochondrial disorders: antioxidants and beyond. *J Child Neurol.* 2014;29(9):1235-40.
686. Marangon K, Devaraj S, Tirosh O, Packer L, Jialal I. Comparison of the effect of alpha-lipoic acid and alpha-tocopherol supplementation on measures of oxidative stress. *Free Radic Biol Med.* 1999;27(9-10):1114-21.
687. Besouw M, Masereeuw R, van den Heuvel L, Levtschenko E. Cysteamine: an old drug with new potential. *Drug Discov Today.* 2013;18(15-16):785-92.
688. Enns GM, Kinsman SL, Perlman SL, Spicer KM, Abdenur JE, Cohen BH, et al. Initial experience in the treatment of inherited mitochondrial disease with EPI-743. *Mol Genet Metab.* 2012;105(1):91-102.
689. Koga Y, Povalko N, Inoue E, Nakamura H, Ishii A, Suzuki Y, et al. Therapeutic regimen of L-arginine for MELAS: 9-year, prospective, multicenter, clinical research. *J Neurol.* 2018;265(12):2861-74.
690. Rai PK, Russell OM, Lightowlers RN, Turnbull DM. Potential compounds for the treatment of mitochondrial disease. *Br Med Bull.* 2015;116:5-18.